

Names of Researchers	Title of Search	No. of Page
أ.م.د. علي عبد العباس عبد الله البكري	Innovative Technology for Remote Control of the Irrigation System by Modern Control Using Renewable Energy	1-15
د. فواز سلطان عبد الله	Computation of hourly solar radiation using ASHRAE model for some Iraqi cities	16-31
د. وسام عبد علي تويج د. نصير كريم قاسم السوداني د. بهاء طعمة جباد د. عباس حمادي الوتار عبد الكريم عبد الحسين كريم الخفاجي	Influence of $\frac{USDP}{ion\ on\ AE}$ nanopowder particle size on the photocatalytic activity	32-37
م.م علي مجيد محمود م.م احمد رؤوف ناصر م.م بهاء ضياء جليل	Solar cell Monitoring and Actuating via Embedded Web Server	38-47
د. حسن وريوش رشا خالد محمد الدباغ فاطمة حامد رجب	Analytical study of solar cell efficiency enhancement	48-58
م.م ضياء نجم عبد الامير د. قصي عبد الجبار جواد م.م احمد عزيز حاشوش	Study the parameters effect on the design of solar energy system for impressed current cathodic protection for oil pipelines	59-74
أ.م.د علي هادي عبد المنعم د. رفاه عبد الهادي رجاء نادر كيظان	Study the Spectral Nonlinear Properties for of Rhodamine (6G) Dyes Doped Polymer (PMMA) Using Z-Scan Technique	75-84
ماجد حسن علي كريم بهلول جمال حمود علي غازي	تصميم وتصنيع مجهز قدرة متناوب متنقل يعمل بالطاقة الشمسية	85-91
د. فلاح ابراهيم مصطفى امل ساجت صبر سهام زهراوي عباس	تأثير السمك والمعاملة الحرارية على التوصيلية المستمرة لاغشية اوكسيد الكاديوم المحضرة بطريقة الترديز بالبلازما	92-95
أ.م.د عباس زغير سلمان م.م روشن طارق احمد	The comparison analysis of fixed angle wind turbine with that of a double output induction generator	96-107
د. جعفر علي كاظم	The possibility of using savonius wind turbine in the lifting system of wells water	108-121
د. عادل محمود صالح محمد كاظم	Effect of magnetic field on fuel consumption and exhaust emission in internal combustion engine (C.I. Engine)	122-135

Names of Researchers	Title of Search	No. of Page
د. نصير كريم قاسم السوداني أ.د. احمد فرحان عطوان الساعدي علاء حسين شنيشل السوداني	System sizing of solar water heating system	136-149
د. عماد قاسم حسين أ.م.د كريم كاظم جاسم د. صباح عبد الحسن كطافة	Thermal design and analysis of printed circuit board for optimum performance	150-161
علي خالد شاكر ماهر كاظم طاهر	Optimization of tilt angle for solar collector located in northern Iraq cities to receive maximum solar radiation	162-177
م.م كاظم حسين صفر	Experiential study on enhancement of single basin solar still using phase change material (paraffin wax)	178-187
مقدام طارق جيجان خليل ابراهيم عباس محمد احمد رشيد	Using paraffin wax as a thermal storage material in a solar air heater	188-197
د. هاشم عبد حسين	An experimental and theoretical investigation of the dynamic effects of rapid rise in the flow rate on characteristics of the riser tube	198-217
د. احمد منعم حسون فرحان خماس	Observed and Predicted daily wind travels and wind speeds in western Iraq	218-227
أ.م.د علي هادي عبد المنعم أ.د هيفاء غازي رشيد علاء بدر حسن	Design of solar radiation Concentration using microlenses array with waveguide	228-233
أ.د جعفر مهدي حسن د.قصي عبد الجبار جواد م.م ضياء نجم عبد الامير	Modeling and design of flat plate solar collector for using different physical and geometrical condition	234-250
م.م حيدر شريف مهدي م. محمد علي فياض م. اياد محمود سلمان أ.م.د سعد طامي حميدي	The investigation of effect dust on the performance of solar collector with different area	251-262
	Effect different s bonding absorber surface collector on efficiency factor	263-274
د. خالد فيصل سلطان	Numerical Assessment of Thermal Energy and Flow of Nanofluids in a Horizontal and an Inclined Tube Filled with a Porous Medium	275-294
د. جمال محمد حمد	دراسة تقييمية للعوامل المؤثرة على كفاءة خلايا الوقود باستخدام النمذجة والمحاكاة	295-300
م.م وفاء محمد عزيز المهندس . وليد خالد حسين	دراسة وتحليل الجدوى العلمية والاقتصادية باستخدام الطاقة النظيفة بديلا عن مصادر الطاقة التقليدية	301-315
احمد عبد الجبار محمود	دراسة الجدوى من استخدام مولد واحد ميكاتريك بالخلايا الشمسية في منفذ عرعر الحدودي	315-322

تقنية مستحدثة للتحكم عن بعد لمنظومة السقي بواسطة السيطرة الحديثة و باستخدام

Innovative Technology for Remote Control of the Irrigation System by Modern Control Using Renewable Energy

E.mail: ali_albakry2000@yahoo.com

قسم هندسة القدرة الكهربائية / الكلية التقنية / مسيب

تقدم هذه الورقة البحثية مقارنة جديدة لأستخدام التقنية الحديثة و الذكية على منظومات الري التقليدية و باستخدام الطاقة المتجددة (الشمسية) من خلال السيطرة على المحركات الطرفية المنصوبة على بوابات التحكم بمرور المياه و كميته في السواقي الرئيسية و الفرعية في قطعة الارض المخصصة للزراعة. تم نصب متحسسات الرطوبة في قطعة الارض المطلوب زراعتها، تقوم هذه المتحسسات بتغذية اشارة مرتدة الى وحدة السيطرة المركزية (PC) سيطرة منطقية مبرمجة (PLC) و التي تقوم بدورها باعطاء الايعاز المناسب و اللازم لعملية التشغيل و السيطرة على عملية السقي حيث تشمل تشغيل و ايقاف المحركات الطرفية المسيطرة على كمية و سريان الماء، و تشغيل منظومة ارسال البيانات اللاسلكية. تتم جميع هذه العمليات بصورة اوتوماتيكية و بدون تدخل المشغل او الفلاح و هذا يقلل الكلفة الكلية لانتاج و خدمة المحصول. البرمجة الخاصة بعملية الري تتم من خلال استخدام لوحة المفاتيح للحاسبة الطرفية في غرفة السيطرة و ارسال. عملية نقل الاشارة يمكن اجراءها بعدة طرق و اهمها الطريقة التي استخدمت عمليا في هذا البحث عن طريق الشبكة العنكبوتية، اذ ان هذه الشبكة تغطي معظم ارجاء العراق و منها المنطقة الوسطى و بالذات مدينة بابل التي تم تطبيق المشروع و انجازه فعليا و لموسم كامل(الصيف). نتائج المشروع كانت مشجعة اذ تمت السيطرة لاسلكيا و بشكل كامل و اوتوماتيكي و عن بعد. بهذا المشروع البحثي العملي التطبيقي تم الحد من الهدر المائي لا سيما و ان البلد يمر بازمة مائية و بحاجة لكل قطرة ماء. التغذية الكهربائية للمشروع تمت باستخدام الطاقة الكهربائية البديلة كمصدر للتجهيز اذ تم الاعتماد على الطاقة الشمسية في توليد الطاقة الكهربائية اللازمة لتشغيل وحدات المشروع و بهذا نكون قد ارحنا حملا كهربائيا عن شبكة التوزيع الكهربائية مهما كان التوفير قليل نسبيا و لكنه خطوة يمكن تعميمها على مساحات اكثر و بطاقات اكبر في المستقبل القريب.

Abstract

This paper offers a new approach to the use of modern technology and smart irrigation systems on the traditional one. As it is to control the process of irrigation wirelessly and remotely, and that by controlling the organization of the irrigation process through the control of terminal motors, installed at the gates that control the flow and quantity of water in the main and sub in a piece of land allocated for agriculture. The sensors of water level had been installed in selected locations in a piece of land that selected to be cultivated, these sensors feed the feedback signals to the central control unit (PC) or (PLC), which in turn give instruct the appropriate and necessary for the operation and control of the process of irrigation, like

opening and closing the operation of the terminal motors which control the quantity and flow of water and the operation of the sending and receiving wireless data system. All the operations of these processes are automatic and without operator intervention. We have a lot of the workforce, which reduces the total cost to produce the corp. Programming process of irrigation is done through the use of the calculator keyboard terminals in the control room and transmitter. The transfer of the operating and control data can be done in several ways and the most important method used in practice in this research through the Web, as this network covers most parts of Iraq, including the central region and in particular the city of Babylon, where the project implemented and accomplished effectively and for the whole season (summer) . Project results have been encouraging, as was controlled wirelessly and in full and automatic and remotely. This practical applied research project was to reduce wastage of water and especially that the country is in crisis and need every drop of water. Power supply for the project has been using the power of alternative source for processing, as has been relying on solar energy to generate electrical power necessary to run the project and that we have lifted some electric load from electrical the Iraqi electrical distribution network, whatever the savings in energy is relatively small, but this step can be generalized to large spaces in the nearest future.

-1

ان التطور السريع للإنترنت في السنوات الأخيرة ساعد كثيرا في امكانية ايجاد ارضية خصبة للعديد من الافكار العلمية التطبيقية في شتى المجالات العلمية، الصناعية، التجارية و اخيرا الزراعية و التي تطورت بدورها لتتزامن مع التطور الحاصل في الشبكة العنكبوتية العالمية. اذ ان السيطرة بكافة انواعها و اهمها السيطرة الذكية (Intelligent Control) اخذت حيزا كبيرا من هذا التطور و في شتى المجالات التطبيقية و اهم هذه التطبيقات الزراعة الحديثة بانواعها الثلاث المعتمدة في الري في العراق و في شتى بقاع العالم ، الا و هي الري بالرش (Sprinkler Irrigation) قيط (Drip Irrigation) (Surface Irrigation) او الري بالغمر كما يسمى. اذ ان امكانية الجمع بين التحكم و التشغيل الآلي للتقنيات المشتركة بين الزراعة الحديثة و المزايا التي تقوم بتقديمها خدمات الشبكة العنكبوتية العالمية (World Wide Web) امكانية كبيرة و يتوفر فيها مجال خصب للكثير من التطبيقات و منها ما يقدمه بحثنا هذا [1]. هي استخدام نظم تكنولوجيا المراقبة، المعلومات و التنفيذ للحد من لعمل الانسان و تدخله جزئيا او كليا و بالتالي تقليل كلفة المنتج سواء اكان صناعيا او زراعي في نطاق التصنيع والتشغيل الآلي اضافة لتقليل الجهد [2]. ان المزوجة بين الخدمات التي تقدمها الشبكة العنكبوتية العالمية (WWW) و السيطرة الحديثة و الذكية (IC) و المعتمدة على استخدام السيطرة المنطقية المبرمجة (PLC) يفتح المجال واسعا لتطبيقات عديدة و متنوعة و منها التطبيقات في مجال الزراعة الحديثة عن طريق التحكم في عملية السقي بواسطة المتحسسات [4] [3], (Scheduled Irrigation) او ذكيا (Smart Irrigation) باستخدام منظومات التحسس و هو التطبيق المستحدث في هذا البحث. جة للتحكم عن بعد اصبح ضروريا جدا في عمليات المراقبة و اعطاء القرار و التنفيذ، اذ كانت هذه العملية تتم سابقا باستخدام منظومات الارسال و الاستقبال اللاسلكية بين المرسل (المشغل الرئيسي) او ما يسمى ب (Transmitter) و المستقبل (العميل) او ما يسمى ب (Receiver) [5]. هذه التقنية فيها الكثير من السلبيات و التي يمكن تلخيصها بعدة نقاط:

-
- ```

graph LR
 InputData[Input Data] --> Junction1(())
 Junction1 --> RemoteWebClient[Remote web client]
 RemoteWebClient --> NetworkInternet[Network/Internet]
 NetworkInternet --> Junction2(())
 Junction2 --> PLC[Local Controller (PLC)]
 PLC --> ExperimentalSetup[Experimental Setup]
 ExperimentalSetup --> InternetDelay[Internet Delay]
 InternetDelay --> Junction1
 ProgrammingRemoteUnit[Programming Remote Unit] --> NetworkInternet
 PLC <--> PCSCADAServer[PC/SCADA Server]
 subgraph RemotePlant [Remote Plant]
 PLC
 ExperimentalSetup
 PCSCADAServer
 end

```

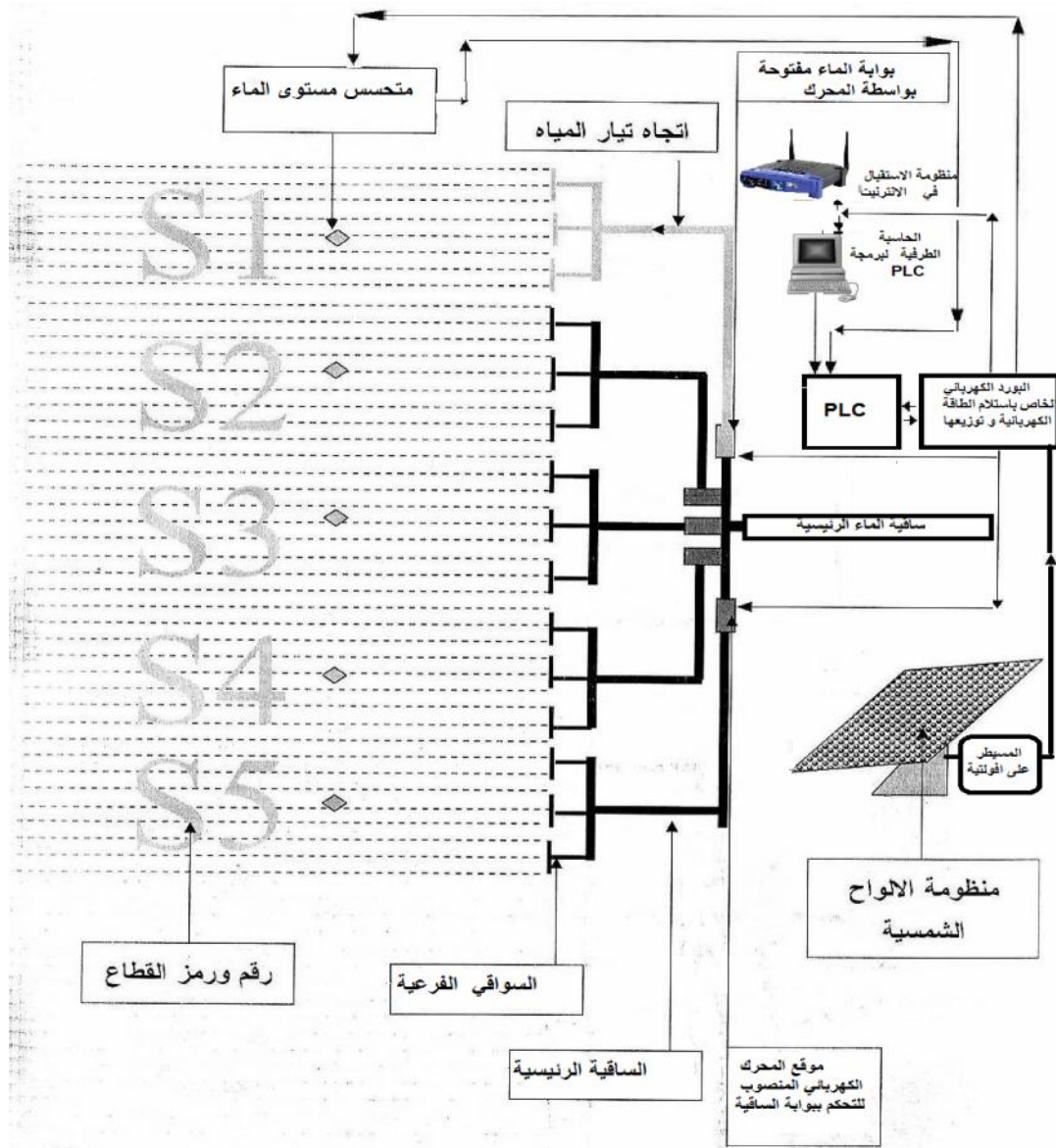
ان الطاقة الشمسية (Solar Energy) تمثل النسبة الاعظم من انواع الطاقة المتجددة المستخدمة عمليا و بالذات في العراق ، اذ ان كثافة الاشعة الشمسية الساقطة و التي تسقط على الاراضي العراقية تعتبر الاكثف عالميا. ان الشمس تمثل المصدر لرئيس للطاقة المشعة الساقطة على الكرة الارضية، اذ ان طاقة الاشعة الكهرومغناطيسية الساقطة تساوي في المتوسط ما يقارب  $1353 \text{ w/m}^2$  [6 7]. لوضع هذا في المنظور، فان الطاقة التي تنتجها 25 فدانا من سطح الشمس ، سيكون كافيا لتلبية الطلب الحالي للطاقة في العالم [8]. عند التعامل مع الطاقة الشمسية ، هناك خياران اساسيان، الأول هو تحويل الطاقة الشمسية مباشرة إلى كهرباء بواسطة الخلايا الفوتوفولتائية ( Photovoltaic Cell). اما الخيار الثاني فهو الطاقة الشمسية الحرارية (Thermal Storage)، و التي يتم فيها استخدام الأشعة الشمسية لتوفير الحرارة إلى نظام الديناميكية الحرارية، وبالتالي خلق الطاقة الميكانيكية التي يمكن تحويلها إلى الكهرباء. في الأنظمة الفوتوفولتائية تمتاز بسهولة التركيب و قلة الكلفة نسبيا بالطريقة الثانية إلا أن كفاءتها تتراوح ما بين 10 15 بينما في نظام الطاقة الشمسية الحرارية، تصل الكفاءة إلى 30 [9 10] و لكن هذه الطريقة تستخدم عند الحاجة الى توليد الطاقة الكهربائية بكميات كبيرة او صناعية بينما الطريقة الاولى تستخدم في الحالتين و تكون اقتصادية لة الكفاءة لذا تم اختيار هذه الطريقة في هذا المشروع البحثي. ان استخدام الطاقة الشمسية في تشغيل معدات الزراعة الحديثة يمثل في اغلب الحالات حلا مثاليا لبعدها عن الاراضي الزراعية عن مصادر الطاقة الكهربائية و بالذات شبكة الكهرباء الوطنية، و بهذا يتحقق هدفا رئيسيا اخر هو احياء و استغلال اراضي زراعية جديدة صالحه للزراعة كانت متروكة سابقا لبعدها عن مصادر المياه و الطاقة.

## 2 - الطريقة المستخدمة في السيطرة على السقي عبر الانترنت

### 1-2 المخطط التفصيلي للمشروع البحثي

تم تنفيذ هذا المشروع البحثي بصورة عملية على قطعة ارض زراعية مساحتها دونم واحد (2500 ) قدرها ( 100 ) ( 25 متر عرض ) و تم تهيئة هذه القطعة (حراثتة، تسوية و تعديل و شق السواقي) و تقسيما قدرها ( 500 ) ( 100 ) ( 5 متر عرض ) حيث تم شق سواقي في كل قطاع و بالتالي يكون عدد السواقي الكلي في عموم القطعة 15 ساقية. تم نصب متحسس لمستوى الماء في (Water Sensor Level) و بهذا سيكون عدد المتحسسات خمسة. و استنادا الى هذا التقسيم لقطعة الارض فان كل قطاع اي كل ثلاث سواقي سيتم السيطرة على ربيها و السيطرة على مستوى الماء في السواقي بواسطة المتحسس المذكور(كون السواقي متماثلة في كل قطاع) و بوابة التحكم بالماء منصوبة على الساقية الفرعية المجهزة للسواقي الثلاث (Servo Motor) يتحكم بفتح و غلق البوابة اعتمادا على الايعاز الواصل اليه من منظومة السيطرة المنطقية المبرمجة (PLC) و التي تعتمد بدورها على الاشارة المرتدة (Feed Back Sensor) و بهذا يكون لدينا خمسة متحسسات و خمس محركات للتحكم ببوابات التحكم بسرمان الماء. يوضح الشكل رقم (2) مخططا يبين جميع اجزاء المشروع البحثي. اذ يتضح من الشكل المذكور منظومة الاستقبال لاشارة الانترنت و التي هي (Access Point)، اذ انه منظم لاستقبال اشارة الانترنت المسموح له باستقبالها وفق سياق تم تنظيمة مسبقا بين منظومة البث او ما يسمى بالخادم (Server) (2) او ما يسمى بالعمل او (Client). الوحدة الاخرى التي تتضح بالشكل هي الحاسبة الطرفية في غرفة السيطرة في موقع العمل و التي تستلم برامج السيطرة من شبكة الانترنت و تقوم بدورها بالسيطرة و تغذية منظومة السيطرة المنطقية المبرمجة (Programmable Logic Control) و التي تقوم بالسيطرة على عملية السقي من خلال الاشارات التنفيذية الخارجة منها الى بورد القدرة الكهربائية الذي يحتوي على المرحلات (Relays) و التي بدورها تقوم بتشغيل الكونكتات التي تسيطر على تشغيل المحركات المنصوبة على بوابات التحكم بسرمان ، اضافة لقيام هذا البورد الكهربائي بتجهيز

الكهرباء لبقية اجزاء المشروع من اجهزة الكترونية ( PLC , PC, Access Point & Sensors ). التغذية الرئيسية للبورء الكهربائي هذا الذي يغذي جميع وحدات المشروع البحثي تتم من خلال منظومة التوليد باستخدام الطاقة الـ (Renewable Energy) اذ تم اختيار الطاقة الشمسية كونها الخيار الامثل للاستغلال من الطاقة المتجددة في الاجواء العراقية كون كثافة الاشعة الساقطة على الاراضي العراقية تعتبر الاكثف عالميا طيلة اشهر السنة مقارنة بالانواع الاخرى الرياح او غيرها.



شكل رقم (2): مخطط يوضح جميع اجزاء المشروع البحثي و طريقة

## 2-2 تصميم منظومة التوليد بالطاقة الشمسية

### 1-2-2 الحسابات التصميمية للأحمال

قبل ان نبدء بأي تصميم لمحطة التوليد باستخدام الطاقة الشمسية، يجب معرفة الحمل المراد ربطه و تشغيله عليها، اذ يتضمن هذا الحمل مايلي:

- منظومة السيطرة المنطقية المبرمجة ال (PLC) (Programmable Logic Control) 30 (P<sub>plc</sub> = 30 w) (12 cm x 10 cm) (8 Input Port) (16 Output Port) و ذلك تحسبا لامكانية تطبيقه و استخدامه للسيطرة على عملية السقي .
- (Servo Motor) عدد خمسة للسيطرة على القطاعات الخمسة من الارض الزراعية 400 (P<sub>m</sub> = 400 w) و بفولتية قدرها 12 – تيار مستمر (12 V - DC).
- تم استخدام مستقبل لأشارة الانترنت نوع (LINKSYS) و بقدرة قدرها 25 (P<sub>Lin</sub> = 25 w).
- (Water Level Sensor) عدد خمسة و بقدرة قدرها 5 (P<sub>s</sub> = 5 w).
- كمبيوتر شخصي لبرمجة ال PLC و لأستقبال البيانات و التعليمات الخاصة بالتشغيل من الطرف الآخر نوع P4 14 100 (P<sub>c</sub> = 100 w).

و بهذا يكون الحمل الكلي:

$$P_T = P_{PLC} + P_m + P_{Lin} + P_s + P_c \quad (1) \dots\dots\dots$$

$$P_T = 30 \text{ w} + 400 \text{ w} + 25 \text{ w} + 5 \text{ w} + 100 \text{ w} = 560 \text{ w}$$

560 (Rated Load = 560 w)، يجب ان يكون التجهيز أعلى او مساوي لهذا الحمل عند تصميم منظومة التوليد باستخدام الطاقة الشمسية لذا تم الأخختيار بأن يكون معدل التوليد للقدرة الكهربائية المجهزة للمنظومة بمقدار 600 (Rated Generated Power) حيث ان الفرق بين التوليد و (2):

$$P_G - P_L = P_{Loss} \quad (2) \dots\dots\dots$$

$$600 \text{ w} - 540 \text{ w} = 60 \text{ w}$$

حيث ان:

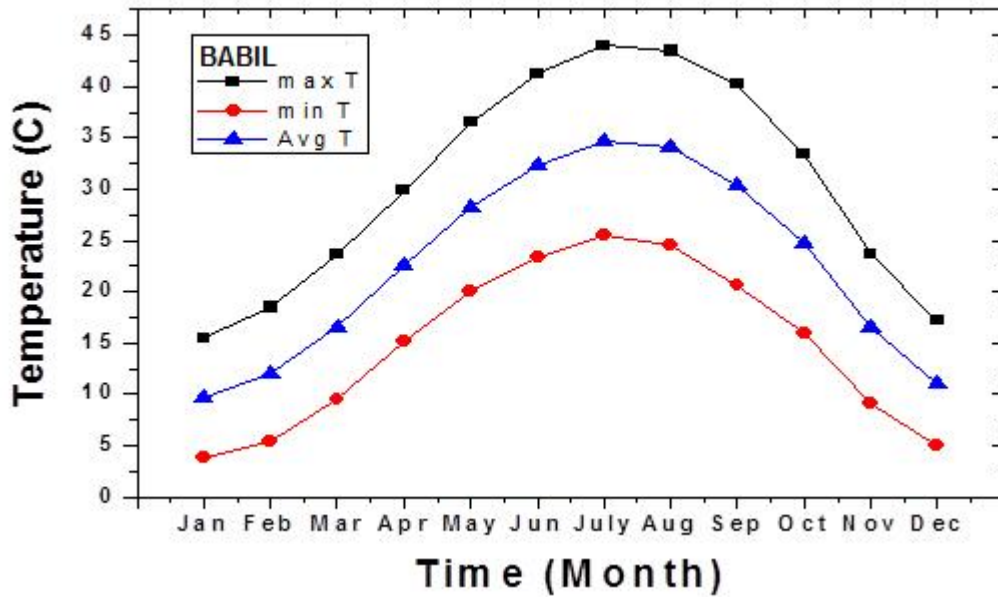
$P_G$  = قدرة توليد منظومة الطاقة الشمسية

$P_L$  = قدرة الحمل الفعلية

$P_{Loss}$  =

## 2-2-2 حساب زاوية ميل الألواح الشمسية

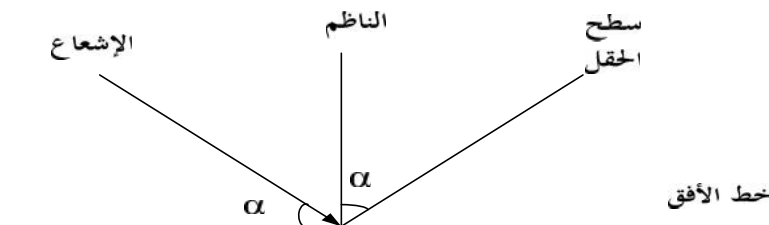
هناك علاقة وثيقة بين زاوية الشعاع الشمسي الساقط حسب اشهر السنة و بالتالي تغير درجة الحرارة للأرض حسب الموقع الجغرافي و التي تتعلق ايضا بكثافة الاشعة الساقطة. اذ يبين الشكل رقم (3) العلاقة بين درجة الحرارة و اشهر 2011 حيث يبين القيمة العظمى ،القيمة الدنيا و المعدل لدرجات الحرارة لمدينة بابل طيلة اشهر السنة و التي تم اختيارها لتنفيذ هذا المشروع البحثي.



(3): يوضح تغير درجات الحرارة مع اشهر السنة في مدينه بابل للعام 2011

يجب تحديد الزاوية التي سيتم بموجبها تحديد ميل حقل الخلايا على الأفق وتدعى هذه الزاوية بزاوية التوجيه وتكون تابعة لخط العرض الجغرافي للموقع وتؤخذ هذه الزاوية كمتوسط على مدار السنة وتوجه الخلايا بموجبها وبعد توجيه حقل الخلايا بمقدار هذه الزاوية يتم تعديل الإشعاع الشمسي الذي يزداد بالنسبة  $1/\cos$  [11].

حيث : زاوية انحراف السطح عن الأفق كما هو مبين في الشكل (4).



شكل رقم (4): زاوية انحراف السطح للألواح الشمسية عن الأفق

من الدراسة التحليلية لحركة الشمس تبين بأن الزاوية المثلى لميل حقل الخلايا الشمسية تتحدد بالعلاقة التالية:

$$\gamma = W - U \quad (3) \dots\dots\dots$$

حيث ان:

:W

U : زاوية ميل الشمس وتؤخذ من الجدول رقم (1).

(1): العلاقة بين زاوية الميلان و اشهر السنة

| الشهر            | 1     | 2     | 3     | 4    | 5     | 6     | 7     | 8     | 9  | 10   | 11    | 12  |         |
|------------------|-------|-------|-------|------|-------|-------|-------|-------|----|------|-------|-----|---------|
| زاوية<br>الميلان | 20.8- | 12.7- | 11.9- | 9.9+ | 18.9+ | 23.1+ | 23.3+ | 13.7+ | 9+ | 8.8- | 18.4- | 23- | 0.1916+ |

ان الموقع الجغرافي لمحطة التوليد باستخدام الطاقة الشمسية في موقع  
مابين دائرتي عرض 29-37 درجة شمالاً وما بين خطي طول 38- 48 درجة شرقاً، اذ يقع في منطقة الفرات الاوسط -  
محافظة بابل و بالذات في قضاء المسيب. لذا فقد تم حساب الموقع الجغرافي للمشروع البحثي هذا باستخدام البرنامج اير  
(Earth Google) وتبين انه يقع بالضبط على خط عرض (33° 10' North) و يرتفع بمقدار 33  
سطح البحر تقريباً. لذا فان هذ المشروع البحثي يقع على خط عرض (33° 10' North) وبأخذ متوسط زاوية ميل الشمس  
:

$$W = 33^{\circ} 10' - 0.1916 = 32^{\circ}.804'$$

يقع في النصف الشمالي من الكرة الأرضية لذا يجب توجيه منظومة الألواح الشمسية باتجاه الجنوب و  
بموازاة الخط الواصل بين الشرق و الغرب، ولكن الجدول ر (1) يظهر الاختلاف الكبير في قيم زاوية ميل الشمس  
وبالتالي زاوية التوجيه لكل شهر من أشهر السنة ولذلك يفضل استخدام أجهزة التتبع ذات المحورين أو ذات المحور الواحد  
لنتم هذه العملية اتوماتيكياً و لكن الكلفة ستكون عالية و الجدوى الاقتصادية ستكون قليلة لكون المسد  
المشروع قليلة (دونم واحد فقط) و ممكن تطوير المشروع مستقبلاً بنصب منظومة التتبع الشمسي لتسيطر على الهيكل  
لذا تم تغيير زاوية الميلان يدوياً و حسب اشهر السنة استناداً على الحسابات في اعلاه.

## 2-3 اختيار الألواح الشمسية ونوعها

استناداً الى الحسابات التصميمية للحمل الكهربائي الكلي للمشروع في الفقرة (2-2-1) و الذي يبلغ (540 w)  
استوجب ان يكون التوليد بقدرة 600 واط تقريباً و هذا يعني اختيار 5 الواح شمسية بقدرة 120 واط لكل منها و بفولتية  
قدرها 12 فولت تقريباً علماً بان الفولتية المتولدة متغيرة ضمن قيم محددة، اذ يمكن السيطرة على الفولتية الخارجة من  
خلال منظم الفولتية (Voltage Controller Cutoff) و يسمى كذلك ب (Voltage Stabilizer)

الذي تم اختياره في ادناه في الاسواق المحلية و بمواصفات جيدة و من منشأ اصلي (ياباني) لذا وقع الاختيار على هذا النوع، اذ تم استخدام خمسة الواح شمسية و بالمواصفات التالية:

Solar panels type: KC120 manufactured by Kyocera of Japan

$P_{max}$ : 120 W

$V_{max}$ : 16.9 V

$I_{max}$  : 7.1 A

Weight : 12 Kg

Dimension (L×W×D) = 1,425 mm × 653 mm × 56 mm

= 0.930 m<sup>2</sup> × 56 mm

و نظرا لأن فولتية التوليد للخلايا الشمسية تتذبذب اعتمادا على مدى كثافة و شدة و زاوية الشعاع الشمسي الساقط، اذ ان الفولتية القياسية العظمى للخلية التي تم اختيارها (KC120 / Kyocera)  $16.9 V =$  يد ذات فولتية قدرها (12 V DC) و هي فولتية مناسبة جدا في حالة التوليد باستخدام الالواح الشمسية لشحن البطاريات المربوطة عليها و التجهيز المباشر للحمل المطلوب لتعويض خسائر الفولتية الناتجة عن التسليك الكهربائي بعد تنظيم هذه الفولتية باستخدام منظم الفولتية (Voltage Regulator) على الفولتية الخارجة من الالواح الشمسية و يحافظ على قيمتها بقيمة مقاربة لل (12 V) و هذا يساعد على حماية الاحمال المربوطة من الزيادة المتوقعة في الفولتية، و ذلك لتذبذب كثافة الاشعة الشمسية الساقطة على الواح الطاقة الشمسية و حسب ساعات النهار و اشهر السنة. اذ تربط الالواح الشمسية الخمسة على التوازي و تربط الفولتية الخارجة عبر منظم الفولتية (Voltage Regulator) منظومة البطاريات و التي تربط بطريقة مشابهه لربط الالواح الشمسية، اذ يساعد هذا المنظم على الحفاظ على فولتية ثابتة لشحن البطاريات اضافة الى وقاية الحمل من زيادة الفولتية و ديمومة الاستقرارية.

#### 4-2-2 منظومة البطاريات (Batteries System):

ان الحسابات التصميمية للبطاريات تعتمد بصورة رئيسية على حسابات التوليد لمنظومة التوليد باستخدام الطاقة الشمسية كما جاء في الفقرة (2-2-1)، لذا فقد تم اختيار بطاريات نوع ( sealed lead acid batteries each of 12 V, 100 AH ) كونها تمثل البطاريات المناسبة و الملائمة للعمل مع منظومة الالواح الشمسية [11] تربط هذه البطاريات على التوازي بأسلوب مشابه لربط الالواح الشمسية لتوليد فولتية قدرها 12 V، وبهذا سنحصل على منظومة بطاريات متكاملة ذات فولتية قدرها 12 V DC و بسعة خزن قدرها 500 امبير- (500 A.H). وجود البطاريات في منظومة التوليد باستخدام الطاقة الشمسية يعتبر ضروري جدا لسببين رئيسيين ، اولهما ان البطاريات تساعد على الحفاظ على استقرارية و موثوقية (Stability & Reliability) فولتية التجهيز و بهذا تعمل البطاريات كمنظم اضافي لفولتية التجهيز يساعد على اخمد كل التغيرات الطارئة في الفولتية سواء اكانت زيادة ام نقصان، اما السبب الثاني و الذي يمثل السبب الرئيسي فهو ضمان استمرارية التشغيل في الاوقات التي تغيب فيها الشمس او تكون كثافة الاشعة الشمسية الساقطة قليلة.

يمثل الشكل رقم (5) التوليد باستخدام الطاقة الشمسية المتكونة من الألواح الشمسية الخمسة المربوطة على التوازي و بقدرة كلية قدرها 600 (120 واط لكل لوح شمسي) منصوبة و مثبتة على الهيكل الحامل لها و الذي يحمل البطاريات الخمسة بسعة كلية قدرها 500 امبير – ساعة و بسعة قدرها 100 امبير – ساعة لكل بطارية، اما من الناحية الاخرى فان هذا الهيكل يوفر حماية للبطاريات من الشعاع الشمسي المباشر و الذي تحجبه الخلايا عن البطاريات و بهذا يساهم هذا التصميم للهيكل في اطالة عمر البطارية و الحفاظ عليها من التلف. الهيكل تم تصميمه ليتمكن من الموقع من تحريكه الى المكان المناسب و بسهولة من خلال تركيبه على عجلات مدولة عدد (6).



( )



( )

(5): ( ) - صورة امامية توضح الألواح الشمسية الخمسة المنصوبة على الهيكل المتحرك و زاوية الميل مع البطاريات الخمسة المثبتة على الهيكل الحامل خلف الألواح الشمسية . ( ) -

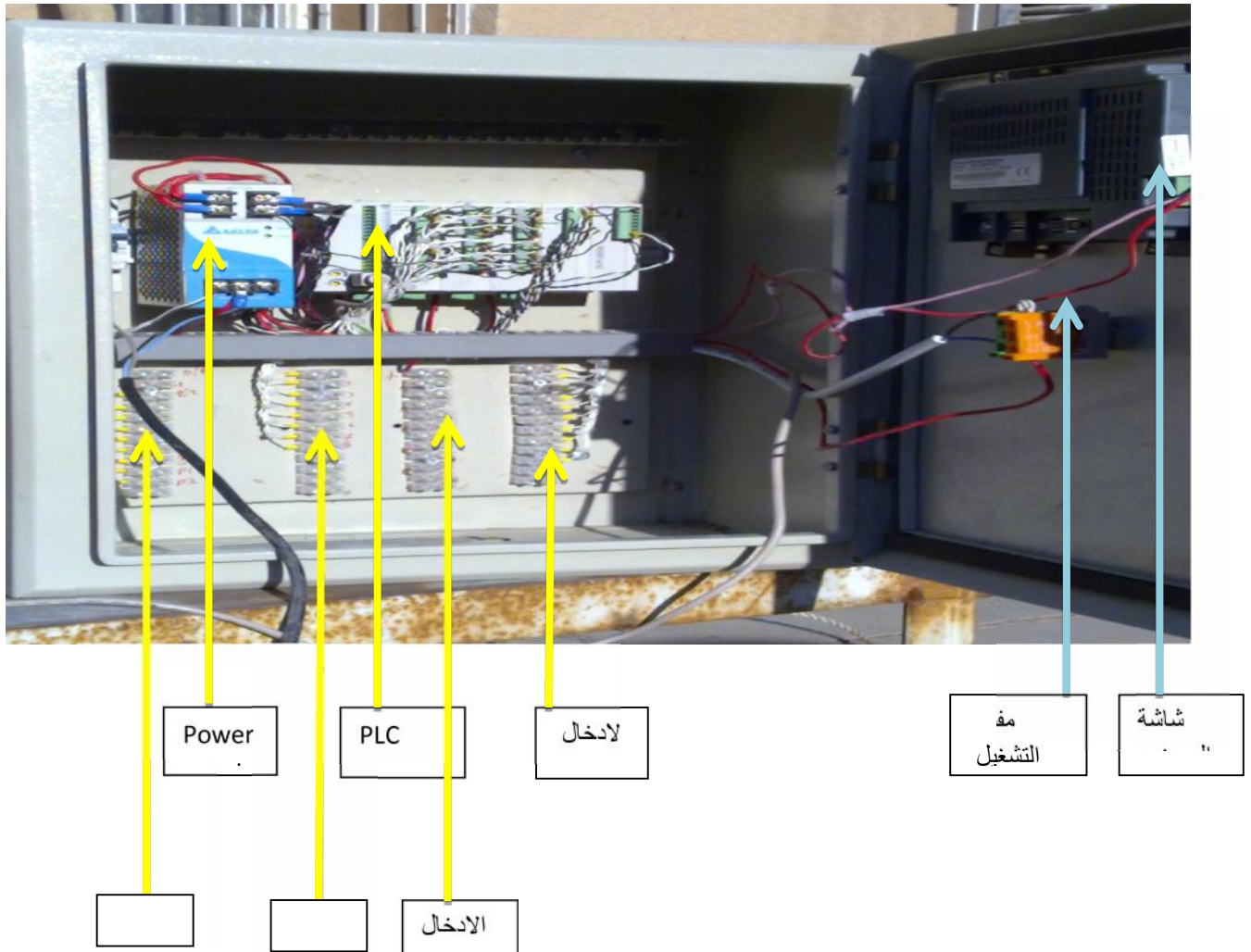
## 3-2 التحكم عن بعد باستخدام شبكة الانترنت

ان الميزات و الخصائص و الخدمات التي تقدمها الشبكة العنكبوتية العالمية او ما تسمى بشبكة الانترنت (INTERNET) جعلت هذا العالم الكبير عبارة عن قرية صغيرة، اذ ساهمت بشكل فعال و حيوي في عملية نشر العلم و التكنولوجيا المتقدمة و الحديثة و في شتى صنوف المعارف العلمية و الانسانية. الجانب الاخر و الذي لا يقل اهمية عن ما ذكر هو امكانية عد بالعمليات الانتاجية، و الصناعية و يشتى فروع العلم كذلك. ان الذي يهمنا في هذا الجانب هو امكانية استخدام شبكة الانترنت في التحكم في عملية السقي لقطعة من الارض قد تبعد مئات او الالاف من الكيلومترات عن مركز السيطرة و التشغيل الرئيسي في جهة الارسال (Server) و التي تعمل كمستقبل او عميل (Client) لغرض مراقبة ما يحدث على الجانب الآخر و البعيد بنفس الوقت و آنيا (On – Line) و هذا الذي تم التركيز عليه في هذا المشروع البحثي العملي التطبيقي و بطريقة مستحدثة ولأول مرة في العراق. اذ تم اختيار قطعة ارض (2500 ) ( 100 25 متر عرضا) في قضاء المسيب في محافظة بابل (33° 10' North) شمالا، و تم تهيئة الموقع للزراعة باستخدام طريقة الري السطحي (الري بالغمر) المتعارف عليه في جميع انحاء العراق و لكن تم هنا بطريقة حديثة و مسيطر عليها، اذ تم تقسيم قطعة الارض هذه الى خمسة قطع او قطاعات مساحة كل منها (500 ) ( 100 5 ) .

سواقي في كل قطاع ليصبح عدد السواقي الكلي 15 ساقية، اذ تم نصب بوابة تحكم معدنية على كل قطاع (اي كل بوابة تحكم بثلاث سواقي). تتم السيطرة على عملية الغلق و الفتح لهذه البوابة بواسطة محرك تيار مستمر (DC Motor) (Servo Motor)، اي ان عدد المحركات المنصوبة على ابواب التحكم مساويا لها (خمس محركات). كل محرك من هذه المحركات مسيطر على تشغيله بواسطة منظومة السيطرة المنطقية (Programmable Logic Control : PLC) التي بدورها تستلم المعلومات المطلوبة من متحسسات مستوى الماء (Water Level Sensor) القطاعات الخمسة في السواقي. تم اختيار منظومة تحكم منطقية ذات ثمانية مداخل (8 I/P Ports) (16 O/P Port) لامكانية الاستفادة من هذه الوحدة المنطقية المبرمجة في تطبيقات لمساحات اوسع و لتطبيقات عملية اخرى اعتمادا على البرمجة اللازمة للقيام بعملية التحكم علما بأن هذا النوع من وحدات التحكم المنطقية تم استخدامه [12]. يرتبط بهذه (PC) (Desktop with monitor)

يقبل عن (P4) او لابتوب عادي بمواصفات متوسطة و ممكن استخدام اي نوع من الموديلات و الشركات المصنعة بحيث لا يتجاوز استهلاك القدرة الكهربائية في كلا الخياريين عن 100 واط لكي نكون ملتزمين بالحسابات التصميمية للمشروع البحثي هذا. اذ تقوم هذه الحاسبة (PC) بنقل البيانات المنقولة عن بعد من المشغل الرئيسي الذي قد يبعد الالاف من الكيلومترات او المئات او اي مسافة اخرى اعتماد على بعد المزرعة عن موقع التشغيل عبر منظومة الانترنت (ان المسافة بين موقع العمل و مركز السيطرة عن بعد في هذا البحث كانت 10 كيلومتر). اذ يتم استخدام برامج خاصة بعملية السيطرة المطلوبة و تحمل التعليمات و ملفات التشغيل عبر الانترنت حيث يتم حجز موقع (Web Site) (IP)، ترسل هذه البيانات من المشغل الرئيسي المسيطر و يسمى بالخادم او (Server)، تستقبل هذه البيانات من قبل شبكة الاستلام في موقع المشروع البحثي او قطعة الارض المراد السيطرة على عملية السقي فيها من قبل هوائي الاستقبال و هي على عدة انواع و تم هنا استخدام ما يسمى ب (Nano- Station) تقوم هذه المحطة المايكروية بدورها بنقل البيانات الى ما يسمى بجهاز ال (Access Point) الذي بدوره يقوم بتغذية الحاسبة (PC) او اللابتوب حيث تم اخذ الاحتمالين في الاستخدام في هذا البحث. عند استلام هذه الحاسبة المعلومات المرسله من الطرف الآخر تقوم الحاسبة الاخرى عند المشغل الرئيسي في جهة الارسال (Server) بالسيطرة كليا على الحاسبة الموجودة في الموقع عن طريق خاصية معروفة في شبكات الانترنت و تسمى (Remote Desktop Connection) (IP) المراد السيطرة عليها. هذا يعني ان الحاسبة الموجودة في جهة الاستقبال اي في الموقع المراد السيطرة عليه (Client) اصبحت السيطرة عليها بكامل محتوياتها و برامجها من قبل المرسل (Server). وحدة السيطرة المنطقية المبرمجة (PLC) يمكن الآن برمجتها و السيطرة على تشغيلها و التحكم بكل عملياتها من قبل ال (Server) حاليا كبديل ل

(Client) و تصبح شاشة العرض جاهزة للمراقبة و التنفيذ من قبل المرسل لتقوم بتشغيل عملية التحكم بالسقي و بصورة اتوماتيكية و آلية كليا اعتمادا على متحسسات مستوى الماء (Water Level Sensor) والذي بدوره يقوم بتغذية البيانات (PLC) و اعتمادا على هذه البيانات يتم التحكم بالمحركات المنصوبة على بوابات السيطرة على (PLC) لا تذهب مباشرة الى محركات التحكم بالبوابات بل تذهب الى بورد السيطرة و القدرة الكهربائية حيث تغذي كل اشارة خارجة من ال (PLC) (Relay) الخاص بالسيطرة في البورد الكهربائي و الذي بدوره يقوم بتغذية الملا (Contactor) (PLC) ضعيفة و غير قادرة على تشغيل هذه المحركات لذا تذهب الى المرحل الذي يغذي الملف الخاص بالكونتكر و الذي بدوره يسيطر على تشغيل المحرك. (LADER) (PLC) يسمى بالسلم المنطقي و هي لغة خاصة ببرمجة منظومة السيطرة المنطقية المبرمجة. الشكل رقم (6) يمثل صورة لمنظومة التحكم المنطقية التي تم استخدامها في مشروعنا هذا و مشاريع اخرى سابقة لفريق العمل [12]. بينما يمثل الشكل (7) صورة لجهاز ال (ACCESS POINT) (LINKSYS) و المستخدم ايضا ك (Client) . (8) فيمثل شكلا تفصيليا موضحا فيه كل اجزاء هذا البحث التطبيقي.



(6): صورة توضيحية لوحدة السيطرة المنطقية المبرمجة (PLC) مؤشر عليها جميع الأجزاء

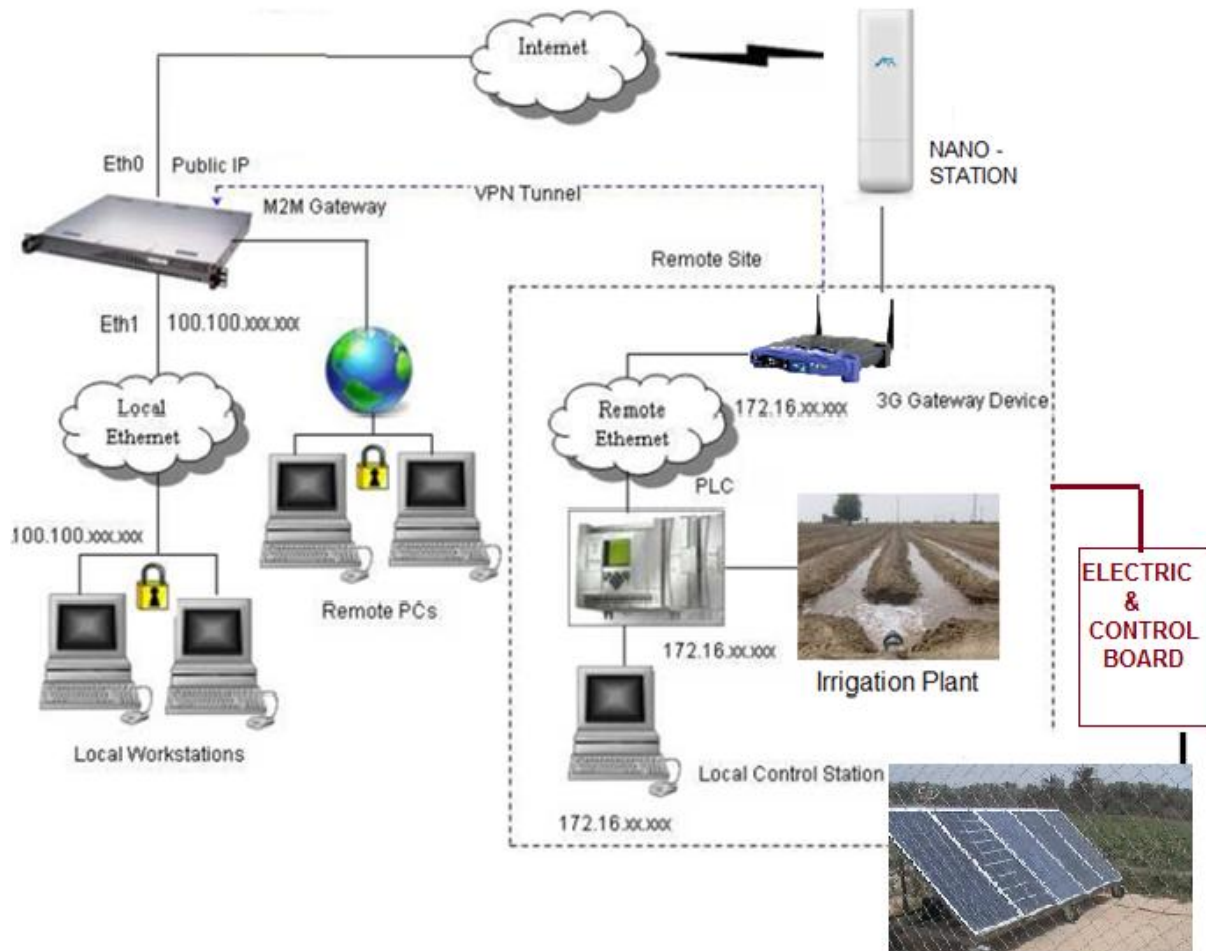


( )



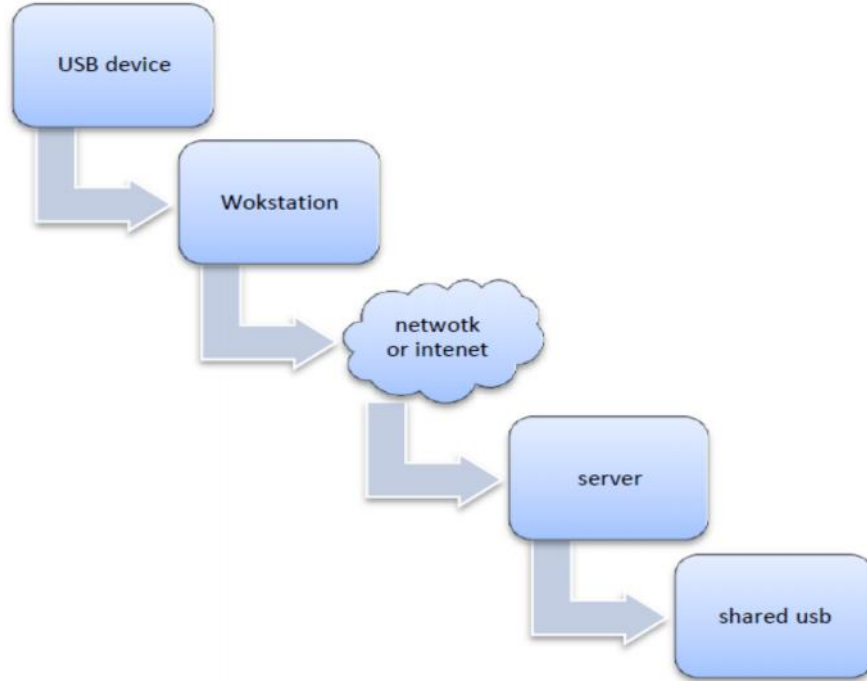
( )

(7): (أ): صورة توضح جهاز الاستقبال في شبكة الانترنت (ACCESS POINT) و الذي يقوم بايصال اشارة الانترنت بعد المعالجة من الهوائي الى الحاسبة. (ب): شكل يوضح محطة الهوائي المايكروية المعروفة ب (NANO - STATION)



(8): رسم توضيحي يبين مخططا تفصيليا لفكرة المشروع البحثي حول استخدام الانترنت في التحكم بالسقي

يوضح الشكل (9) مخططا توضيحا لطريقة انتقال المعلومات الواجب تنفيذها عبر الانترنت



(9) مخططا توضيحا لطريقة انتقال المعلومات الواجب تنفيذها عبر الانترنت

-3

يمثل هذا البحث تحديا كبيرا للطرق التقليدية في السيطرة على عمليات السقي. اذ تمت السيطرة بصورة ذكية من خلال استعمال متحسسات مستوى الماء وهذه الطريقة تقلل من الهدر المائي بصورة كبيرة. ان عملية الجدولة التي تقوم وحدة السيطرة المنطقية المبرمجة استنادا الى البرنامج المعد من قبل المبرمج و حسب الاسبقية في العمل بالنسبة لتشغيل المحركات المسيطرة على بوابات التحكم بكمية و سريان الماء تجعل الحمل ألأني يتناسب مع تصميم منظومة التوليد باستخدام الطاقة الشمسية من ناحية تقليل الكلفة حيث يمثل الحمل الكلي لجميع المحركات اكثر المتولدة. عملية السيطرة عن طريق استخدام شبكة الانترنت لديها افضلية كبيرة اذا ما قورنت بالطريقة التي تستخدم فيها منظومتي ارسال و استقبال لا سلكيتين بما تحمله من مساويء تتعلق بالكلفة العالية و التشويش و التداخل و قلة الموثوقية لهذه الطريقة، فعلى العكس من ذلك كانت الطريقة المستحدثة في السيطرة على السقي عن طريق استخدام التحكم بواسطة الانترنت. ان استخدام الطاقة المتجددة كالطاقة الشمسية في توليد الطاقة الكهربائية اللازمة للمشروع حققت هدفا اضافيا الا و هو رفع بعض الاحمال الكهربائية عن كاهل شبكة الكهرباء الوطنية اضافة لكون هذا النوع من الطاقة نظيف و لا يلوث البيئة. ان هذه الفكرة الجريئة التي ربطت السيطرة على عملية السقي بصورة ذكية مع شبكة الانترنت و استخدام الطاقة الشمسية كمصدر بديل يفتح الباب واسعا لمزيدا من التطبيقات الاخرى اضافة لأمكانية تطبيق هذا المشروع على مساحات كبيرة و في اماكن بعيدة، و بهذا نكون قد ساعدنا باحياء مساحات كثيرة و شاسعة بعيدة عن مصادر الطاقة الكهربائية اضافة الى ترشيد الاستهلاك المائي لا سيما وان تربة العراق بحاجة لكل قطرة ماء اضافة لعجز شبكة الكهرباء الوطنية عن تلبية ح

#### 4- References

- [1] R. Kirubashankar, K. Krishnamurthy, J. Indra, B.Vignesh, "**Design and Implementation of Web Based Remote Supervisory Control and Information System**" International Journal of Soft Computing and Engineering (IJSCE), ISSN: 2231-2307, Volume-1, Issue-4, September 2011.
- [2] Aqeel-ur-Rehman†, Zubair A. Shaikh, Humaira Yousuf, Farah Nawaz, Muneebah Kirmani and Sara Kiran, "**Crop Irrigation Control using Wireless Sensor and Actuator Network (WSAN)**", 978-1-4244-8003-6/10/26.00 ©2010 IEEE.
- [3] Bernard Cardenas-Lailhacar, Michael D. Dukes, Grady L. Miller "**Sensor-Based Control of Irrigation in Bermudagrass**", ASAE Meeting Presentation Paper Number: 052180, ASAE Annual International Meeting, Florida, 17 - 20 July 2005.
- [4] Suhinthan Maheswararajah, Saman K. Halgamuge, *Member, IEEE*, Kithsiri B. Dassanayake, and David Chapman, "Management of Orphaned-Nodes in Wireless Sensor Networks for Smart Irrigation Systems" IEEE TRANSACTIONS ON SIGNAL PROCESSING, VOL. 59, NO. 10, OCTOBER 2011.
- [5] Luis Pay , José M. Azor n, Nicol s M. Garc a, José M. Sabater, Carlos Pérez, Ram n P. "**Process Control and Supervision through Internet**", International Conference on Engineering Education, July 21–25, 2003, Valencia, Spain.
- [6]- Chien J C, "**Concentrating solar thermal power: A viable alternative in china's energy supply**", M Sc Thesis, Lauder Institute Masters Research, 2009.
- [7]- Barlev D, Vidu R & Stroeve P, Innovation in concentraed solar power. University of California, "**Davis Solar Energy Collaborative Workshop**", Davis, CA, May 11, 2010.
- [8]- Cowles G, Robins J, Covin W, Cremmins B, Fitz Gerald C, Foy D, Harwood J, Katz J, Nagy L and Rowlett J, "**The solar energy research and advancement act of 2007**", Program in Environmental Science and Policy, Columbia University, 2008.
- [9]- Payne S and Dutzik T, "**On the rise solar thermal power and the fight against global warming**", Environment America Research & Policy Center, Bernadette Del Chiaro, 2008.
- [10]- Perez-de-los-Reyes C, Porras-Soriano A & Soriano M L, "**Use of flat plate solar collectors and parabolic trough concentrators for greenhouse soil disinfestation**". Spanish Journal of Agricultural Research, vol. 7, No. 2, pp: 315-321, 2009.
- [11] German Aerospace Center (DLR), " **Concentrating Solar Power for the Mediterranean Region Executive Summary**", Institute of Technical Thermodynamics Federal Ministry for the Environment, Germany, 16.04.2005.
- [12] د.علي عبد العباس البكري، د. حميد كاظم الموسوي، السيد احمد كريم، السيد مصطفى حسن، " المتجددة (الشمسية) في تشغيل منظومات الري بالتنقيط و باستخدام السيطرة الذكية بواسطة السيطرة المنطقية (PLC)", المؤتمر العلمي الرابع (دور التعليم التقني في بناء العراق الجديد)، 3-4 نيسان / 2011 الكلية الاسلامية الجامعة، النجف الاشرف، مجلة الكلية الاسلامية الجامعة، العدد 16 2011.

## Computation Of Hourly Solar Radiation Using ASHRAE Model For Some Iraqi Cities

Dr. Fawaz Sultan Abdullah  
Lecturer  
Technical College/Mosul  
[fawazsultan@yahoo.com](mailto:fawazsultan@yahoo.com)  
07701601616

### Abstract

An attempt has been done to estimate clear-sky hourly global solar radiation for some Iraqi cities (Baghdad, Kirkuk, and Nasiriyah) using ASHRAE model. The model was used to calculate hourly solar radiation on four months (January, April, July, October) which represents the four seasons in Iraq cities. The results of ASHRAE model are compared with results those estimated using Collares-Pereira and Rabl (1979) model. The Collares-Pereira and Rabl model is based on monthly mean daily solar radiation that measured at Iraqi meteorological department for five years intervals (2005-2010). Comparison between two models results, show that the results for Iraqi cities provide good estimates of the hourly global radiation. The root mean square error (RMSE) and mean bias error (MBE) are used to verify the results of ASHRAE model.

**Keywords:** Hourly solar radiation, Collares-Pereira and Rabl model, ASHRAE model to estimate the hourly solar radiation.

### حساب قيم الإشعاع الشمسي (الساعية) باستخدام نموذج اشري لبعض مدن العراق

#### الخلاصة

تم التنبؤ بحساب قيم الإشعاع الشمسي (في كل ساعة من ساعات النهار) لبعض مدن العراق (بغداد، كركوك، والناصرية) باستخدام نموذج اشري للسماء الصافية. تم استخدام هذا النموذج لحساب قيم الإشعاع الشمسي لأربع أشهر من السنة (كانون الثاني، نيسان، تموز، تشرين الأول) والتي تمثل قيم الإشعاع الشمسي لكل من الفصول الأربعة في تلك المدن. تم مقارنة نتائج نموذج اشري مع نتائج نموذج كولارس- بيريرا و رابل لسنة (1979). إن نتائج هذا الأخير اعتمدت على قيم المعدل الشهري اليومي للإشعاع الشمسي. إن قيم المعدل الشهري اليومي للإشعاع الشمسي تم الحصول عليها من قبل دائرة الأنواء الجوية العراقية ولفترة خمس سنوات ماضية (2005-2010). تم مقارنة نتائج النموذجين أعلاه، حيث بينت النتائج تقارب القيم ما بين النموذجين المستخدمين من خلال استخدام تقنية (RMSE) و (MBE) لمعرفة نسبة الخطأ الناتج من استخدام نموذج اشري لتخمين قيم الإشعاع الشمسي في كل ساعة من ساعات النهار.

**الكلمات الدلالية:** الإشعاع الشمسي في كل ساعة، نموذج كولارس- بيريرا و رابل، نموذج اشري لتخمين قيم الإشعاع الشمسي.

## INTRODUCTION

The ASHRAE clear sky model [1] is commonly used as a basic tool for solar heat load calculation of air conditioning systems and building designs among the engineering and the architectural communities in the world. The measured hourly values of solar radiation data are not available for large number of stations. Thus, accurate estimation of hourly values of global and diffused solar radiation data is essential for the design and performance evaluation of solar energy systems. Sometimes the design of solar energy devices needs accurate estimations of hourly solar radiation values. At places where hourly radiation values are not available, it has to be estimated from the daily values. There are various methods which allow the conversion of daily solar radiation into hourly values. The distribution of total radiation on a horizontal surface over a day was examined by Liu, et al.,[2], who showed that the ratio of hourly to daily radiation could be correlated with the local day length and hour angle. The hours were designated by the time for the mid point of the hour, and the days were considered to be symmetrical about solar noon. A model for hourly solar radiation has also been developed by Collares, et al.,[3], which is correlated with the local time of day. An attempt has been made to develop a new model to evaluate hourly solar radiation on horizontal surface for Indian locations having different climatic conditions, using least square regression analysis based on the ASHRAE model. Comparison between the estimated and the measured values shows that the constants derived for Indian locations provide good estimates of hourly solar radiation Al-Sadah, et al., [4]. Choudhary, et al.,[5] and Iqbal, et al., [6] have also done similar type of work, while Soler , et al.,[7] and Gopinathan, et al.,[8] have proposed a set of polynomial equations for estimating hourly values. In this paper, the ASHRAE clear-sky model is used to estimate the hourly global solar radiation on horizontal surfaces for (Baghdad, Kirkuk, and Nasiriyah) cities. The values of hourly solar radiation are compared with results that estimated using Collares-Pereira and Rabl model which in turn based on monthly average daily global radiation on horizontal surface that obtained for Baghdad city for the time period (2005-2010), to validate the results of ASHRAE model.

## METHODOLOGY

### 1-ASHRAE Model

The calculations of ASHRAE model is shown in simple expressions as follows:-

#### *Global Solar Radiation:-*

The global solar radiation on horizontal surface is composing of two main components, beam and diffuse solar radiation components as follows,[9]:-

$$I = I_b + I_d \dots\dots\dots(1)$$

Where  $I_b$  is hourly beam radiation component ( $w/m^2$ ), and  $I_d$  is hourly diffuse radiation component ( $w/m^2$ ).

### 1-1 Beam Solar Radiation:-

The direct hourly solar radiation on the surface normal to the sun's ray,  $I_{bn}$ , is represented by [9], as follows:-

$$I_{bn} = A \times \exp[-B / \cos(\theta_z)] \dots \dots \dots (2)$$

Where:  $A$  is the apparent extra-terrestrial solar radiation in ( $w/m^2$ ),  $B$  is the atmospheric extinction coefficient, while  $\theta_z$  is the solar zenith angle (degree). Then the beam radiation component on horizontal surface has been estimated from [9], as follows:-

$$I_b = I_{bn} \times \cos(\theta_z) \dots \dots \dots (3)$$

### 1-2 Diffuse Solar Radiation:-

The diffuse solar radiation on horizontal surface is given by, [9], as follows:-

$$I_d = C \times I_{bn} \dots \dots \dots (4)$$

Where:  $C$  is the diffuse radiation factor (dimensionless). So the monthly average hourly solar radiation can be represented as follows:-

$$I = I_{bn} \times \cos(\theta_z) + C \times I_{bn} \dots \dots \dots (5)$$

The solar zenith angle ( $\theta_z$ ) was evaluated using the following equation as mentioned in, [10], as follows:-

$$\cos(\theta_z) = \cos(u) \cos(L) \cos(h) + \sin(u) \sin(L) \dots \dots \dots (6)$$

Where:  $u$  is the solar declination angle (degree),  $L$  is the latitude of place (degree), and  $h$  is the solar hour angle (degree). The solar declination angle was estimated depending upon number of day through the year, as explained in [10].

$$u = 23.45 \sin \left[ \frac{360(d + 284)}{365} \right] \dots \dots \dots (7)$$

Where:  $d$  is the number of days of the year, start with 1 at January 1, and end at 365 at December 31. The hour angle  $h$  is an angular measure of time and it is positive morning and negative evening. The hour angle can be estimated depending on apparent solar time  $AST$  which equivalent to  $15^\circ$  per hour as mentioned in, [11].

$$h = 15 \times (12:00 - AST) \dots\dots\dots(8)$$

The apparent solar time or ( *AST* ) can be calculated depending on an angular motion of sun across the sky. In this study it is may considered as an Iraqi standard time.

## 2-Collares-Pereira And Rabl Model:

In order to validate the results of ASHRAE model, Collares-Pereira and Rabl develop an empirical correlation based on solar hour and solar sunset angles, which is shown below as follows, [11]:

$$r = \frac{\bar{I}}{\bar{H}} = \frac{f}{24} [r + s \cos(h)] \times \left[ \frac{\cos(h) - \cos(h_{ss})}{\sin(h_{ss}) - \left( \frac{2fh_{ss}}{360} \right) \cos(h_{ss})} \right] \dots\dots(9)$$

Where: *r* is the ratio of hourly total radiation to daily total radiation. *h* is the solar hour angle (degree) which estimated at midpoint between any two sequence hours, *h<sub>ss</sub>* is the sunset hour angle (degree) which is equal to the following formula, [11]:

$$h_{ss} = \cos^{-1}[-\tan(L)\tan(u)] \dots\dots(10)$$

Where the coefficients *r* and *s* shown in above formula are estimated as follows, [11]:

$$r = 0.409 + 0.51 \sin(h_{ss} - 60) \dots\dots\dots(11a)$$

$$s = 0.660 - 0.47 \sin(h_{ss} - 60) \dots\dots\dots(11b)$$

## Data Source

Clear-sky hourly solar radiation on horizontal surface for some Iraqi cities had been estimated using ASHRAE model. The geographical latitudes and longitudes for these cities are shown in table (1).

The original ASHRAE model was modified, by converting the values of solar parameters (A, B, and C) from the twentieth one day of each month to the specified or averaged value at each month to make the calculations of solar radiations suitable for any day in the month as shown in table (2). The values of modified solar parameters are taken from author, [12].The numerical values of A and B for each month are varying throughout the year because of seasonal changes in the dust and water vapor content of the atmosphere and because of the changing earth-sun distance. So the values of A are increasing as the Sun-Earth distance decreasing (especially in Winter season), and they starting to reduce as the distance between Earth and Sun are increasing (which happened in Summer season) and that is clear in table (2). The results of ASHRAE model was verified using Collares-Pereira and Rabl (1979) model which in turn depends on monthly mean daily solar radiation. The values

of monthly mean daily global solar radiation in (MJ/m<sup>2</sup>-day) for Nasiriyah, Kirkuk, and Baghdad cities are obviously in tables (3a,b,c) respectively. These values are taken from Iraqi metrological department for above cities for five years intervals (2005-2010).

The need for radiation data covering entire areas led to the development of radiation models that allow the calculation of radiation parameters within certain margins of error. The accuracy of the estimated values was tested by calculating the Mean Bias Error *MBE*, and the Root Mean Square Bias Error *RMSE*. These values of errors are stated by, [13] as follows:

$$RMSE = \left[ \sum (\bar{H}_{cal} - \bar{H}_{obs})^2 / M \right]^{1/2} \dots\dots\dots(12)$$

$$MBE = \left[ \sum (\bar{H}_{cal} - \bar{H}_{obs}) / M \right] \dots\dots\dots(13)$$

Where *M* is the number of observed points,  $\bar{H}_{cal}$  is the calculated global radiation, and  $\bar{H}_{obs}$  is the observed global radiation on horizontal surface.

## Results And Discussion

The values of hourly solar radiation that estimated using ASHRAE clear-sky model for four months (January, April, July, October) are represented are demonstrated for all daylight hours (5:00 Am-19:00 Pm) for Nasiriyah, Kirkuk,, and Baghdad cities are cleared in Fig. (1). The hourly radiation recorded data for Iraqi locations does not available due to limitation of radiation instruments in Iraqi cities. Then, the estimated hourly solar radiation values can be obtained from monthly mean hourly solar radiation by using Collares-Pereira and Rabl (1979) model.

Figs.(2a,b,c,d) through Figs. (4a,b,c,d) show the hourly global solar radiation that estimated using ASHRAE model and verified using Collares-Pereira and Rabl (1979) model versus daylight hours (5:00Am-19:00Pm) for four months of year as mentioned above for Nasiriyah, Kirkuk, and Baghdad cities respectively. These figures explain the real behavior of hourly solar radiation variation with hours of day from sunrise to sunset times as clear in these figures. The values of hourly solar radiation have two maximum values in each curve: one for solar noon times, when the sun are pointed at highest point in the sky (meridian time), and other at summer month or at June month when the sun is normal or nearly normal on Earth surface of Iraqi cities. In each figure, it is clear that some difference in values of hourly solar radiation between the two above models especially in winter season (January month). Another difference occur due to the precision of instruments that used to measure the monthly or daily solar radiation in these cities. To avoid repeating calculations for twelve months, the calculations of hourly solar radiations were made on four months only (January, April, July, and October) which represents the four seasons in Iraq cities.

The *RMSE* test provides information on the short-term performance of the studied model as it allows a term-by term comparison of the actual deviation between the calculated value and the measured value. [6] has recommended that a zero value for *MBE* is ideal and a low *RMSE* is desirable.

The results of ASHRAE model are presented in tables (4a, b, and c) for Nasiriyah, Kirkuk, and Baghdad cities respectively. These tables show also the values of hourly solar radiation that estimated using Collares-Pereira and Rabl (1979) model as calculated using Eq. (9). Finally, table (5) shows the statistical errors for the above cities in ( $\text{MJ/m}^2\text{-day}$ ) to validity the results of ASHRAE model.

## Conclusions

An attempt has been done to estimate hourly global solar radiation for some Iraqi cities (Baghdad, Kirkuk, and Nasiriyah) using ASHRAE model. The results of ASHRAE model are compared with results of hourly solar radiation that estimated using Collares-Pereira and Rabl (1979) model. The Collares-Pereira and Rabl model is based on monthly mean daily solar radiation that measured at Iraqi meteorological department for five years intervals (2005-2010). Comparison between two models, show a good agreement between the two models. The statistical errors, (root mean square and mean bias errors) are used to show the degree of agreement between original ASHRAE model and Collares-Pereira and Rabl model. The mean bias and the root mean square errors are gave good verification to use the ASHRAE model as a model to estimate the hourly solar radiation for all Iraq cities as shown in table (5).

## References

- [1]ASHRAE, "Handbook of Fundamentals". Atlanta, Georgia: American Society of Heating, Refrigeration, and Air-Conditioning Engineers, chapter 27.1985.
- [2]Liu BYH, Jordan RC. The interrelationship and characteristic distribution of direct, diffuse and total solar radiation. Solar Energy 1960; 4: 1-19.
- [3]Collares-Pereira M, Rabl A. The average distribution of solar radiation correlation between diffuse and hemispherical and between daily and hourly insolation values. Solar Energy 1979; 22: 155- 164.
- [4]Al-Sadah FH, Ragab FM, Arshad MK. Hourly solar radiation over Bahrain. Energy 1990; 15(S): 395.
- [5]N. K. D. Choudhary, "Solar radiation at New Delhi", Solar Energy, Vol. 7, pp. 44-46, 1963.
- [6]M. Iqbal, "A study of Canadian diffuses and total solar radiation data-1, monthly average daily horizontal radiation", Solar Energy, Vol. 22, pp. 87-90, 1979.

- 
- [7]A. Soler and K. K. Gopinathan, "Estimation of monthly mean hourly global radiation for latitudes in the 1°N – 81°N range", Solar Energy, Vol. 52, No.3, pp. 233-239, 1994.
- [8]K. K. Gopinathan and A. Soler, "Techniques for obtaining the monthly mean hourly diffuse radiation from daily values", Solar Energy, Vol. 22, No. 7, pp. 735-742, 1997.
- [9]Duffie, J.A. and Beckman, W.A. "Solar Engineering of Thermal Processes", 2nd edition. John Wiley and Sons: New York, NY. 1991.
- [10]Soteris Kalogirou, "Solar energy engineering: process and systems", Academic Press, London. 2009.
- [11]Beckman, W.A., Klein, S.A., Duffie, J.A. "Solar Heating Design". John Wiley & Sons, New York. 1977.
- [12]K. Bakirici. "Estimation of Solar Radiation by Using ASHRAE Clear Sky Model in Erzurum, Turkey". Energy Source, Part A, 31:208-216. 2009.
- [13]El-Sebaili and A.A. Trabea "Estimation of Global Solar Radiation on Horizontal Surfaces Over Egypt". Egypt. J. Solids. 28. 2005.

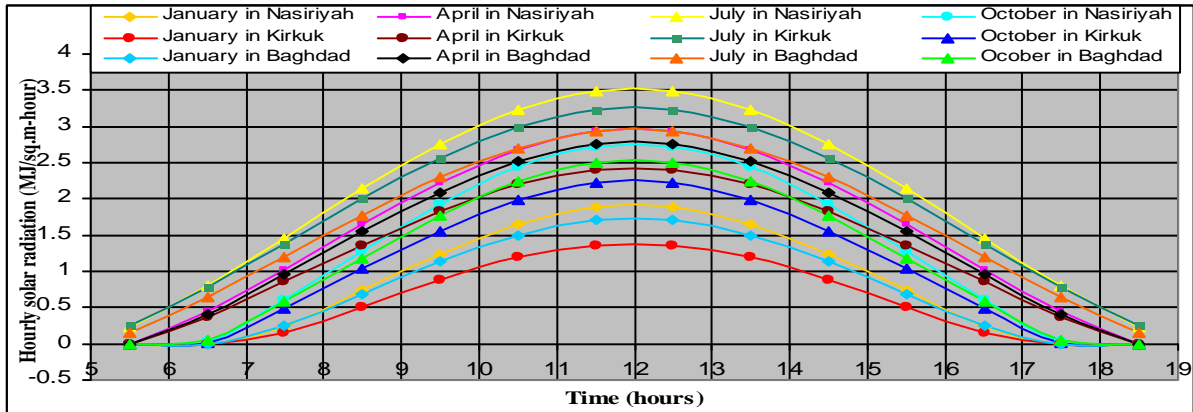


Fig.(1) Computed hourly solar radiation at different seasons using ASHRAE model for Nasiriyah, Kirkuk, and Baghdad cities.

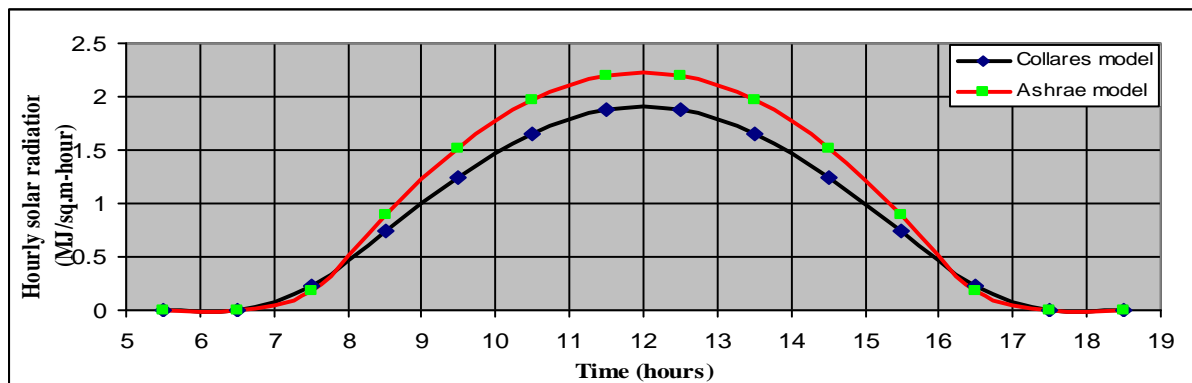


Fig.(2a) Comparison between hourly solar radiations at January month for Nasiriyah city.

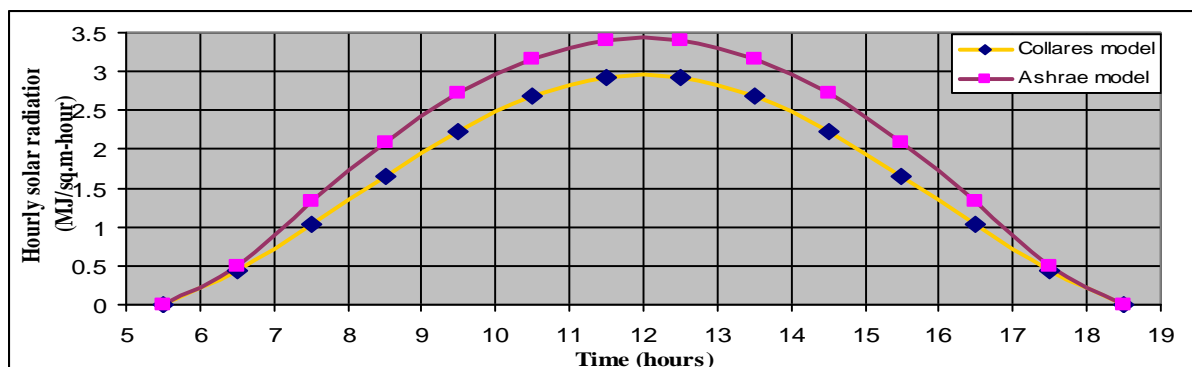


Fig.(2b) Comparison between hourly solar radiations at April month for Nasiriyah city.

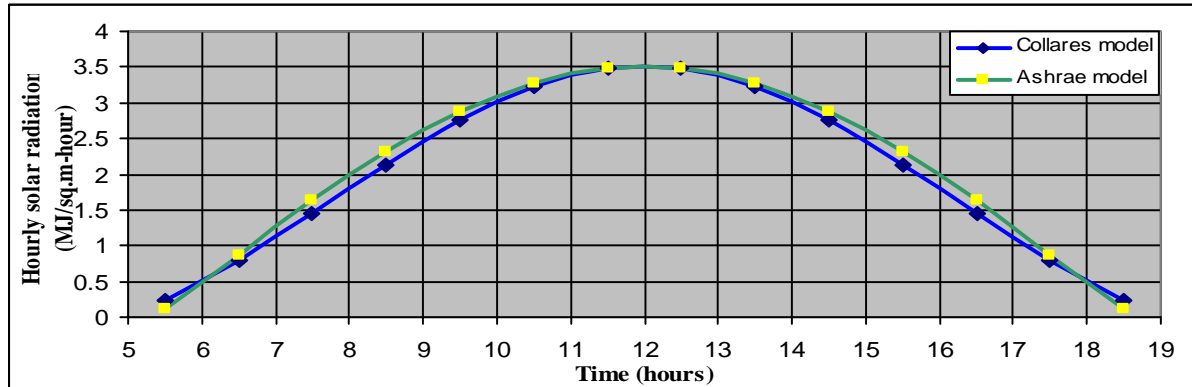


Fig.(2c) Comparison between hourly solar radiations at July month for Nasiriyah city.

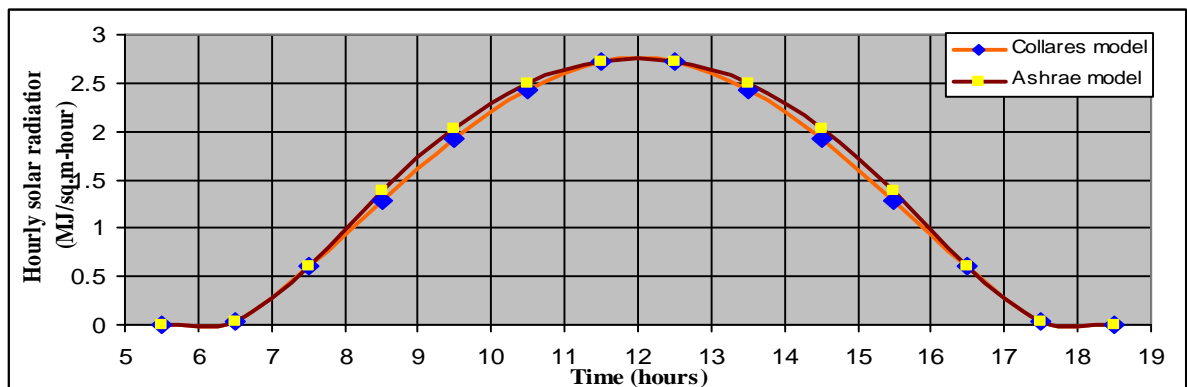


Fig.(2d) Comparison between hourly solar radiations at October month for Nasiriyah city.

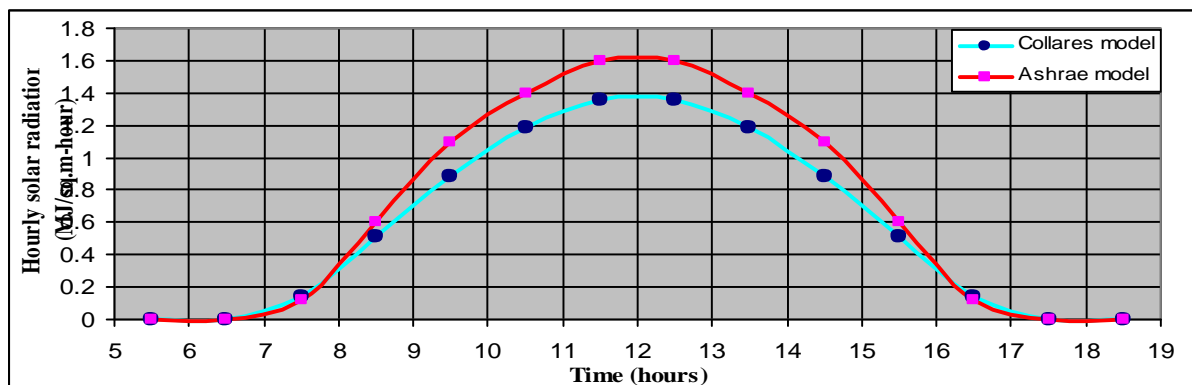


Fig.(3a) Comparison between hourly solar radiations at January month for Kirkuk city.

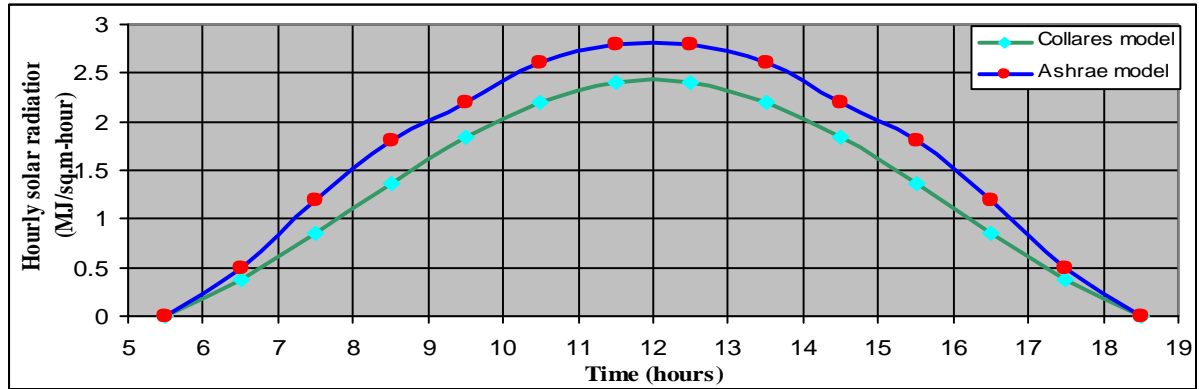


Fig.(3b) Comparison between hourly solar radiations at April month for Kirkuk city.

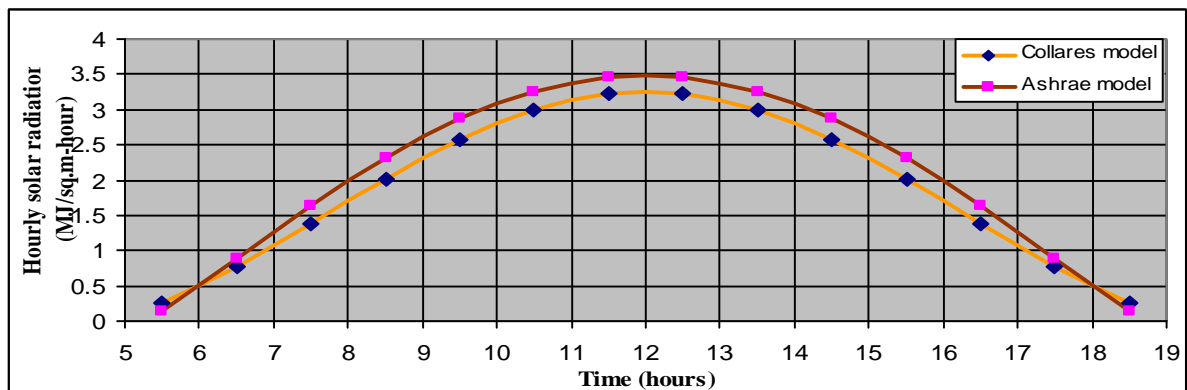


Fig.(3c) Comparison between hourly solar radiations at July month for Kirkuk city.

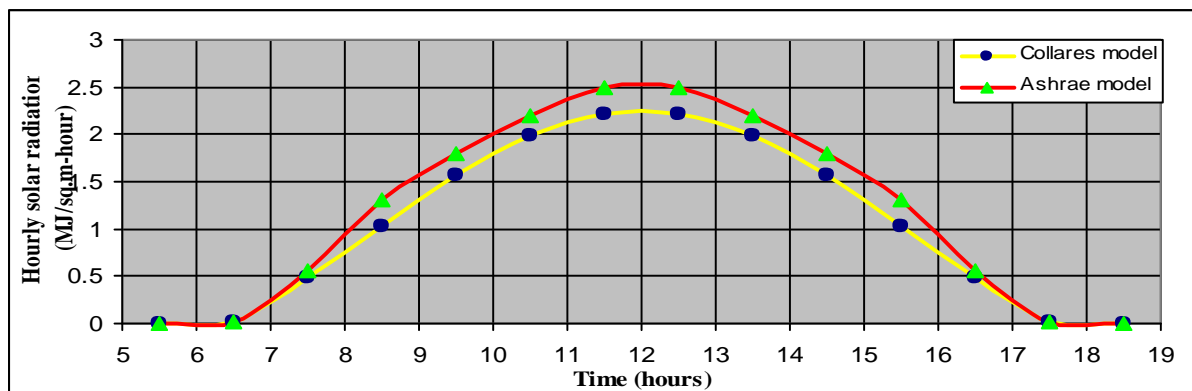


Fig.(3d) Comparison between hourly solar radiations at October month for Kirkuk city.

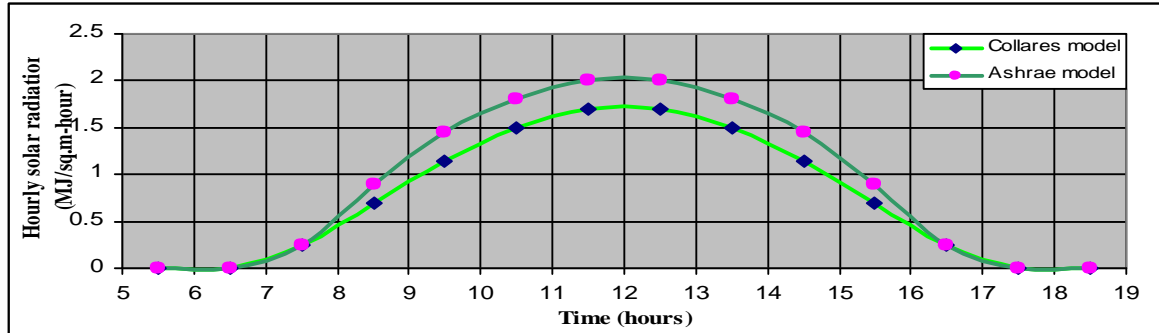


Fig.(4a) Comparison between hourly solar radiations at January month for Baghdad city.

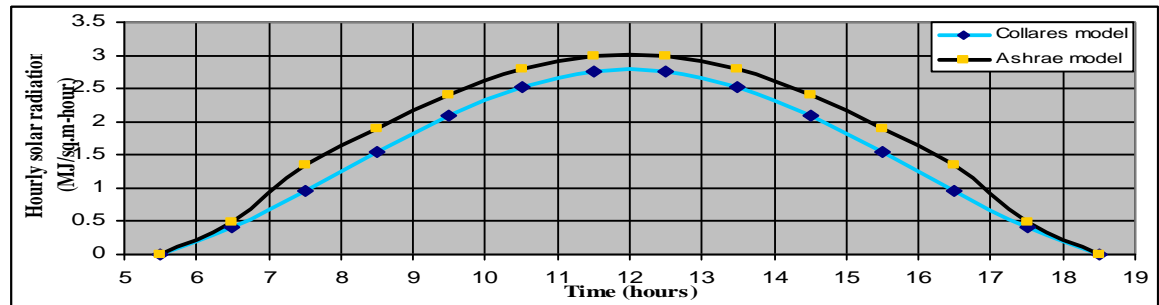


Fig.(4b) Comparison between hourly solar radiations at April month for Baghdad city.

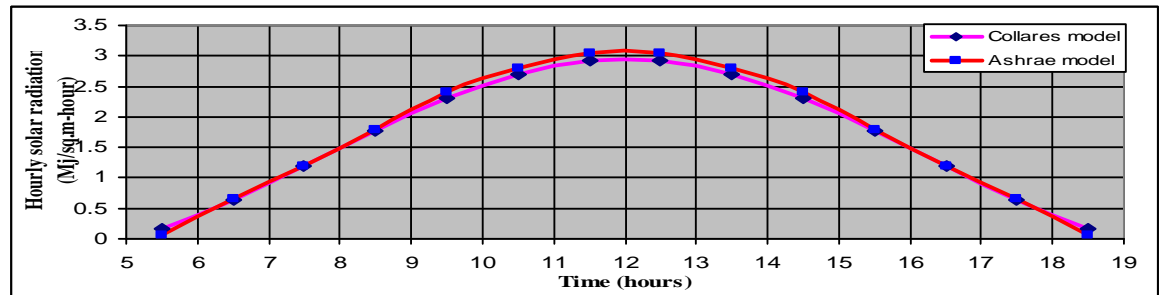


Fig.(4c) Comparison between hourly solar radiations at July month for Baghdad city.

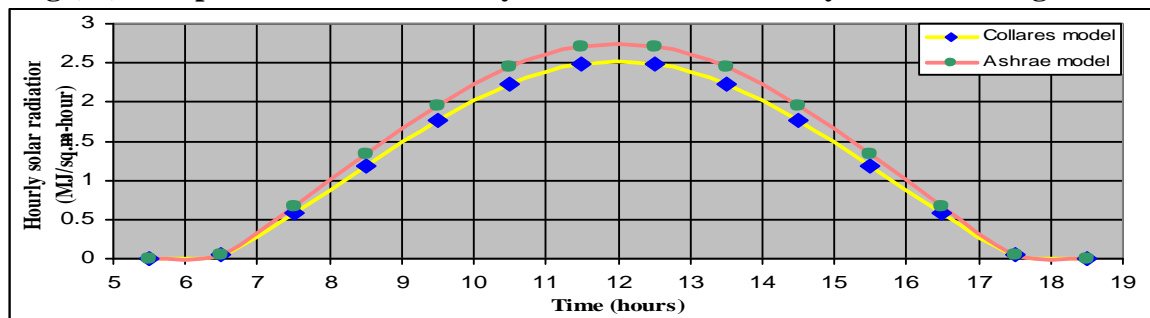


Fig.(4d) Comparison between hourly solar radiations at October month for Baghdad city.

**Table (1) Geographical Latitude and Longitudinal of the Region Locations.**

| City      | Latitude | Longitude | Decimal degrees of Latitude |
|-----------|----------|-----------|-----------------------------|
| Baghdad   | 33°20' N | 44°30' E  | 33.333                      |
| Kirkuk    | 35°28' N | 44°21' E  | 35.466                      |
| Nasiriyah | 31°00' N | 46°16' E  | 31.000                      |

**Table (2) Constants for ASHRAE equations for average values of each month.**

| Months    | Day no. | A (per day)      | B (per day)   | C (per day)   |
|-----------|---------|------------------|---------------|---------------|
|           |         | W/m <sup>2</sup> | Dimensionless | dimensionless |
| January   | 17      | 1229.88          | 0.142         | 0.058         |
| February  | 16      | 1216.25          | 0.144         | 0.060         |
| March     | 16      | 1190.40          | 0.153         | 0.068         |
| April     | 15      | 1144.66          | 0.175         | 0.092         |
| May       | 15      | 1109.68          | 0.192         | 0.116         |
| June      | 11      | 1092.69          | 0.202         | 0.130         |
| July      | 17      | 1084.88          | 0.207         | 0.136         |
| August    | 16      | 1102.97          | 0.202         | 0.124         |
| September | 15      | 1142.12          | 0.182         | 0.098         |
| October   | 15      | 1183.45          | 0.164         | 0.077         |
| November  | 14      | 1213.61          | 0.151         | 0.065         |
| December  | 10      | 1228.00          | 0.145         | 0.059         |

**Table (3a): Monthly mean daily solar radiation values for Nasiriyah city (2005-2010).**

| Months    | Day number | $\bar{H}$ (MJ/m <sup>2</sup> -day) |
|-----------|------------|------------------------------------|
| January   | 17         | 11.529                             |
| February  | 16         | 15.394                             |
| March     | 16         | 19.158                             |
| April     | 15         | 22.105                             |
| May       | 15         | 25.482                             |
| June      | 11         | 28.555                             |
| July      | 17         | 28.182                             |
| August    | 16         | 26.648                             |
| September | 15         | 23.190                             |
| October   | 15         | 18.212                             |
| November  | 14         | 13.098                             |
| December  | 10         | 11.268                             |

**Table (3b): Monthly mean daily solar radiation values for Kirkuk city (2005-2010).**

| Months    | Day number | $\bar{H}$ (MJ/m <sup>2</sup> -day) |
|-----------|------------|------------------------------------|
| January   | 17         | 8.2300                             |
| February  | 16         | 10.594                             |
| March     | 16         | 14.211                             |
| April     | 15         | 17.204                             |
| May       | 15         | 20.535                             |
| June      | 11         | 23.323                             |
| July      | 17         | 23.392                             |
| August    | 16         | 22.114                             |
| September | 15         | 19.600                             |
| October   | 15         | 14.772                             |
| November  | 14         | 9.0600                             |
| December  | 10         | 7.3650                             |

**Table (3c): Monthly mean daily solar radiation values for Baghdad city (2005-2010).**

| Months    | Day number | $\bar{H}$ (MJ/m <sup>2</sup> -day) |
|-----------|------------|------------------------------------|
| January   | 17         | 10.615                             |
| February  | 16         | 14.344                             |
| March     | 16         | 16.508                             |
| April     | 15         | 20.704                             |
| May       | 15         | 23.485                             |
| June      | 11         | 25.649                             |
| July      | 17         | 25.454                             |
| August    | 16         | 23.838                             |
| September | 15         | 21.128                             |
| October   | 15         | 16.808                             |
| November  | 14         | 12.426                             |
| December  | 10         | 10.170                             |

**Table (4a) Monthly mean daily global radiation (MJ/m<sup>2</sup>-day),  
ratio of hourly solar radiation to daily solar radiation (dimensionless),  
hourly solar radiation values in (MJ/m<sup>2</sup>-hour) using Collares-Pereira model,  
and hourly solar radiation values in (MJ/m<sup>2</sup>-hour) using ASHRAE model for Nasiriyah city.**

| Months              | Daylight (hours) |        |        |        |        |        |        |        |        |        |        |        |        |        |
|---------------------|------------------|--------|--------|--------|--------|--------|--------|--------|--------|--------|--------|--------|--------|--------|
| Jan.<br>Day no.=17  | 5-6              | 6-7    | 7-8    | 8-9    | 9-10   | 10-11  | 11-12  | 12-13  | 13-14  | 14-15  | 15-16  | 16-17  | 17-18  | 18-19  |
| $\bar{H}$           | 11.529           | 11.529 | 11.529 | 11.529 | 11.529 | 11.529 | 11.529 | 11.529 | 11.529 | 11.529 | 11.529 | 11.529 | 11.529 | 11.529 |
| $r$                 | 0                | 0      | 0.0175 | 0.0623 | 0.1078 | 0.1447 | 0.1654 | 0.1654 | 0.1447 | 0.1078 | 0.0623 | 0.0175 | 0      | 0      |
| Collares            | 0                | 0      | 0.144  | 0.5127 | 0.8872 | 1.1908 | 1.3612 | 1.3612 | 1.1908 | 0.8872 | 0.5127 | 0.144  | 0      | 0      |
| Ashrae              | 0                | 0      | 0.116  | 0.7985 | 1.4065 | 1.8414 | 2.0672 | 2.0672 | 1.8414 | 1.4065 | 0.7985 | 0.116  | 0      | 0      |
| Apr.<br>Day no.=105 | 5-6              | 6-7    | 7-8    | 8-9    | 9-10   | 10-11  | 11-12  | 12-13  | 13-14  | 14-15  | 15-16  | 16-17  | 17-18  | 18-19  |
| $\bar{H}$           | 22.105           | 22.105 | 22.105 | 22.105 | 22.105 | 22.105 | 22.105 | 22.105 | 22.105 | 22.105 | 22.105 | 22.105 | 22.105 | 22.105 |
| $r$                 | 0                | 0.0207 | 0.0469 | 0.0748 | 0.1007 | 0.1208 | 0.1317 | 0.1317 | 0.1208 | 0.1007 | 0.0748 | 0.0469 | 0.0207 | 0      |
| Collares            | 0                | 0.3559 | 0.8065 | 1.2872 | 1.7131 | 2.1992 | 2.3980 | 2.3980 | 2.1992 | 1.7131 | 1.2872 | 0.8065 | 0.3559 | 0      |
| Ashrae              | 0                | 0.5007 | 1.3188 | 2.0646 | 2.6751 | 3.1071 | 3.3307 | 3.3307 | 3.1071 | 2.6751 | 2.0646 | 1.3188 | 0.5007 | 0      |
| Jul.<br>Day no.=198 | 5-6              | 6-7    | 7-8    | 8-9    | 9-10   | 10-11  | 11-12  | 12-13  | 13-14  | 14-15  | 15-16  | 16-17  | 17-18  | 18-19  |
| $\bar{H}$           | 28.182           | 28.182 | 28.182 | 28.182 | 28.182 | 28.182 | 28.182 | 28.182 | 28.182 | 28.182 | 28.182 | 28.182 | 28.182 | 28.182 |
| $r$                 | 0.0068           | 0.0272 | 0.0509 | 0.0757 | 0.0982 | 0.1154 | 0.1247 | 0.1247 | 0.1154 | 0.0982 | 0.0757 | 0.0509 | 0.0272 | 0.0068 |
| Collares            | 0.1926           | 0.7674 | 1.4368 | 2.135  | 2.7669 | 3.2520 | 3.5149 | 3.5149 | 3.2520 | 2.7669 | 2.135  | 1.4368 | 0.7674 | 0.1926 |
| Ashrae              | 0.0677           | 0.8165 | 1.6101 | 2.322  | 2.9013 | 3.3108 | 3.5226 | 3.5226 | 3.3108 | 2.9013 | 2.322  | 1.6101 | 0.8165 | 0.0677 |
| Oct.<br>Day no.=288 | 5-6              | 6-7    | 7-8    | 8-9    | 9-10   | 10-11  | 11-12  | 12-13  | 13-14  | 14-15  | 15-16  | 16-17  | 17-18  | 18-19  |
| $\bar{H}$           | 18.212           | 18.21  | 18.21  | 18.212 | 18.212 | 18.212 | 18.212 | 18.212 | 18.212 | 18.212 | 18.212 | 18.21  | 18.21  | 18.212 |
| $r$                 | 0                | 0.003  | 0.034  | 0.0705 | 0.1055 | 0.1336 | 0.1482 | 0.1482 | 0.1336 | 0.1055 | 0.0705 | 0.034  | 0.003  | 0      |
| Collares            | 0                | 0.055  | 0.627  | 1.2829 | 1.9175 | 2.4202 | 2.6979 | 2.6979 | 2.4202 | 1.9175 | 1.2829 | 0.627  | 0.055  | 0      |
| Ashrae              | 0                | 0.0005 | 0.672  | 1.469  | 2.1294 | 2.597  | 2.8401 | 2.8401 | 2.597  | 2.1294 | 1.469  | 0.672  | 0.0005 | 0      |

**Table (4b) Monthly mean daily global radiation (MJ/m<sup>2</sup>-day),  
ratio of hourly solar radiation to daily solar radiation (dimensionless),  
hourly solar radiation values in (MJ/m<sup>2</sup>-hour) using Collares-Pereira model,  
and hourly solar radiation values in (MJ/m<sup>2</sup>-hour) using ASHRAE model for Kirkuk city.**

| Months              | Daylight (hours) |        |        |        |        |        |        |        |        |        |        |        |        |        |
|---------------------|------------------|--------|--------|--------|--------|--------|--------|--------|--------|--------|--------|--------|--------|--------|
| Jan.<br>Day no.=17  | 5-6              | 6-7    | 7-8    | 8-9    | 9-10   | 10-11  | 11-12  | 12-13  | 13-14  | 14-15  | 15-16  | 16-17  | 17-18  | 18-19  |
| $\bar{H}$           | 8.230            | 8.230  | 8.230  | 8.230  | 8.230  | 8.230  | 8.230  | 8.230  | 8.230  | 8.230  | 8.230  | 8.230  | 8.230  | 8.230  |
| $r$                 | 0                | 0      | 0.0175 | 0.0623 | 0.1078 | 0.1447 | 0.1654 | 0.1654 | 0.1447 | 0.1078 | 0.0623 | 0.0175 | 0      | 0      |
| Collares            | 0                | 0      | 0.144  | 0.5127 | 0.8872 | 1.1908 | 1.3612 | 1.3612 | 1.1908 | 0.8872 | 0.5127 | 0.144  | 0      | 0      |
| Ashrae              | 0                | 0      | 0.116  | 0.7985 | 1.4065 | 1.8414 | 2.0672 | 2.0672 | 1.8414 | 1.4065 | 0.7985 | 0.116  | 0      | 0      |
| Apr.<br>Day no.=105 | 5-6              | 6-7    | 7-8    | 8-9    | 9-10   | 10-11  | 11-12  | 12-13  | 13-14  | 14-15  | 15-16  | 16-17  | 17-18  | 18-19  |
| $\bar{H}$           | 17.204           | 17.204 | 17.204 | 17.204 | 17.204 | 17.204 | 17.204 | 17.204 | 17.204 | 17.204 | 17.204 | 17.204 | 17.204 | 17.204 |
| $r$                 | 0                | 0.0207 | 0.0469 | 0.0748 | 0.1007 | 0.1208 | 0.1317 | 0.1317 | 0.1208 | 0.1007 | 0.0748 | 0.0469 | 0.0207 | 0      |
| Collares            | 0                | 0.3559 | 0.8065 | 1.2872 | 1.7131 | 2.1992 | 2.3980 | 2.3980 | 2.1992 | 1.7131 | 1.2872 | 0.8065 | 0.3559 | 0      |
| Ashrae              | 0                | 0.5007 | 1.3188 | 2.0646 | 2.6751 | 3.1071 | 3.3307 | 3.3307 | 3.1071 | 2.6751 | 2.0646 | 1.3188 | 0.5007 | 0      |
| Jul.<br>Day no.=198 | 5-6              | 6-7    | 7-8    | 8-9    | 9-10   | 10-11  | 11-12  | 12-13  | 13-14  | 14-15  | 15-16  | 16-17  | 17-18  | 18-19  |
| $\bar{H}$           | 23.392           | 23.392 | 23.392 | 23.392 | 23.392 | 23.392 | 23.392 | 23.392 | 23.392 | 23.392 | 23.392 | 23.392 | 23.392 | 23.392 |
| $r$                 | 0.0094           | 0.0293 | 0.0523 | 0.0758 | 0.0972 | 0.1135 | 0.1223 | 0.1223 | 0.1135 | 0.0972 | 0.0758 | 0.0523 | 0.0293 | 0.0094 |
| Collares            | 0.2206           | 0.7743 | 1.3784 | 2.0007 | 2.5655 | 2.9954 | 3.2279 | 3.2279 | 2.9954 | 2.5655 | 2.0007 | 1.3784 | 0.7743 | 0.2206 |
| Ashrae              | 0.1479           | 0.8885 | 1.6428 | 2.3188 | 2.8698 | 3.2589 | 3.4603 | 3.4603 | 3.2589 | 2.8698 | 2.3188 | 1.6428 | 0.8885 | 0.1479 |
| Oct.<br>Day no.=288 | 5-6              | 6-7    | 7-8    | 8-9    | 9-10   | 10-11  | 11-12  | 12-13  | 13-14  | 14-15  | 15-16  | 16-17  | 17-18  | 18-19  |
| $\bar{H}$           | 14.772           | 14.772 | 14.772 | 14.772 | 14.772 | 14.772 | 14.772 | 14.772 | 14.772 | 14.772 | 14.772 | 14.772 | 14.772 | 14.772 |
| $r$                 | 0                | 0.0017 | 0.0330 | 0.0699 | 0.1057 | 0.1342 | 0.1499 | 0.1499 | 0.1342 | 0.1057 | 0.0699 | 0.0330 | 0.0017 | 0      |
| Collares            | 0                | 0.0158 | 0.4877 | 1.0319 | 1.5612 | 1.9815 | 2.2141 | 2.2141 | 1.9815 | 1.5612 | 1.0319 | 0.4877 | 0.0158 | 0      |
| Ashrae              | 0                | 0.5627 | 0.5624 | 1.3157 | 1.9420 | 2.3865 | 2.6169 | 2.6169 | 2.3865 | 1.9420 | 1.3157 | 0.5624 | 0.5627 | 0      |

Table (4c) Monthly mean daily global radiation (MJ/m<sup>2</sup>-day), ratio of hourly solar radiation to daily solar radiation (dimensionless), hourly solar radiation values in (MJ/m<sup>2</sup>-hour) using Collares-Pereira model, and hourly solar radiation values in (MJ/m<sup>2</sup>-hour) using ASHRAE model for Baghdad city.

| Months              | Daylight (hours) |        |        |        |        |        |        |        |        |        |        |        |        |        |
|---------------------|------------------|--------|--------|--------|--------|--------|--------|--------|--------|--------|--------|--------|--------|--------|
| Jan.<br>Day no.=17  | 5-6              | 6-7    | 7-8    | 8-9    | 9-10   | 10-11  | 11-12  | 12-13  | 13-14  | 14-15  | 15-16  | 16-17  | 17-18  | 18-19  |
| $\bar{H}$           | 10.615           | 10.615 | 10.615 | 10.615 | 10.615 | 10.615 | 10.615 | 10.615 | 10.615 | 10.615 | 10.615 | 10.615 | 10.615 | 10.615 |
| $r$                 | 0                | 0      | 0.0227 | 0.0637 | 0.1074 | 0.1416 | 0.1630 | 0.1630 | 0.1416 | 0.1074 | 0.0637 | 0.0227 | 0      | 0      |
| Collares            | 0                | 0      | 0.2140 | 0.6757 | 1.1382 | 1.5174 | 1.7279 | 1.7279 | 1.5174 | 1.1382 | 0.6757 | 0.2140 | 0      | 0      |
| Ashrae              | 0                | 0      | 0.1787 | 0.8980 | 1.5239 | 1.9707 | 2.2026 | 2.2026 | 1.9707 | 1.5239 | 0.8980 | 0.1787 | 0      | 0      |
| Apr.<br>Day no.=105 | 5-6              | 6-7    | 7-8    | 8-9    | 9-10   | 10-11  | 11-12  | 12-13  | 13-14  | 14-15  | 15-16  | 16-17  | 17-18  | 18-19  |
| $\bar{H}$           | 20.704           | 20.704 | 20.704 | 20.704 | 20.704 | 20.704 | 20.704 | 20.704 | 20.704 | 20.704 | 20.704 | 20.704 | 20.704 | 20.704 |
| $r$                 | 0                | 0.0195 | 0.0461 | 0.0746 | 0.1009 | 0.1217 | 0.1329 | 0.1329 | 0.1217 | 0.1009 | 0.0746 | 0.0461 | 0.0195 | 0      |
| Collares            | 0                | 0.4036 | 0.9627 | 1.5447 | 2.0945 | 2.5198 | 2.7393 | 2.7393 | 2.5198 | 2.0945 | 1.5447 | 0.9627 | 0.4036 | 0      |
| Ashrae              | 0                | 0.4806 | 1.3308 | 2.1261 | 2.7686 | 3.1658 | 3.3954 | 3.3954 | 3.1658 | 2.7686 | 2.1261 | 1.3308 | 0.4806 | 0      |
| Jul.<br>Day no.=198 | 5-6              | 6-7    | 7-8    | 8-9    | 9-10   | 10-11  | 11-12  | 12-13  | 13-14  | 14-15  | 15-16  | 16-17  | 17-18  | 18-19  |
| $\bar{H}$           | 25.454           | 25.454 | 25.454 | 25.454 | 25.454 | 25.454 | 25.454 | 25.454 | 25.454 | 25.454 | 25.454 | 25.454 | 25.454 | 25.454 |
| $r$                 | 0.0068           | 0.0272 | 0.0509 | 0.0756 | 0.0982 | 0.1154 | 0.1247 | 0.1247 | 0.1154 | 0.0982 | 0.0756 | 0.0509 | 0.0272 | 0.0068 |
| Collares            | 0.1602           | 0.6386 | 1.1956 | 1.7744 | 2.3025 | 2.7062 | 2.9249 | 2.9249 | 2.7062 | 2.3025 | 1.7744 | 1.1956 | 0.6386 | 0.1602 |
| Ashrae              | 0.0677           | 0.6566 | 1.221  | 1.809  | 2.444  | 2.871  | 3.0566 | 3.0566 | 2.871  | 2.444  | 1.809  | 1.221  | 0.6566 | 0.0677 |
| Oct.<br>Day no.=288 | 5-6              | 6-7    | 7-8    | 8-9    | 9-10   | 10-11  | 11-12  | 12-13  | 13-14  | 14-15  | 15-16  | 16-17  | 17-18  | 18-19  |
| $\bar{H}$           | 16.808           | 16.808 | 16.808 | 16.808 | 16.808 | 16.808 | 16.808 | 16.808 | 16.808 | 16.808 | 16.808 | 16.808 | 16.808 | 16.808 |
| $r$                 | 0                | 0.0032 | 0.0345 | 0.0705 | 0.1053 | 0.1329 | 0.1482 | 0.1482 | 0.1329 | 0.1053 | 0.0705 | 0.0345 | 0.0032 | 0      |
| Collares            | 0                | 0.0507 | 0.5794 | 1.1843 | 1.7700 | 2.2340 | 2.4904 | 2.4904 | 2.2340 | 1.7700 | 1.1843 | 0.5794 | 0.0507 | 0      |
| Ashrae              | 0                | 0.052  | 0.6719 | 1.333  | 1.959  | 2.456  | 2.707  | 2.707  | 2.456  | 1.959  | 1.333  | 0.6719 | 0.052  | 0      |

Table (5) Statistical errors in (MJ/m<sup>2</sup>-hour) for Iraqi cities.

| Stations  | Months  | MBE    | RMSE   |
|-----------|---------|--------|--------|
| Nasiriyah | January | 0.147  | 0.2117 |
|           | April   | 0.319  | 0.3754 |
|           | July    | 0.072  | 0.1229 |
|           | October | 0.041  | 0.0634 |
| Kirkuk    | January | 0.103  | 0.1485 |
|           | April   | 0.296  | 0.3344 |
|           | July    | 0.199  | 0.2421 |
|           | October | 0.1577 | 0.1973 |
| Baghdad   | January | 0.1614 | 0.2137 |
|           | April   | 0.2361 | 0.2712 |
|           | July    | 0.0379 | 0.0786 |
|           | October | 0.1207 | 0.1477 |

## Influence of $TiO_2$ nanopowder particle size on the photocatalytic activity

Wesam A A Twej<sup>(a)</sup>, Nasser K Alsodany<sup>(b)</sup>, Baha T chiad<sup>(a)</sup>, Abass J Al-Watar<sup>(a)</sup> and Abdulkareem A Al-khafaji<sup>(c)</sup>

(a) university of Baghdad, college of science , (b) ministry of electricity and  
(c) university of Baghdad, college of pure science-Ibn Alhaitham

### Abstract:

There are several parameters which affect the photocatalytic activity of nanopowder titanium dioxide ( $TiO_2$ ). One of the important parameters is the grain size of  $TiO_2$  particles. In the present work a comparison between two grain sizes of  $TiO_2$  particles has been utilized. The results clarified that; the reduction of  $TiO_2$  grain size led to enhancement of the photocatalytic activity. A new method for the evaluation of the photocatalytic activity has been presented and achieved. This method based on titration of hydrogen peroxide ( $H_2O_2$ ) with further bi-product of ( $H_2O_2$ ) yield from  $TiO_2$  irradiation by UV source. The degradation percentage of potassium permanganate was calculated from the  $H_2O_2$  titration measurements. Totally degradation was achieved after 20 min for the sample of (10nm, 0.05 gm) but 60 min for the sample of (10 nm, 0.01gm),and 60 min for the sample of (50 nm, 0.05 gm), while it reaches 50% after 60 min for the sample of (50 nm, 0.01 gm).

### تأثير حجم جسيم المسحوق النانوي لثاني اوكسيد التيتانيوم ( $TiO_2$ ) على كفاءة المحفز الضوئي

1- د. وسام عبد علي تويج، 2- د. نصير كريم السوداني، 3- د. بهاء طعمه جواد، 4- د. عباس حمادي الوتار، 5- عبد الكريم عبد الحسين كريم الخفاجي

1- جامعة بغداد-كلية العلوم، 2-وزارة الكهرباء، 3- جامعة بغداد-كلية العلوم، 4- جامعة بغداد-كلية العلوم  
5-جامعة بغداد-كلية التربية للعلوم الصرفة- ابن الهيثم

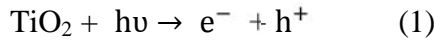
### الخلاصة

هناك عدة متغيرات تؤثر على فعالية المحفز الضوئي للمسحوق النانوي لثاني اوكسيد التيتانيوم ( $TiO_2$ ). احد اهم هذه المتغيرات هو حجم حبيبة جسيمات الـ ( $TiO_2$ ) في العمل الحالي تم دراسته الفرق بين حجمين مختلفين لحبيبات هذه الجسيمات. والنتائج اوضحت ان تقليل حجم جسيم مسحوق ثاني اوكسيد التيتانيوم يؤدي الى تحسين كفاءة المحفز الضوئي، وكذلك تم انجاز طريقه جديده لحساب كفاءة المحفز الضوئي، هذه الطريقه تستند الى المعايير بالتحليل الكمياري لبيروكسيد الهيدروجين بالإضافة للذي ينتج من خلال تشيع ثاني اوكسيد التيتانيوم بمصدر أشعة فوق البنفسجية. نسبة الانحلال المئوي لمحلول برمكانات البوتاسيوم تم حسابها من خلال قياسات المعايير بالتحليل الكيماوي . الانحلال الكلي تم الوصول اليه بعد 20دقيقه للنموذج(10نانومتر، 0,05غم) ولكن 60 دقيقه للنموذج (10نانومتر، 0,01غم) و60 دقيقه للنموذج(50نانومتر ، 0,05غم) بينما تصل الى 50% بعد 60دقيقه للنموذج (50نانومتر ، 0,01غم).

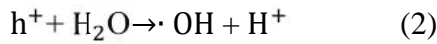
## 1. Introduction

Titanium dioxide (TiO<sub>2</sub>) exists in three crystalline structures: rutile, anatase, and brookite. It is a semiconductor of a band gap equal to 3.2eV in anatase phase. Anatase phase of TiO<sub>2</sub> possess strong hole trapping sites on surface which results in higher lifetime of the carriers compared to rutile phase, and this results in anatase being a better photocatalytic material than rutile [1-4]. Photocatalytic activity of TiO<sub>2</sub> strongly depends on its phase structure, crystallite size and specific surface areas [5]. Because the photodegradation reactions occur at the surface of the particles, a large surface area and a short distance to the surface is wanted. This can be achieved by making the particle size very small [6].

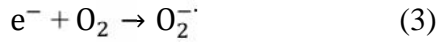
If TiO<sub>2</sub> is irradiated by photons of an energy equal or more than its energy gap, electrons are promoted from the valence band to the conduction band leaving positive holes in the valence band.[7,8]



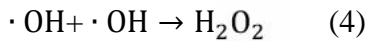
The positive hole (h<sup>+</sup>) reacts with either surface bound water (H<sub>2</sub>O) or pollutant to produce hydroxyl radical (·OH) . [8]



On the other hand, the electron reacts with oxygen to produce superoxide anions (O<sub>2</sub><sup>-</sup>) [7, 8]



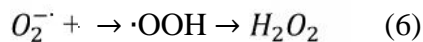
These radicals O<sub>2</sub><sup>-</sup> and ·OH in solution can react to give Hydrogen peroxide H<sub>2</sub>O<sub>2</sub>. [9,10]



Further hydroxyl.[9,10]

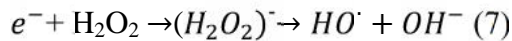


And hydroperoxyl radicals.[9,10]



An electron is generated when an acidic solution is irradiated in the presence of titanium dioxide.

Hydrogen peroxide will be decomposed by this electron [9,10,11].



A process with similar principle where  $H_2O_2$  reacts with  $KMnO_4$  at room temperature in a solution acidified by  $H_2SO_4$  and forms a manganite salt was designed.

Hydrogen peroxide forms as a bi-product of a radical reaction during the irradiation of the acidic solution of potassium permanganate with the addition of photoactive titanium dioxide and immediately reacts with the present  $KMnO_4$ .

The decrease of permanganate is then determined by titration of hydrogen peroxide and the degradation percentage of  $KMnO_4$  was calculated from the volume of hydrogen peroxide used during the titration.

## 2. Experiment

### 2.1. Materials

The following materials were used:

Titanium dioxide anatase nanopowder of particle size (10 and 50 nm), was purchased from M. K. Impex Corp., Canada. ( $H_2O_2$ ) Hydrogen peroxide, ( $KMnO_4$  0.15 M), analytical grade potassium permanganate and sulfuric acid ( $H_2SO_4$ ) (purity 99.9 %) all were supplied by Gainland Chemical Company, U.K. and deionized water supplied by Al Mansor Co.

### 2.2. Procedures

All the preparations and measurements were done in physics lab. college of science, university of Baghdad. Potassium permanganate solution was prepared by dissolving the permanganate with distilled water at concentration of 0.5 mol/L. Add 10 ml of potassium permanganate to (10 ml) of sulfuric acid in a petri dish under magnetic stirrer, as shown in fig1.

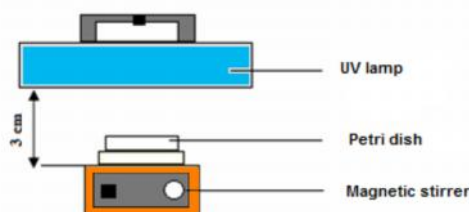


fig. 1: Schema of experiment

A volume of hydrogen peroxide was added to the solution above until its color was bleached completely, this volume of  $H_2O_2$  is denoted as ( $V_0$ ). Add a definite amount of titanium dioxide to the solution under a magnetic stirrer and then irradiated by UV source for several time intervals.  $V_1$  represents the volume of  $H_2O_2$ , which was added to the permanganate solution after the UV irradiation. The results were evaluated by degradation percentage (DP) [6].

$$DP = \frac{V_0 - V_1}{V_0} * 100$$

This test will be repeated for several time intervals and at different weights of  $\text{TiO}_2$  nanopowder. Finally a comparison between two  $\text{TiO}_2$  nanopowders of grain sizes (10 and 50 nm) were made. The judgment point for insuring totally photodegradation of permanganate solution in this work was the optically absorbance measurement using UV-VIS spectrometer fixed at the peak wavelength absorption which is at 550 nm. The permanganate solution was bleached as a result of the access addition of  $\text{H}_2\text{O}_2$  to the solution. When the absorption peak intensity of the permanganate solution is vanished, this indicates that, the permanganate was completely photodegraded. The study was started by immersing 0.01 gm and 0.05 gm of both 10 and 50 nm  $\text{TiO}_2$  nanopowder and dispersed in 10 ml of  $\text{KMnO}_4$  solution at concentration of ( 0.5 mol / L ). The mixtures were acidified by 10 ml, dilute solution of  $\text{H}_2\text{SO}_4$  under ultrasonic, then irradiated by fixed power lamp (6 W, UVC source) at different time intervals.

### 3. Results and Discussion

The study can be divided into two parts according to  $\text{TiO}_2$  weight and particle size

#### 3.1. The effect of $\text{TiO}_2$ weight

Firstly; the effect of  $\text{TiO}_2$  weight, by measuring the photodegradation percentage, has been studied. Figure (1) shows that, as the UV irradiation time increases the degradation percentage of the permanganate solution increased exponentially and reaching the saturation after about one hour at a degradation percentage of 50% for( 0.01 gm , $\text{TiO}_2$  nanopowder 50 nm ).

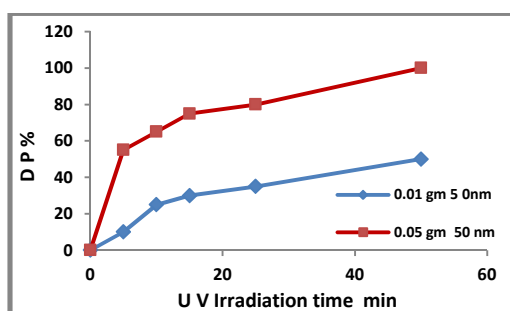


*Fig.1. degradation % vs. irradiation time for 0.01 gm and 0.05gm of 50 nm  $\text{TiO}_2$ .*

This may be attributed to the insufficient amount of  $\text{TiO}_2$ . Now 0.05 gm of  $\text{TiO}_2$  nanopowder of grain size 50 nm has photodegradation activity to bleach only half amount of 10 ml of the mentioned permanganate solution. While the photodegradation percentage increase clearly reaching 100 % after the same time of UV irradiation, when the  $\text{TiO}_2$  nanopowder quantity doubled five times. Now, when the particle size of the  $\text{TiO}_2$  nanoparticle was reduced from 50 to 10 nm as shown in figure 2.

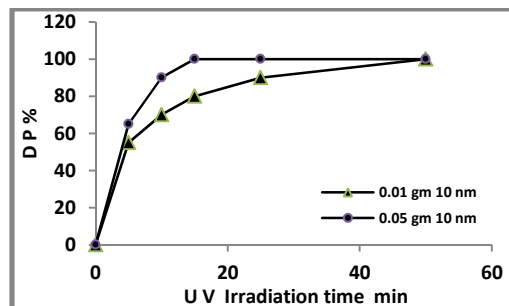


**Fig.2. degradation % vs. irradiation time for 0.01 and 0.05 gm of 10 nm TiO<sub>2</sub>.**

The photodegradation percentage reaches 100% after 20 min. for (0.05 gm), and reaches 100% after less than 60 min. for ( 0.01 gm ).

### 3.2. Effect of particle size

The effect of nanopowder particle size on the photodegradation percentage has been studied. Starting from small amount of TiO<sub>2</sub> nanopowder weight (0.01 gm) we measured the PD %. From figure 3 one can see that the sample of 50 nm has a weak photodegradation activity in comparison with that of 10 nm for the same weight of nanopowder.

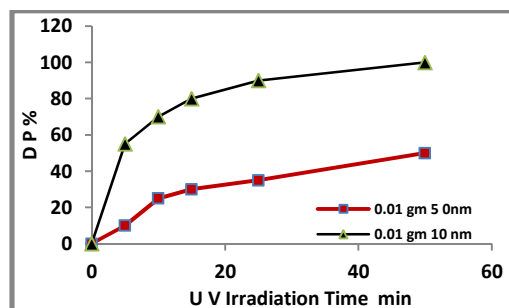


**Fig.3. DP vs. irradiation time for 0.01 gm of 10 and 50 nm TiO<sub>2</sub>.**

When the amount of the TiO<sub>2</sub> nanopowder increased from 0.01 to 0.05 gm, the PD % increased rapidly for the samples of size of 10 nm, where it reached 100% after 20 min in comparison of one hour for the 50 nm sample.

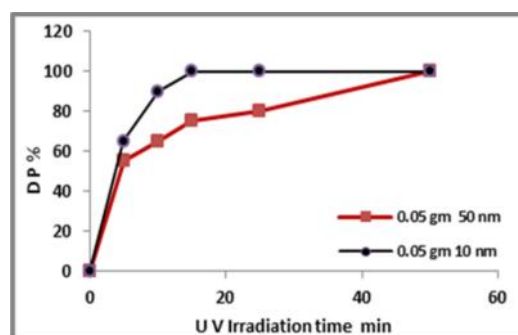


**Fig.4. degradation % vs. irradiation time for 0.05gm of 10 and 50 nm TiO<sub>2</sub>.**

The results were summarized in the table 1:

| <i>Table 1.The effect of grain size and TiO<sub>2</sub> amount on the time of degradation percentage</i> |                    |                   |            |
|----------------------------------------------------------------------------------------------------------|--------------------|-------------------|------------|
| <b>Grain size(nm)</b>                                                                                    | <b>Weight (gm)</b> | <b>Time (min)</b> | <b>Dp%</b> |
| <b>10</b>                                                                                                | 0.01               | 60                | 100%       |
| <b>10</b>                                                                                                | 0.05               | 20                | 100%       |
| <b>50</b>                                                                                                | 0.01               | 60                | 50%        |
| <b>50</b>                                                                                                | 0.05               | 60                | 100%       |

#### 4. Conclusion:

This work concluded that the degradation percentage was doubled when 10nm grain size for the same amount weight of nanopowder TiO<sub>2</sub> was used in compare with 50nm grain size. Therefore; photocatalytic activity is increased with reducing the grain size of TiO<sub>2</sub> nanopowder. This method has several advantages compared to other methods which based on decolorization of dyes. The evaluation of photocatalytic activity goes faster by using this method.

#### References

1. Murat Kurtoglu, *Ph.D thesis ( Effect of doping on the photocatalytic, electronic and mechanical properties of so;-gel titanium dioxide films)* Drexel University, 2011.
- 2..Fujishima,K.Hashimoto,T.Watanabe:(TiO<sub>2</sub>Photocatalysis:Fundamentalsand plications); BKC, Tokyo;1999.
- 3.Wang R. Hashimoto K, Fujishima A” light induced amphilic surface” *Nature*, 388 431-432, 1997.
- 4.Gupta S M and Tripathi M “ A review of TiO<sub>2</sub> nanoparticles” *Chinese Sci. Bull.* V 56 no. 16 1639-1657, 2011.
- 5.Qi Kaihong, *Ph.D thesis ( study of photocatalytic activities of nanoscaled metal oxides on textiles)* Hong Kong Polytechnic University, 2008
- 6.Anna-Karin Gustavsson. *M.Sc. thesis ( solar photocatalytic degradation of Rhodamine B by TiO<sub>2</sub> nanoparticle composites )* . University of Gothenburg, 2010
- 7.Masatoshi N “Hydrophilic and photocatalytic properties of the SiO<sub>2</sub>/ TiO<sub>2</sub> double layers” *thin solid films*,496, 131-135, 2006.
- 8.Kenneth J.klabunde and Ryan M.Richards (*Nanoscale materials in Chemistry*) second edition, by Wiley. 2009
- 9.Akira F, Tata N, Donald A” *Titanium Dioxide Photocatalysis” J PCPP*, 1, 1-21, 2000.
10. Kazuhito H, Hiroshi I and Akira F” *TiO<sub>2</sub> photocatalysis: A historical overview and future prospects” Japanese J of applied physics*, 44,12,8269-8285, 2005.
- 11.Howard A.Foster, Iram B.Ditta, Sajnu Varghese, Alex Steele.” *Photocatalytic disinfection using titanium dioxide: Spectrum and mechanism of antimicrobial activity” Appl. Microbial Biotechnol.* (2011) 90:1847-1868.

## Solar cell Monitoring and Actuating via Embedded Web Server

Ali M. Mahmood

Ahmed R. Nasser

Bahaa D. Jalil

Control and Systems Eng. Dept.  
University of Technology

[alimmj81@yahoo.com](mailto:alimmj81@yahoo.com)

[arn111984@yahoo.com](mailto:arn111984@yahoo.com)

[bahaoy@yahoo.com](mailto:bahaoy@yahoo.com)

### Abstract

The energy of the sun is free to use because it is a natural permanent source, which makes the solar cell system cheaper and completely non-polluting so it can be used in a wide variety of locations in the world Wherever there is sun. Monitoring systems for solar cell becomes very important when there are a large number of solar cells panels over high distances. Monitoring allows early detection if the output falls below the required level or one of the solar cell panel goes down. The aim of this paper is to design remotely monitor and actuator system for a solar panel via the Internet by using the Embedded Web Server to ensure reliable performance for solar cells. Finally it will use the data logger system that continuously store the data gathered from the solar system to check the previous reading.

### المراقبة والتحكم للخلايا الشمسية عبر خادم الويب المضمن

#### الخلاصة

إن الطاقة الشمسية مجانية للاستغلال وذلك لأنها مصدر طبيعي دائم، وهذا يجعل نظام الخلية الشمسية ارخص وغير ملوث للبيئة لذا يُمكن أن تستعمل في مختلف مواقع العالم حيثما تكون هناك شمس. أنظمة المراقبة للخلايا الشمسية أصبحت مهمة جداً في حال وجود عدد كبير من الألواح الشمسية على مساحات بعيدة. تُسمح أنظمة المراقبة للكشف المبكر في حالة حدوث أي إخفاق في منظومة الخلايا الشمسية إلى أقل من المستوى المطلوب. إن هدف هذا البحث هو تصميم نظام مراقبة وتحكم للخلايا الشمسية عن بعد باستخدام الإنترنت والذي يتم باستعمال خادم الويب المُضمن لضمان الأداء الموثوق للخلايا الشمسية. أخيراً سوف يتم استعمال نظام تسجيل البيانات الذي يُخزن البيانات المأخوذة بشكل مستمر من الخلايا الشمسية وذلك لتدقيق القراءة السابقة.

**Keywords:** Solar cell, Embedded Web Server, Monitoring & Actuating Systems, Data Logger, HTML

### 1. Introduction

The basic idea of a solar cell is to convert light energy into electrical energy. The energy of light is transmitted by photons, small packets of light. Electrical energy is stored in electromagnetic fields, which in turn can make a current of electrons flow. Thus a solar cell converts light, to electric current. The electrical characteristics (current, voltage, or resistance) vary when light is falling upon it which, when exposed to light, can generate and an electric current without being attached to any external voltage source. Solar power is an efficient alternative to fossil fuels and some alternative energy sources, as it gives off no carbon dioxide waste and uses the natural energy from our sun to generate electricity. Solar panels are available for a wide range of applications, including powering individual gadgets, electronic devices and vehicle batteries. To interact with solar system. During the operation, it is needed to monitor and control of individual solar panels to allow the remote control center to track the panels on their individual performance. The monitored panels can be

quickly switched off in the case of failure, overload, fire, environment hazards (tornados), or other troubles. The most important parameters in solar system that needed to monitor are voltage, current and temperature. Therefore the Solar system owners or service providers can automatically track the work of the panels and determine if service or maintenance is required. To make the design more powerful the solar parameters are stored by using data logger to recapture them when there are needed [1,2].

## 2. Embedded Web Server

It is a Web server software that resides permanently within a hardware device. It is widely used because it allows access to the software via a Web. The general purpose web servers compose of an operating system, the web pages or the application and a huge amount of memory and sometimes a special hardware [3].

The central function unit to get access on an embedded system via Web browser is the Web server. Such Web servers bring the desired HTML pages (HTML=Hyper Text Markup Language) and pictures over the worldwide Internet or a local network to the Web browser. This happen HTTP-based (Hyper Text Transfer Protocol). Web server (HTTP server) and browser (HTTP client) build TCP/IP applications. The embedded web-server, with a built-in TCP-IP connectivity protocol is used to allow receiving and sending digital commands for actuating and monitoring purpose without the need to have a dedicated server PC or even special software [4].

In order to make a web based monitoring system, The following technology is used ; HTML, Java and web server to observe and control the system with one computer has been used and already present a LAN which is connected to internet. The architecture of the overall system is divided into two sides the solar side shown in Figure (1). It is composed of three parts; embedded web server, sensors and solar cell panel. The client side contains its own user interface , in the form of web pages to interact with the remote system by using the standard web browsers as shown in Figure (2).

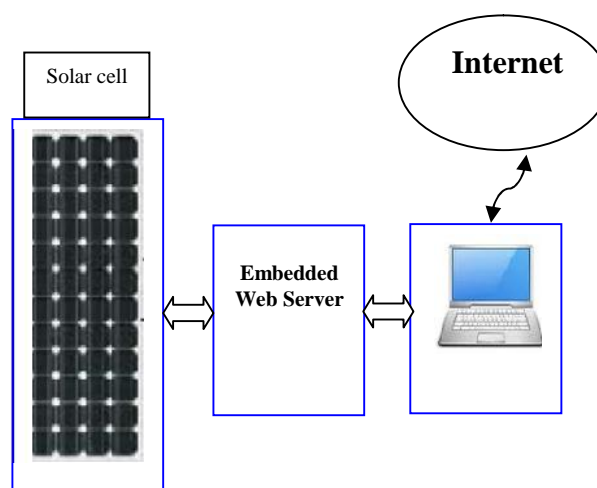


Figure (1) : Solar cell Side

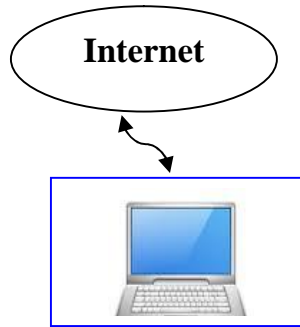


Figure (2): Solar cell Monitoring & Actuating (client) Side

### 3. Solar Cell Monitoring

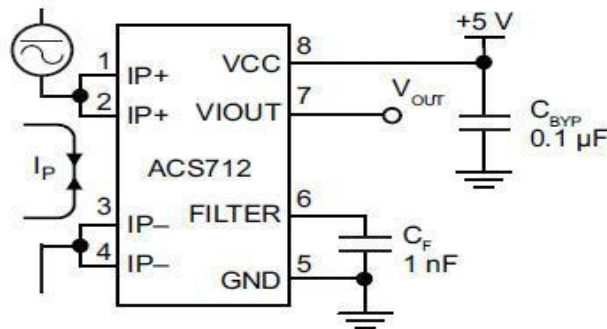
To interact with a solar system during its operation we need to monitor and control the individual solar panels that allows for the remote control center to track the panels on their individual performance and allows the panels to be quickly switched off in the case of failure, overload, fire, environment hazards (tornados), or other troubles. When the solar panel get covered with dust the performance will degrade. So it is needed to monitor the most important parameters in solar system (voltage, current and temperature) to inform the control center which panel need to be cleaned and to ensure high power supply performance. when there is a large number of solar panels over long distances, it will be feasible to monitor the parameters of the solar cells via the internet and this can be done by using the Embedded web servers. Monitoring means reading the solar cell parameters from the outside world to the computer to do some calculations or to investigate from actual value of them. The challenges in particular are how to develop an effective monitoring technologies to compensate for the decentralized nature of remote power generation. Currently, solar monitoring technologies are expensive, limited in their application, and for the most part proprietary[5]. To achieve the system monitoring it is needed a hard ware to interface the solar with computer for this purpose the Microcontroller is used as shown in the following section.

#### 3.1. ATmega 328 Microcontroller

The Atmel is a high performance 8-bit AVR RISC-based microcontroller. It combines 32KB ISP flash memory with read-while-write capabilities, 1KB EEPROM, 2KB SRAM, 23 general purpose I/O lines, 32 general purpose working registers, three flexible timer/counters with compare modes, internal and external interrupts, serial programmable USART, a byte-oriented 2-wire serial interface, SPI serial port, 6-channel 10-bit A/D converter (8-channels in TQFP and QFN/MLF packages), programmable watchdog timer with internal oscillator, and five software selectable power saving modes. The device operates between 1.8-5.5 volts. By executing powerful instructions in a single clock cycle, the device achieves throughputs approaching 1 MIPS per MHz, balancing power consumption and processing speed.

#### 3.2. Current Monitoring

To get the solar current the main component used is the ACS712 sensor from Allegro Micro Systems to measure the current as shown in Figure (3). It provides inexpensive solutions for AC or DC current sensing in industrial systems. The device is not intended for wide applications but is usually used in motor control , switched-mode power supplies, over current fault protection, load detection and management.

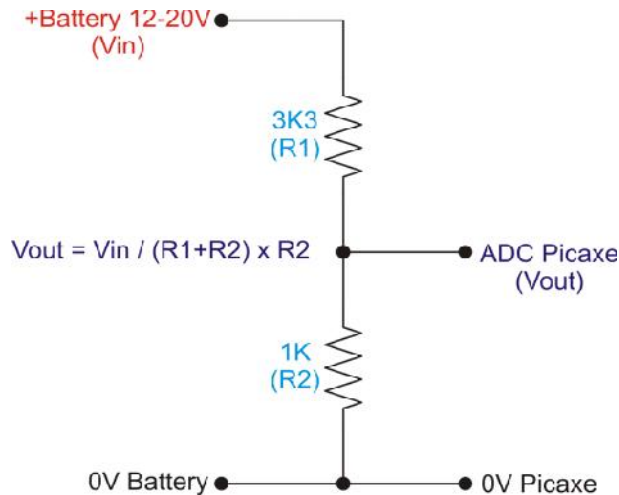


Figure(3): ACS712 Current sensor

In This work it is used one of the three models of ACS712. Other models can be chosen depending on the maximum measured current (5-20-30A) [6,7]. From its pin configuration, the voltage across VIOUT and ground PIN is proportional to current flowing between IP+ and IP-, which makes ACS712 very easy to use. It needs two capacitors for filtering the power supply and output while requiring a power supply of 5V. For 5A model, the value that links the proportionality of output voltage and input current measurements is sensitivity which has a typical value of 185mV/A.

### 3.3.Voltage Monitoring

Monitoring battery voltage can do easily by the Atmega328 with a simple voltage divider circuit in Figure (4), where it can be control loads, generators, or notifications based on battery voltage [8].



Figure(4): Voltage Divider Circuit

Where the voltage divider comes in, it scales the 0 – 12 v battery voltage to a lower range of 0– 5 volts. The mathematical calculation of the battery voltage and resistor values is shown in Figure (4). It can also be useful to express this equation in terms of R1 or R2 when selecting resistors.

$$V_{out} = \left( \frac{R_2}{R_1 + R_2} \right) \times V_{in} \quad (1)$$

### 3.4. Temperature Monitoring

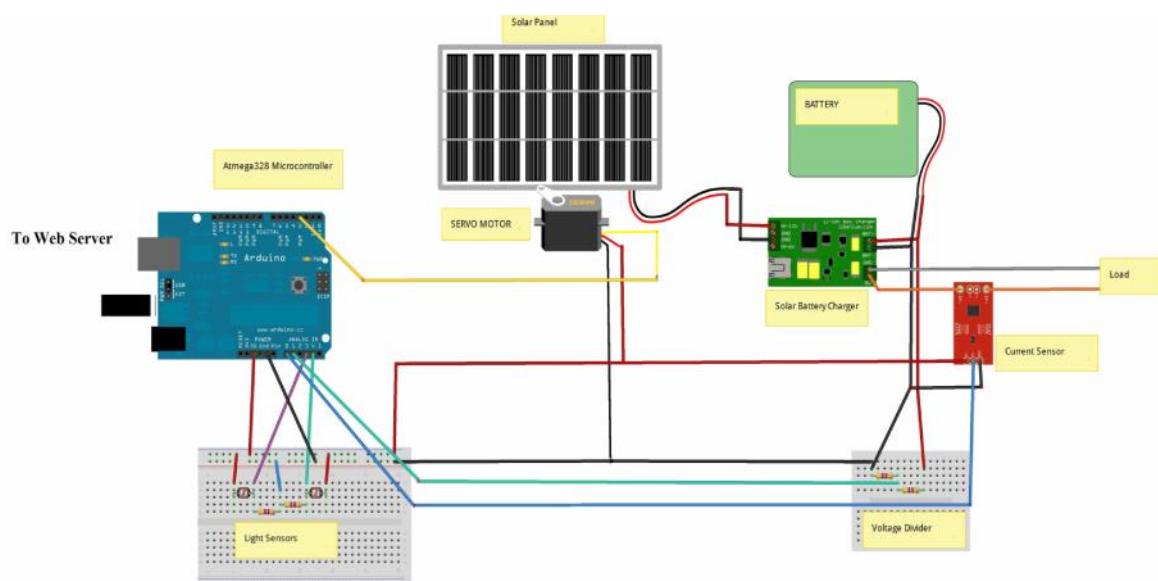
LM35 is a temperature sensor from National Semiconductor that have a high accuracy. The output of analog voltage and has a measurement range of  $-55^{\circ}\text{C}$  to  $+150^{\circ}\text{C}$  with an accuracy of  $\pm 0.5^{\circ}\text{C}$ . Output voltage is  $10\text{mV} / ^{\circ}\text{C}$  [9]. Output ports can be directly connected to Atmega328 microcontroller, because Atmega328 has 6 ADC ports (analog input). Analog inputs on the microcontroller has a 10-bit resolution, which can provide output  $2^{10} = 1024$  discrete values. When used 5V supply, the resulting resolution is  $5000\text{mV}/1024 = 4.8\text{mV}$ . Because the LM35 has a resolution output of  $10\text{mV} / ^{\circ}\text{C}$ , then the resolution of the thermometer are made with microcontroller is  $10\text{mV}/4.8\text{mV} \sim 0.5^{\circ}\text{C}$ .

### 4. Solar Cell Actuating

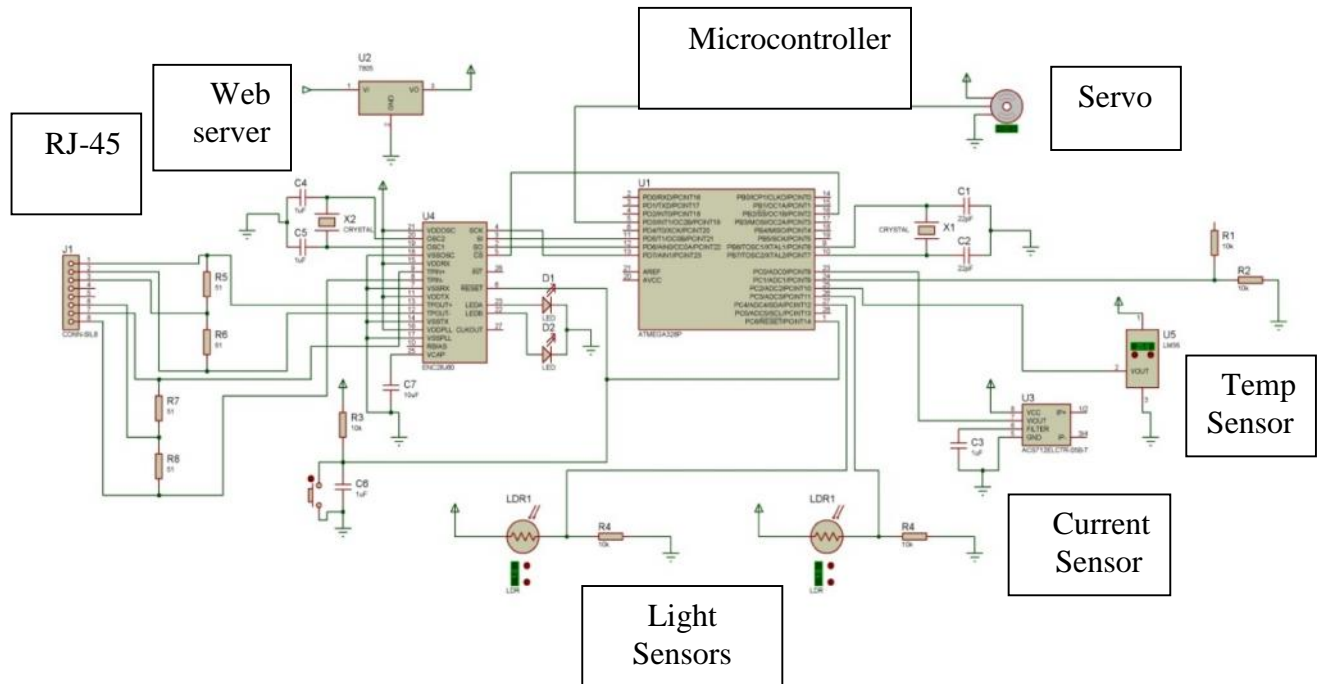
It is used two light sensors to track a solar cell panel as shown in Figure (5). The light sensors are fixed at 90 degree to each other. The sensors are shielded, so they will see the brightest light levels when pointing directly at the light source. When light source moves the light moved from the sensor causing changing its resistance. The tracking of the sunlight for a solar panel, approve the maximum sunlight intensity that applied on the solar cell, so that both sensors need to see the same intensity of light. For solar cell sunlight tracking it must read both of the input sensor values and compare between them, 0 difference means they are at the same light level, a -ve error value means the light is brighter to the right, and a +ve error value means the light is brighter to the left. The servo motor is disciplined with a position value.

### 5. Data Logger System

The data logger that used in this work is a database that records solar cell parameters such as voltage, current and temperature that are equipped with the embedded web server and the microcontroller board for data storage. The data recorded by the loggers utilize web page to view the collected data. The data collected by the logger can be plotted with recording date or time as shown in Figure (10).



Figure(5): Complete Circuit Diagram (Microcontroller board)



Figure(6): Schematic Diagram of the Overall Design

## 6. Circuit Test and Simulation Results

The circuit is designed and simulated by using Virtual Bread Board (VBB) Simulation program. Virtual Breadboard or 'VBB' is a development and an emulation environment for embedded applications that use microcontrollers featuring Makeable Breadboard layouts that bring designs to life faster and more cost effectively. Figure (7) shows the program main screen. After wiring the overall circuit in Figure(6) using VBB program and loading the microcontroller with the software discussed in section 7. The circuit is simulated by the same program and during simulation the monitoring web page shown in Figure (10) shows the online results that used for monitor solar cell parameters such as voltage , current and temperature. After run the simulation for 24 hours it can display the recorded results by using data logger web page as shown in Figure(11) and plot the results as shown in Figure(12).

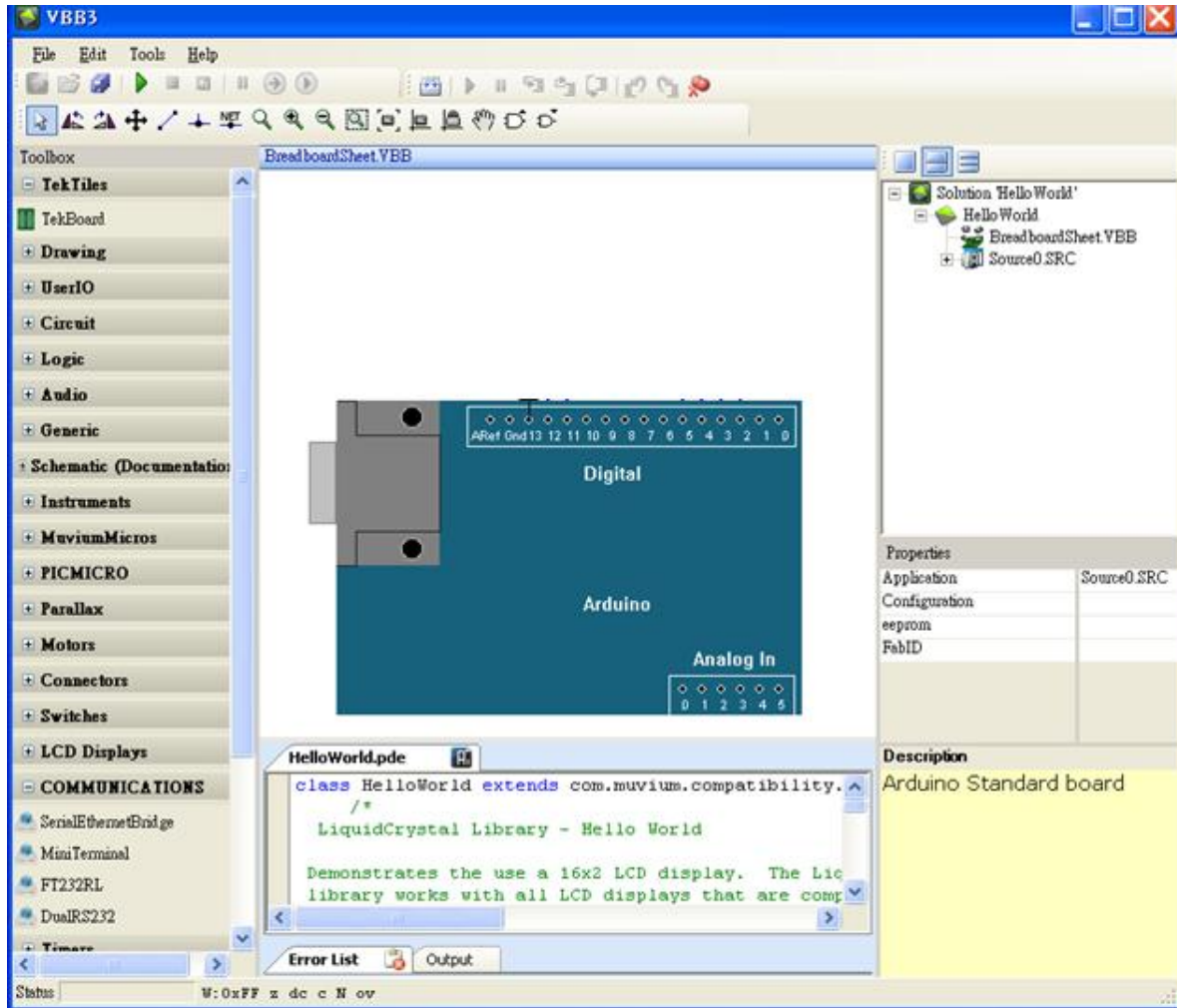
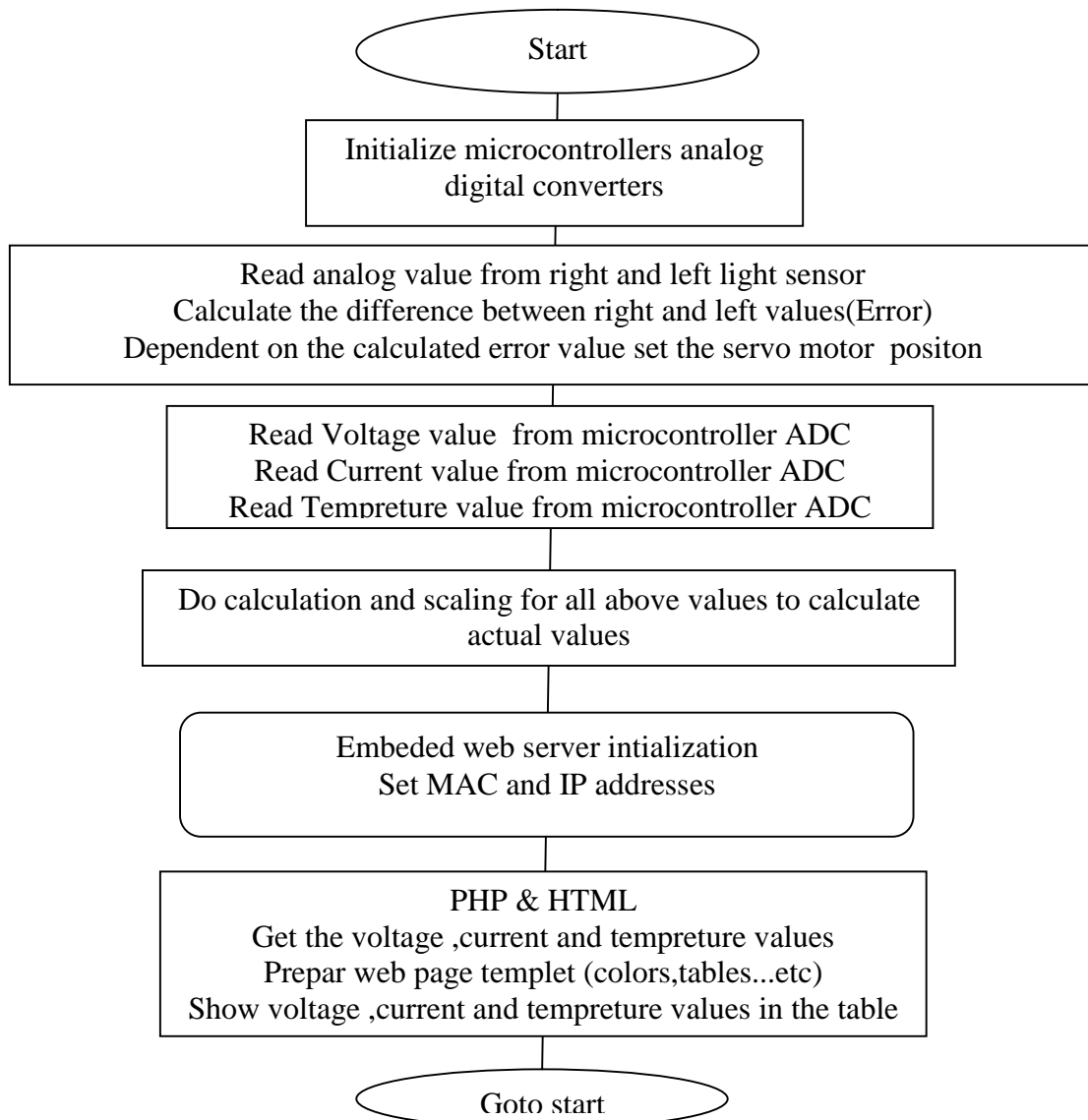


Figure (7): Virtual Bread Board (VBB) Simulation program.

## 7. Software development:

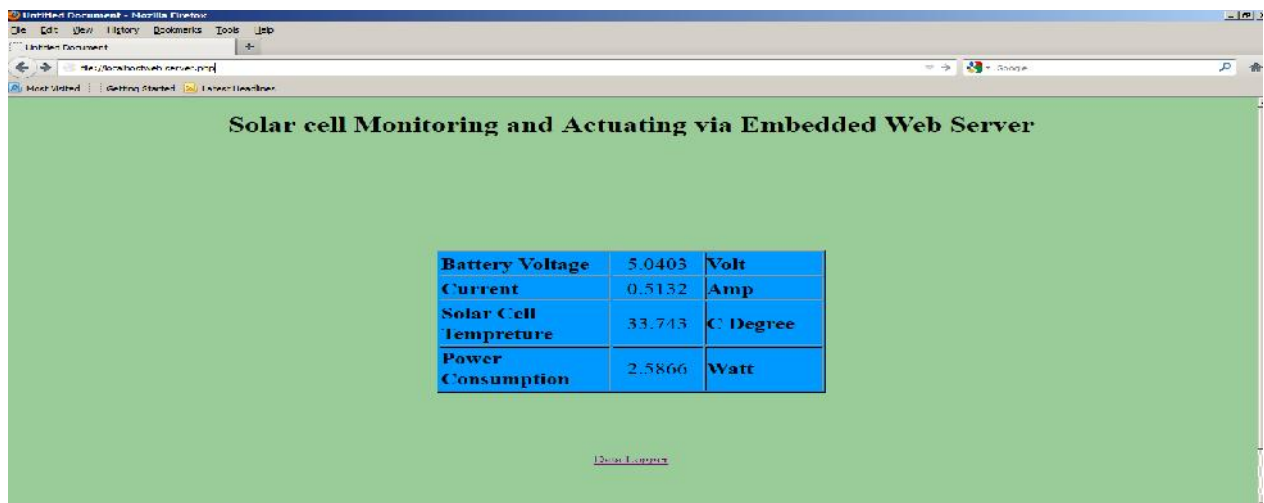
The main processing unit used in this work it is the Atmega 328 microcontroller which mentioned in the section 3.1.1. This microcontroller can program by using C++ language. The software used for program this type of microcontroller is developed by Atmel corporation is AVR Studio which can convert C++ code into hex code used for programming microcontroller. The Embedded web server software is developed by using both of PHP and HTML web programming languages. Which provide the user interfaces for monitoring the data variables reads from the microcontroller such as (Voltage ,Current..etc) .The software flow diagram is shown in Figure(8).



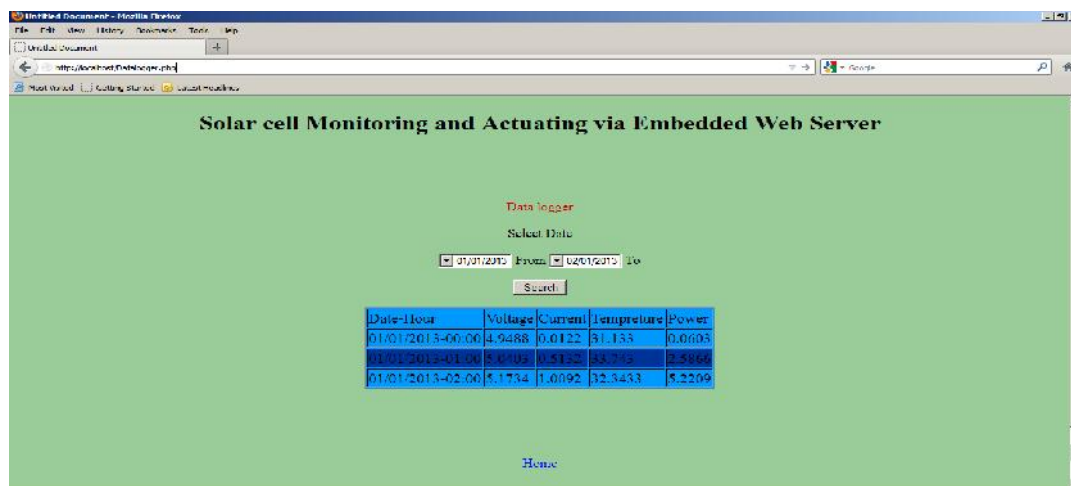
**Figure (8):Software Flow Diagram.**



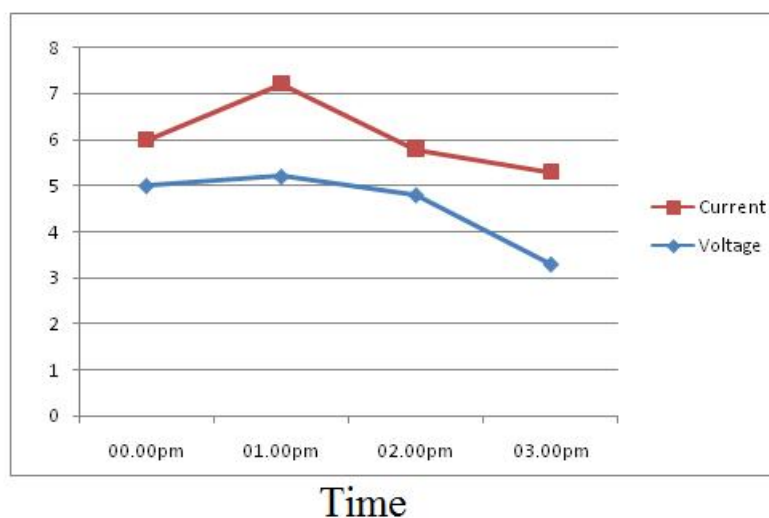
**Figure(9): Complete circuit diagram (Embedded web server board)**



Figure(10): Embedded Web Server Home page



Figure(11): Embedded web server Data logger page



Figure(12): Embedded Web Server Data logger plotting page.

## Conclusions

- 1.The using of Embedded web server is very powerful since it is depended on Internet protocols (TCP /IP ).
2. The Embedded web server is very effective and favorable approach since it can check the solar system in any location in the world.
3. Reading the solar parameters (current and voltage) serves as a great indicator if something goes wrong with the system, where avoiding system failure will lead to energy saving .
4. System actuator involve sun tracking to invest the maximum sun light leading to maximum energy.
5. One of the primary benefits of using data logger is the ability to automatically collect data on a 24-hour basis. Upon activation, data loggers are typically deployed and left unattended to measure and record information for the duration of the monitoring period.

## References

- [1] Gwinyai Dzimano, “MODELING OF PHOTOVOLTAIC SYSTEMS”, Master thesis, The Ohio State University,2008.
- [2] C. De falco, m. Porro, r. Sacco, and m. Verri, “Multiscale Modeling And Simulation Of Organic Solar Cells”,2012.
- [3] Olivetti S.p.A.,”Embedded Web Server” , Gruppo Telecom Italia Via Jervis, 77 - 10015 Ivrea (ITALY),2009.
- [4] Deepak C.Karia, Vispi Adajania, Manisha Agrawal and Swapnil Dandekar, “Embedded Web Server Application Based Automation and Monitoring System”, roceedings of 2011 International Conference on Signal Processing, Communication, Computing and Networking Technologies (ICSCCN 2011).
- [5] Daniel Schermuk, Ezequiel Esposito,”Home Automation System using LPC1769”, UNIVERSITY OF BUENOS AIRES,2011.
- [6] Bimal Aklesh Kumar, “Solar Power Systems Web Monitoring”, The 2nd Symposium on Renewable Energy Technologies (SoRET), October 2011.
- [7] Michael Peffers, Muhammed Khan, Michael Gannon, Ahmad Buleybal, “UCF Wireless Solar Panel Monitoring System”, School of Electrical Engineering and Computer Science, University of Central Florida, Orlando, Florida, 32816-2450,2011. [8] Susan Connell,” EcoDog Introduces Advanced Residential Solar Power Monitoring”, Jennings & Associates Communications, Inc,2010.
- [9] Nikolas Wolfe , “An Open-Source Monitoring System for Remote Solar Power Applications”, CIS 4914 Senior Project,2009.
- [10] Hossein Mousazadeh,et al,” A review of principle and sun-tracking methods for maximizing solar systems output”, Renewable and Sustainable Energy Reviews 13 (2009) 1800–1818.

## Analytical Study of Solar Cell Efficiency Enhancement by Using Nd-YAG Laser

<sup>(1)</sup>**Hassan W. Hilou**

Assist.Prof. Al-Mamon University College, College of engineering, Baghdad, Iraq; e-mail: hassanwhilou@yahoo.co.uk

<sup>(2)</sup>**Fatema H. Rajab**

Assist.Lec. Laser & optoelectronics Dept., College of Engineering, Al-Nahrain University, Baghdad, Iraq; e-mail: hamid\_fatema@yahoo.com

<sup>(3)</sup>**Rasha K. Mohammed**

Assist.Lec. Laser & optoelectronics Dept., College of Engineering, Al-Nahrain University, Baghdad, Iraq; e-mail: rashakhalid\_2004@yahoo.com

### ABSTRACT

Surface texturing plays a critical role in silicon solar cell performance, affecting both reflectance and light trapping. Laser based tooling offers the possibility of cost reduction and efficiency enhancement.

In this paper, theoretical study of laser texturing to enhance the efficiency of solar cell has been performed. The laser system used in this work is Nd-YAG laser with wavelengths of 1.064 $\mu$ m, 532  $\mu$ m, and 335  $\mu$ m. The pulse duration of laser was 50 $\mu$ s and energy is 0.1J.

The average efficiency of the laser texturing solar cell has been calculated to be 16.1524%, 16.2180% and 16.3953%, respectively. These values are compared with the untextured surface, which is having efficiency of 10.6%.

The comparison between the three results was made to find the optimum efficiency enhancement. It has been found that the higher increasing of efficiency is achieved with higher wavelength.

**Keywords:** Solar cell, Laser surface texturing, Energy enhancement.

### دراسة تحليلية لتحسين كفاءة الخلية الشمسية باستخدام ليزر نديموم ياك

#### الخلاصة

التنسيج السطحي يلعب دوراً حاسماً في أداء خلية السيليكون الشمسية، يؤثر على كل من معامل الانعكاس و انحصار الضوء. الاعتماد على أداة الليزر يعرض إمكانية تحسين الكفاءة وتخفيض التكلفة.

في هذه الدراسة النظرية لتنسيج الليزر تمت تحسين كفاءة الخلية الشمسية. إن نظام الليزر الذي استعمل في هذا العمل هو ليزر النديميوم ياك بأطوال الموجة من  $1.064 \mu\text{m}$  و  $532 \mu\text{m}$ ، و  $335 \mu\text{m}$ . مدة نبض الليزر كانت  $50 \mu\text{s}$  وطاقة  $0.1 \text{ J}$ . الكفاءة المتوسطة لليزر لتنسيج الخلية الشمسية حسبته لكي تكون  $16.1524\%$ ،  $16.2180\%$  و  $16.3953\%$ ، على التوالي. هذه القيم مقارنة بسطح الغير منسج، التي سيكون عندها كفاءة  $10.6\%$ . تمت المقارنة بين النتائج الثلاث لإيجاد تحسين الكفاءة القصوي. وقد استنتجت هذه الدراسة ان الزيادة الأعلى للكفاءة منجزة بطول الموجة الأعلى.

## INTRODUCTION

It has been a long time, since the finding of photovoltaic effect by Bequerel in 1839. Recently, rapid industrial growth, urbanization, and increasing demands for consumer electronics, all of those lead to a very fast depletion of existing energy resource. Furthermore, in the past years, the awareness of the negative impacts of fossil fuel consumption on the environment has been increase. This leads to a very active alternative energy research. One of the solutions of above problem is the silicon solar cell. The solar cells or “photovoltaic device” can convert optical power from Sun to electricity. It is the best candidate for the next generation energy sources. They are low cost and easy to be fabricated. However, one of the major drawbacks is its fairly low absorption coefficient. Many approaches have been proposed to enhance the light trapping efficiency, such as adding back reflector , designing periodic arrays of metal nanoparticles, modulating surface textures for enhancing light trapping, two-dimensional photonic crystal, using light scattering textured back electrodes, using diffraction grating , and photonic crystal back reflector, etc. [1].

For thin-film solar cells, light absorption is usually proportional to the film thickness. However, if freely propagating sunlight can be transformed into a guided mode. The optical path length significantly increases and results in enhanced light absorption within the cell.

Surface texturing is a common technological process in solar cell manufacturing aiming at a reduction of the light reflection losses. The standard alkaline texturing of multicrystalline silicon for solar cells is not effective because of random orientation of the grains. In this paper a method of laser texturisation has been proposed numerically to overcome these difficulties [2].

## LASER SURFACE TEXTURING

The idea of texturing the top of Si wafer surface is to aid the coupling of light into a p-n structure and to increase the optical path length in the absorber. There are many type of texturing technique as chemical texture, plasma texture, lithograph texture, and laser texturing [3].

Lasers find widespread application in materials processing. They are successfully applied in industrial processes including welding, cutting, drilling, ablation deposition and surface treatment. Lasers are used to generate coherent and monochrome light that is characterized by small divergence of the beam, small diameter of the spot and very high power density of radiation. Lasers applied in surface engineering generate infrared light whose power density is in the range  $10^3$ - $10^8$  W/cm<sup>2</sup>. Laser radiant flux incident on the non-transparent surface of material is partially reflected and absorbed. The amount of incident laser radiant flux that is reflected and/or absorbed depends on the wavelength of laser beam, physical properties of material and its surface. The quantity of heat absorbed by the material at the point of laser beam interaction depends on its absorption coefficient, wavelength and power density of laser beam and time of exposure. The higher is the temperature of heated material the higher is absorption of incident radiation. The highest temperature of upper layer is obtained at point that corresponds to place related to the highest power density. Distribution of temperature on the top surface corresponds to the distribution of power density in the cross-section of laser beam. The heat accumulated in the top layer penetrates inwards material as a consequence of heat transfer. As a result, upon laser processing so-called heat affected zone with structural defects may be created [4].

## LASER-GROOVED BURIED CONTACTS

Any discussion on laser-based efficiency enhancement processes within c-Si cell production should always start with laser-grooved contacts (LGBC).

LGBC as an overall process captures so many of the drivers behind currently proposed efficiency enhancement scheme: locally doped selective-emitter formation, high conductivity electroless plated contacts, reduced finger line-width shading, and increased metallization

aspect ratios. Figure (1) illustrates a schematic of the LGBC process with an SEM image of a laser groove at the front surface, prior to metallization [1].

Scribe quality is achieved by optimizing several laser output parameters: short pulse width enable clean material ablation, high average powers, high – finesse output beams to allow focusing with micron scale resolution, short wavelength laser output at either 532nm (green) or 355nm (UV) where absorption properties in c-Si are orders of magnitude more favorable in comparison to lower cost 1064nm IR lasers. Also increased lifetime ratio (decreased laser damage) are obtained when scribing lines using short-wavelength 355nm (UV) or 532nm (green) lasers as shown in Figure (2) [5].

## THEORETICAL ANALYSIS

This work analyses possible implementation of laser treatment in texturing of silicon solar cells. Texturisation enhances the absorption of light through the following phenomena of incoming light rays that are reflected from one tilted (by texturing) surface may strike another surface resulting in an improved probability of absorption, and therefore reduced reflection. This paper presents the results of increasing the efficiency of a solar cell by using laser texturing technique. Three different wavelengths are used and a comparison is made between the results associated with these wavelengths.

Various approximation to the intensity distribution within the focus of a laser beam are possible, while consider the total laser power ( $P$ ) is incident over a circular area  $A^2$  and the intensity within this area is constant at the value. In practice, the distribution of intensity within the focus is a complex function of position and time but laser-induced thermal effects do not seem to be overly sensitive to this distribution provided that the temperature (i.e., thermal effect) is sampled away from the immediate in which the interaction occurs. For this reason, it is often convenient to assume as above that all “fine structure” in the intensity distribution is eliminated and that the thermal effect is the same as that which would be produced by absorption of the equivalent total power over a circular area ( $P/\pi A^2$ ) whose radius may be chosen empirically.

Consider the case of heating a large block of material with laser radiation focused onto the surface as shown in Figure (3) [6].

If the solid is taken to be homogeneous and isotropic, the conduction of heat is [6]:

$$\nabla^2 T - \frac{1}{a} \frac{\partial T}{\partial t} = - \frac{A(x,y,z,t)}{K} \quad (1)$$

Where  $a$  is the thermal diffusivity.

The time-independent temperature distribution in the solid is obtained by solving equation (1) for the applied power ( $P$ ) for ( $t > 0$ ) over the circle  $x^2 + y^2 = A^2$ ,  $z=0$ , of the semi-infinite region:

$$-\infty \leq x \leq +\infty, -\infty \leq y \leq +\infty, 0 \leq z \leq +\infty$$

The solution at the point whose cylindrical coordinates ( $r, z$ ) is then :

$$T(r, z, t) = \frac{P\epsilon}{2\pi AK} \int_0^\infty J_0(m'.r).J_1(m'.A). \left\{ e^{(-m'z)}.erfc \left[ \frac{z}{2(at)^{1/2}} - m'(at)^{1/2} - e^{(m'z)}.erfc \left[ \frac{z}{2(at)^{1/2}} + m'.(a.t)^{1/2} \right] \right\} \cdot \frac{dm'}{m'} \quad (2)$$

Where  $\epsilon$  is the fraction of the energy absorbed from the beam, and  $J_0$  are Bessel Functions of the first kind.

The texturing process was made by laser beam. The laser beam caused a spot after each run depending on the above equation. The area of the honeycomb (arrays of spots) texturing was calculated by the following procedure [7]. The spot is taken as a sector of parabolic shape.

$$y^2 = p x \quad (3)$$

Where:

Y is the depth

X is the radius

The surface area of this section can be calculated as:

$$S_r = 2\pi \int_a^b y \sqrt{1 + \left[ \frac{dy}{dx} \right]^2} dx \quad (4)$$

The area of the top planner is

$$A=r^2\pi \quad (5)$$

The increase in the efficiency of the textured solar cell can be calculated from the reduction in the reflectance effects on the  $J_L$ . With textured surface, there is a reduction in the total reflectance and the cell should show a power conversion larger than the planer cell.

Then the change in short circuit current density will follow the relation.

$$\frac{\Delta J_{sc}}{J_{sc}} = \frac{(1-R_T)-(1+R_o)}{1-R_o} = \frac{1-R_T}{1-R_o} - 1 \quad (6)$$

Where:

$R_o$ : total reflection of surface.

$R_T$ : total reflection of the textured surface.

The increases in the surface area of the device will also increase the dark current density by the following factor:

$$\frac{\Delta J_o}{J_o} = \frac{S_r - A}{A} = \frac{S_r}{A} - 1 \quad (7)$$

Where:

$A$  is the original planar area.

$S_r$  is the total surface area of the textured device.

This leads generally in a reduction of the open-circuit voltage.

$$\Delta V_{oc} \approx \frac{KT}{q} \left\{ \ln \left[ \frac{J_{sc} + \Delta J_{sc}}{J_o + \Delta J_o} \right] - \ln \left[ \frac{J_{sc}}{J_o} \right] \right\} = \frac{KT}{q} = \ln \left[ \frac{1 + \frac{\Delta J_{sc}}{J_{sc}}}{1 + \frac{\Delta J_o}{J_o}} \right] \quad (8)$$

The net gain in power conversion efficiency is [8]

$$\frac{\Delta \eta}{\eta} = \frac{\Delta P}{P} = \frac{\Delta J_{sc}}{J_{sc}} + \frac{\Delta V_{oc}}{V_{oc}} \quad (9)$$

## RESULTS AND DISCUSSION

The integration of the equation (2) has been evaluated numerically to determine the temperature at any point in the solid at any time.

The integration of the mathematical function included in equation (2) has been solved numerically using the Trapezoidal rule as per the following function [9]:

$$\int_0^m f(x)dm = \frac{m-0}{2n} (y_0 + 2y_1 + 2y_2 + 2y_3 + \dots + y_n) \quad (10)$$

Where n the number of sub-intervals.

Computer program has been written in MATLAB environment to find the form of hole in solar cell of specifications shown in Table (1) to enhance it using Nd-YAG laser with three wavelengths and single energy.

The shape of the hole which had been constructed by using laser pulse was presented in Figure (4). This figure shows the relationship between radius and depth using Nd-YAG laser with wavelength=1064nm, energy=0.1J and tp=50μs. It is clear from the figure that the radius of resulted hole = 2.8mm and depth =47μm.

On the second hand, the second harmonic generation of Nd -YAG laser with wavelength=532nm is used to generate hole with r=2.6mm and z=38μm as shown in Figure (5). Also, the third harmonic generation of Nd-YAG laser with 355nm is used to generate hole with r=2.3mm and z=26μm as shown in Figure (6).

The equations (3-9) are applied for the calculations of the increase in the efficiency for textured solar cell.

The increase in efficiency using 1063nm is about 52.3810%. The untextured quarter of the solar cell give the efficiency of 10.6%. The textured cell should have an efficiency  $(10.6 + 10.6 * \frac{\Delta\eta}{\eta})$  that is equal (16.1524%). whereas the increase of efficiency using 532nm and 355nm are given in Table (2).

## CONCLUSIONS

1. The success of laser-based processes within the generation high efficiency silicon cell depends strongly on the correct choice of laser type.
2. The texturing process is one of useful processes to enhance the solar cell efficiency using solid state (Nd-YAG) pulse laser.
3. The best diameter caused by laser beam is 2.3mm with the depth of 26μm.
4. The best increasing of efficiency is 54.6727% using third harmonic generation of Nd-YAG laser.

## REFERENCES

- [1] T. H. Chang<sup>1</sup>, et al, "Efficiency enhancement in GaAs solar cells using self-assembled microspheres", OPTICS EXPRESS 6521, Vol. 17, No. 8, 13 April 2009.
- [2] D. M. Waters, et al, "surface Analysis of CdTe after Various Pre-Contact Temperature" , Presented at the 2<sup>nd</sup> World Conference and exhibition on Photovoltaic Solar Energy Conversion: Vienna, Austria, 6-10 July,1998.
- [3] M. A. Green, "Silicon Solar Cell, Advanced Principle and Practice", Center for Photovoltaic Device and System university of New South Wales Australia, 1995.
- [4] L.A. Dobrzański , et al, " Application of laser in multicrystalline silicon surface processing", journal of Achievements in Materials and Manufacturing Engineering, VOLUME 24 ISSUE October 2007.
- [5] S. Clara, "laser processing enables high efficiency silicon cell concepts", photovoltaic world, coherent Inc., April 2009.
- [6]W. W. Duley, "CO<sub>2</sub> Laser Effects and Applications", Academic press, 1976.
- [7] G. B.Thomas and R. L.Finney," Calculas and Analytic Geometry" , Addison – Welsly Publishing Company, 1988.
- [8] R. J. Roredd and P.M. Holm, "The Design of Anisotropic Etched Solar Cell, Vol. 11, 1984.
- [9] J. L. Buchanan and P. R. Turner, "Numerical Methods and Analysis", 1st Ed., Mc Graw-Hill, 1992.

**Table (1):The characteristics of textured solar cell**

|                       |                         |
|-----------------------|-------------------------|
| Type                  | p-type                  |
| Dopant                | Boron                   |
| Resistivity           | 40Ω/seq                 |
| Diameter              | 10cm                    |
| Thickness             | 500μm                   |
| Reflectivity          | 0.35,0.65,0.8           |
| Melting temp.         | 1412 c                  |
| Boiling temp.         | 3350 c                  |
| Thermal conductivity  | 0.14 W/mm.K             |
| Thermal diffusivities | 80 mm <sup>2</sup> /sec |

**Table (2):The characteristics of textured solar cell**

| Wavelength λ(nm) | radius r(mm) | Depth Zm(μm) | Δ efficiency % | Efficiency % |
|------------------|--------------|--------------|----------------|--------------|
| 1063             | 2.8          | 47           | 52.3810        | 16.1524      |
| 532              | 2.6          | 38           | 52.9997        | 16.2180      |
| 355              | 2.3          | 26           | 54.6727        | 16.3953      |

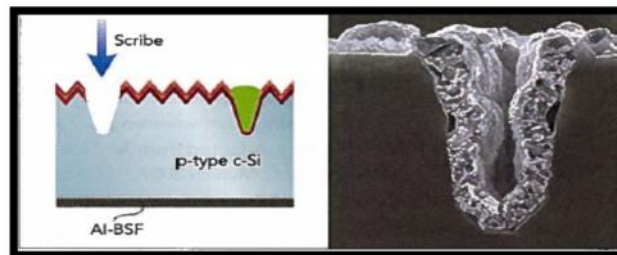


**Figure (1): Laser grooved buried contacts [1].**

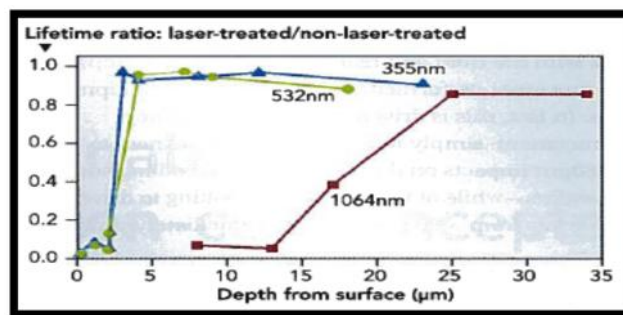


**Figure (2): Life time ratio [5]**

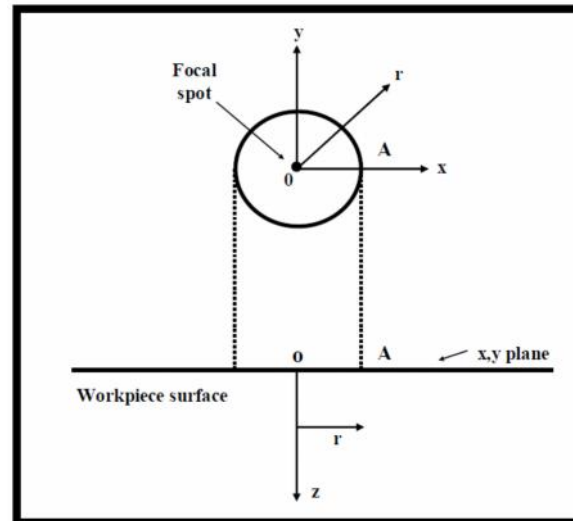


Figure (3): Coordinate system [6].

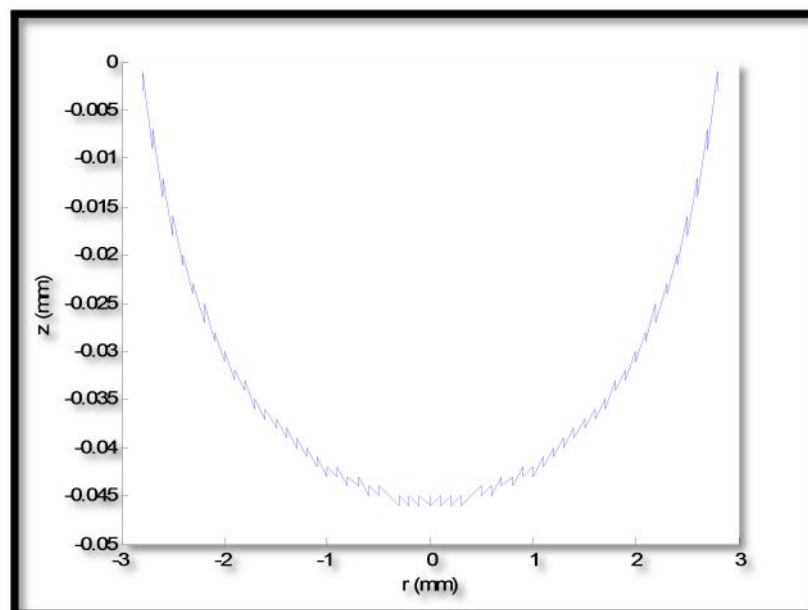


Figure (4): the form of hole in solar cell using 1064nm.

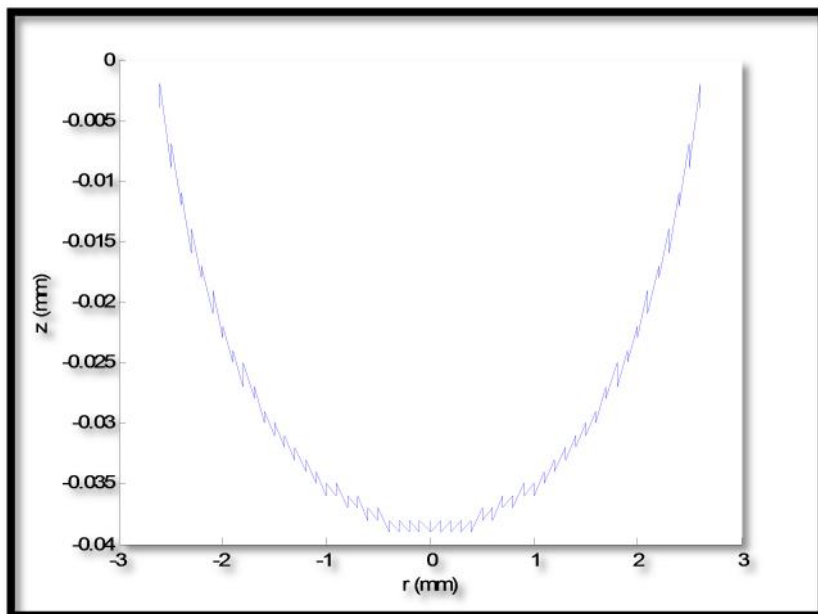


Figure (5): the form of hole in solar cell using 532nm.

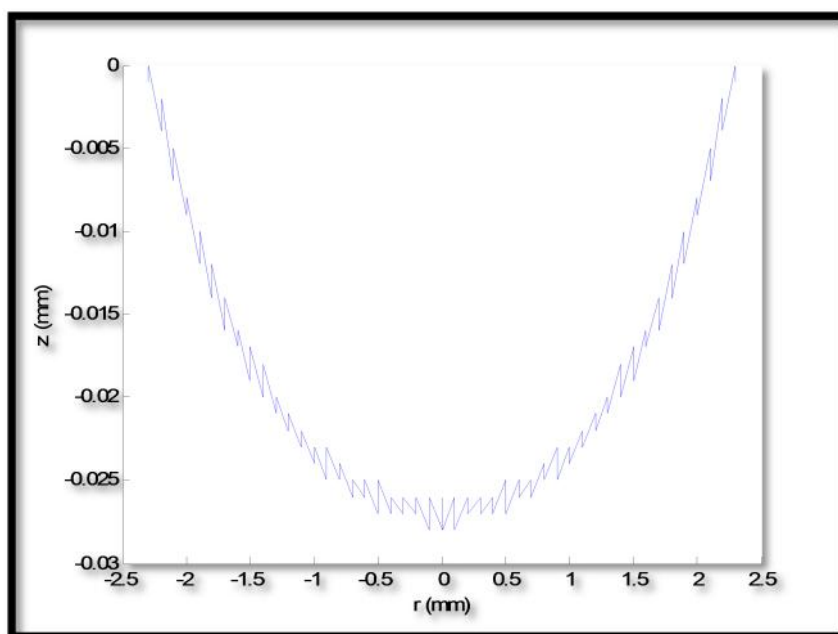


Figure (6): the form of hole in solar cell using 355nm.

## Study the parameters effect on the design of solar energy system for impressed current cathodic protection for oil pipelines

Dheya N. Abdulamer<sup>\*</sup>, Dr. Qusay A. Jawad<sup>\*</sup>, Ahmed A. Hassosh<sup>\*\*</sup>

Energy and Renewable Energies Technology Center, University of Technology

<sup>\*\*</sup>Materials Engineering department, University of Technology

### Abstract:

Cathodic protection represent the main solution for protection of oil pipelines against corrosion. There are two types of cathodic protection, the first one known as sacrificial cathodic protection, while the other called impressed cathodic protection. In this research, study the parameters effect (soil resistivity, anode geometrical and groundbed states) were done to design solar energy system as main source for impressed current required for protection. Design of impressed current cathodic protection using solar energy based on various factors. Low soil resistivity (25 .cm) required low potential (3.024, 3.218 and 4.079 V) for two anodes with ( 48, 24.9 and 6.02 cm) length of anode and (0.027, 0.0234 and 0.0158 shape factor ) respectively. In this context, nine PV panels (13 W) is fair enough in the low soil resistivity (25 .cm) with K=0.0158. Solar energy have been used in this research because of it represent clean energy and it is good solution for protect oil pipelines at the land very far from power station.

**Keywords :** Solar Energy, Impressed Current Cathodic Protection (ICCP)

دراسة العوامل المؤثرة على تصميم نظام الطاقة الشمسية للحماية الكاثودية بالتيار المضغوط لخطوط انابيب النفط

ضياء نجم عبد الامير<sup>\*</sup>، د. قصي عبد الجبار جواد<sup>\*</sup>، احمد عزيز حاشوش<sup>\*\*</sup>

<sup>\*</sup> مركز تكنولوجيا الطاقة والطاقة المتجددة، الجامعة التكنولوجية

<sup>\*\*</sup> قسم هندسة المواد، الجامعة التكنولوجية

الخلاصة:

تعتبر الحماية الكاثودية من الطرق الاساسية الضرورية لحماية انابيب النفط من التآكل. هنالك نوعين من الحماية الكاثودية، يدعى النوع الاول الحماية الكاثودية بالتضحية، بينما الاخرى تدعى الحماية الكاثودية باستخدام التيار المضغوط

. تم خلال هذا البحث دراسة اثر العوامل المختلفة ( مقاومة التربة، الابعاد الهندسية ووضعية الانود في التربة) لغرض تصميم نظام الطاقة الشمسية كمصدر رئيسي لضغط التيار المطلوب للحماية . اظهرت النتائج ان التربة ذات المقاومة فولتية منخفضة من المصدر بحدود (3.024 3.218 4.079) لقطين باط (25 . )  
( 6.02 24.9 ) (0.0158 0.0234 0.027) على التوالي. بهذا السياق يتبين ان تسعة الواح شمسية ذات قدرة قدرها (13 ) تكون ملائمة لهذه التربة. استخدمت الطاقة الشمسية في هذا البحث وذلك لكونها من الطاقات النظيفة بالاضافة الى ذلك يمكن استخدامها في المناطق النائية والبعيدة عن محطة توليد الطاقة الكهربائية.

### List of symbols:

- I is total protective current  
A is total structure surface area in square feet  
 $I_i$  is required current density  
CE is coating efficiency.  
N is number of anodes required  
 $A_1$  is anode surface area in square feet per anode  
 $I_1$  is recommended maximum current density output in milliamperes.  
 $L_f$  is life in years  
W is weight of one anode in pounds.  
 $R_a$  is the anodes' resistance  
S is the center-to-center spacing between anode backfill columns in feet.  
L is the wire length in feet.  
 $R_s$  is the structure-to-electrolyte resistance  
 $R_c$  is the coating resistance in ohms per square feet  
 $A_c$  is the coated pipe area in square feet.  
 $R_T$  is total circuit resistance.  
is soil resistivity in ohm-centimeters  
 $d_s$  Diameter of steel pipe  
 $L_s$  length of steel pipe  
d anode diameter  
 $R_w$  wire resistance

$L_w$  wire length

$W_P$  Energy per day of solar panel

$W_L$ : Energy of required load (watts).

$B_c$  Battery capacity

$N_{PV}$  Number of PV panels

$N_b$  Number of batteries required

HSCBCI High Silicon Chromium Bearing Cast Iron

## 1. Introduction:

Cathodic protection is an electrochemical technique in which a cathodic (protective) potential is applied to an engineering structure in order to prevent corrosion from taking place, and this implies that Ohm's law,  $E=IR$ , can be used to control the potential, as well as the current [1]. There are two principal methods of applying cathodic protection. The impressed current technique and the use of sacrificial anodes. Impressed current cathodic protection (ICCP) systems are used throughout the world to provide cathodic protection for pipelines, ship hulls, offshore production platforms, water and wastewater treatment equipment, tank farms, and underground storage tank systems [2]. Figure (1) illustrates the use of an external power supply to provide the cathodic polarization of the structure. The circuit comprises the power source, an auxiliary or impressed current electrode, the corrosive solution, and the structure to be protected. The power source drives a positive current from the impressed current electrode through the corrosive solution and onto the structure. The structure is thereby cathodically polarized (its potential is lowered), and the positive current returns through the circuit to the power supply. Thus, to achieve cathodic protection, the impressed current electrode and the structure must be in both electrolytic and electronic contact. The power supply is usually a transformer/rectifier that converts AC power to DC. Typically, the DC output will be in the range 15–100V and 5–100 A, although 200 V/200A units are not unknown. Thus, fairly substantial driving voltages and currents are available. Where mains power is not available, diesel or gas engines, solar panels, or thermoelectric generators have all been used to provide suitable DC [3].

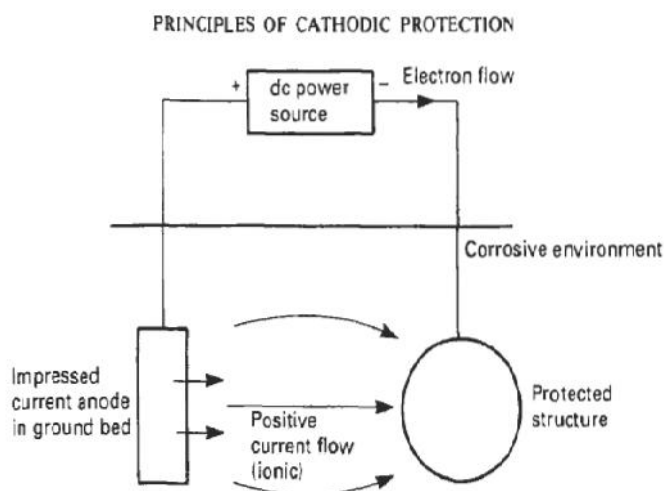


**Figure (1) : Impressed Current Cathodic pretection technique**

## 2. Theoretical background:

Before the system is designed, certain preliminary information must be gathered. The steps required when designing Impressed current cathodic protection systems are as follows:

### 1. Current requirement:

A critical part of design calculations for cathodic protection systems on existing structures is the amount of current required per square foot (called current density  $I_i$ ) to change the structure's potential to - 0.85 volt. A well coated structure will require a very low current density (about 0.05 milliamperes per square foot); an uncoated structure would require high current density (about 10 milliamperes per square foot). The average current density required for cathodic protection is 2 milliamperes per square foot of bare area.

Current requirements can be calculated using equation (1), based on coating efficiency and current density desired. The efficiency of the coating as supplied will have a direct effect on the total current requirement.

$$I = (A) (I_i) (1.0 - CE) \dots\dots\dots(1)$$

(2) Selecting anode. As with the galvanic system, the choice of anode is arbitrary at this time economy will determine which anode is best. The anodes used most often are made of high silicon chromium-bearing cast-iron (HSCBCI). When impressed current-type cathodic protection systems are used to mitigate corrosion on an underground steel structure, the auxiliary anodes often are surrounded by a carbonaceous backfill. The backfill materials commonly used include coal coke breeze, calcined petroleum coke breeze, and natural graphite particles. The backfill serves three basic functions:

- (a) it decreases the anode-to-earth resistance by increasing the anode's effective size,
- (b) it extends the system's operational life by providing additional anode material, and
- (c) it provides a uniform environment around the anode, minimizing deleterious localized attack.

(3) Calculated number of anodes needed to satisfy manufacture's current density limitations. To determine the number of anodes needed to meet the current density limitations, use equation -2

$$N = I / ( A_1 I_1 ) \dots\dots (2)$$

(4) Calculated number of anodes needed to meet design life requirement. Equation -3 is used to find the number of anodes:

$$N = L_f (I) / 1000 ( W ) \dots\dots (3)$$

(5) Calculated number of anodes needed to meet maximum anode groundbed resistance requirements. Equation -4 is used to calculate the number of anodes required:

$$Ra = \frac{... * K}{N L} + \frac{... * P}{S} \dots\dots(4)$$

**Table 1: Anode paralleling factors (P) for various numbers of anodes (N) installed in parallel [4].**

| N  | P       | N  | P       |
|----|---------|----|---------|
| 2  | 0.00261 | 14 | 0.00168 |
| 3  | 0.00289 | 16 | 0.00155 |
| 4  | 0.00283 | 18 | 0.00145 |
| 5  | 0.00268 | 20 | 0.00135 |
| 6  | 0.00252 | 22 | 0.00128 |
| 7  | 0.00237 | 24 | 0.00121 |
| 8  | 0.00224 | 26 | 0.00114 |
| 9  | 0.00212 | 28 | 0.00109 |
| 10 | 0.00201 | 30 | 0.00104 |
| 12 | 0.00182 |    |         |

**Table 2: Shape functions (K) for impressed current cathodic protection anodes where L is effective anode length and d is anode/backfill diameter [4].**

| L/d | K      |
|-----|--------|
| 7   | 0.0158 |
| 30  | 0.0234 |
| 60  | 0.0270 |

The soil resistivities (25, 50, 600, 1000, 5000 .cm) were represent moderate to severe conditions of large extent of land in north Iraq – Turkey pipeline extending from Nineva to Um – Qaser in Basrah as shown in the table 3. This condition without effect of bacteria and any obstacle [5].

**Table 3: Soil resistivity in the large extent of Iraq land [5].**

| <b>Concentration<br/>NaCl %</b> | <b>NaCl<br/>content<br/>g/l</b> | <b>Conductivity<br/><math>\mu\Omega/\text{cm}</math></b> | <b>Resistivity<br/><math>\Omega.\text{cm}</math></b> |
|---------------------------------|---------------------------------|----------------------------------------------------------|------------------------------------------------------|
| 0.01                            | 0.1                             | 200                                                      | 5000                                                 |
| 0.05                            | 0.5                             | 1000                                                     | 1000                                                 |
| 0.1                             | 1                               | 1666.66                                                  | 600                                                  |
| 1                               | 10                              | 20000                                                    | 50                                                   |
| 3                               | 30                              | 40000                                                    | 25                                                   |

(6) Determined total circuit resistance. Determining the total circuit resistance which will be used to calculate the rectifier size needed.

(a) Calculate anode groundbed resistance. Use equation -4.

(b) Calculate groundbed header cable resistance. The cable is typically supplied with a specified resistance in ohms per 100 feet. The wire resistance ( $R_w$ ) then is calculated from equation -5:

$$R_w = \text{Ohms (L)} / 1000 \text{ ft} \dots\dots(5)$$

(c) Calculate structure-to-electrolyte resistance using eq – 6 :

$$R_c = R / A_c \dots\dots(6)$$

(d) Calculate total circuit resistance. To calculate the total resistance, equation -7 is used :

$$R_T = R_a + R_w + R_c, \dots\dots(7)$$

(7) Calculate required voltage  $V_{\text{req}}$ . Equation -8 is used to determine voltage output ( $V_{\text{rec}}$ ) of the rectifier:

$$V_{\text{req}} = (I)(R_T)(150\%) \dots\dots (8)$$

Besides the more common rectifiers being marketed, a solar cathodic protection power supply (for D.C. power) may be considered for remote sites with no electrical power. Three factors that should be considered when specifying a solar cathodic protection power supply are:

1. The cost of the solar cathodic protection power supply in dollars per watt of continuous power.
2. The solar cathodic protection power supply's much higher initial cost compared to selenium rectifiers operated by A.C. power.
3. The additional maintenance required for a solar cathodic protection power supply, mainly to keep the solar panels free of dirt deposits [4].

### 3. Design of Impressed current cathodic protection (ICCP) system:

The first step in the design involves calculating the total current required (I) for protecting steel pipe against corrosion which has been described as indicated in the table (4). Equation (1) has been used for determined (I). Ground bed anode resistance  $R_a$ , wire resistance  $R_w$ , pipeline to soil resistance  $R_c$  and the total circuit resistance have been estimated using equations (4, 5, 6 and 7) respectively. The data obtained from these equations depend mainly on the variations of soil resistivity ( ), number of anodes, paralleling factor (P), anode shape factor (K) and anode dimensions. Table (1) referred to variations number of anodes and paralleling factor (P) have been used, while table (2) include the variations of anode shape (K) and anode dimensions. Equation. 8 was used to evaluate of rectifier voltage that should be employed for generate current density required to shift voltage in to cathodic polarization. Data of soil resistivity derived from table (3), which is represent Soil resistivity in the large extent of Iraq land. Energy per day of solar panel can be calculated using the following equation 9.

$$W_p = 6.93 W_L \dots\dots\dots(9)$$

Equation (10) is used to estimate battery capacity for 24 hours .

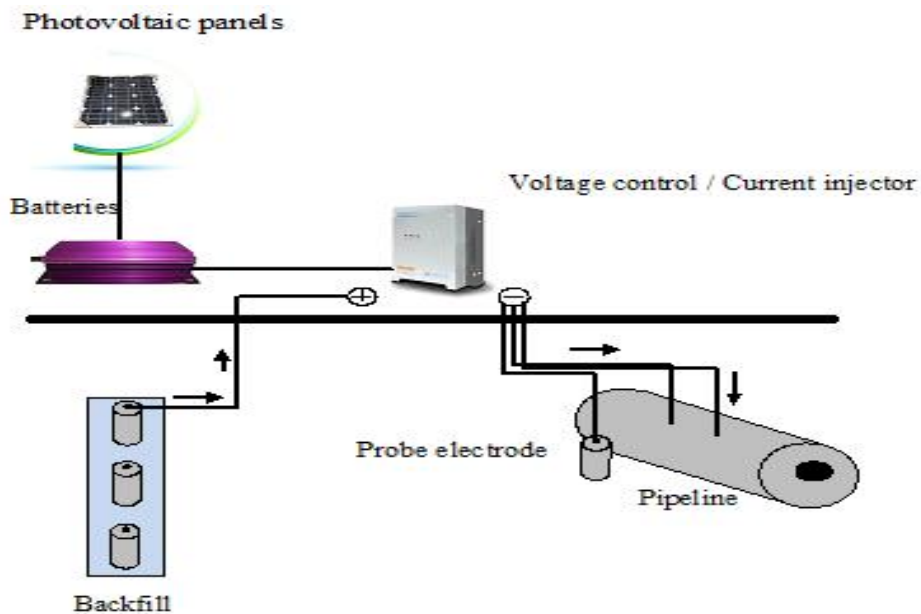
$$B_c = 35.7 W_L \dots\dots\dots(10)$$

Number of PV panels and Batteries required can be estimated by the following equations [6];

$$N_{PV} = \frac{W_p}{13} \dots \dots \dots (11)$$

$$N_b = \frac{B_c}{200} \dots \dots \dots (12)$$

Arrangement of impressed cathodic protection system using solar panels can be shown in the Fig.(2).



**Figure(2): ICCP using solar panels**

The output current from impressed cathodic protection can be designed for 15 year under the following conditions that mentioned in the table (4), which represent the main consideration for design impressed cathodic protection for 100 m oil pipeline .

**Table (4): Boundary conditions for design ICCP using solar energy**

| Structure           | Description                                                                                                                                   |                                                                                                                 |
|---------------------|-----------------------------------------------------------------------------------------------------------------------------------------------|-----------------------------------------------------------------------------------------------------------------|
| <b>Steel pipe</b>   | $d_s = 30 \text{ cm}$                                                                                                                         | $L_s = 10000 \text{ cm}$<br>$CE = 85\%$<br>$R_c = 2000 \text{ } \Omega \cdot \text{cm}$<br>$I_i = 6 \text{ mA}$ |
| <b>HSCBCI anode</b> | Case 1: $d = 12 \text{ cm}$<br>$K = 0.027$<br>$D = 0.8$<br>$L/D = 60$<br>$s = 457.2 \text{ cm}$                                               | $L = 48 \text{ cm}$                                                                                             |
|                     | Case 2: $d = 10 \text{ cm}$<br>$K = 0.0234$<br>$D = 0.83$<br>$L/D = 30$<br>$s = 457.2 \text{ cm}$                                             | $L = 24.9 \text{ cm}$                                                                                           |
|                     | Case 3: $d = 12 \text{ cm}$<br>$K = 0.0158$<br>$D = 0.86$<br>$L/D = 30, s = 457.2 \text{ cm}$                                                 | $L = 6.02 \text{ cm}$                                                                                           |
| <b>Copper Wire</b>  | $R_w = 0.15 \text{ } \Omega / 1000\text{ft}$                                                                                                  | $L_w = 2500 \text{ cm}$                                                                                         |
| <b>PV module</b>    | Model: LJ-C12/308<br>Size: $520 * 520 * 22 \text{ mm}$<br>$P_{\max} = 13 \text{ W}$<br>$V_{oc} = 13.8 \text{ V}$<br>$I_{sc} = 1.17 \text{ A}$ |                                                                                                                 |
| <b>Battery</b>      | Deep cycle 12V/ 200 Ah                                                                                                                        |                                                                                                                 |

#### 4. Results and Discussion:

The resistance of anode in the different soil and relationship it with number of HSCBCI anodes shown in the figures (3, 4 and 5). High values of anode resistance (43.86, 72.21 and 198.37 ) respectively were found with high soil resistivity (5000 .cm). Increased the anode number lead to decrease anode resistance in the various soil resistivities. The behavior of curve was changed in to straight line .

Voltage required to shift in to cathodic polarization is shown in the figures (6, 7 and 8) which are representing the relationship between required voltage and number of HSCBCI anodes in the different soils. As previously figures, the same behavior can be found, where the values of voltage decreased with increment of anodes number. Minimum values of voltage about (2.75-3.7 V) existed in the (50 and 25 .cm) soil resistivity.

Huge numerical data obtained to evaluate the number required of PV panels and batteries that provides exactly power to protect 100 m oil pipeline against corrosion in the different soil which have various electrical resistivity. In this context, figure (9) shows the relationship between number of PV panels required and number of anodes in different soil resistivity. As expected, high number of PV panels required (30) panels (13 W) for high soil resistivity (5000 .cm), and this values decrease with increasing number of anodes. While the number of PV panels decreased with falling of soil resistivities to (1000, 600, 50 and 25 .cm) as shown in figures (9, 10 and 11).

Batteries number depend mainly on the calculated required power ( total current per surface area by the voltage required). Figures (12, 13 and 14) show the relationship between number of batteries with anodes number.

Because of high soil resistivity (5000 .cm), so high number of PV panels and batteries required to adjust in to required power for cathodic protection. In contrast, number of batteries required decrease during falling of soil resistivity.

Anode dimension and anode shape factor have great effect of the values obtained of PV panels and batteries number. In general, number of PV panels and batteries increased with increasing the anode shape factor and decreasing the length of anode.

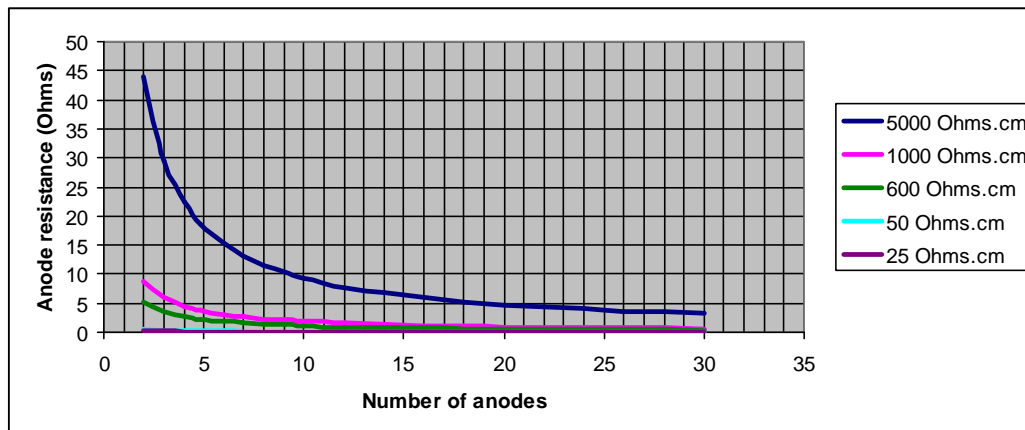


Figure (3):  $R_a$  Vs number of anodes at 1.57 ft length of anode,  $K = 0.0270$ ,  $S = 15$  ft

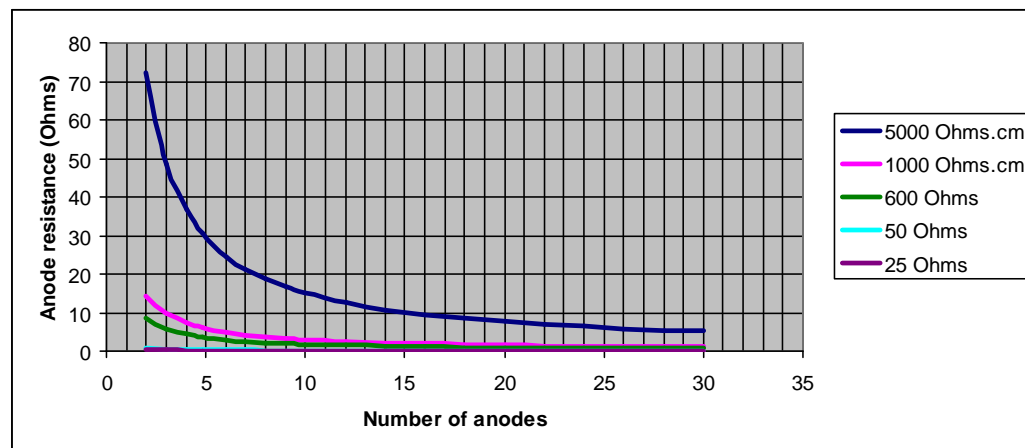


Figure (4):  $R_a$  Vs number of anodes at 0.82 ft length of anode,  $K = 0.0234$ ,  $S = 15$

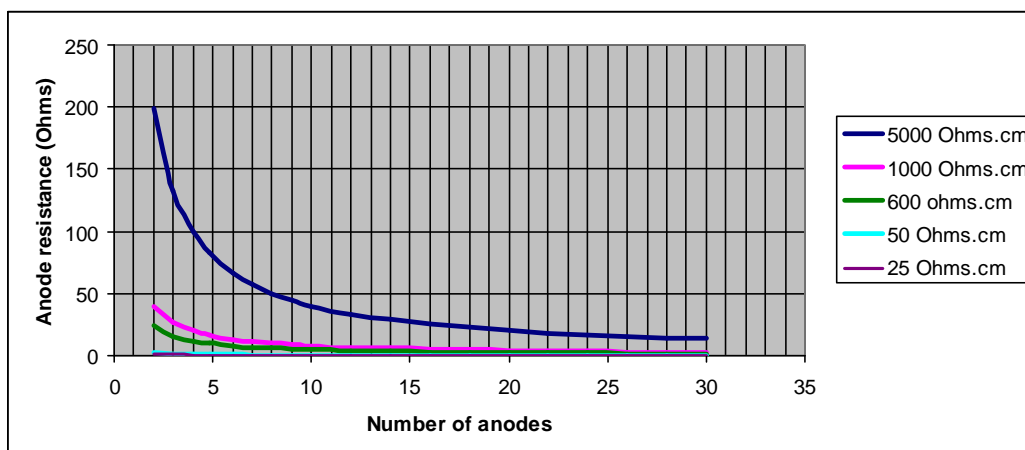


Figure (5):  $R_a$  Vs number of anodes at 0.2 ft length of anode,  $K = 0.0158$ ,  $S = 15$  ft

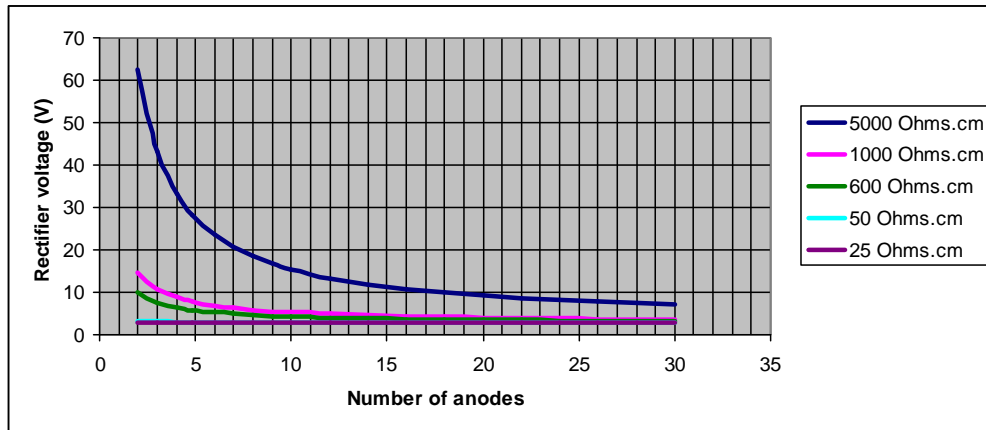


Figure (6):  $V_{req}$  VS number of anodes at 1.57 ft length of anode,  $K = 0.0270$ ,  $S = 15$  ft

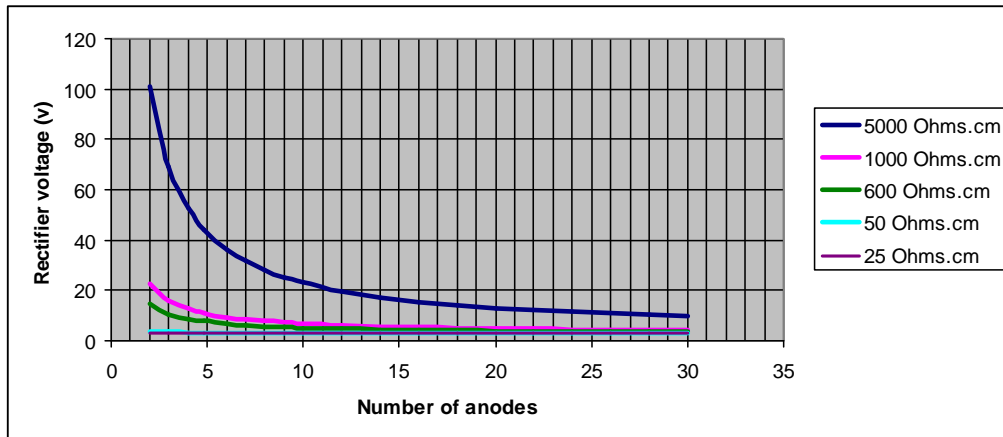


Figure (7):  $V_{req}$  VS number of anodes at 0.82 ft length of anode,  $K = 0.0234$ ,  $S = 15$  ft

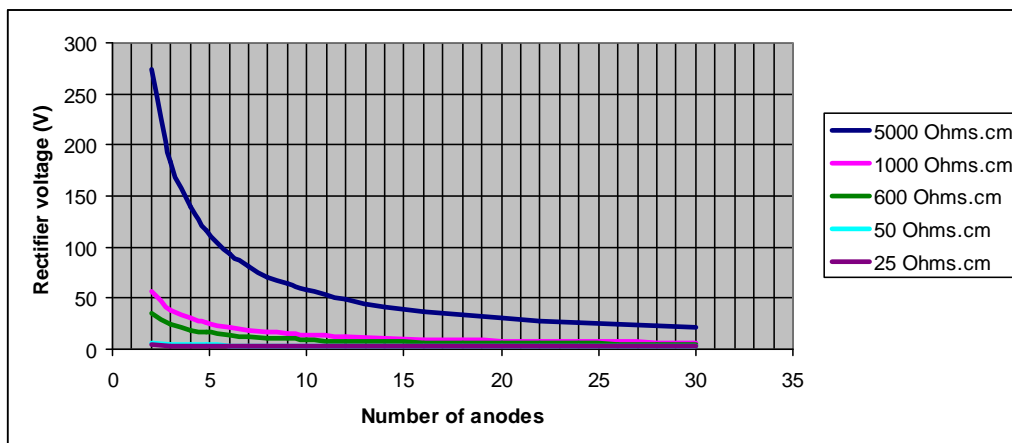


Figure (8):  $V_{req}$  VS number of anodes at 0.2 ft length of anode,  $K = 0.0158$ ,  $S = 15$  ft

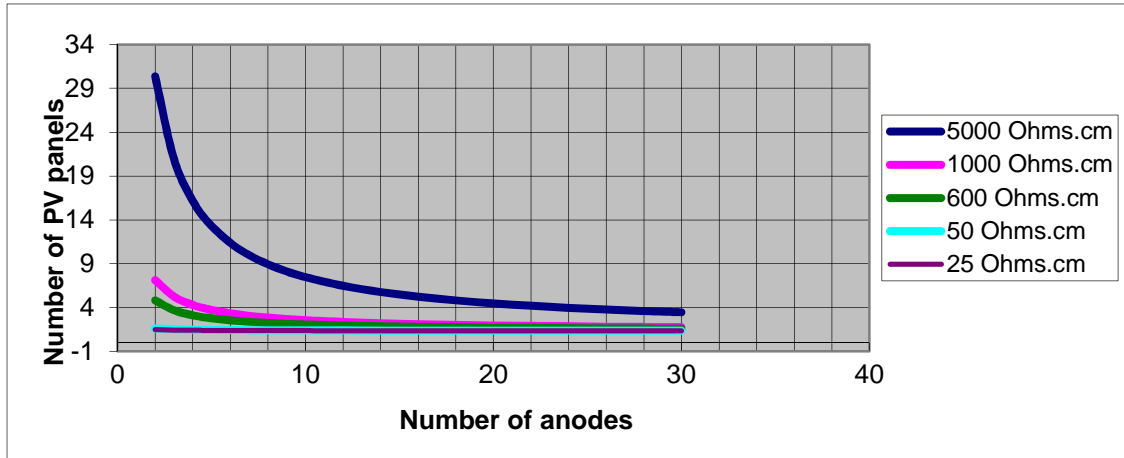


Figure (9):  $N_{pv}$  Vs number of anodes at 1.57 ft length of anode,  $K = 0.0270$ ,  $S = 15$  ft

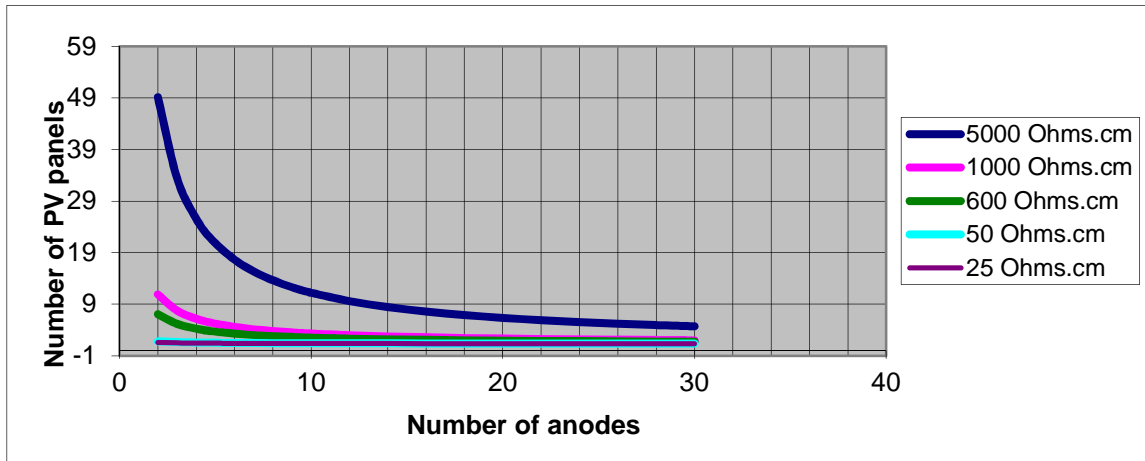


Figure (10):  $N_{pv}$  Vs number of anodes at 0.82 ft length of anode,  $K = 0.0234$ ,  $S = 15$  ft

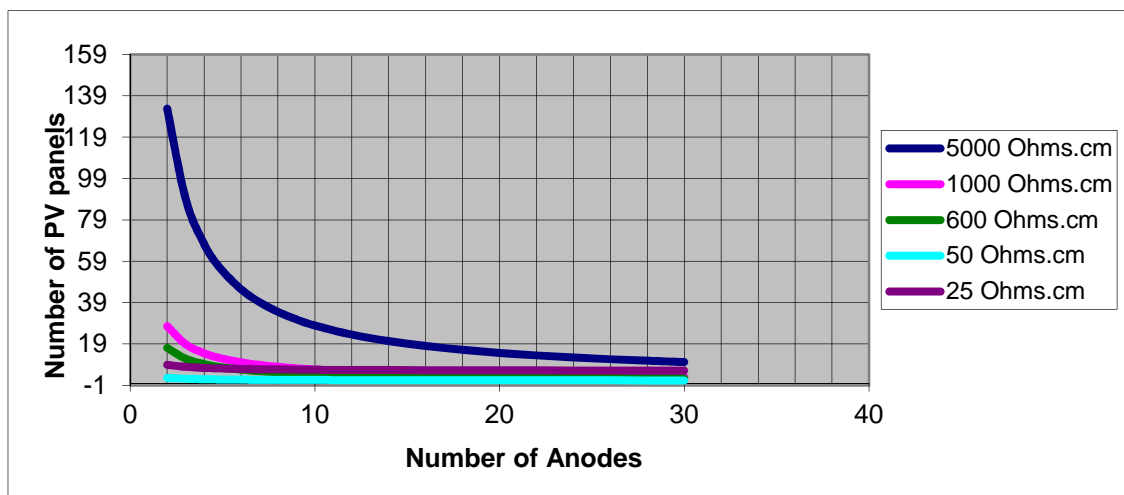


Figure (11):  $N_{pv}$  Vs number of anodes at 0.2 ft length of anode,  $K = 0.0158$ ,  $S = 15$  ft

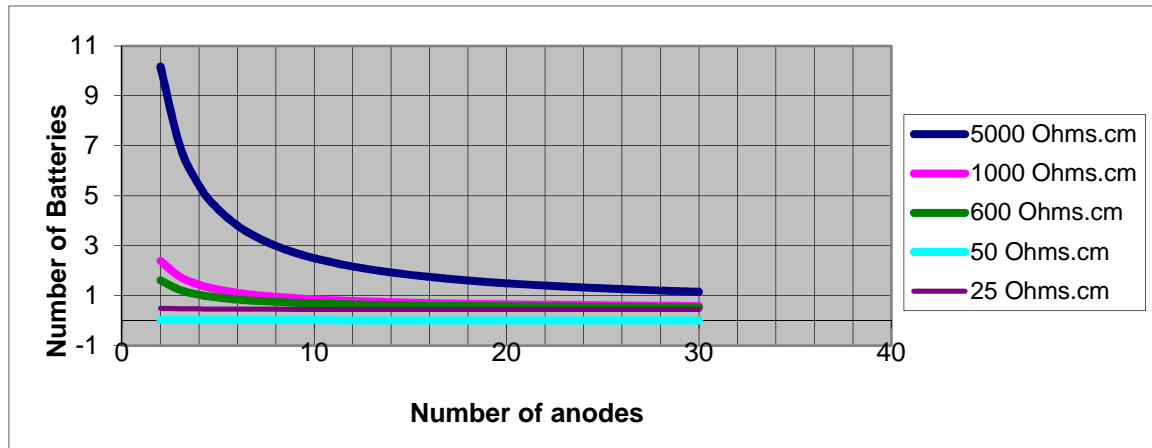


Figure (12):  $N_b$  Vs number of anodes at 1.57 ft length of anode,  $K = 0.0270$ ,  $S = 15$  ft

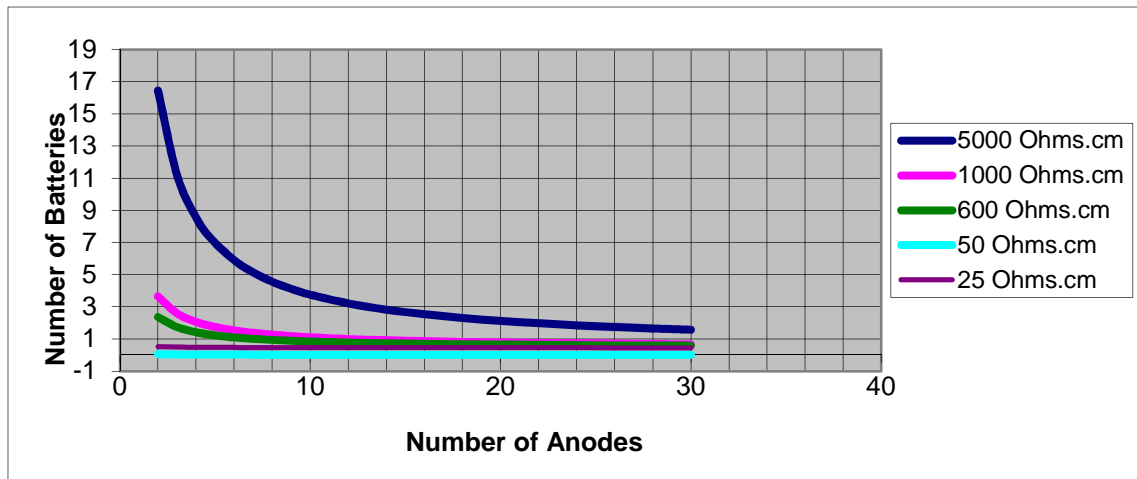


Figure (13):  $N_{pv}$  Vs number of anodes at 0.82 ft length of anode,  $K = 0.0234$ ,  $S = 15$  ft

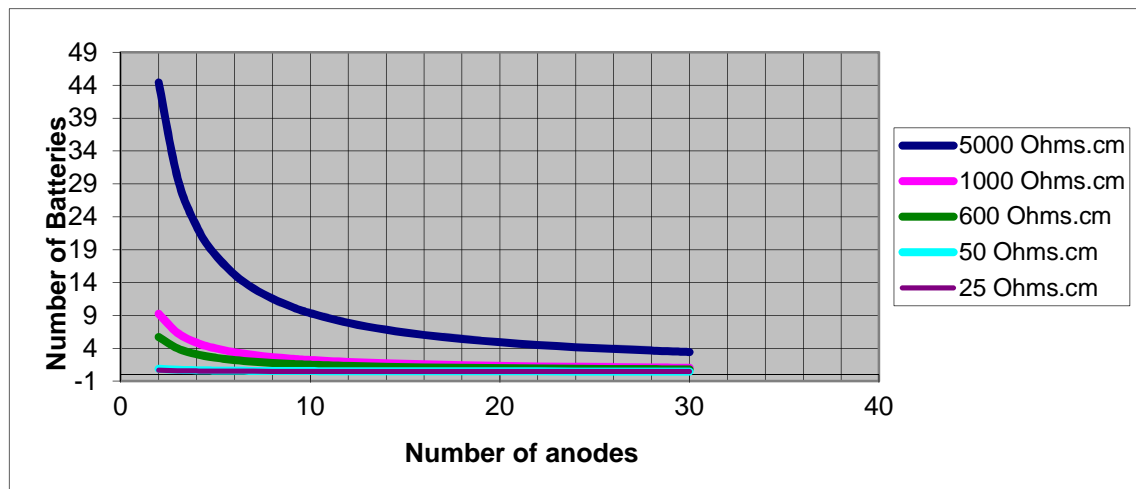


Figure (14):  $N_{pv}$  Vs number of anodes at 0.2 ft length of anode,  $K = 0.0158$ ,  $S = 15$  ft

## Conclusions:

Design of (ICCP) using solar energy based on various factors. High soil resistivity (5000 .cm) required high potential (62.59, 101.28 and 273.49 V) for two anodes with ( 48, 24.9 and 6.02 cm length of anode and (0.027, 0.0234 and 0.0158 shape factor ) respectively. However, number of PV panels and batteries required depend on the load (required power), very high number of PV panels and batteries necessary in the high soil resistivity, these values decreased with increment of anodes number, at the same time, these values increased with decrease of anode length and shape factor of anode.

## References

- [1] PEREZ N., Electrochemistry and corrosion science, Kluwer academic publisher, USA 2004.
- [2] James B, Bushman, P.E., Impressed Current Cathodic Protection System design, Bushman & Associates, Inc., Medina, Ohio USA.
- [3] Ashworth V., Principles of Cathodic Protection, Elsevier, 2010.
- [4] UNIFIED FACILITIES CRITERIA (UFC), Cathodic Protection, Iraq Virtual Science Library, USA, 2005.
- [5] Hafiz, M.H, Modeling of Pipeline Corrosion Control by Cathodic Protection, Ph.D, Thesis, Department of Production and Metallurgy Eng. University of Technology, 2006.
- [6] "How to Design Solar PV System", available at <http://www.leonics.com>.

## Study the Spectral Nonlinear Properties for of Rhodamine (6G) Dyes Doped Polymer (PMMA) Using Z-Scan Technique

Rajaa Nader<sup>(1)</sup> , Ali Hadi Al-Hamdani <sup>(2)</sup>, Rafah Abdul Hadi <sup>(1)</sup>

<sup>1</sup> University of Baghdad .College of Science for Women –physics department

<sup>2</sup> University of Technology – Laser & Optoelectronics Engineering Department

E-mail:ali- [alhamdani2003@yahoo.com](mailto:alhamdani2003@yahoo.com)

### Abstract :

The spectral properties and the nonlinear optical properties of the Rhodamine (6G) films dyes doped (PMMA) have been studied at concentration ( $1 \times 10^{-5}$  M/L) and deferent thickness (1,2 ,3, 4.5 ,5.5 mm) also spectral properties are studied by recording their (absorption and fluorescence) spectra . the nonlinear optical properties were measured by z-scan technique .The results showed that the fluorescence intensity decreases with the increasing in thickness . the quantum efficiency of the filme dye R(6G) has been calculated we found that its increased with increasing of the thickness . with increased the thickness both the nonlinear refractive index ( $n_2$ ) and nonlinear absorption conefficient ( ) were decreased.

**Key words :** Z-scan, nonlinear refractive index ( $n_2$ ) , nonlinear absorption conefficient , Rhodamind 6G , Absorpence, Fluorescence.

### دراسة الخصائص البصرية اللاخطية لصبغة الرودامين (6ج) المطعمة ببولي ميثا اكرليت باستخدام تقنية المسح الضوئي

(1) علي هادي الحمдاني <sup>(1)</sup> رفاه عبد الهادي  
<sup>(1)</sup> قسم الفيزياء- كلية العلوم للبنات -  
<sup>(2)</sup> التكنولوجيا- قسم هندسة الليزر والبصريات

:

في هذا البحث تم دراسة الخصائص الطيفية والخصائص البصرية اللاخطية لأغشية صبغة الرودامين (6ج) المطعمة ببولي ميثا اكرليت وهذه الأغشية بتركيز ( $1 \times 10^{-5}$ ) (1 2 3 4.5 ,5.5) ملليمتر . درست الخصائص الطيفية بتسجيل اطياف ( الامتصاص ، الفلورة ) ، اما الخصائص البصرية اللا خطية فتم قياسها بواسطة تقنية المسح الضوئي . أظهرت النتائج ان شدة الفلورة تقل بزيادة السمك . الكفاءة الكمية لأغشية صبغة الرودامين (6ج) وأظهرت النتائج انها تزداد بزيادة السمك . وأوضحت النتائج ان يقل بزيادة السمك .

## Introduction

The intense interest in dye laser research has been motivated by the dye lasers' ability to provide continuously tunable coherent radiation in the visible and near ultraviolet regions of spectrum [1,2]. Dyes are excellent systems for academic interest to help understand various phenomena due to their high fluorescence quantum yield and broad gain bandwidth [3]. mostly Dye molecules are used to generate tunable laser sources optical shutters, optical signal-processing devices, two-photon microscopy, upconversion lasers, optical limiting, optical data storage, and three-dimensional microfabrication[4]. Organic material can show very high nonlinear coefficients, because of the large variety of these compounds at high intensities. [5].

Z-scan technique has proved to be one of the most convenient methods for nonlinear optical measurements because of its many attractive features such as simplicity and high accuracy; widely used to study the nonlinear refraction and nonlinear absorption of materials. Z-scan technique based on the principles of spatial beam distortion, it will be shown that for many practical cases, nonlinear refraction and its sign can be obtained from a simple linear relationship between the observed transmittance changes and the induced phase distortion without the need for performing detailed calculations [6]. There are two different geometries in Z-scan technique: (i) The geometry in which a finite aperture is kept before the detector which known as a closed-aperture (CA) Z-scan, and (ii) the geometry in which the aperture is removed to focus all the transmitted light into the detector is referred to an open-aperture (OA) Z-scan [7].

W. Zhang and M. G. Kuzyk (2007) studied the effect of a thin optical medium on a high order Gaussian beams with higher angular mode number by using Z-scan technique for a dispersed-1 doped poly(methyl methacrylate) (DR1/PMMA) thin sample. The nonlinearity of DR1/PMMA is due to photo-induced trans-cis-trans isomerisation of DR1 molecules followed by reorientation in the direction perpendicular to the polarization of the incident laser beam [8].

A. Nag, and D. Goswami (2009) study the Solvent effect on two-photon absorption and fluorescence of rhodamine dyes [9].

## Materials and methods

Rhodamine 6G or named as Rhodamine590 which belongs to the Xanthenes family, Molecular formula:  $C_{28}H_{31}N_2O_3Cl$ , Molecular weight: 479.02 gm/mol. Its Appearance Pale red crystalline powder which purchased from Himedia Laboratories Pvt.Ltd . India

The polymer which used in this work is poly (methyl methacrylate) (PMMA) Chemical formula  $(C_5O_2H_8)_n$ , Molecular Weight , (84000gm/mol), refractive index : 1.49.

## Spectroscopic Measurement :

The measurement of the absorption spectra of the samples are taken by using a spectrophotometer (Metertech, SP8001,UV/VIS spectrophotometer) and the emission spectra taken by using (Spectrofluorometer –model F96PR) .

## Measuring of Quantum efficiency ( $q_{fm}$ ) :

Quantum efficiency defining as the ratio between the number of quanta emitted and the number of quanta absorbed [10] :

$$Q_{fm} = \text{number of quanta emitted} / \text{number of quanta absorbed} \dots\dots\dots(1)$$

## Z - scan System :

The experimental setup of closed and open aperture z- scan is shown in figure (1). The laser which used in the present work is a home built CW laser beam of 532 nm Nd: YAG (SHG)(COHERENT-Copass215M-50 diode-pumped laser) focused by a lens of (20)cm focal length . the optical detector type (SOLO2 R2) .

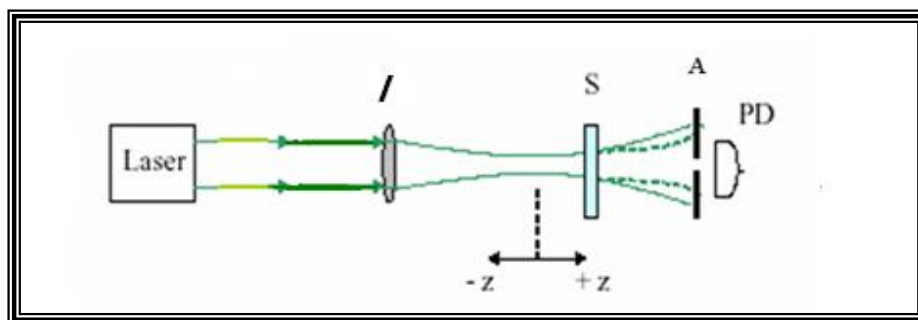


Figure. 1: The setup of z- scan system [4]

## Results and Discussion

The absorption and fluorescence spectra of R(6G) in PMMA with different thickness (1,2,3,4.5,5.5 mm) respectively are shown in Figure (2) . From these figures we can observed

that( R6G) absorption spectrum did not shifted with increase thickness . the fluorescence spectrum followed shifted peaks to shorts wavelength ( blue shift ) when increasing the thickness . Table (1) shows the wavelength of the absorption , fluorescence spectra, and the quantum efficiency of the dye doped in PMMA. From the results of calculation by using computer model ( mtlab 6.5) and equation (1) . the quantum efficiency increase with thickness increase. The nonlinear properties of PMMA doped of R6G were measured by the z-scan techniques at the difference thickness (1,2,3,4.5,5.5 mm) concentration ( $1 \times 10^{-5}$  M/L).

Figure (3) shows the closed – aperture z- scan curves by using 532(nm) laser , this figure represents the normalized transmittance as a function of sample position (z) Figures (3a,3b, 3c, 3e) shows the experimental result of dye films at difference thickness (1, 2,3,5.5 mm). A valley – peak structure in the profile indicates positive effect of refractive nonlinearity , i.e self –focusing. Figure (3d) indicates negative refractive index film of thickness (4.5mm), i.e self- defocusing ,also a peak – valley profile displayed in this figure. The measurable quantity  $T_{p-v}$  can be defined as the difference between the normalized peak and valley transmittances ,  $T_P - T_V$  . The variation of this quantity as a function of  $|\phi_o|$  is given by :

$$T_{p-v} = 0.406|\phi_o| \dots\dots\dots(2)$$

Where  $\phi_o$  : nonlinear phase shift, The on-axis phase shift is related to the nonlinear refractive index ( $n_2$ ) by :

$$\phi_o = n_2 I_0 L_{eff} k \dots\dots\dots(3)$$

Where  $I_0$  is the intensity of the laser beam at focus  $z=0$  , k is the wave number, ( $k = 2\pi / \lambda$  ),  $\lambda$  : is the wavelength of the beam.

$L_{eff}$ : the effective thickness of the sample, can be determined from the following .formula

$$L_{eff} = (1 - \exp(-\alpha_o L)) / \alpha_o \dots\dots\dots(4)$$

L : the sample thickness length ,  $\alpha_o$  : the linear absorption coefficient . [11]

Figure (4) shows the open – aperture z- scan curves by using 532(nm) laser , this figure represents the normalized transmittance as a function of sample position (z). Figures ( 4b , 4c ,4d ) indicates that the absorption coefficient at films of thickness (2,3,4.5)mm are saturable absorption (SA), this process occurred when the nonlinear absorption coefficient  $\beta < 0$ , which can be appeared when a strong light absorption between two levels causes saturation (bleaching) of the corresponding electronic transition. The two levels involved surface plasmon resonance ground and excited state [12] , Figures (4a,4e) ) indicates that the absorption coefficient at films thickness (1,5.5)mm are two -photon absorption, the two-photon absorption process occurred when the nonlinear absorption coefficient  $\beta > 0$  [13], The measured of the nonlinear absorption coefficient using by eq. :

$$T(Z) = 1 - (I_0 L_{eff} [1+z] / 2)^2 \dots\dots\dots(5)$$

We found that the nonlinear absorption coefficient ( ) decreased with an increase in thickness as in figure (5). Also the nonlinear refractive index ( $n_2$ ) decreased with an increase in thickness as in figure (6). The experimentally determined values of  $T_{p-v}$ ,  $n_2$  and are given in Table (2) .

### Conclusion :

From the results , the effective of nonlinear properties of the thickness , i.e (the nonlinear absorption and nonlinear refraction) decreased with an increasing in the thickness at constant concentration, Also the behavior of nonlinear optical absorption change from two photon absorption to saturable absorption.

### Reference

- [1] S. Stephen, and F –Jacobs; Murray Sargent , James F. Scott, and Marlon O. Scully ;Laser Application to Optics and Spectroscopy; Addison –Wesley Publishing Company ,( 1975).
- [2] J. B. Birks,;Organic Molecular Photophysics;Willy – Interscience, London,( 1970).
- [3] R. LAJA ; Study of optical properties and lasing of organic dyes under single and multiphoton excitation , 2007.
- [4] N. K. M. Naga Srinivas, S. Venugopal Rao, and D. Narayana Rao ; Saturable and reverse saturable absorption of Rhodamine B in methanol and water; School of Physics, University of Hyderabad, Hyderabad 500 046, India (2003)
- [5] I.C. Khoo, ;Liquid Crystals; 2nd ed. Wily-Interscience, Canada, (2007).
- [6] M. Sheik-Bahae, A.A. Said, Tai-Huei Wei, D. J. Hagan, and E. W. Van Stryland, ;Special 30th Anniversary Feature; (2007).
- [7] S.R. Rama Chari, H.S. Mishra, Rawat, and S.M. Oka, ;Applied Physics B; 62, (1996)
- [8] Weiya Zhang and Mark G. Kuzyk, "Physics Optics", 27 sep., (2007).
- [9] Amit Nag, Debabrata Goswami ; Solvent effect on two-photon absorption and fluorescence of rhodamine dyes; India ,(2009)
- [10] A.K.R.Darzi,;Fluorescence Life Time Measurement of Rhodamine "B"&"6G" in Different Solvent using Mode-Locked Nd:Class Laser, M.sc.Thesis Baghdad University (1977).
- [11] R.KRekha and A .Ramalingam, "Non- linear characterization and optical limiting effect of carmine dye "Centre for Laser Technology , India (2009)
- [12] M. G. Papadopoulos, A. J. Sadlej and J. Leszczynski; Nonlinear optical properties of matter, Springer, Netherlands, (2006).
- [13] W. T. Silfvast ; Laser Fundamentals", 2nd ed. Syndicate of the University of Cambridge, New York, (2004).

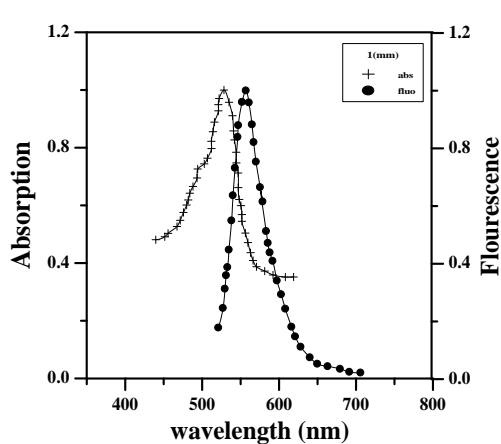


Fig.(2a)

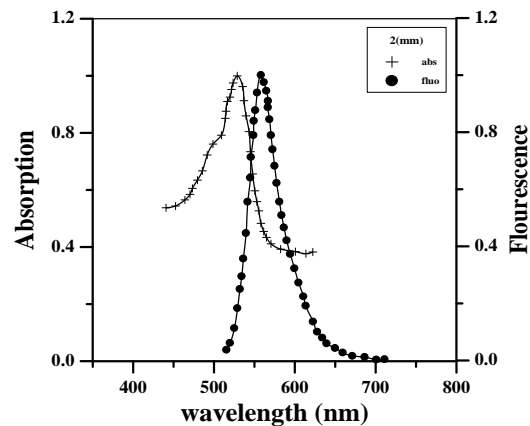


Fig.(2b)

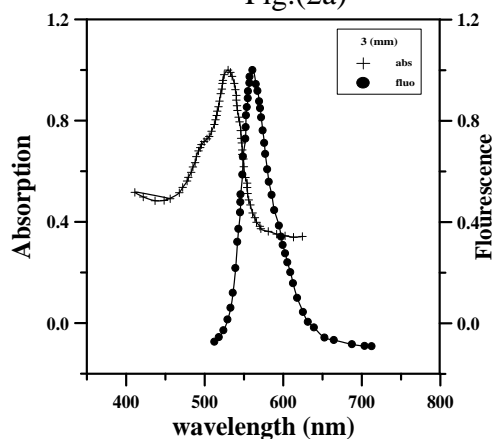


Fig.(2c)

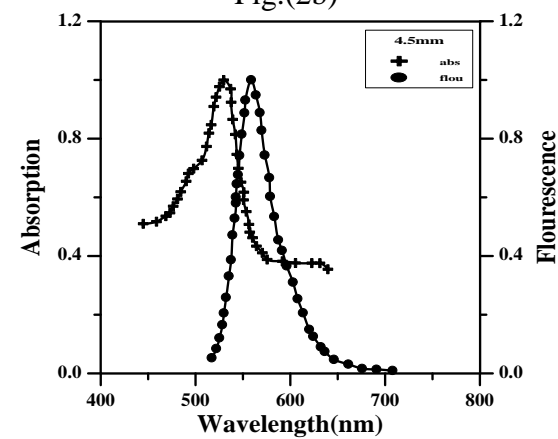
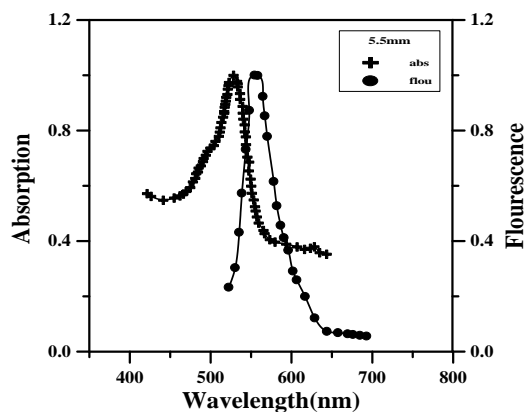
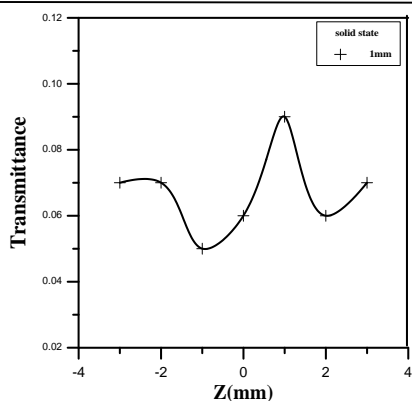


Fig.(2d)

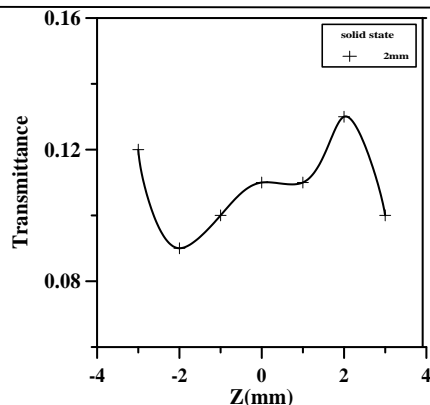


Fig(2e)

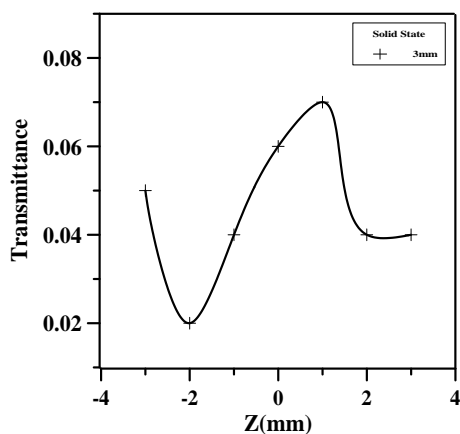
**Figure( 2) :** The absorption and Fluorescence spectrum of R6G dye doped PMMA for different thickness (1,2,3,4.5,5.5 mm) at concentration  $1 \times 10^{-5}$  M/L



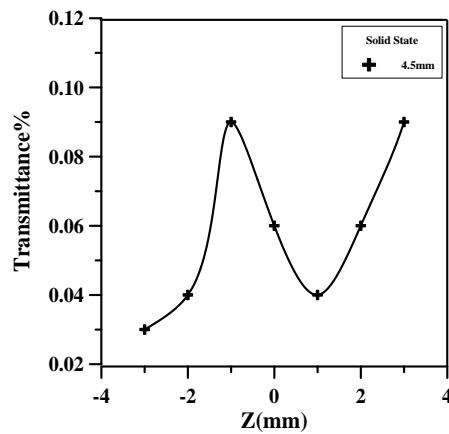
Fig(3a)



Fig(3b)



Fig(3c)



Fig(3e)

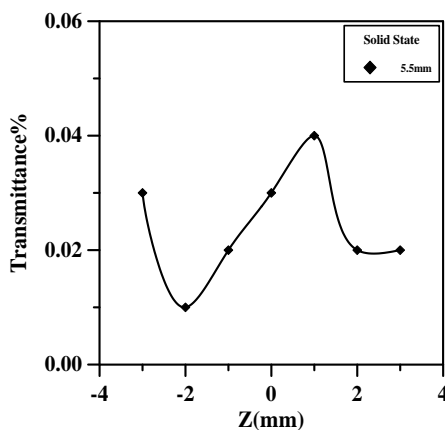
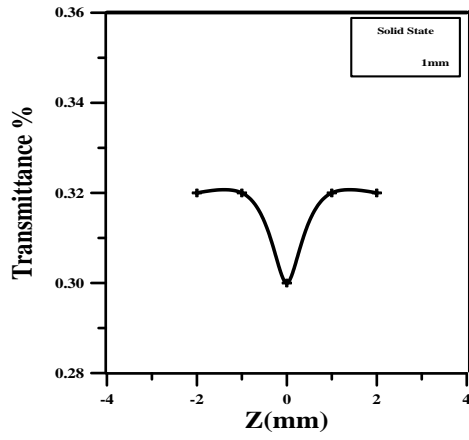
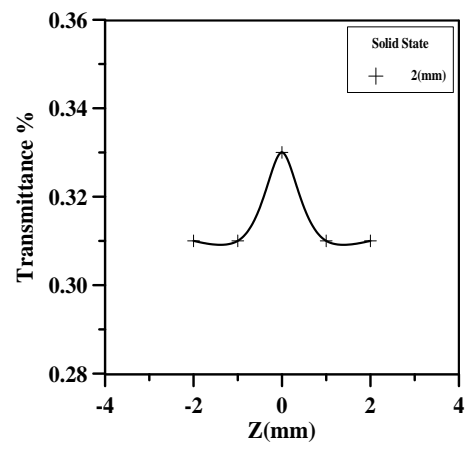


Fig (3e)

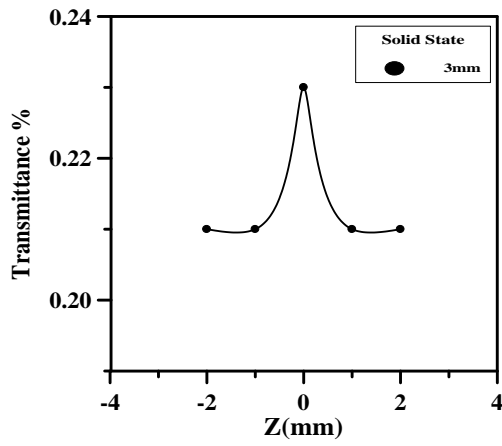
**Figure (3):** closed - aperture z- scan of R6G dye doped PMMA for different thickness (1,2,3,4.5,5.5 mm ) at concentration  $1 \times 10^{-5}$  M/L



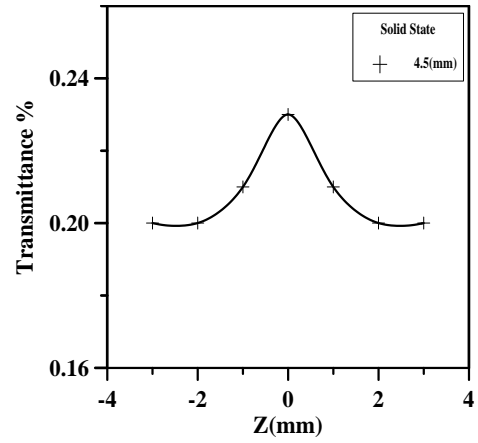
Fig(4a)



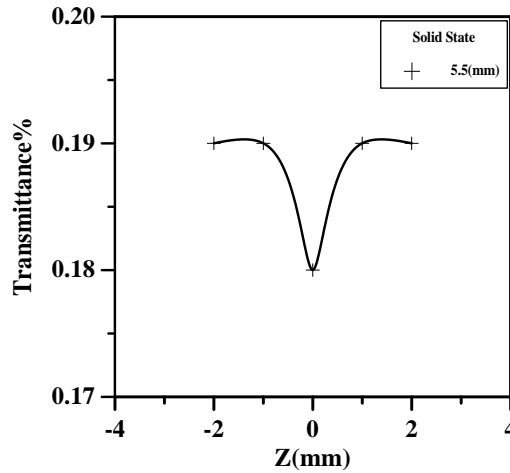
Fig(4b)



Fig(4c)



Fig(4d)



Fig(4e)

Figure (4): Open - aperture z- scan of R6G dye doped PMMA for different thickness (1,2,3,4.5,5.5 ) mm at concentration  $1 \times 10^{-5}$  M/L

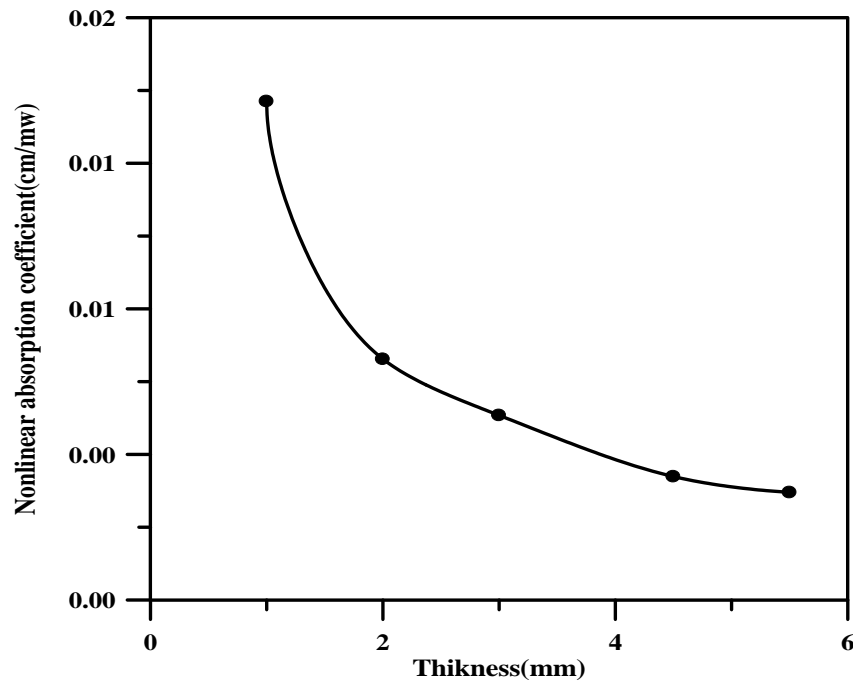


Figure (5): The relation between Nonlinear absorption and the Thickness of Rh6G dye doped PMMA

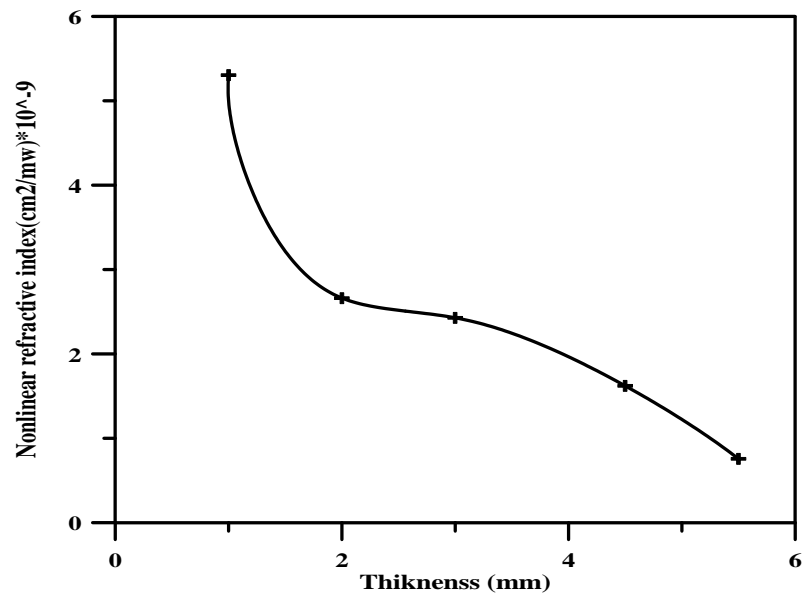


Figure (6): The relation between Nonlinear refractive and the Thickness of Rh6G dye doped PMMA

**Table(1): Absorption and Fluorescence spectra and the Quantum efficiency of R6G**

| Thickness(mm) | $\lambda$ max abs.nm | $\lambda$ max flu.nm | Quantum efficiency |
|---------------|----------------------|----------------------|--------------------|
| 1             | 528                  | 556.9                | 78%                |
| 2             | 528                  | 558.2                | 85%                |
| 3             | 528                  | 561                  | 87%                |
| 4.5           | 528                  | 558.8                | 93%                |
| 5.5           | 528                  | 554.5                | 96%                |

**Table (2): Nonlinear parameters of R6G dys doped PMMA**

| Thickness<br>(mm) | $\Delta T_{p-v}$ | $\Delta \Phi$ | $n_2$<br>cm <sup>2</sup> /mw | $\beta$<br>cm/mw |
|-------------------|------------------|---------------|------------------------------|------------------|
| 1                 | 0.04             | 0.09          | $5.305 \times 10^{-9}$       | 0.0137           |
| 2                 | 0.04             | 0.09          | $2.66 \times 10^{-9}$        | 0.0066           |
| 3                 | 0.05             | 0.123         | $2.42 \times 10^{-9}$        | 0.005            |
| 4.5               | 0.05             | 0.123         | $1.62 \times 10^{-9}$        | 0.0033           |
| 5.5               | 0.03             | 0.07          | $0.756 \times 10^{-9}$       | 0.0029           |

## تصميم وتصنيع جهاز قدرة تيار متناوب متنقل يعمل بالطاقة الشمسية Design and Manufacture a Mobile Photovoltaic AC Power Generator

ماجد حسن علي ، كريم بهلول ،  
مركز بحوث الطاقة والبيئة/ مجمع وزارة العلوم والتكنولوجيا/ الجادرية.

### Abstract

In this research we design and manufacture mobile solar power supply using solar energy (1KW) composed of solar panels (150W) connected in parallel to give (24Volts) passing through control box containing of batteries capacity (150Ah). The system provides alternating electrical energy for the required loads (220Volts – 5.4 Amp).

### الخلاصة

إن طلب الطاقة يزداد حول العالم بالنظر للتوسع في كل مناحي الحياة وهذا بدوره يؤدي إلى زيادة في تلوث البيئة كون توليد الكهرباء بالطرق التقليدية يحتاج إلى حرق الوقود ، لذلك فإن الطاقة الشمسية هي أحد الحلول الجيدة في الكهرباء النظيفة وخاصة للمناطق النائية البعيدة عن مصادر الطاقة. في هذا البحث تم تصميم وتصنيع مولد كهرباء متنقل يعمل بالطاقة الشمسية Off- Grid (1 كيلو واط) مؤلف من تسعة ألواح شمسية قدرة الواحدة (150 ) ية مقدارها (24 فولت) ويمر تيار الألواح المستمر عبر منظم شحن إلى البطاريات الثمانية (أربعة مجموعات كل مجموعة بطاريتين على التوالي وعلى التوازي فيما بينها ، كل بطارية سعتها 150 أمبير/ ) لتعطي سعة مقدارها (600 أمبير/ ساعة) (3)

نتاج طاقة كهربائية متناوبة لتشغيل الحمل المطلوب (220 4.5 أمبير). على عربة بعجلتين بطريقة فنية بحيث يمكن رزم الألواح وإنزالها داخل العربة عند عدم الاستخدام أو النقل من ثم نشرها بالزاوية المطلوبة حسب الموقع أثناء التشغيل. يمكن سحب هذا المولد الشمسي المتنقل بواسطة سيارة أو جرار زراعي إلى أي مكان لغرض الاستخدام ، وبينت الدراسة أن مقدار تيار الألواح الشمسية يزداد بزيادة الإشعاع الشمسي لغرض الإسراع بعملية شحن البطاريات واستخدام المنظومة لإنتاج الطاقة الكهربائية.

### المقدمة

نظومات الألواح الشمسية الفوتوفولتائية فوائدها عديدة أهمها أنها صامتة وغير ملوثة للبيئة حيث لاتصدر عنها الغازات الدفئة كما هو الحال عند استخدام الوقود التقليدي الكهرباء ، كما أن هذه المنظومات الشمسية يقلل من الاعتماد على الكهرباء التقليدية ويوفر بعض المبالغ لقائمة الكهرباء لمدة أكثر (25 سنة) الذي هو عمر الألواح الشمسية ويعتبر هذا استثمار " طويل الأمد " [1]. هناك نوعان من منظومات الكهرباء بالطاقة الشمسية أحدهما يربط مع الشبكة الكهربائية ويسمى (Grid Type) ولا يحتوي على بطاريات والأخرى مستقلة وبعيدة عن الشبكة الوطنية (off – grid) والتي تم استخدامها في البحث وتحتوي على بطاريات للخرن وأن المكونات الأساسية للنوعين (2,1) [2].

إنتاج الكهرباء العاملة بالطاقة الشمسية ذات البطاريات مناسبة البعيدة عن مصادر الطاقة التقليدية لأن عملية مد أ الكهرباء مكلفة للغاية ، كما أنه يمكن استخدام هذه المنظومات لتشغيل الأجهزة

العاملة بالتيار المستمر والمتناوب . إن البطاريات المستخدمة في المنظومات الشمسية تشبه إلى حد ما بطاريات السيارات ق بسيط أنها مصممة لسحب تيار عالي الشدة (Deep Discharge) ويفضل أن تكون محكمة ولا تحتاج إلى صيانة أو إضافة المحلول إليها أثناء الاستخدام [3] هناك بعض العوامل المؤثرة على مقدار القدرة الخارجة من المنظومة الشمسية الفوتوفولتائية وهي:

- 1- القياسية (STC) (Standard Test Conditions)  
حيث أن مواصفات اللوح الشمسي تعتمد على طريقة التصنيع هل هو من بلورات السليكون الأحادية أم الثنائية ومواصفات  $1000 / 25$  .
- 2- : تقل طاقة اللوح الشمسي المتولدة مع زيادة درجة الحرارة حيث تختلف خواص السليكون 75 ويفقد اللوح الشمسي 15% من طاقته عند هذه الدرجة.
- 3- الغبار : إن مقدار الغبار المتراكم على الألواح الشمسية يؤدي إلى ضياع 25% في حالة عدم تنظيفه لمدة شهر.
- 4- ضياعات التيار جرا .
- 5- ضياعات التحويل من التيار المستمر (DC) إلى التيار المتناوب (AC).  
الكهرباء الشمسية المتنقلة عبارة عن صديقة للبيئة وتعمل في الأيام المشمسة والغائمة وأثناء الليل وتعتمد ساعات تشغيلها على قدرة الألواح الشمسية ومقدار الإشعاع الشمسي في المنطقة المراد نصب هذه المولدة فيها [4]. في هذا البحث تم تصميم وتصنيع عربة قدرة متنقلة يمكن سحبها وقطرها بأي واسطة نقل ومجهزة بكل مستلزمات انتاج الكهرباء من الطاقة الشمسية (ألواح، بطاريات، منظومات سيطرة وغيرها) وتسمى أيضا (Mobile Stand Alone System).

#### الجانب النظري

إن المكونات الأساسية لمنظومة تجهيز الكهرباء من الطاقة الشمسية هي :

- 1- الألواح الشمسية (PV modules).
  - 2- (Solar charge controller).
  - 3- (Inverter).
  - 4- البطاريات (Batteries).
  - 5- (Load).
- (1) أدناه يمكن الشمسية المطلوبة :

$$W_p = \frac{1.3 \times h \times W_L}{I} \dots\dots\dots (1)^{[5]}$$

حيث أن :

$W_p$ : الألواح الشمسية (واط)

$h$ : عدد ساعات التشغيل

$W_L$ : ( )

$I$ : معدل الإشعاع الشمسي اليومي لمدينة = 5.5 Kw / m<sup>2</sup> / day

ولغرض حساب قدرة العاكس فإنه لا يمكن أن تكون القدرة الداخلة إليه (قدرة الألواح) أقل من قدرة الحمل، أي أن قدرة العاكس يجب أن تكون أكبر بمقدار 25% - 30% من قدرة الحمل أما بالنسبة لتشغيل المحركات والضواغط فإن العاكس يجب أن يكون ذا قدرة أكبر بثلاث مرات من قدرة الحمل لأن لهذه الأجهزة تيار بدء عالي (High Starting Current) بالإضافة إلى ذلك يجب أن يكون العاكس يعمل بنفس فولتية النظام [5]

سعة البطاريات فيكون (2) هي:

$$B_c = \frac{1.3 \times h \times W_L}{0.85 \times 0.6 \times V_n} \times d_{aut} \dots \dots \dots (2)^{[5]}$$

حيث أن :

B<sub>c</sub>: Battery capacity  
W<sub>L</sub>: total watt  
h: Hours per day  
0.85: for battery loss  
0.6: depth of discharge  
V<sub>n</sub>: nominal battery voltage  
d<sub>aut</sub>: autonomy (عدد الايام الغائمة)

(3) هي الأساس :

ايجاد

$$SC = I_{sh} \times 1.3 \dots \dots \dots (3)^{[5]}$$

حيث أن :

SC: solar charge controller rating  
I<sub>sh</sub>: total short circuit current of PV array

ومن خلال المعادلات أعلاه تم حساب قدرات أجزاء المنظومة حيث كانت قدرة الألواح (1350 )  
1500 و سعة البطاريات 600 أمبير/ ساعة ومنظم شحن ذو تيار 40 أمبير.

#### الجانب العملي

تم تصنيع عربة معدنية بالأبعاد (2.5 × 1.5 × 0.5) م مجهزة بعجلات قياس 14  
وسيلة نقل إلى المكان المناسب والمطلوب . يت هيكل للألواح الشمسية على العربة بميل زوايا مختلفة مع الأفق حسب  
الموقع المراد نصب المنظومة فيه كما ويمكن رزم هذا الهيكل مع الألواح بطريقة إنزلاقية  
وضع مكونات المنظومة (بطاريات، عاكس، منظم شحن) في حوض العربة أسفل الألواح الشمسية . كان عدد الألواح  
الشمسية 9 150 واط لتعطي قدرة إجمالية 1350 ريات 600 أمبير/ ساعة. ولغرض  
تشغيل المنظومة تم استخدام حمل كهربائي مكون من (هيتز كهربائي بقدرة 500 واط، مبردة هواء بقدرة 250  
ومحرك كهربائي بقدرة 200 واط) واستمر التشغيل لمدة (6 ساعات) متواصلة دون أي مشكلة حيث أثبتت المنظومة  
كفاءتها خلال العملية، وأن ال (3) يبين المخطط الكهربائي للمنظومة أما الشكل رقم (4) فيوضح صورة للمنظومة  
أثناء النصب والتشغيل.

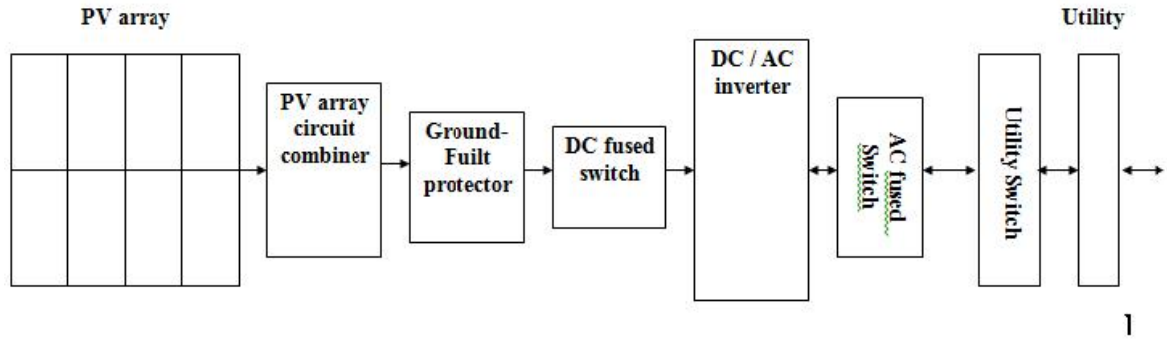
#### النتائج والمناقشة

(3,2,1) تم حساب قدرة الألواح الشمسية وسعة البطاريات وقدرات العاكس ومنظم الشحن  
وتم اختبار المنظومة في تشغيله (950 ) (6 ) متواصلة حيث أخذت البيانات باستخدام جهاز  
قياس الإشعاع الشمسي المباشر (solar meter) ومقارنته بقراءة التيار الخارج من الألواح الشمسية حيث بينت  
(5) زيادة التيار مع زيادة الإشعاع الشمسي وهذا نتيجة زيادة حركة الالكترونات خلال السليكي  
وبالتالي زيادة التيار. إن عملية استخدام منظومات انتاج الكهرباء الشمسية المتنقلة مناسبة في أوقات الكوارث والأحداث  
المأساوية البعيدة عن مراكز المدن والتي تفنقر للطاقة الكهربائية وتمتاز بما يلي :  
1- الوثوقية العالية.

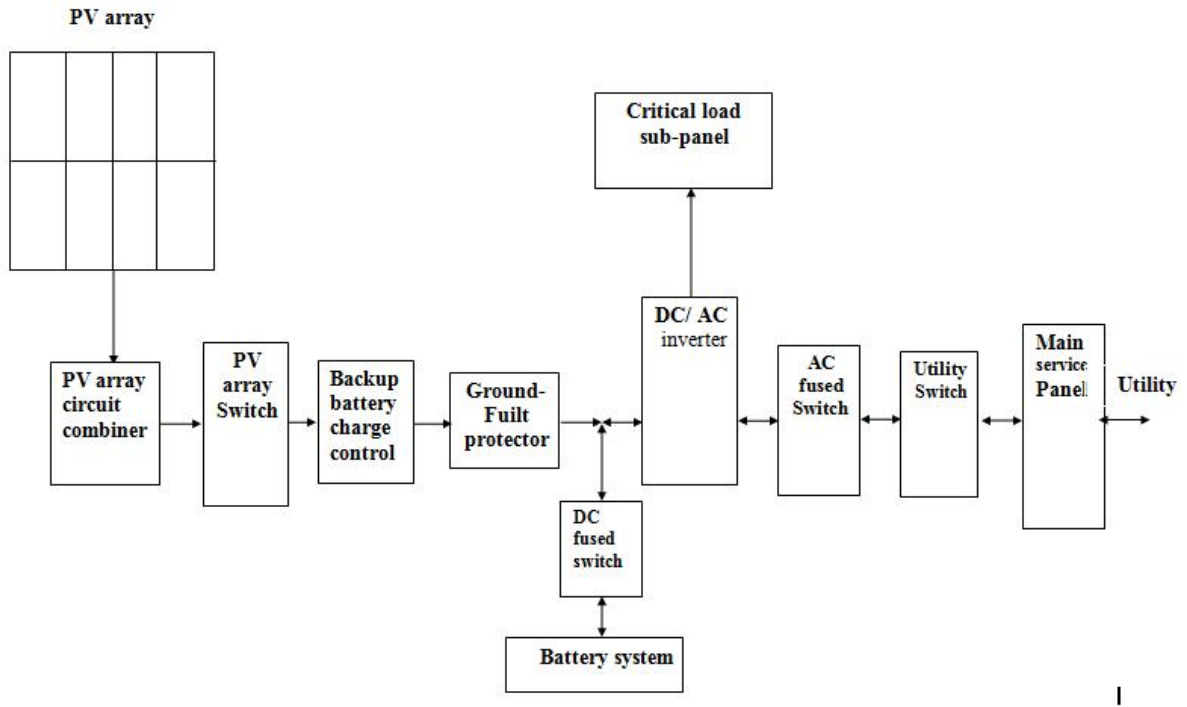
- 2 .
- 3- سهولة النقل والنصب والتشغيل.
- 4- مجدية اقتصاديا حيث لو تمت المقارنة بين المنظومة الشمسية قيد البحث والتي قدرتها (1 كيلو واط) وسعرها (18000) أخرى تعمل بالبنزين وقدرتها (1 كيلواط) ولنفس فترة التشغيل (10 ات يوميا) لكليهما :
- 1- سعر المولدة العاملة بالبنزين = 100 .
- 2- 1080 دولار بنزين سنويا".
- 3- 129,6 دولار زيت محرك سنويا".
- عمر هذه المنظومة سنة واحدة وعليه يصبح سعرها السنوي (1309,6) 25 سنة الذي هو عمر الشمسية يصبح السعر (32740) دولار في حين ان سعر المنظومة الشمسية هو (18000) .

## Reference

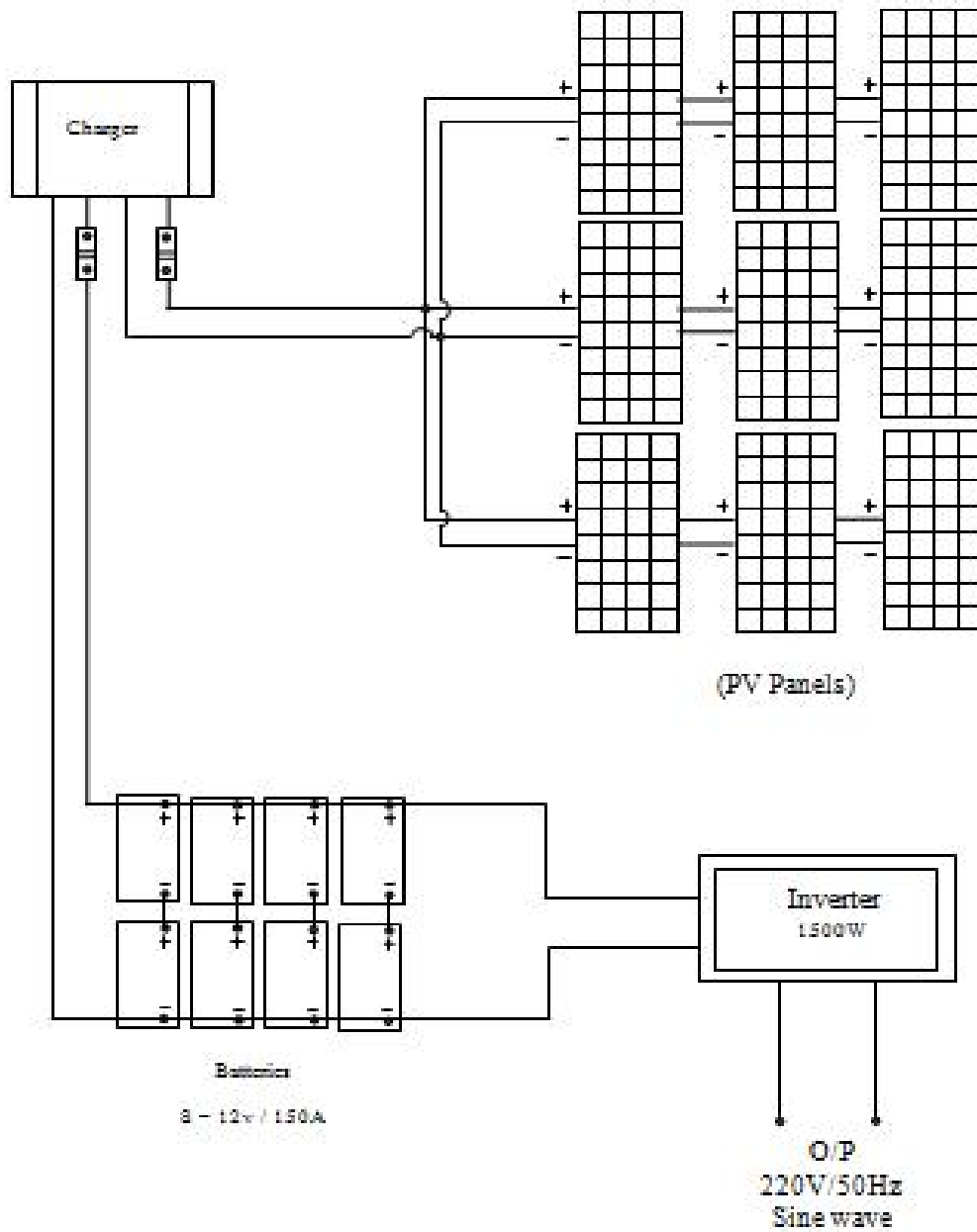
- 1- [http:// www.altenergymag.com](http://www.altenergymag.com) "Mobile Solar Power" 2009 .
- 2- "A Guide to Photovoltaic (PV) System Design and Installation" California Energy Commission, Version 1.0 Jun 14, 2001 .
- 3- "PV Systems with Battery Storage" U. S. Department of Energy, 2006 .
- 4- [http:// www.energy.ca.gov](http://www.energy.ca.gov) "Factors Affecting PV Output", 2001.
- 5- [http:// www.leonics.com](http://www.leonics.com) "How to Design Solar PV System" 2010 .



شكل رقم (1) المبدأ الأساسي لعمل منظومة توليد كهرباء شمسية مرتبطة مع الشبكة [2]



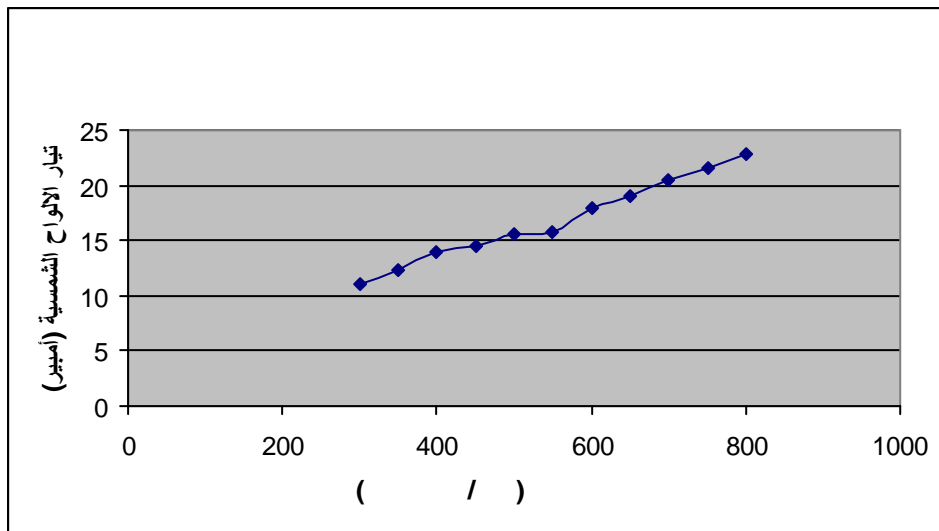
شكل رقم (2) المبدأ الأساسي لعمل منظومة توليد كهرباء شمسية مستقلة [2]



شكل رقم (3) المخطط الكهربائي لمجهز القدرة 1000 واط



(4) جهاز القدرة المتنقل



(5) العلاقة بين تيار الألواح الشمسية والاشعاع

## تأثير السمك والمعاملة الحرارية على التوصيلية المستمرة لأغشية CdO المحضرة بطريقة التريز بالبلازما

د. فلاح إبراهيم مصطفى      أمل ساجت صبر      سهام زهراوي عباس  
ر.فيزياويين أقدم      ر.فيزياويين      ر.فيزياويين

### الخلاصة:

تم تحضير أغشية رقيقة أكسيد الكاديوم على أرضيات من الزجاج نوع بايركس بطريقة التريز بالبلازما بمساعدة المجال المغناطيسي. تم دراسة تغير التوصيلية المستمرة كدالة لدرجة الحرارة ضمن المدى الحراري (303-493)K. أظهرت النتائج وجود طاقتي تنشيط  $E_{a1}(eV) = 0.075$  و  $E_{a2}(eV) = 0.78$  لأغشية رقيقة لسمك 100nm مع وجود طاقتي تنشيط  $E_{a1}(eV) = 0.07$  و  $E_{a2}(eV) = 0.75$  لأغشية رقيقة لسمك 300nm عند مدى من درجات الحرارة (303-373)K و (373-483)K على التوالي. وأجريت المعاملة الحرارية على الغشاء المحضرة بسمك 300nm لمدة ساعة واحدة بدرجة حرارة  $220^{\circ}C$  وتغيرت طاقتي التنشيط إلى  $E_{a1}(eV) = 0.073$  ,  $E_{a2}(eV) = 0.8$  . حيث أن زيادة السمك تؤدي إلى زيادة التوصيلية المستمرة ونقصان طاقة التنشيط ، بينما أدت المعاملة الحرارية إلى نقصان التوصيلية المستمرة وبالتالي زيادة طاقة التنشيط.

## Effect of thickness and heat treatment on (D.C) conductivity of CdO thin films prepared by Plasma sputtering method

F.I.Mustafa      A.S.Sabr      S.Z.Abbas

### ABSTRACT :

In this study we prepare CdO films by using plasma sputtering method on substrate from glass type Pyrex , we used system of dipole sputtering with magnetic field. we studied the electrical properties include determining of (D.C.)conductivity in the temperature rang (R.T-493)K the result showed two mechanisms with two value of activation energy . the influence of increasing in thickness due increasing in (d.c.)conductivity . It also includes study of effect of heat treatment at (  $220^{\circ}C$  ) on (d.c.) conductivity.

### المقدمة:

الخواص الكهربائية للأغشية الرقيقة تعتمد بصورة رئيسية على طريقة تحضير الأغشية وتؤدي الى معرفة ميكانيكية التوصيل الكهربائي ونوع حاملات الشحنة وتركيزها . إن مادة أكسيد الكاديوم ذات لون بني غامق، يمتلك تركيب بلوري مكعب متمركز الاوجه (FCC) [1]، ويمتلك أكسيد الكاديوم فجوة طاقة ممنوعة (2.5eV). يتم تحضير أكسيد الكاديوم بصورة مباشرة من التسخين الشديد لعنصر الكاديوم (Cd) في الهواء، وهو شبه موصل من النوع السالب (n-type) وهي تمتلك توصيلية عالية. يستخدم أكسيد الكاديوم في المنظومات الشمسية لزيادة كفاءتها بسبب

امتلاكه معامل امتصاص عالي ويستخدم كمواد شفافة حرارية لشبابيك المركبات والطائرات وكمرايا عاكسة حرارياً للنوافذ الزجاجية [ 2].

#### طريقة العمل :

تم تحضير أغشية اوكسيد الكاديوم على أرضيات من الزجاج نوع بايركس بطريقة التريز بالبلازما في وسط فراغي 0.1mbar وبسمك ( 300,100)nm وتم قياس سمك الاغشية بالطريقة الوزنية باستخدام العلاقة التالية :

$$d = \frac{\Delta w}{\rho \cdot A}$$

حيث:

d: يمثل السمك

$\Delta w$  الفرق في الوزن ،

... الكثافة ،

A هي مساحة القاعدة

#### الجزء النظري:

يتم حساب التوصيلية المستمرة ( $\sigma_{dc}$ ) من دراسة تغير المقاومة للأغشية مع درجة الحرارة باستخدام العلاقة الآتية [ 3] :

$$\sigma_{dc} = 1/\rho_0 = L/R_e b t \dots\dots\dots(1)$$

$R_e$ : مقاومة الغشاء ، b: عرض القطب (cm) ، L: المسافة بين قطبي الألمنيوم (cm)

t: سمك الغشاء (cm)

وباستخدام العلاقة التالي يتم حساب طاقة التنشيط:

$$\ln \sigma = \ln \sigma_0 \exp^{(-E_a / K_B T)} \dots\dots(2)$$

ومن خلال رسم العلاقة البيانية بين ( $\ln \sigma_{dc}$ ) ومقلوب درجة الحرارة ( $1000/T$ ) ومن ميل المنحني الميل يتم حساب طاقة التنشيط ( $E_a$ ) بالنسبة لشبه موصل من نوع (n-type) من خلال ضرب الميل بثابت بولتزمان ( $K_B$ ) بوحدات (eV) وحسب المعادلة التالية :-

$$E_a = 0.08625 * \text{slope} \dots\dots\dots(3)$$

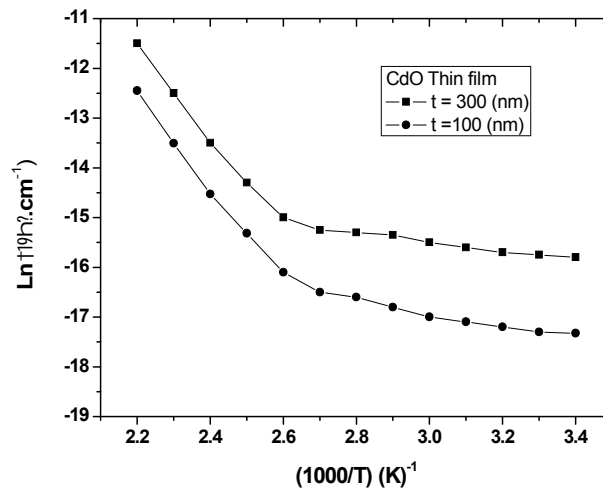
حيث الثابت (0.08625) ناتج من تحويل ثابت بولتزمان إلى وحدات (eV/K) [ 4] .

## النتائج والمناقشة:

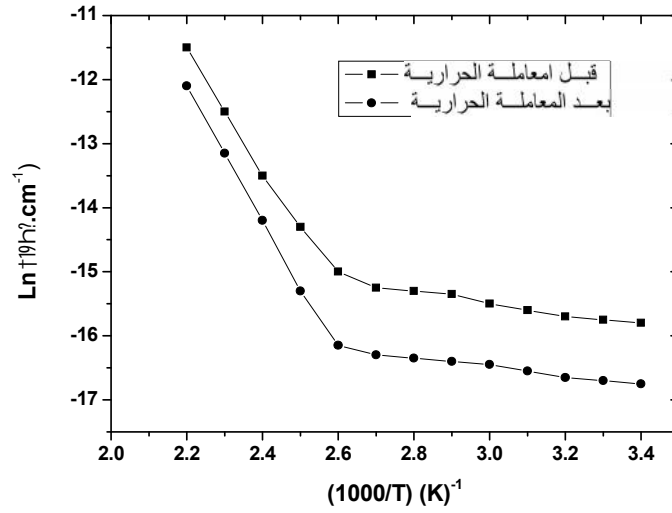
تم حساب التوصيلية الكهربائية المستمرة ( $\sigma_{dc}$ ) لأغشية CdO مع تغير درجة الحرارة ضمن المدى الحراري من درجة حرارة الغرفة (R.T) ولغاية 493K وعند الضغط الجوي من خلال تغير المقاومة ( $\rho_0$ ) لجميع الأغشية مع تغير درجة الحرارة باستخدام المعادلة رقم (1)، وتم حساب طاقة التنشيط (Ea)eV من المعادلة (2)، نلاحظ ان قيم التوصيلية تزداد مع زيادة درجة الحرارة [ 5 ] إذ إن زيادة درجة الحرارة تؤدي الى زيادة وتنشيط عدد الكثرونات وينتج من ذلك زيادة التوصيلية . حيث ان جميع الاغشية تمتلك توصيلية عالية بحدود  $(9 \times 10^{-2})(\Omega.cm)^{-1}$  . وكذلك التوصيلية تزداد بزيادة السمك ، وعند ملاحظة الشكل (1) يتبين وجود طاقتي تنشيط للمركب (CdO) وان طاقة التنشيط الأولى تقع ضمن المدى الحراري 303-373K أما طاقة التنشيط الثانية فتقع ضمن المدى الحراري 373-483K كما موضح في الجدول (1) حيث أنها تقل بزيادة السمك . يوضح الشكل (2) تأثير المعاملة الحرارية على التوصيلية المستمرة لأغشية CdO ويتضح من خلاله ان التوصيلية المستمرة للأغشية المحضرة بسمك 300 nm تقل بعد المعاملة بدرجة حرارة 220 °C وهذا ينفق مع المصدر [ 5 ] حيث تؤدي المعاملة الحرارية الى تقليل العشوائية وبالتالي تقليل عرض ذبول المستويات الموضعية وبذلك تزداد قيمة فجوة الطاقة الواقعة بين حزمتي التكافؤ والتوصيل وبذلك تزداد طاقة التنشيط [ 6 ] كما موضح في جدول رقم (1).

جدول(1) يوضح قيم طاقات التنشيط لجميع الأغشية

| Thickness (nm)            | E <sub>a1</sub> (eV) | E <sub>a2</sub> (eV) |
|---------------------------|----------------------|----------------------|
| 100                       | 0.075                | 0.78                 |
| 300                       | 0.07                 | 0.75                 |
| 300 بعد المعاملة الحرارية | 0.073                | 0.8                  |



الشكل (1) يمثل تغير التوصيلية مع مقلوب الحرارة للأغشية المحضرة باختلاف السمك



الشكل (2) يمثل تغير التوصيلية مع مقلوب الحرارة لغشاء CdO المحضر بسمك (300)nm

## References

- 1- M M .Islam ,M R. Islam. (2008), " Optical and Electrical Characteristics of CdO thin films deposited by Spray Paralysis Method ", *Journal of Bangladesh Academy* 32
- 2- R S.Rusu,G.I.Rusu,(2005) " On the electrical and optical characteristics of CdO thin films " *J. Optoelectronics and Advanced Materials*, 7 pp.823-828
- 3- V.Ganesan, S.Potadar.(2009) "Structural, optical and electrical of copper selenide film[1] s ". *32:pp.37-42Indian Academy of Sciences*
- 4- A.R.Bulu, V.S.Nagarethinam .(2012 ) " Effect of the solution concentration On the structural and electrical properties of CdO " *J Of Electron Device* 12 pp.739-749
- 5- Amrut S Lanje, (2011) "Luminescence and electrical resistivity properties of CdO nanopartical " *Indian JOurnal of Pure &Applied Physics* 49 pp. 234-238
- 6- R. S Rusu<sub>a</sub>, G.I.Rusu<sub>b</sub> .(2005) "The electrical and optical characteristics of CdO thin films" *J of Optoelectronics and Advance Materials* 7 PP.1511-1516

## The comparison analysis of fixed pitch angle wind turbine with that of a double output induction generator

Dr. Abbass Z. Salman  
Assistance. Prof

Roshen T. Ahmed  
Assistance lecturer

Energy and renewable energies technology center  
University of technology

### Abstract

The characteristic matching of a fixed pitch angle wind turbine with that of a double output induction generator (DOIG) has been analytically study in this research.

The stator and rotor electrical output of a generator has been fed into an infinite bus-bar via a static power conditioner in the rotor circuit. A direct current mathematical model is used to represent the steady state performance of the generator power conditioner network system.

Performance curves, power coefficient versus tip speed ratio,  $C_p(\ )$  is represented by a polynomial function. A nonlinear equation for the wind speed is result from the mechanical power balance which can be equated from the relation between input and output of the (DOIG) at any given generator speed.

By using Newton-Raphson method the nonlinear equation obtained can be solved numerically.

### المقارنة التحليلية لاداء المستقر لتوربينه هوائية مع الاداء المستقر للمولد الحثي ذو المخرجين

#### الخلاصة

يقدم البحث طريقة رياضية لتحليل الاداء والموائمة بين التوربين الهوائي ذو الزاوية الثابتة مع المولد الحثي ذو المخرجين.

الطاقة الكهربائية للجزء الثابت والدوار في المولد تغذي الشبكة العامة عن طريق مكيف قدرة استاتيكي في دائرة العضو الدوار.

استخدمت منظومة رياضية لتمثيل مواصفات حالة استقرار المولد.

وقد تم وصف الاداء المستقر للنظام الكهربائي (المولد ومكيف القدرة الاستاتيكي والشبكة) عن طريق دائرة تيار مستمر مكافئة ووصف الاداء المستقر للتوربين عن طريق نموذج رياضي.

وبمساواة القدرة الميكانيكية الخارجة من التوربين بالقدرة الميكانيكية الداخلة للمولد امكن الحصول على نموذج رياضي موحد يصف الاداء المستقر للنظام الكهربائي والتوربين عندما يتم ربطهما معا وبحل هذا النموذج امكن ايجاد مدى تشغيل التوربين ومتطلباتها.

## Introduction

As a result of the growing demand for use of electricity in all areas of life, the use of electric power generators by wind also increased as a result of easy access to the wind and is not affected by the environment of any that clean source of energy also it is inexhaustible. One of these schemes is the DOIG connected to an infinite bus-bar using a static power conditioner in the rotor circuit. The DOIG used in this research is a slip-ring rotor induction machine. The wind energy will drive the machine and connected from stator and rotor terminals to the network. By this type of connection the stator voltage and frequency will be fixed with that of the network. The speed dependent rotor voltage and frequency are interfaced with the network using a static power conditioner which consists of a diode bridge and an inverter bridge thyristor connected together through a d.c. link of high inductance. Equivalent induction machine circuit has been used to computing steady state performance characteristics[1]. This work presents an analytical approach matching the steady state characteristics of a fixed pitch angle wind turbine with that of a DOIG connected to an infinite bus-bar via a diode bridge d.c. link reactor-inverter bridge-thyristor scheme in the rotor circuit. From wind speed and wind turbine generator speed a mathematical modelling is derived which give us the steady state performance of the wind turbine. Equating the wind turbine output mechanical power to the electrical system input power at any generator speed results in a nonlinear equation for the unknown wind speed which can be solved using Newton-Raphson method [2].

## System modeling

The system used was shown in figure (1), optimum power transfer from the generator to the network can be obtained by adjusting the firing delay angle ( ) according to the generator speed. The steady state behavior of the electrical system modeling is based on the following assumptions:

- d. c. direct current is assumed to be completely smoothed and ripple free.
- Neglecting all valves forward voltage drop and commutation in the inverter.
- Commutation effect in the diode bridge on the rectified voltage is considered.
- Ignoring all mechanical losses, iron and magnetic saturation.
- Fundamental components are considered.

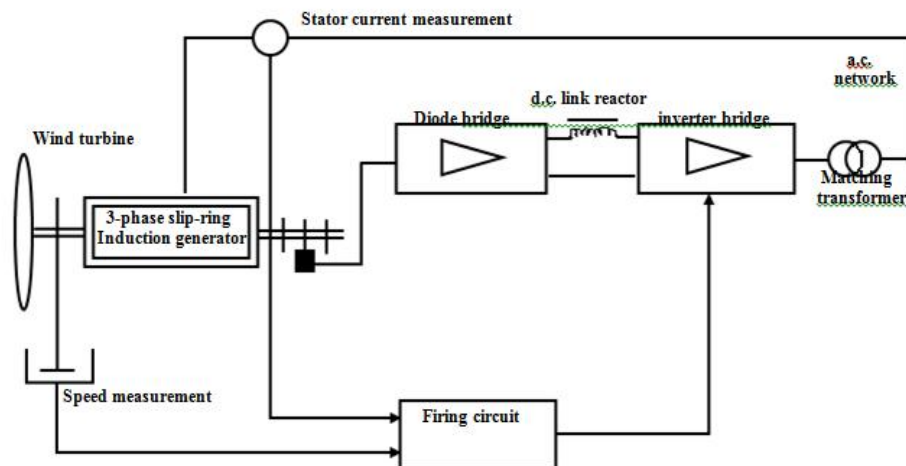


Fig 1. Single line diagram of the system

It is convenient to represent each phase of the induction generator by its so called transformer type equivalent, by applying Thevenin theorem to the conventional induction machine equivalent circuit shown in figure 2(a, b) by ignoring the ratio of the stator winding resistance  $R_s$  to its self reactance ( $X_s + X_m$ ) one can get the Thevenin voltage  $\underline{V}_{th}$  and impedance  $Z_{th}$  as:

$$\underline{V}_{th} = \dagger_1 (1-b) \underline{V}_s'' = \dagger_1 \underline{V}_s'' - b \dagger_1 \underline{V}_s'' \quad \dots\dots\dots(1)$$

And

$$Z_{th} = R_{th} + jX_{th} = (1-b) \dagger_s^2 R_s'' + j(1-b) \dagger_1 X_{\dagger s}''$$

$$Z_{th} = \dagger_1^2 R_s'' - b \dagger_1^2 R_s'' + j \dagger_1 X_{\dagger s}'' - j b \dagger_1 X_{\dagger s}'' \quad \dots\dots\dots(2)$$

$\dagger_1$  and  $b$  are given by:

$$\dagger_1 = \frac{X_m''}{X_{\dagger s}'' + X_m''} = \frac{1}{1 + \dagger_s} \quad \dots\dots\dots(3)$$

And

$$b = \frac{n_s}{n} \quad \dots\dots\dots(4)$$

Where

|                       |                                   |
|-----------------------|-----------------------------------|
| $\underline{V}_s''$   | Stator referred phase voltage     |
| $I_s''$               | Stator referred phase current     |
| $\underline{V}_r$     | Rotor phase voltage               |
| $I_r$                 | Rotor phase current               |
| $R_s''$               | Stator referred resistance        |
| $\underline{V}_{th}$  | Thevenin voltage                  |
| $\dagger_s$           | Stator leakage coefficient        |
| $X_{\dagger s}''$     | Stator referred leakage reactance |
| $X_m''$               | Referred magnetizing reactance    |
| $R_r$                 | Rotor resistance                  |
| $X_{\dagger r}$       | Rotor leakage reactance           |
| $n_s$                 | Synchronous speed                 |
| $n$                   | Rotor speed                       |
| $R_{th}$ and $X_{th}$ | Thevenin resistance and reactance |

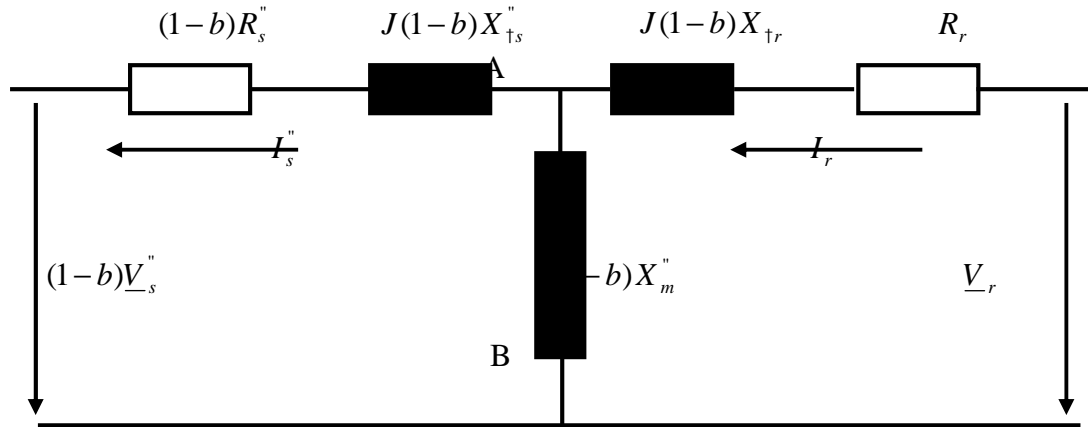


Fig 2(a) Induction machine equivalent circuit conventional

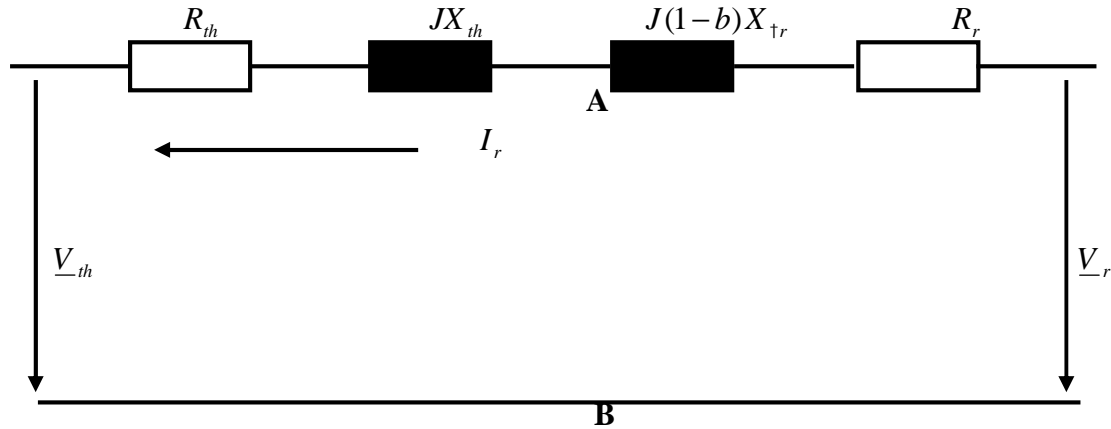


Fig 2(b) Induction machine equivalent circuit transformer type

Since there is a diode bridge in the generator rotor circuit, the fundamental rotor current lags behind the rotor voltage by the commutation angle caused by the generator leakage reactance[3].

The average d.c. voltage  $V_{dr}$  at the diode d.c. terminal is given by:

$$V_{dr} = V_{drs} + \Delta V_x + \Delta V_r \dots\dots\dots(5)$$

This equation describes the steady state behavior of the network-generator-diode bridge system. Figure (3a) represents Equation (5) as follows:

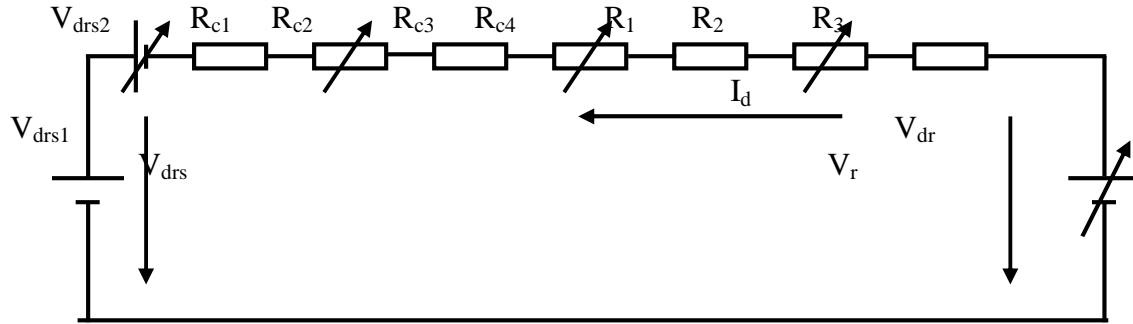


Fig 3a System d.c. equivalent circuit according to the voltage equation

1) The two opposite d.c. voltage source represent the  $V_{drs}$

$$V_{drs} = V_{drs1} - V_{drs2} \dots\dots\dots(6)$$

$V_{drs1}$  and  $V_{drs2}$  can be represent by a.c. voltage  $V_{th}$  as:

$$V_{drs1} = \frac{3}{f} \sqrt{6} \dagger_1 V_s'' \dots\dots\dots(7)$$

And  $V_{drs2} = bV_{drs1} \dots\dots\dots(8)$

2) The voltage drop across two resistance  $R_{c1}$ ,  $R_{c3}$  and the two variable resistance (Proportional)  $R_{c2}$  and  $R_{c4}$  is the average d.c. voltage change ( $\Delta V_x$ )

$$\Delta V_x = (R_{c1} + R_{c2} + R_{c3} + R_{c4}) I_d \dots\dots\dots(9)$$

Where:

$$R_{c1} = \frac{3}{f} \dagger_1 X_{ts}'' \dots\dots\dots(10)$$

$$R_{c2} = -bR_{c1} \dots\dots\dots(11)$$

$$R_{c3} = \frac{3}{f} X_{tr} \dots\dots\dots(12)$$

$$R_{c4} = -bR_{c2} \dots\dots\dots(13)$$

3) Finally the voltage drop across  $R_1$ ,  $R_3$  and variable resistance  $R_2$  represent the voltage change term  $\Delta V_r$

$$\Delta V_r = (R_1 + R_2 + R_3) I_d \dots\dots\dots(14)$$

Where:

$$R_1 = 2 \dagger_1^2 R_s'' \dots\dots\dots(15)$$

$$R_2 = -bR_t \dots\dots\dots(16)$$

$$R_3 = 2R_r \dots\dots\dots(17)$$

According to the assumption used

$$I_d = \sqrt{\frac{3}{2}} I_r \quad \dots\dots\dots(18)$$

### Control strategy and performance equations

The control strategy is to keep the d.c. voltage across the  $V_{di}$  at zero by kept the inverter delay angle at  $90^\circ$  during the speed range of the generator stator current is less than rated value. By this strategy the generators work most efficiently, Any d.c. voltage  $V_{di}$  except zero value will shift the power speed curve to a lower power at same speed.

By applying this control strategy to figure 3a we get:

$$V_{dr} = 0 = V_{drs1} - V_{drs2} + (R_{c1} + R_{c2} + R_{c3} + R_{c4} + R_1 + R_2 + R_3) I_d \quad \dots(19)$$

Solving equation 19 we get

$$I_d = \frac{V_{drs1} - V_{drs2}}{R_{c1} + R_{c2} + R_{c3} + R_{c4} + R_1 + R_2 + R_3} \quad \dots\dots\dots(20)$$

Finally the range of the stator current and the direct current reach there rated values  $I_{sn}$  and  $I_{dn}$  respectively. By substitution of  $I_d = I_{dn}$  in equation 19 and using equations 8,11,13 and 16 one get:

$$b_n = 1 + \frac{R_3 I_{dn}}{V_{drs1} + (R_{c1} + R_{c2} + R_1) I_{dn}} \quad \dots\dots\dots(21)$$

Where  $b_n$  = Generator rated speed

The other control strategy is to control the inverter d.c. voltage  $V_{di}$  by adjusting the inverter firing delay angle to keep this current constant all over the speed range above the rated speed as soon as the direct current attains its rated value  $I_{dn}$  at the rated speed  $b_n$ .

The power relation obtained from figure 3a is:

$$P_1 = V_{drs1} \times I_d \quad \dots\dots\dots(22)$$

$P_1$  = Electrical power

$$P_{cs} = (R_1 + R_{c1}) I_d^2 \quad \dots\dots\dots(23)$$

$P_{cs}$  = Stator copper losses

$$P_2 = -V_{di} \times I_d = -V_{dr} \times I_d \quad \dots\dots\dots(24)$$

$P_2$  = Electrical power absorbed by the network

$$P_{cr} = (R_3 + R_{c3}) I_d^3 \quad \dots\dots\dots(25)$$

$P_{cr}$  = Rotor copper losses

$$P_{out} = P_1 + P_2 \quad \dots\dots\dots(26)$$

$P_{out}$  = Total electrical power

By combining equations 6, 11, 13, 16, 19 and 22 to equation 25 the DOIG internal mechanical power is:

$$\begin{aligned} P_{mg} &= P_{mgs} + P_{mgr} = (P_1 + P_{cs}) + (P_2 + P_{cr}) \\ &= b[V_{drs1} + (R_1 + R_{c1} + R_{c3})I_d]I_d \quad \dots\dots\dots(27) \\ &= [V_{drs2} - (R_2 + R_{c2} + R_{c4})I_d]I_d \end{aligned}$$

The above equation show that the input mechanical power  $P_{mg}$  is divided between the stator  $P_{mgs}$  and rotor  $P_{mgr}$ , so that the d.c. equivalent circuit shown in figure 3a must be rearranged to the form in figure 3b[4].

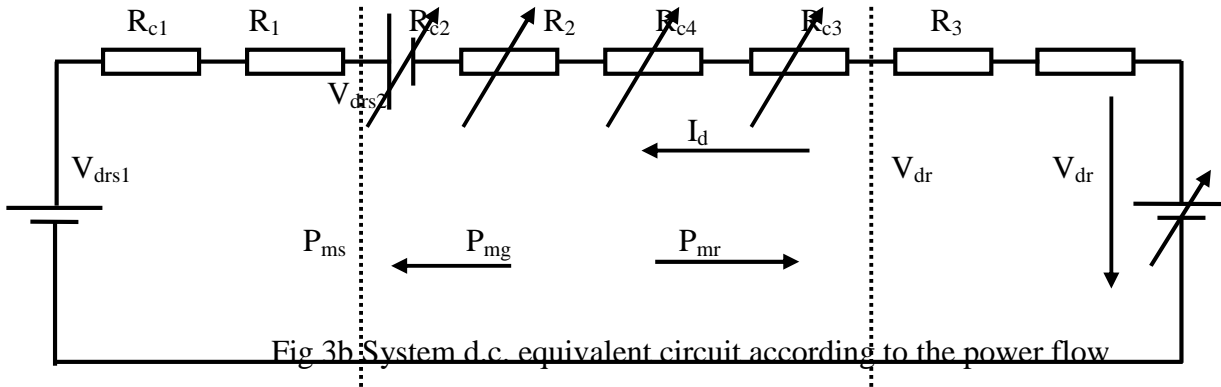


Fig 3b: System d.c. equivalent circuit according to the power flow

## Wind turbine

The equation below show the power available in wind.

$$P_{mt} = C_p \left( \frac{1}{2} \rho A V_w^3 \right) \quad \dots\dots\dots(28)$$

Where:

$\rho$  = Air density

A = Air swept by the turbine

$C_p$  = Turbine performance coefficient

$V_w$  = Wind speed

$C_p$  depends on number of blades and blade pitch angle.

$$\lambda = \frac{V_T}{V_w} = \frac{2fRn}{V_w} = \frac{2fRn_s \frac{n}{n_s}}{V_w} = \frac{b}{V_w} \quad \dots\dots\dots(29)$$

Where  $\lambda$  is the wind speed ratio, from equation 29 one can notice that the tip speed  $V_T$  is proportional to the rotor speed  $n$  and the radius of the turbine blade  $R$ .

Figure 4 shows the relation between wind turbine performance coefficient and the tip wind speed ratio for a two blade wind turbine having a fixed pitch angle of  $1^\circ$ .

$$C_p = -0.007 \lambda^2 + 0.135 \lambda - 0.128 \quad \dots\dots\dots(30)$$

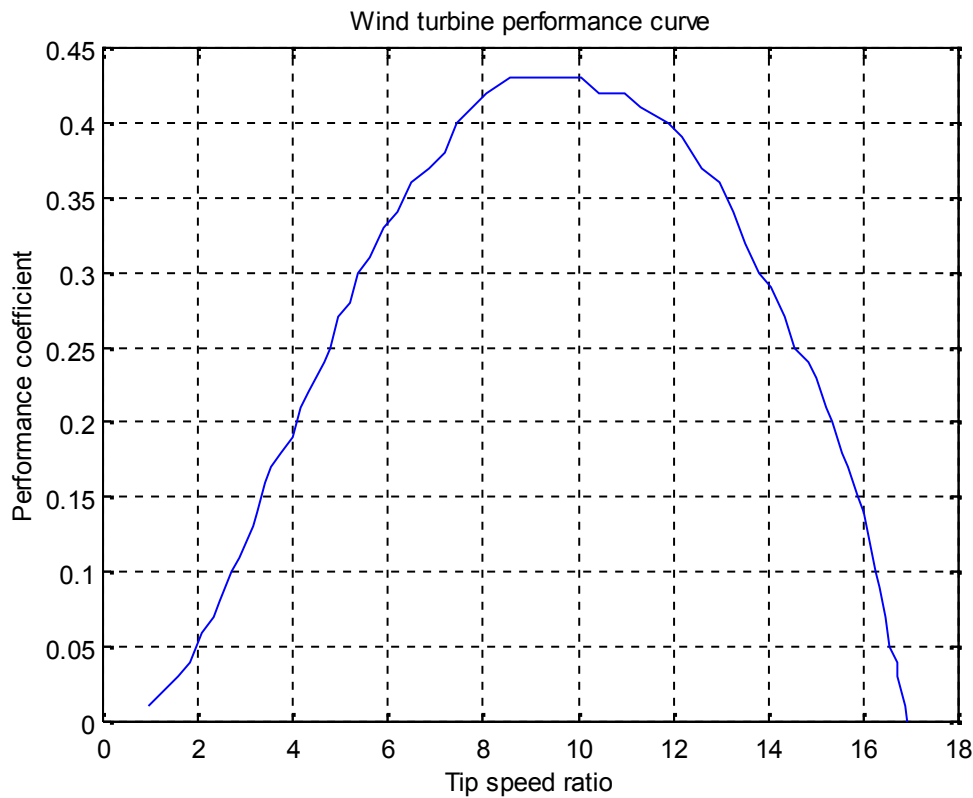


Fig 4 Wind turbine performance

Introducing equation 29 into 30 we get

$$C_p = -0.007 \left( \frac{b}{V_w} \right)^2 + 0.135 \left( \frac{b}{V_w} \right) - 0.218 \quad \dots\dots\dots(31)$$

Grouping equations 28 to 31 the turbine output mechanical power is:

$$P_{mt} = K.C_p \left( \frac{b}{V_w} \right)^3 = K \left( -0.007b^2V_w + 0.135bV_w^2 - 0.218V_w^3 \right) \quad \dots\dots\dots(32)$$

With the constant

$$K = \frac{1}{2} \rho A (2fRn_s)^3 \quad \dots\dots\dots(33)$$

The assumption used for evaluation the constant K is that the turbine is designed to get optimum values of  $C_{pmax}$  at rated wind speed  $V_{wn}$  corresponding to generator rated speed  $b_n$ . At this speed the generator input mechanical power is its rated value  $P_{mgn}$ .

From figure 4 we get

$$C_{pmax} = 0.43 \text{ at } \lambda_n = 9.35 \quad \dots\dots\dots(34)$$

By substitution  $P_{mt} = P_{mgn}$ ,  $C_p = C_{pmax}$ ,  $b = b_n$  and  $\omega = \omega_n$  in equation 32 we get

$$K = \frac{P_{mgn}}{C_{pmax}} \left( \frac{\omega_n}{b_n} \right)^3 \dots\dots\dots(35)$$

And finally the turbine mechanical output power is

$$P_{mt} = \frac{P_{mgn}}{C_{pmax}} \left( \frac{\omega_n}{b_n} \right)^3 \left( -0.007b^2V_w + 0.135bV_w^2 - 0.128V_w^3 \right) \dots\dots\dots(36)$$

### Algorithm of matching

The generator is connected to the power system at the cut-in wind speed  $V_{wci}$  where the power is enough to overcome the mechanical and no load losses. The speed is double the generator synchronous speed  $b=2$ , the generator input mechanical power  $P_{mg}$  is computed at any value of generator speed by solving the electrical system mathematical model during the speed range within which the given speed lies. The determined generator input mechanical power  $P_{mg}$  as determined in equation 27 is balanced by the turbine output mechanical power  $P_{mt}$  equation 36, and its result in a nonlinear relation as shown in equation below.

$$P_{mg} = \frac{P_{mgn}}{C_{pmax}} \left( \frac{\omega_n}{b_n} \right)^3 \left( -0.007b^2V_w + 0.135V_w^2 - 0.128V_w^3 \right) \dots\dots\dots(37)$$

The above equation is solved using Newton-Raphson method. Having obtained  $V_w$  the corresponding required performance parameters  $\omega$  and  $C_p$  of the turbine are determined using equations 29 and 30.

### Results and discussion

A 3-phase, 4-pole, 50-Hz, Y-connected, slip-ring induction machine is used in the digital simulation of the mathematical module in figure 1. The parameters of the machine are:  $R_s=2.22$ ,  $R_r=3.83$ ,  $X_s=X_r=5$ ,  $X_m=74$  the stator to rotor transformation ratio is 2:1 and the base values are:

Base current  $I_b = I_{dn} = 10.8$  A, base voltage  $V_b = V_{tn} = 220$  V,  $V_i = 110$  V, and the base power  $P_b = P_{tn} = 2.48$  KW.

These data are used for different generator speed and the results obtained are shown in Figure 5 there are two operating range:

- 1) the range from cut-in wind speed  $V_{wci}$  to the rated wind speed  $V_{wn}$ :  
the tip wind speed ratio reduce from its maximum to its rated value  $\omega_n$  while the performance coefficient increase from zero to its maximum  $C_{pmax}$ , figure 5b show the operating range of the wind turbine, from the intersection point of  $C_p(\omega)$  with  $\omega$  axis upward to the point  $(\omega_n, C_{pmax})$ .  
The firing delay angle is kept constant at  $90^\circ$ .
- 2) the range from the rated wind speed to the cut-out wind speed  $V_{wco}$ :

The inverter control angle is adjusted in order to keep the direct current  $I_d$  constant. This will cause in maintaining the stator electrical output power constant at its rated value independent of speed. Accordingly, the mechanical power needed by the stator remains

constant. But the rotor output electrical power and consequently the resultant output electrical power as well as the total mechanical input power each increase approximately linear with the wind speed. Both the power coefficient and the tip to wind speed ratio decrease from the point  $(n, C_{pmax})$  downward on the curve  $C_p()$  until the cut-out wind speed is attained, all the curves obtained by using matlab programming language [5].

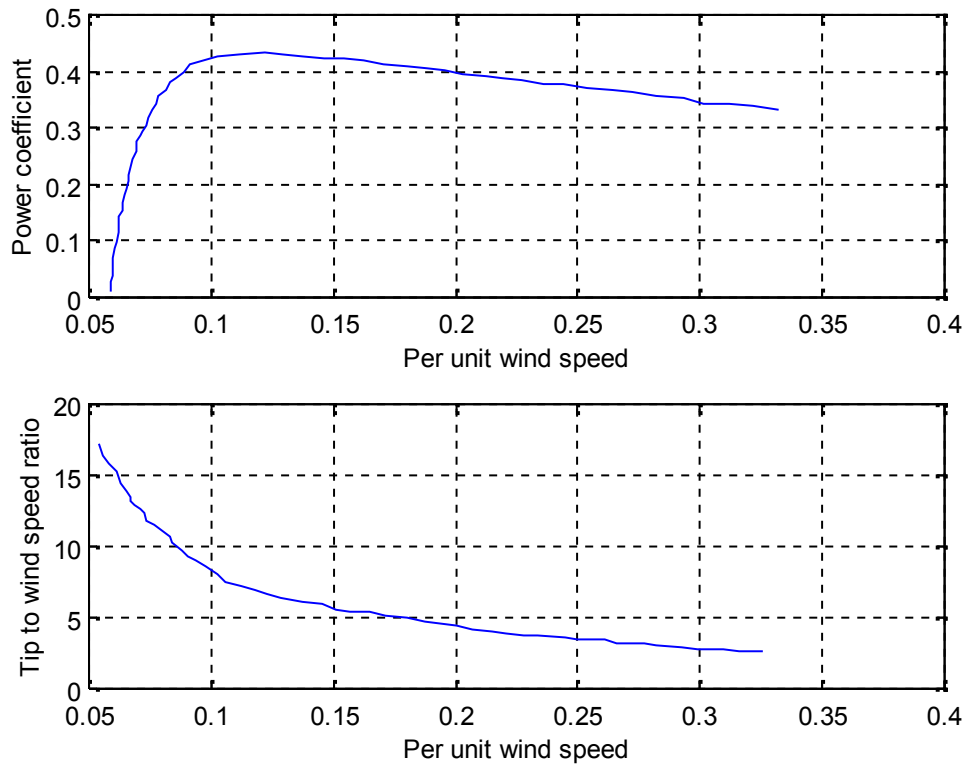


Fig 5a System steady state performance characteristics

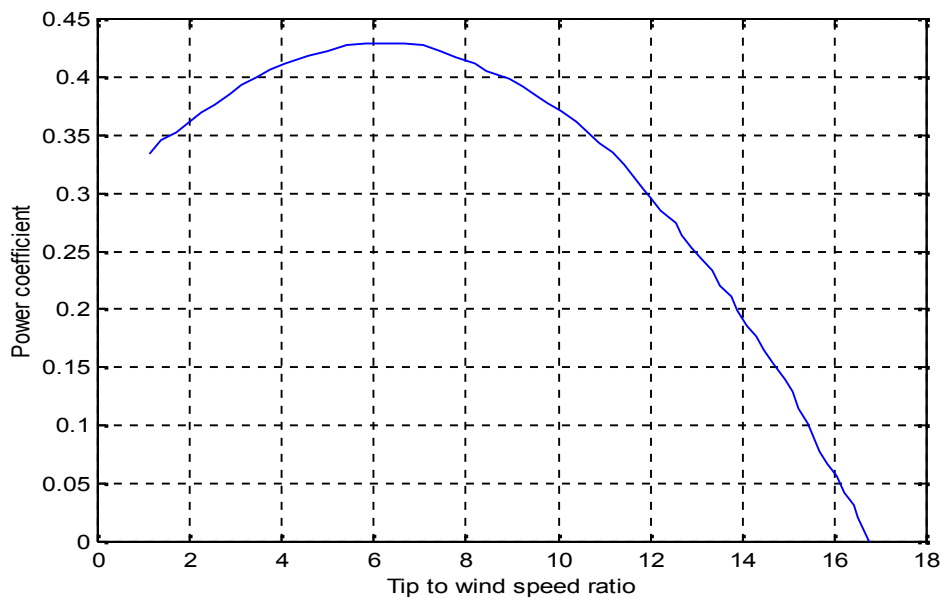


Fig 5b System steady state performance characteristics

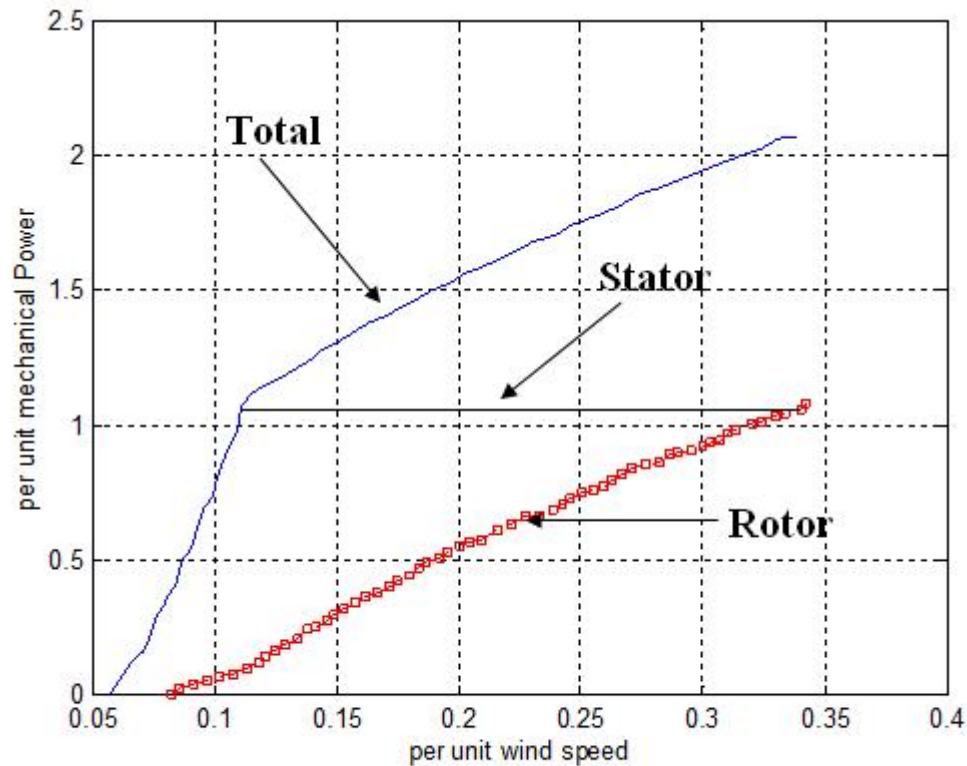


Fig 5c System steady state performance characteristics

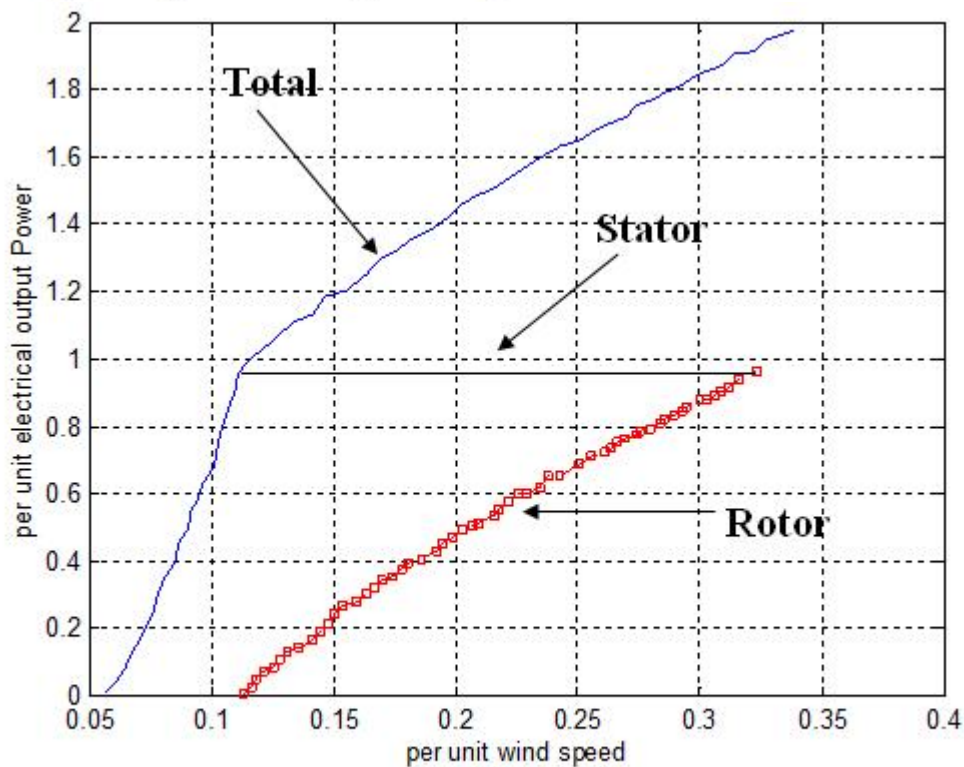


Fig 5d System steady state performance characteristics

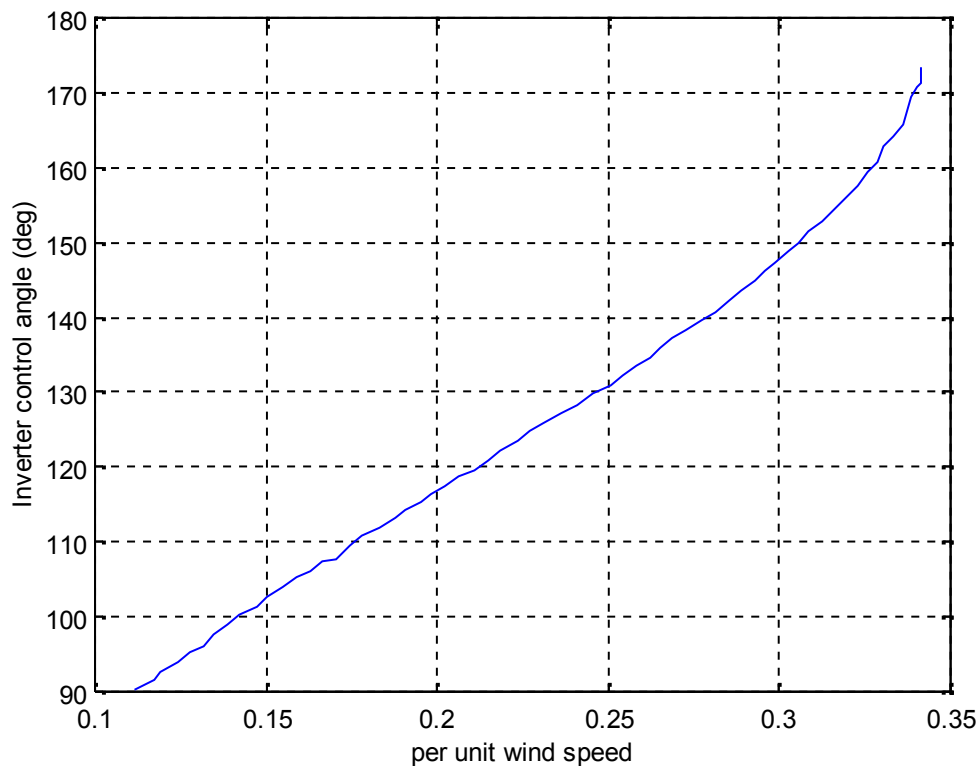


Fig 5e System steady state performance characteristics

## Conclusion

Matching the characteristics of a wind turbine with that of a DOIG was analytically approached and presented. A d.c. module is derived that describe the electrical system steady state. A mathematical model described the turbine steady state performance is derived using curve fitting method.

From the mechanical balance a unified model for the electrical system and the turbine is estimated, this model is solved numerically to obtain the turbine operating conditions under the specified DOIG control strategy.

## Reference

1. Johnson, C.C. and Smith, R.T.: Dynamic of wind generators on electric utility networks, IEEE trans, Vol. AES-12, No. 4, July 1976, pp. 483-493.
2. Salameh, Z. and Kazda, L. : Analysis of the steady state performance of the double output induction generator, IEEE transaction on energy conversion, Vol. EC-1, No. 1, March 1986, pp. 26-32.
3. J. Wilkie, W. E. Leithead, C. Anderson. "Modelling of wind turbines by simple models", Wind Engg. Vol. 14, No. 4, 1990, pp 247-260
4. Andrew C. Clegg, "Self tuning and force control of a hydraulic manipulator", 2000.
5. From internet website, <http://www.rebelwolf.com>.

## Study the possibility of using Savonius wind turbine in the lifting system of wells water

Dr. Jaafar Ali Kadum

Energy and Renewable Energies Technology Center- University of Technology

### Abstract:

Water is the important source of life, and the availability of water has become more crucial than ever before. The demand for water grows along with the world's population. The mankind need of water for irrigate land addition to industrial demand, as well as clean water for drinking purposes.

This research deals with the study of the possibility of using wind power to generate the energy needed to raise the wells water for the purpose of agriculture in remote areas. Been studying different types of wind turbines and water lift pumps,

The selection of appropriate species to build an integrated system, Characterized simply designed and the possibility of building and sustaining at low-cost and simple technique, and thus chosen the savonius wind turbine and water reciprocating pump suitable fit and match the turbine work.

Finally mathematical model was constructed for the compatible system of savonius wind turbine connected to water reciprocating, to calculate the amount of water that can be raised by this system, depending on wind speed and well water depth and the size of the turbine.

Computational results show that the small savonius turbine size  $2m^2$  with suitable reciprocating pump, can raise the amount of water about  $40 m^3$  / day from a well depth of 10 m at average wind speed of 5 m / s.

If it possible to raise this amount of water by a cheap small size simple design and installation system, at average wind speed of 5 m/s at western lands of Iraq, this is considered as a good achievement.

### دراسة إمكانية استخدام توربين الرياح نوع سافونوس في منظومة رفع مياه الآبار.

#### الخلاصة:

الماء هو مصدر مهم للحياة، وتوفير الماء أصبح أكثر أهمية من أي وقت مضى. الطلب على المياه ينمو جنبا إلى جنب مع نمو عدد سكان العالم، البشرية تحتاج الماء لري الأراضي وكذلك للطلب الصناعي. بالإضافة إلى الماء التنظيف لأغراض الشرب.

البحث درس إمكانية استخدام طاقة الرياح في توليد الطاقة اللازمة لرفع ماء الآبار لغرض الزراعة في المناطق النائية، في هذا البحث تم دراسة أنواع مختلفة من توربينات الرياح ومضخات رفع المياه، واختيار الأنواع المناسبة منها لبناء منظومة متكاملة، تتميز ببساطة تصميمها وإمكانية بنائها وإدامتها بكلفة منخفضة، وبذلك تم اختيار توربين الرياح نوع سافونوس ومضخة ماء ترددية تلائم عمل التوربين.

وأخيرا تم بناء موديل رياضي خاص لمنظومة توربين الرياح نوع سافينوس مرتبط مضخة الماء الترددية، لحساب كمية الماء التي يمكن أن تجهزها المنظومة، اعتمادا على سرعة الرياح وعمق البئر وحجم التوربين. نتائج الحسابات تبين إن توربين سافينوس صغير بحجم  $2\text{ م}^2$  مع مضخة ماء ترددية ملائمة يمكن أن ترفع كمية ماء مقدارها  $40\text{ م}^3$  /يوم من بئر بعمق 10م عند سرعة رياح معدلها 5م/ثا. إذا أمكن رفع كمية ماء بهذا الحجم بمنظومة صغيرة بسيطة التصميم والتركيب وبسعر قليل عند متوسط سرعة رياح 5م/ثا في المناطق الغربية من العراق، فإن ذلك يعتبر إنجاز جيد.

## 1- Introduction:

In addition to the problem of water leakage in the remote area, also the source of energy to pump water is also a big problem, developing electrical grids system is often too expensive. because remote villages are frequently located too far away from existing grid lines and electrical power stations. Even if fuel is available within the country, transporting that fuel to remote areas is difficult and the maintenance of the pump engines is really big challenger, additional to the economical problem of many people.

Wind is a pure, clean source of energy that we have been used successfully for long centuries. Wind machines have been used since ancient times to drive machines to pump water in many parts of the world. Early wind pumps Persia and China were of the vertical axis wind turbine type and it is thought the technology arrived in Europe from the eleventh century. [1]

Since the beginning, two types of windmills and turbines have been built to use this renewable source: some machines with horizontal axis of rotation (HAWT) and some other with vertical axis (VAWT). The first type is the most common today, but growing market asks for machines with different properties to fit different wind speeds and engineering requests.

Savonius wind turbines were designed by the Finnish engineer Sigurd J. Savonius in 1922, but Johann Ernst Elias Bessler (born 1680) was the first to attempt to build a horizontal windmill of the Savonius type in the town of Furstenburg in Germany in 1745. Savonius turbines are used whenever the construction cost and maintenance is much more important than efficiency.[2]

This paper presents a review on the performance of Savonius wind turbines. This type of turbine is unusual and its application for obtaining useful energy from air stream is an alternative to the use of conventional wind turbines. Simple construction, high start up and full operation moment, wind acceptance from any direction, low noise and angular velocity in operation, reducing wear on moving parts, are some advantages of using this type of machine.

In general the wind water pumping system is consist of two main parts first the turbine to generate the mechanical power, and the second is the water pump, so they must be discussed separately and then matching them in one system.

### A-The wind Turbines:

Wind power was first used long time ago by many civilizations during mankind history to produce mechanical energy or for navigation. Only with the use of coal and oil in the last two centuries its importance decreased, but during the last decades the interest on this topic grew as much as the possible business around it.

Classification of the Wind Turbine:

Wind Turbines have various classifications among them, the main classifications being horizontal axis wind turbine (HAWT) and vertical axis wind turbines (VAWT). Fig(1) show the general classification of the wind turbines.

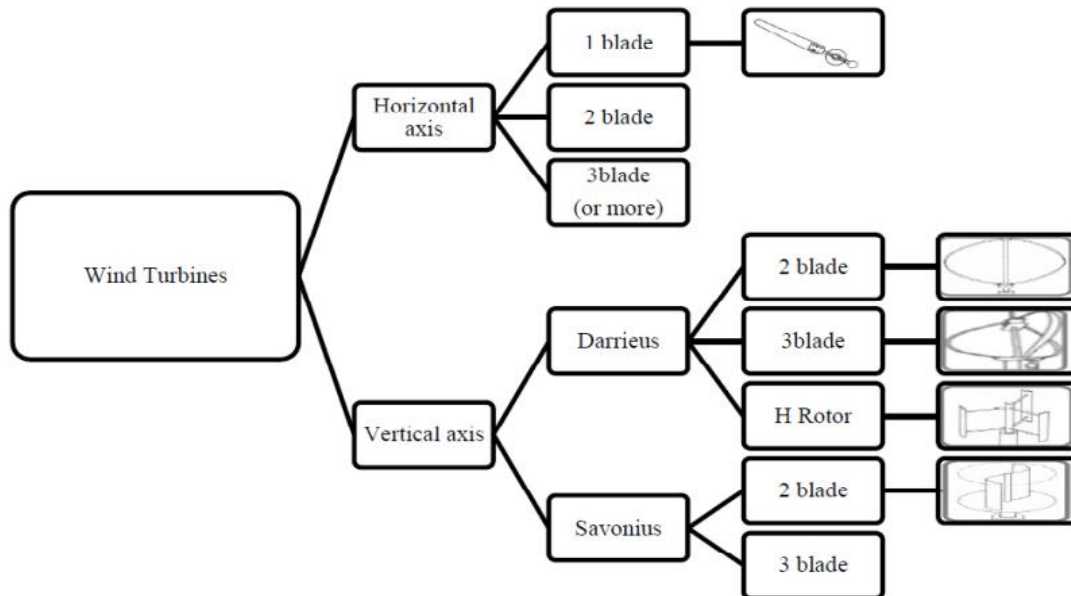


Fig.(1) General classification of the wind turbine .[3]

Main Characteristic of horizontal axis wind turbine:

- Higher efficiency than other types.
- Variable blade pitch control which gives the turbine optimum performance.
- As wind energy increases with height, the tower of the turbine gives access wind speed.
- Due to inherent large structures, construction costs are very high.
- Wind turbine operation at high speed leads to production of noise.
- Require an additional yaw control mechanism to turn the rotor toward the wind direction.
- more complexity and expansively than vertical type.

Main Characteristic of vertical axis wind turbines:

- not required a tower structure, as VAWTs' are mounted closer to the ground
- They don't require yaw mechanisms.
- These are located closer to the ground and hence easier to maintain.
- These have lower start-up speeds than their horizontal counterparts.
- These have a lower noise.
- Are more efficient in gusty winds.
- Can be significantly less expensive to build.
- simple in design and low maintenances cost.
- have lower efficiency as compared to HAWT's

- Because of their low height they cannot capture the wind energy at higher altitudes.

Fig. (2) Shows the performance of different types of wind turbines according to tip speed ratio. Ref.[ 4]

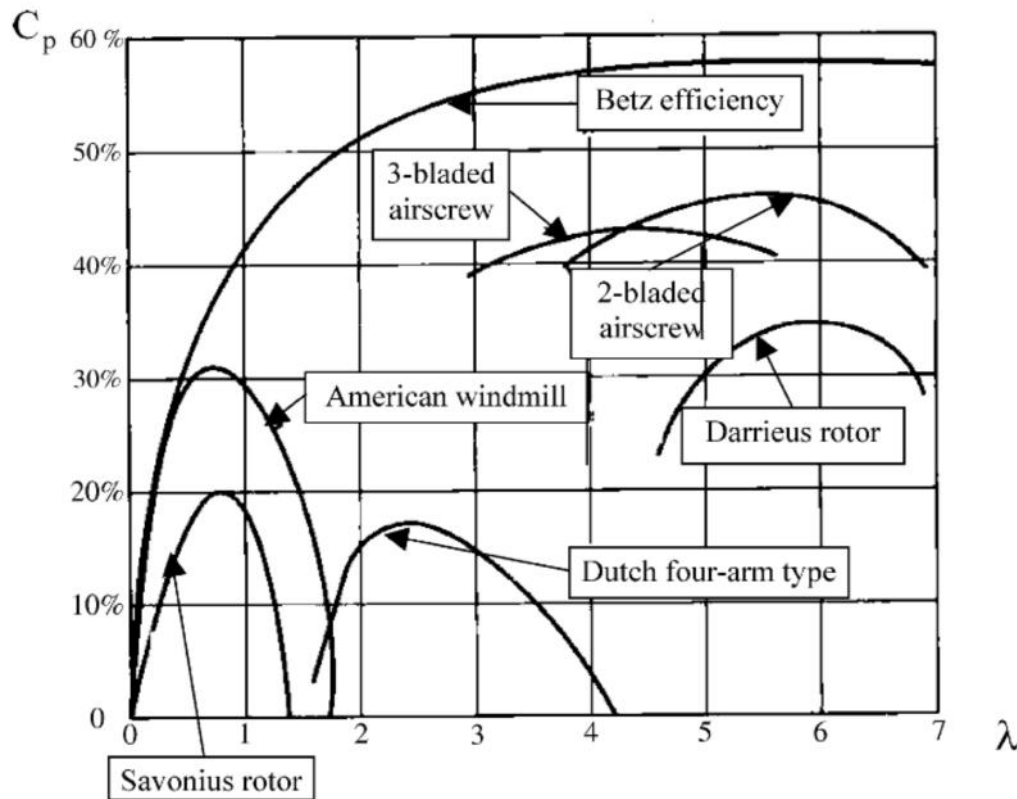
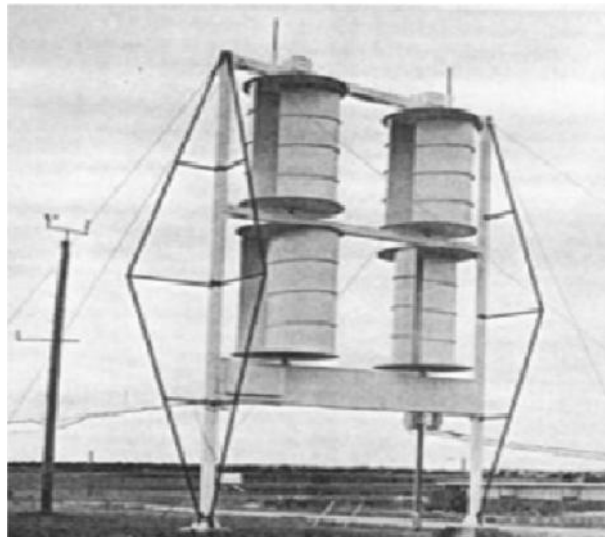


Fig.( 2)  $C_p$ - $\lambda$  diagram for different type of wind turbines [4]

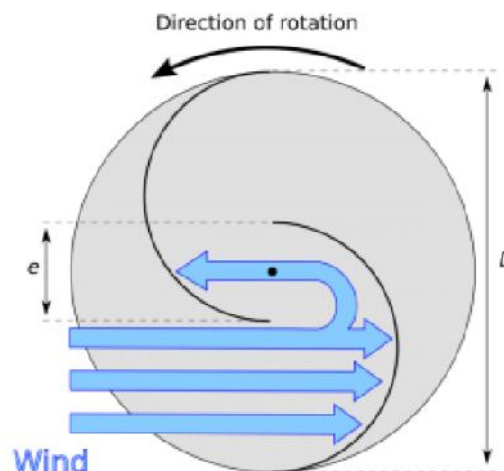
This scheme is the result of an extensive study results of various turbine types, as it demonstrates that the multi blade horizontal axis wind turbines is the most performers from the other systems. It work at high rotational speed, so it is not working at low wind speed less than 4 m/s, so it is unsuitable for Iraqi weather in, the chart also shows the multi blade horizontal wind turbine has high performance at lower tip speed ratio, It is already frequently used at medium wind speed. This type needs a tower to lift the rotor as well as system is needed to direction guide toward the wind, so it is not easy to construct and maintain. Savonius wind turbine appear as the simplest type and will be selected for many reasons. When cost or reliability is much more important than efficiency and more it works at low rotational speed and high rotational torque fits to simple water reciprocating water pump works. The Savonius turbine is one of the simplest turbines aerodynamically, it is a drag-type device, consisting of two or three scoops. Savonius and other vertical-axis machines are good at pumping water and other high torque operation, low rpm applications so it is not suitable for electricity generation. They can sometimes have long helical scoops to give smooth torque. Savonius wind turbine work at low tip speed ratio approximately one [4], so it cannot rotate faster than the wind speed, Much of the savonius wind turbine swept area near the ground, making the overall energy extraction less effective due to lower wind speed at lower

heights. so it can be employed for some purpose such as pumping water or grinding grain. How can the Savonius wind turbine work, aerodynamically because the turbine scoops curvature, the scoops experience less drag when moving against the wind than when moving with the wind. The differential drag causes the Savonius turbine to spin. Fig.(3) Show a simple Savonius wind turbine.



Fig(3) Simple constructed Savonius wind turbine[5]

Savonius turbine is the simplest geometry and its construction is cheap. It starts rotating at lower wind speeds as compared to its counterpart wind turbines, having a high starting torque. It produces low noise and can make use of the wind flowing in any horizontal direction to its rotation. However, in spite of these advantages, this wind turbine faces one main disadvantage of having low efficiency. Fig(4) show the aerodynamic interference and reaction of the wind with the turbine scoops.



Fig(4) The aerodynamic reaction of the wind with the turbine scoops.

Parameters that affect the performance of a Savonius wind turbine:

There are many parameters effecting on Savonius performance such as the end plates shape, aspect ratio, buckets spacing, buckets overlap, number rotor stages, Reynolds number, and turbulence size [4].

#### B-The Water Pumps:

Water pumping technology developed in parallel with the sources of power available at the time. Indeed the first process to lift water was by cupped their hands and lifted water from a stream chose the 'pumping' technique appropriate to them. Modern devices such as centrifugal pumps have reached a high state of development and are widely used, particularly in developed countries, only because suitable power sources such as diesel engines and electric motors became available

The use of wind power for pumping water should be feasible if

- winds of at least 2.5-3 m/s are present 60% or more of the time.
- the water source can be pumped continuously without excessive drawdown.
- storage is provided, typically for at least 3 days' demand, to provide for calm periods without wind.
- a clear sweep of wind to the windmill is secured, i.e. the windmill is placed above surrounding obstructions, such as trees or buildings within 125 m.

Types of pumps:

The main applications of pumps in small community water supply systems are:

- Pumping water from wells.
- Pumping water from surface water intakes.
- Pumping water into storage reservoirs and the distribution system.

Pump classification according to mechanical principles

- Reciprocating piston.
- Rotary fines.
- Diaphragm
- Axial-flow (propeller)
- Centrifugal
- Air lift

Another type of pump with limited application in water supply systems.

Technical information on the water pumps types:

#### 1- Reciprocating (plunger)

The type of reciprocating pumps used for small water supplies. there are Several types may be considered as mentioned in table(1).[6]

Table(1) Types of reciprocating pumps and there specifications.

| Type of pump               | Depth range  | Characteristics and applicability                                                                                          |
|----------------------------|--------------|----------------------------------------------------------------------------------------------------------------------------|
| 1. Reciprocating (plunger) |              | Low speed of operation; hand, wind or motor powered; efficiency range 25–60%                                               |
| a. Suction                 | Up to 7 m    | Capacity range: 0.5-1 l/s; suitable to pump against variable heads; valves and pump buckets require maintenance attendance |
| b. Suction: treadle pump   | Up to 6 m    | capacity range: 0.5-2.5 l/s; mostly used for irrigation but also feasible for water supply if water is treated             |
| c. Lift (direct action)    | Up to 15 m   | As for suction                                                                                                             |
| d. Low lift: rower pump    | Up to 3-6 m  | capacity: 0.5-2 l/s mostly used for irrigation but also feasible for water supply if water is treated                      |
| e. Lift (high lift)        | Up to 180+ m | As for suction                                                                                                             |

Reciprocating pumps have a plunger (or piston) that moves up and down (reciprocates) in a closed cylinder for positive displacement of water. On the upward stroke the plunger forces water out through an outlet valve, and at the same time water is drawn into the cylinder through an inlet valve. The downward stroke brings the plunger back to its starting position, and a new operating cycle can begin. Fig.(5) show the principal of pump operation.

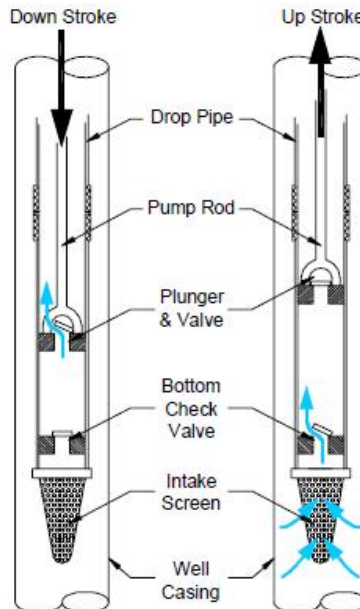


Fig.(5).Show the component of the Reciprocating pumps.[6]

Because of the fact that the cylinder and plunger are located below the water level, this pump can lift water from wells as deep as 180 m or even more. The forces created by the pumping increase with the depth to the water.

## 2-Diaphragm pump

Diaphragm pumps are positive displacement pumps. There are two entirely different types. Conventional diaphragm pumps are more commonly used as dewatering pumps than as pumps for drinking water supply. The main part of the pump is its diaphragm, a flexible disc or tube made of rubber or metal. Non-return valves are fitted at the inlet and outlet. It can pump water up to 45 m Fig. (6) show composition of this pump.

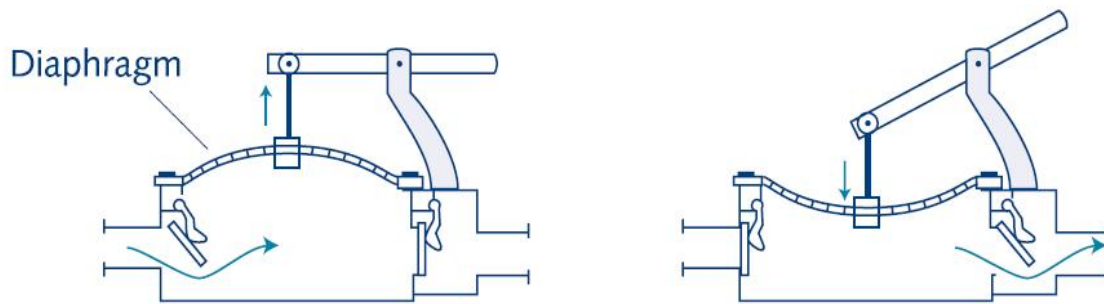
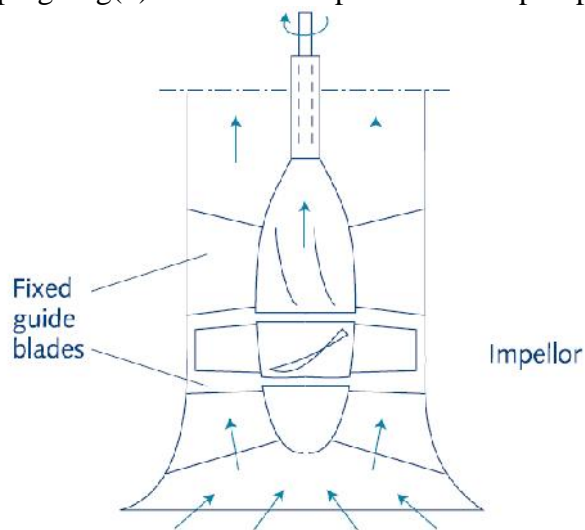


Fig. (6) Show composition of this pump.[6]

## 3- Axial-flow pumps

In the axial-flow type of pump, radial fins or blades are mounted on an impeller or wheel, which rotates in a stationary enclosure (called a casing).it can pump water up to 5-10m, it is high capacity low lift pumping. Fig(7) show the component of this pump.



Fig(7) Show the component of axial flow pump.

#### 4-Centrifugal pumps

The essential components of a centrifugal pump are the impeller and the casing as shown in Fig.( 8). The impeller is a wheel with vanes radiating from the centre to the periphery. When rotated at a sufficiently high speed, the impeller imparts kinetic energy to the water and produces an outward flow due to the centrifugal forces. The casing is so shaped that the kinetic energy of the water leaving the impeller is partly converted to useful static head pressure. Technical information of centrifugal pump are mention in table(2) [6].

Table (2) Types and technical information of centrifugal pumps.

|                             |             |                                                                                                                                  |
|-----------------------------|-------------|----------------------------------------------------------------------------------------------------------------------------------|
| 4. Centrifugal              | Depth range | High speed of operation - smooth, even discharge; efficiency (range 50-85%) depends on operating speed and pumping head          |
| a. Single-stage             | 20-35 m     | Requires skilled maintenance; not suitable for hand operation; powered by engine or electric motor                               |
| b. Multi-stage shaft-driven | 25-50 m     | As for single stage; motor accessible, above ground; alignment and lubrication of shaft critical; capacity range 25-10,000 l/min |
| c. Multi-stage submersible  | 15-50 m     | High capacity at low lift; very low efficiency especially at greater lifts; no moving parts in the well; well casing             |

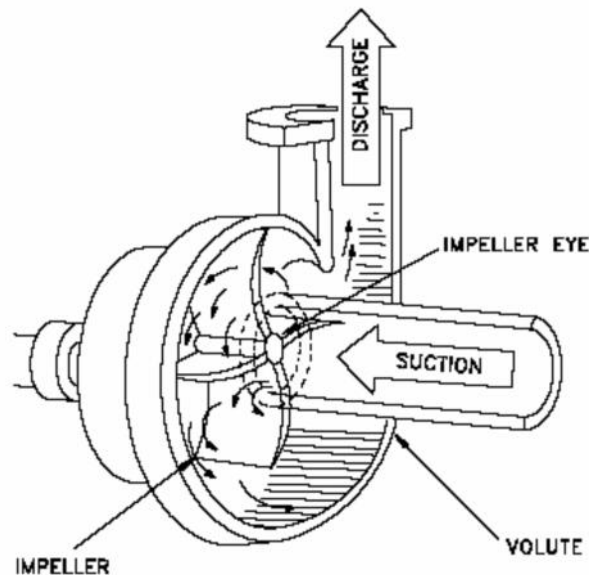


Fig.( 8).The essential components of a centrifugal pump. [6]

Comparison and pump selection:

In selecting a pump type for a specific purpose the following technical criteria need to be considered:

- Rate volume of delivery water required.
- Vertical distance from pumping level to delivery level.
- Durability of basic components (including corrosion resistance)
- Weight of below ground parts
- Availability and cost of spares
- Ease of maintenance

From the previous pump technical specification, the lift reciprocating pumps is simple in design, maintenance, cheap in cost, operate at low rotational speed, high efficiency it is suitable for Savonius wind turbine [7] ,[8] .

## 2- Theory:

Kinetic Energy in the Wind

The kinetic energy of air mass moving at a velocity can be expressed mathematically as is Eq (1).

$$E = \frac{1}{2} m \hat{v}^2 \dots\dots\dots(1)$$

$$P = \frac{\partial E}{\partial t} \dots\dots\dots(2)$$

Where E is the kinetic energy,  $\hat{v}$  is the air velocity, and P is the extracting power.

The rate of change of kinetic energy of the air flowing at a certain velocity  $v$  through a certain volume is the power possessed by the moving wind. This is the amount of wind energy passing through cross-section per unit time.

At a certain given velocity  $v$ ,

$$P = \frac{1}{2} \frac{\partial m}{\partial t} \hat{v}^2 \dots\dots\dots(3)$$

The rate of air mass change flowing through area (A) can be determined in Eq.(4) as.

$$\frac{\partial m}{\partial t} = \rho A \hat{v} \dots\dots\dots(4)$$

substitute Eq. (4) in Eq. (3), gate the power equation.

$$Power = \frac{1}{2} \rho A \hat{v}^3 \dots\dots\dots(5)$$

It is the wind flowing energy at a certain velocity  $v$ .

Wind energy converters using aerodynamic drag:

The first fundamental difference which considerably influences the actual power depends on which aerodynamic forces are utilized for producing mechanical power. All bodies exposed to an airflow experience an aerodynamic force the components of which are defined as aerodynamic drag in the direction of flow, and as aerodynamic lift at a right angle to the direction of flow. The real power coefficients obtained vary greatly in dependence on whether aerodynamic drag or aerodynamic lift used Fig.(9) show the simple representation of the drag machine. [9].

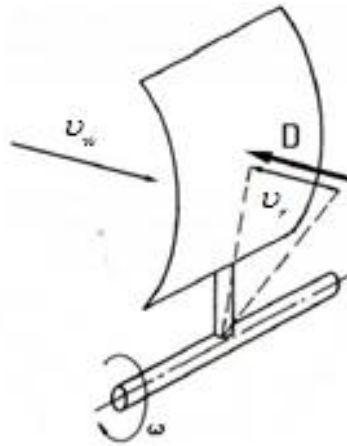


Fig.(9) Wind Flow conditions and aerodynamic drag forces.

The air push the surface A with air velocity  $\hat{v}_w$  the power capture P of which can be calculated from the aerodynamic drag D, the area A and velocity  $\hat{v}_r$  with which it moves:

$$P = D \hat{v}_r \dots\dots\dots(6)$$

The relative velocity  $\hat{v}_r = \hat{v}_w - \hat{v}$  which effectively impinges on the drag area is decisive for its aerodynamic drag. Using the common aerodynamic drag coefficient  $C_d$ , the aerodynamic drag can be expressed as:

$$D = C_D \frac{Q}{2} (\hat{v}_w - \hat{v}_r)^2 F \dots\dots\dots(7)$$

Where Q is the free-stream airflow. The resultant power is:

$$P = C_D \frac{Q}{2} (\hat{v}_w - \hat{v}_r)^2 A \hat{v}_r \quad (w) \dots\dots\dots(8)$$

If power is expressed again in terms of the power contained in the free-stream airflow, the following power coefficient is obtained:

$$C_P = \frac{P}{P_o} = \frac{\frac{Q}{2} C_D A (\hat{v}_w - \hat{v}_r)^2 \hat{v}_r}{\frac{Q}{2} \hat{v}_w^3 A} \dots\dots\dots(9)$$

Analogously to the end approach described before, it can be shown that  $C_p$  reaches a maximum value with a velocity ratio of  $\hat{v}_r / \hat{v}_w = 1/3$ . The maximum value is then.

$$C_{P,Max} = \frac{4}{27} C_D \dots\dots\dots(10)$$

The order of magnitude of the result becomes clear if it is taken into consideration that the aerodynamic drag coefficient of a concave surface curved against the wind direction can hardly exceed a value of (1,3). Thus, the maximum power coefficient of a pure drag-type rotor becomes:

$$C_{P,Max.} \approx 0.2 \dots\dots\dots(11)$$

For horizontal wind turbine the max. power coefficient at Betz's limit  $C_p = 0.593$

#### Water Demand:

Planning a water supply system depends mainly on water demand. The level of water demand is the sum of supplying water for villages, livestock, and irrigation. Water demand for a village is estimated from population size and daily per capita water consumption. Once these factors are known, daily demand can be estimated. Daily water demand does not provide enough information though, because water consumption varies over 24 hours. Peak hour demand has to be estimated for a water supply system to be reliable any time of the day. The peak hour demand is the hour when water consumption is the highest, usually at noon. In contrast, consumption is usually lowest at night. Estimating water demand for livestock is similar to figuring the water supply for a village. Water demand is estimated from the number of cattle and other animals using the system, multiplied by per capita water consumption. Typical daily water consumption for farm animals is presented in table (3).[10]

Table (3) Typical daily water consumption for farm animals.

| Type of animals  | Daily water consumption (liter/animal) |
|------------------|----------------------------------------|
| Dairy cow        | 80                                     |
| Beef brood cows  | 50                                     |
| Horses and mules | 50                                     |
| calves           | 30                                     |
| Sheep and goats  | 10                                     |
| chickens         | 0.1                                    |

water demand for various types of crop irrigation is presented in Table( 4).

Table(4) Estimated maximum daily water demand for various types of crop irrigation.

| Type of crops | Daily water requirement ( $m^3/1000m^2$ ) |
|---------------|-------------------------------------------|
| Rice          | 10                                        |
| Cereals       | 4.5                                       |
| Sugar cane    | 6.5                                       |
| Cotton        | 5.5                                       |

As a guideline, the following steps can be used to estimate the water demand for crop irrigation.

1. Determine the size and shape of the irrigation plot.

2. Estimate the water resources and the wind and solar energy resources of the area.
3. Determine the type of crop that will be harvested on the plot.
4. Estimate the water demand from Table (4).

To find the relation shape between the amount of water delivery from the well pump powered by the wind energy as the follow.

Power obtain from the Savonius wind turbine = Power required to rise the water from the well.

$$P_{wind\ turbine} = P_{Rise\ water}$$

$$\frac{1}{2} \rho_{air} C_p A_{turbine} \hat{v}_{wind}^3 = g_{pump} \rho_{water} g h \dot{Q}_w \dots\dots\dots(12)$$

$$\frac{1}{2} \times 1.2 \times 0.2 \times A_{tur.} \hat{v}_{wind}^3 = 0.6 \times 10^3 \times 9.81 \times h \times \dot{Q}_w$$

$$\therefore \dot{Q}_w \approx 2 \times 10^{-5} \frac{A_{tur.} \times \hat{v}_{wind}^3}{h_{well}} \times 86400 \dots\dots\dots m^3 / d$$

$$\dot{Q}_w \approx 1.728 \frac{A_{tur.} \times \hat{v}_{wind}^3}{h_{well}} \dots\dots\dots m^3 / d \dots\dots\dots(13)$$

### 3- Result:

Savonius wind turbines is relatively low efficient than other type wind turbine, so it can be used whenever the low construction cost and maintenance is much more important than efficiency.

The quantity of water pump depends on the turbine projection area and cubic of the wind speed and inversely to the water well depth.

For example a Savonius wind turbine of 1m<sup>2</sup> size at 5m/s mean wind speed can produce 40m<sup>3</sup>/d at well depth of 10m.

Computational results show that the amount of water extracted by the small Savonius turbine system is practice acceptable and due to the fact that the low construction costs and locally available technology, this requires building a small size model and experience in one of the farms in the desert of Iraq.

### 3- Conclusion:

Mean wind speeds of 4 m/s are available over 50% of Iraq lands, which is suitable for wind water pumping, while there are wide region in the west of Iraqi lands that has a wind speed up to 5m/s, which is excellent suitable for water well pumping.

The performance of Savonius turbine can be developed, from about C<sub>p</sub>= 0,2 to 0,4 by optimizing rotor design. There are many parameters effecting on Savonius performance such as the end plates shape, aspect ratio, buckets spacing, buckets overlap, number rotor stages, Reynolds number, and turbulence size.

According to the available wind velocity which is very low, it's very difficult to design the blade profile using the metal. Thus we must decided to use plastic material as its density is much more lower than the metal, as using the plastic barrels which has a good ability for weather wear resistance.

increase the capacity of the system is by increasing the turbine size according it is directly proportional relationship, therefore there are no limits viability of this system to produce the required quantity. Proposed building basin to store water for the period low wind speeds.

#### Reference:

- 1- Renewable Energy Water Pumping Systems Handbook Period of Performance: April 1–September 1, 2001
- 2- *Wind Power for Homes and Business: Renewable Energy for the 1990s and Beyond*. Post Mills, VT: Chelsea Green Publishing Company. Gipe, P. (1993).
- 3- JL Menet(2004),A double step Savoniusrotor for the local generation of electricity: a design study, Renewable Energy 29 (2004), Page(1843–1862)
- 4- M.H.Simmonds and A. Bodek(1964) , Performance test of a Savonius Rotor, Microfiche Reference Library, Technical Report T10, McGill University, January 1964.
- 5- UK Saha , S Thota, D Maity(2008), Optimum design configuration of Savonius rotor through wind tunnel experiments ; Journal of Wind Engineering and Industrial Aerodynamics 96 (2008),Page (1359– 1375).
- 6- McGowan, R. and Hodgkin, J. (1992). *Pump selection: a field guide for energy efficient and cost effective water pumping systems for developing countries*. Revised ed. (WASH technical report; no. 61). Arlington, VA, USA, Water and Sanitation for Health Project.
- 7- Fraenkel, P. (1997). *Water-pumping devices: a handbook for users and choosers*. 2nd ed. London, UK, Intermediate Technology Publications.
- 8- IRC (1988). *Handpumps: issues and concepts in rural water supply programmes*. (Technical paper series; no. 25). The Hague, The Netherlands, IRC International Water and Sanitation Centre.
- 9- M.A.Kamaji, S.B.Kedare, S.V.Prabhu(2009), Experiments on a single stage modified Savonius rotor , Page (1064-1073).
- 10- Renewable Energy Water Pumping Systems Handbook Period of Performance: April 1–September 1, 2001

## Effect of Magnetic Field on the Fuel Consumption and Exhaust Emissions in Internal Combustion Engine (C. I. Engine)

**Dr. Adil Mahmood Salih**  
Machines & Equipment Eng.Dept  
University of Technology

**Eng. Mohammed Kadhim Allawi**  
Technical College Baghdad Foundation  
of Technical Education

### Abstract

The combustion efficiency in most internal combustion engines are not up to (90%) so that a part of the fuel does not burn and comes out with the exhaust gases, leading to increase flowing fuel consumption and increasing emissions in the atmosphere. Therefore, several attempts have been made to increase the combustion efficiency and reduce emissions. The phenomenon is clear at the maximum load. In this work a new way to reduce the fuel consumption by using magnetic field, to ensure the complete combustion. This leads to obtain a maximum thermal efficiency and reduce the emissions by subjecting the fuel to force magnetic flux of the magnet installed at the entrance of the of fuel flowing, leading to more efficient combustion. From the experimental results, a reduction in the fuel consumption (L/h) in compression ignition engine (C.I. engine) was obtained up to (3%), brake specific fuel consumption (bsfc) up to (2.877%) and brake thermal efficiency raised to about (3%). The exhaust gas emissions showed a reduction nearly by (13.8 %) of CO, (7.8 %) of CO<sub>2</sub> and (10.8%) of HC. Lotus engine simulation (LES) program was used to study the effect of same parameters in experimental testing, this program gives the best performance of engine at maximum brake power, and the same input data given to the program is taken from the results of experimental results. For fuel consumption (L/h) for (C.I. engine) for two different values of (A/F), the use of magnetic field reduced the fuel consumption to about (2.83%). For brake thermal efficiency for (C.I. engine) for different values of (A/F), brake thermal efficiency for higher (A/F) increased. For (C.I. engine) using different values of the cetane number (48.5, 50, 55), when the cetane number increased, the brake specific fuel consumption (bsfc) decreased compared with other values of cetane number. Brake specific fuel consumption (bsfc) decreased but is very low when density changes of diesel fuel during the days of the week.

تأثير المجال المغناطيسي على استهلاك الوقود وملوثات العادم في محرك الاحتراق الداخلي (محرك الاشتعال الانضغاطي)

### الخلاصة

ان كفاءة الاحتراق في أغلب محركات الاحتراق الداخلي هي لا تتجاوز (90%) وهذا يعني ان قسما من الوقود سوف لا يحترق ويخرج مع غازات العادم مما يؤدي الى زيادة استهلاك الوقود وزيادة الملوثات في المحيط لذا أجريت عدة

محاولات لزيادة كفاءة الاحتراق وتقليل نسبة الملوثات وتكون هذه الظاهرة واضحة عند أقصى حمل. لذا تم استخدام طريقة جديدة لتقليل استهلاك الوقود وهي استخدام المجال المغناطيسي لضمان الاحتراق التام مما يؤدي الى حصول على أعلى كفاءة حرارية والحد من الملوثات حيث يخضع الوقود الى قوة الفيض المغناطيسي من المغناطيس المثبت على انبوب جريان الوقود مما يؤدي الى زيادة كفاءة الاحتراق. والنتائج التي حصلنا عليها من الجانب العملي قللت استهلاك الوقود في محرك الاشتعال الانضغاطي بحدود ( 3% ) واستهلاك الوقود المكبحي بحدود ( 2.38% ) و ملوثات غازم العادم تظهر انخفاض واضح بنسب ( 13.8% ) لغاز احادي اوكسيد الكربون و ( 7.8% ) لغاز ثنائي اوكسيد الكربون و ( 10.8% ) للهيدروكربونات غير المحترقة . باستعمال برنامج اللوتس محاكاة محرك لدراسة تأثير نفس المدخلات في الاختبار العملي حيث هذا البرنامج يعطي أفضل أداء للمحرك عند اعظم قدرة مكبحة وان البيانات المدخلة الى البرنامج تاخذ من نتائج النتائج العملية، استهلاك الوقود لمحرك الاشتعال الانضغاطي لقيمتين مختلفتين لنسبة (الهواء/ الوقود ) باستخدام مجال مغناطيسي يؤدي الى تقليل استهلاك الوقود بنسبة (2.83%). الكفاءة الحرارية المكبحة لمحرك الاشتعال الانضغاطي لقيم مختلفة لنسبة (الهواء/ الوقود ) حيث يلاحظ زيادة الكفاءة الحرارية المكبحة كلما زادت نسبة (الهواء/ الوقود ) . محرك الاشتعال الانضغاطي يستخدم قيم مختلفة لعدد السيتان ( 5.48,50,55 ) حيث كلما زاد عدد السيتان قل استهلاك الوقود المكبحي ، استهلاك الوقود المكبحي يقل لكن بنسبة بسيطة عند تغير كثافة وقود الديزل خلال ايام الاسبوع

## Nomenclature

| Symbol          | Meaning                         | Unit       |
|-----------------|---------------------------------|------------|
| A/F             | Air to fuel ratios              |            |
| bp              | Brake power                     | KW         |
| bsfc            | Brake Specific fuel consumption | kg/(kW.hr) |
| CO              | Carbon monoxide                 |            |
| CO <sub>2</sub> | Carbon dioxide                  |            |
| C.I.engine      | Compression ignition engine     |            |
| HC              | Unburned hydrocarbons           | ppm        |
| ho              | Differential manometer          | cm         |
| m <sub>a</sub>  | Air mass flow rate              | kg/sec     |
| m <sub>f</sub>  | Fuel mass flow rate             | kg/sec     |

## INTRODUCTION

Since the invent of the internal combustion engine in the late 19th century, a great number of research studies have been conducted to improve the engine performance, decrease the engine fuel consumption and reduce the unwanted exhaust emissions. Emissions and fuel consumption are two major worldwide environmental century. Given the large number of vehicles manufactured worldwide (estimated 15-20 million road vehicles per year); transportation is one of the largest sources of both emissions and fuel consumption in the world. One major solution to decrease emissions and fuel consumption in transportation is the use of cleaner and more efficient combustion in engines. Many of experimental studies which present evidences of the benefits of magnetic treatment were occurred. For motor vehicles, much fuel economy and noticeable soot suppressions could be approached when the magnetic treatment was introduced [1]. Charles H. Sanderson [2], 1977. In his invention, he showed a method and apparatus for treating liquid fuel in an internal combustion engines by passing it through a magnetic field prior to mixing it with air in the carburettor or the fuel injector. Farrag A.El Fatih, Gad M.saber [3]. Experiments reveal that the magnetic effect on fuel consumption reduction was up to 15%. CO reduction at all idling speed was range up to 7%. The effect on NO emission reduction at all idling speed was range up to 30%. The reduction of CH<sub>4</sub> at all idling speed was range up to 40%. The experiments of Faris et.al, [4], 2012, research comprised the using of permanent magnets with different intensity (2000, 4000, 6000, 9000) Gauss, which installed on the fuel line of the two-stroke engine, and study of its impact on gasoline consumption, as well as exhaust gases. For the purpose of comparing, the results necessitated the search for experiments without the use of magnets. The overall performance and exhaust emission tests showed a good result, where the rate of reduction in gasoline consumption ranged between (9-14) %, and the higher the value of a reduction in the rate of 14 % was obtained using field intensity 6000 Gauss as well as the intensity 9000 Gauss. It was found that the percentages of exhaust gas components (CO, HC) were decreased by 30%, 40%, respectively, but CO<sub>2</sub> percentage increased up to 10%. Al-Dossary , Rashid [5] , studied the effect of magnetic field on internal combustion engine with unleaded gasoline .Al-Dossary found that the effect of magnetic field on CO was the most significant at most engine's loads and speeds.

## 2- Methodology

The effect of the magnetic field on fuel (diesel Iraqi) used in the engines and its impact on the amount of consumption, as well as emission of exhaust gases, the appropriate method was examined. We include below the description of the materials and equipment used.

### 2.1. Magnetic devices

Magnetic devices Fig (1) used in this research were manufactured in the U.S.A. Accepted Laboratory Tested EPA. The fuel is subjected to the lines of forces from permanent magnets mounted on fuel passage lines. The magnet for producing the magnetic field is oriented so that its (South Pole) is located adjacent the fuel line, and its (North Pole) is located spaced apart from the fuel line. Applying a magnetic field to ionizing fuel to be fed to

combustion devices, one can ensure more complete combustion, obtaining a modification of the fuel economy, improving the fuel efficiency and reducing polluting emissions.



Fig (1). The Magnetic devices

## 2.2. Engine

The engine used in the experimental work is compression ignition engine (C.I. engine) type (FIAT) model (TD133), 4 cylinders, 4 strokes; the displacement volume at this engine is (3.666L). The engine was coupled to a hydraulic dynamometer to measure the brake torque. Fig (2) shows the experimental rig of (C.I. engine), and table (1) lists the main technical specifications of this engine.

## 2.3. Measurement of brake torque

The hydraulic dynamometer, type [isi lingegneria didattica] was used to measure the brake torque of (C.I. engine) by using friction fluid. Water was used as the friction fluid.

## 2.4. Fuel consumption

The glass tube, was used to measure the fuel consumption of the (C.I. engine). This glass tube has a constant volume (100) ml, and a stop watch was used to measure the fuel consumption of this volume.

## 2.5. Air consumption

The air supplied to compression ignition engine was measured by use an air box, orifice and the manometer used to measure the pressure differential between the atmosphere and pressure in the air box.

## 2.6. Measurement of engine speed (rpm)

The measuring of the engine speed of compression ignition engine (C.I. engine) was carried out by using instrument tachometer used to measure the rotation speed of a shaft engine. This instrument usually displays the revolutions per minute (rpm). Tachometer has been fixed the shaft engine test rig by coupling.

## 2.7. Gas analyser

The exhaust gas analyser type (2000-4) was used to analyse the emissions of exhaust, as shown in Fig (3). The analyser detects the CO-CO<sub>2</sub>-HC contents.

## 2.8. Calibration

To ensure that all the data read from the measuring devices are correct, a calibration was done to all measuring device.



Fig (2). The experimental rig  
of (C.I. engine)



Fig (3) .The exhausts gas analyser  
type (mod 488 Italy)

The following equations were used in calculating engine performance parameters: [6]

- 1- The brake specific fuel consumption.

$$bsfc = \frac{\dot{m}_f}{bp} \times 3600 \quad \dots\dots(1)$$

- 2- Brake thermal efficiency is defined as in Eq.

$$\eta_{bth} = \frac{bp}{\dot{m}_f L.C.V} \quad \dots\dots\dots (2)$$

- 3- Air mass flow rate

$$\dot{m}_{a, act} = \frac{12\sqrt{(h_o)}}{3600} \times \rho_{air} \quad \dots\dots\dots (3)$$

- 4- Fuel mass flow rate

$$\dot{m}_f = \frac{vf \times 10^{-6}}{time} \times \rho_f \quad \dots\dots (4)$$

- 5- Air-fuel ratio

$$A/F = \frac{\dot{m}_a}{\dot{m}_f} \quad \dots\dots\dots (5)$$

- 6- Brake power

$$bp = \frac{2\pi \times N \times T}{60 \times 1000} \quad \dots\dots\dots (6)$$

### 3- RESULTS and DISCUSSIONS

The experimental and engine simulation results of fuel consumption, break specific fuel consumption, break thermal efficiency and emission were discussed.

#### 3.1. Experimental results

To demonstrate the impact of the use the magnet experiments were conducted in two groups.

Group 1:-

Experiments were carried out without using of magnets at a different speed at full load as shown the Fig (4).

Group 2:-

Experiments were carried out using the magnet as shown in Figure (5) for the same speed names in the first groups.

Figure (6) represents the amount of fuel consumed (L/h) with the engine speeds for (C.I. engine) for using magnetic field and without. The values of fuel consumption (L/h) increase when the engine speeds are increased .By using of a magnetic field, the amount of consumed fuel (L/h) is less than without using by about (3%).

Figure (7) shows the relation between brake specific fuel consumption (bsfc) and engine speed with using magnetic field and without of (C.I. engine) . It can be seen that the brake specific fuel consumption (bsfc) decreased nearly by (N=1600 rpm), and when the magnetic field was used, this reduction was measured to be approximately by (2.877%).

The brake thermal efficiency results are shown in Fig (8) of (C.I. engine) for different engine speeds. The using of magnetic field increased the brake thermal efficiency by about (3%), and the maximum value of the brake thermal efficiency for using of magnetic field operation is at (N= 1600 rpm).

Figure (9) shows the effect of magnetic field on the present of (CO) of the (C.I. engine), indicating that the present of (CO) decreases when the engine speed is increased, and the using of magnetic field reduced the amount of the present of (CO) by about (13.8%).

It was found that the reducing percentage of the gases (CO<sub>2</sub> and HC) were up to (7.8%, 10.8%), respectively for the (C.I. engine), as shown in Figures (10) and (11).

### 3.2. Engine simulation results

Engine performance including ,fuel consumption (L/h), brake specific fuel consumption (bsfc) and brake thermal efficiency were studied using leaded diesel fuel with and without magnetic effect. Figure (12) show the network of (C-I- engine) used in this study.

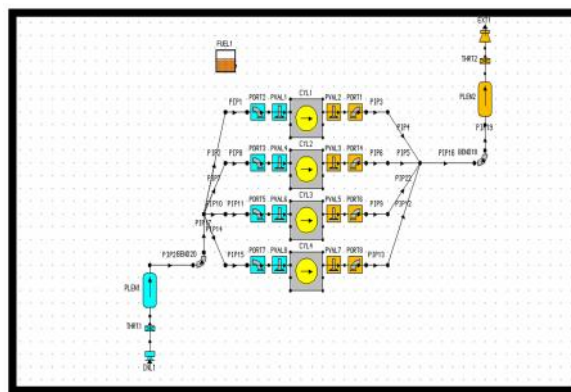


Fig (12). The network model of (C-I- engine).

Figure (13) shows the relation between the fuel consumption (L/h) and engine speeds with two different values of air to fuel ratio [A/F =32.8, the average value of air to fuel ratios of

the experimental results of testing without using magnetic field] and air to fuel ratios  $[A/F = 33.86$ , the average value of air to fuel ratios of the experimental results of testing with using magnetic field] for (C.I. engine), the using of magnetic field ( $A/F = 33.86$ ) reduced the fuel consumption by about (2.83%).

The comparison between the engine simulation and the experimental results the Fig (14) show the relation between ( $m \cdot f$ ) and engine speed of (C.I. engine) working at max loading .From Fig (14) the trend of curves is similarly to the ( $N=1800$  rpm) .

Figure (15) shows the relation between brake thermal efficiency and engine speed for different values of ( $A/F$ ), we can see from Fig (15) that the brake thermal efficiency is higher for ( $A/F$ ) (33.86) than ( $A/F$ ) (32.8), and the max value of brake thermal efficiency is at ( $N=1600$  rpm).

Figure (16), for three different values of cetane number (48.5, 50, 55), table (2) and at ( $A/F=25$ ), it is noted that when the cetane number increased, the fuel consumption decreased as compared with the other values of cetane number.

Figure (17) clarifies the effect of brake specific fuel consumption (bsfc) on engine speed for different densities of diesel fuel during the days of the week, density of diesel fuel was provided from (AL- Najaf) refineries as shown in table (3). In Fig (17) the effect of changing the densities is very low upon (bsfc).

## 4- CONCLUSIONS

### 4.1. Experimental Conclusion

- 1- For fuel consumption (L/h) with the engine speeds, for (C.I. engine) using magnetic fields, the amount of consumed fuel (L/h) is less than without using by about (3%).
- 2- For Brake specific fuel consumption (bsfc) with the engine speeds, for (C.I. engine) using magnetic fields, the amount of (bsfc) is less than without using by about (2.877%).
- 3- Brake thermal efficiency with the engine speeds, for (C.I. engine), was relatively improved with the magnetic field intensity by about (3%).
- 4- Focusing on emission, it was found that CO of the (C.I. engine) decreased when the engine speed was increased and the using of magnetic field reduced the amount of the present of (CO) by about (13.8%).
- 5- For (C.I. engine), the present of (CO<sub>2</sub> and HC) by using magnetic field was lower than without using by about (7.8%, 10.8%), respectively.

## 4.2. Engine simulation Conclusion

- 1- For fuel consumption (L/h) with the engine speeds for (C.I. engine) with two different values of (A/F), the using of magnetic field ( $A/F = 33.86$ ) reduced the fuel consumption by about (2.83%).
- 2- Concerning the fuel consumption (L/h) and engine speeds for (C.I. engine), when the cetane number increased, the fuel consumption decreases as compared with other values of cetane number.
- 3- For brake thermal efficiency with the engine speeds of (C.I. engine) for different values of (A/F) brake thermal efficiency was higher when (A/F) increased.
- 4- For brake specific fuel consumption (bsfc) and engine speed of (C.I. engine) when changing the density of diesel fuel during the days, the effect of changing the density was very low upon (bsfc).

## References

- 1-S. Mingdong et al, study on the Combustion Efficiency of Magnetized Petroleum Fuels, Chinese Science Bulletin, (1984),
- 2- Charles H. Sanderson. Method and apparatus for treating liquid fuel .U.S. Pat. 4,050,426 .Jun.23, 1977.
- 3-Farrag A.El Fatih,Gad M.saber "Effect of Fuel Magnetism on Engine Performance and Emissions", Australian Journal of Basic and Applied Sciences, 4(12): 6354-6358, 2010.
- 4- Ali S. Farisa, Saadi K. Al-Naserib, Nather Jamal, Raed Isse, Mezher Abed, Zainab Fouad, Akeel Kazim, Nihad Reheem, Ali Chaloob, Hazim Mohammad, Hayder Jasim, Jaafar Sadeq, Ali Salim, Aws Abas, " Effects of Magnetic Field on Fuel Consumption and Exhaust Emissions in Two-Stroke Engine". 18 ( 2012 ) 327 – 338 .
- 5- Al Dossary, Rashid. M. A., "The Effect of Magnetic Field on Combustion and Emissions", Master's Thesis, King Fahd University of Petroleum and Minerals, 2009.
- 6- ام. ال. ماثيور واربي شارما "محركات الاحتراق الداخلي" ترجمة الدكتور يونس عبد المالك الفخري، الجامعة التكنولوجية

Table (1)

|                           |                                     |
|---------------------------|-------------------------------------|
| <b>FIAT diesel engine</b> |                                     |
| Engine type               | 4cyl., 4-stroke                     |
| Engine model              | TD 313 Diesel engine rig            |
| Combustion type           | DI, water cooled, natural aspirated |
| Displacement              | 3.666 L                             |
| Valve per cylinder        | two                                 |
| Bore                      | 100 mm                              |
| Stroke                    | 110 mm                              |
| Compression ratio         | 17                                  |

Table (2)

|                                  |       |       |       |
|----------------------------------|-------|-------|-------|
| <u>Cetane number</u>             | 48.5  | 50    | 55    |
| Relative Density at 15 °C (g/ml) | 0.838 | 0.846 | 0.856 |
| Lower heating value (KJ/Kg)      | 42360 | 42870 | 43180 |
| H/C Ratio                        | 1.8   | 1.87  | 1.99  |
| Alkaline %                       | 72    | 80    | 96    |
| <u>Olifines (%)</u>              | 2     | 1     | 2     |
| <u>Aromatics (%)</u>             | 26    | 19    | 2     |

Table (3)

| Type of prod | Type of prod. Test             | Sat   | Sun   | Mon   | Tue   | Wed   | The   | Fri   |
|--------------|--------------------------------|-------|-------|-------|-------|-------|-------|-------|
| Gas oil      | Density Kg/m <sup>3</sup> @15C | 841.8 | 843.3 | 845.9 | 843.8 | 842.3 | 843.3 | 842.8 |
|              | Cetan NO                       | 56.0  | 56.0  | 56.0  | 56.0  | 56.0  | 56.0  | 56.0  |

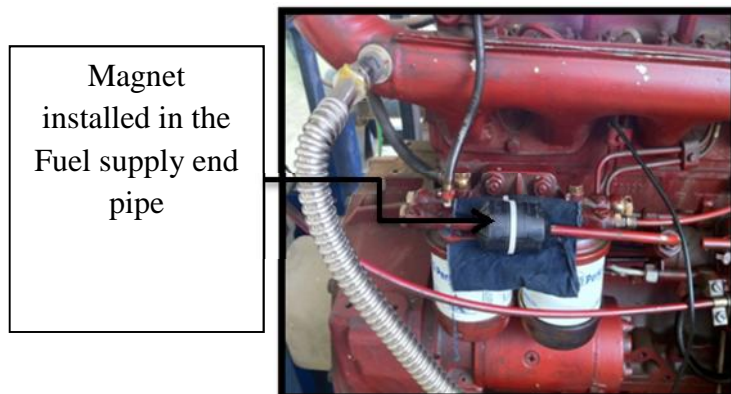


Fig (4) Magnet installed in the fuel supply end pipe

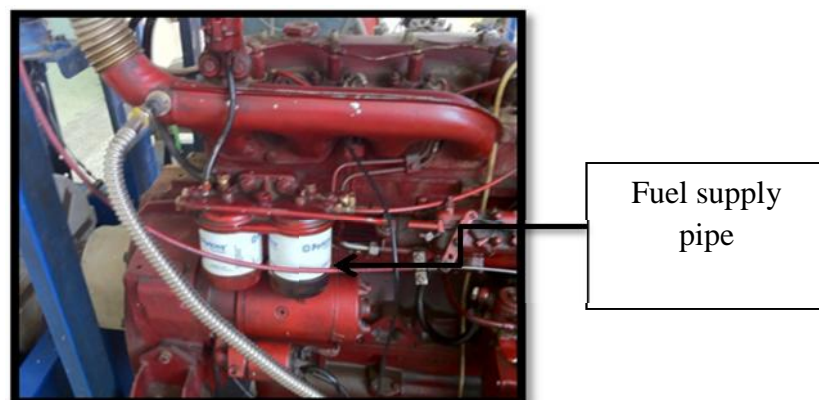


Fig (5) The Fiat compression ignition engine rig

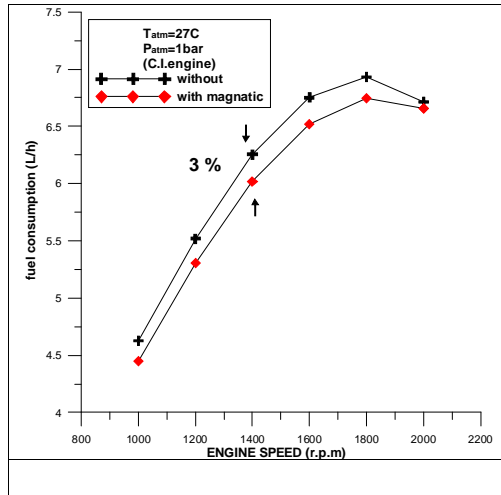


Fig (6). Fuel consumption (L/h) as function of engine speed of (C.I. engine) for with magnetic field and without

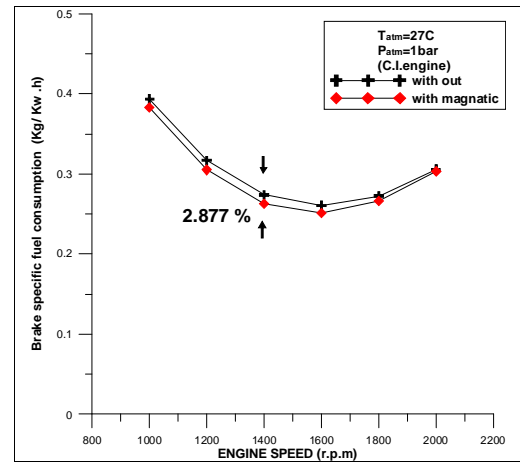


Fig (7). Brake specific fuel consumption (bsfc) as function of engine speed of (C.I. engine) for with magnetic field and without

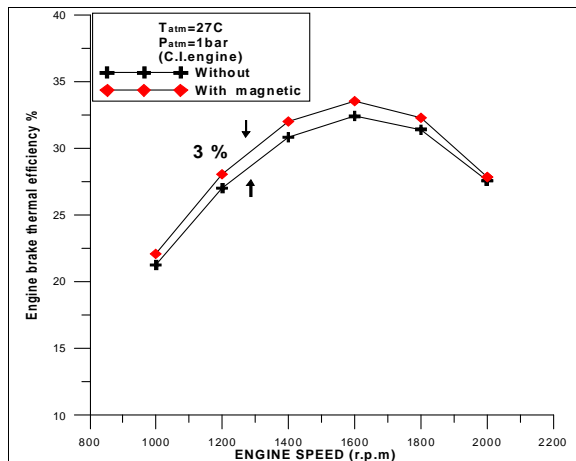


Fig (8). Brake thermal efficiency as function of engine speed of (C.I. engine) for using magnetic field and without

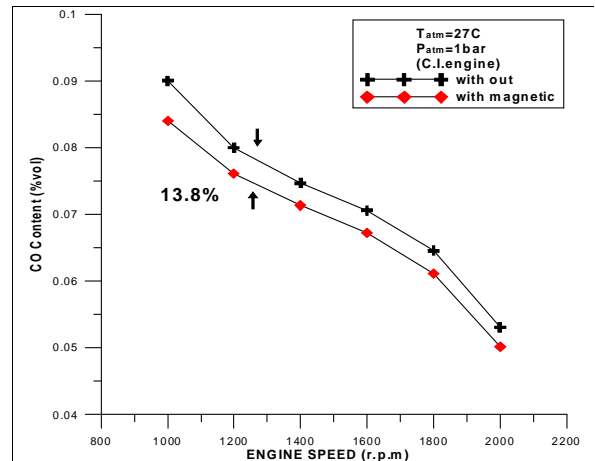


Fig (9). The present of (CO) as function of engine speed of (C.I. engine) for using magnetic field and without

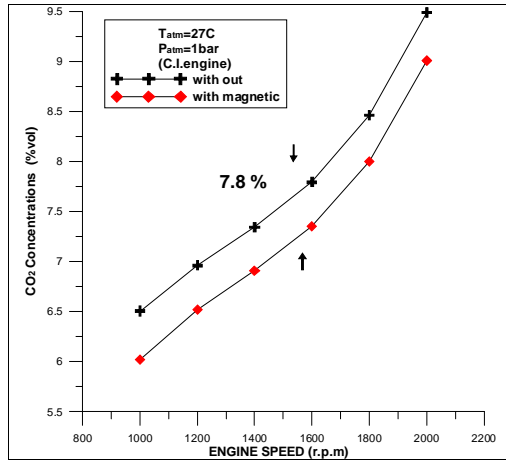


Fig (10). The present of (CO<sub>2</sub>) as function of engine speed of (C.I. engine) for using magnetic field and without

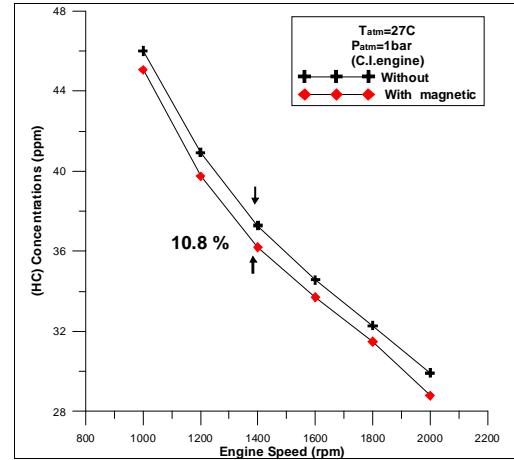


Fig (11). The (HC) concentration (ppm) as function of engine speed of (C.I. engine) for using magnetic field and without

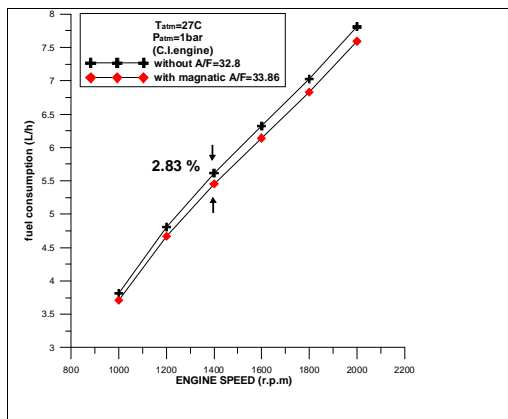


Fig (13). The relation between the fuel consumption (L/h) and engine speeds with two different values of air to fuel ratio.

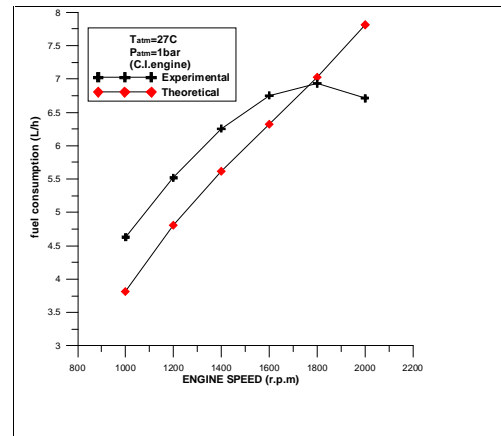


Fig (14). The relation between the fuel consumption (Experimental & Theoretical) with the engine speeds for (C.I. engine) without using magnetic field.

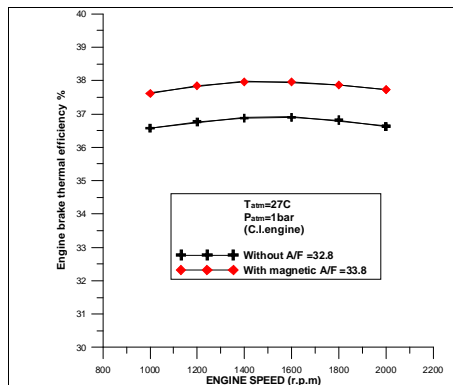


Fig (15). Brake thermal efficiency as function of engine speed of (C.I. engine) for with magnetic field and without

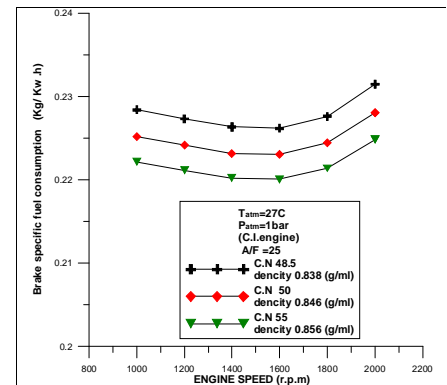


Fig (16). The brake specific fuel consumption (bsfc) as function of engine speed of (C.I. engine) for different values of cetane number

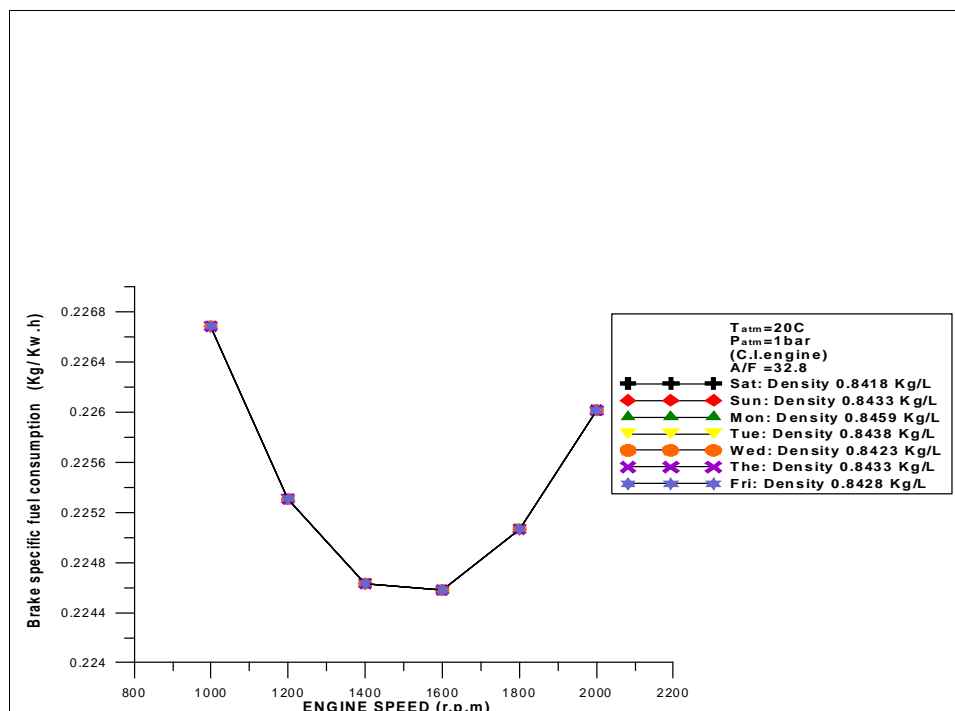


Fig (17). The brake specific fuel consumption (bsfc) as function of engine speed of (C.I. engine) for different densities of diesel fuel

## System Sizing of Solar Water Heating System in Iraq

Al-Sudany Naseer K. <sup>(1)</sup> , Al-Sa'ady Ahmed F. <sup>(2)</sup> , Al-Sudany Ala'a H. <sup>(2)</sup>

<sup>(1)</sup> Ministry of electricity, Renewable Energy and Environment Center.

<sup>(2)</sup> Al-Mustansiriyah University, College of Education, Physics Department.

### Abstract

This research aims to introduce solar water heating system in Iraq domestic sector, residential sector, public sector, industrial sector and government sector in order to reduce the load from the national electricity grid. In this research the consumers were classified into five groups depending on number of persons in their families which were (2-4), (4-6), (6-8), (8-10) and (10-12) persons and calculate the required energy to heat the water for each month and for all groups. After that the resulted energy from the solar water heating system was calculated. Finally, the required area of solar heater was calculated for each group. The results indicated that the total saving energy by using solar heaters for three million consumer is about (10TWh) for residential sector and (3TWh) for the governmental sector which can cover load about (2200 MW) and work 24h daily during the year.

This can be represented 1/3 of total production power at the present time. From the economic point of view, the calculations appeared that the return of investment (ROI) for all solar heaters at work operation time reach to only 26 months depending on the price of on solar heater which about 750\$, and can save 1.2 billion dollars each year by work of these systems which was calculated depending on the price of electrical energy kWh which about 10 cent/kWh.

### حجم النظام المستخدم في أنظمة تسخين الماء بالطاقة الشمسية

د.نصير كريم قاسم<sup>(1)</sup> أ.د.احمد فرحان عطوان<sup>(2)</sup> م.م. علاء حسين شنيشل<sup>(2)</sup>

### الخلاصة

يهدف هذا المشروع إلى إشاعة استخدام السخان الشمسي من قبل المواطنين في دورهم السكنية، وكذلك من قبل دوائر الدولة والمؤسسات الحكومية، بهدف تخفيف العبء عن منظومة الكهرباء الوطنية. تم في هذا البحث تصنيف المستهلكين إلى خمسة أصناف اعتماداً على عدد أفراد العائلة، حيث يشمل الصنف الأول العوائل المكونة من (2-4) فرد، بينما يضم الصنف الثاني العوائل التي تضم (4-6) فرد، والصنف الثالث العوائل التي تضم (6-8) فرد، والصنف الرابع العوائل (8-10) فرد، والصنف الخامس العوائل التي تضم (10-12) فرداً، وتم كذلك حساب الطاقة اللازمة لتسخين الماء لكل شهر من الأشهر التسعة ولجميع الأصناف من المستهلكين. كذلك تم حساب الطاقة الناتجة باستخدام السخان الشمسي ذو الأنابيب. وبالتالي حساب المساحة المطلوبة من السخان الشمسي لكل صنف من أصناف المستهلكين. بينت الحسابات التي

تم الحصول عليها من هذه الدراسة أن الطاقة الكلية التي يمكن ترشيدها باستخدام السخانات الشمسية لثلاثة ملايين مشترك تقدر بـ (10TWh) للقطاع السكني، و(3TWh) للقطاع الحكومي، والتي تغطي حملا قدرته بحدود (2200MW) يعمل 24 ساعة يوميا خلال السنة، والتي تمثل 3\1 القدرة الإنتاجية الكلية في الوقت الحاضر. ومن الناحية الاقتصادية، أظهرت الحسابات أن إعادة الكلفة الكلية لجميع السخانات تتم خلال فترة تشغيل تصل إلى 26 شهر فقط اعتمادا على أن سعر السخان الواحد يصل إلى 750 دولار أمريكي. كما ويمكن توفير مبلغ 1.2 مليار دولار كل سنة جراء تشغيل هذه الأنظمة، والذي تم حسابه على أساس أن كلفة إنتاج الطاقة الكهربائية تبلغ 10cent /kWh.

## **1. Introduction**

The human comfort and adaptation to every existing condition of any context has been always the main reason for the investigation and research of new technologies which will assist the way of living and consequently to lead to further development [1]. Fossil fuels are consumed at greater rate than formed now in Earth layers under heat and pressure and will disappear completely after some definite time period in the future. Energy consumption worldwide is around 10 billion tons of coal equivalents per year. The share of oil in total consumption is 40%, share of gas and coal are 50% [2]. adverse influence of energy production processes and combustion of transport fuel on environment grow, causing the raise of greenhouse gas (GHG) emissions and global warming, acids rains, growth of air, water and earth pollution, etc [3]. In accordance with the forecasts, concentration of CO<sub>2</sub> will rise by 75-350% in 2100 as compared with the level as of 1850 that cause to increase the temperature of the atmosphere near Earth's surface [4].

The energy sector has to put efforts in renewable energy as well as energy optimization measures. Renewable energy, such as wind power, solar (heat & power), geothermal (heat & power), can take the place of current primary energy supply sources or improvements can also be made in energy conversion, transportation and distribution. There is a large theoretical potential to use solar energy to cover heat demands in buildings [1]. The impacts on environment are significantly less from renewable energy sources compared with impacts caused by combustion of fossil fuels [5].

Since Iraq receives high solar radiation about 2000kWh/m<sup>2</sup>/year, it is therefore necessary to go to the solar energy technologies options instead of conventional sources of energy to support the Iraqi economy and to reduce the potential on the Iraqi National Electricity Grid by using thermal solar energy and photovoltaic conversion [6]. Solar collectors are the heart of most solar energy systems which absorbs the sun's light energy and changes it into heat energy. Domestic hot water is the second-highest energy demand in the typical household in all over the world [7].

Today solar water heating systems are being used for single family houses, apartment buildings, schools, car washes, hospitals, restaurants, agricultural farms and different industries.

## 2.The Intensity of Solar Radiation in Iraq

The rate at which solar energy enters a collector aperture, divided by the aperture area is called the aperture irradiance [8]. Theoretically Iraq is considered at the second level of solar exposure radiation. The daily averaged solar insolation map of Iraq can be shown in figure 1 which have established that almost all of Iraq has the potential areas for establishing large – scale solar utilities, thus, the annual average of energy received daily from the sun ranges between 4.5 – 5.4 kWh/m<sup>2</sup> and in Baghdad is about 5 kWh/m<sup>2</sup> which make Iraq is among the most suitable countries for solar applications [9]. solar radiation in Baghdad are listed in table 1.

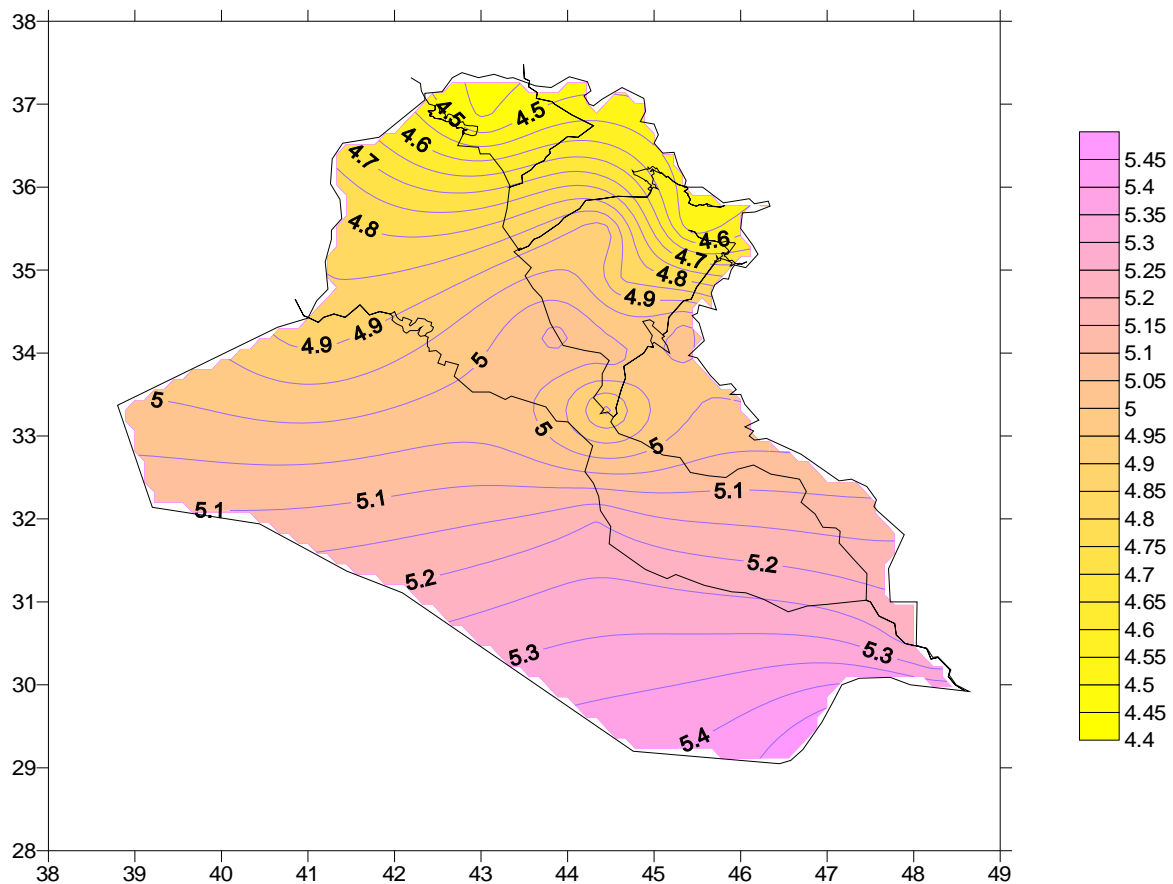


Figure (1) Daily-averaged solar insolation for different locations in Iraq [9].

Table(1): Average daily and annually global horizontal solar radiation in Baghdad [10]

| Month                              | Se<br>p | Oc<br>t | Nov  | Dec  | Ja<br>n | Fe<br>b | Mar | Ap<br>r | Ma<br>y | Annua<br>l |
|------------------------------------|---------|---------|------|------|---------|---------|-----|---------|---------|------------|
| Insolation kWh/m <sup>2</sup> /day | 5.8     | 5.0     | 4.32 | 4.25 | 4.6     | 5.6     | 5.6 | 5.0     | 5.2     | 1360       |

### 3.Flat Plate and Evacuated-Tube Solar Collectors

There are many types of solar thermal collectors, such as concentrating solar collectors, Flat-plate thermal solar collector and Evacuated-Tube Collectors [8]. Each evacuated tube consists of two glass tubes made from extremely strong borosilicate glass. The outer tube has very low reflectivity and very high transmissivity that radiation can pass through. The inner tube has a layer of selective coating that maximizes absorption of solar energy and minimizes the reflection, thereby locking the heat. The ends of the tubes connected to the copper header are fused together and a vacuum is created between them. The vacuum is created as an insulator and does not allow short wave radiation to escape through the glass tube. This process is shown in Figure 2. The absorber plate is mostly of aluminum or copper that painted black so as to allow it to absorb maximum amount of solar radiation [11]. The selective coating enables the use of the solar energy spectrum to generate heat. This produces greater thermal efficiency in bright sunshine but also gives high efficiency in diffuse sunlight conditions [12].

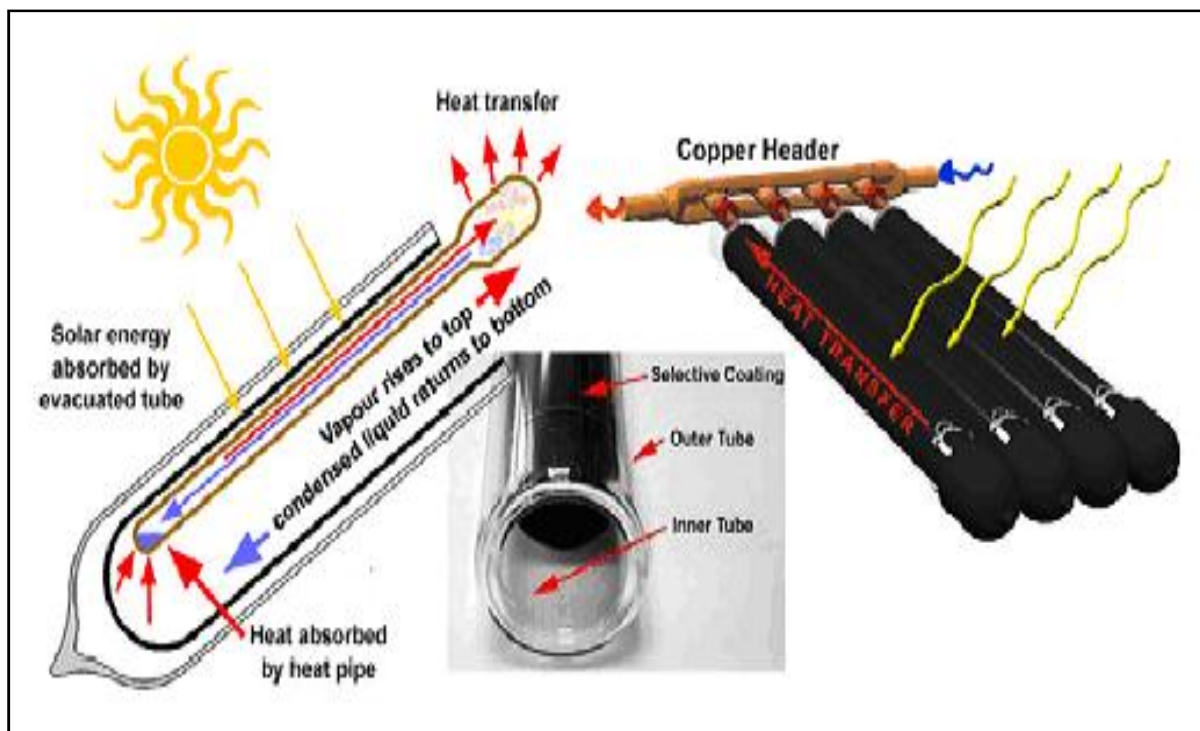


Figure (2) Design and working of evacuated (or vacuum) tubes pane[11].

Evacuated tube collectors are superior to flat plate collectors in a number of ways [13]:

1. Due to the cylindrical shape of the evacuated tube, the sun is perpendicular to the surface of the glass for most of the day. Flat plate collectors have the disadvantage that the sun is

only perpendicular to the collector at noon and thus a proportion of the sunlight striking the surface of the collector is likely to be reflected.

2. As the name suggests, air is evacuated from the evacuated tube to form a vacuum. This greatly reduces conductive and convective heat losses from the interior of the tube. As a result, wind and cold temperatures have minimal effect on the efficiency of the evacuated tubular collector.
3. Suntrap all-glass evacuated tubular collectors can be used in subzero temperatures without the system sustaining damage. Flat plate systems often require expensive and complicated "antifreeze" systems to be installed.
4. Evacuated tubes are strong, long lasting, inexpensive if one of the tubes is broken, and easy to replace.
5. Due to the high efficiency absorption of solar radiation even during overcast conditions, combined with excellent insulation properties of the tube, evacuated tube collectors will heat water all year round (back-up heating system required for particularly overcast or rainy weather).
6. Due to the various advantages of evacuated tube collector over flat plate collectors, a smaller collector can be used to provide the same heating performance. Flat plate solar collector can produce similar heat output to evacuated tubular collector, but generally only during warm, still, sunny conditions. When averaged over an entire year, evacuated tube collector heat output per net  $m^2$  of collector area, is superior to flat plate.

#### **4. Energy Balance of Solar Water Heating**

The most important problems which determine the feasibility of using solar water heating is the energy balance for effective working of this system. The convert of incident solar energy on solar water heating collector into heat energy depends on many factors, the most important of them is:

- Solar collector efficiency.
- Solar collector area.
- Size of water that required to heat.
- The required temperature.

The work efficiency of solar collectors is related to the type of technology which determine the thermal and optical efficiency that associated the conversion of solar energy into heat. In general, the optical losses is about 20% from the incident solar radiation by

reflection and absorption from the optical window of solar collector. While the thermal losses depends in most cases on type of technology. Thus, for flat plate collector it reach to 40%, but for evacuated tube collector is 25% and for heat pipe collector is 10%.

## **5. Design Calculations of Solar Water Heating system**

It can get high benefit from solar heater when the design calculations are used according to the ambience that the system installed in it. In this research evacuated tube solar water heater was used in calculations which the most computable for Iraq ambience. The primary calculations can be summarized into the following steps:

- Calculate the volume of daily required hot water.
- Calculate the required energy to heat the water (kWh).
- Guess the losses of energy resulted from store the hot water (kWh).
- Calculate the final size that required from solar collector.
- 

### **5.1 Determine The Daily Hot Water Demand**

The daily required of hot water can be classified according to the need of persons into three primary groups as in the following:

- Little use that the human can use about 10-20 liter every day.
- Middle use that the human can use about 20-40 liter every day.
- extreme use that the human can use about 40-80 liter every day.

In this research the consumers were classified into five groups depending on number of persons in the family, these groups were (2-4), (4-6), (6-8), (8-10) and (10-12) persons, where the daily required of hot water was calculated for each group depending on the average using, after that the required energy to heat the water was calculated for each month from the nine months and for all groups of consumers depending on the following parameters:

- The volume of required hot water.
- The temperature of required water which about 60°C.
- The temperature of supplied water to solar collector which vary from month to other.

The quantity of daily required energy to heat the required water can be calculated by using the following equation [14]:

$$Q_{hw} = V_{hw} C_w \Delta T \text{ (Wh/day)} \quad (1)$$

Where  $V_{hw}$  is the volume of hot water (kg),  $C_w$  is the specific heat capacity of water and  $\Delta T$  is the difference between ambient water temperature and required temperature. The minimum ambient temperature in Baghdad are listed in table 2.

Table(2): minimum ambient temperature for Bagdad [15]

|                    | Sep  | Oct  | Nov  | Dec | Jan | Feb | Mar | Apr  | May  |
|--------------------|------|------|------|-----|-----|-----|-----|------|------|
| Feeding water Temp | 23.0 | 19.0 | 12.0 | 6.0 | 4.0 | 5.0 | 9.0 | 15.0 | 21.0 |

## 5.2. Required Area of Solar collector

The required area of solar collector can be calculated depending on resulted energy from solar energy by using Heat Pipe Evacuated Tube Solar Water Heater System, Evacuated Tube and Flat Plat Solar Collectors which have efficiencies (70-75%) and can get 1000 kWh/m<sup>2</sup>/270day, (50-60%) and can get 800 kWh/m<sup>2</sup>/270day and (35-40%) and can get 540 kWh/m<sup>2</sup>/270day, respectively by using the following equations [16]:

$$A_{sc} = \frac{Q_{yrq}}{\eta_{solar} I_{max}} \approx \frac{Q_{yrq}}{Q_{sc}} \quad (2)$$

Where  $A_{sc}$  is the required solar collector area,  $Q_{yrq}$  is the yearly required energy to heat the water,  $\eta_{solar}$  solar collector efficiency,  $I_{max}$  maximum solar radiation and  $Q_{sc}$  is the yearly energy gain by solar collector for each square meter which depends on the collector type. Annual energy savings (electricity in this example) can be estimated using the following equation [16]:

$$E_s = A_{sc} I_{ave} \eta_{solar} 365 / \eta_{aux} \quad (3)$$

Where  $E_s$  is annual energy savings [kWh/yr],  $I_{ave}$  is average solar radiation [kWh/m<sup>2</sup>/day] and  $\eta_{aux}$  is auxiliary heater efficiency which assume 0.88 for electricity.

## 5.3. Storage Losses

To decrease the thermal losses resulted from store 200 liter hot water for one or two days, it is important to use Stratification procedures as in the following:

- It must avoid the mixing of hot with cold water in storage tank.

- Ideally, the storage tank must have large length and small diameter.
- The ratio between the high to diameter for storage tank must be 2.5:1.

It must use insulator with very high quality, i.e, High insulation levels Losses of 1.08kWh/L/annum.

## 6. Results and Discussions

### 6.1. Evaluate The Daily Hot Water Demand Energy

The results of average daily of required energy for different volumes of hot water according to the consumers classification are shown in figure 3. The results showed that the average required energy to heat water with volume 200 liter to 60°C for (6-8) persons family is (12.24 kW/m<sup>2</sup>/day), whereas the required energy to heat the same quantity of water for needed season which about 270 day from September to May is (3300 kWh/m<sup>2</sup>/270day) when the thermal losses caused by energy storage was not take into account, but after the thermal losses enter to the calculations which about 216 kWh/m<sup>2</sup>/270day the overall required energy to heat 200 liter became 3500 kWh/m<sup>2</sup>/270day. The results also indicate that the maximum required energy to heat required water is 13 kWh/m<sup>2</sup>/270day at January because of the ambient temperature is minimum value at this month.

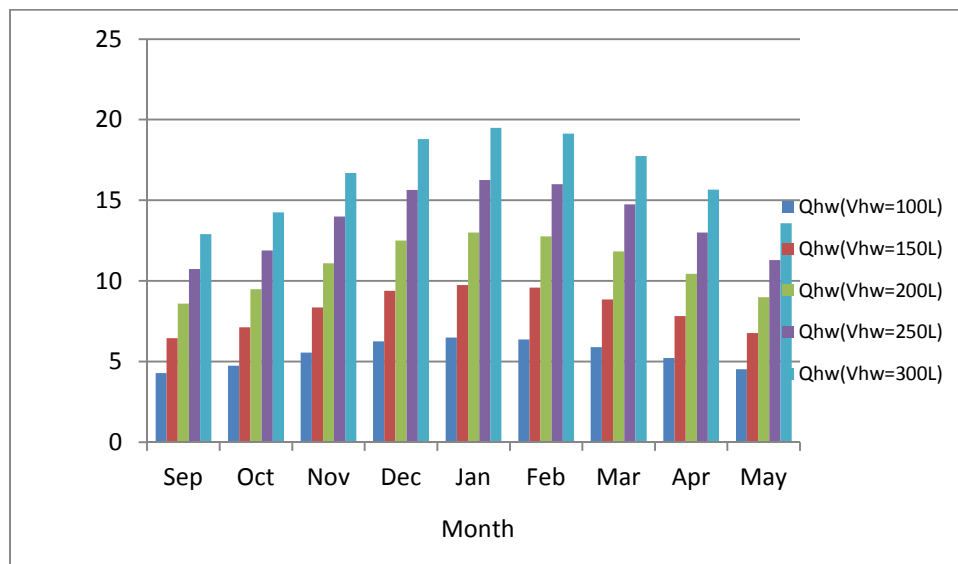


Figure (3): Average daily required energy for different volumes of hot water (kWh)

## 6.2. Required Area of Solar collector

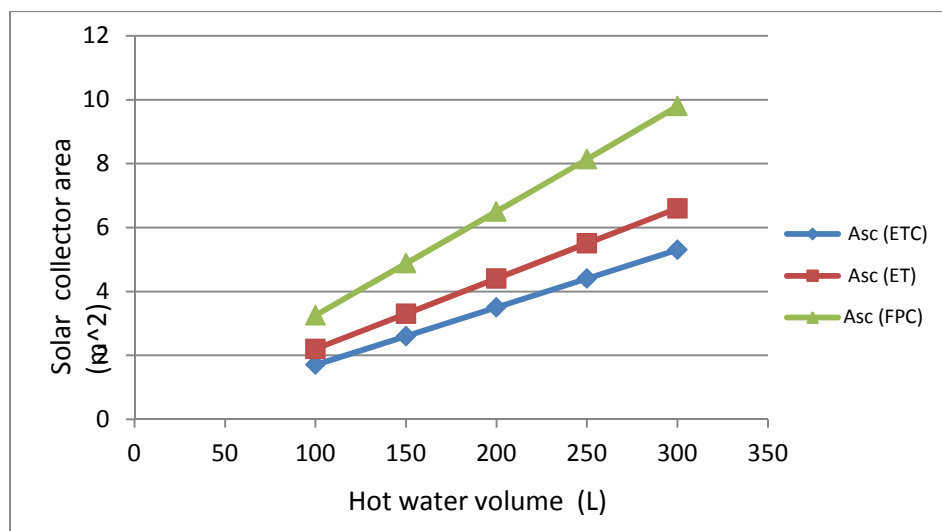
The results appears that the required solar collector area to cover the need of (6-8) persons family with volume of hot water 200 liter are 3.5 m<sup>2</sup> of Heat Pipe Evacuated Tube Solar Water Heater System, 4.4 m<sup>2</sup> of Evacuated Tube collector and 6.5 m<sup>2</sup> of Flat Plat Collectors according to the following calculations:

- Flat Plate:  $540\text{kWh/m}^2/\text{year} = 3500/540 = 6.5\text{m}^2$
- Evacuated Tube:  $800\text{kWh/m}^2/\text{year} = 3500/800 = 4.4\text{m}^2$
- Heat Pipe Evacuated Tube:  $1000\text{kWh/m}^2/\text{year} = 3500/1000 = 3.5\text{m}^2$ .

Other results of calculations are listed in table 3 and are shown in figure 4.

Table(3): Solar collector area calculated for different Iraqi families

| Consumer (person) | Hot Water Vol. L | Losses Energy kWh/yr. | Req. Energy kWh/yr. | Req. Energy kWh/yr. | Collector Area m <sup>2</sup> ETC | Collector Area m <sup>2</sup> ET | Collector Area m <sup>2</sup> FPC |
|-------------------|------------------|-----------------------|---------------------|---------------------|-----------------------------------|----------------------------------|-----------------------------------|
| 2-4               | 100              | 108                   | 1650                | 1760                | 1.7                               | 2.2                              | 3.25                              |
| 4-6               | 150              | 162                   | 2480                | 2640                | 2.6                               | 3.3                              | 4.88                              |
| 6-8               | 200              | 216                   | 3300                | 3500                | 3.5                               | 4.4                              | 6.5                               |
| 8-10              | 250              | 270                   | 4140                | 4400                | 4.4                               | 5.5                              | 8.14                              |
| 10-12             | 300              | 324                   | 5000                | 5300                | 5.3                               | 6.6                              | 9.8                               |



figure(4): Required solar collector area calculated for three types with different Iraqi families

### 6.3. Storage Losses

depending on the area of required solar collector and the average daily of solar radiation that incident on Baghdad, the resulted thermal energy from solar energy was calculated. The results indicate that this energy was agreement with required thermal energy for heat process. Table 4 demonstrate the average daily solar energy resulted from solar collector by using Heat Pipe Evacuated Tube Solar Water Heater.

Table(4): Collected solar energy for different Iraqi families by using Heat Pipe Evacuated Tube Solar Water Heater.

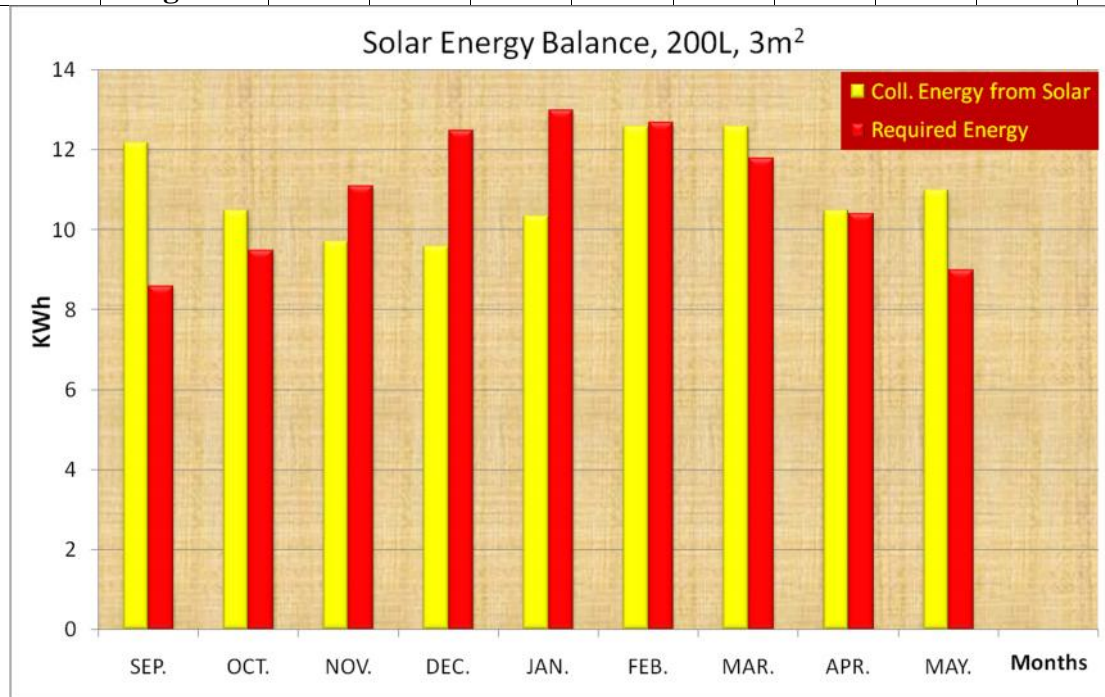
| Area(m <sup>2</sup> ) | Sep       | Oct       | Nov       | Dec       | Jan       | Feb       | Mar       | Apr       | May       | Annual (kWh/yr.) |
|-----------------------|-----------|-----------|-----------|-----------|-----------|-----------|-----------|-----------|-----------|------------------|
| 1.7                   | 6.9       | 5.95      | 5.5       | 5.4       | 5.86      | 7.14      | 7.14      | 5.95      | 6.18      | 1680             |
| 2.6                   | 10.5<br>5 | 9.1       | 8.42      | 8.3       | 9         | 10.9<br>2 | 10.9<br>2 | 9.1       | 9.46      | 2575             |
| 3.5                   | 14.2      | 12.2<br>5 | 11.3<br>4 | 11.1<br>5 | 12        | 14.7      | 14.7      | 12.2<br>5 | 12.7<br>4 | 3460             |
| 4.4                   | 17.8<br>6 | 15.4      | 14.2<br>5 | 14        | 15.1<br>8 | 18.5      | 18.5      | 15.4      | 16        | 4350             |
| 5.3                   | 21.5      | 18.5<br>5 | 17.1<br>7 | 16.9      | 18.3      | 22.2<br>6 | 22.2<br>6 | 18.5<br>5 | 19.3      | 5240             |

### 6.4. Solar energy balance

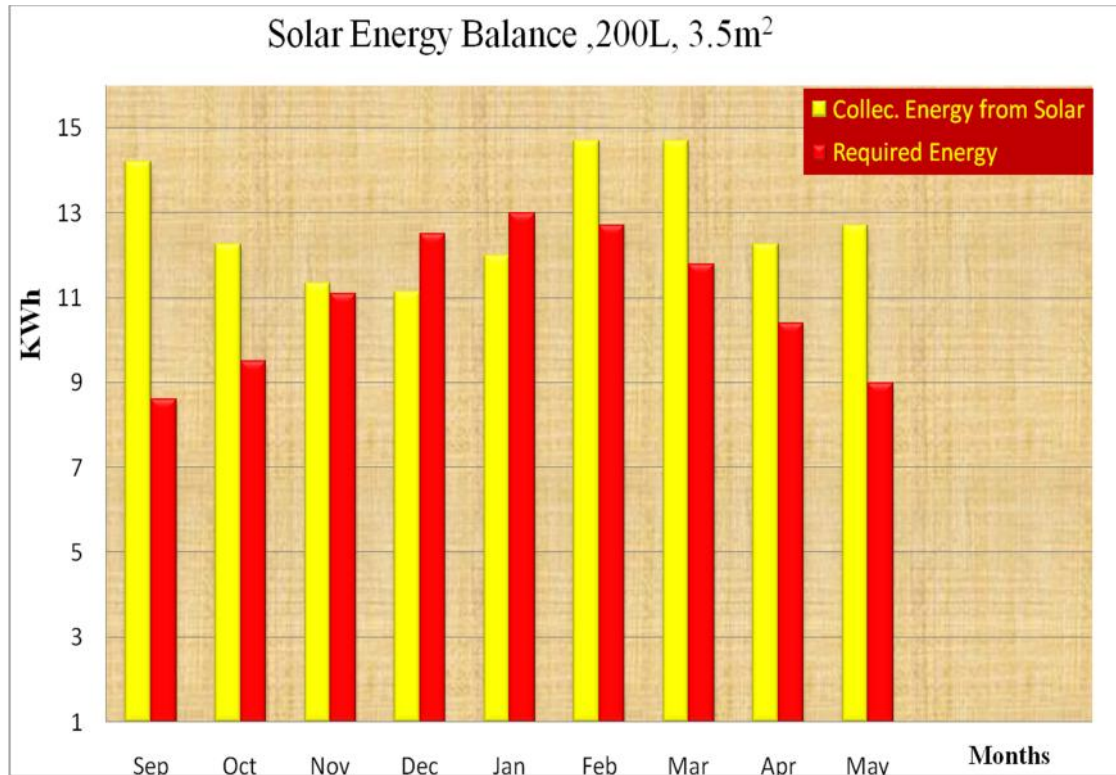
Table 5 displays the results of solar energy balance for solar water heater with area 3, 3.5 and 4 m<sup>2</sup> to heat 200 liter water and figures 5, 6 and 7 shows these results respectively. This research depend on the group that contain (6-8) persons because of most of Iraqi families consist of this number of persons, therefore the calculations concentrate on this group of families. The results indicate that the collected energy by 3m<sup>2</sup> heat pipe evacuated tube solar collector is more than the required energy in September, October, March, April and May. While it is less than in November, December, January and February which lead to shortage at these months. In the 3.5m<sup>2</sup> collector there is shortage only at January and December , but there is no shortage when the area of solar collector is 4m<sup>2</sup>.

Table(5): Solar energy balance for solar heater area with efficiency 70% and 200 liter water

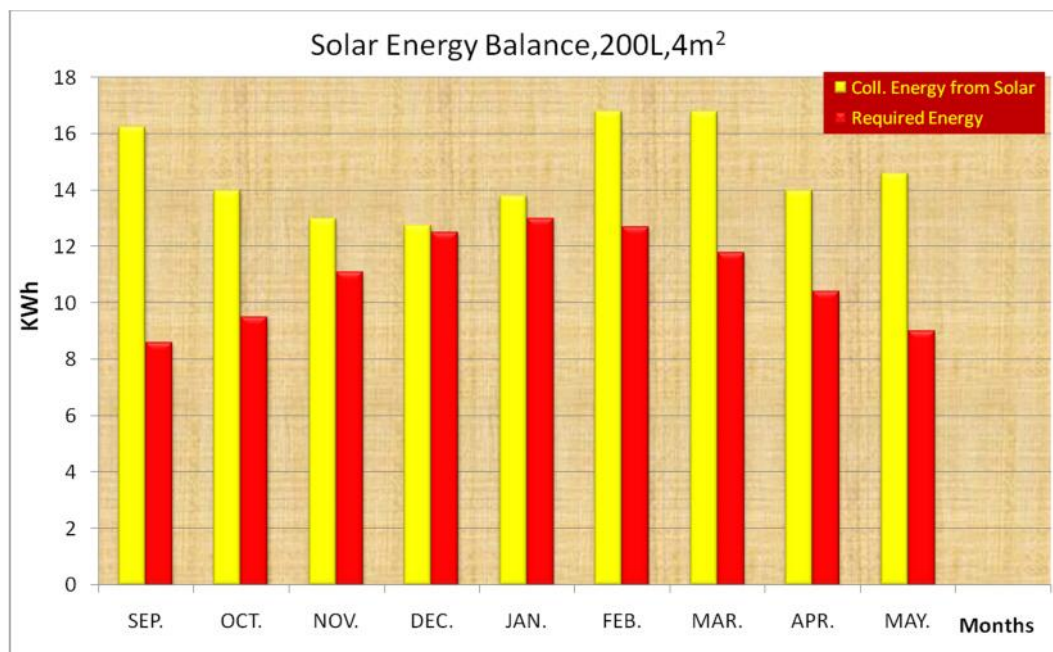
| Area of collector s |                    | Sep   | Oct   | Nov   | Dec   | Jan   | Feb   | Mar   | Apr   | May   |
|---------------------|--------------------|-------|-------|-------|-------|-------|-------|-------|-------|-------|
| 3.0m <sup>2</sup>   | Req.Eg. KWh        | 8.6   | 9.5   | 11.1  | 12.5  | 13.0  | 12.76 | 11.83 | 10.44 | 9.0   |
|                     | Eg.Coll.by SE. KWh | 12.18 | 10.5  | 9.7   | 9.6   | 10.35 | 12.6  | 12.6  | 10.5  | 11    |
|                     | Saving Eg. %       | 142 % | 111 % | 87%   | 77%   | 80%   | 99%   | 106 % | 101 % | 122 % |
| 3.5m <sup>2</sup>   | Req.Eg. KWh        | 8.6   | 9.5   | 11.1  | 12.5  | 13.0  | 12.76 | 11.83 | 10.44 | 9.0   |
|                     | Eg.Coll.by SE. KWh | 14.2  | 12.25 | 11.34 | 11.15 | 12    | 14.7  | 14.7  | 12.25 | 12.74 |
|                     | Saving Eg. %       | 165 % | 129 % | 102 % | 89%   | 92%   | 115 % | 124 % | 117 % | 142 % |
| 4.0m <sup>2</sup>   | Req.Eg. KWh        | 8.6   | 9.5   | 11.1  | 12.5  | 13.0  | 12.76 | 11.83 | 10.44 | 9.0   |
|                     | Eg.Coll.by SE. KWh | 16.24 | 14    | 13    | 12.75 | 13.8  | 16.8  | 16.8  | 14    | 14.6  |
|                     | Saving Eg. %       | 189 % | 147 % | 117 % | 102 % | 106 % | 132 % | 142 % | 134 % | 162 % |



Figure(5): Solar energy balance for solar heater with area 3.5 m<sup>2</sup>



Figure(6): Solar energy balance for solar heater with area 3.5 m<sup>2</sup>



Figure(7): Solar energy balance for solar heater with area 4 m<sup>2</sup>

## **6.5. Electrical Energy Saving**

The conversion efficiency of electrical energy to thermal energy is 100% and the cost of electrical energy production by classical methods (use of fossil fuels) is about 10 cent/kWh, therefore:

- ❖ Cost Saving = Displaced energy x cost per Unit.
- ❖ Electricity = 3500 kWh/year x 0.1\$/kWh = 350\$ per year.
- ❖ 3.5m<sup>2</sup> cost approx. 750\$ installed.
- ❖ Annual Saving: 350\$/year.
- ❖ Payback: 2.2 Years.

## **7. Conclusions**

1. Insert 3000000 solar water heater for three million consumers in the electrical system distribution in the residential sector and 1000000 consumer in the government sector lead to save the consumption of electrical energy load about 2000 MW.
2. Saving of 1.2 billion dollars each year by work these solar systems, when the cost of electrical energy production is about 0.1\$/kWh.
3. Insert 300000 solar water heater for three hundred thousand consumers in the electrical system distribution in the residential sector and the government sector lead to save the consumption of electrical energy load about 120 MW.
4. It may be return the cost of all solar heaters at the period of about 26 months.

## **References**

1. Nicolas S. E., "**Asphalt Solar Collector and Borehole Storage Design study for a small residential building area**", M.Sc. thesis, Department of Energy and Environment, Chalmers University of Technology, Sweden, 2010.
2. KEY WORLD ENERGY STATISTICS 2010. International Energy Agency. Pdf file (<http://www.iea.org>).
3. DIERET - Distance Internet Education on Renewable Energy Technologies. INFORSE. 2005,CD version.
4. United Nations Framework Convention on Climate Change: <http://unfccc.int>.
5. REN21 Renewable Energy Policy Network. —Renewables 2005-2009 Global Status Reports.Washington, DC: Worldwatch Institute. [www.ren21.net](http://www.ren21.net).
6. Hamza, MSc. Thesis, "**Evaluation the performance of Evacuated tube solar water heating system**" Baghdad University, college of Engineering, Mechanical Engineering Department, 2009.

7. Goswami , D. Yogi, "**Advances in Solar Energy**" 2<sup>nd</sup> An Annual Review of Research and Development, Vol. 17, American Solar Energy Society, University of South Florida USA, 2007.
8. William B. S. and Michael G., "**Power from the Sun**", J.T.Lyle Center for Regenerative Studies, 2001.
9. NASA, "**Surface Meteorology and Solar Energy – Available Table**" Atmospheric science Data Center, 2008.
10. Nasa Research Center "**Measuring Solar Radiation Incident on Earth**" STS-107, Space Research and you, NP288-HQ, http, 2002.
11. Siddharth A., Shobhit C., Udayakumar R. and Muhammad A., "**Thermal analysis of evacuated solar tube collectors**", Journal of Petroleum and Gas Engineering Vol. 2(4), pp. 74-82, April 2011.
12. Ruchi S., Sumathy K., Samee U. K., " **Performance Improvement of a Heat Pump Assisted Solar Water Heating System**", International Conference on Renewable Energies and Power Quality (ICREPQ'12), 2012.
13. SOLAVIS, "**Flat Plate Collectors v. Evacuated Tubes – A brief Overview**" www.solavis.com.au, 2008.
14. "A World Leader in Solar Thermal Collectors Technical Design Guide", Thermomax Ltd. Company, 107-06/D, 2006.
15. Weather underground.com, History for Baghdad Iraq.
16. US Army Corps of Engineering, "**Central Solar Hot Water Systems Design Guide** ", 2011.

## Thermal Design and Analysis of Printed Circuit Board for Optimum Performance

Emad Q. Hussein<sup>\*</sup>, Kareem K. Jasim<sup>\*\*</sup>, Sabah A. Gitaffa<sup>\*\*\*</sup>

<sup>\*</sup> Mechanical Engineering Department, University of Kerbala  
<sup>\*\*</sup> Energy and Renewable Energies Technology, University of Technology  
<sup>\*\*\*</sup> Electrical Engineering Department, University of Technology

### Abstract

This paper deals with the thermal Analysis and design of printed circuit board PCB, to calculate the thermal effects generated by components on the board. In this paper we graphically evaluate the temperature distribution on a proposed PCB, at steady state thermal condition. The analysis done with the parameters set to appropriate real values. This paper covers common causes of thermal problems on a PCB and how to address those problems quickly and effectively using the PCB thermal analysis capabilities and Optimize PCB thermal design by doing thermal analysis and simulation early in proposed your design. In the present work, computational procedures together with a computer program are established to calculate the results of the computations include:

- Increasing of Nusselt number at different locations from board edge with increased air velocity.
- Decreasing the value of convection heat transfer coefficient at start of edge board.
- Thermal resistance of convection is decreased with increasing of convection heat transfer coefficient.

Temperature of component is proportional with air velocity increased because of increasing heat transfer coefficient.

### Keywords

Thermal design of PCB, Heat transfer, Thermal analysis, Nusselt number

### خلاصة

هذا البحث يتعامل مع التحليل الحراري وتصميم لوحة الدوائر المطبوعة PCB لحساب التأثير الحراري المتولد على اجزاء اللوحة. حيث تم تقييم البيانات وتوزيع درجة الحرارة على اللوحة في حالة الاستقرار الحراري مع الأخذ بنظر الاعتبار قيم تقريبية حقيقية. في هذا البحث تغطي الأسباب الشائعة للمشاكل الحرارية على لوحة PCB وكيفية معالجة هذه المشاكل بشكل سريع وفعال وذلك باستخدام قابلية التحليل الحراري للوحة والتصميم الحراري الامثل عن طريق المحاكات في وقت مبكر من التصميم المقترح. في العمل الحالي تم اجراء الحسابات جنباً الى جنب مع برنامج حسابي انشئ وكانت النتائج كما يلي :-

- زيادة رقم نسلت في مواقع مختلفة عن حافة اللوحة مع زيادة سرعة الهواء.
- انخفاض قيمة معامل انتقال الحرارة بالحمل في بداية حافة اللوحة.
- انخفاض المقاومة الحرارية مع زيادة معامل الحمل الحراري. انخفاض درجة الحرارة الاجزاء مع زيادة سرعة الهواء بسبب زيادة معامل الحمل الحراري.

## List of symbols

- $A_1$  Exposed surface area of the component  
 $A_2$  Effective area of the component  
 $a$  Flow area over the PCB less component obstructions  
 $b$  Component length (streamwise)  
 $C_p$  Specific heat of air  
 $d$  Component width  
 $e$  Height that the component protrudes from the PCB  
 $F$  Flow rate of the air  
 $H_F$  Height of the flow channel above the PCB  
 $h$  Heat transfer coefficient  
 $k_b$  Thermal conductivity of the board without copper  
 $k_a$  Thermal conductivity of air  
 $k_c$  Thermal conductivity of the copper  
 $k_l$  Thermal conductivity of the leads  
 $L$  Length of the leads.  
 $M$  Number of components perpendicular to the flow direction  
 $N$  Number of components in the flow direction  
 $n$  Number of leads per component  
 $q$  Heat load on the component  
 $Q_t$  Total heat dissipated upstream of the component  
 $\rho$  Density of the fluid  
 $R$  Thermal resistance of the component to air  
 $R_i$  Interface resistance between the component and the PCB  
 $r_c$  Resistance across the air gap del  
 $r_l$  Lead resistance between the case and the PCB  
 $T_l$  Local air temperature  
 $T_a$  Ambient air temperature  
 $u$  Velocity of air  
PCB Printed circuit board

## 1. Introduction

Printed circuit board (PCB) is a board made from an insulating, non-conductive material that has conductive metal tracks (electronic interconnects) called races as shown in Fig. (1). Integrated circuits and components are soldered to the board, and the metal traces between terminals connect the various devices and components [1].

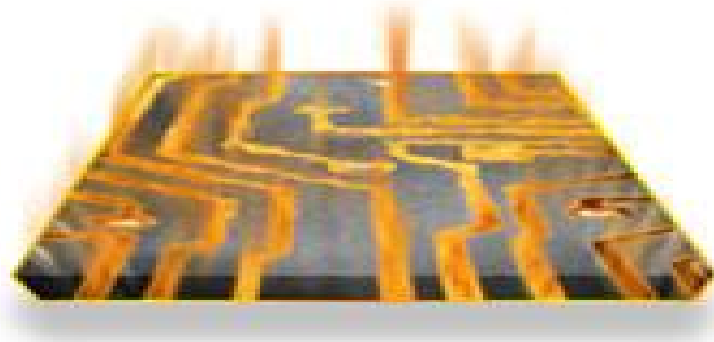


Fig. (1) Printed circuit board with metal tracks

Conjugate conduction – convection heat transfer is becoming a very active field due to variety of its industrial applications, such as the cooling of electronic equipment. In the electronics industry, engineers are looking for the best ways to cool their electronic packages, which may be as small as a printed board assembly or as big as a "rack", which is a system composed of many printed board assemblies. However, efficient cooling cannot be achieved without understanding the heat transfer from each specific package and determining the flow and thermal fields [2]. However, today's more complex and smaller device dimensions along with closer packing result in higher heat density and elevated operating temperatures. Higher operating temperatures decrease the service life of the device or module. Any temperature sensitive materials used in a module can degrade and wear out more quickly. Other failure mechanisms, such as metal migration, can occur, particularly when both high temperature and humidity conditions are present. Here, metal whiskers or dendrites can grow from the conducting lines. With lines being spaced closer together in today's devices, shorts between lines can occur and cause device failure. Additionally, when temperatures fluctuate, device interconnections and other components can fatigue from expansion and contractions due to thermal stress and eventually fail [3]. Higher temperatures also increase the electrical resistance of the conducting lines within a device or module, slowing the signal speed and reducing performance. As devices become more complex, conducting paths become longer and this performance reduction is more significant. For all of the above reasons, it's critical to minimize temperature of the electronics by designing efficient ways of carrying away their generated heat [4,5]. The more significant factors effect on cooling of printed circuit board are; heat source distribution from PCB, thermal conductivity of the PCB plate, size of the PCB, and radiation heat transfer between two surfaces is proportional to the fourth power of temperature [6,7].

## 2. Thermal Simulation Tools

The basic kinds of thermal modeling and analysis tools include the following; general purpose tools for analyzing any kind of structure, computational fluid dynamics (CFD) tools for system flow/heat transfer analysis, and PCB application specific tools for detailed PCB

and component modeling [8]. Some components on a PCB will generate little heat, others a great deal; a CPU in a PC can generate up to 100W! In addition to any internally generated heat, the temperature experienced by any part of a PCB will be affected by

- heat generated by other components on the board
- heat generated by neighbouring equipment
- absorption of sunlight by the equipment casing
- heat associated with the surroundings.

If this heat is not removed, devices will become hotter, and their behavior may change significantly, so that the circuit no longer behaves in the way it was designed to, and may even fail. Also, whilst high temperatures themselves can be damaging, repeated operational variations cause thermally-induced mechanical stresses which can be even more harmful. Such 'thermal cycling' may be quite severe, even in everyday applications. For example, circuitry housed near the engine of a car experiences both the high temperatures developed by the engine when the car is being driven, and rapid cooling when the engine is switched off. But repetitive thermal cycling occurs in all electronic devices to some extent; even a desktop PC is stressed every time it is switched on for a period and then turned [9].

### 3. Theoretical Model

This study calculates the average heat transfer dissipation pressure drops and cooling efficiency for PC Board in free stream flow, with isothermal ( constant temperature ) components, here the heat is evenly distributed throughout the component. The power levels of all components are assumed equal. The component temperature calculated is the mean case temperature. For purposes of reliability assessment, the junction temperature is of greater interest. This is largely controlled by the components internal structure, the manufacturer's internal resistance values can be used for further thermal analysis under most circumstances.

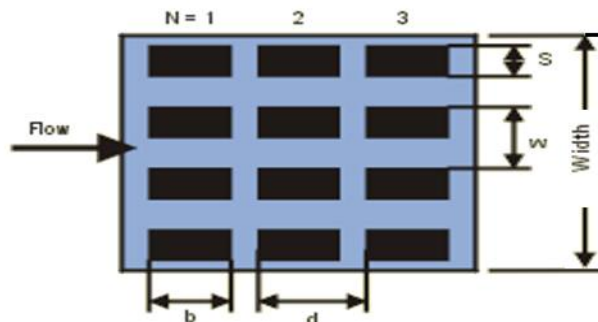


Fig.(2) Physical domain for PCB

For this analysis, the conductance should be less than  $0.03 \text{ W/}^{\circ}\text{C}$  [5]. In this model each component and the surrounding PCB area is treated in isolation, the PCB area being the rectangle formed cutting midway between components. It is then assumed that, the heat is dissipated by this isolated component and area of PCB is equal to the component power. The heat path is by convection from the exposed surfaces and conduction through the leads and stand-off gap into the PCB [7]. The component temperature  $T_c$  can be written as,

$$T_c = T_l + q * R \quad (1)$$

And the local air temperature  $T_l$  can be evaluated from,

$$T_l = T_a + \frac{Q_t}{F * \rho * C_p} \quad (2)$$

The total heat dissipated upstream from the component is calculated as:

$$Q_t = q * M * (N - 1) \quad (3)$$

The flow rate of air ,  $F$  over the PCB can be evaluated from,

$$F = u * (N_b * a) \quad (4)$$

Where,  $a$  is the flow area over the PCB , is given by

$$a = W_b * H_F - (M * S * e) \quad (5)$$

The thermal resistance of the component to air can be written as

$$R = 1 / (h * A_1 + \frac{1}{(R_i + \frac{1}{A_2 * h})}) \quad (6)$$

Where,  $A_1$  is the exposed surface area, is given by

$$A_1 = S * b * 2e(S + b) \quad (7)$$

The area between the component and PCB is not included in this area because the generally small distance between component and PCB inhibits convection. The leads generally inhibit convection from the sides of the chip, therefore the stand-off gap is included in the effective depth package. The thermal interface resistance  $R_i$  can be calculated as [8,9],

$$R_i = \frac{1}{\left(\frac{1}{r_c}\right) + \left(\frac{1}{r_l}\right)} \quad (8)$$

Where ;

$$r_c = \text{del} / (k_a * S * b)$$

$$r_l = L / (k_l * n * A_l)$$

Where, **del** refers to the air gap between the component and the PCB, the rectangles **d \* w** of the PCB are not isothermal and ,therefore the effective area of the component  $A_2$  is calculated as,

$$A_2 = 2(d' * w') - S * b \quad (9)$$

Where;

$$d' = E_2 * d + b(1 - E_2)$$

$$w' = E_1 * w + S(1 - E_1)$$

Where;  $E_1$  and  $E_2$  are the two PCB fin efficiencies in the lateral and stream wise directions respectively. These are calculated as follows,

$$E_1 = \frac{\tanh M_1}{M_1} \quad (10)$$

$$E_2 = \frac{\tanh M_2}{M_2} \quad (11)$$

Where;

$$M_1 = \left( \frac{w - S}{2} \right) * (2h/C_1)^{0.5}$$

$$M_2 = \left( \frac{d - b}{2} \right) * (2h/C_2)^{0.5}$$

Where;  $C_1$  and  $C_2$  are the conductance's of the PC Board in the lateral and stream wise directions respectively, both conductance's are calculated the same way. The conductance of the PC Board is given by,

$$C_1 = k_b * t + k_c * \phi_1 \quad (12)$$

$$C_2 = k_b * t + k_c * \phi_2 \quad (13)$$

Where,  $\phi_1$  and  $\phi_2$  are the ratios of the volume of copper on the PC Board in the direction of interest per unit plan area of PCB (lateral and stream wise), depending on flow velocity  $u$ . The heat transfer coefficient,  $h$  is evaluated by using Will's Correlation[9], when the flow velocity is between 0.2 and 8.0 m/s;

$$h = 5.3 \frac{b}{a} + G \frac{(\rho * u)^{0.8}}{(N * d)^{0.36}} \left( \frac{d}{b} - 1 \right)^{0.13} \quad (14)$$

Where;  $G$  is equal to 6.2 when no card guides are used at the PCB leading edges, and 7.6 when card guides are not used.

#### 4. Simulation and Results

The program for analysis is developed to obtain numerical solution of the thermal analysis of PCB. The following data are considered numerical values for the model parameters are taken from [10], and tabulated in Tables (1, 2, and 3).

**Table 1. PC Board properties**

| Description                                         | Symbol                                  | Value      | Units                          |
|-----------------------------------------------------|-----------------------------------------|------------|--------------------------------|
| Width of PCB (lateral to flow)                      | $\frac{b}{w_b}$                         | 0.250      | m                              |
| Height of flow channel above PCB                    | $\frac{w_b}{H_F}$                       | 0.017      | m                              |
| Conductivity of the board (no copper)               | $\frac{w_b}{H_F k_b}$                   | 0.294      | W/m.°C                         |
| Thickness of the board                              | $\frac{t}{t_b}$                         | 0.0016     | m                              |
| Volume of copper per area of PCB (lateral to flow)  | $\frac{h}{p \cdot i_1}$                 | 0.00000722 | m <sup>3</sup> /m <sup>2</sup> |
| Volume of copper per area of PCB (parallel to flow) | $\frac{h \cdot i_1}{p \cdot i_2}$       | 0.00000444 | m <sup>3</sup> /m <sup>2</sup> |
| Conductivity of the PCB copper                      | $\frac{H_F \cdot i_1}{h \cdot i_2 k_c}$ | 360        | W/m.°C                         |

**Table 2. Component properties**

| description                             | Symbol                 | Value      | Units          |
|-----------------------------------------|------------------------|------------|----------------|
| Number of components (parallel to flow) | $N$                    | 10         | None           |
| Length (parallel to flow)               | $b$                    | 0.030      | m              |
| Pitch (parallel to flow)                | $d$                    | 0.033      | m              |
| Number of components (lateral to flow)  | $M$                    | 8          | None           |
| Width (lateral to flow)                 | $S$                    | 0.015      | m              |
| Height (protruding into flow)           | $e$                    | 0.004      | m              |
| Heat Load per component                 | $q$                    | 0.5        | W              |
| Air gap between PCB and component       | $del$                  | 0.000257   | m              |
| Number of leads per component           | $n$                    | 16         | None           |
| Length of leads                         | $L$                    | 0.001      | m              |
| Cross-sectional area of one lead        | $\frac{A}{A_L}$        | 0.00000025 | m <sup>2</sup> |
| Thermal conductivity of leads           | $\frac{L}{A_L k_{el}}$ | 287.0      | W/m.°C         |

**Table 3. Air flow properties**

| Description                                            | Symbol                 | Value   | Units             |
|--------------------------------------------------------|------------------------|---------|-------------------|
| Ambient temperature (at entrance)                      | $\frac{t_a}{T_a}$      | 25      | °C                |
| Average flow velocity in free flow area between boards | $\frac{nbol}{t_a u}$   | 0.5~2.5 | m/s               |
| Thermal conductivity of air                            | $\frac{t}{t_a k_{ca}}$ | 0.028   | W/m.°C            |
| pecific heat of air                                    | $\frac{u}{k_{ca} C_p}$ | 1006    | J/kg.°C           |
| Air density                                            | $\rho$                 | 1.2     | kg/m <sup>3</sup> |

The analysis done with the parameter set to appropriate real values. The following results are obtained:

1. The behavior of the Nusselt number with distance from board edge at different values of velocity of air is shown in Fig. (3). This figure shows that, the Nusselt number proportional with distance from board edge, due to increase velocity of air.
2. Fig.(4) shows the relation between the convection heat transfer coefficient with distance from board edge at varying velocity of air. It shows that, the heat transfer coefficient decreases with distance from the edge of the board until to reach approximate constant value.
3. The behavior of overall thermal resistance at different location from board edge as shown in Fig. (5).The graph shows that the overall thermal resistance proportional with decreases heat transfer coefficient at the same location on the board.
4. The variation of the component temperature at different locations from board edge at velocity of air is shown in Fig. (6).This figure shows that, the temperature of component inversely proportional with air velocity increases, due to increase heat transfer coefficient.

## 5. Conclusion

In the present work, a computational procedure together with a computer program are established, the following are the main conclusions obtained from the present research;

- The Nusselt number will increase when locations becomes far from board edge, also with increase air velocity.
- Approaching boundary (edge board), the value of convection heat transfer coefficient would decrease.
- The overall thermal resistance is proportional with increasing heat transfer coefficient at different value of velocity of air.
- The temperature of component is inversely proportional with air velocity increase, due to increase convection heat transfer coefficient.

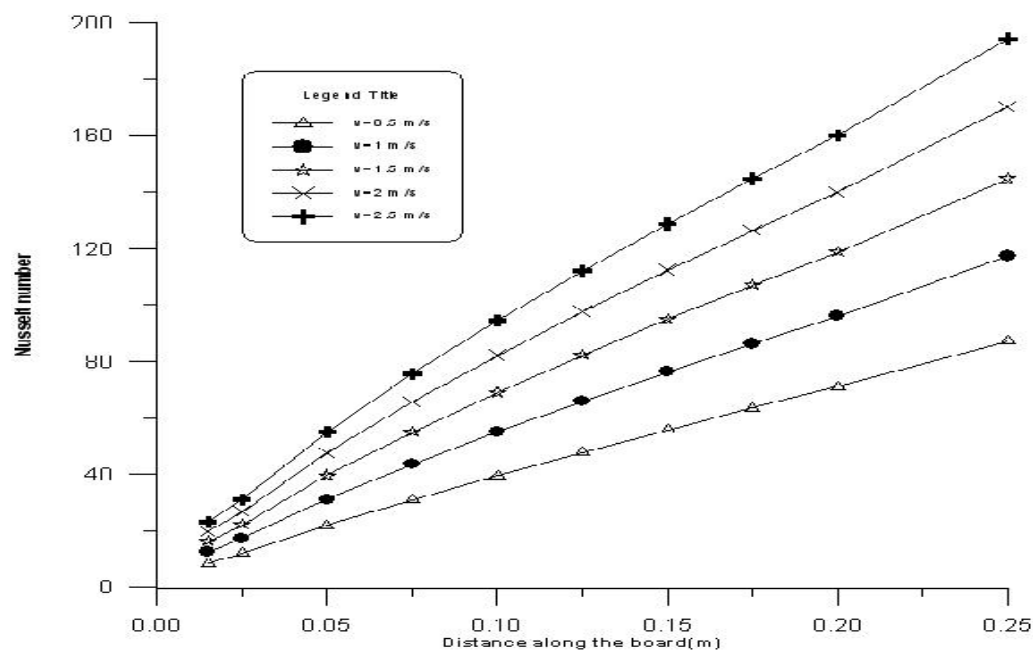


Fig. (2) Variation of Nusselt number along different distance from the edge of the board

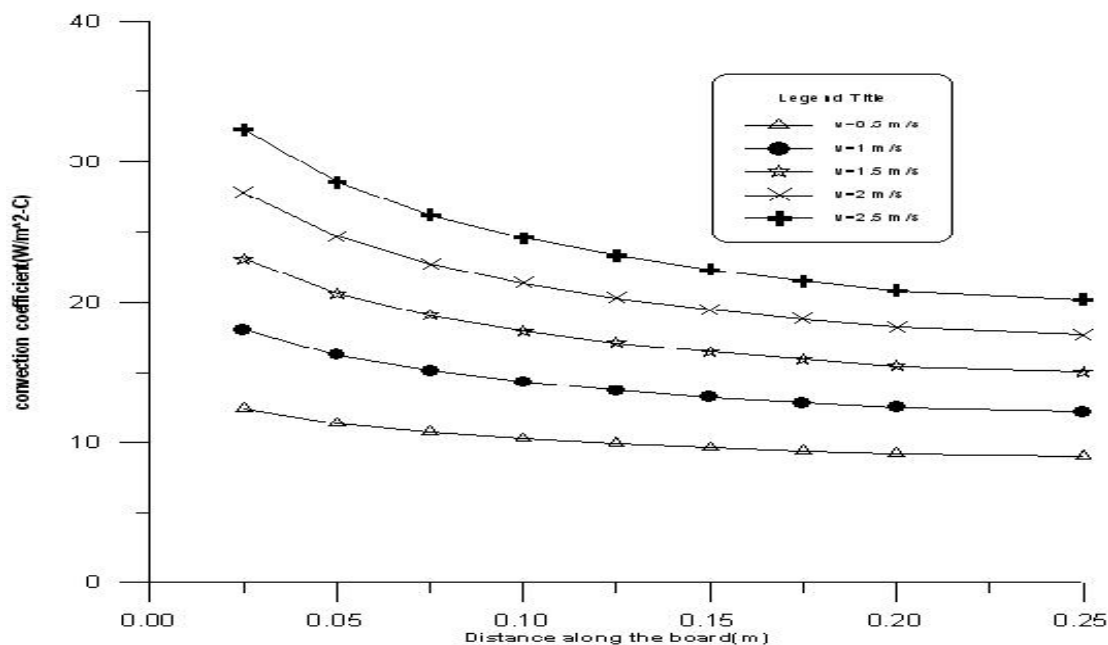


Fig. (3) Variation of convection heat transfer coefficient along different distance from the edge of the board.

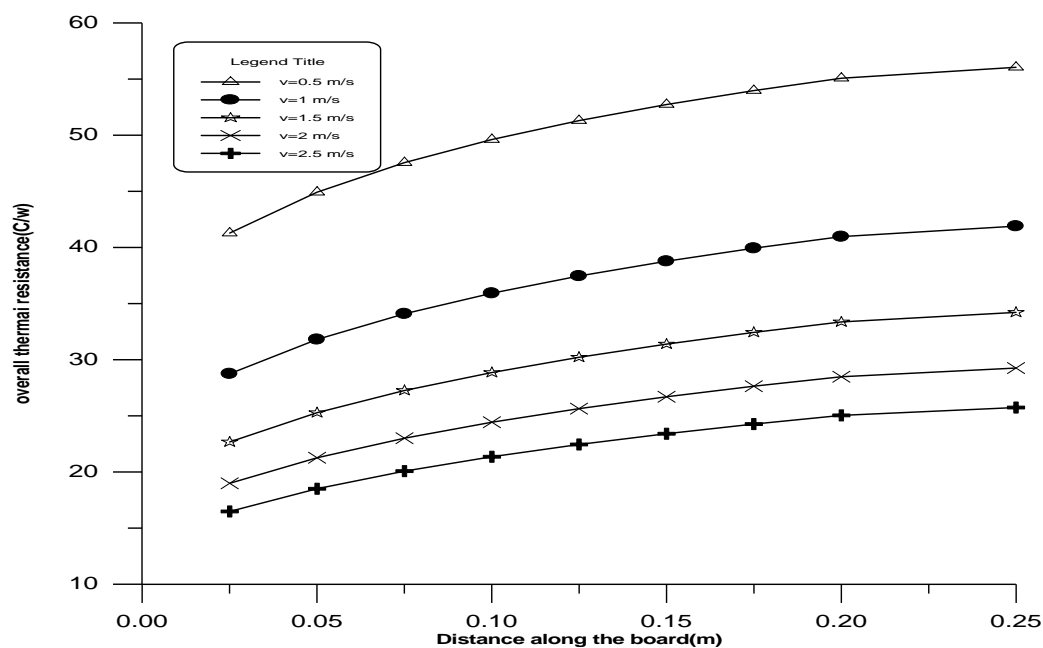


Fig. (4) The variation of overall thermal resistance along different distance from the edge of the board.

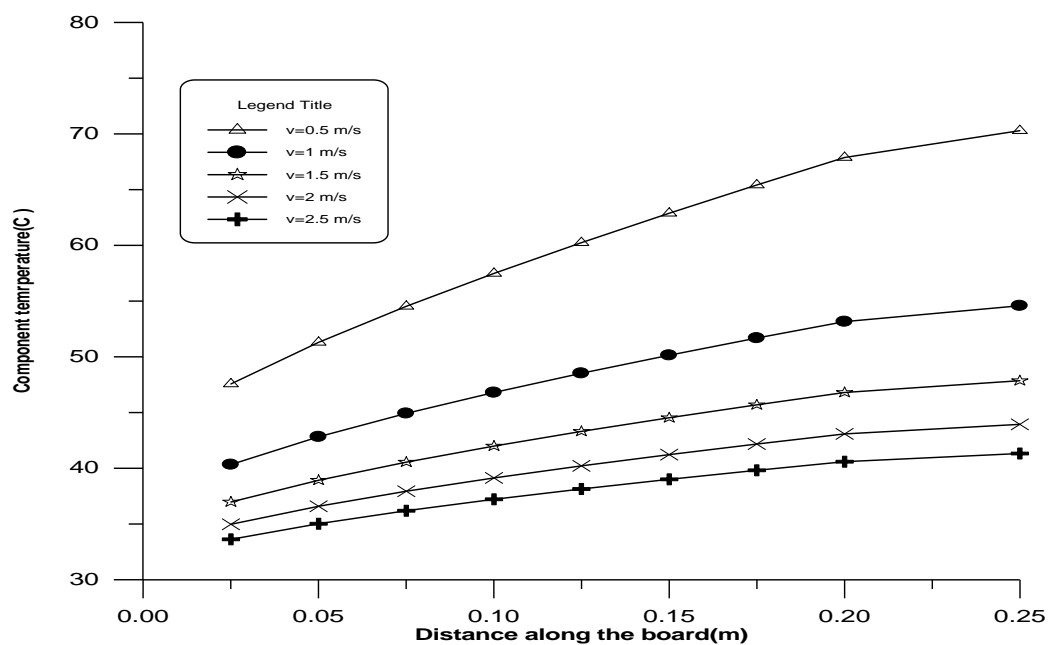


Fig. (5) Variation of component temperature along different distance from the edge of board.

## References:

- [1] Electronic Production“ Thermal Analysis of Air Cooled PCB's ”, Parts 1-4, May - August 1983.
- [2] C. Simpson, “ The Fundamental of Thermal Design ” Electronic Design, pp. 95–100, September ,1991.
- [3] Courtney R. Furnival “ Thermal and High Current Multilayer Printed Circuit Boards With Thermion T-lam and Hybrid Boards” January 2001.
- [4] M.Afrid and A Zebib ” Natural Convection Air Cooling of Heated Components Mounted on A Vertical Wall” May, 2001.
- [5] Rajaram, Dr. S.” Thermal Design of Electronic Equipment for Reliability & Performance” AT&T Bell Laboratories, Whippany USA. p 20 – 42,2006.
- [6] Eric Madsen, Ansoft Corporation “ PCB Thermal Analysis Power Dissipations and Thermal Boundary Conditions” Issue of Printed Circuit Design Magazine, February 2001.
- [7] Huang Chunyue“ Thermal Fatigue Life Analysis and Forecast of PBGA Solder Joints on the Flexible PCB Based on Finite Element Analysis” International Conference Shanghai, July 2008.
- [8] David S. Steinberg “Cooling Techniques for Electronic Equipment” Text book 2008.
- [9] Dave Steinberg” Preventing Thermal Cycling and Vibration Failures in Electronic Equipment” Text Book 2010.
- [10] Charles A. Harper” Electronic materials and processes handbook ” Mc Graw-Hill, ISBN 0-07-140214-4, 2003.

## Optimum Tilted Angle Of Photovoltaic Cell located in northern Iraq Cities to get maximum generated electric power

Ali Khalid Shaker Al-Sayyab and Maher Kadhim Taher

Refrigeration and Air Conditioning Department, Basra Technical College, Foundation of Technical Education

### ABSTRACT:

Photovoltaic cell need to be inclined at the optimum angle to maximize the receiving solar energy then maximize the out but electric power . In this study, the collector surface is assumed to be facing toward south, solar global radiation on a tilted surface was estimated using a mathematical model which programed in engineering equation solver EES program to find an optimum tilted angle depending on the maximum solar radiation.

In this work find an optimum tilted angle of photovoltaic cell located in Arbil city (latitude  $36^{\circ} 15''$ ), Sulaymaniyah city ( $35^{\circ} 35''$ ), Dahuk ( $36^{\circ} 50''$ ) and Kirkuk ( $35^{\circ} 30''$ ) which are taken as northern Iraq cities only, the tilted angle varied with range from  $0^{\circ}$  to  $90^{\circ}$ . The results show the optimum tilted angle of of Arbil city is  $34^{\circ}$ , Dahuk city is  $34^{\circ}$ , for Sulaymaniyah city is  $33^{\circ}$  and for Kirkuk city is  $33^{\circ}$ . And these cities are nearly in optimum tilted angle due to nearly in latitude.

### الخلاصة:-

يتطلب اماله الخلية الضوئية بزوايه ميل مثلى لتحقيق أقصى قدر من الطاقة الشمسية المستقبلية ,بالتالي تحقيق أقصى قدر من القدرة الكهربائية المولدة. في هذه الدراسة، افترض توجيه الخلية نحو الجنوب، وقدرت كميه الاشعاع الشمسي على باستخدام النموذج الرياضي حيث تم برمجته في برنامج EES للعثور على زاوية مائلة الأمثل اعتمادا على

في هذا العمل تم ايجاد افضل زوايه ميلان لخلايا الضوئية التي تقع في مدينة اربيل (خط العرض  $36^{\circ} 15'$ ) مدينة السليمانية ( $35^{\circ} 35'$ )، دهوك ( $36^{\circ} 50'$ ) التي تؤخذ كمدن شمال العراق فقط، تم تغيير زوايه الميلان من  $0$  إلى  $90$  درجة. اظهرت النتائج ان زاوية الميلان الأمثل لمدينة اربيل هي  $34$  درجة، لمدينة دهوك هي  $34$  درجة، لمدينة السليمانية هي  $33$  و لمدينة كركوك هي  $33$  درجة. وهذه المدن هي متقاربة في زاوية الميلان الأمثل نظرا إلى تقاربها في خط العرض.

## 1- Introduction:-

The quest for clean, sustainable sources of energy is becoming more popular with the concerns over global warming. Scientific communities have determined that carbon dioxide emissions from the use of fossil fuels, contribute to the greenhouse effect. In Iraq the most electric power is generated by using thermal power plant that use fossil fuel to generate steam which required for its permanency to generate electric power, since more carbon dioxide emissions from burning fossil fuel. For there more the electric power that generated by these plant is not sufficient for population requirements. There for must be found an alternative electric source friendly to the climate have no greenhouse effect, Over the past decade, increasing awareness of climate change hazards and energy security considerations has forced the global community to focus on renewable energy sources.

Solar energy is a clean, virtually inexhaustible source of heat and energy unlimited and harnessing for heat and electricity produces no air or water pollution. The use of solar energy technologies can only help our environment by decreasing CO<sub>2</sub> emissions and reducing drain-off pollution from fossil fuel power plants.

Solar technology applications function efficiently at ambient temperatures and pressures, create no noise, limit pollution through available disposal and recycling programs for dead battery systems and solar panels, and can be installed in a modular manner. Besides these advantages Furthermore, quality and longevity of photovoltaic devices and systems, and profitable lifecycle features of whole photovoltaic systems. Photovoltaic cells are the one of common type of the form of solar energy using, which convert solar radiation into electricity. The performance of the Photovoltaic cells is highly dependent on its orientation, cell tilted angle, optical and geometric properties, macro and microclimatic conditions, geographical position, and the period of use (Ashok Kumar,2011).

And to maximize the power generated by this plant many steady where adopted to obtained the optimum tilted angle and orientation ,which show that The optimum tilt angle depends on latitude ( ), solar declination or days of the year (Koray.2006). Kamal Skeiker show the changing of the tilt angle of PV cell located in Syria by 12 times in a year achieves a solar radiation of approximately 30% more than the case of a solar collector fixed on a horizontal surface, Can Ertekin(2008) study the effect of collector location and tilted angle for many place in turkey showed that tilt angles are high during the autumn (September to November) and winter (December to February) and low tilt angles during the summer (March to August)

. Hamid Moghadam and et.al(2011) find the optimum tilt angle for two different Iranian cities, Zahedan city (Lat.=29.49) and Bandar Abbass city (Lat.=27.18),The results, in the same time step, show that the increase of latitude led to the increase of the optimum tilt angle.

## **2- MATHEMATICAL METHOD FOR THE OPTIMUM TILTED ANGLE**

The total daily irradiation on a horizontal plane is the combination of two components, the direct irradiation and the diffuse irradiation from the sky (Ashok Kumar,2011)

In this study the Bernard-Menguy-Schwartz model is used to find the optimum tilt angle ( $\beta$ ) of photovoltaic cell solar collector in northern Iraq cities because it's more simple correlation than other authors and predicted to northern hemisphere more accurate (Romdhane.2009)(Al Sayyab Et.al .2012)

In Bernard-Menguy-Schwartz model the direct radiation under three conditions of sky:

Clear Sky:

$$I_D = 1230e^{\left(\frac{-1}{3.8 \sin(h_s+1.6)}\right)} \dots\dots (1)$$

Very Clear Sky:

$$I_D = 1210e^{\left(\frac{-1}{6 \sin(h_s+1)}\right)} \dots\dots (2)$$

Polluted Sky:

$$I_D = 1260e^{\left(\frac{-1}{2.3 \sin(h_s+3)}\right)} \dots\dots (3)$$

The diffused radiation for any sky conditions:-

$$D_H = 125(\sin(h_s))^{0.4} (4)$$

The total radiation received by the horizontal plane:-

$$G_H = D_H + I_D \sin(h_s) \dots\dots (5)$$

Diffuse and total radiations receipts by the inclined collector plane:

$$D_i = \frac{1+\cos(\beta)}{2} D_H + \frac{1-\cos(\beta)}{2} G_H \alpha \dots\dots (6)$$

$$G_i = I_D \cdot \cos(\theta) + D_i \quad (7)$$

Where the factor  $\alpha$  is the coefficient of reflexion of the ground located in front of the collector (usually taken equal to 0.2).and the angle  $\theta$  formed between the normal of the collector and the solar rays at solar midday define by:

$$\theta = 90 - (\beta + h_s) \dots\dots (8)$$

$$h_s = 90 - \varphi + \delta \dots\dots (9)$$

Duration of the day:

$$\Delta D = \frac{2}{15} \arccosh(-\tan(\varphi) \cdot \tan(\delta)) \dots (10)$$

$$\delta = 23.45 \sin\left(360^\circ \frac{(284 + N)}{365}\right) \dots (11)$$

Received energy:

$$E = \frac{2}{\pi} \times G_i \times \Delta D \quad (12)$$

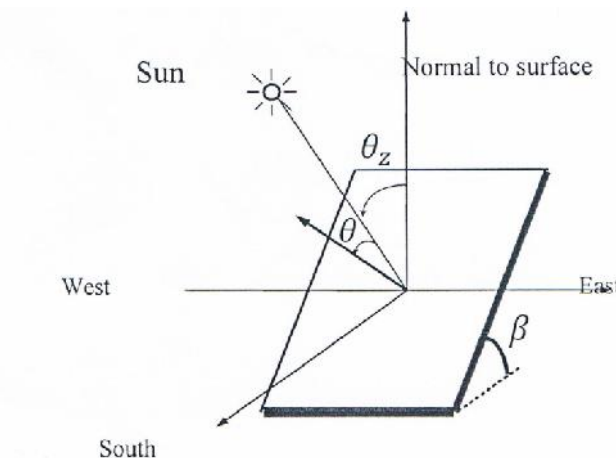


**Fig (1) Common Angles in solar application [Hamdy et al,2006]**

### 3- RESULTS AND DISCUSSION:-

#### 3. 1- Monthly Optimum Tilted Angle:-

##### A) Effect of Declination angle on optimum monthly tilted angle:-

Monthly tilt angle is a fixed value for the solar collectors in each month. the effect of tilted angle variation on the photovoltaic cell performance located in Arbil city is shown in Fig (2), (3) , and (4), from this figures, as the tilted angel of photovoltaic cell increased the collected solar energy flux will increased gradually, due to increase the amount of the normal solar radiation that incident to the cell surface, until the flux reach to a maximum value ,after this value of tilted angle the collected solar energy flux will decreased as tilted angle increased ,there for this angle will be obtained as the optimum tilted angle for this month. Also these figure show that the optimum tilted angle of each months will different from each other due to the earth declination angle varies with number of day variation over the year ,Fig (5) ,so declination angle have main effect on azimuth angle of sun ray.

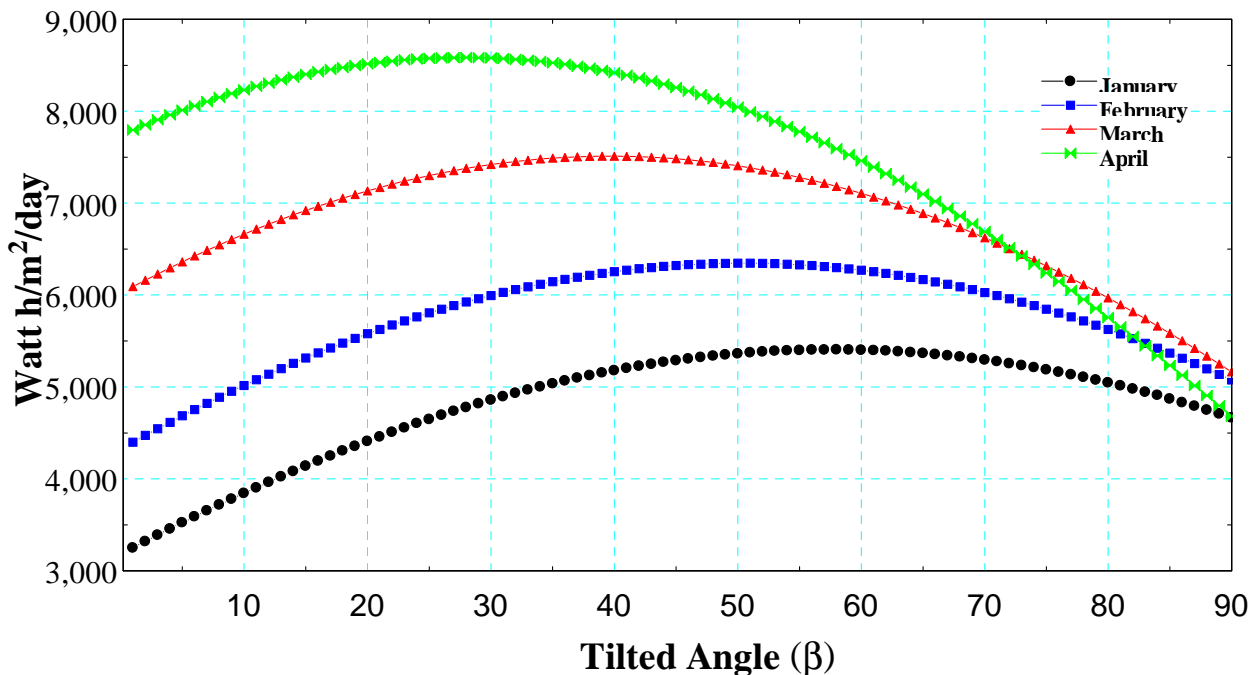


Fig (2) Effect of PV Cell Tilted Angle Variation on Collected Solar Flux located at Arbil city months of (January, February, March and April)

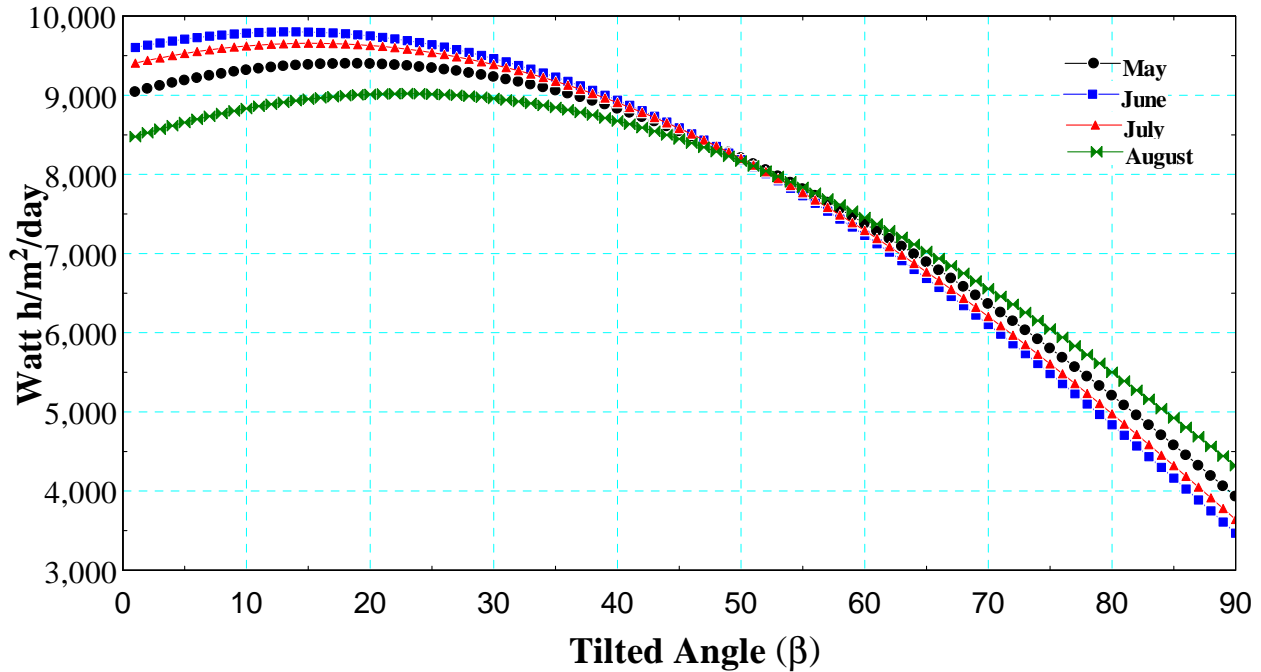


Fig (3) Effect of PV Cell Tilted Angle Variation on Collected Solar Flux located at Arbil city months of (May, June, July and August)

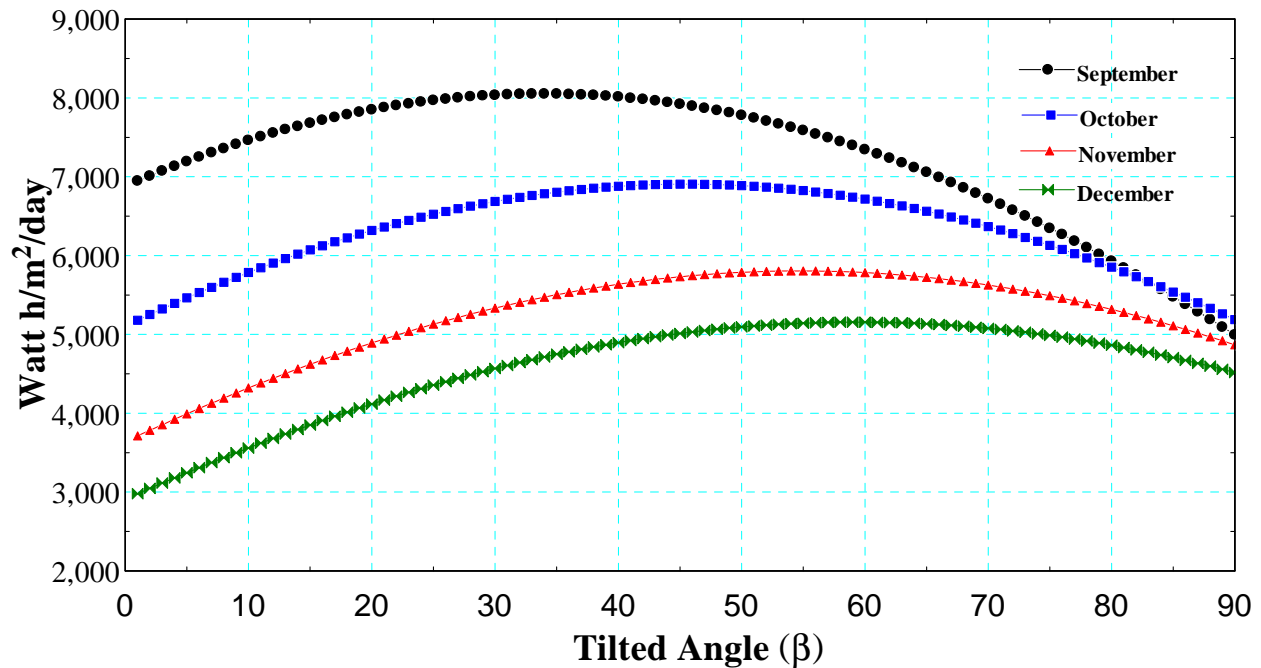


Fig (4) Effect of PV Cell Tilted Angle Variation on Collected Solar Flux located at Arbil city months of (September, October, November and December)

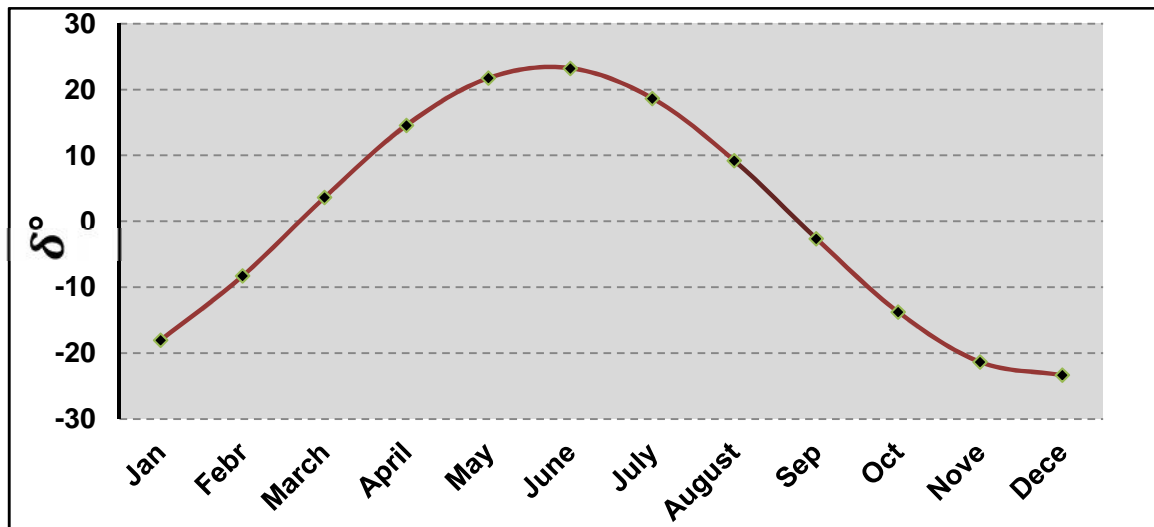


Fig (5) Declination angle variation with number of day

#### B) Effect of Declination angle on solar energy flux:-

When sun beam passes through atmosphere layer some of the sun's direct radiation is scattered by nitrogen, oxygen, and other molecules, and by aerosols, water droplets, dust, and other particles with diameters comparable to the wavelengths (Gates 1966). As the declination angle increased this will decreased the path of the sun ray and this will decreased the solar beam absorbing and scattering and increased the flux of solar energy that reaches to earth surface, so as mentioned in Fig. (5) the declination angle reaches maximum value at Jun and this make this month have maximum solar flux as shown in fig (5) and Fig. (6).

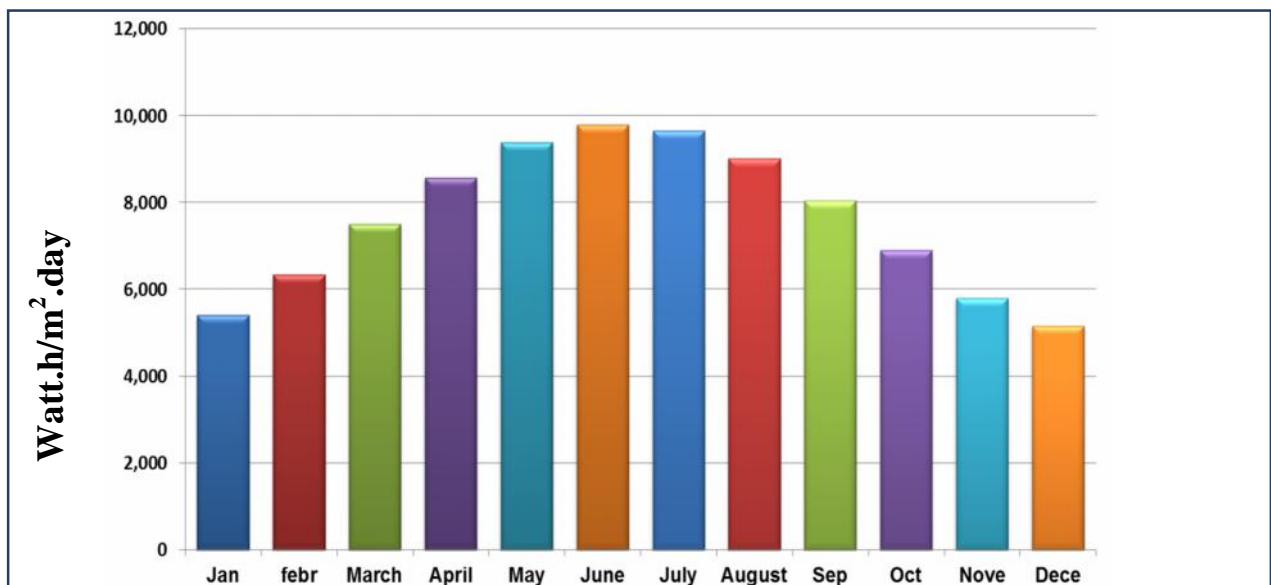
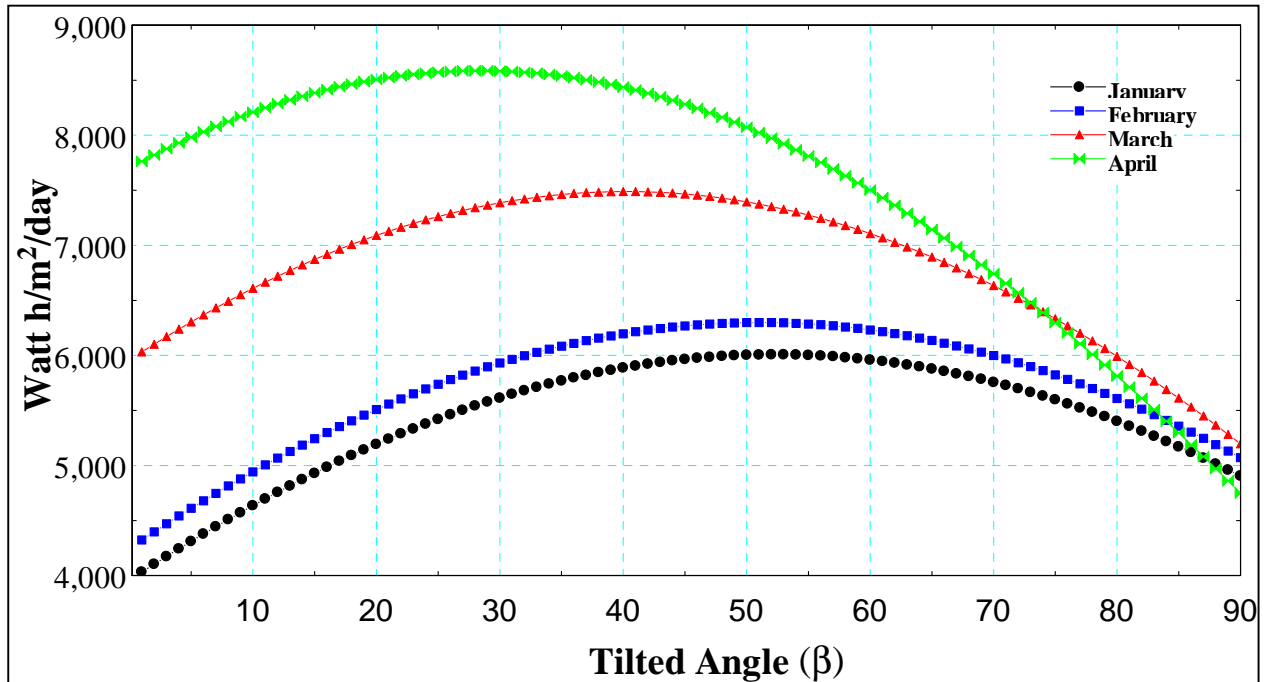


Fig (6) Effect of Declination angle Variation on Collected Solar Flux by PV cell located at Arbil City with optimum tilted angle

figures (7) , fig(10) and fig (13) show the effect of latitude on optimum tilted angle for cell located in different cities, Dahuk ,Sulaymaniyah and Kirkuk respectively , these figures show that these cities have different monthly optimum tilted angle for the same months due to the different in latitude of these cities Table (1).



**Fig (7) Effect of PV Cell Tilted Angle Variation on Collected Solar Flux located at Dahuk city months of (January, February, March and April)**

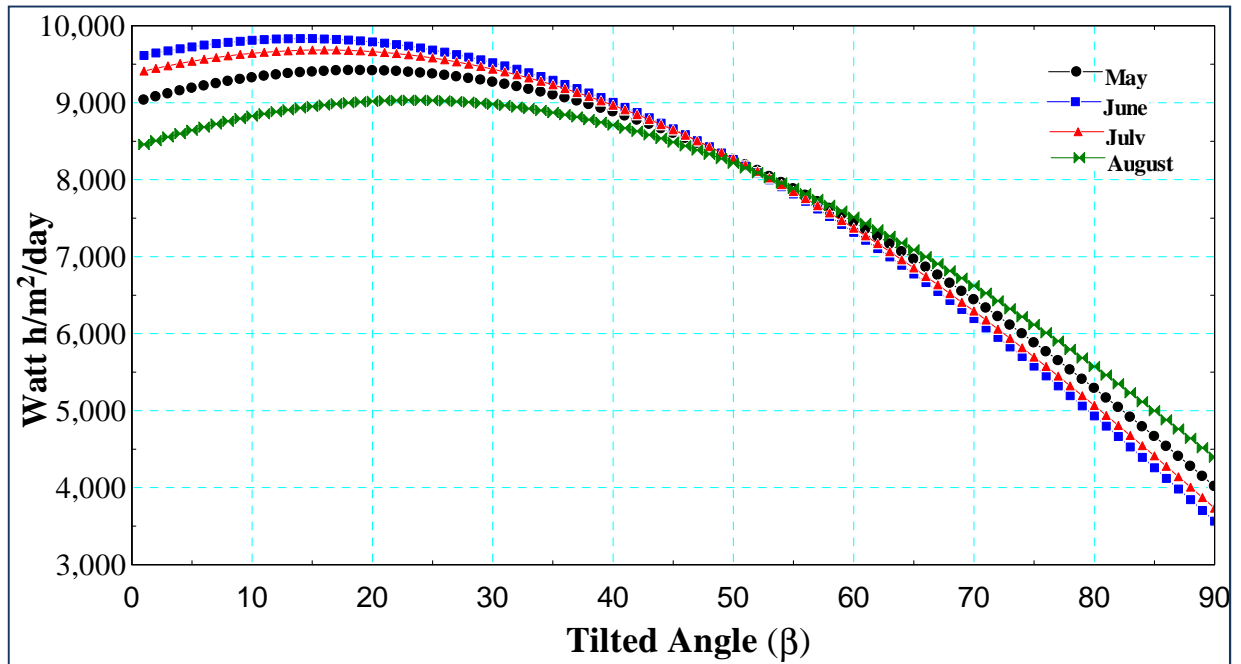


Fig (8) Effect of PV Cell Tilted Angle Variation on Collected Solar Flux located at Dahuk city months of (May, June, July and August)

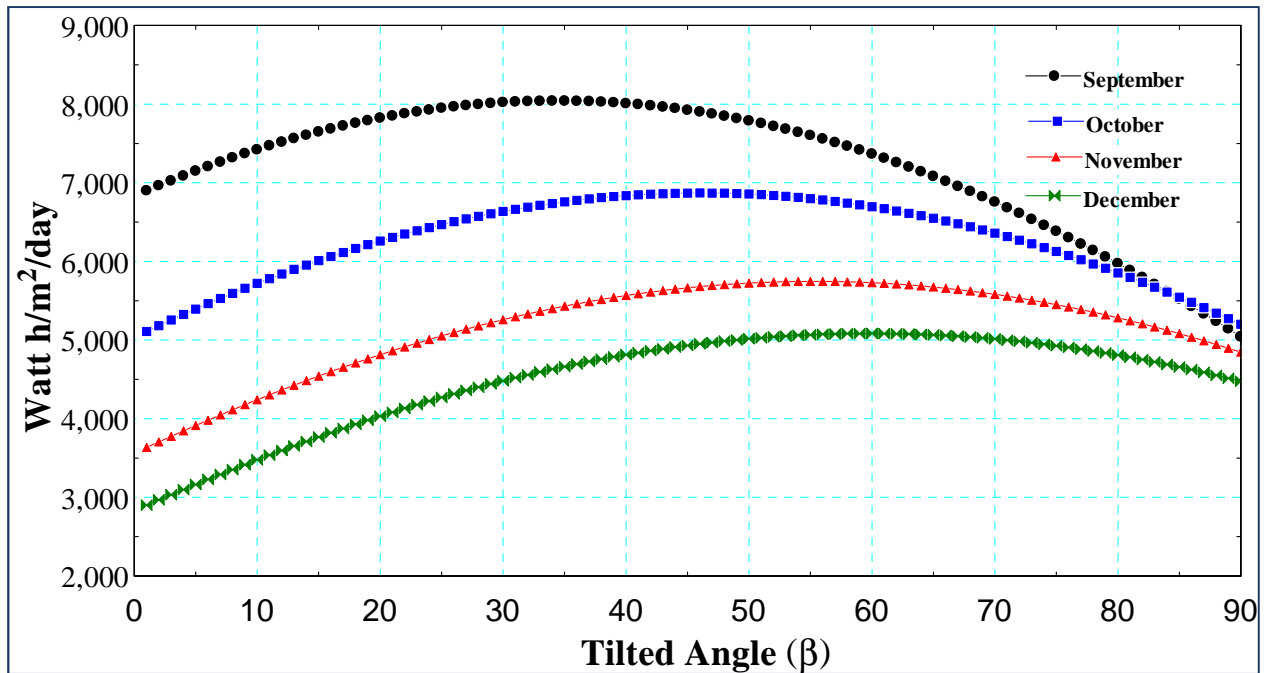


Fig (9) Effect of PV Cell Tilted Angle Variation on Collected Solar Flux located at Dahuk city months of (September, October, November and December)

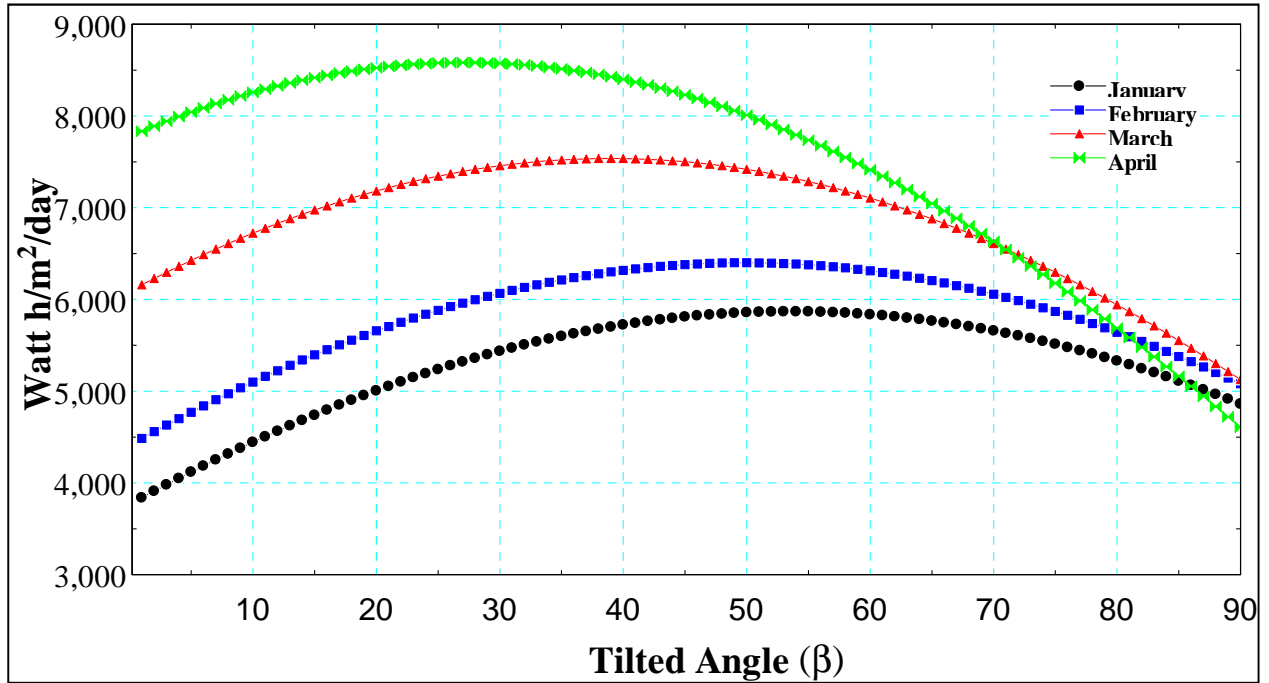


Fig (10) Effect of PV Cell Tilted Angle Variation on Collected Solar Flux located at Sulaymaniyah city months of (January, February, March and April)

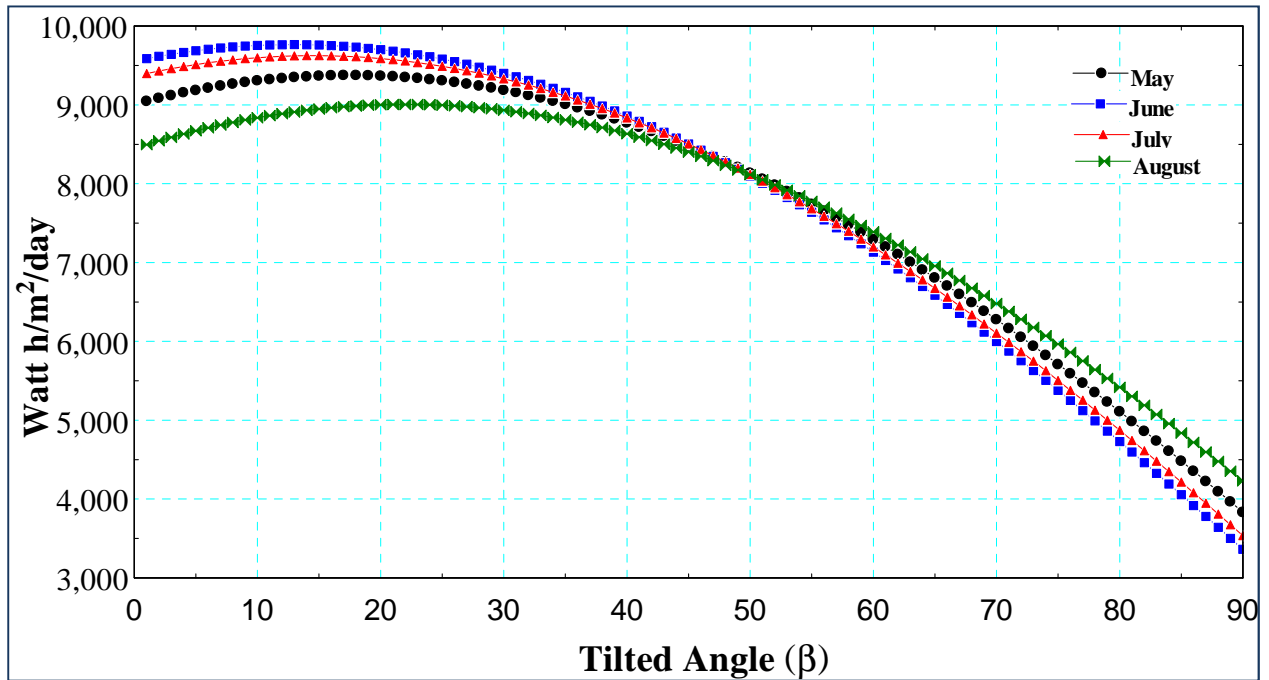


Fig (11) Effect of PV Cell Tilted Angle Variation on Collected Solar Flux located at Sulaymaniyah city months of (May, June, July and August)

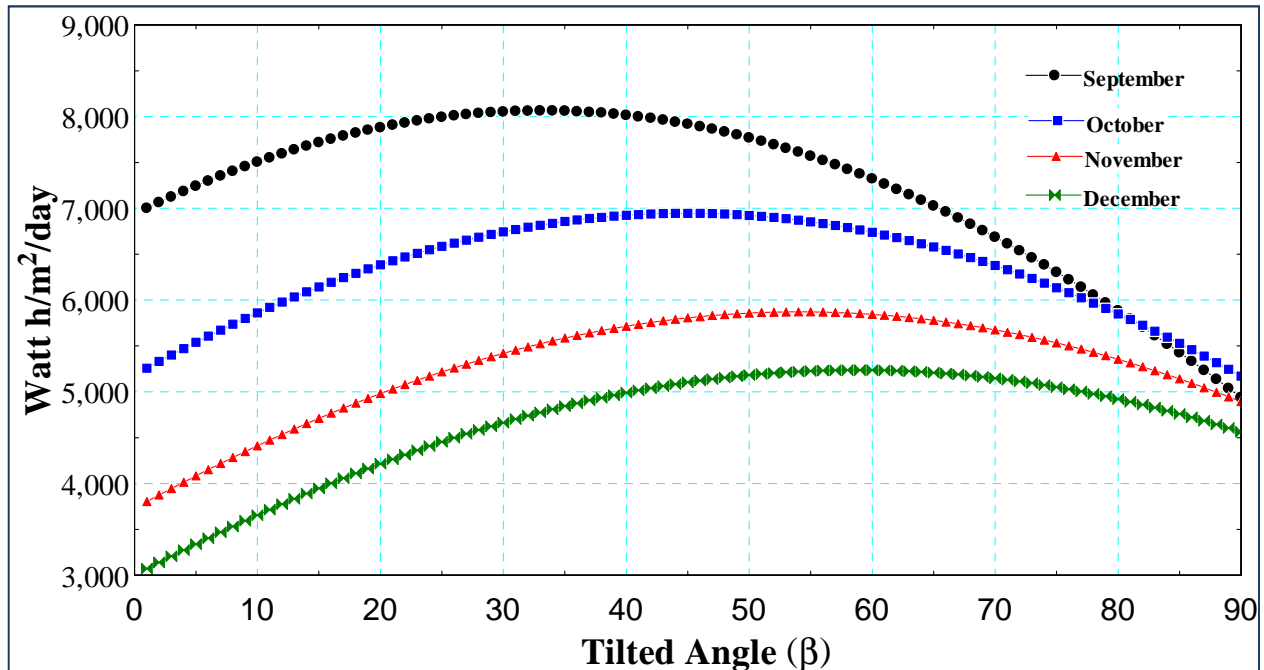


Fig (12) Effect of PV Cell Tilted Angle Variation on Collected Solar Flux located at Sulaymaniyah city months of (September, October, November and December)

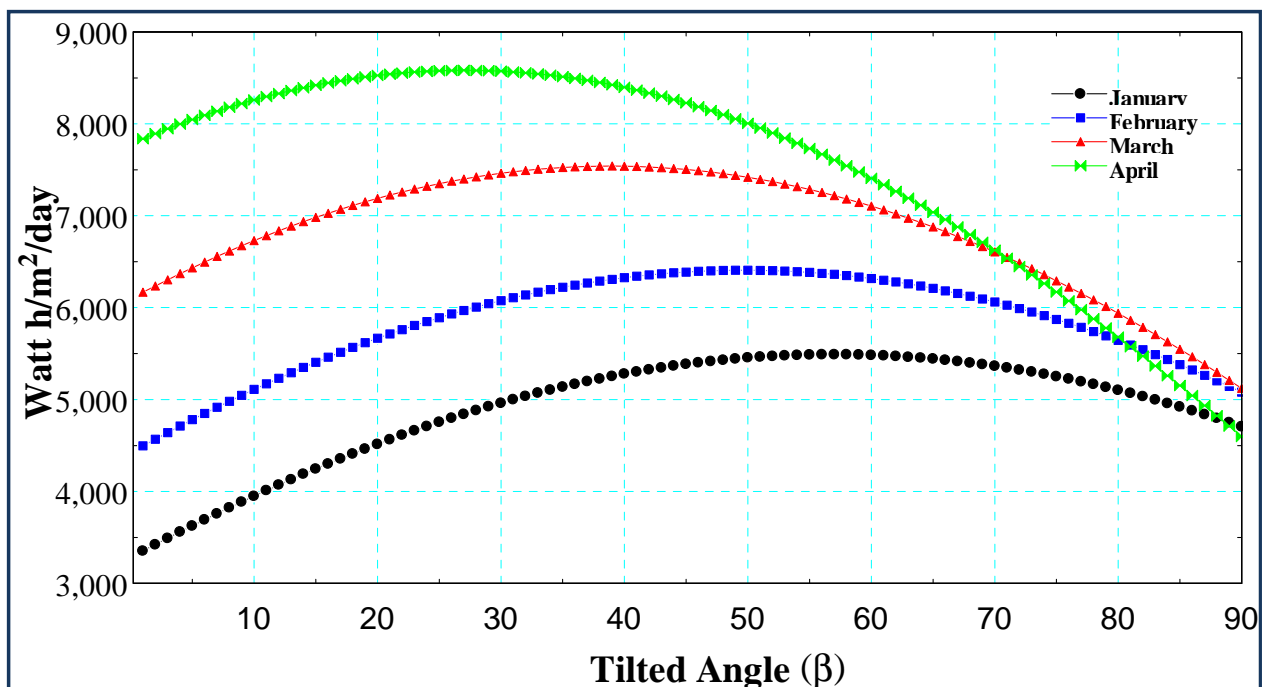


Fig (13) Effect of PV Cell Tilted Angle Variation on Collected Solar Flux located at Kirkuk city months of (January, February, March and April)

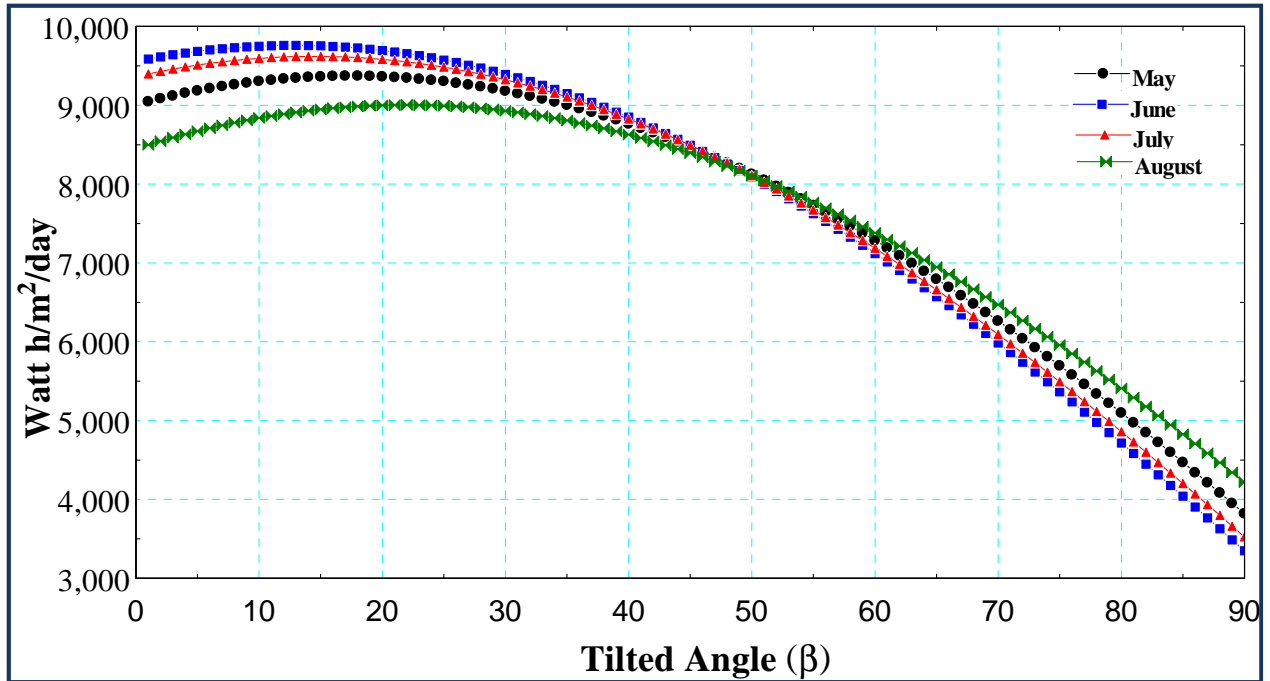


Fig (14) Effect of PV Cell Tilted Angle Variation on Collected Solar Flux located at Kirkuk city months of (May, June, July and August)

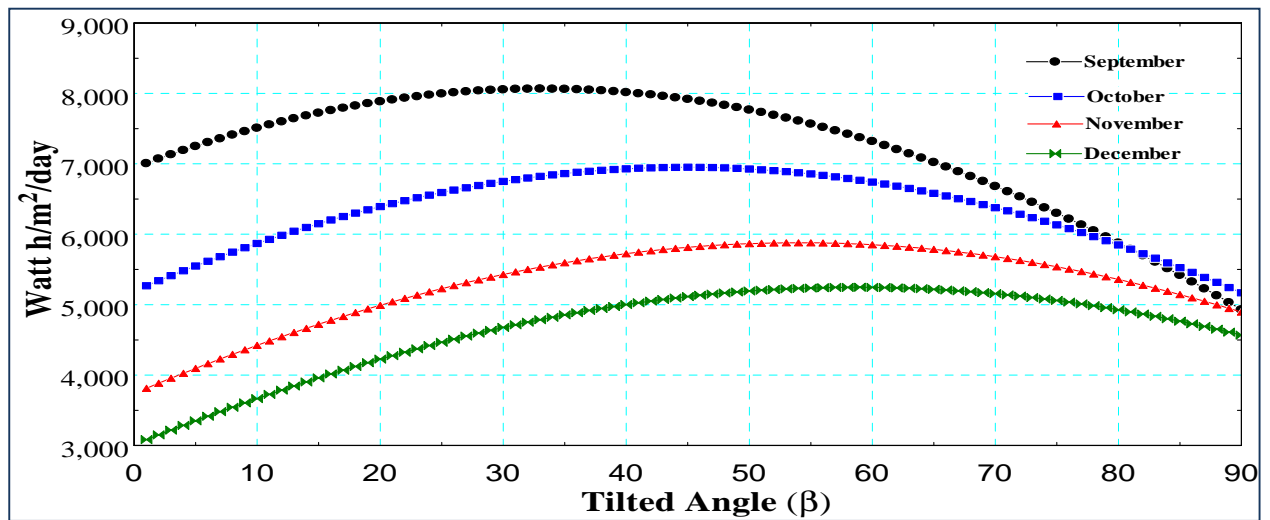


Fig (15) Effect of PV Cell Tilted Angle Variation on Collected Solar Flux located at Kirkuk city months of (September, October, November and December)

### 3.2 Yearly Optimum Tilted Angle:-

To find the yearly optimum tilted angle, the photovoltaic cell tilted angle will varied over range from  $0^{\circ}$  to  $90^{\circ}$ , the variation of tilted angle will be adopted over the days of the year, and an average value of collected solar energy will take as method to find the collected energy by any tilted angle. From Figures (16, 17, 18 and 20) shows that there is one angle give maximum solar flux per day over the year and this angle can be taken as yearly optimum tilted angle, so that these figures show the different latitude give different yearly optimum tilted angle also this angles are not equal to latitude of these cities and .this refutes the claim of many study that take optimum tilted angle equal to latitude.

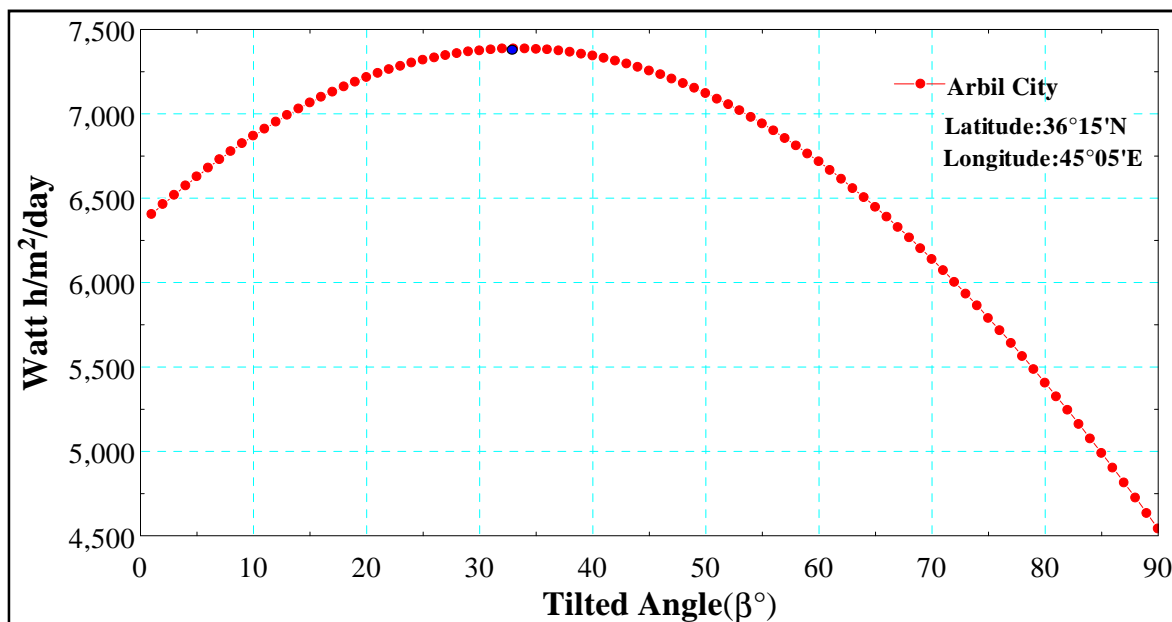


Fig (16) Optimum Yearly Tilted Angle of PV Cell located at Arbil city

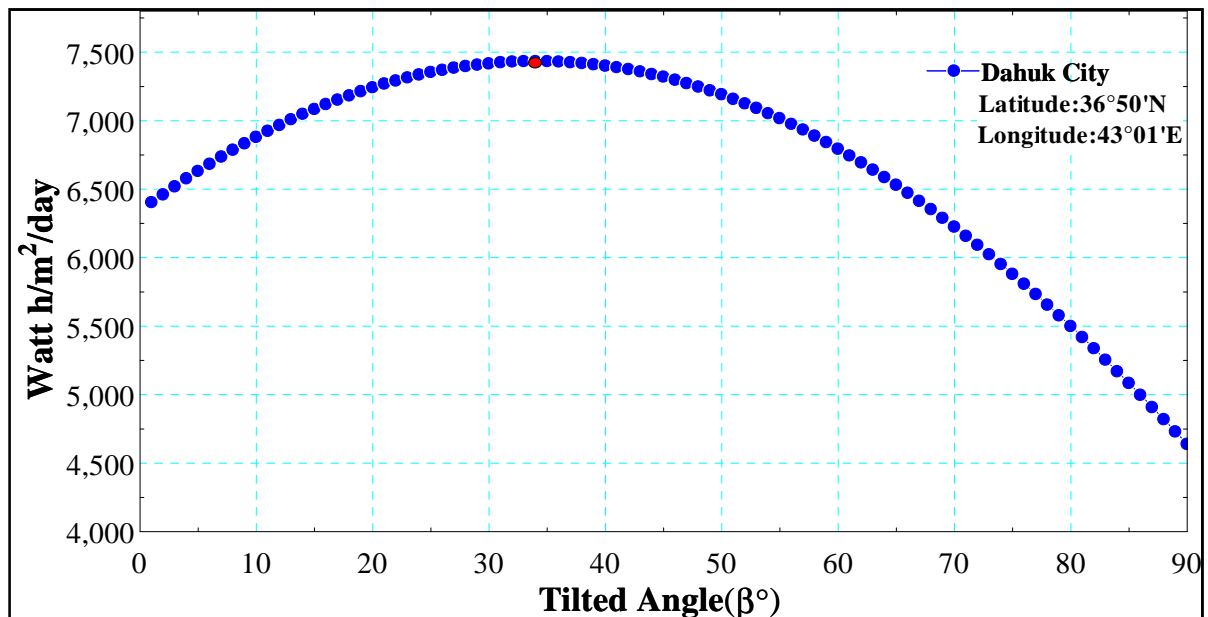


Fig (17) Optimum Yearly Tilted Angle of PV Cell located at Dahuk city

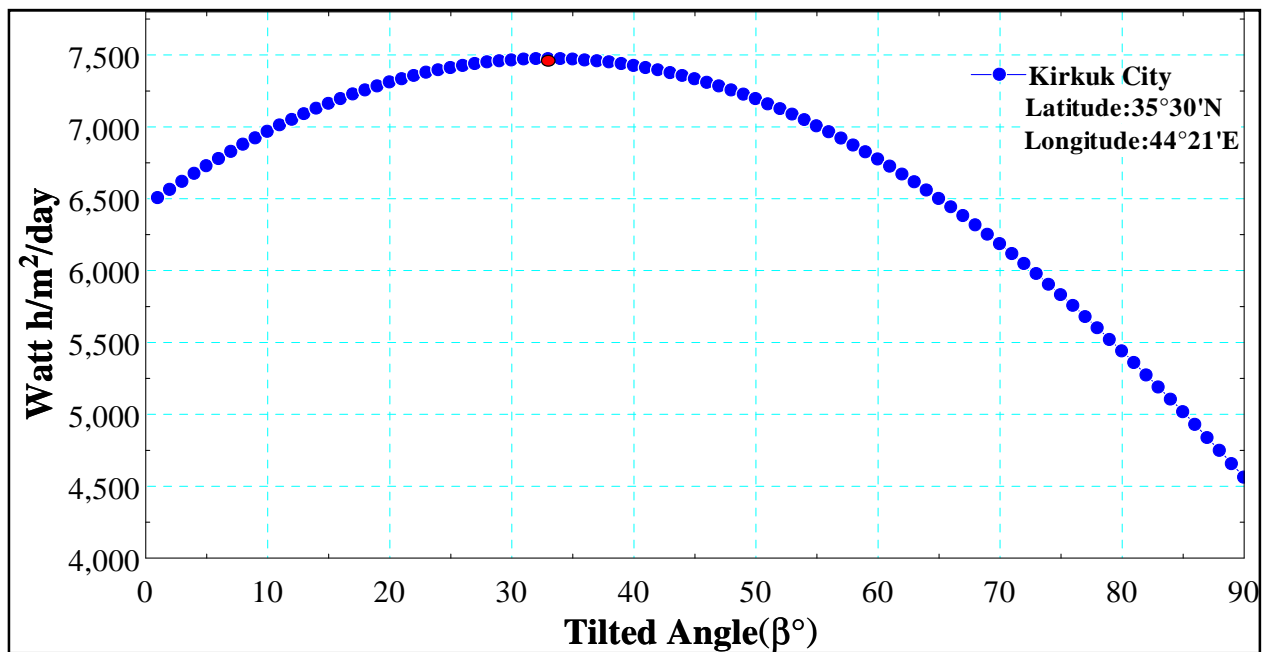


Fig (18) Yearly Optimum Tilted Angle of PV Cell located at Kirkuk city

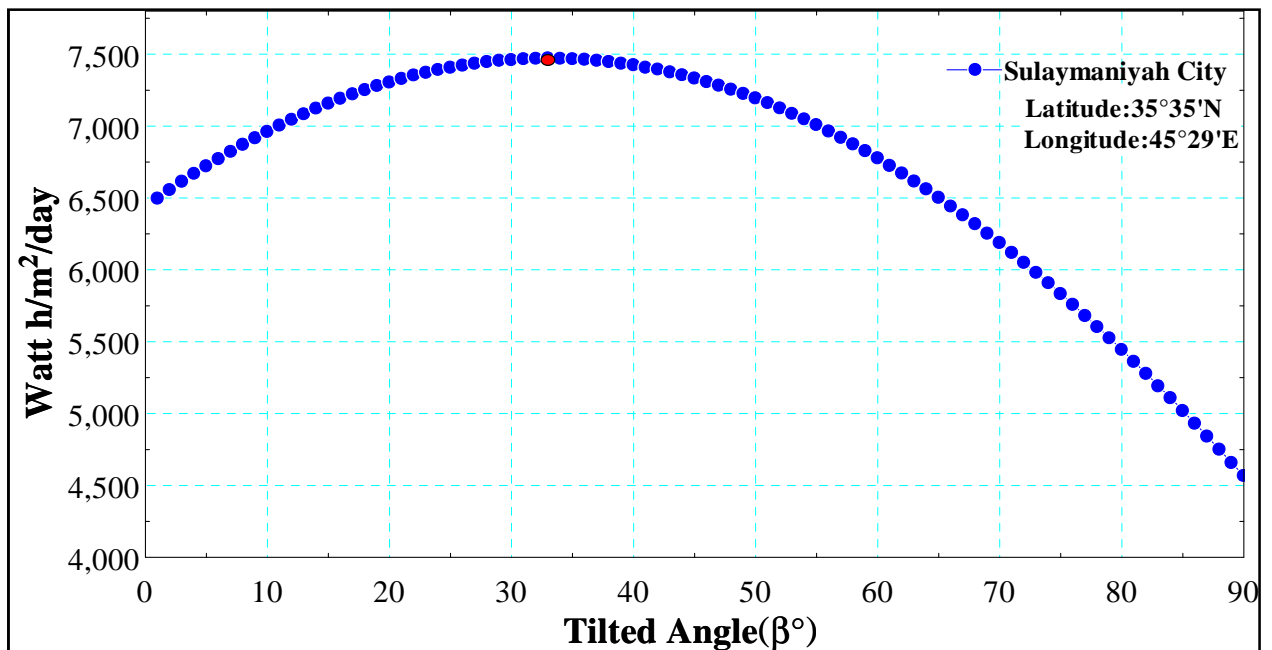


Fig (19) Yearly Optimum Tilted Angle of PV Cell located at Sulaymaniyah city

**Table (1) Effect of City Latitude on Optimum Monthly Tilted Angle**

| Optimum Monthly Tilted Angle |         |          |       |       |     |      |      |        |           |         |          |          |
|------------------------------|---------|----------|-------|-------|-----|------|------|--------|-----------|---------|----------|----------|
| City                         | January | February | March | April | May | June | July | August | September | October | November | December |
| Arbil                        | 58      | 51       | 40    | 28    | 18  | 14   | 15   | 22     | 34        | 45      | 55       | 60       |
| Dahuk                        | 53      | 50       | 41    | 28    | 19  | 14   | 16   | 23     | 35        | 46      | 56       | 59       |
| Sulaymaniyah                 | 54      | 50       | 39    | 27    | 17  | 13   | 15   | 22     | 33        | 45      | 54       | 58       |
| Kirkuk                       | 57      | 49       | 39    | 27    | 18  | 13   | 14   | 22     | 33        | 45      | 55       | 59       |

#### 4) Conclusion:-

**From this study conclude that:-**

- 1) The optimum tilted angle of photovoltaic cell dose not equal to the latitude of the city which the cell located in it.
- 2) The optimum monthly tilted angle will different from month to other due to the declination angle variation over the month of the year
- 3) In Iraq June represent the period of the maximum solar flux over the year.
- 4) The yearly optimum tilted angle of Arbil city is  $34^{\circ}$  ,Dahuk city is  $34^{\circ}$  ,for Sulaymaniyah city is  $33^{\circ}$  and for Kirkuk city is  $33^{\circ}$ . And these cities are nearly in optimum tilted angle due to nearly in latitude (Arbil = $36^{\circ} 15''$  ,Dahuk = $36^{\circ} 50''$  ,Sulaymaniyah = $35^{\circ} 35''$  and Kirkuk = $35^{\circ} 30''$ )

## REFERENCES

- ASHRE HVAC application, use of solar energy, 1999.
- Can Ertekin , Fatih Evrendilek and Recep Kulcu ,Modeling Spatio-Temporal Dynamics of Optimum Tilt Angles for Solar Collectors in Turkey. Sensors 2008, 8, 2913-2931.
- Tom Markvart and Luis Castafier Practical Handbook of Photovoltaics: Fundamentals and Applications, 2003.
- Kyoto Protocol to the United Nations Frame work Convention On Climate Change .1998, UNITED NATIONS, FCCC/INFORMAL/84.
- Ashok Kumar, 2011 “optimization Of Tilt Angle for Photovoltaic Array” International Journal of Engineering Science and Technology (IJEST), Vol. 3 No. 4 Apr 2011.
- KORAY ULGEN,Optimum Tilt Angle for Solar Collectors,Energy Sources, Part A, 28:1171–1180, 2006.
- Vilela, O.C.; Fraidenraich, N.; Tiba, C., Photovoltaic pumping systems driven by tracking collectors: experiments and simulation. Solar Energy jorنال, 2003, vol.74 no.1, 45-52.
- Kamal Skeiker ,2009 Optimum tilt angle and orientation for solar collectors in Syria , Energy Conversion and Management , 2009.50.2439–2448.
- Hamdy K. Elminir , Ahmed E. Ghitas, F. El-Hussainy, R. Hamid a,M.M. Beheary, Khaled M. Abdel-Moneim,Optimum solar flat-plate collector slope:Case study for Helwan, Egypt. Energy Conversion and Management 47,2006,624–637.
- Hamid Moghadam, Farshad Farshchi Tabrizi and Ashkan Zolfaghari Sharak, Optimization of solar flat collector inclination, Desalination, Volume 265, Issues 1–3, 15 January 2011, Pages 107-111,2009.
- Frank Kreith, D. Yogi Goswami ,Handbook of Energy Efficiency and Renewable Energy, 2007.
- Soulayman, S. S. H.,On the optimum tilt of solar absorber plates. Renewable Energy, 1991. 1, 551-554.
- Romdhane Ben Slama ,Incidental Solar Radiation According to the Solar Collector Slope - Horizontal Measurements Conversion on an Inclined Panel Laws, The Open Renewable Energy Journal, 2009, 2, 52-58.
- Tian Pau Chang ,Study on the Optimal Tilt Angle of Solar Collector According to Different Radiation Types, International Journal of Applied Science and Engineering, 2008. 6, 2: 151-161.

## Experimental Study on Enhancement of Single-Basin Solar Still Using Phase Change Materials (Paraffin wax)

Kadhim H. Suffer  
Nahrain University.  
College of Engineering.  
Mechanical Engineering Department.  
Kadhim\_Askar@yahoo.com

### Abstract

An enhancement of single slope solar still by using (Paraffin wax) as a phase change material (PCM) was experimentally studied. Single-basin solar still can be used for water desalination. Probably, they are considered the best solution for water production in remote, arid to semi-arid, small communities, where fresh water is unavailable. However, the amount of distilled water produced per unit area is somewhat low which makes the single-basin solar still unacceptable in some instances. The purpose of this work is to study the effect of using a PCM as capsules in a solar still as a thermal storage media, and thus enhance the productivity of water. Experimental results show that the productivity of distilled water was enhanced with use PCM. The daily water productivity is increased by 34%. Also the best efficiency of 78.6 % occurred when using PCM compared with efficiency of 60 % when only water used in still. Therefore it is concluded that the productivity of water still per unit area increased.

Keywords: Single basin type, Solar still, Desalination, PCM capsules, thermal energy storage.

### دراسة تطبيقية لتحسين أداء مقطر شمسي أحادي الحوض باستخدام مادة متغيرة الطور (شمع البرافين)

#### الخلاصة

تم دراسة تحسين أداء مقطر شمسي أحادي الحوض باستخدام مادة متغيرة الطور (شمع البرافين) عملياً. أن المقطر الشمسي يستخدم عادة لتقطير المياه غير النقية التي تحتوي على الأملاح والشوائب الأخرى. وفي الأماكن النائية التي لا يوجد فيها الماء النقي بالكمية المطلوبة. لذلك يكون المقطر الشمسي الحل الأمثل لتوفير الماء النقي. لكن الكمية التي ينتجها المقطر الشمسي لوحدة المساحة تكون قليلة. لذلك يلجأ إلى البحث على زيادة الإنتاجية للمقطر وهذا هو الغرض من هذه الدراسة، والفكرة هي زيادة إنتاجية مقطر شمسي أحادي الميل باستخدام مادة متغيرة الطور مثل (شمع البرافين) داخل كبسولات مصنوعة من أنابيب نحاسية محكمة الغلق ومطلية باللون الأسود من الخارج تغمر داخل الماء الموجود في المقطر الشمسي. النتائج التطبيقية بينت أن استخدام المادة المتغيرة الطور يعطي زيادة بإنتاجية المقطر بمقدار 34% وبكفاءة 78.6% مقارنة مع إنتاجية المقطر عندما تكون كفاءته 60 % في حالة استخدام الماء فقط في المقطر الشمسي. لذلك نستنتج أن استخدام المادة المتغيرة الطور أعلاه تعطي زيادة في إنتاجية المقطر لنفس وحدة المساحة.

الكلمات المرشدة: المقطر أحادي الميل، المقطر الشمسي، التقطير، كبسولة المواد متغيرة الطور، خزن الطاقة الحرارية

## Nomenclature

|           |                                               |
|-----------|-----------------------------------------------|
| $A_p$     | Still basin area ( $m^2$ ).                   |
| $h_{fgw}$ | Latent heat of vaporization of water (kJ/kg). |
| $I(t)$    | Solar radiation intensity ( $W/m^2$ ).        |
| $m_w$     | Distillated water (kg/s).                     |
| PCM       | Phase Change Materials.                       |
| $T_a$     | Ambient temperature ( $^{\circ}C$ ).          |
| $T_b$     | Back temperature ( $^{\circ}C$ ).             |
| $T_g$     | Glass temperature ( $^{\circ}C$ ).            |
| $T_s$     | Steam temperature ( $^{\circ}C$ ).            |
| $T_w$     | Water temperature ( $^{\circ}C$ ).            |
| $\eta$    | Efficiency (%).                               |

## 1. Introduction

Solar energy is an important alternative energy source that likely will be more utilized in the future. One main factor which limits the application of solar energy is that it is a cyclic time-dependent energy resource. Therefore, solar systems require energy storage to provide energy during the night and overcast periods [1]. Distillation is one of many processes that can be used for water purification. The energy required to evaporate water is the latent heat of vaporization of water. This has a value of 2260 kJ/kg. This means that to produce 1 liter (i.e. 1kg since the density of water is 1kg/litre) of pure water by distilling brackish water requires a heat input of 2260 kJ. Many others work for development and enhancement water still as, Radhwan A. M. [2] studied the transient performance of a stepped solar still with built-in latent heat thermal energy storage. The basin was placed on a slab filled with a layer of paraffin wax (phase change material, PCM) that acts as a latent heat thermal energy storage system (LHTESS). The still performance parameters investigated were analyzed, and the results compared with the case of a still without the LHTESS. The results showed that the still with LHTESS has an efficiency of 57%, and the total daily yield is about 4.6 L/m<sup>2</sup>. This finding is important since heat could be provided to the greenhouses at night and when it is most needed. El-Sebaili A. A., et al. [3] studied the transient mathematical models for a single slope-single basin solar still with and without phase change material (PCM) under the basin liner of the still. Numerical calculations have been carried out, using stearic acid as a PCM, when the still is used without the PCM. The PCM is more effective for lower masses of basin water on winter season. Akash B. A. et al. [4] studied the effect of using different absorbing materials in a single-basin solar still, and thus enhancing the productivity of water. Experimental result shows that the productivity of distilled water was enhanced for some materials. Black dye was the best absorbing material used in terms of water productivity. It resulted in an enhancement of about 60 %. Badran O.O. [5]. Performance of a single slope solar still using different operational parameters was studied experimentally. For this study the still productivity increased up to 51% when combined enhancers such as asphalt basin liner and sprinkler have been applied to the still. The study also showed that the daily production of still can be increased by reducing the depth of the water in the basin. Gowtham M. et al. [6] work to improve the productivity of solar still by concentrating solar thermal energy through a parabolic trough concentrator. These studies improved the evaporation rate of the system. This is done through increasing the energy storage capacity through paraffin wax as latent heat storage material. Productivity improved by 54%. Medugu D. W. and

Ndatuwong L. G. [7] developed theoretical analysis of the heat and mass transfer mechanisms inside this solar still. The measured performance was then compared with results obtained by theoretical analysis. The results clearly show that the instantaneous efficiency increases with the increase of solar radiation and with the increase of feed water temperature. The distillation efficiency of the still is 99.64% as compared to the theoretical analysis. Naim M. M. and Abd El Kawi M. A. [8]. Constructed a novel continuous single-stage solar still that makes use of a phase change energy storage mixture (PCESM) for promoting energy usage has been devised and constructed. Results indicated that the use of an energy storage material led to a larger productivity of distilled water and that the larger the concentration of the saline water the lower the productivity of the still. Ighodalo O. A., Ebhodaghe F. A. [9] studied the performance evaluation of a solar still for salty water desalination. The still was tested using two different materials, aluminum painted black and black leather as the absorber. They are concluded the daily temperature and type of absorber materials are factors that can influence the distillate yield. The low cost of production is as a result of the materials employed in the fabrication. Murugave K. K. et al. [10] Modeling and Verification of Double Slope Single Basin Solar Still Using Laboratory and Actual Solar Conditions. It is found that the production rate increases with the increases of water and glass temperature. But at higher operation temperature, the production rate increases with the decrease in temperature difference between water and glass. Khalifa A. N. and Hamood A. M. [11] studied on the verification of the effect of water depth on the performance of basin type solar. A good number of the investigations on the effect of brine depth are cited in this study. An experimental study was subsequently conducted to verify this trend by an experimental investigation on a solar still that was constructed and tested with five different brine depths, namely 1, 4, 6, 8 and 10 cm. This study validated the decreasing trend in productivity with the increase of brine depth and showed that the still productivity could be influenced by the brine depth by up to 48%.

## 2. Experimental set up

The experimental setup shown in Figs. 1, 2 and 3 is one of the simplest types of solar stills. Two stills were used in this work, one used with water only, and the other still used with the copper pipes filled by paraffin wax and immersed in water, the stills have an effective area of 0.6 m<sup>2</sup>. It has a top cover of transparent glass, and the interior surface of its basin is blackened to enable absorption of solar energy. The stills frames are insulated from the outer surface by insulating material. The identical fixed solar stills are faced due south. The temperatures of the glass cover, the water and vapour inside the stills and bottom of stills plate from the system are measured by thermocouples of the same type. Radiation shields are used with the thermocouples wherever necessary. All thermocouples are connected to a digital electronic thermometer is used. The water level was 3 cm in the stills. Different parts of the stills will be explained in the following:

### 2.1. Basin liner

This is the major part of the solar still has a base dimensions 100 cm long and 60 cm width fig.3; It's made of galvanized steel, the glass cover is tilted at an angle of 15° and the still is oriented due south. Four copper-constantan thermocouples are embedded at different points in the still to measure the temperature.

## 2.2 PCM capsules

In this work twenty PCM capsules are used, these capsules are made from copper pipes have 95 cm long and 12.5 mm inside diameter and filled with a paraffin wax, two ends are closed by copper welding, the total length of pipes was 19 meters. These capsules are painted by blackened color to increase the absorbent of solar radiation fig. 2.

## 2.3 Paraffin wax

The paraffin wax used has the following properties; Typical melting point about 35 °C and having a density of around 0.9 g/cm<sup>3</sup> and penetration at 25 °C is equal to 34, oil content (max) is 1.5 % , color (SAYBOLT) solidification point is 30 °C, latent heat was (2.244 kJ/kg. K) Conductivity is 0.27 W/m°C, specific heat is 2890J/kg °C and it is insoluble in water, but soluble in ether, benzene, and certain esters.

## 2.4. Insulating material

The sides and bottom of the system are insulated with 50-mm-thick rigid Styrofoam insulation board that have a density of 40 kg/m<sup>3</sup> and 0.045 W/m<sup>2</sup> °C thermal conductivity.

## 2.5. Measuring instruments

Various types of instruments were used such as:

- (1) Pyranometer (The daystar meter): To measure the total radiation in W/m<sup>2</sup>.
- (2) Glass beaker: To collect and measure the distillate water.
- (3) Temperature thermometer type (TM-925) to measure temperature at various points in the still by thermocouples (type-K). The accuracy of this device is in the range of 0.1°C for the temperature measurements between -50.0to 1300.0 °C ± (0.4% + 0.8°C)
- (4) Air speed meter.

## 3. Result and discussions.

The experiments results are presented in the form of graphs, to show the effect of using PCM in solar still output and to highlight the effect of using PCM on the glass temperature, basin water temperature and the distillation accumulation. All the experiments were taken in different days during the April, May and July 2012 in clear sky weather conditions. The speed of the air outside the stills was 3.5 m/s.

Fig. 4 shows the solar intensity versus time of the day. The intensity of solar radiation reaching the earth surface varies from zero during the night to about 900 W/m, on a clear noon. Hence, the radiation intensity depends on the hour of the day.

Fig. 5 shows the variation of different variables of solar still in case using water in still, it can be seen that the temperature of the steam is the maximum followed by the temperature of water that has been heated by the basin in a convection process due to incident rays, then the temperature of the inner glass where the condensation occur, then the outer glass that transmit the incident rays, and it is in contact with the surrounding, and the minimum temperature will be the ambient temperature. While fig. 6 summarizes Different variables were measured hourly as (glass, ambient, water, back plate and steam) temperatures. It is seen that these temperatures increases with time due to the increased rate of heat transfer by conduction from the water to the PCM as the solar radiation intensity increases. The PCM started to melt after four hours from the beginning of still exposure to solar radiation, afterwards, the PCM remains nearly constant until it melts completely; then, it decreases slowly with time after

sunset when the discharging process of the heat stored within the PCM begins. However, the temperatures of the water and the other elements of the still decrease faster with time due to the decreased ambient temperature. This is caused a significant difference between water temperature and temperature of PCM during the night period, therefore this difference make the water continues to evaporate until these temperatures are equals. For this reason the productivity of still with use PCM increased. Fig. 7 shows the hourly variation of productivity ( $\text{kg/m}^2 \text{ h}$ ) for 24 hour. It shows that the highest production was at 15 pm when water in one still and highest production was at 16 pm water with PCM in other still is used. The latent energy stored in the PCM keeps the system operational during the night to deliver distillate output. However, the decreasing trend of all above temperatures show that the quantity of distillate output is reduced due to little difference in the temperature of glass cover and ambience that continues until next day morning. Further, the productivity for given mass of water in the basin of the still with PCM has been plotted for daytime and night hours to understand the operational characteristics of the system. The PCM enhances the productivity of the system by 34 % due to PCM being as heat as source under discharge mode during night. Fig.8 presents the variation of daily accumulative productivity in two stills. A better productivity it appears for still with PCM, and this is because during night the PCM acts as the heat source for basin water, this gives to heatens to higher temperature difference between water and glass due to lower ambient temperature. The amount of heat transferred from the PCM to the water increases the productivity which is found to increase from  $2.07 (\text{kg/m}^2 \text{ on day})$  in still without PCM, to  $2.78 (\text{kg/m}^2 \text{ day})$  in still with PCM. Fig.9 presents the variation of daily efficiency for tow stills which is calculated form formula;

$$y = \frac{m_w * h_{fgw}}{I(t) * A_p} * 100$$

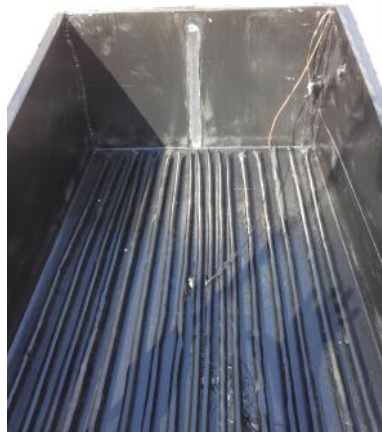
A better efficiency of 60 % has taken place at 15:00 h, for water in still, water temperature was ( $58^\circ \text{C}$ ) and a quantity of distillate water of about ( $0.29 \text{ kg/m}^2 \text{ h}$ ) compared with efficiency of 78.6 % has taken place at 16:00 h and water temperature is ( $60^\circ \text{C}$ ) with a quantity of distillate water of about ( $0.36 \text{ kg/m}^2 \text{ h}$ ) in still with PCM.

#### 4. Conclusions

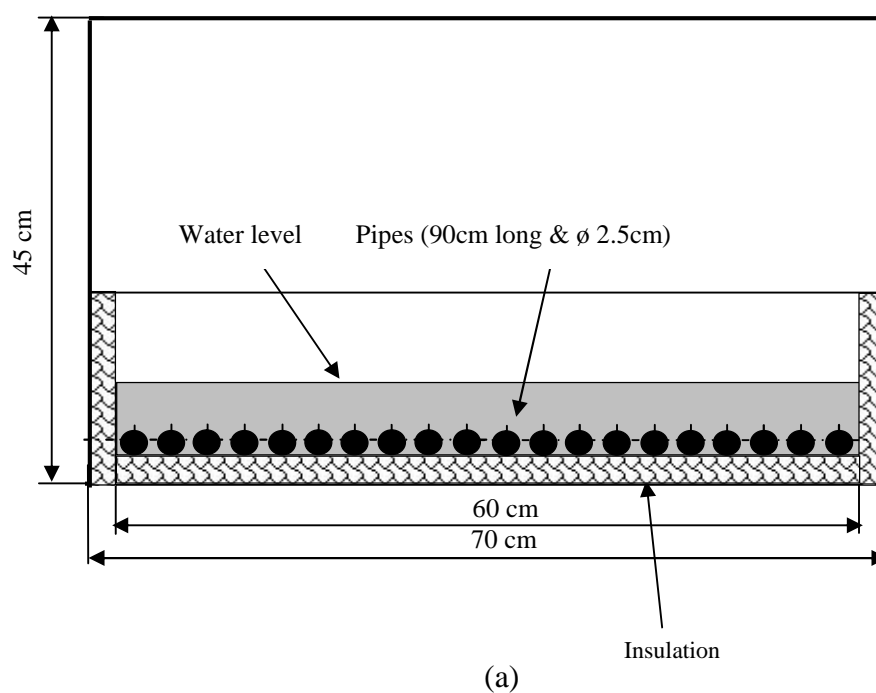
This study shows the potential of integration of phase change material with solar still system for producing potable water throughout the day and night. The preliminary results show that the system dramatically increases the productivity of 34 % with PCM as compared to conventional solar stills. Further it was found that the highest productivity rate varied with the least water depth in the basin of solar still system. Also it can be concluded that the better efficiency 78.6 % was taken when using PCM compared with efficiency 60 % when only water was in the still. It was noticed that the behavior of increase in the productivity with the increase in the solar radiation and this result is in agreement with those reported by Radhwan A. M. [2], El-Sebaai A. A., et al. [3], Akash B. A. et al., [4] and Naim and Abd Elkawi [8].



**Fig. 1. Experiment water stills photo.**



**Fig. 2. Front photo for arrangement of PCM capsules inside basin liner still.**



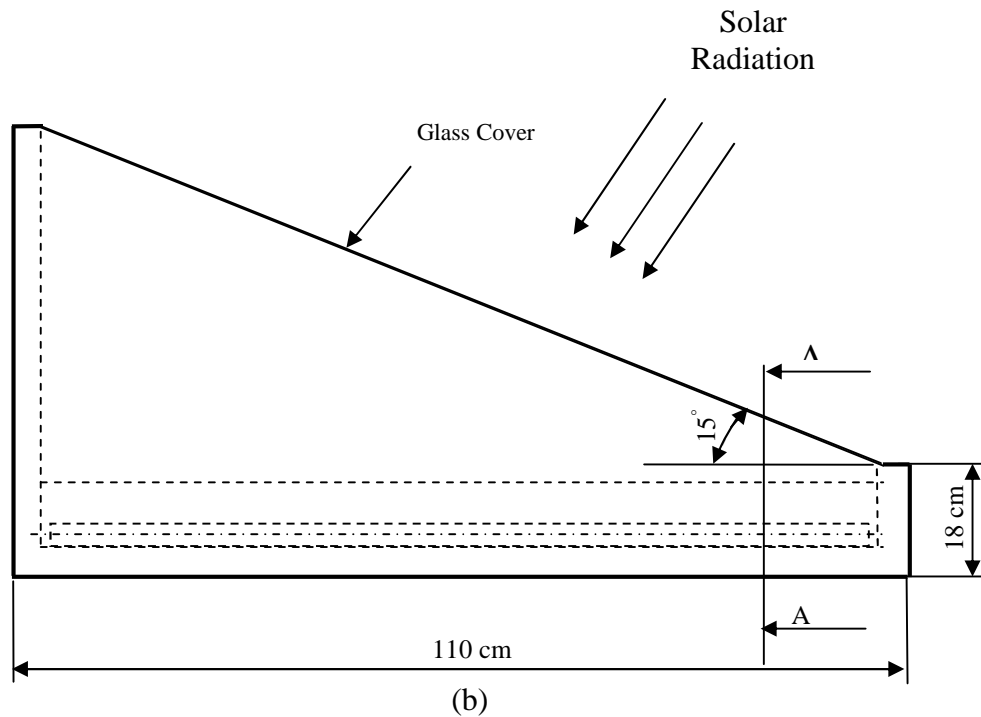


Fig. 3. Still drawing, (a) Section A-A, (b) Side View

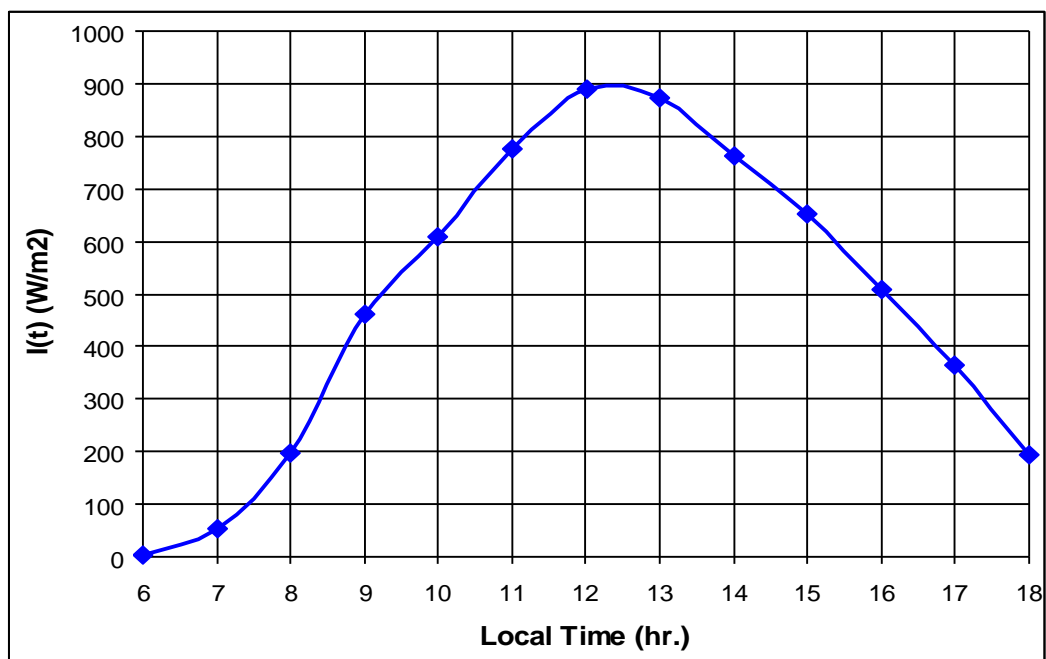


Fig. 4. The solar radiation intensity versus time of the day.

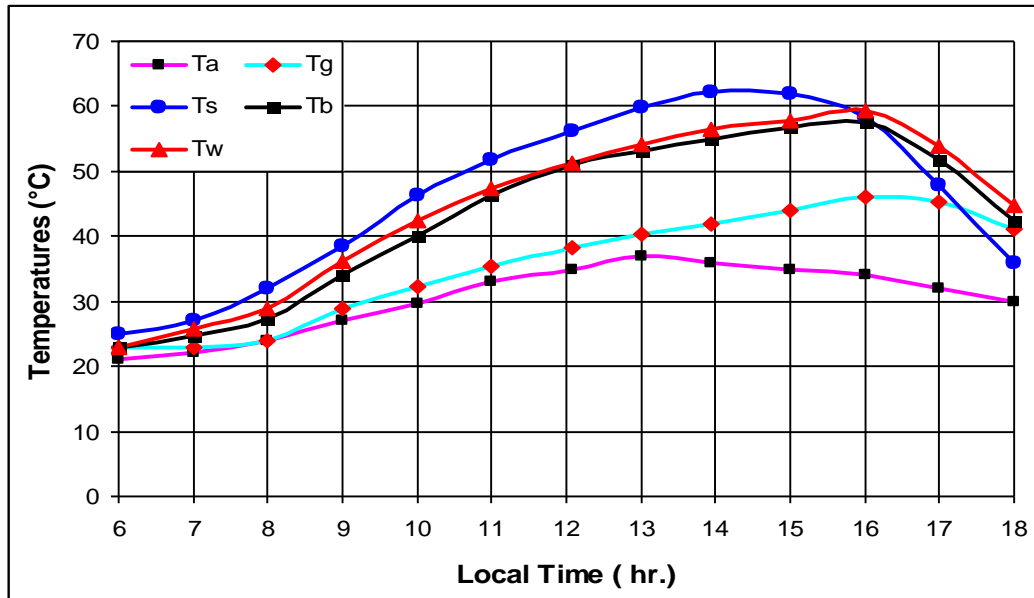


Fig. 5. The hourly variation of water, glass, back plate, steam and ambient temperatures when using water only.

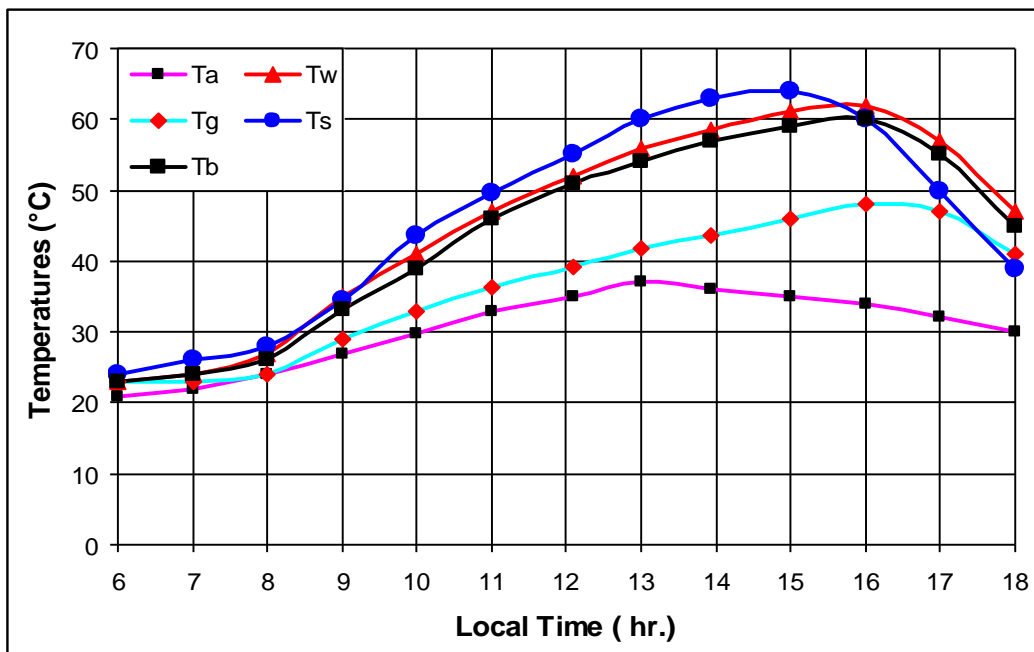


Fig. 6. The hourly variation of water, glass, back plate, steam and ambient temperatures when using wax in the copper pipes.

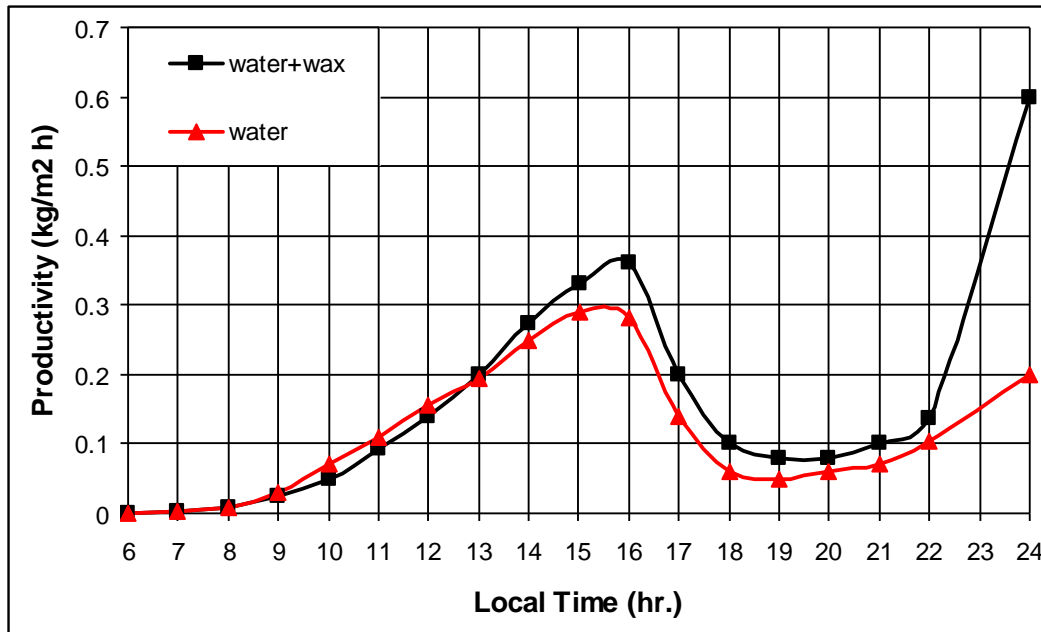


Fig. 7. Variation of productivity for 24 hour for use (a) only water in the still, (b) wax in the copper pipes.

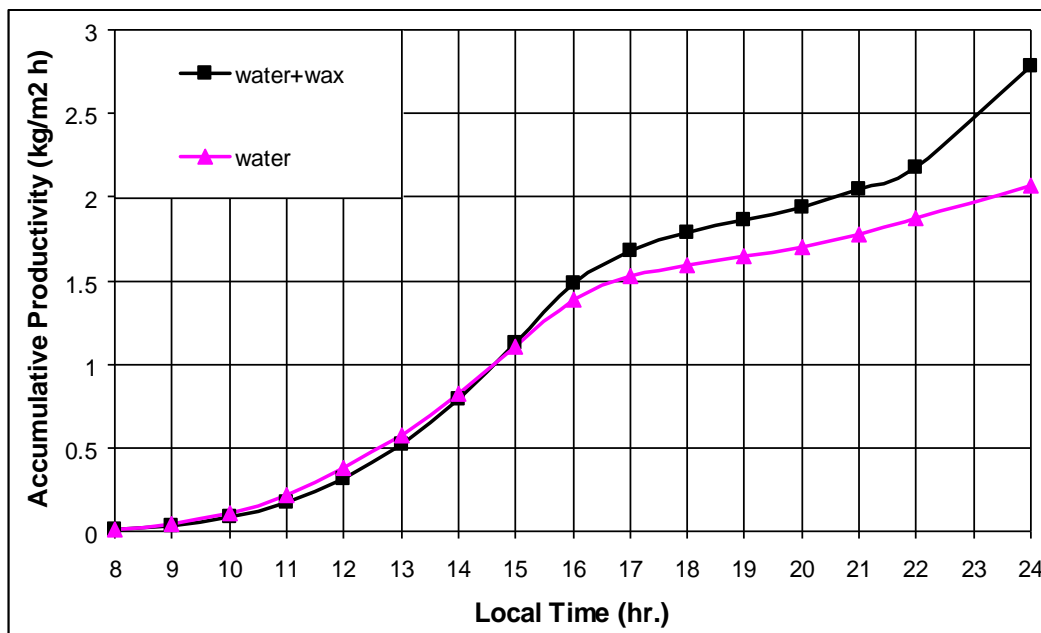


Fig. 8. Variation of accumulative productivity for 24 hour for use (a) only water in the still, (b) wax in the copper pipes.

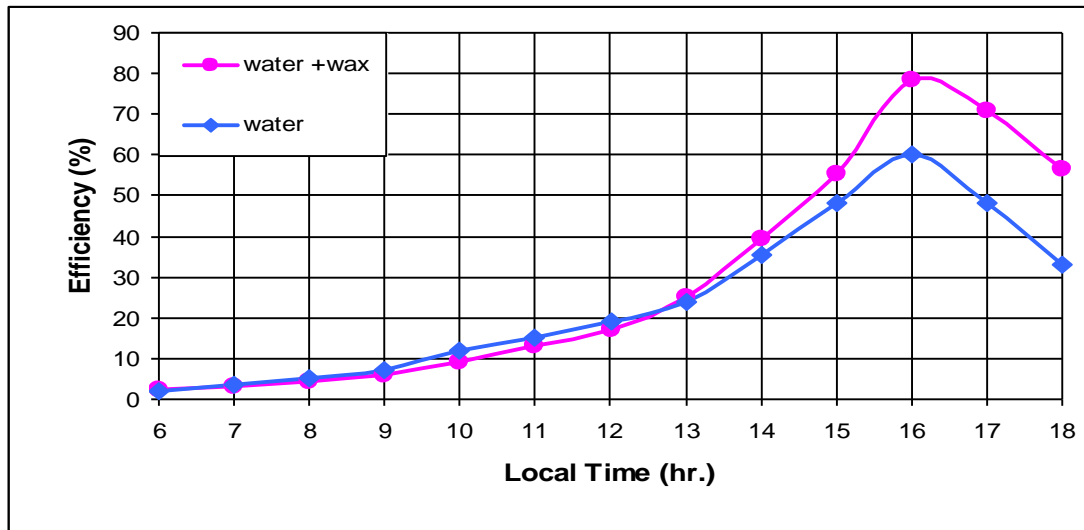


Fig. 9. Variation of daily still efficiency

## 5. References

- [1] Dincer, I., Rosen, M. A. THERMAL ENERGY STORAGE, John Wiley & Sons, Ltd, England, 2002.
- [2] Radhwan A. M. "Transient performance of a stopped solar still with built-in latent heat thermal energy storage", Desalination, Vol. 171, pp. 61-76, 2003.
- [3] El-Sebaei A. A., Al-Ghamdi A. A., Al-Hazmi F. S., Faidah A. S. "Thermal performance of a single basin solar still with PCM as a storage medium", Elsevier Journal Applied Energy, Vol. 86, pp. 1187-1195, 2009.
- [4] Akash B. A., Mohsen M.S., Osta O., Elayan Y. "Experimental evaluation of a single-basin solar still using different absorbing materials", Renewable energy, Vol. 14, pp. 307-310, 1998.
- [5] Badran O.O., "Experimental study of the enhancement parameters on a single slope solar still productivity", Elsevier Journal, Desalination, Vol. 209, pp. 136-143, 2007.
- [6] Gowtham M., Chander M. S., Mallikarujanan K.V.Sri Saila and .Karthikeyan N., "Concentrated Parabolic Solar Distiller with latent heat storage capacity", International Journal of Chemical Engineering and Applications, Vol. 2, pp. 185-188, 2011.
- [7] Medugu D. W., Ndatuwong L. G., "Theoretical analysis of water distillation using solar still", International Journal of physical Sciences, Vol. 4 (11), pp. 705-712, November, 2009.
- [8] Naim M. M., Abd El Kawi M. A., "Non-conventional solar stills Part2. Non-conventional solar stills with energy storage element", Elsevier Journal Desalination, Vol. 153, pp. 71- 80, 2002.
- [9] Ighodalo O. A., Ebhodaghe F. A., "Performance Evaluation of a Solar Still for Salty Water Desalination", Journal of Emerging Trends in Engineering and Applied Sciences, Vol. 2, pp. 338-341, 2011.
- [10] K. Kalidasa Murugavel, Kn. K. S. K. Chockalingam and K. Srithar, 2009, "Modeling and Verification of Double Slope Single Basin Solar Still Using Laboratory and Actual Solar Conditions", Jordan Journal of Mechanical and Industrial Engineering, Vol. 3, pp 228 – 235, 2009.
- [11] Khalifa A. N. and Hamood A. M., "On the verification of the effect of water depth on the performance of basin type solar still", Solar Energy, Vol. 83, pp. 1312–1321, 2009.

## USING PARAFFIN WAX AS A THERMAL STORAGE MATERIAL IN A SOLAR AIR HEATER

Miqdam T Chaichan\* Khaleel I Abaas\* Mohammed A Rasheed\* Hussein A Kazem\*\*

\* Machines and Equipment Engineering Department, University of Technology/Baghdad

\*\* Faculty of Engineering, Sohar University, Sohar, Sultanate of Oman

### Abstract

This paper deals with an experimental investigation of a designed and fabricated air heater consisting of two cases. The first case used concrete as the main part of the air heater. The second case used paraffin wax as phase change material (PCM) accompanied with concrete as the main part of the air heater. Tests were conducted in January and February, 2012 in Baghdad – Iraq weathers.

Results show that the exit air temperature was increased highly for the second case compared with the first case and the efficiency of system was improved and the maximum storage efficiency achieved was 54.13% higher than the concrete case. The air heating gained was in its maximum value at the second case and the maximum increment achieved was 54.97% at Feb.

**Keywords:** Phase change material, solar heating system, air temperature, discharge process.

استخدام الشمع البارافيني كمادة لل تخزين الحراري في سخان هواء شمسي

### الخلاصة

تبين هذه الورقة بحث عملي لسخان هواء شمسي مصمم ومصنع لدراسة حالتين، في الحالة الأولى تم استخدام الكونكريت كجزء رئيسي من سخان الهواء، وفي الحالة الثانية استخدم الشمع البارافيني كمادة متغيرة الطور (PCM) شتراك مع الكونكريت كجزء اساسي من سخان الهواء، تمت التجارب في شهري  
اجواء مدينة بغداد – 2012

تبين النتائج أن درجات حرارة الهواء الخارج تزداد بشكل كبير للحالة الثانية مقارنة بالحالة الأولى وتحسن كفاءة النظام، وكانت أعلى كفاءة خزن تم الوصول لها هي 54.13% كونكريت، وكانت قيمة الحرارة المكتسبة العظمى التي تم الحصول عليها هي للحالة الثانية ومقدار الزيادة كان 54.97% مقارنة بالحالة الأولى لشهر فبراير.

### 1. Introduction:

Increasing energy consumption, shrinking resources and rising energy costs will have significant impact on our standard of living for future generations. In this situation, the development of alternative, cost effective sources of energy for residential housing has to be a priority (Ahmed, 2011). Solar radiation, along with secondary solar resources such as wind and wave power, hydroelectricity and biomass, accounts for most of the available renewable energy on Earth. Only a minuscule fraction of the available solar energy is used. Solar energy is the radiant light and heat from the Sun that has been harnessed by humans since ancient times using a range of ever-evolving technologies (Chaichan, 2011).

Solar technologies are either passive solar or active solar depending on the way they capture, convert and distribute sunlight (Bendea, 2009). Passive solar heating systems using air as the circulating fluid can be used effectively for space heating, particularly in small

spaces such as field huts or refuges (Szymocha, 2005). Air heating collectors have been occasionally used since World War II, mostly for low temperature space heating applications.

Many air heaters were penetrated after 1973 oil crisis, as a part of considerable interest in alternative energies. Stacuna-nathan, 1973 tested passing air between multiple glazing before heat it, and it was found that collector efficiency gained about 10 to 15%.

Modern heaters designs have focus mainly on improving convective heat transfer at the absorber. Mittal, 2006 investigated using wire mesh as a backing material, with air flowing between the absorber and second glazing through the mesh, achieving collector efficiency about 70%. Mohamad, 1997 found that a backing bed of porous media improved heat transfer as well as pre-worming the air by first running it between two glazing plates. This also helps in improving collector efficiency by reducing the overall heat losses. Efficiency achieved was about 75%. Ramadan et al, 2007 used double pass heating in addition to a limestone packing above the absorber plate and passing air through it to improve efficiency.

Latent heat thermal energy storage systems, using phase change materials (PCM) to store heat, have many applications. They are used in solar heating systems in houses and greenhouses to store heat collected during high isolation periods and subsequently liberate heat during the night or other periods, in air conditioning systems to shift peak heating and cooling loads to off-peak hours (Zang, 2006); and in space stations to bridge the eclipse period when no solar energy is available (Regin, 2009). In comparison with other thermal energy storage systems, they potentially have less weight and volume. They also absorb and release heat at a suitable predetermined temperature (Raj, 2011).

Many authors (Regin, 2008 & Bilir, 2005) confirmed that the thermal energy storage systems using PCMs have been recognized as one of the most advanced energy technologies to enhance the energy efficiency and sustainability of buildings. An interesting feature of PCMs is that they can store latent energy as well as sensible energy. Their high latent heat storage capacity combined with friendly energy systems employing endogenous energies, such as solar thermal energy, can reduce the energy consumption of buildings in a passive and sustainable way (Mahmud, 2009). The systems incorporating PCMs benefit also from the isothermal nature of the phase change process (Hazami, 2009).

Assis et al. (2007) experimentally studied the melting of the PCM in a spherical shell which includes the visualization of the process, and compared it with the transient numerical solution performed using the Fluent 6.0 software. A generalized correlation was suggested for the molten fraction, in terms of Fourier number, Stefan number and Grashof number.

Cho (2000) experimentally investigated the thermal characteristics of paraffin in a spherical capsule packed inside a storage tank at different values of the Reynolds number and inlet temperatures. They concluded that the phase change period for the capsule at the edge of the storage tank was shorter than that at the center of the storage tank, because the porosity at the center was smaller than at the edge of the storage tank.

The main goal of the present work is to design a latent thermal energy storage system incorporating PCM, taking advantage of solar energy, which is an abundant resource in Iraq climates, for space heating during the winter season in Baghdad, Iraq.

## 2. Experimental Setup

Two air heaters boxes were designed and fabricated to carry out this study. The two air heaters consist of the following:

- a- The wood box: the boxes were made of wood 1cm thickness to guarantee good thermal insulation. The boxes are opened from above where the glass is fitted. The boxes dimensions were (1 m length, 0.5 m width and 0.15 m height). The front and rear end converge to reduce air flow losses at these two points. Air drawing fan was fitted at the exit, its function was to draw air from the air heater and deliver it to conditioned space. The entrance was fabricated just as the exit with circular form of diameter size 10 cm. The perpendicular distances from the entrance and existence to the air heater (divergent zone for the entrance and convergent zone for the exit) were 35 cm.
- b- The air heater: two air heaters were built. The first one was fabricated from concrete (sand, cement and pebbles) 12 cm thicknesses. Ten copper pipes (2.58 cm dia and 1 m long) were fixed inside the concrete block. These pipes were opened from its ends to allow air to pass through. The air gains transmitted heat from concrete to pipes while it is passing through it to the conditioned space. This crossing air was considered the base of comparison in the present study. Three essential parts form this air heating system, these parts are: a single transparent glass, isolated duct and the storage unit which is consist of a single row of cylinders. This unit works to satisfy two goals; absorb and storage the solar energy. The concrete block face was painted with absorbent black paint. The total mass of the concrete material is about 80 kg.  
 The second air heater was fabricated in the same dimensions of the first one. It was built from concrete also but three rows of copper pipes (each one consists of 10 pipes) were fitted inside it uniformly. The middle row pipes were open ends used for air passing. The higher and lower rows were closed ends filled with paraffin wax which is the PCM used in this study. Wax weight used in this study was 9.72 kg. The design takes into consideration many con-cerns such as, the integration with PCM storage unit, the simpl-icity of construction, dismantlement, and hand-ling the PCM unit. The experimental trials consist of two different processes, such as charging and discharging. The charging process is done by heating the PCM bed from concrete temperature (at constant temperature), until the entire PCM changed its phase completely. During the discharging process, heat is supplied through the heated PCM bed to concrete and air. Table 1 illustrates some of concrete and parrafin wax specifications.
- c- Glass: 2mm thickness glass was fixed at the top of the two boxes to cover the concrete wall and the entrance cone. It was fixed by silcon material to prefent any air leakage 3 cm above the concrete wall. Exposing the aluminun chips for sun rays was the reason for covering the entrance cone with glass.
- d- Thermocouples: six copper-constantant thermocouples were fixed in six palces inside concrete block. Two were fixed at the block top, two at the middle and two at the bottom of the block. The avarage of these thermocouples was consid-ered as the concrete temp-erature. Four thermocouples were fixed in each PCM layer. It was distri-buted in a way that its avarage can be considered as the higher and lower wax temperature. Two mercury thermometers were fixed in the air entrance and exit to meas-ure its temperature in each case.
- e- Exit air velocity measuring device: Exit air velocity was measured by (Anom-eter). All the measuring devised were calibrated and there accuracy was found as will be seen in uncrtinaty paragaph.
- f- Aluminum reflectors: two wooden sections were covered from one side with aluminum foils and used as reflectors. They were used to insure concentrating the sun rays on the

air heater at the morning and noon periods. After sunset these sections were used as covers for the air heaters to prevent any heat transfer by radiation or convection to the surrounding.

g- The Fan: A constant speed fan (10 cm dia. and 100 W powers) was used to maintain a laminar flow.

A schematic diagram of the experimental setup used in this study is given in Figure 1 & 2, while Figure 3 represents a photo of the air heater.

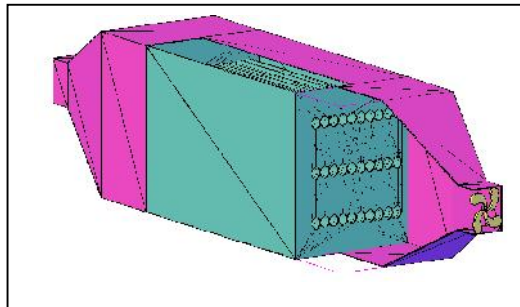


Fig.(1), a schematic diagram of the experimental setup used in this study

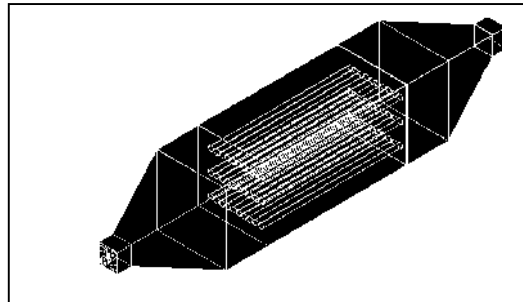


Fig.(2), a schematic diagram of the experimental setup used in this study



Fig. (3), Photograph for the air heater used in the study

## Test Procedure

Experimental measurements tests were conducted for the air heaters at the following cases:

- 1- First case: Concrete wall alone inside the air heater box.
- 2- Second case: Concrete wall with PCM pipes inside the air heater box.

Tests were conducted from 1/ 1/ 2012 to 15/2/ 2012 in Baghdad city-Iraq winter weathers. The incident solar intensity for the former mentioned period was taken from the Iraq Meteorology Organization. Measures were taken for the studied cases at the same time and day. The temperatures were measured for several days in each month at a rate of two times per week. The average of these measured readings were considered as the hourly temperatures for each studied month. The measures started at 7.00 AM and continued until the wall temperature equalized entering air temperature.

The following equations were used to calculate storage energies and heating efficiency for each part of the used systems.

- 1- The stored energy in concrete wall:

$$Q_c = m_c c_{p_c} \Delta T_{h_c} \quad (\text{kJ}) \quad (1)$$

- 2- The stored energy in paraffin wax

$$Q_w = m_w c_{p_w} \Delta T_{h_w} \quad (\text{kJ}) \quad (2)$$

- 3- Air mass flow rate

$$m_a = \rho_a Q \quad (3)$$

- 4- Air volume flow rate

$$Q = A V \quad (4)$$

- 5- Heat transfer by air

$$Q_a = m_a c_{p_a} \Delta T_{h_a} \quad (\text{kW}) \quad (5)$$

- 6- First case (Concrete) thermal storage efficiency (first case)

$$\eta_{storage} = \frac{Q_c}{I A} \quad (\%) \quad (6)$$

- 7- Second case (Concrete+PCM) thermal storage efficiency

$$\eta_{storage} = \frac{Q_c + Q_w}{I A} \quad (\%) \quad (7)$$

- 8- System heating efficiency

$$\eta_{heat} = \frac{Q_{air}}{I A} \quad (\%) \quad (8)$$

### 3. Results and Discussions

Fig. 4 shows the air heating process parts temperatures, inlet cold air, exit hot air and concrete wall temperature. Concrete wall temperature increases highly due to solar intensity starting from 8 AM until 2 PM. After 2 PM the wall temperatures reduces due to solar intensity declines accompanied with cold air entering causing exit air temperatures to be reduced and drops. The air temperature increment rate at Jan. was 61.8% while at Feb. was 57.92%. These results indicate that the air heating system can be used for Baghdad City weathers efficiently.

Fig. 5 represents temperatures details for the second case tested in this study where PCM was added to the concrete wall. Temperature increase and reduction still the same as fig.3, except for in this case warming time extended for about two to three hours more. Concrete temperature relatively maintained the same temperatures as case one, putting in mind, that concrete mass in this case less than case one, whereas PCM pipes take place, on the account of concrete mass. At the time of warming (from 7 AM to 2 PM) concrete temperatures exceeded all other temperature. After 2 PM concrete sensible heat gained at the last period reduced faster than PCM. Wax temperature after 2 PM exceeded all other temperatures depending on its stored sensible and latent heats. The air temperature increment rates were 78.92 and 65.08% for Jan. and Feb. respectively. It can be realized from figures 3 & 4 results that the increment rates at Jan. are higher than that at Feb. This is due to the higher inlet air temperatures introduced to the air heater at Baghdad Feb. days.

Fig. 6 represents air stored energy for the two studied cases versus time. It is clear from the figure that the second case stored the highest energy in air. This case contains the effect of concrete sensible heat in addition to wax sensible and latent heat. For comparison purposes, the increments in air stored energy at Jan. were 52.59 for case 2 compared with case 1. The increments were 54.97 for case 2 compared with case 1 at Feb. It can be observed that higher heat was gained at Feb. due to higher solar intensity in Baghdad City region.

Fig. 7 demonstrates the tested systems efficiencies versus time. It is clear that higher system efficiency can be achieved using the second case (concrete+wax). Increments in system efficiency percentages were 49.38 at Jan. and 54.13 at Feb. for cases2 compared with case 1.

Fig. 8 illustrates the tested system thermal storage efficiency versus time. Case 2 still rank the highest thermal efficiency due to availability of concrete sensible heat storage added to wax sensible and latent heat storage. The increments in thermal storage efficiencies were 44.39% at Jan, while at Feb. it were 49.19% for case 2 compared to case 1.

Fig. 9 shows the charging period of PCM. This period starts from the first daytime but it appears clearly starting from 11 AM and it expands till 2 PM. In this period PCM temperature increased to reach wax melting point, at which it settles until all the wax melting is completed. The liquid wax temperature starts to increase higher than melting point for the rest of the charging period. Wax phase changing in addition to sensible heat which it stores after melting ensures high thermal energy storage.

Fig. 10 represents the discharge period of PCM. This period starts around 2 PM and it expands until all the stored energy is used. PCM temperatures reduced in this period and paraffin wax started to lose its sensible stored energy until it reaches melting point. At this point it settles until all wax changes its phase to solid phase. After all the wax is solidified its

temperature reduces in high rate due to two reasons. The first one is the time of this operation takes place after 2:30 PM where the solar intensity starts to drop and inlet air temperatures stated to reduce more.

#### 4. Conclusions

Two cases were studied in the present paper, simple case of air heater made of concrete, in the second heater PCM was added to the system. The tests were conducted at Baghdad city winter days between 1-1-2012 to 15-2-2012. The results indicate the following:

1- Adding PCM to concrete (case 2) improves the air heater system. Compared with case 1 (concrete heater) for Jan. and Feb. respectively the following is resulted: the gained temperatures increased with about 61.8. The air stored energy was improved about 54.97. The system efficiency was improved to 54.13%.

2- Adding PCM to concrete system improves the charging period. It also decelerates the system temperature lose at discharging period. This addition helps the system to warm air for longer time.

3- The results demonstrate that case 2 air heating system is adequate for air heating purposes in Iraqi winter weathers.

Table (1), Specifications of concrete and paraffin wax used in present study

|                                            | Concrete | Paraffin wax |
|--------------------------------------------|----------|--------------|
| Density s ( $\text{kg/m}^3$ )              | 2300     | 930          |
| Density l ( $\text{kg/m}^3$ )              |          | 830          |
| Cp s ( $\text{kJ/kg h}$ )                  | 880      | 1850         |
| Cp l ( $\text{kJ/kg h}$ )                  |          | 2384         |
| Heat storage capacity s ( $\text{kJ/kg}$ ) | 8.8      | 212          |
| Heat storage capacity l ( $\text{kJ/kg}$ ) |          | 175          |

#### References

- [1]- Ahmed S T & Chaichan M T, A study of free convection in a solar chimney sample, Engineering and Technology J, vol. 29, No. 14, pp: 2986-2997, 2011.
- [2]- Chaichan M T & Abaas Kh I, Practical investigation for measurement of concentrating solar power prototype for several target cases at Iraqi summertime weathers, 1<sup>st</sup> Scientific Conference for Energy & Renewable Energies Applications, UOT, Baghdad, Iraq, 2011.
- [3]- Bendea C, Rosca M, Karitas K, High solar fraction heating and cooling systems, Analele Universit ii din Oradea Fascicula de Energetic , vol. 15, 2009.
- [4]- Szymocha K, Advanced thermal solar system with heat storage for residential house space heating, SESCOI 2005 Conference, British Columbia Institute of Technology, Burnaby, British Columbia, Canada, August 20 - 24, 2005.

- 
- [5]- Stacunanathan S & Deonarine S, A tow-pass solar air heater, Solar Energy, vol. 15, No. 1, pp: 41-49, 1973.
- [6]- Mittal M &Varshney L, Optimal thermohydrolic performance of a wire mesh packed solar air heater, Solar Energy, vol. 80, No. 9, pp: 1112-1120, 2006.
- [7]- Mohamad A, High efficiency solar heater, Solar Energy, vol. 60, No. 2, pp: 71-76, 1997.
- [8]- Ramadan M, Al-Sebaili A, Aboul-Enein S & Al-Bialy E, Thermal performance of a packed bed double-pass solar air heater, Energy, vol. 33, No. 8, pp: 1524-1535, 2007.
- [9]- Zang Y P, Lin K P, Yang R, Di H F &Jiang Y, Preparation, performance and thermal application of shape-stabilized PCM in energy efficient buildings, Energy and buildings, vol. 38, No. 10, pp: 1262-1269, 2006.
- [10]- Regin F, Solanki F S C & Saini J S, An analysis of a packed bed latent heat thermal energy storage system using PCM capsules: Numerical Investigation, Renewable energy, vol. 34, pp: 1765-1773, 2009.
- [11]- Raj A & Velraj V R, Heat transfer and pressure drop studies on a PCM-heat exchanger module for free cooling applications, Intl. Journal of thermal sciences, available online, 2011.
- [12]- Regin F, Solanki A S C & Saini J S, Heat transfer characteristics of thermal energy storage system using PCM capsules: A review, Renewable & Sustainable Energy Reviews, vol. 12, pp: 2438-2458, 2008.
- [13]- Bilir L & Ilken Z, Total solidification time of a liquid phase change material enclosed in cylindrical/Spherical containers, Applied Thermal Engineering, vol. 25, pp: 1488-1502, 2005.
- [14]- Mahmud A, Sopian K, Alghoul M A & Sohif M, Using a paraffin wax-aluminum compound as a thermal storage material in a solar air heaters, ARPN Journal of Engineering and Applied Sciences, vol. 4, No. 10, 2009.
- [15]- Hazami M, Kooli S, Lazâar M, Farhat A & Belghith A, Energy and exergy efficiency of a daily heat storage unit for buildings heating, Revue des Energies Renouvelables, vol. 12, No. 2, pp: 185 – 200, 2009.
- [16]- Assis E, Katsman L, Ziskind G & Letan R, Numerical and experimental study of melting in a spherical shell, Intl. Journal of Heat and Mass Transfer, vol. 50, pp:1790-1804, 2007.
- [17]- Cho K & Choi S H, Thermal characteristics of paraffin in a spherical capsule during freezing and melting processes, Intl. Journal of Heat and Mass Transfer, vol. 43, pp: 3183-3196, 2000.

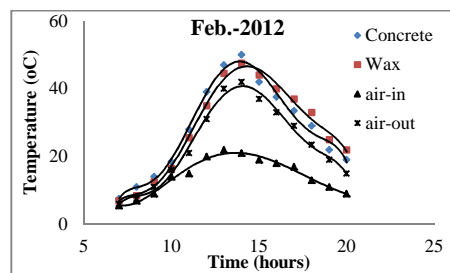
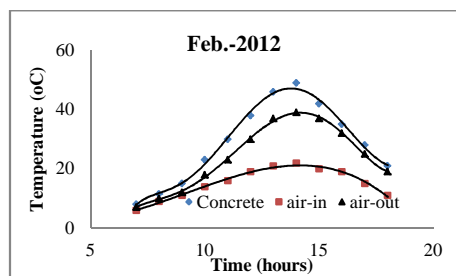
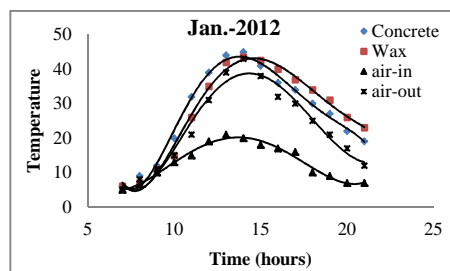
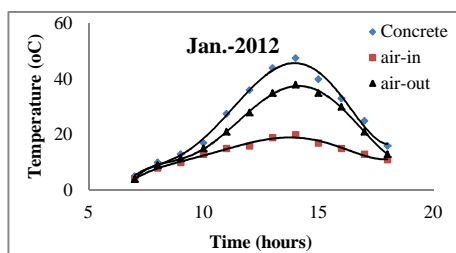


Fig. (4), Temperatures of air heater parts for the first case

Fig. (5), Temperatures of air heater parts for the 2<sup>nd</sup> case

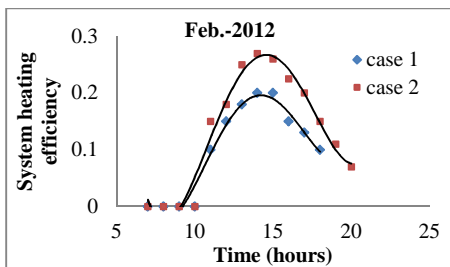
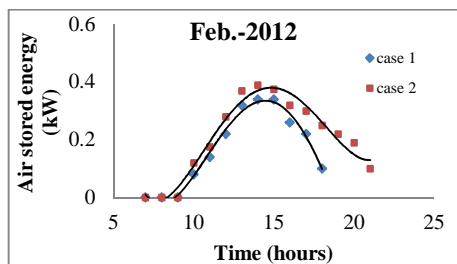
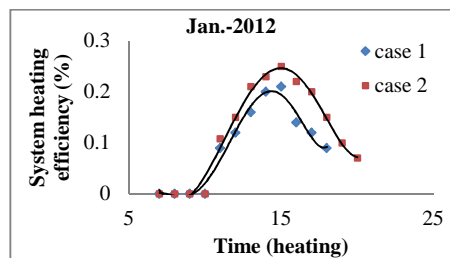
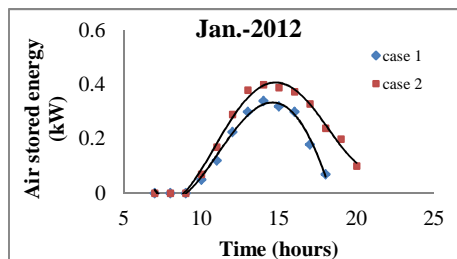


Fig. (6), Air stored energy for the two studied cases

Fig. (7), System heating efficiency for the two studied cases

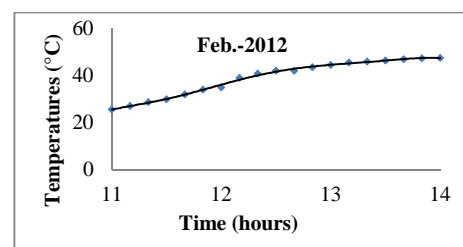
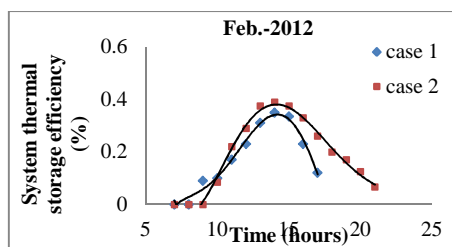
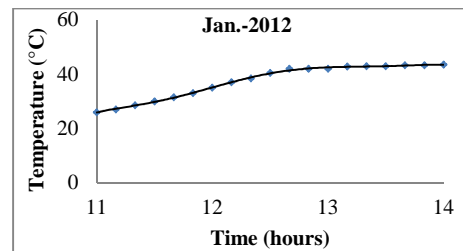
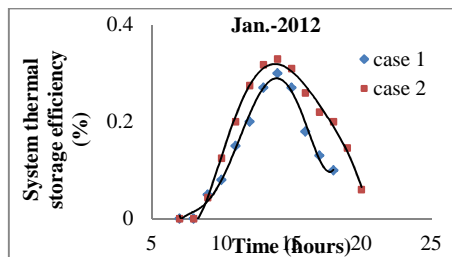


Fig. (8), System heating efficiency for the two studied cases

Fig. (9), PCM charging behavior for paraffin wax (case 2)

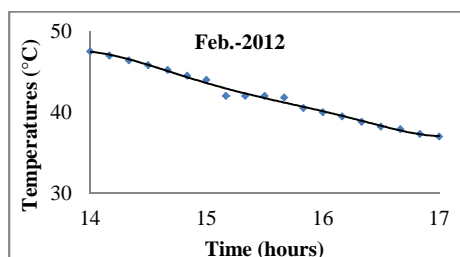
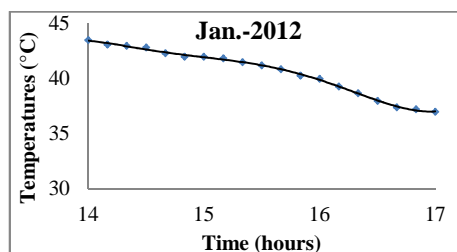


Fig. (10), PCM discharging behavior for paraffin wax (case 2)



## Nomenclature:

$A_d$  -The drum area at normal operating level ( $m^2$ )  
 $C_p$  - Specific heat at constant pressure ( $KJ/kg.k$ )  
 $D_i$  ,  $D_o$  - inter and outer drum diameter (m)  
 $h_{fg} - h_{fg} = h_g - h_f$  entropy of evaporation ( $KJ/kg$ )  
 $h_c$  - Condensation enthalpy ( $KJ/kg$ )  
 $h_f$  - Specific enthalpy of saturated liquid water ( $KJ/kg$ )  
 $h_s$  - Specific enthalpy of steam ( $KJ/kg$ )  
 $h_g$  - Specific enthalpy of dry super heated ( $KJ/kg$ )  
 $h_w$  - Specific enthalpy of feed water ( $KJ/kg$ )  
 $K$  - Friction coefficient in down comer-riser loop  
 $L$  - Drum water level (m)  
 $L_s$  - Level variations caused by changes of the amount of steam in the drum (m)  
 $L_w$  - Level variations caused by changes of the amount of water in the drum (m)  
 $m_s$  - Mass flow rate of steam exiting the boiler to turbine ( $Kg/s$ )  
 $m_w$  - Mass flow rate of water ( $Kg/s$ )  
 $Q$  - Heat flow rate ( $KJ/h$ )  
 $Q_f$  - Feed water flow rate ( $KJ/h$ )

$Q_s$  - Steam water flow rate ( $KJ/h$ )  
 $t_d$  - Residence time of the steam in the drum(s)  
 $T_s$  - Saturation temperature for steam ( $^{\circ}C$ )  
 $V_d$  - Volume of boiler drum ( $m^3$ )  
 $V_{dc}$  - Volume of down comer ( $m^3$ )  
 $V_r$  - Volume of riser ( $m^3$ )  
 $V_{sd}$  - Volume of steam in drum ( $m^3$ )  
 $V_{sd}^0$  - Volume of steam in drum at equilibrium ( $m^3$ )  
 $V_{wd}$  - Volume of water in drum ( $m^3$ )  
 $V_{wt}$  - Total volume of water in drum ( $m^3$ )  
 $X$  - Mass fraction of steam in the flow (-)

## Greek symbol

$\Gamma$  - Volume fraction of steam in the flow (-)  
 $S$  - Parameter in empirical formula (-)  
 $\dots_g$  - Density of saturated steam ( $Kg/m^3$ )  
 $\dots_w$  - Density of water ( $Kg/m^3$ )

## Introduction

Water circulation in natural circulation drum boilers is one of the critical problems in boiler technology. Poor water circulation may cause tube rupture resulting in unscheduled boiler shutdown that may interrupt plant operation. Such poor circulation may arise from operational-type problems such as rapid rises in boiler load causing rapid rises in the heat flux as a result of rapid rises in fuel flow rates. It is known that each boiler tube experiences different heating conditions due to the no uniformity of heat flux distribution in the furnace. During the last few years, some boiler explosions were attributed to poor water circulation [1, 2]. As a result, calculations and measurements of water circulation and other operating parameters, such as steam quality and void fraction, have become more important not only for boiler manufacturers but also for large industrial establishments as well as insurance companies. Adequate water circulation is necessary to cool tubes that form boiler walls. Criteria are required to determine the potential for tube overheating. These criteria can be applied using circulation modeling and calculations to identify problem areas. Modeling the steam generator system including drum boiler, riser and down comer is one of the important problems [3, 4]. The motive force driving the steam/water mixture through the tubes in a natural circulation system is the difference in density between cooler water in the down

comer circuits and the steam/water mixture in the riser tubes. This flow must be adequate to cool the tubes and prevent overheating. Normally, overheating of riser tubes are due to one of two reasons. The first occurs under steady-state conditions when the tubes are partially blocked such that the pressure losses increase. As a result the mass flow rate of water decreases at the same heat flux causing less heat transfer to the water and consequent overheating of the tube metal. The second cause occurs when sudden rise in the heat flux occurs and is followed by an increase in the steam quality. As a result, circulation decreases as a result of increase in the pressure [5, 6]. A schematic picture of a boiler system is shown in Figure (1, a, b), the heat ( $Q$ ) supplied to the riser's causes boiling. Gravity forces the saturated steam to rise causing a circulation in the riser-drum-down comer loop. Feed water is supplied to the drum and saturated steam, ( $q_s$ ), is taken from the drum to the super heaters and the turbine [7].

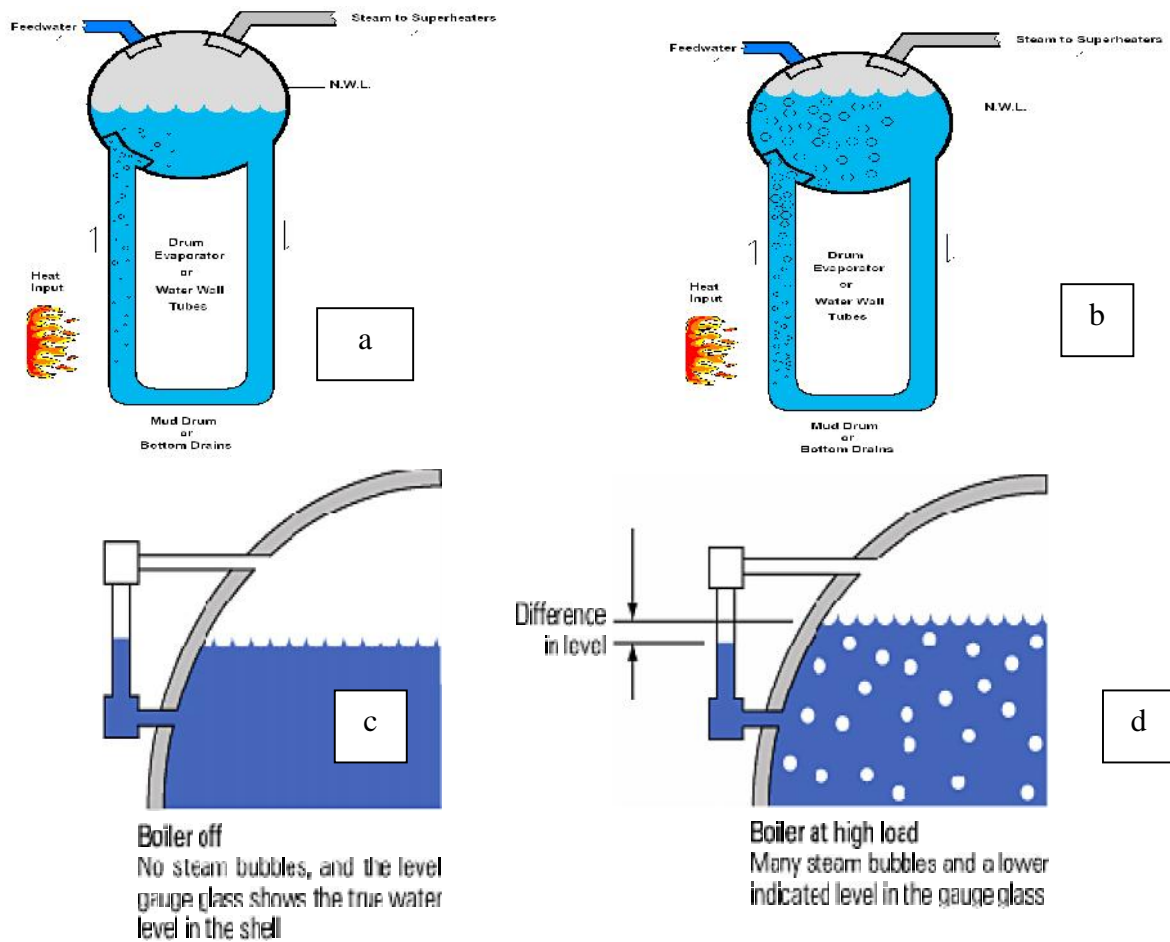


**Figure (1) Bubbles effect on the drum level, a - Low firing rate - High firing rate, c - Neutral drum level, d - Rise drum level [7]**

**Astrom and Bell [8]** developed a model of nonlinear dynamic system and describes the complicated dynamics of the physical plant. It was shown that the dynamic fuzzy model gives in some appropriate sense accurate global nonlinear prediction and at the same time that

its local models are close approximations to the local linearization of the nonlinear dynamic system.

**Kim and Choi [9]** developed a model for water level dynamics in the drum–riser–down comer loop of a natural circulation drum-type boiler. The model is based on basic conservation rules of mass, momentum, and energy, together with the constitutional equations. The work provides an investigation of the response of water level dynamics to changes in steam demand and/or heating rate.

**The present work** aims at developing, utilizing nonlinear modeling, a numerical procedure for the dynamic simulation of natural circulation steam generator system and investigating the dynamic response of the pressure in the drum, steam quality at the exit of the riser tubes to rapid variations in fuel flow rate (heat input) and experimental measurement of upper drum parameters (drum pressure and drum water level) under these vibrations to optimize the steam generator operation to prevent the overheating of the riser tubes.

#### **Theoretical work:-**

The theoretical work was included: - calculations of heat transfer coefficient and wall temperature, in addition of the governing equations of boiler were solved numerically.

#### **Heat transfer coefficient calculation**

The two-phase (liquid and vapor) flow pattern in a pipe depends on many parameters such as the flow velocity, the quality of the mixture, the properties of the two phases (density, viscosity and surface tension) and the pipe geometry as well as its orientation. The flow patterns in horizontal tubes are slightly different due to the effect of gravity.

A large number of empirical and semi-empirical correlations are available to predict heat transfer coefficients for the flow boiling regimes in vertical and horizontal tubes. Some of these correlations have been widely tested and are practically used. The calculation of the heat transfer coefficient includes a convection evaporation term and nucleate boiling term and is expressed as [10, 11, 12]

$$h = h_l [C_l (Co)^{c_2} (25F_r)^{c_5} + BO^{c_4} F_k] \quad (1)$$

$$Nu = 0.023 (Re_e)^{0.8} (Pr)^{0.4} \quad (2)$$

$$F_r = \frac{G^2}{\rho_l^2 g D} \quad (3)$$

$$BO = \frac{q}{G h_{fg}} \quad (4)$$

$$CO = \left( \frac{1-x}{x} \right)^{0.8} \left( \frac{\rho_v}{\rho_l} \right)^{0.5} \quad (5)$$

### Wall temperature calculations

To calculate the inside and outside wall temperatures of the riser tube [13, 14, and 15]:

$$qfD_o = \frac{T_i - T_{sat}}{R_{conv}}, \quad (6)$$

$$R_{pipe} = \frac{\ln(D_o / D_{in})}{2fK_{pipe}}, \quad R_{conv.} = \frac{1}{fD_i h} \quad (7)$$

The system considered includes the drum, riser and down comer, the presence of steam below the liquid level in the drum causes the shrink-and-swell phenomenon which makes level control difficult. The outflow from the risers passes through a separator to separate the steam from the water. In spite of the complexity of the system it turns out that its gross behavior is well captured by global mass and energy balances. The balance thermal equation for burning process can be obtained from the following equation: [16, 17, 18 and 19]:-

$$\frac{d(m_g H_{gf})}{dt} = A.C_{pA}.TA + k_{comb}.B.H_{cn} - G_e C_{pg}.T_g - K_{Re}(T_m^4 - T_s^4) \quad (8)$$

Where A - Air, B - the fuel flow, Ge - the evacuated gas, Kcomb - the burning coefficient . The heat exchange to furnace zone (convection, conduction and radiation) and the water from pipes, at the saturation temperature Ts, is equivalent with a direct heat exchange through radiation.  $T_m$  is the middle temperature of burning gases. From the law of perfect gases [20,21and 22]:-

$$m_g H_{gf} = \frac{VC_{vg} P_f}{R} \quad (9)$$

$$\frac{VC_{vg}}{R} \frac{dp_f}{dt} = .C_{pA}.TA + k_{comb}.B.H_{cn} - G_e C_{pg}.T_g - K_{Re}(T_m^4 - T_s^4) \quad (10)$$

$$a_{11} \frac{dV_{wt}}{dt} + a_{12} \frac{dP}{dt} = \dot{m}_w - \dot{m}_s \quad (11)$$

$$a_{21} \frac{dV_{wt}}{dt} + a_{22} \frac{dP}{dt} = \dot{Q} + m_w h_w - m_s h_g \quad (12)$$

$$a_{32} \frac{dP}{dt} + a_{33} \frac{dX}{dt} = \dot{Q} - x h_{fg} \dot{m}_{dc} \quad (13)$$

$$a_{42} \frac{dP}{dt} + a_{43} \frac{dX}{dt} + a_{44} \frac{dV_{sd}}{dt} = \left(\frac{\ddot{m}_g}{T_d}\right)(V_{sd}^0 - V_{sd}) + \frac{(h_w - h_f)}{h_{fg}} \dot{m}_w \quad (14)$$

The governing equations consist of conservation of mass and energy of the total system. The equations governing the phase change in the drum include the steam and water volumes inside the drum and the rate of steam condensation and the equations governing the flow

circulation in the riser–down comer loop, which govern the transport of the mass , energy and momentum.

Thus, a set of four differentials nonlinear equations representing the time dependence of the state variables of the pressure, steam quality, total water volume and steam volume in the drum can be presented as follows [23, 24 and 25]. The coefficients of these four equations are given by

$$a_{11} = \dots_f - \dots_g = \dots_{fg} \quad (15)$$

$$a_{12} = V_{wt} \frac{\partial \dots_f}{\partial p} + v_{st} \frac{\partial \dots_g}{\partial p} \quad (16)$$

$$a_{21} = \dots_f h_f - \dots_g h_g \quad (17)$$

$$a_{22} = V_{wt} (h_f \frac{\partial \dots_f}{\partial p} + \dots_f \frac{\partial h_f}{\partial p}) + V_{st} (h_g \frac{\partial \dots_g}{\partial p} + \dots_g \frac{\partial h_g}{\partial p}) - V_t + MC_p \frac{\partial T_s}{\partial P} \quad (18)$$

$$a_{32} = (\dots_f \frac{\partial h_f}{\partial P} - X h_{fg} \frac{\partial \dots_f}{\partial P})(1-r)V_r + (1-X)h_{fg} \frac{\partial \dots_g}{\partial P} + \dots_g \frac{\partial h_g}{\partial P} r V_r +$$

$$(\dots_g + X \dots_{fg}) h_{fg} v_r \frac{\partial r}{\partial P} - V_r + M_r C_p \frac{\partial T_s}{\partial P} \quad (19)$$

$$a_{33} = ((1-X)\dots_g + X \dots_f) h_{fg} V_r \frac{\partial r}{\partial x} \quad (20)$$

$$a_{42} = V_{sd} \frac{\partial \dots_g}{\partial P} + \frac{1}{h_{fg}} \{ \dots_g V_{sd} \frac{\partial h_g}{\partial P} + \dots_f V_{wd} \frac{\partial h_f}{\partial P} - V_{sd} - V_{wd} + M_d C_p \frac{\partial T_s}{\partial P} \}$$

$$+ X(1+S)V_r [r \frac{\partial \dots_g}{\partial P} (1-r) \frac{\partial \dots_f}{\partial P} + (\dots_g - \dots_f) \frac{\partial r}{\partial P}] \quad (21)$$

$$a_{43} = X(1+S)(\dots_g - \dots_f) V_r \frac{\partial r}{\partial x} \quad (22)$$

$$a_{44} = \dots_g \quad (23)$$

## The numerical solution

### A. The initial conditions

To obtain the initial conditions, the following equations must be solving:-

$$\dot{m}_w = \dot{m}_s \quad (24)$$

$$\dot{Q} = \dot{m}_s (h_g - h_w) \quad (25)$$

$$\dot{Q} = Xh_{fg} \sqrt{\frac{2 \dots_f A_{dc} (\dots_f - \dots_g) g r V_r}{k}} \quad (26)$$

$$\dot{m}_r = \dot{m}_{dc} \quad (27)$$

$$\dot{m}_{ct} = \dot{m}_w (h_f - h_w) / h_{fg} \quad (28)$$

$$r = \frac{\dots_f}{\dots_{fg}} \left[ 1 - \frac{\dots_s}{x \dots_{fg}} \ln \left( 1 + \frac{\dots_{fg}}{\dots_g} \right) \right] \quad (29)$$

$$Q = \dot{m}_{dc} (x h_{fg}) \quad (30)$$

$$V_{sd} = V_{sd}^0 - \frac{t_d (h_f - h_w)}{\dots_g h_{fg}} m_w \quad (31)$$

$$V_{wt} = V_{wd} + V_{dc} + (1 - r) V_r \quad (32)$$

$$t_d = \frac{\dots_g}{m_{sd}} V_{sd}^0 V_{wd} + V_{dc} + (1 - r) V_r \quad (33)$$

## B. The constants and boundary conditions

The operational data are taken from power plant characteristics such as, drum pressure, steam mass flow rate, drum volume, riser and downcomer volumes, water surface area, feed water temperature and thermal conductivity of the pipe material. There are many constants according to the boundary conditions as following [26, 27]:-

**I -** Convection number  $\leq 0.65$  ( $C1 = 1.136$ ,  $C2 = -0.9$ ,  $C3 = 667.2$ ,  $C4 = 0.7$  and  $C5 = 0.3$ ).

**II-** Convection number  $\geq 0.65$  ( $C1 = 0.6683$ ,  $C2 = -0.2$ ,  $C3 = 1058$ ,  $C4 = 0.7$  and  $C5 = 0.3$ ) the convection number calculated from equation (5).  $C5 = 0$  for vertical tubes and  $C5 = 0$  for horizontal tubes if  $Fr$  is greater than 0.04.  $Fk = 1$  for water (a fluid dependent parameter),  $hL$  is the single phase heat transfer coefficient and is calculated from the Dittus– Boelter equation (1).  $S = 0.3$  (Empirical value used for calculation the coefficients in equations 21 and 22).

## C. The solution procedure

A numerical scheme for the solution of the governing differential equations was established. The dynamic response of the system's state variables due to rapid changes in fuel flow rate (heat input) was investigated. The present model was used for the prediction of possible tube overheating was devise. The solution procedure can be summarized: - equations (1)–(7) were used to calculate the heat transfer coefficient and metal temperature. Equations (11)–(14) were solved simultaneously using an explicit method time step is 0.3 s for a total time 200 s. The

coefficients in these equations were obtained from Equations (15)–(23). As well as other main boiler parameters calculated from others equations.

## Experimental work

The experimental work was applied on the steam generator of Didacta – Italia power plant. All the parameters are measured after the plant reached to thermal equilibrium state and any others data are taken from the technical characteristics of steam generator. The experimental work included the measurements and calculation of the main parameters as the following:-

### A. Measurements

The test was performed for the changes in drum pressure and drum water level in response to step variations in firing rate ( increasing of heat input by 10% and 20%). The measurements provide firing rate variations with time. The following parameters are measured:-

#### 1. Measurement of drum level

The drum level has a complicated geometry d11 (glass gauge 113 mm length) as shown in figure (2) in steam generation unit. To measure the drum level response with firing rate, read drum level directly from the glass gauge (d11) with the same time when we measure the drum pressure at increasing the firing rate by (10% and 20%). The drum has a complicated geometry. The linearized behavior can be described by the wet surface ( $A_d$ ) at the operating level. The deviation of the drum level ( $l$ ) measured from its normal operating level is [29]:-

$$L = \frac{V_{wd} + V_{sd}}{A_d} = L_s + L_w \quad (34)$$

To measure the drum level response with firing rate change, read drum level directly from the glass gauge (d11) with the same time when we measure the drum pressure at increasing firing rate by (10% and 20%) . Repeat the same procedure above but in opposite i.e. drum level response with decreasing firing rate by 10 %, and 20%

#### 2- Measurement of drum pressure

The drum pressure Gage (PI) in steam generation unit as shown in figure (2) changes with variation of firing rate (heat input), to measure this variation, we start the plant and let the plant run a long enough to reach stabilization i.e. until steam pressures and temperatures in the various points of the circuit and the cooling water temperature at outlet from the condenser remain constant. When stabilization is reached, record the drum pressure measurements with the time under increasing of firing rate by 10% and 20%. At each change, we are read the drum pressure by Gage (PI) with time.

#### 3- Measurement of differential pressure

$\Delta p$  = differential pressure (mm Hg) measured by using of a calibrated diaphragm.

#### 4- Measurement of feed water

Feed water volume ( $V_{f.w.}$ ) measured directly as shown in figure (2)

#### 5- Measurement of fuel level

Fuel level measured from fuel tank as shown by figure (2)

## B- Calculation procedure

The value of mass flow rate of steam ( $m_s$ ) can be calculated from the following equation after measure the value of the differential pressure ( $\Delta p$ ) mm Hg [29]:-

$$m_s = r \cdot v \frac{f d^2}{4} \sqrt{2 \Delta p} [kg / s] \quad (35)$$

Where,  $r$  - coefficient of discharge = 0.60845,  $v$  - expansibility factor = 0.99658,  $d$  - orifice diameter = 20.5 mm, internal pipe diameter = 27mm,

Steam temperature ( $T_s$ ) measured directly from the control unit in steam power plant (Electric control and command board). Also the data of burner are taken from the technical characteristics of burner such as, rate of consumption ( $m_f$ ) can be calculating from the following equation [29]:-

$$m_f = \frac{L_f \cdot 0.8}{\dagger_f} \cdot 3600 [kg / h] \quad (36)$$

Where,  $L_f$  = level reading of fuel tank, 0.8 = specific weight of the fuel,  $\dagger_f$  = measured time.

Feed water mass flow rate ( $m_w$ ) calculated by measured of feed water volume ( $V_{f.w.}$ ), and time of boiler operation ( $\dagger_{b.p.}$ ),  $v_{f.w.}$  was taken from tables (according to pressure and temperature of boiler), then ( $m_w$ ) can be calculate from the following equation [29]:-

$$m_w = \frac{\dot{V}_{f.w.}}{v_{f.w.}} \quad \dots(37)$$

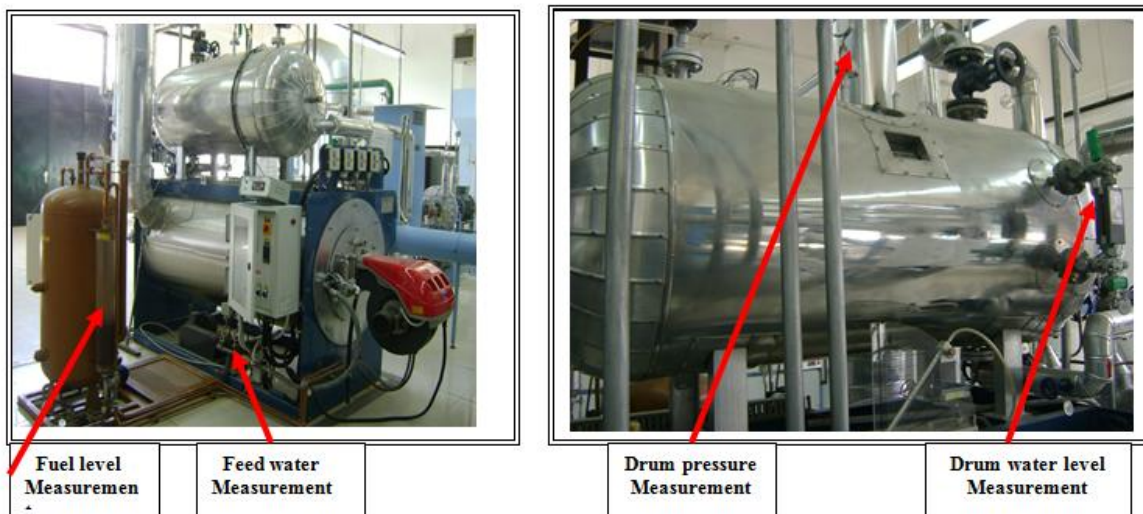


Figure (2) Steam generation unit of power plant (Didacta- Italia)

## Results and discussion

Figure 3 presents an experimental and theoretical behavior of drum pressure with time; the fluctuation of drum pressure with time is due to the firing rate variations with time as shown in figure 4.

Figure 5 presents the change of the pressure as a result of sudden increase in heat input ( $Q$ ), and shows that the pressure increases at a constant rate of  $dP/dt$  as a result of a step rise in the heat input of 10% and for the case of 20% step rise in the heat input in order to explain the increase in the drum pressure.

Figures (6 and 7) are provided and present the response of the mass flow rates in risers and downcomers for the two cases of step rise in heat input. The riser mass flow exhibits a sudden increase as a result of increase in the heat input. As the heat input, is increased, a sudden increase from the steady-state value in the mass flow rate in the riser occurs.

However, the downcomer flow exhibits a gradual increase with time. Thus, the outlet of the riser first increases and then decreases to match the flow in the downcomer. Thus, the difference between the riser and downcomer mass flow rates, increases suddenly causing increase in the mass flow rate into the drum and the volume of steam–water in the drum.

The difference between both of the two flow rates diminishes at around 30 s from the moment of the step rise in heat input. This is followed by a continuous gradual decrease in the risers and downcomers mass flow rates. The case of 20% step rise shows similar trends but with higher magnitudes of flow rates in risers and downcomers. As well, the difference between the riser and downcomers at start of the rise is much higher for the case of 20%. Consistent with the increase in heat input, the quality at exit of the riser increases as a result of increased rate of evaporation. The quality increases first at a high rate during the first 10 s. Figures (8 and 9) are present the dynamics of steam and water volumes in the drum under the water level. The difference between the mass flow rate in the risers and downcomers along with the increase in the quality leads to a rise in the mass of water as well as steam in the drum. As well, as shown in Figures (8 and 9), the volume of the steam within the liquid (under water level) in the drum,  $V_{sd}$ , increases as a result of a combined increase in the riser flow rate and the quality at exit of the riser. The increase in the riser flow rate and the quality cause high increase in steam flow into the drum, which results in increase in  $V_{sd}$ .

Figure (10) indicates that the rate of condensation as a result of increase in pressure increases suddenly and then continues to increase but at a lower rate. The main cause of condensation is due to the increase in the pressure at the same saturation temperature  $T_s$ .

Figure (11) shows that the total volume of water in the system,  $V_{wt}$ , increases. The increase in  $V_{wt}$  is a result of increase of  $V_{wd}$  and the condensation of the steam under the water level in the drum. Consistent with the increase in the total water volume,  $V_{wt}$ , Figure 9 shows a decrease in the total steam volume,  $V_{st}$ , according to the relation  $V_{st} + V_{wt} = V$ .

The response of heat transfer coefficient,  $h$ , is shown in figure (12) and the response of the liquid heat transfer coefficient;  $h_L$  is presented in figure (13). As shown in Figure (12),  $h$  decreases during the first ten seconds. This is followed by increase in  $h$  with time. Despite that the case of 20% exhibit higher values of  $h$ , the rate of increase in  $h$  is slower for the case of 20%.

Figure (14) explain the variation of temperature difference between the metal and saturated steam for step rise in heat input.

Figure (15) exhibits the distribution of the void fraction that indicates a rapid increase in the first few seconds then followed by a continuous reduction in its value. As a result, the heat transfer coefficient decreases as shown in figure (12). This explains the behavior of the heat transfer coefficient,  $h$ , in figure (12).

Figure (16) provides a comparison of the water level due to liquid and steam contents. The small differences are due to the steam contribution to water level the present calculations and those of kim and choi , show that the volume of bubble continue to increase at a lower rate rather than decrease .

## Conclusions

The present model is used to investigate the dynamic effects of rapid changes in fuel flow rate on the overheating of the riser tubes in natural circulation water tube boilers. The system under consideration includes the drum, riser and down comer as its major components. A numerical scheme for the solution of the governing differential equations was established. The dynamic response of the system's state variables due to rapid changes in fuel flow rate and steam flow rate was investigated.

The results indicate that increasing the heat flux by 10% and by 20% can lead to high variations in pressure, steam quality and water level in the drum. As well, the changes in the heat transfer coefficient lead to a temperature increase in the riser metal temperature. The riser temperature increases due to the increase in the steam temperature and due to the dynamic influence resulting from increase in the heat flux .The experimental and theoretical results of the water level in the drum are in reasonable comparison and with kim and choi results.

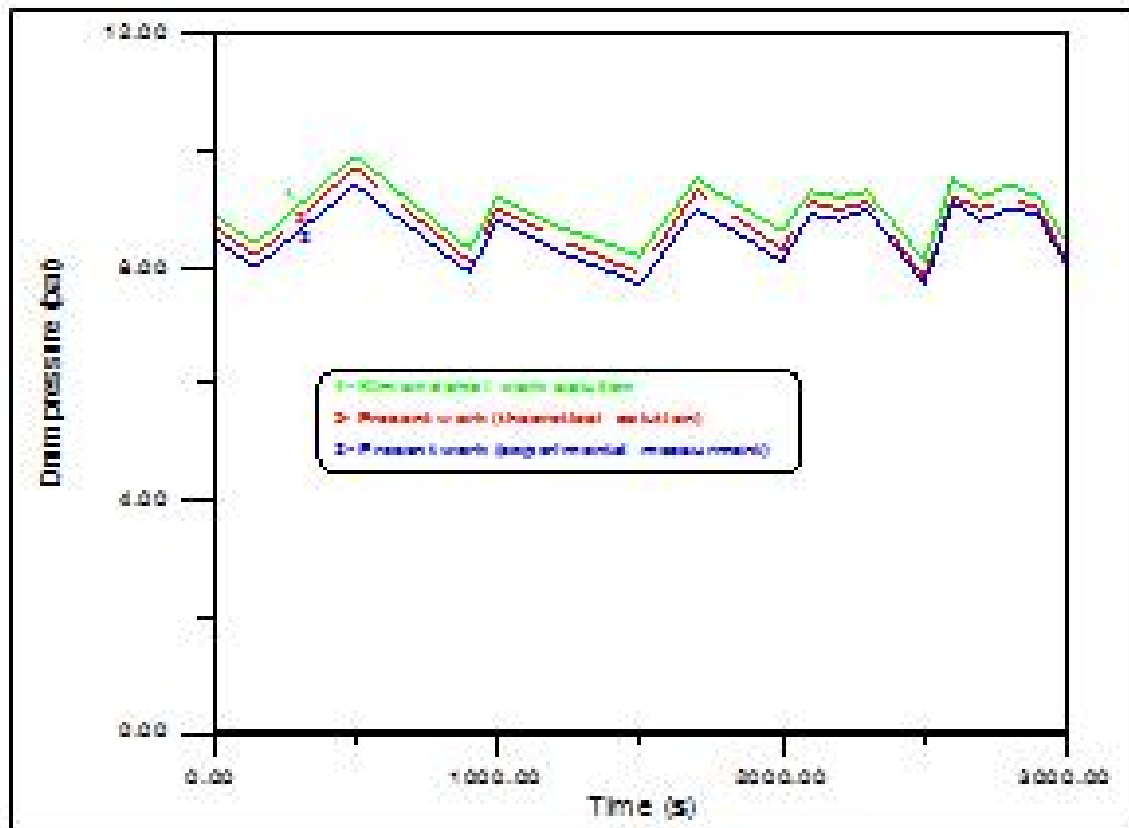


Figure (3) Response of drum pressure to variations in firing rates

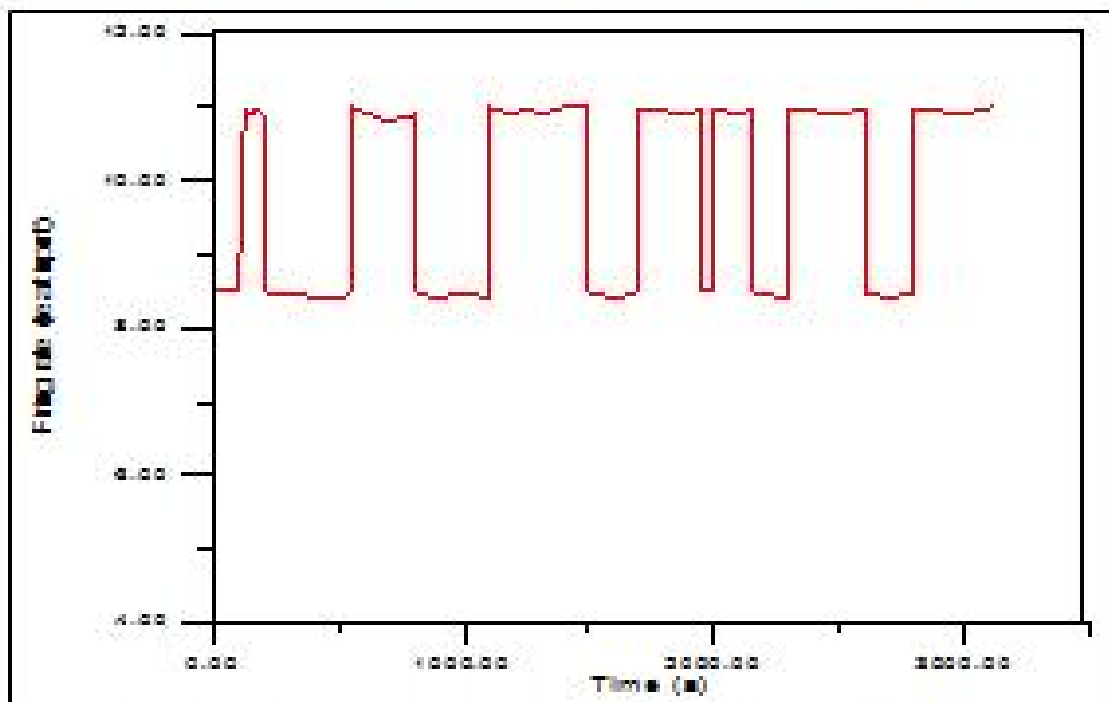


Figure (4) Experimental measurements for distribution firing rate

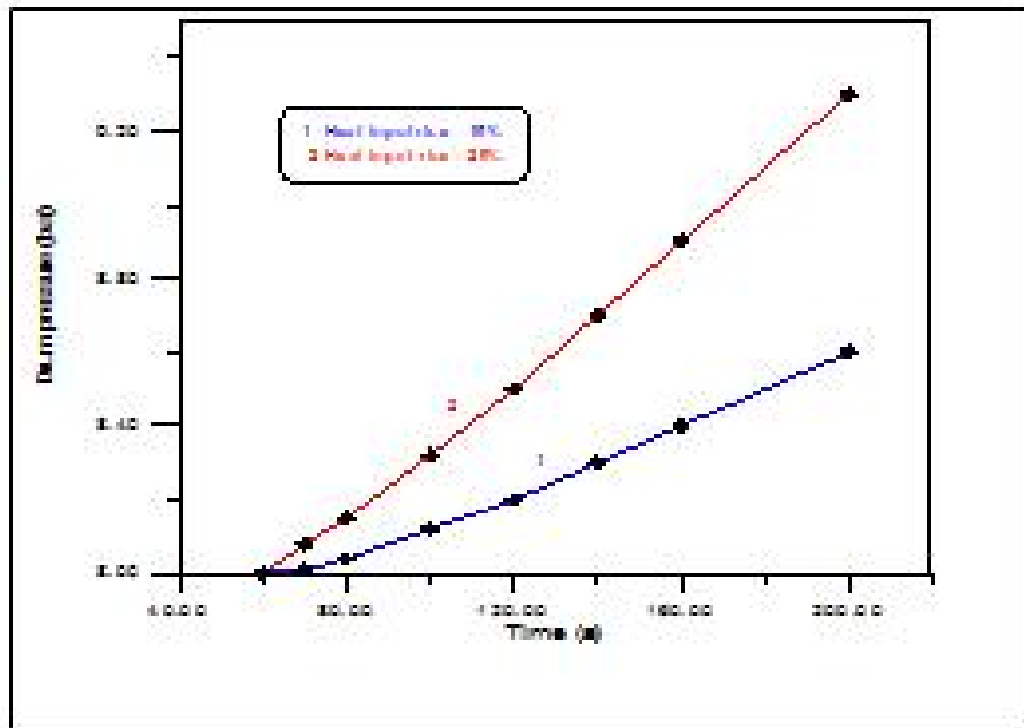


Figure (5) Variation of drum pressure for step rise in heat input

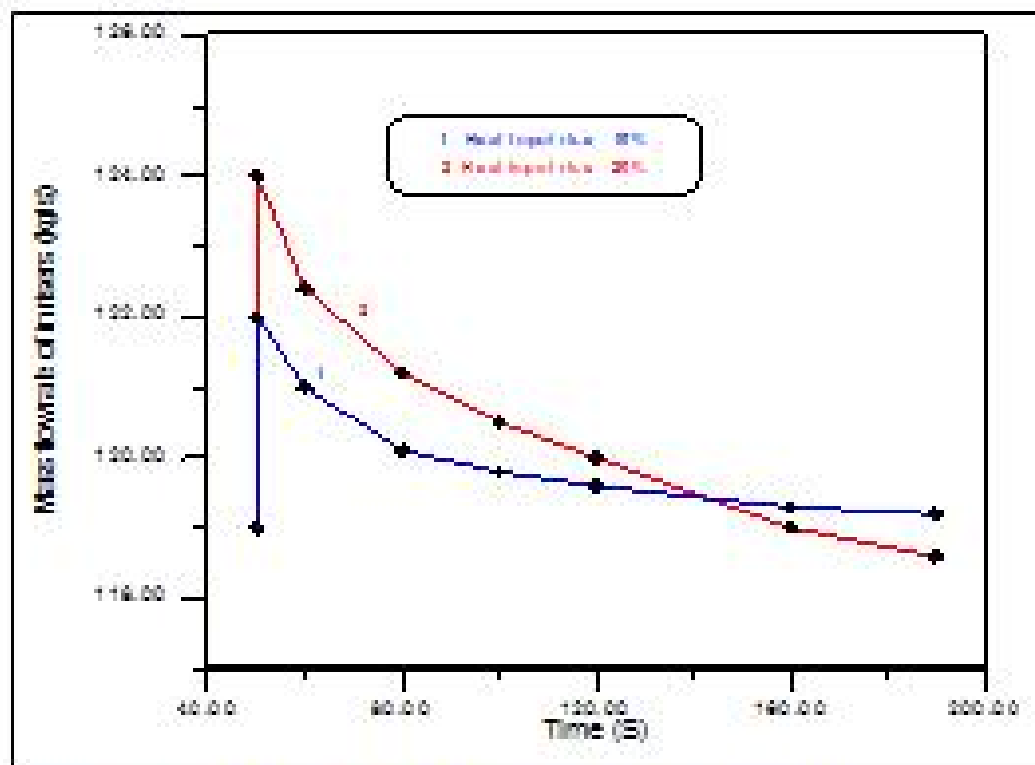


Figure (6) Variation of mass flow rate in risers for step rise in heat input

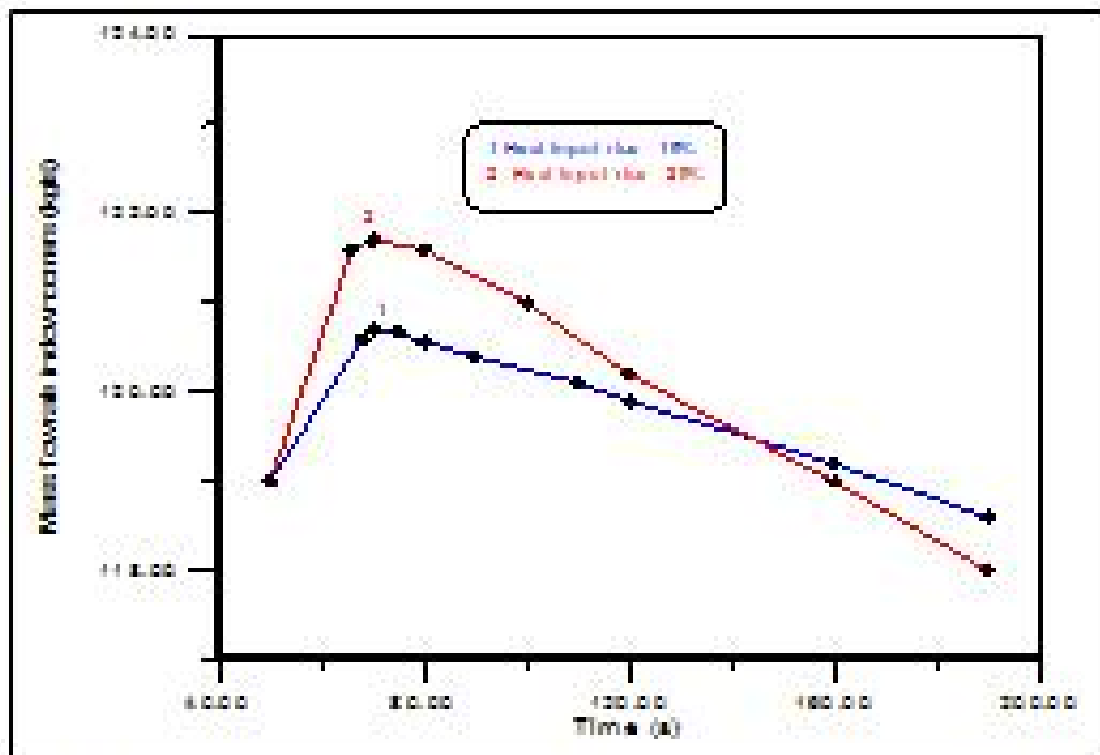


Figure (7) Variation of mass flow rate in development for step rise in heat input

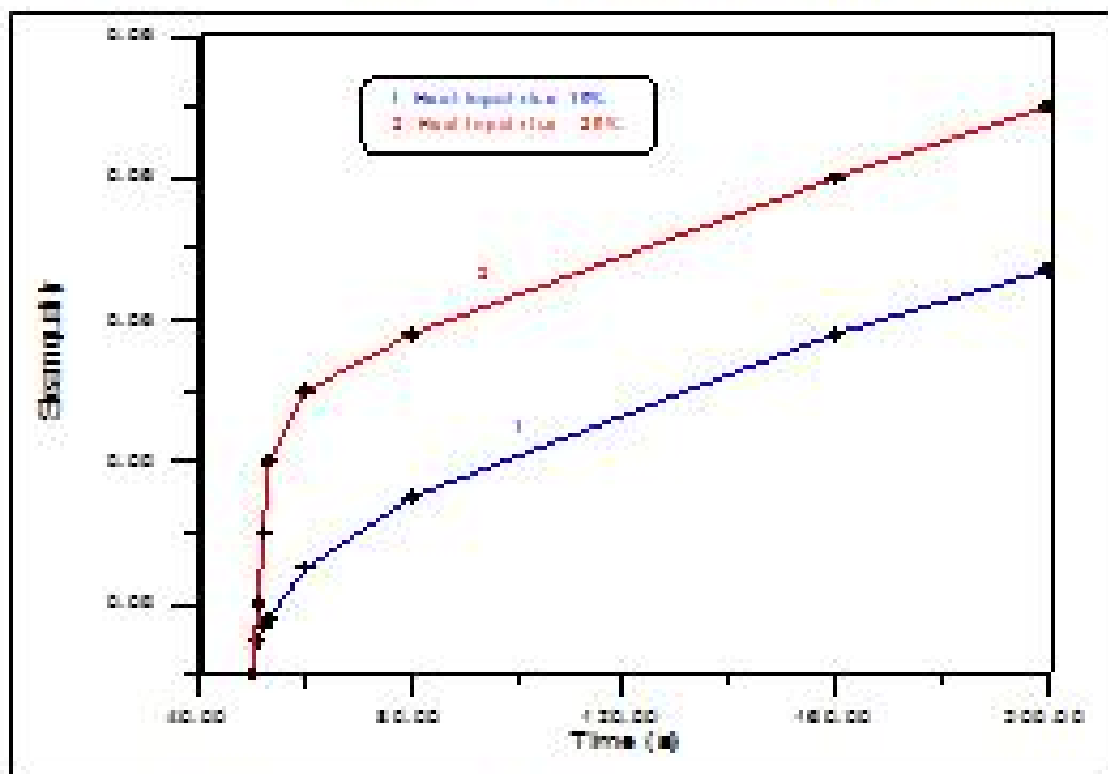


Figure (8) Variation of steam quality for step rise in heat input

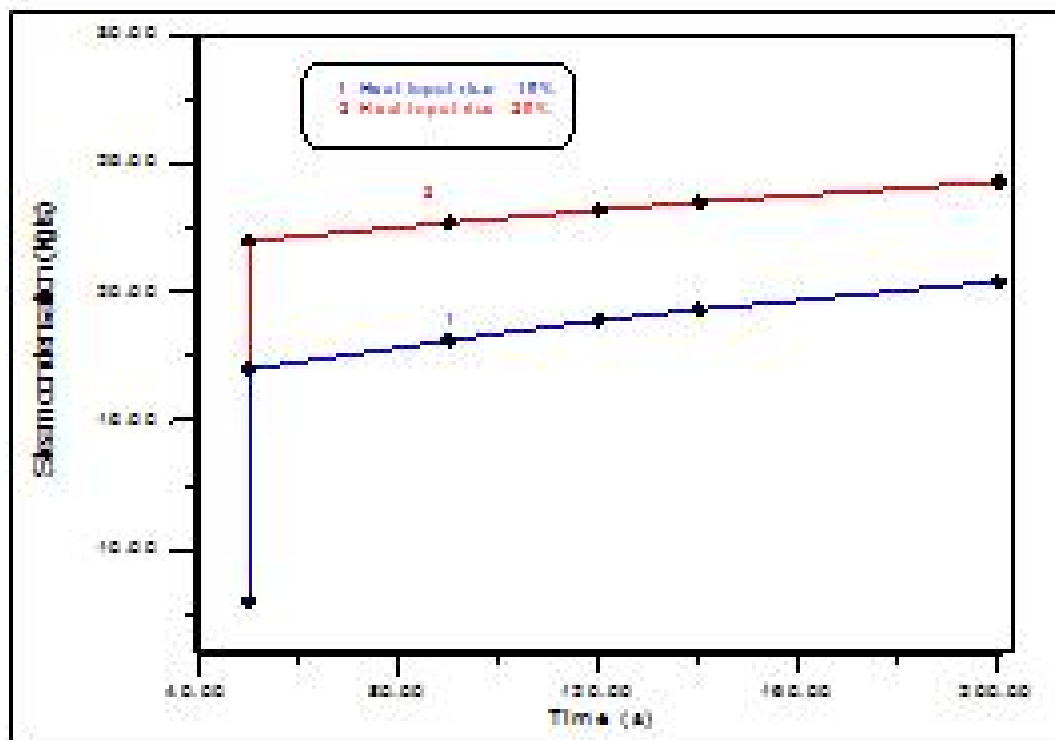


Figure (9) Variation of steam condensation for step rise in heat input

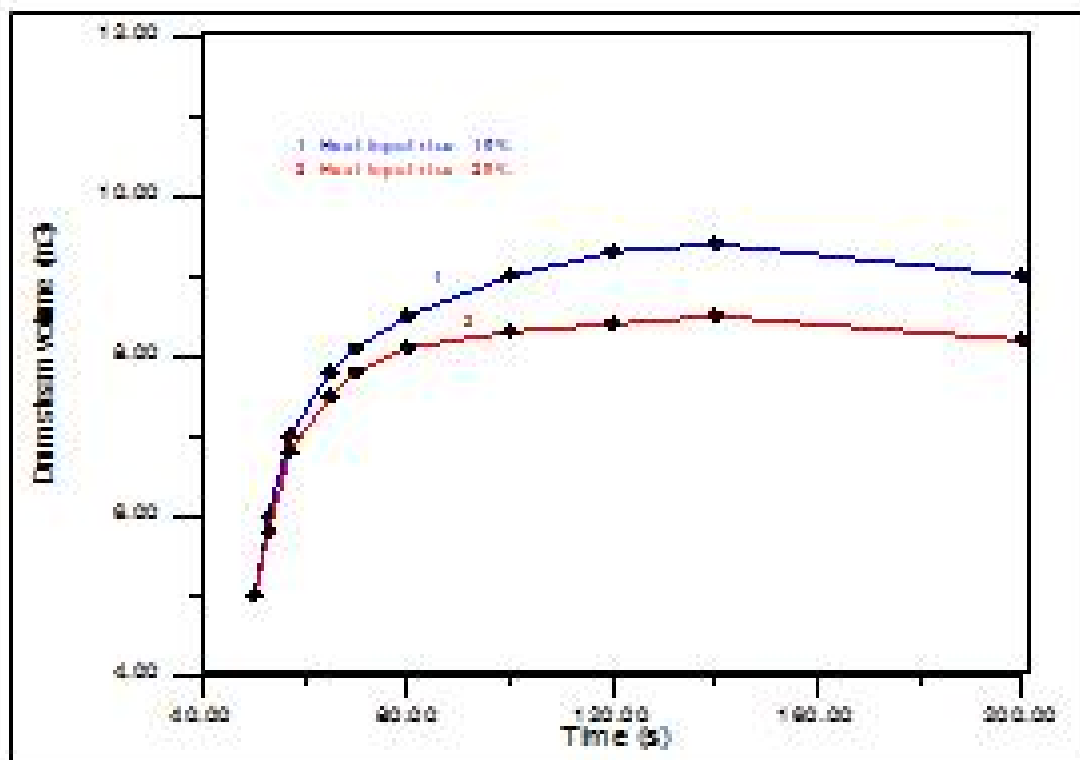


Figure (10) Variation of steam volume for step rise in heat input

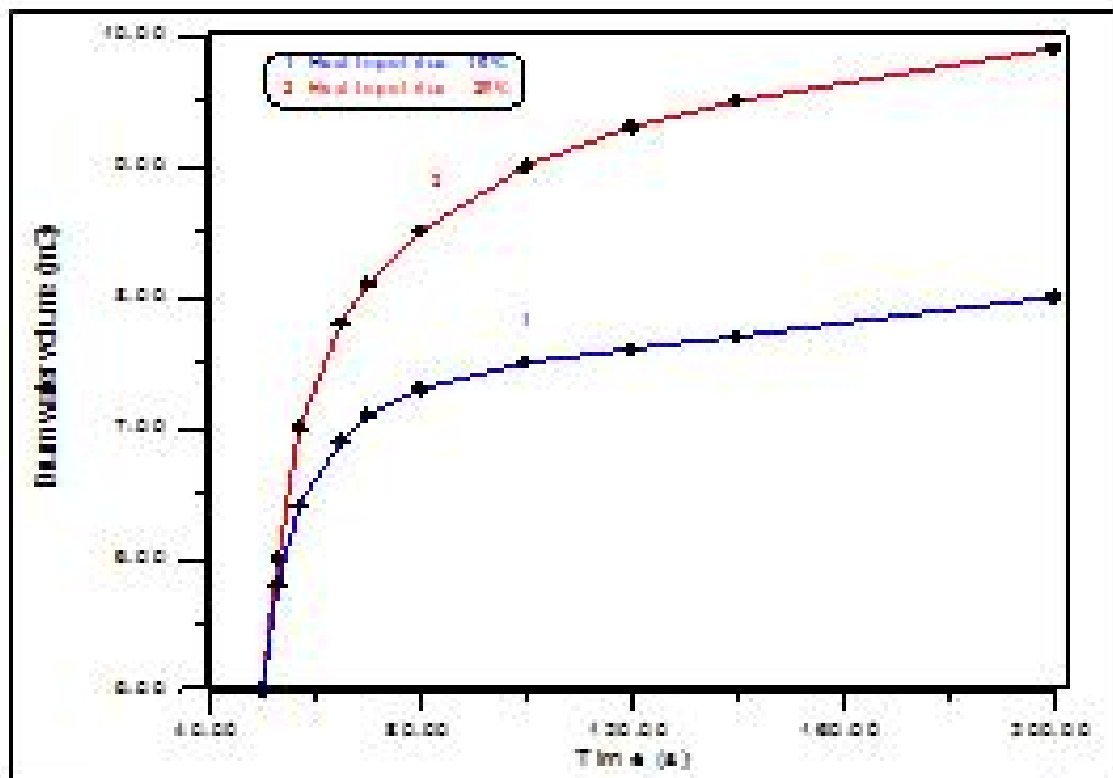


Figure (11) Variation of water volume for step rise in heat input

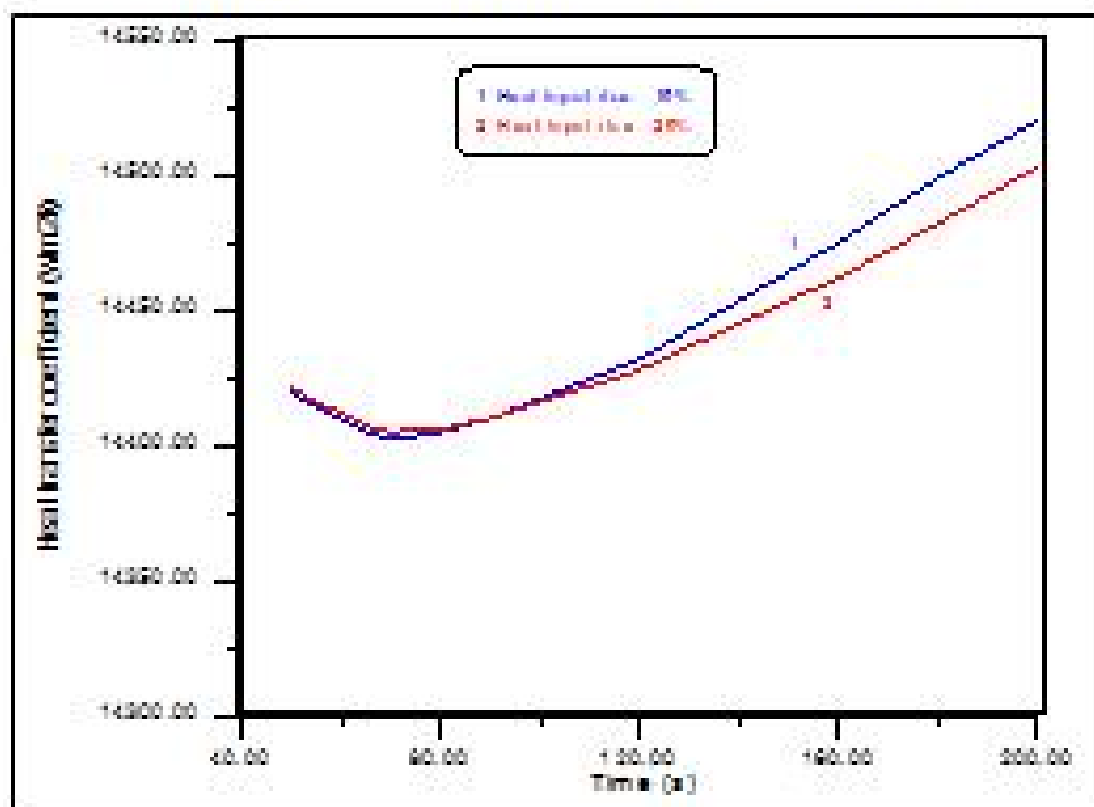


Figure (12) Variation of heat transfer coefficient for step rise in heat input

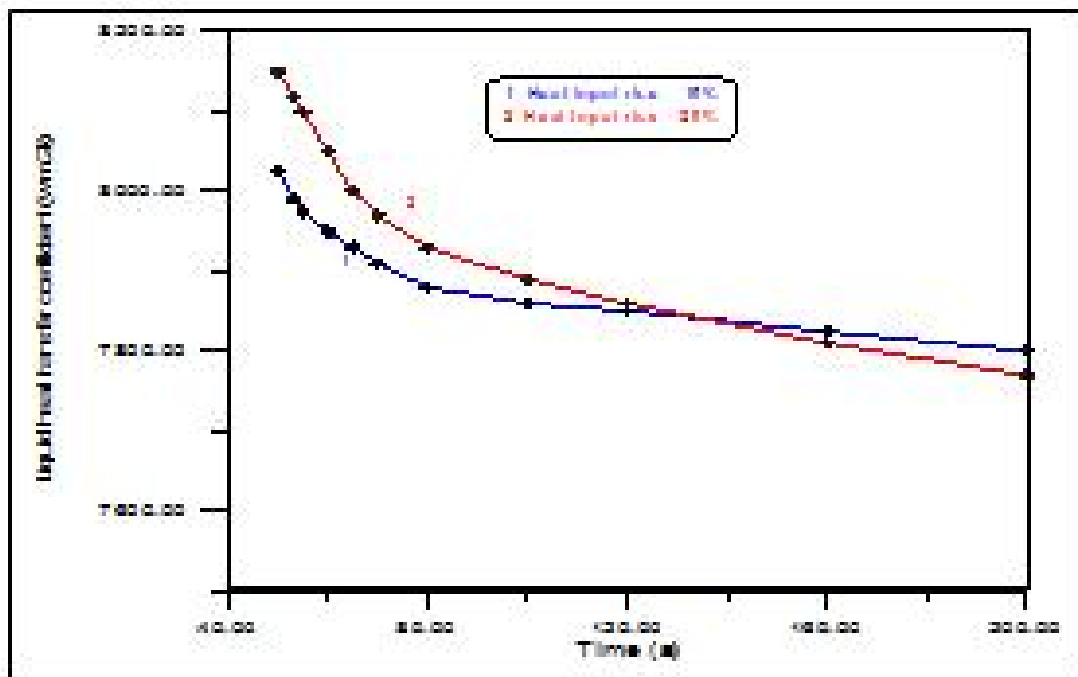


Figure (13) Variation of liquid heat transfer coefficient for step rise in heat input

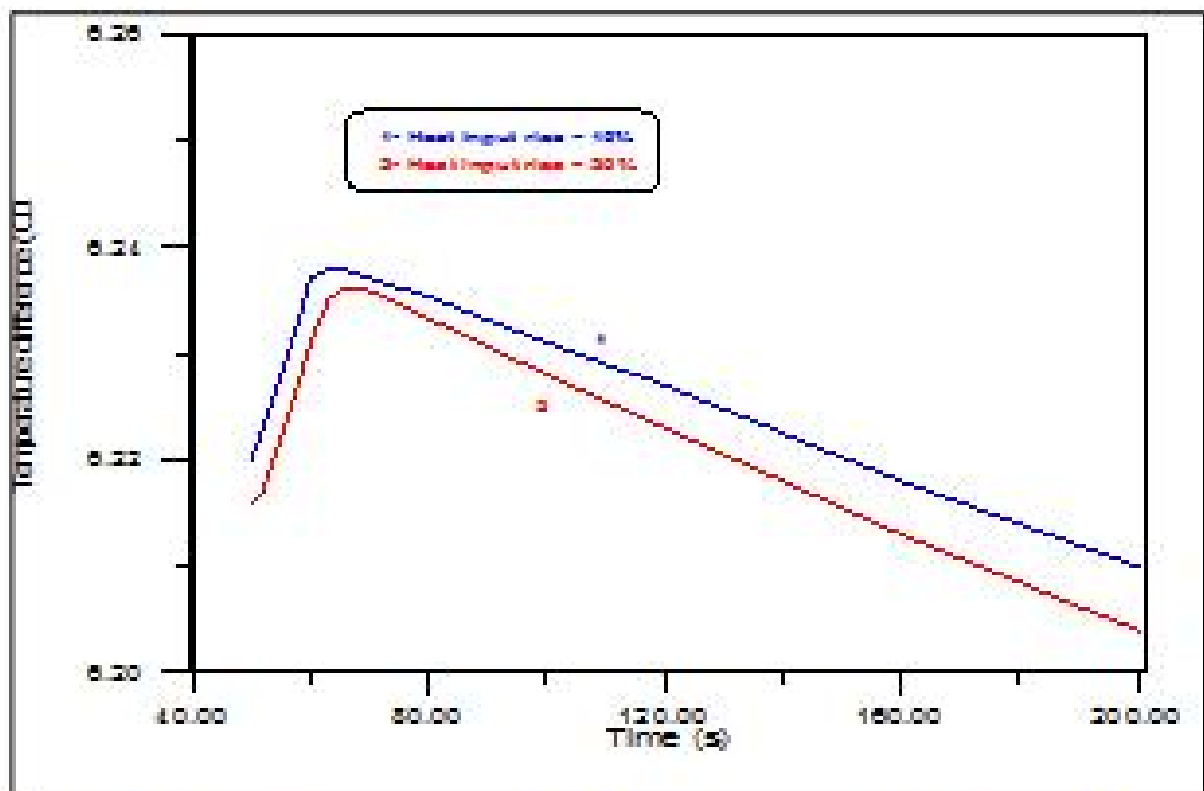


Figure (14) Variation of temperature difference between the metal and saturated steam for step rise in heat input

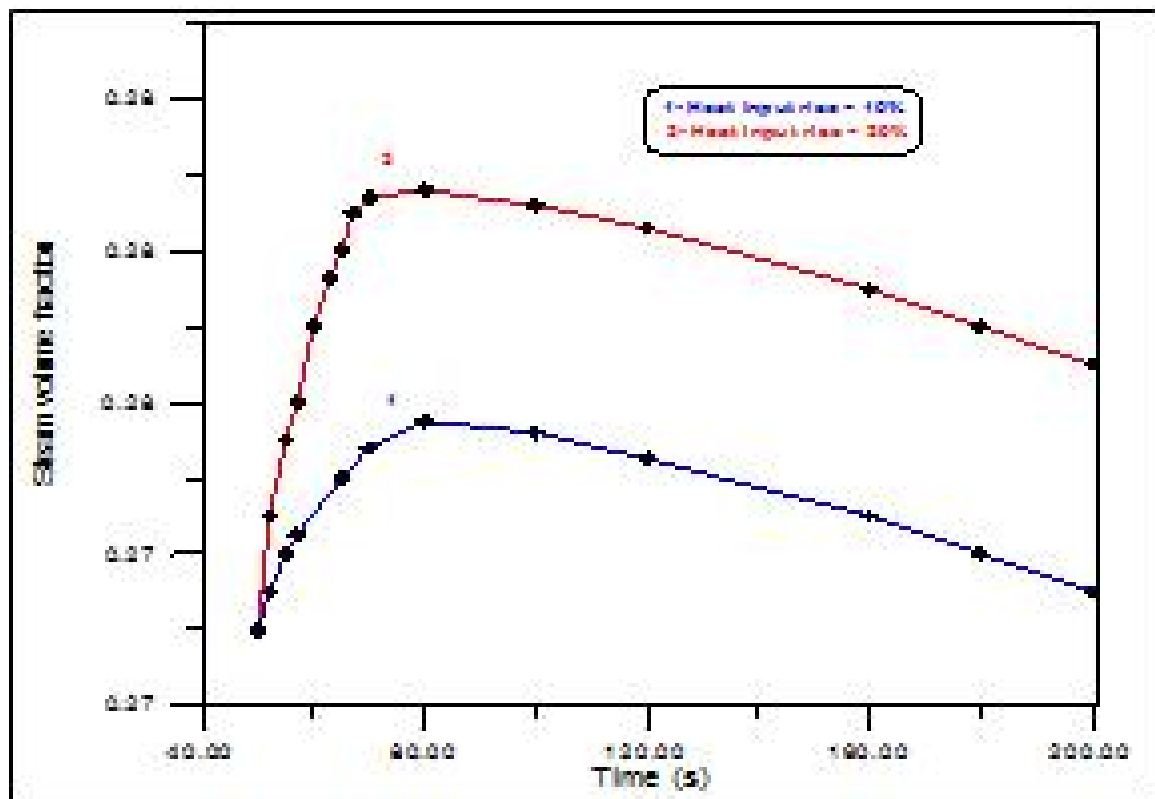


Figure (15) Variation of steam volume fraction for step rise in heat input

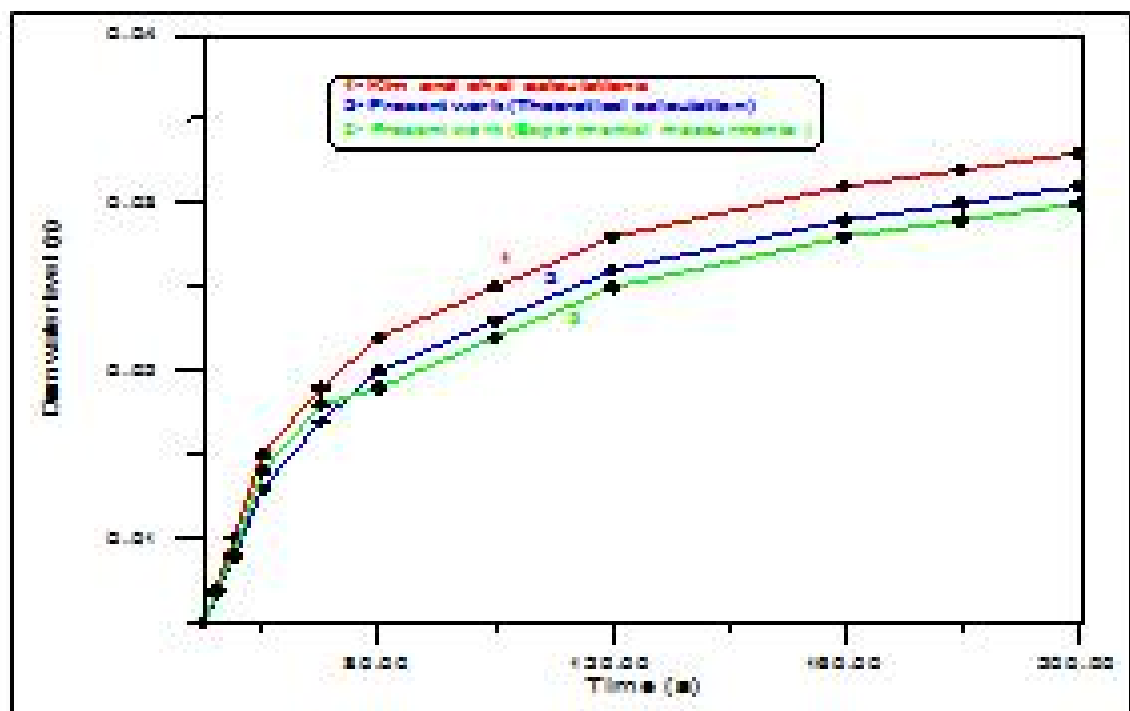


Figure (16) Comparison of drum water level Variation for step rise in heat input

## References

1. Taler, J., W glowski, B., Gr dzieł, S., Duda, P., Zima, W., Monitoring of Thermal Stresses in Pressure Components of Large Steam Boilers, VGB PowerTech, Vol. 82, Nr. 1, (2002), pp. 73-78.
2. Sreedhar R, Fernandez B, Masada GY. Sliding control retrofit for a thermal power plant. Proceedings of the 4<sup>th</sup> IEEE Conference on Control Applications, Albany, NY, U.S.A., 28–29 September 1995; 409–414.
3. Duda, P., Taler, J., Numerical Method for the Solution of Non-Linear Two-Dimensional Inverse Heat Conduction Problem Using Unstructured Meshes, International Journal for Numerical Methods in Engineering 48, (2000), pp. 881-899.
4. Nomura M, Sato Y. Adaptive optimal control of steam temperatures for thermal power plants. IEEE Transactions on Energy Conversion 1989; 4(1):25–33.
5. Flynn ME, O' Malley MJ. A drum-boiler model for long term power system dynamic simulation. IEEE Transactions on Power Systems 1999; 14(1):209–217.
6. Habbi H, Zelma M, Bouamama B. A dynamic fuzzy model for a drum-boiler-turbine system. Automatica 2003; 39:1213–1219.
7. Garduno-Ramirez R, Lee KY. Multiobjective optimal power plant operation through coordinate control with pressure set point scheduling. IEEE Transactions on Energy Conversion 2001; 16(2):115–122.
8. Astrom KJ, Bell RD. Drum-boiler dynamics. Automatica 2000; 36:363–378.
9. Kim H, Choi S. A model on water level dynamics in natural circulation drum-type boilers. International Communications in Heat and Mass Transfer 2005; 32:786–796.
10. Chen P, Shamma JS. Gain-scheduled L1-optimal control for boiler-turbine dynamics with actuator saturation. Journal of Process Control 2004; 14:263–277.
11. Peng H, Ozaki T, Haggan-Ozaki V, Toyoda Y. A nonlinear exponential ARX model-based multivariable generalized predictive control strategy for thermal power plants. IEEE Transactions on Control Systems Technology 2002; 10(2):256–262.
12. Daren Y, Zhiqiang X. Nonlinear coordinated control of drum boiler power unit based on feedback linearization. IEEE Transactions on Energy Conversion 2005; 20(1): 204–210.
13. Li B, Chen T, Yang D. DBSSP—A computer program for simulation of controlled circulation boiler and natural circulation boiler start up behavior. Energy Conversion and Management 2005; 46:533–549.
14. International Formulation Committee (IFC). A formulation of the thermodynamic properties of ordinary water substance. The 1967 IFC Formulation for Industrial Use, 1967.

15. Hewitt GF, Roberts DN. Studies of two-phase flow patterns by simultaneous X-ray and flash photography. Report AERE-M2159, Atomic Energy Research Establishment, Harwell, 1969.
16. Hewitt GF. Gas– Liquid Flow, in Handbook of Multiphase Systems. Hemisphere Publishing: New York, 1982.
17. Collier JG. Convective Boiling and Condensation. McGraw- Hill Book Company (UK) Ltd.: Maidenhead, 1972.
18. Hewitt GF, Shires GL, Bott PR. Process Heat Transfer. CRC Press: USA, 1994.
19. Taitel Y, Dukler AE. A model for predicting flow regime transitions in horizontal and near horizontal gas-liquid flow. AIChE Journal 1976; 22:47–55.
20. Chen JC. A correlation for boiling heat transfer to saturated fluids in vertical flow. Industrial & Engineering Chemistry, Process Design and Development 1966; 5(3): 322–339.
21. Shah MM. A new correlation for heat transfer during boiling flow through pipes . ASHRAE Transactions 1976; 82(2):66–86.
22. Shah MM. Chart correlation for saturated boiling heat transfer: equations for further study. ASHRAE Transactions 1982; 88(1):185–196.
23. Bjorge RW, Hall GR, Rohsenow WM. Correlation of forced convection boiling heat transfer data. International Journal of Heat and Mass Transfer 1982; 25:753–757.
24. Gungor KE, Winterton RHS. A general correlation for flow boiling in tubes and annuli. International Journal of Heat and Mass Transfer 1986; 29:351–358.
25. Klimenko VV. A general correlation for two-phase flow heat transfer. International Journal of Heat and Mass Transfer 1988; 31:541–552.
26. Klimenko VV. A generalized correlation for two-phase forced flow heat transfer, second assessment. International Journal of Heat and Mass Transfer 1990; 33:2073–2088.
27. Kandlikar SG. A general correlation for saturated two-phase flow boiling heat transfer inside horizontal and vertical tubes. Journal of Heat Transfer 1990; 112:219–228.
28. Steiner D, Taborek J. Flow boiling heat transfer in vertical tubes correlated by an asymptotic model. Heat Transfer Engineering 1992; B(2):43–69.
29. Basu P, Cheng LM. An experimental and theoretical investigation into the heat transfer of a finned water wall tube in a circulating fluidized bed boiler. International Journal of Energy Research 2000; 24(4):291–308.

## Observed and Predicted Daily Wind Travels and Wind Speeds in Western Iraq

Ahmed Hasson, Farhan A. Khammas  
Department of Mechanical Engineering  
College of Engineering,  
Nahrain University, Iraq, Baghdad

[dr\\_ahasson@yahoo.com](mailto:dr_ahasson@yahoo.com)

[far\\_1961ah@yahoo.com](mailto:far_1961ah@yahoo.com)

### Abstract

Calculated daily travel and wind speeds variations were determined. An empirical equation of diurnal changes in wind speeds developed for Western Iraq can be aware of the wind erosion and atmospheric dust storms cause. Wind speed is one of the priority factors to reduce the wind erosion by apply techniques or change environmental systems in that region. Wind speed calculated based upon the measured hourly values of wind speed for the period of 2000-2010. Results of research indicate that Western Iraq has a potential of wind speed have significantly during October through March , so land cover is needed and the best land cover is grow perennial biodiversity and artificial land cover which can reduce on soil removal. Besides, there has been a lack of precise metrological measurements to aid to monitoring and prediction of high – resolution winds in mulched lands.

The study shows that using long-term average gives better results since extremes tend to be smoothed out as more data are averaged. The difference between the measured and calculated wind speed can be simulated within 6% - 27% with mean of 18%.

A good relationship between daily wind travel and mean wind speed for day and night maximum and minimum wind speeds was obtained

**Key words:** Wind speed, Day-night winds, Wind erosion

### مسار حركة الرياح وسرعتها المقاسة والمتوقعة في غرب العراق

قسم الهندسة الميكانيكية  
كلية الهندسة- جامعة النهرين

الاختلافات المحسوبة لحركة وسرعة الرياح قد قيست ، طورت التغيرات بواسطة المعادلات العددية لمنطقة غرب والتي تعكس أهمية انجراف التربة والعواصف الترابية. تعتبر سرعة الرياح من العوامل الرئيسية التي تؤثر على تعرية التربة وذلك لتأثيرها على تغيير النظام البيئي للمنطقة. جمعت القراءات لعناصر الرياح في المنطقة من فترة 2000-2010 وقد دلت النتائج بان المنطقة لها طاقة كامنة لسرعة الرياح وذلك لشهر تشرين بامس الحاجة اليها في تلك الفترة ونظراً لعدم توفر القراءات التي تخص سرعة وحركة الرياح التي قد تساعد في رصد الرياح. ان القراءات المتوفرة ولمدة فترة طويلة قد ساعدت على الحصول على معدلات ومن ثم حسابها وقد استنتجت من الحسابات فروقات مابين النتائج المحسوبة والمقاسة لسرعة الرياح والتي كانت تتراوح بين 6% - 27% 18% لحركة الرياح اليومية لفترة النهار والليل .

## INTRODUCTION

Wind erosion and dust storms are a serious problem in many parts of the world. It is worse in drylands areas most susceptible to wind erosion on agricultural land include much of Western Iraq deep sandy soils generally are considered to be high erodible. The study of wind speed and direction is one of the priority factors to reduce the wind erosion by apply techniques or change farming systems in that area.

Data has been recorded by climatological stations across Western Iraq for many years, but automation is now phasing out reporting of this useful indicator of wind erosion.

Wind erosion physically removes the lighter, less dense soil constituents such as organic matter, nitrogen, phosphorus, clays, and silts which depend on the wind speed. Hasson (2008) found that 7,75% of accumulated dusts was organic materials. Thus it removes the most fertile part of the soil and lowers soil productivity (Lyles, 1975). Lyles (1975) estimated that top soil loss from wind erosion causes annual yield reductions.

Broad scale wind erosion rates can be approximated using meteorological data which reports the frequency of occurrence of dust events (dust storms and local dust events) weighted according to their intensity as a Dust Storm Index (DSI)(Mc Tainsh, 1998) . The Eastern Wind model is an indicator of wind erosion under natural conditions, without the impact of land use activities. The model predicts the level of wind erosion by utilizing both wind erosivity (the power of the wind to erode) and land type erodibility (the susceptibility of the land to erosion). Wind erosivity is measured using wind run data, and land type erodibility is measured using precipitation and evaporation parameters to estimate effective soil moisture, which when averaged annually, approximates vegetation cover.

The relationship of wind speed variations to atmospheric stability has been studied by Oke who concluded that the greater the transfer of horizontal momentum towards the surface, the greater the surface layer winds.

The study has dealt with different micro-climatologically parameters data types. These include latitude, date, daily wind travel, wind speed, ambient temperature, daylength, night length.

During the night time the wind speed used to be calm when buoyancy is reduced and little vertical exchange occurs. Peak wind speed occurs near noon when solar heating promotes vertical exchange resulting in greater momentum transfer toward the surface.

A one dimensional model of the neutral planetary boundary layer is used to predict the wind velocity and coefficient of eddy diffusivity throughout the 2-km planetary layer (Mc Tainsh 1990) who concluded that the wind speed prediction error was 1.2 of the observed values.

Average wind speed estimate from the data base have been systematically compared with corresponding wind speed estimate from buoy measurements and model prediction, and very good agreement has been found,(Raghavan, 1988).

The objectives of this study is construct a wind speed model for predicting diurnal changes in wind speed and to evaluate its relation to air temperature for Western Iraq. This study includes a comparison between the measured and calculated diurnal variation of daily wind speed.

## MEASUREMENTS

The study performed in the, Western Iraq, which is at latitude 33° N, longitude, 44° E. The climate of the study area is semi-arid and sub-tropical. Mean annual precipitation is 420 mm

with > 80% of its value is falling from May to October. Mean monthly temperature range from 14C in winter and 45C in summer. The average monthly wind speed is the highest during the summer months.

The measurements of microclimatological parameters include wind speed and air temperature data were collected from Metrological Station . The data were recorded continuously (24 hours) on hourly basis for long-term[ 2000 to 2010 ], using automatic computer connected on-line with the data acquisition system.

### CALCULATION PROCEDURE

The model uses a truncated sine wave function for the period from sunrise to sunset and an exponential decay function from early sunset to sunrise. An input for the model includes daylength (determined by date and latitude) and maximum and minimum daily wind speed. The following equations are used for calculation of the wind speed (m/s) during day-time (WSd) and night-time (WSn).

$$WSd = (WS_{max.} - WS_{min.}) \sin [(n/y + 2a)] + WS_{min.} \quad (1)$$

$$WSn = (WS_s - WS_{min.}) \exp [(-bn)/z] + WS_{min.} \quad (2)$$

Where  $WS_{max.}$  and  $WS_{min.}$  are maximum and minimum wind speed (m/s).  $WS_s$  is the wind speed at the sunset (m/s).  $y$  and  $z$  are day and night length number of hours (h).  $n$  is the number of hours from the hour of minimum wind speed to sunset (h).  $N$  is the number of hours from sunset to the hour of minimum wind speed(h).  $a$  is the time-lag in maximum wind speed (h) and  $b$  is a coefficient that controls wind speed decrease at night. To calculate the values of the variables  $a$  and  $b$  the non-linear error minimization technique developed by [5] was used taking into account the monthly mean of diurnal wind speed for successive years period (2000 to 2010) for West Midland region. The results show that the values of  $(a)$  and  $(b)$  were constants for the side (1.2 and 3.1), respectively. The day-length ( $y$ ) and night-length ( $z$ ) were computed from the data and from latitude by a method developed by (Powel, 1996) and effective photoperiod day developed by (Sellers, 1965).

### RESULTS AND DISCUSSION

#### RELATIONSHIPS BETWEEN DWT, WSD AND WSN

The hourly values for wind speed is not always available, while the total wind speed travel is available more often. For this reason a relation between daily wind travel (DWT) and mean wind speed for the day (WSd) and night (WSn) could be useful.

The hourly values of wind data for the experiment period were used to develop a regression equation. Linear regression analysis from software program package was used to analyze the data set ( a method of minimization method). The resulting relationship was given in Table 1.

The scatter diagram of the hourly values of wind speed (WSd,WSn) vs. the hourly wind travel were plotted in Fig. 1.

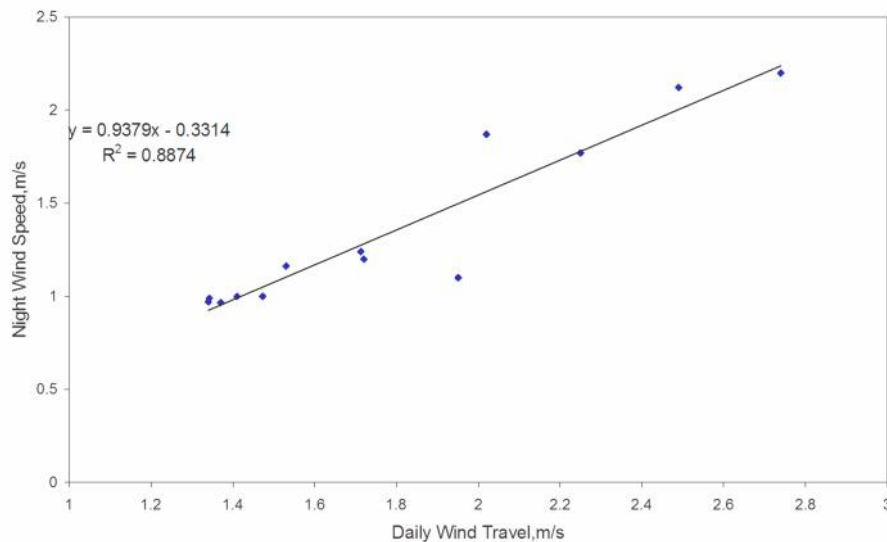


Fig. 1. Relationships between night wind speed and average monthly daily wind travel

#### RELATIONSHIPS BETWEEN DWT, WS<sub>MAX.</sub> AND WS<sub>N</sub>

The scatter diagram of daily wind travel vs. average maximum and minimum wind speed was plotted in Fig. 2. An average maximum wind speed during the afternoon hours (12:00 to 15:00 h) and average minimum wind speed during the morning hours (03:00 to 06:00 h) were used instead of the instantaneous maximum and minimum daily wind speed to get more accurate approximation. The resulting regression equation using these data was:

$$WS_{max.} = 1.297 (DWT) - 0.921 \text{ (m/s)}$$

$$R^2 = 0.921$$

$$WS_n = 0.622 (DWT) + 0.544 \text{ (m/s)}$$

$$R^2 = 0.713$$

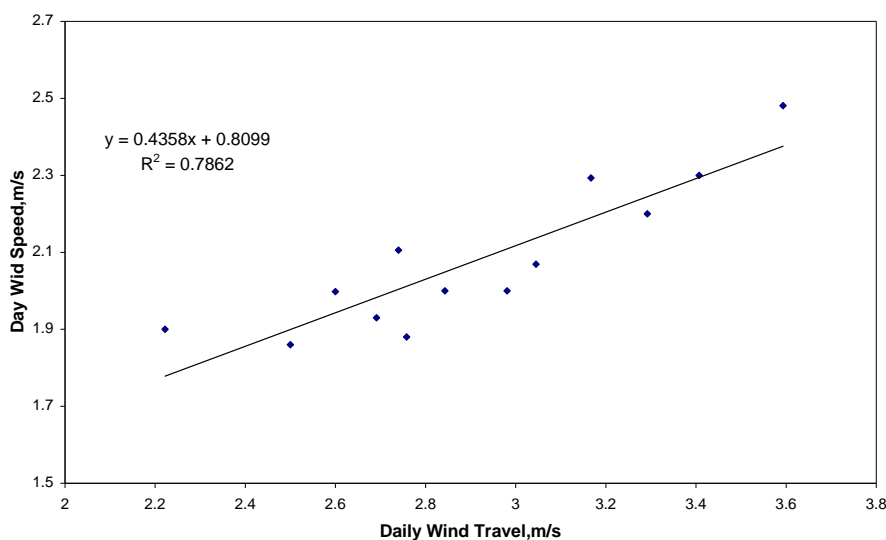


Fig. 2. Relationships between maximum wind speed and average monthly daily wind travel

## OBSERVED - CALCULATED WIND SPEEDS

The measured and calculated data of wind speed for the recording period were shown in Fig.3. The figure shows that the linear relationship exists between the values. By fitting the data points in the figure, the following equation was formed with a high correction coefficient,  $R^2 = 0.982$ .

$$WSc = 1.042 (WSm) + 0.1934 \quad (\text{m/s})$$

Where : WSm and WSc are measured and calculated wind speeds respectively.

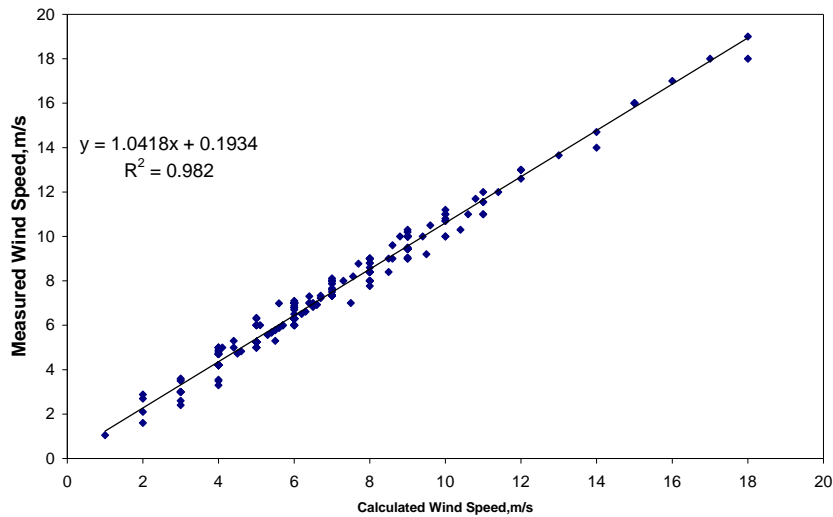


Fig.3. Relationships between calculated and measured wind speeds

Table1. The expansion coefficient in  $Y = a_1 + ax$  equation the correlation coefficient ( $R^2$ ).

| Case | Interce | Slop | $R^2$ |
|------|---------|------|-------|
| WSd  | 0.810   | 0.43 | 0.78  |
| WSn  | 0.331   | 0.93 | 0.88  |
| WSma | 0.124   | 1.30 | 0.92  |
| WSn  | 0.544   | 0.62 | 0.71  |

## EVALUATION OF WIND SPEEDS ESTIMATION

Closeness of the calculated wind speeds to the measured values were checked by comparing: (1) the differences between the calculated and measured wind speeds averaged over the recording period and (2) standard deviation of the averaged difference is defined as:

$$D = 1/n \quad (WSc - WSm)$$

$$S.D = \sqrt{[(WSc - WSm) - nD] R_s / n - 1}$$

Where:  $W_{Sc}$  and  $W_{Sm}$  are calculated and measured wind speed (m/s) respectively, and  $n$  is the number of observations. Table 2. gives the value of average differences,  $D$  and standard deviation of the differences,  $S.D.$  for the values of calculated wind speeds. The  $S.D.$  of the average differences was the greatest in February (1.7 m/s) and tends to decrease (0.4 m/s) in March.

Table 2. Average differences and standard deviation of the differences between the observed and calculated wind speed, m/s.

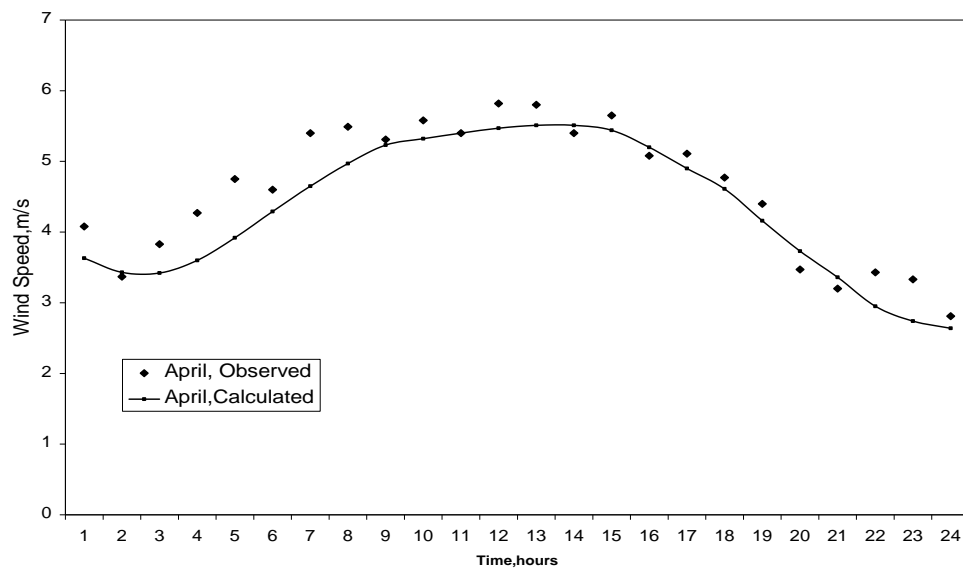
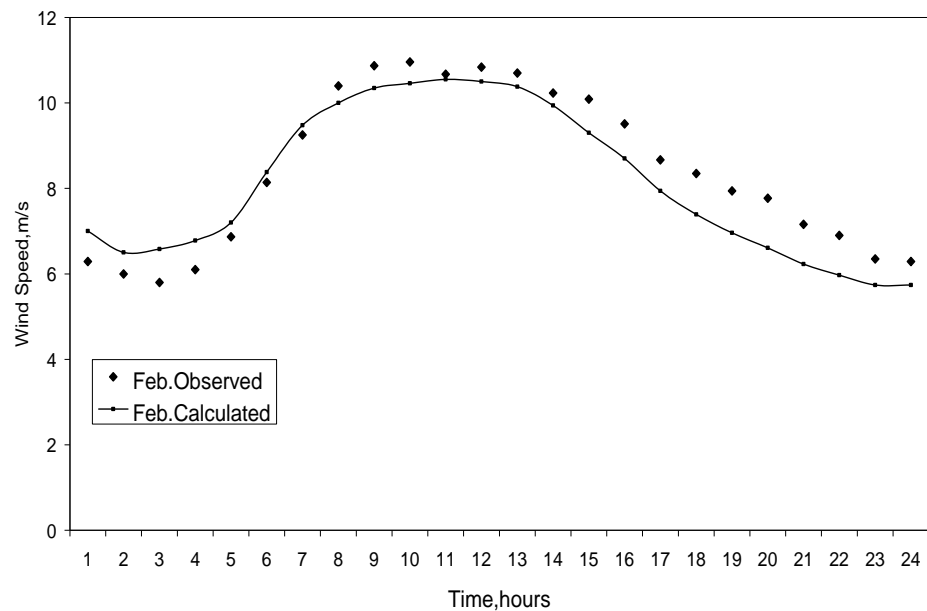
| Months            | Average Differences [ D ] | Standard Deviation [ S.D.] |
|-------------------|---------------------------|----------------------------|
| January           | -0.02                     | 1.658                      |
| February          | -0.40                     | 1.747                      |
| March             | -0.02                     | 0.409                      |
| April             | -0.02                     | 0.964                      |
| May               | -0.38                     | 0.554                      |
| June              | -0.39                     | 1.154                      |
| July              | -0.01                     | 1.270                      |
| August            | -0.02                     | 1.087                      |
| September         | -0.01                     | 0.635                      |
| October           | -0.29                     | 1.706                      |
| November          | -0.03                     | 1.670                      |
| December          | -0.36                     | 1.554                      |
| Annual,2000- 2010 | -0.16                     | 0.481                      |

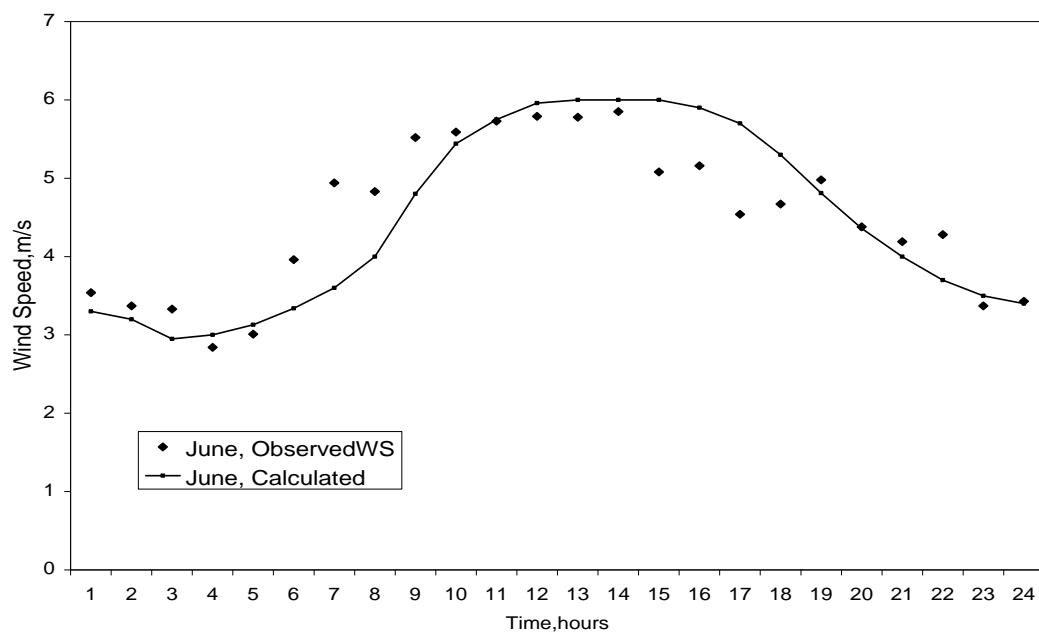
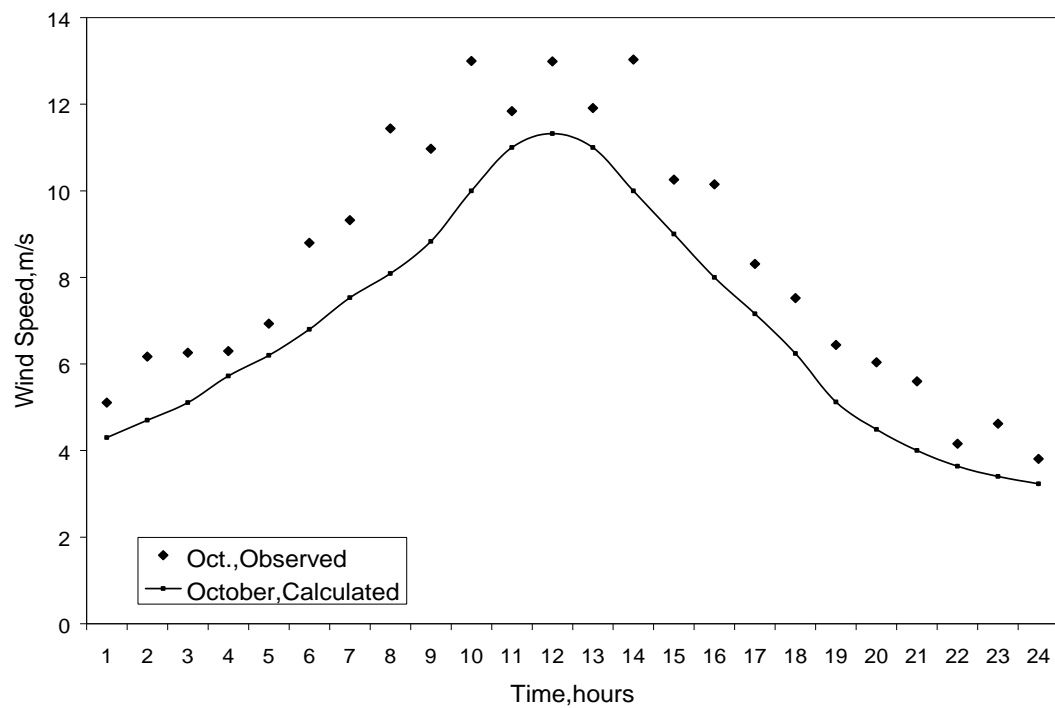
Figure 4. shows that the method does well in calculating the mean monthly diurnal wind speeds compared to the measured values. Also, the seasonal changes in the pattern are well represented in the calculation method. During October through March the most effective wind speeds can be occur, so we suggest perennial and tagasaste are the best fodder to be grown to reduce land exposure and reduce wind speeds. Table 2 shows the average differences and standard deviation of the differences between the observed and calculated wind speed, m/s. The annual differences  $D$  and  $SD$  are -0.16 and 0.48. The standard deviation is high annually compared with the monthly average.

## CONCLUSIONS

The wind model has potential applications in dust storms and agricultural, biological, of Western Iraq research and application models. An analysis wind speed and air temperature was performed for the Western of Iraq region for the period of 2000 – 2010. A sine exponential model for the diurnal variation of wind speed estimation was used for this purpose. The study shows that using long-term average gives better results since extremes tend to be smoothed out as more data are averaged. The difference between the measured and calculated wind speed can be simulated within 6% - 27% with mean of 18%.

A good relationship between daily wind travel and mean wind speed for day and night maximum and minimum wind speeds was obtained.





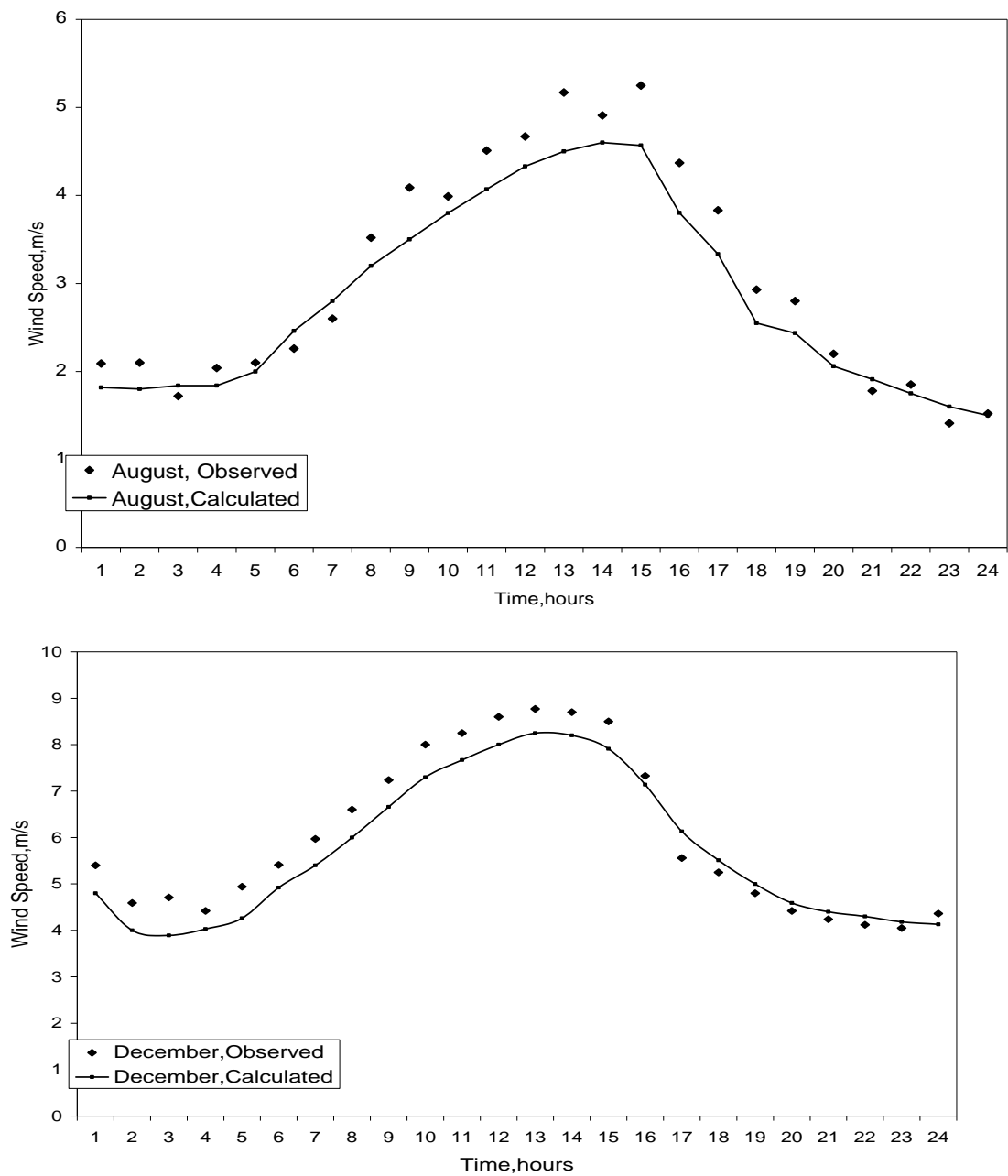


Fig. 4. Comparison between calculated and observed wind speeds

## REFERENCES

- [1]. Hasson, A. (2008) Atmospheric dust properties and it effects on the light transmittance and crop production. Agriculture, Food and Environ Journal, SIJ. Vol. 2, No.1.
- [2]. Mc Tainsh, G.H. (1998). "Dust Storm Index". In: Sustainable Agriculture: Assessing.
- [3]. Raghavan, N. and S. Basu,(1988) Prediction of wind speed, direction and diffusivity under neutral conditions for tall stacks. Journal of Applied Meteorology, 27: 3pp, 261-268 .
- [4]. Manaldo, F.M., Donald, R. T. Beal, R. C. Picher, G. and P. Pablo Clement-Colon. (2001). Comparison of SAR-Derived wind speed with model predictions and ocean measurements. IEEE Transactions on Geosciences and Remote Sensing J., 39:12.
- [5] powell,M. J.D. (1965), A method of minimizing a sum squares of a nonlinear function without calculating derivations. computer. Journal 7: 303-307.
- [6] Sellers, W.D. (1965) Physical climatology, University of Chicago, Weily Publishing.
- [7] Hasson A., Sabeh, S. and Jarrad D. (1999). determination of effective photoperiod above critical level on sensitive physiology processes. Journal of solar Energy Research, 6(1): 13-26.

## Design of solar radiation Concentration using microlenses array with waveguide

Ali H. Al-Hamdani <sup>(1)</sup>, Hayfa G. Rashid <sup>(2)</sup>, Alaa B. Hasan <sup>(3)\*</sup>

(1)Laser and Optoelectronics Engineering Department, University of Technology,

(2)College of Education, Al-Mustansirya University,

(3) College of Education, University of Baghdad, Iraq

(\*) Corresponding Author, *Email:alaaajizany@yahoo.com*

### Abstract

A new approach of solar concentrator has been proposed and used to collect sunlight. The proposed design consists two-dimensional of (20x20) rectangular microlens array (100% fill factor) that coupled into a planar waveguide. Localized facets prisms of symmetrical angle (120°, 60°) were placed at the focus of each lens. The irradiance was measured at each side of the waveguide by Photovoltaic cells (PV) were fixed at there. The results illustrate that the cladding materials and their thicknesses affect the optical efficiency of the system significantly.

**Keywords:** Microlenses array; Waveguide; Photovoltaic cell; Total internal reflection (TIR); Zemax.

### Introduction

The high expensive fabrication of common solar concentrators with tracking system, Leads to Development of new design of solar concentrator microlenses array. This system provides high optical efficiency by collecting light at lens apertures to convert solar photons directly into electricity. Optics for solar concentration typically consists of lenses or mirrors focusing onto secondary elements that eliminate intensity variations at the PV cell. A common approach places dozens of lenses into a shared platform, each focusing onto independent secondary optics and solar cells <sup>[1]</sup>.

Previous work presents an approach to solar concentration where sunlight collected by each lens in a two-dimensional lens array is coupled into a shared, planar waveguide using localized features placed at each lens focus <sup>[2]</sup>. Orthogonal concentration method to further confine sunlight within planar solar collectors. Radial-oriented couplers create micro-optic solar concentrators <sup>[3]</sup>.

In this work; the proposed concentrator design replaces discrete optics with a 2D lens array and a common slab waveguide. Sunlight collected by the array focuses onto localized prisms mirrors positioned to reflect light at angles that exceed the critical angle for total internal reflection, and therefore couple into the waveguide. Coupled light is homogenized as it propagates towards the exit aperture at the slab edges.

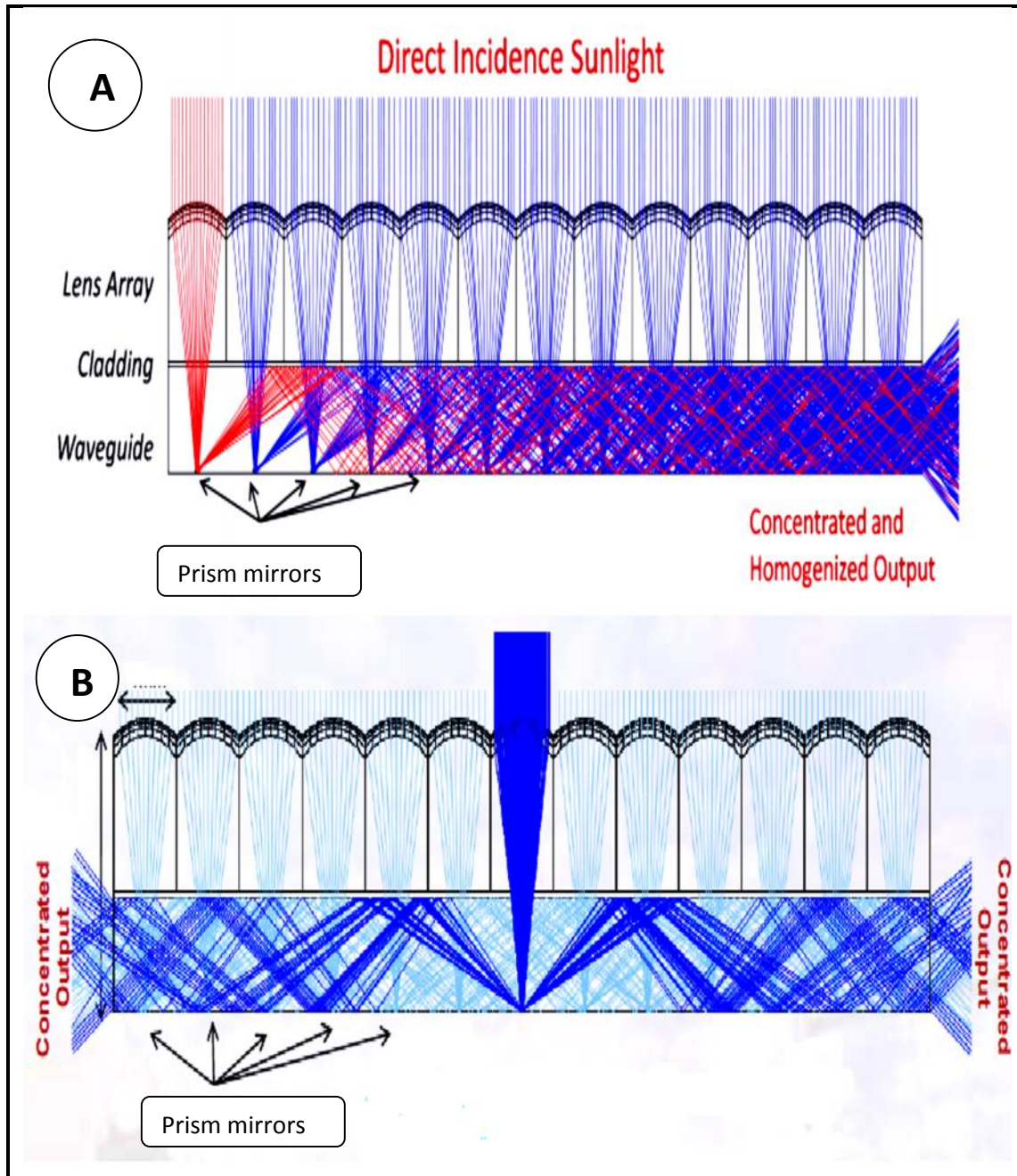


Figure (1): Microlenses array shared with waveguide slab: A. single side ray propagation, B. double sides ray propagation.

### Optical design

Sunlight collected by each lens of the array to focus coupled into a common slab waveguide using prism mirrors. Rays that reflected at prisms facets with angle defined by Snell's Law propagate via waveguide slab by exceeding critical angle, this operation satisfied total internal reflection (TIR) within the waveguide to the exit aperture. The waveguide transports and collects sunlight over the entire input aperture to one or two side of waveguide, which depends on the prism angle.

Waveguide slab has two samples:

- Symmetrical angle ( $120^\circ$ ) and
- Asymmetrical angle ( $60^\circ$ )

The samples gives double sides and single side ray propagation into slab respectively as shown in figure (1) <sup>[2]</sup>. A low refractive index cladding has been used to prevent energy losses in ray propagation by refraction and grantee large critical angle to get high efficiency optical system <sup>[4]</sup>. The performance of the micro-optic slab concentrator has been simulated by non-sequential ray tracing with the aid (Zemax) optical design program <sup>[5]</sup>. The best choice of materials and thickness of microlenses array, cladding and waveguide are important, all summarized in table (1).

Table (1): Microlens array, cladding and waveguide materials and their dimensions.

|                                                                                    |                                                                                                                                                                                                                                                                                                                                                                                                                                                                                        |     |       |                  |       |                     |       |     |       |                  |       |        |       |      |       |
|------------------------------------------------------------------------------------|----------------------------------------------------------------------------------------------------------------------------------------------------------------------------------------------------------------------------------------------------------------------------------------------------------------------------------------------------------------------------------------------------------------------------------------------------------------------------------------|-----|-------|------------------|-------|---------------------|-------|-----|-------|------------------|-------|--------|-------|------|-------|
| Individual lens aperture                                                           | <div> <div> diameter (1 mm)</div> </div>                                                                                                                                                                                                                                                                                                                                                                                                                                               |     |       |                  |       |                     |       |     |       |                  |       |        |       |      |       |
| Microlens array (acrylic)                                                          | <div> <div>thickness (1 mm)</div> <div>refractive index (1.49)at 550 nm</div> </div>                                                                                                                                                                                                                                                                                                                                                                                                   |     |       |                  |       |                     |       |     |       |                  |       |        |       |      |       |
| Waveguide slab (BK-glass)                                                          | <div> <div>refractive index (1.49)at 550 nm</div> <div> <div>dimensions (20x20x3 mm)</div> <div>refractive index (1.51)at 550 nm</div> </div> </div>                                                                                                                                                                                                                                                                                                                                   |     |       |                  |       |                     |       |     |       |                  |       |        |       |      |       |
| Cladding materials                                                                 | <div> <div>refractive index (1.51)at 550 nm</div> <div> <div>thickness (0.1 mm)</div> <div>refractive index at 550 nm [ ]</div> </div> </div> <table border="1"> <tr> <td>Air</td><td>1.000</td></tr> <tr> <td>MgF<sub>2</sub></td><td>1.377</td></tr> <tr> <td>MgF<sub>2</sub>-E</td><td>1.389</td></tr> <tr> <td>LiF</td><td>1.392</td></tr> <tr> <td>CaF<sub>2</sub></td><td>1.433</td></tr> <tr> <td>N-FK56</td><td>1.434</td></tr> <tr> <td>SRF2</td><td>1.437</td></tr> </table> | Air | 1.000 | MgF <sub>2</sub> | 1.377 | MgF <sub>2</sub> -E | 1.389 | LiF | 1.392 | CaF <sub>2</sub> | 1.433 | N-FK56 | 1.434 | SRF2 | 1.437 |
| Air                                                                                | 1.000                                                                                                                                                                                                                                                                                                                                                                                                                                                                                  |     |       |                  |       |                     |       |     |       |                  |       |        |       |      |       |
| MgF <sub>2</sub>                                                                   | 1.377                                                                                                                                                                                                                                                                                                                                                                                                                                                                                  |     |       |                  |       |                     |       |     |       |                  |       |        |       |      |       |
| MgF <sub>2</sub> -E                                                                | 1.389                                                                                                                                                                                                                                                                                                                                                                                                                                                                                  |     |       |                  |       |                     |       |     |       |                  |       |        |       |      |       |
| LiF                                                                                | 1.392                                                                                                                                                                                                                                                                                                                                                                                                                                                                                  |     |       |                  |       |                     |       |     |       |                  |       |        |       |      |       |
| CaF <sub>2</sub>                                                                   | 1.433                                                                                                                                                                                                                                                                                                                                                                                                                                                                                  |     |       |                  |       |                     |       |     |       |                  |       |        |       |      |       |
| N-FK56                                                                             | 1.434                                                                                                                                                                                                                                                                                                                                                                                                                                                                                  |     |       |                  |       |                     |       |     |       |                  |       |        |       |      |       |
| SRF2                                                                               | 1.437                                                                                                                                                                                                                                                                                                                                                                                                                                                                                  |     |       |                  |       |                     |       |     |       |                  |       |        |       |      |       |
| (*) all the selected materials are transparent to solar radiation <sup>[6]</sup> . |                                                                                                                                                                                                                                                                                                                                                                                                                                                                                        |     |       |                  |       |                     |       |     |       |                  |       |        |       |      |       |

Waveguide slab function was to collect, homogenize and transport the energy to a common exit aperture. For the planar waveguide concentrator the geometric concentration ratio ( $C_{geo}$ ) were defined as the ratio of length of the waveguide divided by the thickness that is to say, the ratio input to output areas of the optical system. Optical efficiency ( ) is the fraction of light which reaches the output aperture and principally includes Fresnel reflections, material absorption and waveguide decoupling losses. The flux concentration ( $C_{flux}$ ) is the product of the geometric concentration ratio and optical efficiency <sup>[2]</sup>.

$$C_{flux} = \frac{\text{slab length}}{\text{slab thickness}} \times \text{efficiency} = C_{geo} \times \eta \quad (1)$$

V grooves or called "prisms mirror", were proposed and implemented in Zemax optical design program as rectangular volume object. The design done by collecting several segments of this object in parallel array of dimensions (20x1 mm). Such the yield (35%) ray coupling area which produces double sided of ray propagation at edges of waveguide slab.

The same object arrangement were also adapted to design another V grooves with asymmetrical angle ( $60^\circ$ ). This leads to (30%) ray coupling area that produces single sided of ray propagation at the edge of waveguide slab as shown in figure (2).

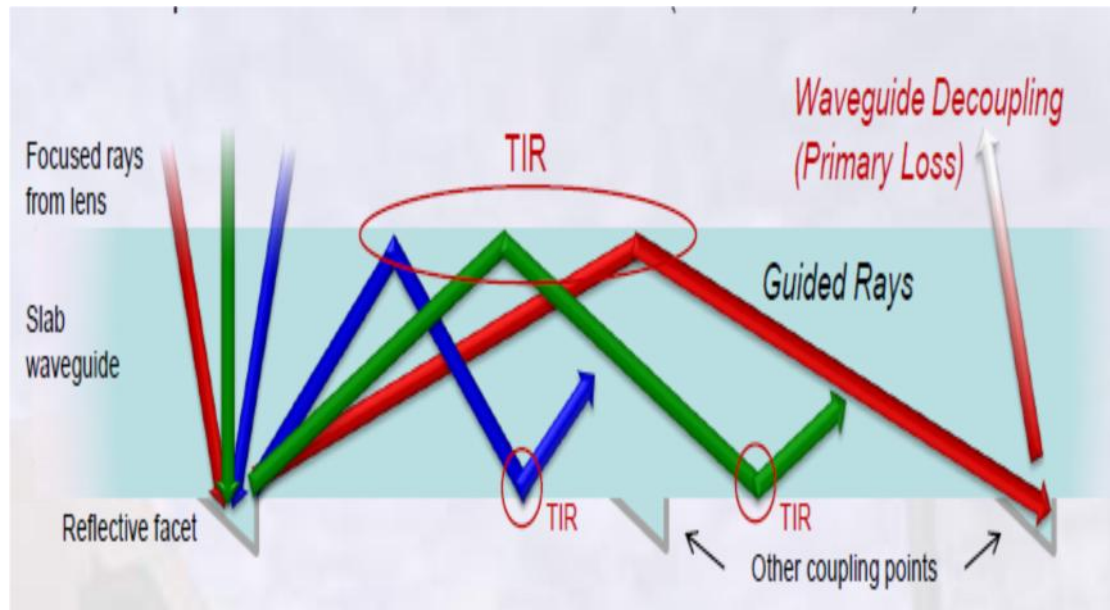


Figure (2): Ray propagation in waveguide slab concentrator.

## Result and discussion

The design of symmetrically angle ( $120^\circ$ ) prism couples rays into the slab, guiding light towards two opposing edges. To collect the concentrated light in two simply places PV cells at each output edge were used. Another design of asymmetrically angle ( $60^\circ$ ) prism couples rays into the slab, guiding light towards one way of edge, to collect the concentrated light at PV cells at output edge. These facets occupy a small fraction of the total waveguide surface and enable high geometric concentrations despite decoupling loss when light strikes a subsequent coupling region. These prisms reflect incident light at angle ( $60^\circ$ ) which exceed critical angle and achieve (TIR) into slab as shown in figure (2). Variable thickness of cladding has been used over the range (0.1- 1mm) in the two samples above. Figure (3) shows degradation of optical efficiency by increasing of cladding thickness in single sided sample, while another sample (double sided) shows slightly variation in optical efficiency by increasing of cladding thickness (maximum value of optical efficiency in (0.7mm) cladding thickness which means the most appropriate focal shift to cover coupling area). This may due to cladding thickness which lead to shifting of lens focus (defocus) that appropriate to ray coupling in wide range of prism area (35%) in double sided sample, while single sided sample has narrower range of coupling area. Despite of single sided configuration has lower path optical length than double sided (number of TIR rays in single sided less than rays of

double sided). Lower negligible energy losses may be achieved in comparison with coupling area <sup>[7]</sup>. Figure (3) shows variation of optical efficiency vs. material indices and their thickness. Its clear high optical efficiency was achieved when air is cladding. The prism angle is responsible of ray's redirection inside waveguide slab, so the angle value determines if rays exceed critical angle or not, (120°) symmetrical and (60°) asymmetrical angle gives roughly (60°) redirected ray angle at another slab surface (boundary surface between slab and cladding) which exceeds critical angle if air cladding has been used, and satisfy (TIR) that gives high efficiency. Another cladding materials satisfy (TIR) at critical angle greater than (65°), and the prism angle partially achieves this critical angle by marginal rays that incident to lenses, this system ensures partially (TIR) that gives low efficiency.

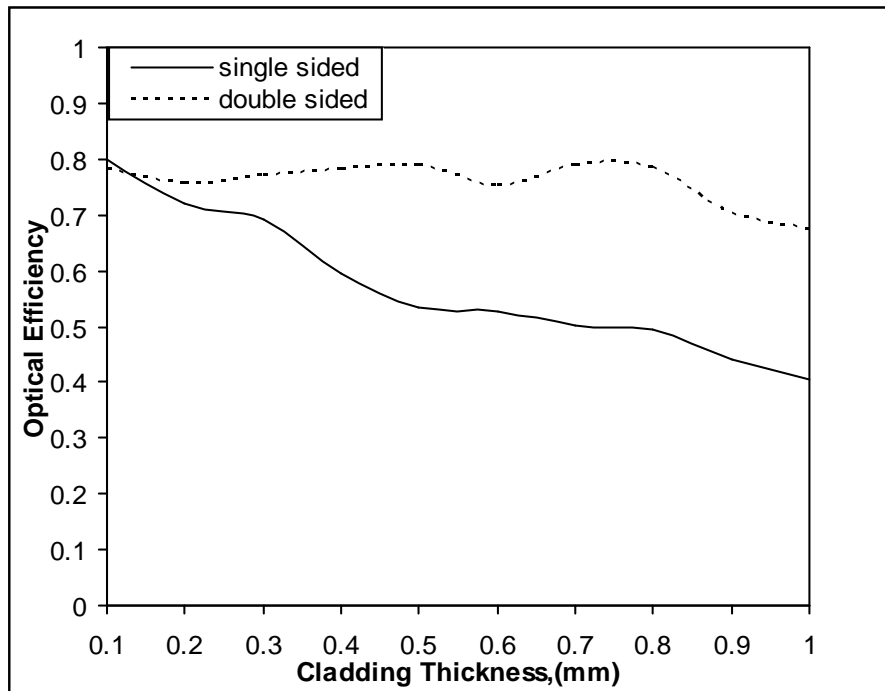
### Conclusion

The micro-optic slab concentrator integrates multiple, focusing apertures with a common waveguide to direct solar energy to a single or double PV cell. A slab waveguide can be used as secondary optics to collect and homogenize sunlight focused by a two-dimensional lens array using the hybrid non imaging approach. Reflective facets designed on the backside of the waveguide act as fold mirrors to couple sunlight into the waveguide at angles which exceed the critical angle for TIR. The system becomes essentially planar while opening a new design space for CPV. Focal length, waveguide thickness and materials selection lead to suitable designs for small and large-scale applications.

### References

1. Miyashita T. "Standardisation for microlenses and microlens arrays" Jap. Jnl. of Appl. Phys. **46**, (8), 5391-5396(2007).
2. Karp. J. H, Tremblay. E. J and Ford. J. E. "Planar Micro Optic Solar Concentrator" Optics Express **18**, (2), 1122-1133(2010).
3. Ford. J. E, Karp. J. H and Tremblay. E.J. "Radial Coupling Method for Orthogonal Concentration within Planar Micro-Optic Solar Collectors" Osa. Solar **22**, (7), 220-230 (2009).
4. Zemax "user's guide", (9), Ch. 15 (2000).
5. O'Neill. M. J. and Others," Stretched Lens Array (SLA) Photovoltaic Concentrator Hardware Development and Testing" 3rd World Conference on Photovoltaic Energy Conversion, USA, 11-18 (2003).
6. Li. L. and Yi. Y. "Design and Fabrication of a Freeform Microlens Array for Uniform Beam Shaping". Microsyst. Technol. **17**, 1713–1720 (2011).
7. Akatay. A and Urey. H. "Design and Optimization of Microlens Array Based High Resolution Beam Steering System". Optics Express **15**, (8), 4523- 4528 (2007).

**A**



**B**

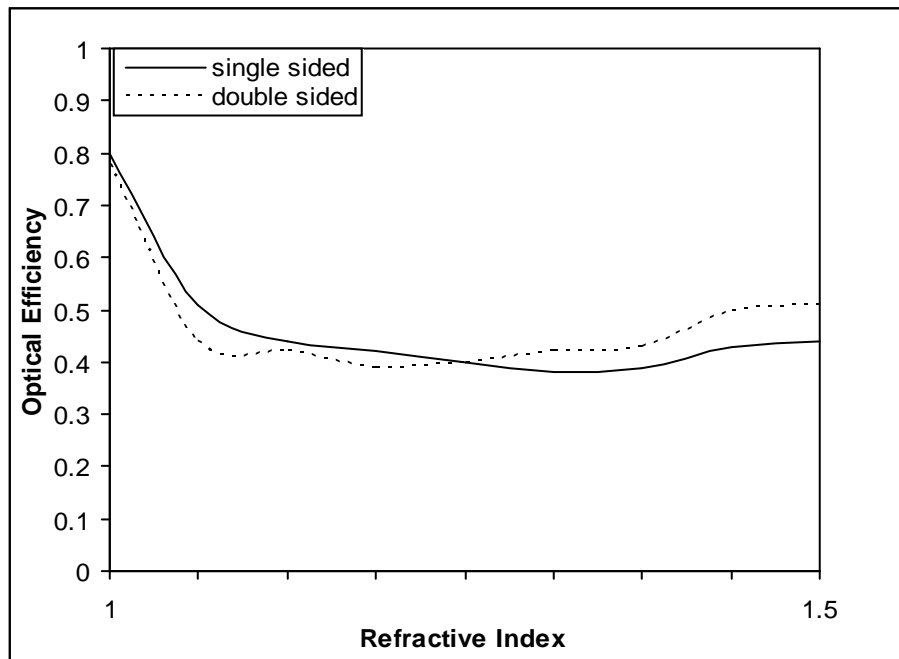


Figure (3): optical efficiency of waveguide concentrator against:  
 (A) Cladding thickness varied,  
 (B) Material refractive indices (n).

For single and double sides ray propagation.

## Modeling and design of flat plate solar collector using different physical and geometrical conditions

Prof. Dr. Jafar Mehdi Hassan

Mechanical Engineering department, University of Technology

Dr. Qusay A. Jawad

Msc. Dheya N. Abdulamer

Energy and Renewable Energies Technology Center, University of Technology

### Abstract

This paper deals with collecting solar radiation from the sun and transfer the received energy to a fluid which passing through pipes or channels which are integrating with the collector absorber plate that has a physical properties characterized by high absorptive solar radiation called the absorption surface, typically a metal plate, usually copper, steel, or aluminum materials with tubing of copper in thermal contact with the plates. In this paper simple and efficient thermal system has been designed to utilize the available sun light by simple design of flat plate solar collector under different conditions which includes:

Unglazed cover, Glazed cover (single or double glazing), Different working fluids, Different physical properties of pipes, Different climatic conditions. For each case of above it was found outlet fluid temperature, instantaneous efficiency and modifier angle factor.

### نمذجة وتصميم مجمع شمسي ذو لوح مستوي باستخدام ظروف فيزيائية وهندسية مختلفة

أ.د جعفر مهدي حسن

قسم هندسة المكنان والمعدات - الجامعة التكنولوجية

د. قصي عبد الجبار جواد، ضياء نجم عبد الامير

مركز تكنولوجيا الطاقة والطاقة المتجددة- الجامعة التكنولوجية

### الخلاصة:

يتعامل البحث الحالي مع تجميع الاشعاع الناشئ من المصدر الشمسي و نقل الطاقة المستلمة الى المائع الذي يمر خلال انابيب او قنوات لها اتصال مع لوح المجمع الماص والذي يملك خواص فيزيائية تتصف بقدرتها على امتصاص الاشعاع الشمسي والذي يدعى بالسطح الممتص، الألواح مصنعة من مواد فلزية عادة منة النحاس، الفولاذ او الالمنيوم. هذا البحث يمثل نظام حراري كفوء سهل صمم لاستخدام الضوء الشمسي المناسب بواسطة تصميم بسيط للوح بسيط مستوي لمجمع شمسي تم دراسته وفق ظروف متغيرة للعمل وهي:

غطاء غير زجاجي، غطاء زجاجي ( طبقة زجاجية واحدة او طبقتين)، موائع بظروف فيزيائية مختلفة للانابيب، ظروف مناخية مختلفة .

لكل حالة من الحالات اعلاه تم ايجاد درجة حرارة المائع، الكفاءة الانية للمجمع الشمسي والعامل الزاوي المعدل.

## Abbreviations

- $r_c$  Collector efficiency.  
 $q_{tube}$  Energy collected above the tube region, Watts.  
 $q_u$  Total energy gain of the collector, Watts.  
 $C_b$  Bond conductance  
 $T_{fi}$  Inlet fluid temperature, °C.  
 $T_{fo}$  Outlet fluid temperature, °C.  
 $G_T$  Incident Solar Radiation,  $W/m^2$ .  
Incident Angle of Beam Radiation, deg.  
Collector slope, deg.  
 $T_{amb}$  Ambient Temperature, °C.  
 $V_{wind}$  Wind speed, m/s.  
 $F^l$  Collector efficiency factor.  
 $G_d/G_T$  Diffuse Radiation proportion.  
 $R$  Relative Humidity.

## 1. Introduction

In the recent years solar energy has been strongly promoted as an active energy source. One of the simplest and most direct applications of this energy is the conversion of solar radiation into heat. Hence way that the domestic sector can lessen its impact on the environment is by the installation of solar flat plate collectors for heating water.

Although it should be said that some of these collectors have been in service for the last 40-50 years without any real significant changes in their design and operational principles.

A typical flat-plate collector consists of an absorber in an insulated box together with transparent cover sheets (glazing)[1].

The absorber is usually made of a metal sheet of high thermal conductivity, such as copper or aluminum, with integrated or attached tubes Fig(1). Its surface is coated with a special selective material to maximize radiant energy absorption while minimizing radiant energy emission. The insulated box reduces heat losses from the back and sides of the collector [2,3].

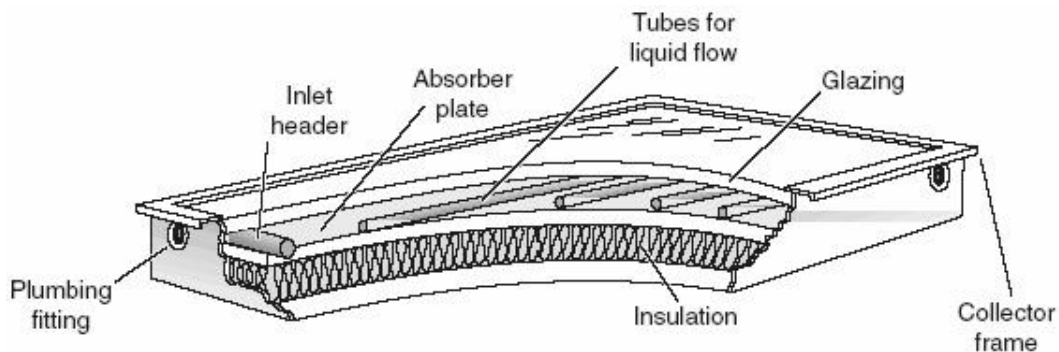


Fig.(1) flat plate solar collector [3]

The flow distribution through the finned tubes of a collector clearly affects the operational efficiency of the collector system. Therefore, the more uniform the flow through the tubes, then the higher efficiency of the collector, and vice versa [4, 5]. The flow distribution can be evaluated by temperature measurements at various points of the collector [6].

The energy loss through the top of solar collector is the result of convection and radiation between the parallel plates. The loss per unit area through the top is equal to the heat transfer from the absorber plate to the cover. This process of losing energy illustrated in Fig (2)

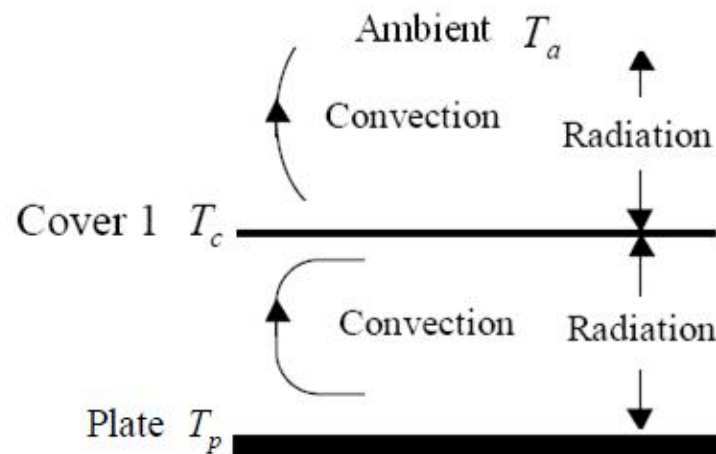


Fig.(2) Heat transfer mechanisms through a collector with a single cover [6]

There are another source of heat losses which are the back and edge heat losses of the collector where the energy loss through the back of the collector is the outcome of the conduction through the back insulation and the convection and radiation heat transfer from the back of the collector to surroundings. The magnitudes of the thermal resistance of convection and radiation heat transfer are much smaller than that of conduction, and therefore it can be assumed that all the thermal resistance from the back is due to the insulation [7].

To guarantee that the collector can withstand high thermal loads, the highest temperature in the collector should be less than the melting point of the parts that is assembled from. Stagnation temperatures are the highest temperatures of the covers and absorber plate that can be obtained from the collector. They take place when the collector is not working, i.e. when the working fluid does not circulate. In this case, the useful gain from the collector is zero[8].

The collector can reach temperatures up to 200°C when no liquid flows through it and therefore all the materials used must be able to resist such heat. The absorber is usually made of metallic materials such as copper, steel or aluminum. The collector housing can be made of plastic, metal or wood, and the glass front cover must be sealed so that heat does not escape, and the collector itself is protected from dirt, insects or humidity.. The absorber plate which covers the full aperture area of the collector must perform three functions: absorb the maximum possible amount of solar irradiance, transfer this heat into the working fluid at a minimum temperature difference and lose a minimum amount of heat back to the surroundings.

Since the temperature of the absorber surface is above ambient temperature, the surface re-radiates some of the heat it has absorbed back to the surroundings. This loss mechanism is a function of the emittance of the surface for low-temperature, long-wavelength radiation. Many coatings that enhance the absorption of sunlight (short-wavelength radiation) also enhance the long wavelength radiation loss from the

surface. A good coating will produce an absorber surface that is a good absorber of short-wavelength solar irradiance but a poor emitter of long-wavelength radiant energy

Normally the absorber is covered with one or more transparent cover sheets to reduce convective heat loss. However convective loss is not completely eliminated because a convective current exists between the absorber and the cover sheet, so transferring heat from the absorber to the cover sheet. External convection then produces a net heat loss from the absorber as it cools the cover sheet.

## 2. Theoretical background

Under steady conditions, the useful heat delivered by solar collector is equal to the energy absorbed in the metal surface minus the heat losses from the surface directly and indirectly to the surroundings. This principle can be stated in the relationship:

$$Q_u = A_c [HR (\tau \cdot r)_e - U_L (t_p - t_a)] \quad (1)$$

Where  $Q_u$  is the useful energy delivered by collector, [Watts] or [cal hr<sup>-1</sup>].  $A_c$  is the collector area, [m<sup>2</sup>].  $HR$  is the solar energy received on the upper surface of slopping collector, [W m<sup>-2</sup>] or [kcal hr<sup>-1</sup> m<sup>-2</sup>].  $H$  is the rate of incident beam or diffuse radiation on a unit area of surface of any orientation.  $R$  is the factor to convert beam or diffuse radiation to that on the plane of collector.  $\tau$  is the fraction of incoming solar radiation that reaches the absorbing surface, transmissivity (dimensionless).  $\alpha$  is the fraction of solar energy reaching the surface that is absorbed, absorptivity (dimensionless).  $(\tau \cdot \alpha)_e$  is the effective transmittance absorptance product of cover system for beam and diffuse radiation.  $U_L$  is the overall heat loss coefficient.  $t_p$  is the average temperature of the upper surface of the absorber, [°C] and  $t_a$  is the atmospheric temperature, [°C]. The factors in eq. 1 depend on the collector design, operating conditions, solar energy and atmospheric temperature. The energy balance equation on the whole collector can written as:

$$A_c [HR (\tau \cdot r)_e + HR (\tau - r)_d] = Q_u + Q_l + Q_e \quad (2)$$

Where  $Q_u$  = rate of useful heat transfer to a working fluid in the solar heat exchanger.  $Q_l$  = rate of energy losses from the collector to the surroundings.  $Q_e$  = rate of energy storage in the collector. Collector efficiency  $r_c$  is the collector performance and is defined as the ratio of useful gain over any time period to the incident solar energy over the same time period.

$$r_c = \frac{\int Q_u d_T}{\int HR d_T} \quad (3)$$

$$\frac{d^2 T}{dx^2} = \frac{U_L}{Ku} (T - T_r - \frac{S}{U_L}) \quad (4)$$

The equation .4 becomes

$$\frac{d^2 \Theta}{dx^2} - m^2 = 0 \quad (5)$$

The general solution is :

$$x = C_1 \sinh mx + C_2 \cosh mx \quad (6)$$

The constants  $C_1$  and  $C_2$  are found by substituting boundary conditions. The eq. 6 becomes:

$$\frac{T - T_a - S/U_L}{T_b - T_a - S/U_L} = \frac{\cosh mx}{\cosh m \left( \frac{W - D}{2} \right)} \quad (7)$$

The energy conducted to the region of the tube per unit length in the flow direction is

$$q_{fin base}^1 = \frac{K u m}{U_L} [S - UL(T_b - T_a)] \tanh \left( \frac{W - D}{2} \right) m \quad (8)$$

The equation. 8 accounts for the energy collected to only one side of a tube. The useful gain of the collector also includes the energy collected above the tube region. The energy gain for the region:

$$q_{tube} = D[S - U_L(T_b - T_a)] \quad (9)$$

Hence, the total energy gain of the collector tubes per unit length in the flow direction may be expressed as:

$$q_u = q_{fin base} + q_{tube section} \quad (10)$$

Ultimately, the useful gain from the eq. 8 must be transferred into the fluid. The resistance to heat flow to the tube from the plant due to the wall thickness of the tube. Hence

$$q_u = \frac{T_b - T_f}{\frac{1}{C_b} + \frac{1}{f D_i h_{fi}} + \frac{1}{C_w}} \quad (11)$$

Where  $C_b$  = the conductance of the bond.  $C_w$  = the conductance of the tube wall and  $h_{fi}$  = the local film heat transfer coefficient. The bond conductance is given as :

$$C_b = \frac{K_b b}{y} \quad (12)$$

Where  $K_b$  = bond conductivity,  $b$  = bond length and  $y$  = bond average thickness. The useful energy gain of the fluid can then be expressed in terms of the known dimensions, the

physical parameters and the local fluid temperature by solving the eq.11 for  $T_b$  and substituting to obtain  $q_u$  from eq.10.

$$q_u = WF^1 [S - U_L (T_f - T_a)] \quad (13)$$

Where

$$F^1 = \frac{1/U_L}{W \left[ \frac{1}{UL[D + (W - D)F]} + \frac{1}{C_b} + \frac{1}{C_w} + \frac{1}{f D_i h_{fi}} \right]} \quad (14)$$

For temperature distribution in the flow direction, consider the energy balance on the fluid element flowing through a pipe which is receiving a uniform heat flux  $q_u$  so that :

$$m \cdot C_p T_f \Big|_y - m \cdot C_p T_f \Big|_{y+dy} + \Delta y q_u = 0 \quad (15)$$

Driving through by  $y$  and finding the limit  $\rightarrow y \rightarrow 0$  and substituting in Eq.15.

$$m \cdot C_p \frac{dT_f}{dy} - WF^1 [S - U_L (T_f - T_a)] = 0 \quad (16)$$

If the assumption is made that  $F^1$  and  $U_L$  are constant ( and independent of  $y$  ), than the solution of the differential equation for the temperature at any position (if subject to the condition that inlet fluid temperature is  $T_{fi}$ ) is :

$$\frac{T_f - T_a - S/U_L}{T_{fi} - T_a - S/U_L} = e^{-(U_L W F^1 y / m \cdot C_p)} \quad (17)$$

If the collector has length  $L$  in the flow direction, then the outlet fluid temperature  $T_{fo}$  is found by substituting  $L$  for  $y$  in the eq. 17.

$$T_{fo} = T_a + \left( \frac{S}{U_L} \right) - \left[ \frac{S}{U_L} - (T_{fi} - T_a) \right] e^{-U_L F^1 A_c / m \cdot C_p} \quad (18)$$

Where :  $A_c = WL$ , the area of collector. The total useful energy collection rate  $Q_u$  may be expressed as :

$$Q_u = m \cdot C_p (T_{fo} - T_a) \quad (19)$$

Substituting for  $T_{fo}$  already derived, gives:

$$Q_u = A_c F_R [S - U_L (T_{fi} - T_a)] \quad (20)$$

Where

$$F_R = \frac{G C_p}{U_L} [1 - e^{-u_L F^1 I G C_p}] \quad (21)$$

$F_R$  has been termed as the heat removal factor of the collector.

### 3. Modeling and Design:

The following tables represent steps of the main considerations that tack into account during modeling flat plate solar collector using *EES* soft program.

**Table 1. Test conditions**

| State | $G_T$<br>( $W/m^2$ ) | $G_d / G_T$<br>(%) | $\theta$<br>(deg) | $\beta$<br>(deg) | $T_{amb}$<br>( $^{\circ}C$ ) | $V_{wind}$<br>(m/s) | $R$<br>(%) |
|-------|----------------------|--------------------|-------------------|------------------|------------------------------|---------------------|------------|
| A     | 1000                 | 2                  | 30                | 30               | 15                           | 3.5                 | 20         |
| B     | 1000                 | 2                  | 30                | 30               | 25                           | 3.5                 | 20         |
| C     | 1000                 | 2                  | 30                | 30               | 35                           | 3.5                 | 20         |

Efficiency curves based on temperature difference :  $T_{av} - T_a$

**Table 2. Dimensions of collector**

| Overall dimensions |       |       | Absorber dimensions |           |
|--------------------|-------|-------|---------------------|-----------|
| L (m)              | W (m) | t (m) | $L_p$ (m)           | $W_p$ (m) |
| 2.91               | 1.221 | 0.079 | 2.4                 | 1.137     |

Where: L = Length, W= Width (m), t = Thickness (m),  $L_p$  = Length,  $W_p$  = Width

**Table 3. Properties of glass Cover**

|                 | Properties of Cover 1 |              |              |               | Properties of Cover 2 |              |              |               |
|-----------------|-----------------------|--------------|--------------|---------------|-----------------------|--------------|--------------|---------------|
|                 | Solar Spectrum        |              | Long- wave   |               | Solar Spectrum        |              | Long- wave   |               |
| Number of Cover | n                     | $\tau_{c,s}$ | $\epsilon_c$ | $\tau_{c,IR}$ | n                     | $\tau_{c,s}$ | $\epsilon_c$ | $\tau_{c,IR}$ |
| 1               | 1.526                 | 0.891        | 0.88         | 0             | 0                     | 0            | 0            | 0             |
| 2               | 1.526                 | 0.891        | 0.88         | 0             | 1.526                 | 0.891        | 0.88         | 0             |

Where:  $d_{cp}$  = Cover- plate air spacing = 1.8 cm,  $d_{c1,c2}$  = Cover 1- cover 2 air spacing = 0.5 cm

**Table 4. Properties of Plate material**

| Plate Material | $K_{pl}$ (w/m.K) | $t_p$ (cm) | $d_n$ | $\epsilon_{pl}$ |
|----------------|------------------|------------|-------|-----------------|
| Cu             | 380              | 0.02       | 0.88  | 0.15            |

Where:  $K_{pl}$ = user defined conductivity,  $t_p$  = Thickness,  $d_n$  = Absorptance,  $\epsilon_{pl}$  = Emittance

### Edge and back insulation

Conductivity of edge insulation = 0.04 w/m . K

Conductivity of back insulation = 0.04 w/m . K

**Table 5. Number and dimension of tube**

| $N_t$ | $d_i$ ( cm ) | $d_o$ ( cm ) |
|-------|--------------|--------------|
| 10    | 1.6          | 1.8          |

Where:  $N_t$  = Number of Tubes,  $d_i$  = Inner diameter,  $d_o$  = Outer diameter  $l_t$  = Tube to Tube spacing

**Table 6. Properties of Fluid**

| Material | Composition (%) | $V'$<br>(L/min) | $P_{in}$ (KPa) | $K_b$ ( w/m.K) |
|----------|-----------------|-----------------|----------------|----------------|
| Water    | 0               | 4.75            | 200            | 400            |

Where:  $V'$  = Volumetric flow rate,  $P_{in}$  = Inlet pressure,  $K_b$  = Plate tube bond conductance

### 4. Results and discussion:

The effects of temperature and number of glass cover have great effects on the instantaneous efficiency of flat plate solar collector. Figure (3), at 15 °C for single cover glass of flat plate solar collector show that the instantaneous efficiency start from 0.625 and decrease to 0.25 at  $\Delta T/GT$  less than 0.09 m<sup>2</sup> K/W. As compared with same conditions, but the flat plate solar collector has double cover glass, figure (6) show the instantaneous efficiency start from 0.6 at  $\Delta T/GT$  equal to 0.01 m<sup>2</sup> K/W then decrease to 0.3 and match with the experimental.

Figures (9) and (12) extremely have the same data that obtained during figures (3) and (6), just decrease in instantaneous efficiency occurred at  $\Delta T/GT$  equal to 0.08 m<sup>2</sup> K/W. The divergence of data can be detected obviously in figure (15), where the instantaneous efficiency decrease to 0.325 at  $\Delta T/GT$  equal to 0.07 m<sup>2</sup> K/W, while figure (18) show the instantaneous efficiency of solar collector match with experimental at  $\Delta T/GT$  less than 0.07 m<sup>2</sup> K/W. It is clear from figure (21) the instantaneous efficiency of solar collector start closely to experimental then divergence between of them reached to maximum value during increase of  $\Delta T/GT$ , in contrast, the opposite behavior can be found in figure (24), where the small match between instantaneous efficiency and experimental occurred at  $\Delta T/GT$  equal to 0.06 m<sup>2</sup> K/W.

Temperature distribution during solar collector can be observed in figure (5), which is represent solar collector has single glass cover exposure into 15 °C. The temperature measured on the glass cover reach in to 49.75 °C and temperature of tube approached to 142.4 °C. For same exposure temperature (i.e 15 °C) on solar collector has double glass cover, the temperature distribution found to be 42.7 °C on the second glass cover, while

80.62 °C measured on the first glass cover. The temperature calculated of tube attended in to 157.1 °C as indicated in figure (8), the same behavior of tube temperature as shown in figure (17) which is represent solar collector has single glass cover exposure in to 35 °C. While collector has double glass cover exposure into same conditions, so that figure (20) show the tube temperature found to be equal in to 172 °C

Temperature developed in collector exposure in to 25 °C have single and double glass cover are 150.4 °C and 164.4 °C as indicated in figures (11) and (14) respectively . Extremely small match of tube temperature as compared with figure (14) can be found in collector has single glass cover exposure in to 45 °C as shown in figure (23), where the temperature developed about 167.6 °C.

Maximum tube temperature can be found 180 °C, in collector has double cover glass exposure in to 45 °C.

## 5. Conclusions:

In general, range of the instantaneous efficiency of flat plate solar collector start from 0.6 and decrease to 0.25 for all physical and geometrical conditions have been used. In this context, match between the module and experimental has been found clearly at  $\Delta T/GT$  less than 0.07 m<sup>2</sup> K/W during flat plate solar collector has double glass cover.

Tube temperature of flat plate solar collector has single and double glass cover exposure into 15 °C, 25 °C, 35 °C and 45 °C respectively are 142.4 °C, 157.1 °C , 150.4°C, 164.4 °C, 158.8 °C, 172 °C, 167.6 °C and maximum tube temperature can be found 180 °C, in collector has double cover glass exposure in to 45 °C.

## References:

1. U.S. Department of Energy - Energy Efficiency and Renewable Energy Solar Energy Technologies Program. <http://www1.eere.energy.gov/solar/>
2. Duffie, J. A., and W. A. Beckman, Solar Engineering of Thermal Processes, John Wiley and Sons, New York, 1991.
3. Charles Smith, History of Solar Energy Revisiting, Past Solar Power Technology Review, Iraqi Virtual library, 1995.
4. G.F Jones and N. Lior, Flow distribution in manifold solar collectors with negligible buoyancy effects. Solar Energy 52, 289–300, 1994.
5. Solar Thermal Tech. Sandia National Labs: <http://solstice.crest.org/renewable>
6. V. Weitbrecht, D. Lehmann, A. Richter, Flow distribution in solar collectors with laminar flow conditions, Solar Energy Volume 73, 433-441, 2002.
7. V. Kienzlén, J.M. Gordon and J.F Kreider, The reverse flat plate collector: A stationary, non evacuated, low-technology, medium-temperature solar collector, J. Solar Energy Engineering, Vol. 110, 23-30, 1988.
8. IORDANOU, GRIGORIOS "Flat-Plate Solar Collectors for Water Heating with Improved Heat Transfer for Application in Climatic Conditions of the Mediterranean Region" Msc. thesis Durham university ,2009.

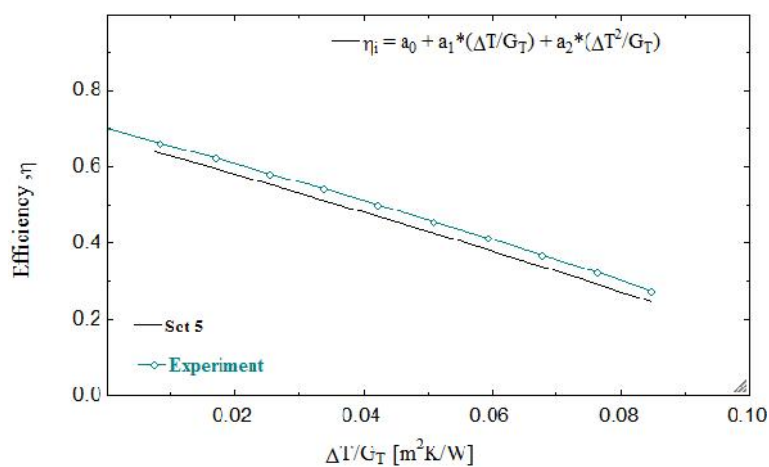


Figure (3) : Instantaneous Efficiency of collector at single glass cover and 15 °C

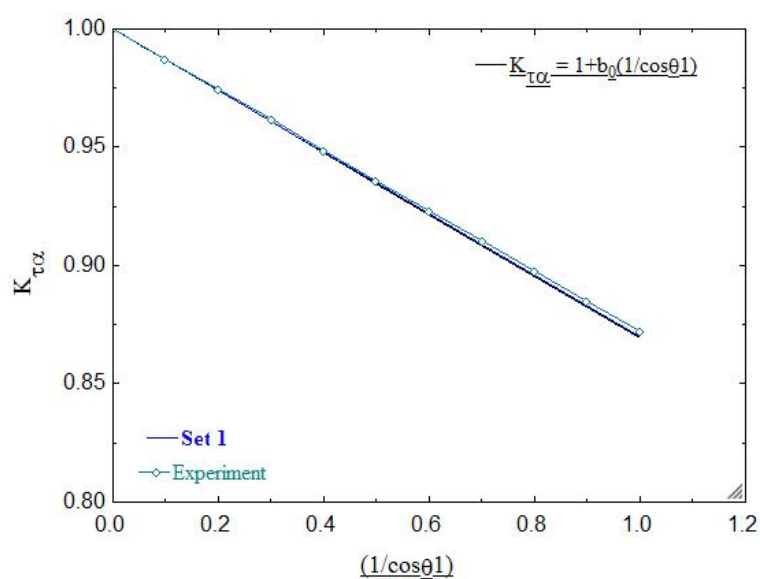


Figure (4): Incident Ingle Modifier at single glass cover and 15 °C

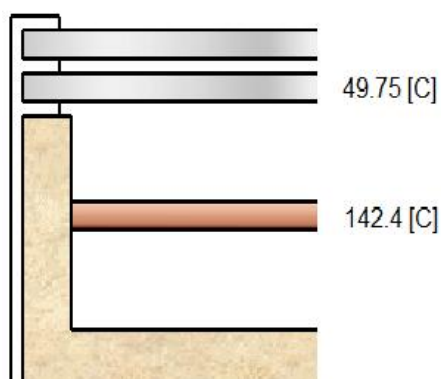


Figure (5) : Temperature distribution at single glass cover and 15 °C

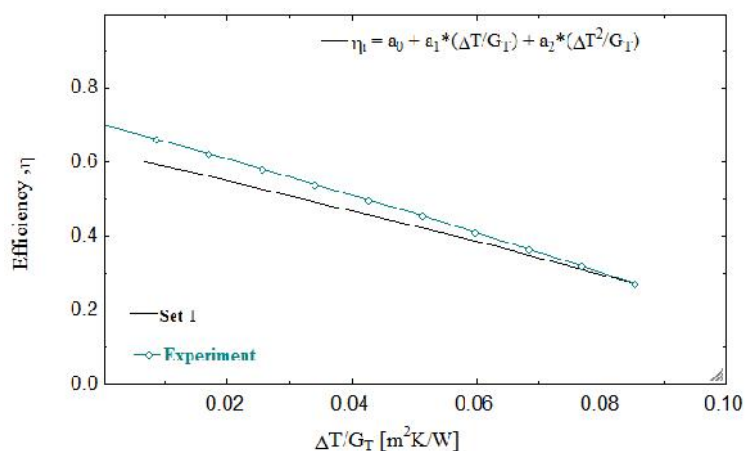


Figure (6) : Instantaneous Efficiency of collector at double glass cover and 15 °C

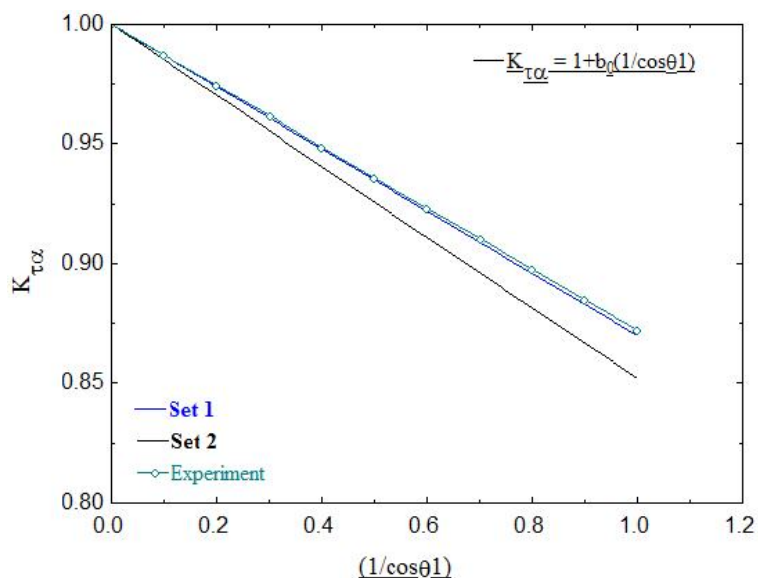


Figure (7): Incident Ingle Modifier at double glass cover and 15 °C

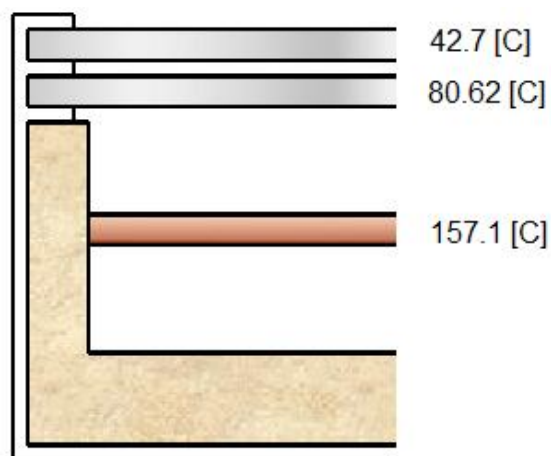


Figure (8) : Temperature distribution at double glass cover and 15 °C

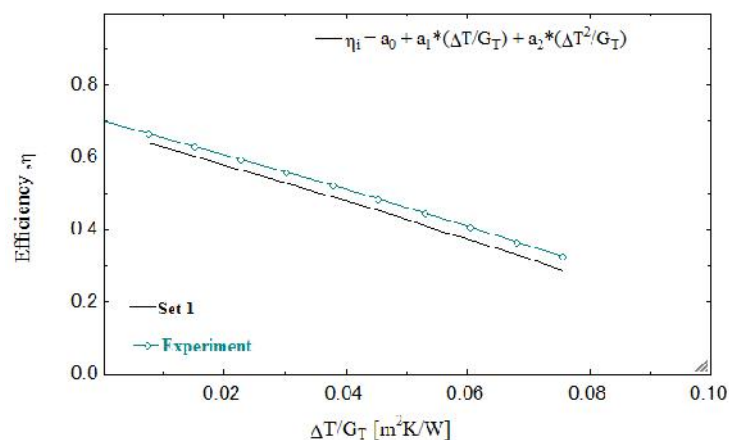


Figure (9) : Instantaneous Efficiency of collector at single glass cover and 25 °C

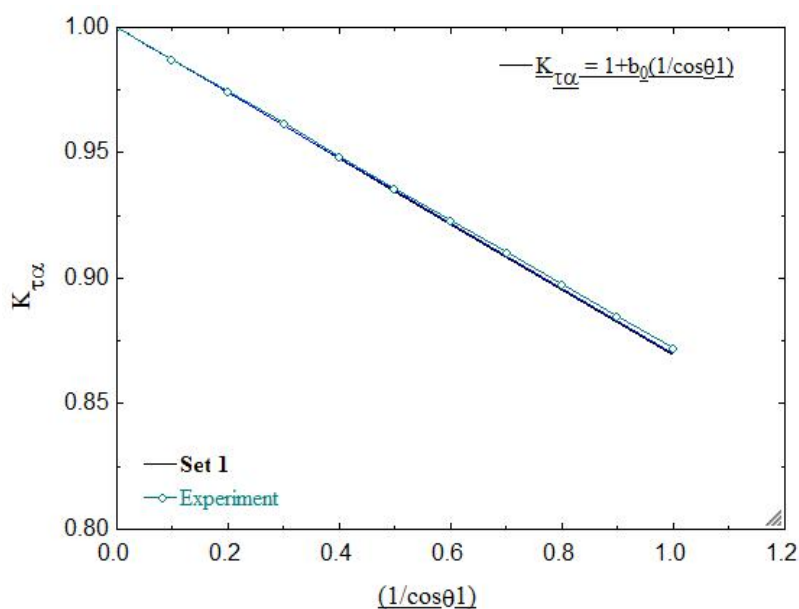


Figure (10): Incident Ingle Modifier at single glass cover and 25 °C

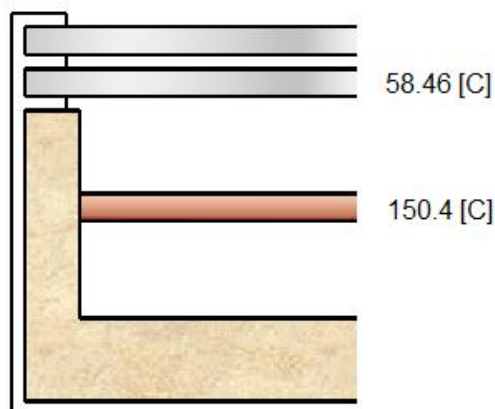


Figure (11) : Temperature distribution at single glass cover and 25 °C

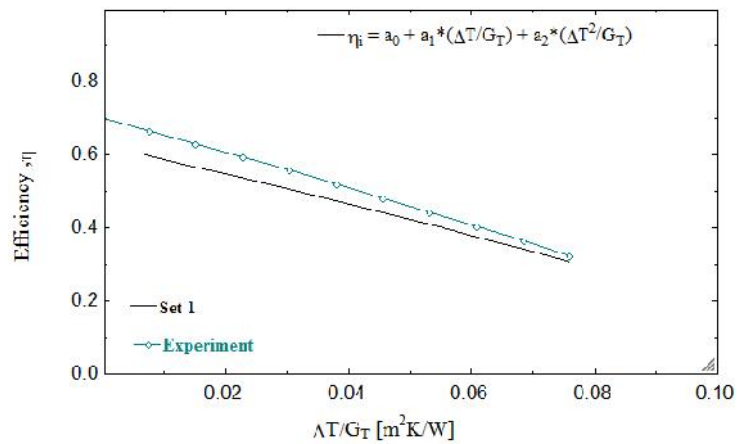


Figure (12) : Instantaneous Efficiency of collector at double glass cover and 25 °C

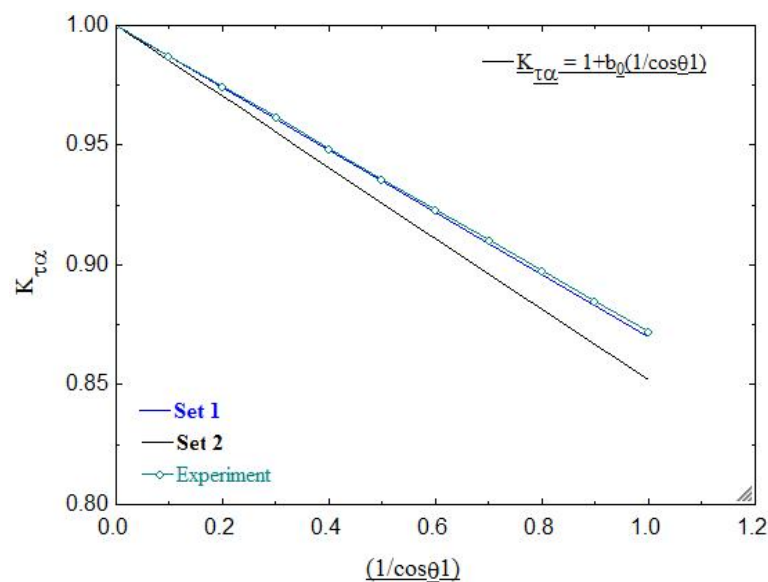


Figure (13): Incident Ingle Modifier for at double glass cover and 25 °C

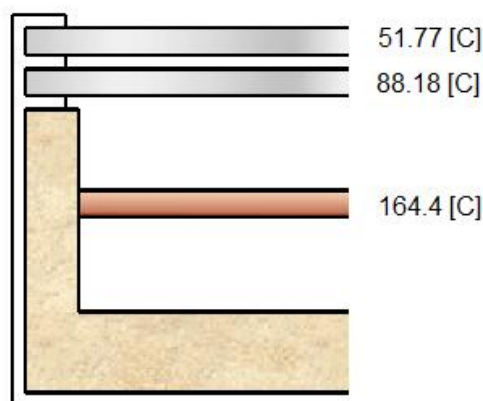


Figure (14) : Temperature distribution at double glass cover and 25 °C

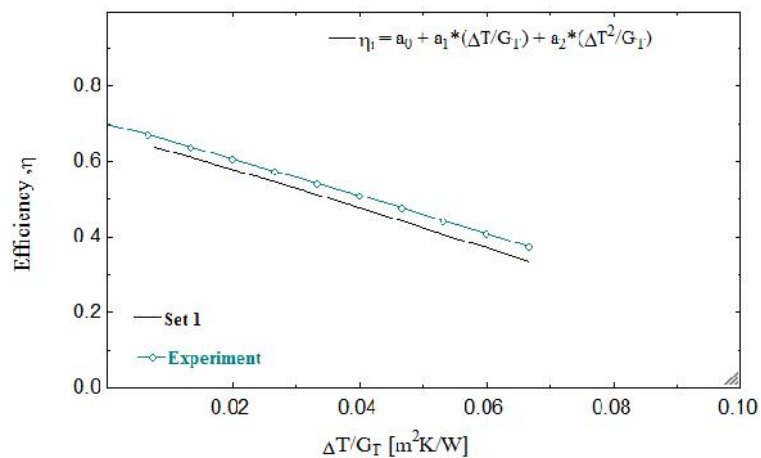


Figure (15) : Instantaneous Efficiency of collector at single glass cover and 35 °C

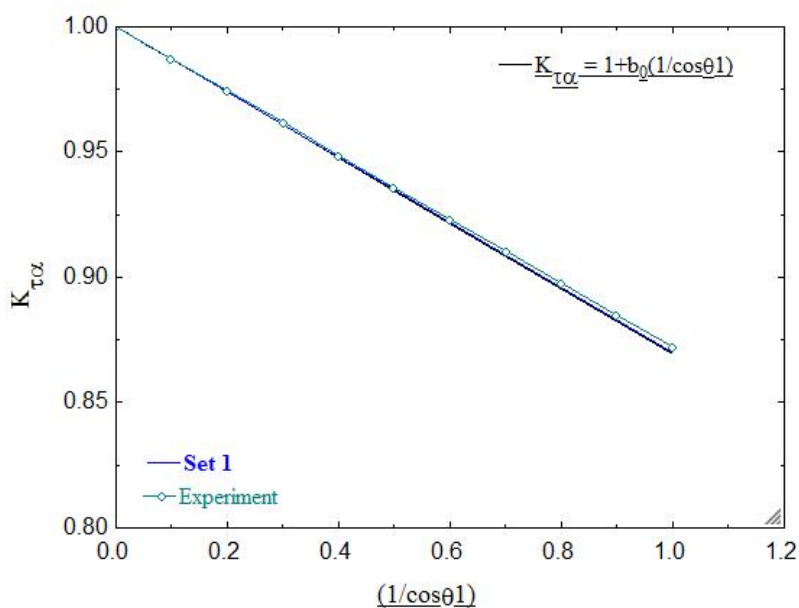


Figure (16): Incident Ingle Modifier at single glass cover and 35 °C

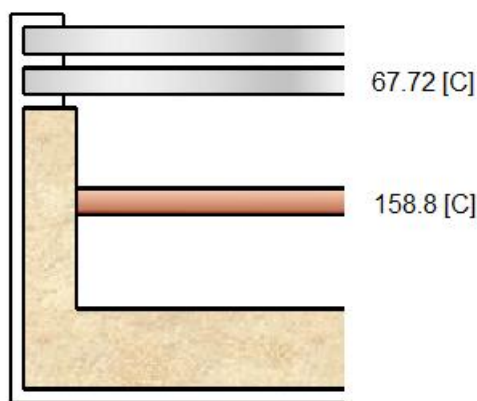


Figure (17) : Temperature distribution at single glass cover and 35 °C

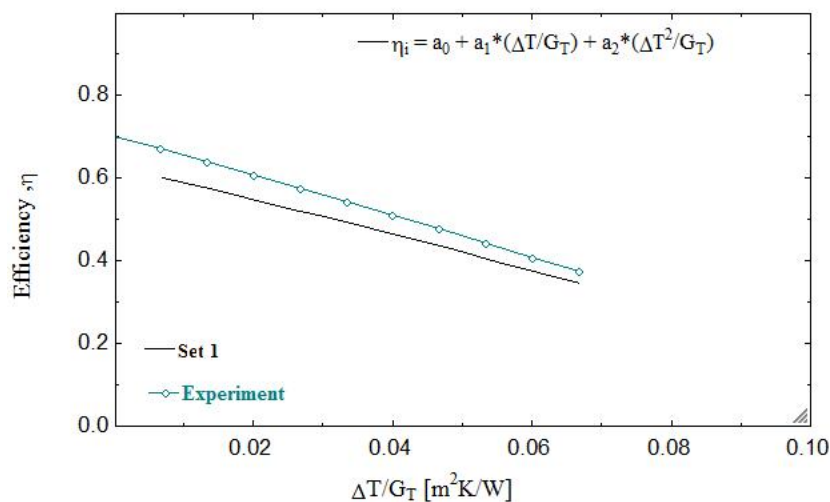


Figure (18) : Instantaneous Efficiency of collector at double glass cover and 35 °C

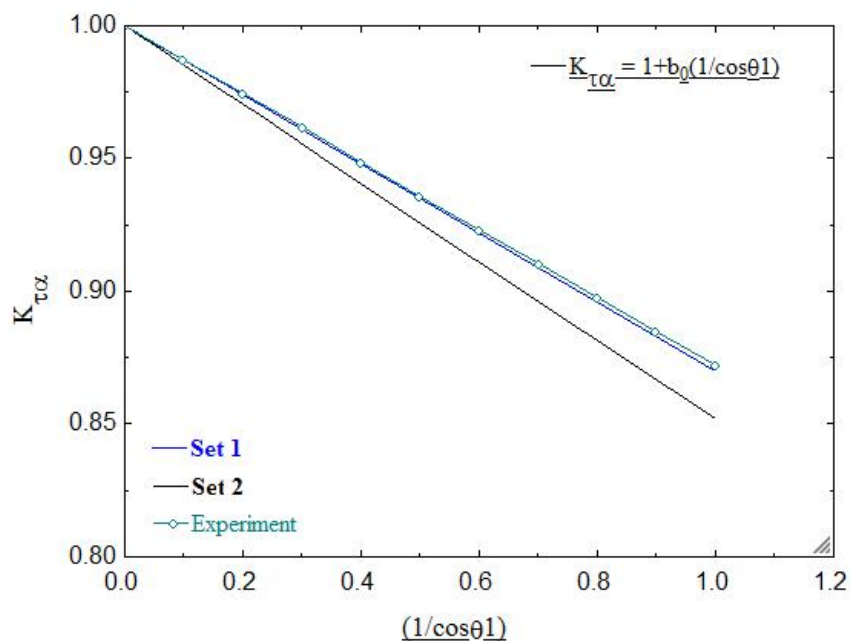


Figure (19): Incident Ingle Modifier at double glass cover and 35 °C

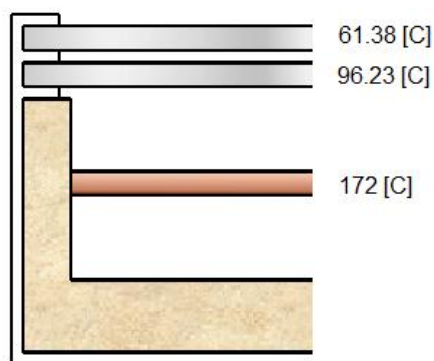


Figure (20) : Temperature distribution at double glass cover and 35 °C

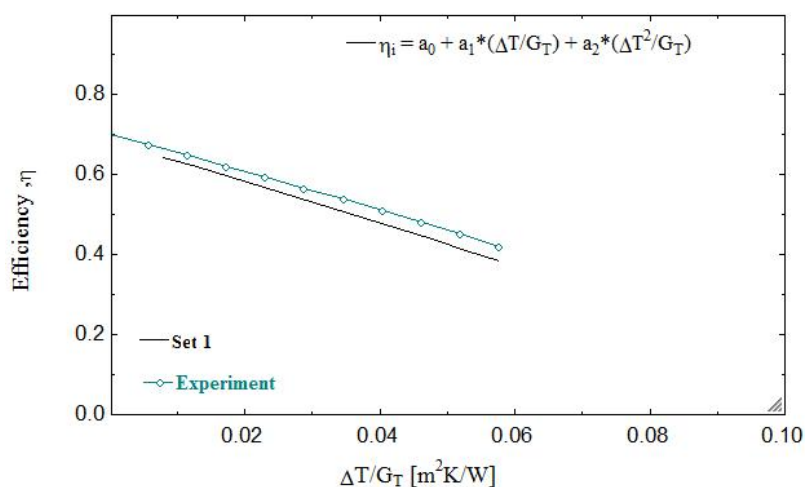


Figure (21) : Instantaneous Efficiency of collector at single glass cover and 45 °C

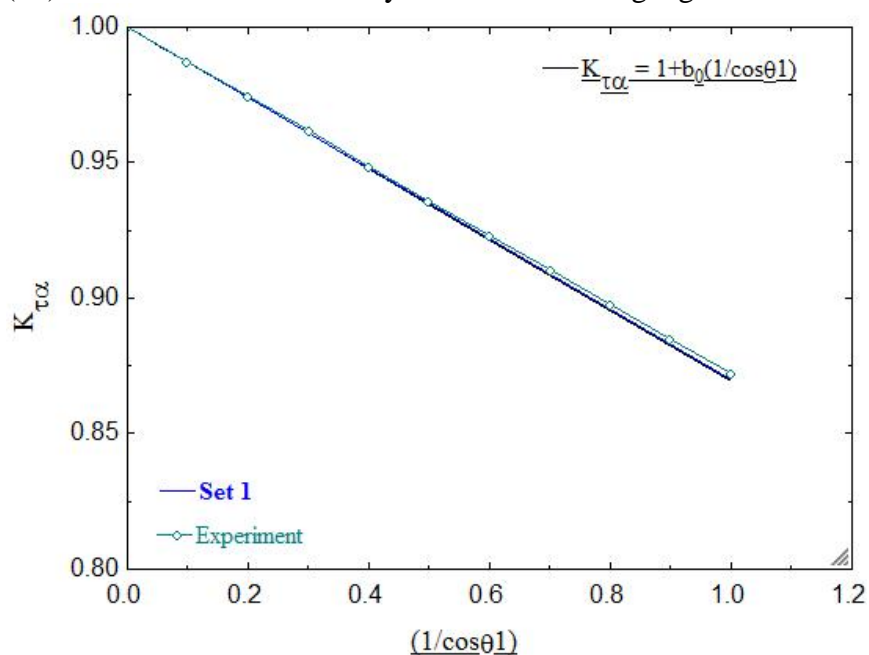


Figure (22): Incident Ingle Modifier at single glass cover and 45 °C

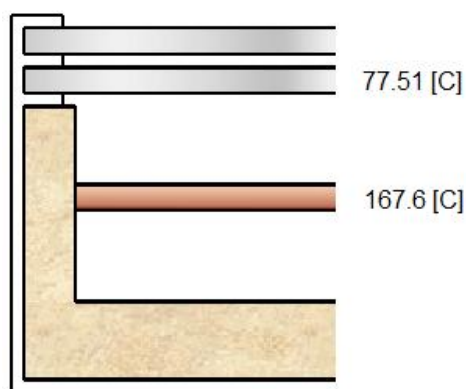


Figure (23) : Temperature distribution at single glass cover and 45 °C

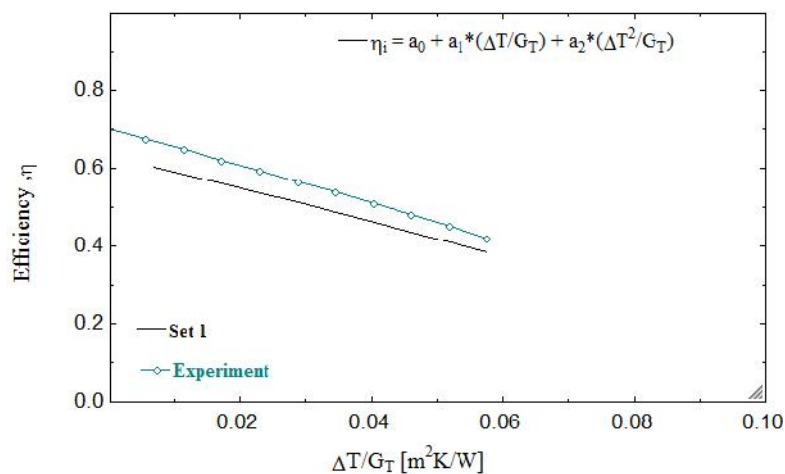


Figure (24) : Instantaneous Efficiency of collector at double glass cover and 45 °C

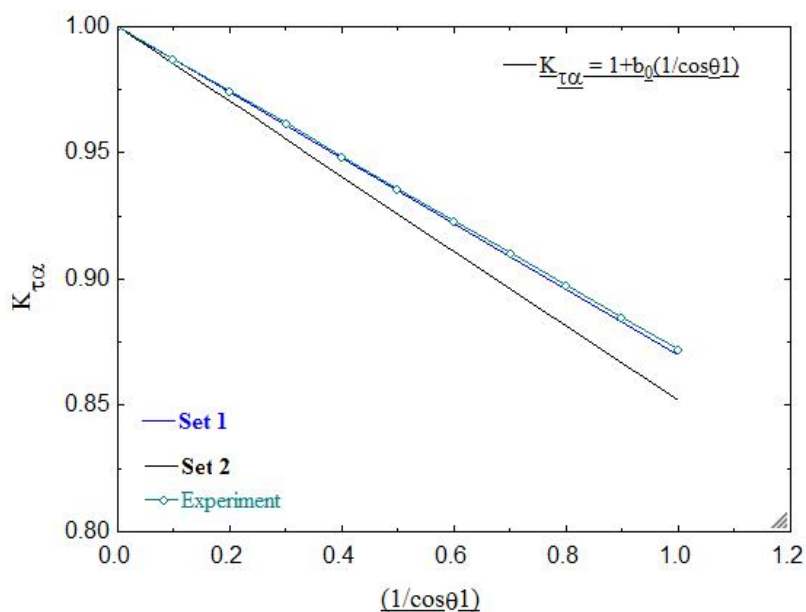


Figure (25): Incident Ingle Modifier at double glass cover and 45 °C

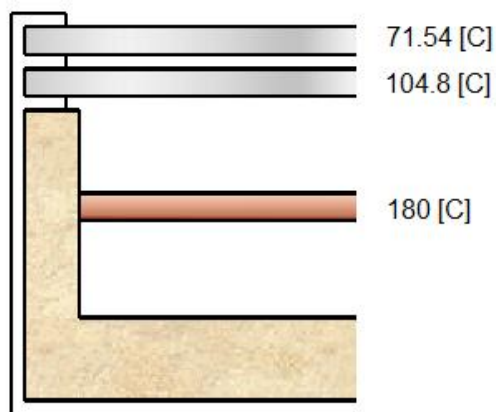


Figure (26) : Temperature distribution at double glass cover and 45 °C

## The Investigation of Effect Dust on the Performance of Solar Collectors with Different Area

Mohammed Ali Fayad  
Lecturer

Ayad M. Salman  
Lecturer

Haider S. Mahde  
Assist. Lecturer

Energy and Renewable Energies Technology Center  
University of Technology

### Abstract

According to the increasing work in the field of renewable energy particularly solar energy to replace the traditional energy sources, therefore we have to think about the protection and maintenance of these renewable energies as long as possible.

Reaching for studying the use of two types of solar collector-flat plate collector, tested and examined under the same climatic conditions of Iraq for months January and February, and hours of operation of the system starts at eight in the morning until four o'clock pm, the first type vacant surface of the dust and the second type contains dust, which reduce the absorption of sunlight. I've been in this research to calculate the effect of dust on the solar collector and note the difference on the performance of solar collector and evaluate its performance through the results. The study proved the accuracy and convergence of results with many of the results of previously published study showed that the solar collector vacant from dust gives better performance compared with the solar collector, which contains dust.

### الخلاصة

نظراً للإقبال الذي نشهده في مجال الطاقة الشمسية والبحث عن بدائل ممكن من خلالها الاستغناء عن الطاقة ليدية ، فلذلك يجب التفكير في حماية وصيانة هذه البدائل والحفاظ عليها أطول فترة ممكنة. استخدام نوعين من الجامع الشمسي من النوع اللوح المستوي المناخية للعراق للأشهر كانون الثاني وشباط ولساعات اشتغال المنظومة تبدأ من الساعة الثامنة صباحاً ولغاية الساعة خالي سطحه من الأتربة و يحتوي على الأتربة والتي تقلل من امتصاص أشعة لقد تم في هذا البحث حساب تأثير الأتربة على الجامع الشمسي وملاحظة الفرق على أداء الجامع الشمسي وتقييم أدائه من خلال النتائج. وأثبتت الدراسة دقة وتقارب النتائج مع العديد من النتائج المنشورة سابقاً وأظهرت الدراسة أن الخالي من الأتربة يعطي أداء أفضل مقارنة مع الجامع الذي يحتوي على الأتربة .

## Nomenclature

| <i>Symbols</i>  | <i>Definition</i>                                                                         | <i>Units</i>      |
|-----------------|-------------------------------------------------------------------------------------------|-------------------|
| $A_c$           | Area of solar collector                                                                   | $m^2$             |
| $C_p$           | Specific heat of water                                                                    | $J/kg.^{\circ}C$  |
| $D$             | External diameter of tube                                                                 | $m$               |
| $D_i$           | Internal diameter of tube                                                                 | $m$               |
| $F_r$           | Factor of solar collector                                                                 | -                 |
| $F_l$           | Efficiency factor of solar collector                                                      | -                 |
| $h_w$           | Wind heat transfer coefficient                                                            | $W/m^2.^{\circ}C$ |
| $h$             | Heat transfer coefficient between fluid and internal tube wall                            | $W/m^2.^{\circ}C$ |
| $L$             | Length tube of solar collector                                                            | $m$               |
| $\dot{m}$       | Mass flow rate of water                                                                   | $kg/sec$          |
| $N$             | Number of riser                                                                           | -                 |
| $n$             | Number of glass covers                                                                    | -                 |
| $Q_{Coll}$      | Solar energy collected                                                                    | $W$               |
| $Q_{CLoss}$     | Energy lost from the solar collector to the environment                                   | $W$               |
| $Q_{Stor}$      | Energy stored in the tank                                                                 | $W$               |
| $R$             | Ratio of total solar radiation                                                            | -                 |
| $S$             | Solar energy absorbed                                                                     | $W$               |
| $s$             | Inclination angle of the solar collector                                                  | degree            |
| $t$             | Time                                                                                      | hr                |
| $T_a$           | Air temperature                                                                           | $^{\circ}C$       |
| $T_{f,i}$       | Inlet water temperature from solar collector                                              | $^{\circ}C$       |
| $T_{f,o}$       | Outlet water temperature from solar collector                                             | $^{\circ}C$       |
| $T_{f,m}$       | Mean external temperature from solar collector                                            | $^{\circ}C$       |
| $T_{p,m}$       | absorbed plate mean temperature                                                           | $^{\circ}C$       |
| $T_p$           | Temperature of absorbed plate                                                             | $K$               |
| $T_s$           | Temperature of water tank                                                                 | $^{\circ}C$       |
| $U_L$           | Coefficient of thermal losses from solar collector                                        | $W/m^2.^{\circ}C$ |
| $U_t, U_b, U_e$ | Coefficient of thermal losses from the upper and lower surface and behind solar collector | $W/m^2.^{\circ}C$ |
| $W$             | Distance between centers of two tubes                                                     | $m$               |
| $\eta_{Coll}$   | Efficiency of solar collector                                                             | %                 |
| $\varepsilon$   | Permeability coefficient                                                                  | -                 |
| $\rho_r$        | Reflection coefficient                                                                    | -                 |
| $\tau$          | Emission factor                                                                           | -                 |

## 1. INTRODUCTION

Solar water heating systems require relatively little attention. But, as with any thermal system, some basic maintenance is essential to keep the system functioning smoothly. The systems should be checked periodically to improve collector efficiency. Renewable energy and energy efficiency offer the prospect for a sustainable energy future with important links to the past. The Role of Maintenance is improvement of performance and to obtain the highest durability and reliability, all solar water heaters require some level of maintenance. Unfortunately, most owners do not attend to the maintenance needs of their systems as they should.[1]. Solar water heaters most of the time are called “domestic hot water systems”. These systems use the solar radiation heat either water or a heat transfer fluid, such as water-glycol antifreeze mixture in collectors generally mounted on the roof. The heated water is then stored in storage tank. The systems should be checked periodically by maintenance to improve solar heating efficiency, [2]. [close 1962], Has presented a mathematical model for prediction the system temperature and water mass flow rate of a natural circulation solar water heater for clear sunny days and no drain-off during the day,[3]. [Phillips and Cook 1975] Studied the natural circulation from a flat plate collector to a hot liquid storage tank experimentally and analytically. The absorber plate served as a conduit for the water flowing from the collector to the storage tank. The results were presented for both the experimental and theoretical investigation in terms of dimensionless parameters which were said to be useful in system design in the prediction of system performance. The cases of both a fully mixed and a fully stratified tank were considered theoretically and the experimental measurements were found to be closer to the stratified case,[4]. [Thomas. Mueller,2002] Described manual for all maintenance involved in the operation, inspection, repair and maintenance of liquid solar heating system. The manual is designed to be used in the field by the personal performing. Thus increasing life time and reducing maintenance costs,[5]. [Nimmo et.al. 1978] Presented an analytical and experimental study of a solar water heater under a forced circulation condition. The mathematical model was presented to predict the performance of solar water heaters for which the meteorological data and draw off of hot water from the storage tank at arbitrary times during the day would be available at 15 minute intervals,[6]. [C.L. Gupta and H.P. Garg 1986 ], developed a computer model for thermal performance of domestic solar water heaters which employed thermosyphon circulation between collector and storage tank also they showed that, reducing the elevation of the storage tank reduces the water flow rate,[7]. [Antonis.M.Psarompas, 2001], studied and

measured the water temperature distributions along the solar collector tubes, absorber plate temperature profiles at various location along the collector, [8].

## 2. Flat-Plate Solar Collectors

Flat-plate solar collector can collect all components of the sun's energy. Flat-plate types are the most-used type of collectors. The typical flat-plate collector consists of a black absorber plate with tubes running through or attached to it to take the collected heat away. Above this surface is a glazing, usually glass, to help trap the heat. Insulation surrounds the absorber to retard the loss of heat from the collector. A typical flat plate collector system is shown in figure (1), [9].

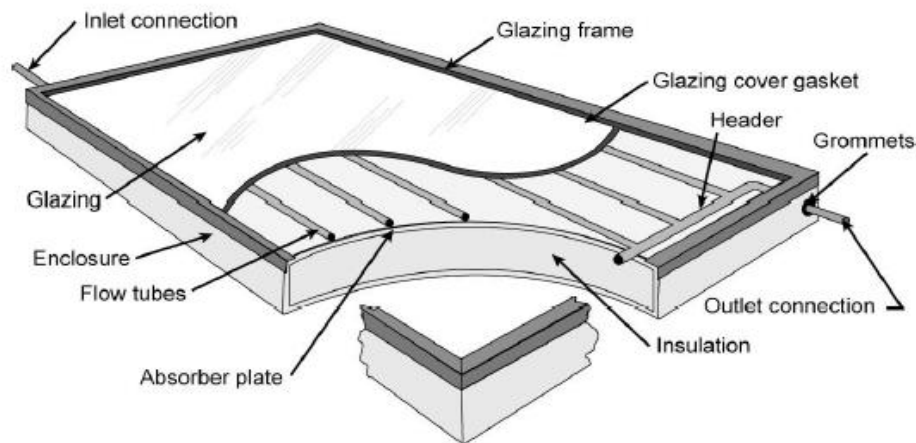


Fig. 1. Schematic representation of a typical flat plate collector [9].

### 2.1 Cleaning Glazing:

The cleaning of the glazing should be done by regular maintenance, if the rain or snow is not enough to clean it. The maintenance procedure should ensure keeping the collector cover clean; dirt reduces the amount of radiation that can reach the collector. The frequency of cleaning will depend on the degree of atmospheric pollution.

## 3. Effect of Dust on the Solar Collector:

The effect of dust on the performance of the flat plate collectors is determined in terms of comparisons between collectors which have accumulated dust and clear collectors. The dust accumulated on the transparent cover decreases the transmission of radiation and thus decrease the useful energy received from collectors. The effect on instantaneous efficiency, useful collector heat flux, temperature rise across the collector and mean storage tank water

temperature. The average percentage reduction of the useful heat is about 12.5 % for collectors with dust accumulation of one month. This values is obtained as follows:

Percentage reduction of useful heat for each hour

$$\frac{(Q_{coll.}) without dust - (Q_{coll.}) with dust}{(Q_{coll.}) without dust}$$

Then averaging this value over the hours of the day [10]. The dust accumulated on the flat plate collector as shown in figure (2).

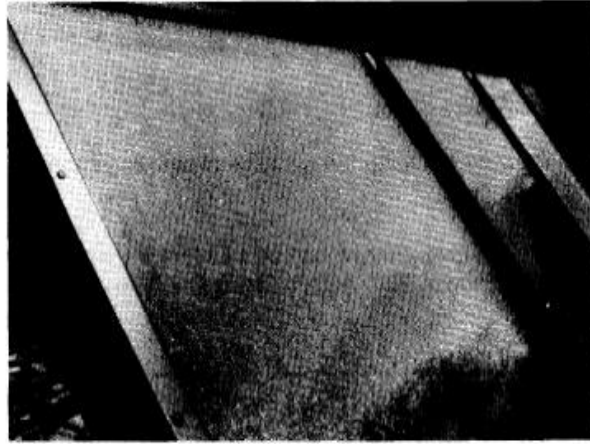


Figure (2) flat plate collector cover is contains dust [10].

#### 4. Theoretical Mathematical Calculation of Solar Collector.

For a basic flat plate collector, the energy balance involving the distribution of incident solar energy can be represented as [2, 11]:

$$Q_{coll.} = A_c Fr [S - U_l (T_{pm} - T_a)] \quad (1)$$

Where;

$T_{pm}$  : Mean temperature absorbed plate of solar collector( $C^0$ )

$T_a$  : is the air temperature.

The absorber solar radiation energy by solar collector can expressed by :

$$S = \frac{H R \dagger_a (1 - d) (1 - z)}{3.6} \quad (2)$$

Where;

H: total solar radiation ( $kJ/m^2.h$ )

$$R = K_b R_b + K_b \left(1 + \frac{\cos(s)}{2}\right) + \dots_r \left(\frac{1 - \cos(s)}{2}\right) \quad (3)$$

Where,

d is the factor takes into account the impact of dust on the glass cover.

z factor effect of the compound the edge of the solar collector on the absorber plate.

$K_b$ ,  $k_d$  represent the proportion of the direct radiation to total radiation and the proportion of scattered radiation to total radiation respectively.

To calculate the emission factor is[4].

$$\ddagger_a = (\ddagger_1 \times \ddagger_2 \times \dots \ddagger_n) \times r_p \times (0.395) \quad (4)$$

The main temperature of absorber plate is calculated by :

$$T_{p,m} = T_{f,m} + Q_{Coll} R_{p-f} \quad (5)$$

The collector heat removal factor is [12]:

$$F_R = \frac{G C_p}{U_L} \left[ 1 - e^{-\frac{U_L F_1}{G C_p}} \right] \quad (6)$$

Where;

$C_p$  : specific heat at constant pressure.

$G$  : flow rate per unit area of collector.

The collector efficiency factor (F1) is constant for any collector design and fluid flow rate.

The collector efficiency factor can be determining by:

$$F_1 = \frac{\frac{1}{U_i}}{W \left[ \frac{1}{U_i [D + (W - D) F]} + \frac{1}{h_i A_i} + \frac{1}{C_b} \right]} \quad (7)$$

Where;

F : Efficiency factor of solar collector

$h_i$  : inside heat transfer coefficient between the fluid and inside area .

$C_b$  : bond conductance.

W, D can be explained in figure:

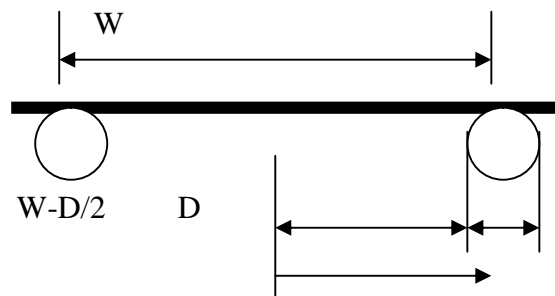


Fig. (3). Explain the distance and diameter of tubes.

The bond conductance is calculated by:

$$C_b = \frac{K_b b}{x} \quad (8)$$

Where,

b = is the thickness of welding line

K<sub>b</sub>= conductivity thermal coefficient (400kW/m.°C)

For the purpose of calculating the overall heat loss coefficient of the solar collector is used the following equation:

$$U_L = U_t + U_b + U_e \quad (9)$$

To calculate the coefficient heat loss from the upper surface of the solar collector is using the following formula:

$$U_t(s) = (1 - (s - 45)(0.00259 - 0.00144 v_p)) U_t(45) \quad (10)$$

$$U_t = \left( \frac{N}{(344 / T_p) [(T_p - T_a) / (N + f)]^{0.31} + \frac{1}{h_w}} \right)^{-1} + \frac{(T_p + T_a)(T_p^2 + T_a^2)}{[v_p + 0.0425 N (1 - v_p)]^{-1} + [(2N + f - 1) / v_g] - N} \quad (11)$$

$$f = (1.0 - 0.04h_w + 5.0 \times 10^{-4} h_w^2)(1 + 0.058N)$$

$$h_w = 5.7 + 3.8V$$

To calculate the coefficient of thermal losses from the lower surface and sides of solar collector, as the sides of solar collector isolated the same material, U<sub>b</sub>, U<sub>e</sub> becomes as:

$$U_b = \frac{K}{L} \quad (12)$$

$$\left. \begin{aligned} U_{edge} &= \frac{K}{L} \\ U_e &= \frac{KA_e}{A_c} \end{aligned} \right\} \quad (13)$$

Where,

K= Heat conductivity

L = Length tube of solar collector

Q<sub>u</sub> could be written it be following in form

$$Q_u = \dot{m} C_p (t_{fo} - t_{fi}) \quad (14)$$

t<sub>fo</sub>, t<sub>fi</sub> are the outlet water temperature and inlet water temperature.

To calculate the energy drawn from the heat tank and the thermal heat losses from the tank is by using the two equations respectively ,the following:

$$Q_{SLoss} = (UA)_s \left( \frac{T_{fo} + T_s}{2} - T_a \right) \quad \dots(15)$$

the solar energy collected is calculated by using the following equation :

$$q_{Stor} = m_s C_p (T_{fo} - T_s) \quad \dots(16)$$

The temperature of the water outside from solar collector is calculated from following equation:

$$T_{fo} = T_{fi} + \left( \frac{F_r A_c}{\dot{m} C_p} \right) (S - U_L (T_{fi} - T_a)) \quad (17)$$

the mean fluid temperature can be found by:

$$t_{fm} = t_{fi} + \frac{\frac{Q_u}{A_c}}{U_l F_r} \left( 1 - \frac{Fr}{F1} \right) \quad (18)$$

The collector heat removal factor is:

$$Fr = \frac{G C_p}{U_l} \left[ 1 - e^{-\frac{U_l F1}{G C_p}} \right] \quad (19)$$

Where;

$C_p$  : specific heat at constant pressure.

$G$  : flow rate per unit area of collector.

Solar collector efficiency gives the collector performance, which is the ratio of the useful energy gain to the incident solar energy and is expressed as [13]:

$$\eta_{coll \cdot hour} = \left( \frac{Q_u}{A_c H R} \right) 100 \% \quad (20)$$

Where;  $\eta_{hour}$  : is the hourly solar collector efficiency.

## 5. Results and Discussion

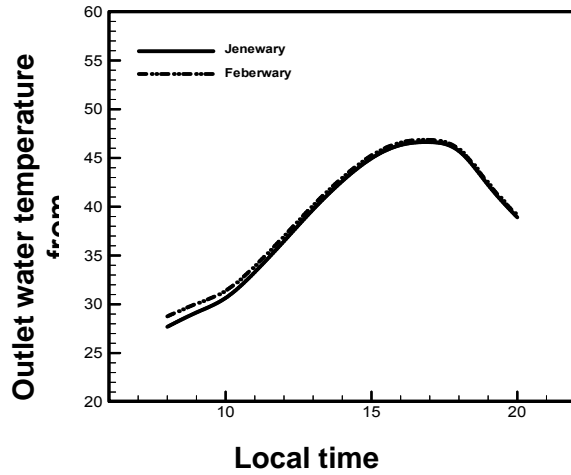


Fig. 1. Show relationship between Local Time Vs. Outlet

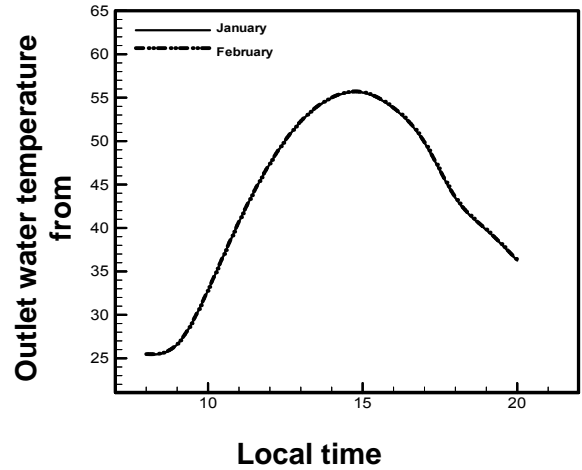


Fig. 2. Show relationship between Local Time Vs. Outlet

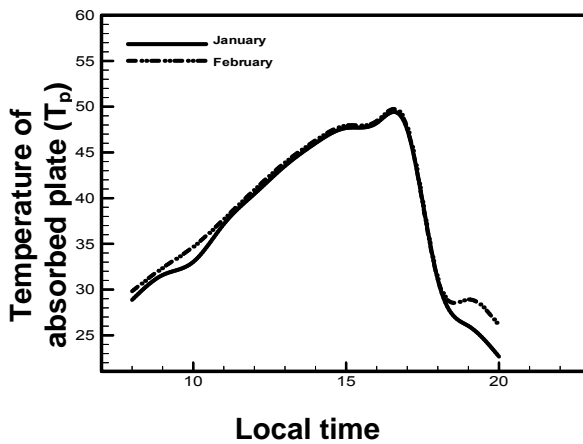
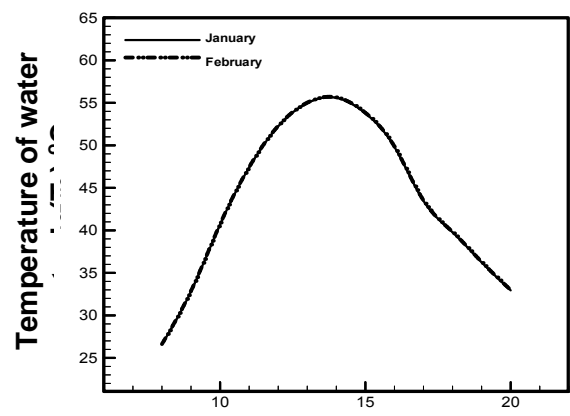
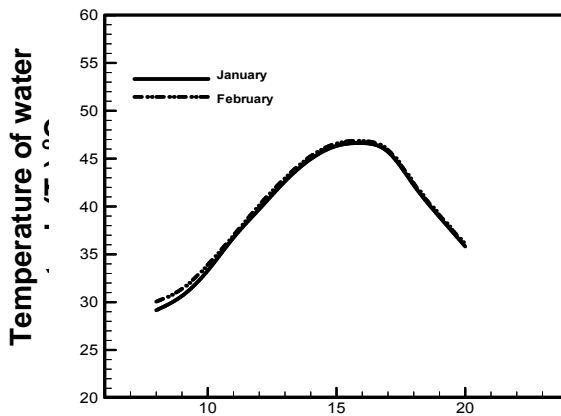


Fig. 5. Show relationship between Local time Vs. Temperature of absorbed plate with dust.

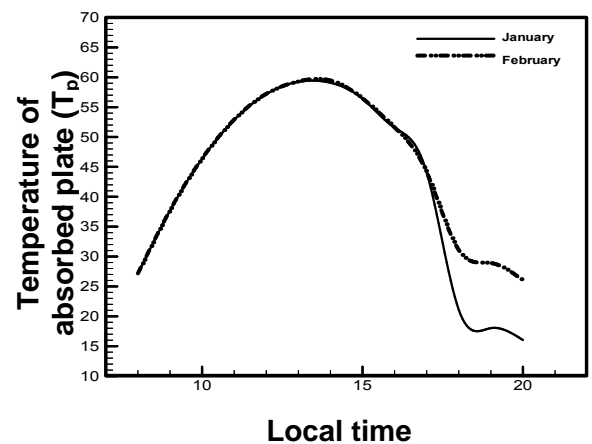


Fig. 6. Show relationship between Local time Vs. Temperature of absorbed plate without dust.

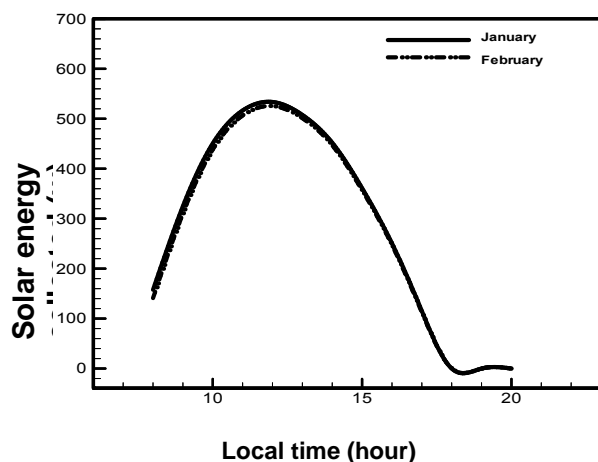


Fig. 7. Show relationship between Local time Vs. Solar energy collected with dust.

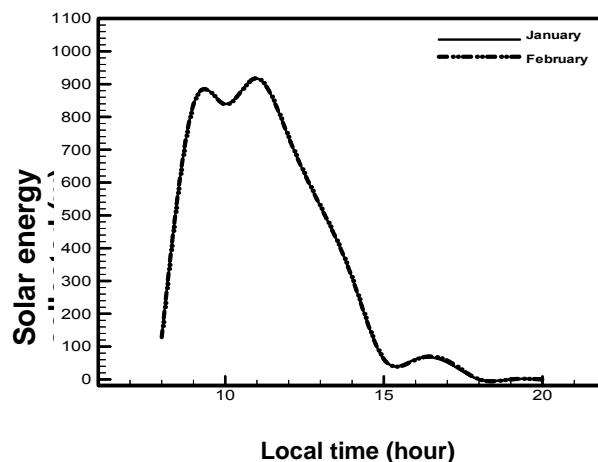


Fig. 8. Show relationship between Local time Vs. Solar energy collected without dust.

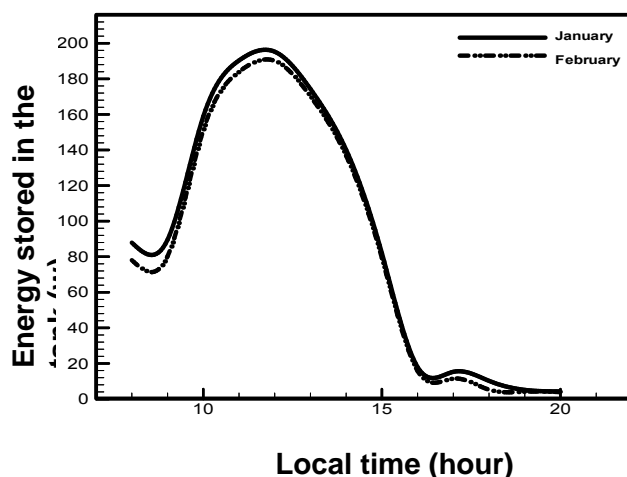


Fig. 9. Show relationship between Local time Vs. Energy stored in tank with dust.

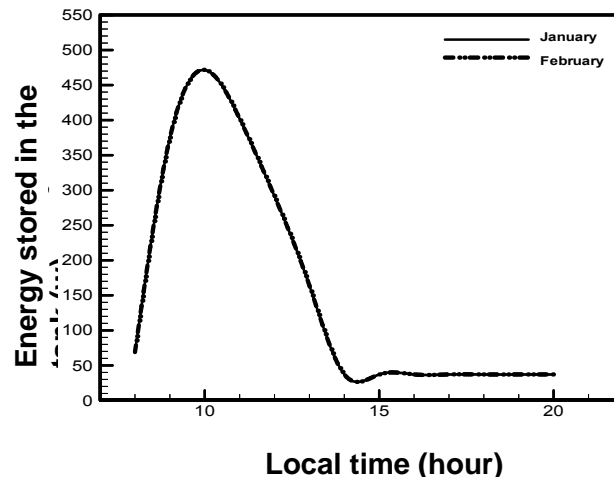


Fig. 10. Show relationship between Local time Vs. Energy stored in tank without dust.

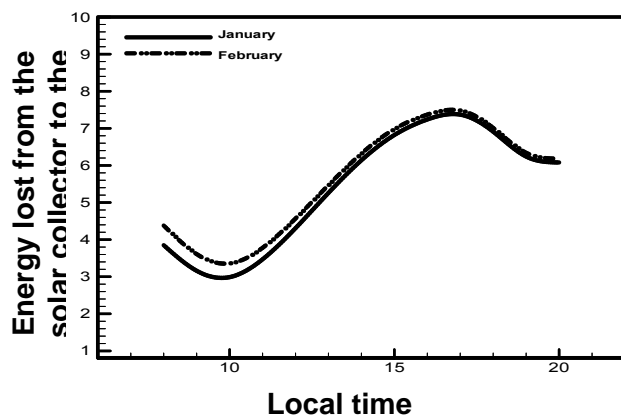


Fig. 11. Show relationship between Local time Vs. Energy lost from the solar collector to the environment with dust.

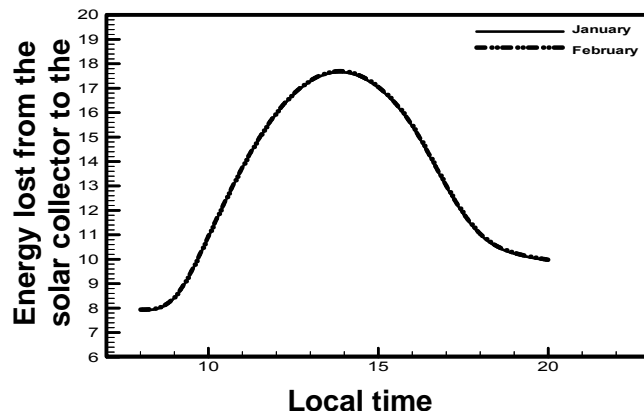


Fig. 12. Show relationship between Local time Vs. Energy lost from the solar collector to the environment without dust.

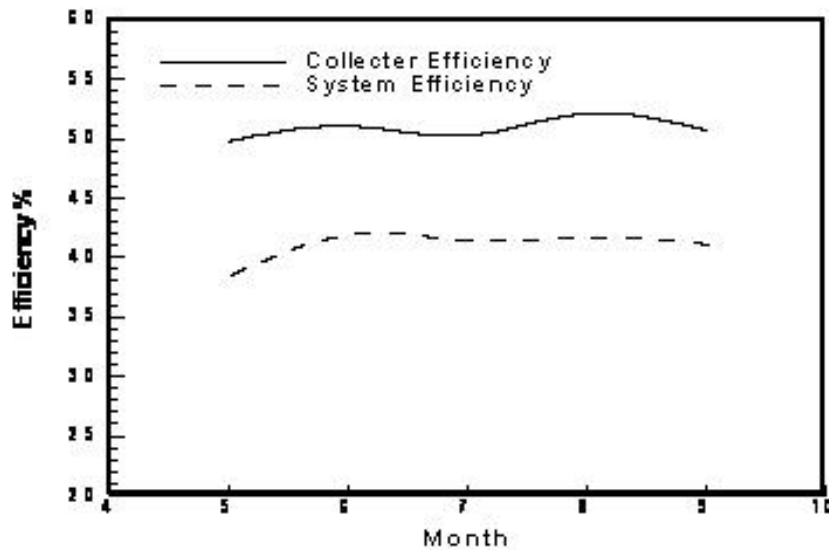


Figure (13) Change in efficiency of solar collector through January and February month.

The gathering dust on the surface glass of the solar collector have negative effect on the efficiency because reduce the amount of radiation of the window to the absorber surface. The succeeding of the system depend on the performance of flat plate collector .

Figures (1 and 2) We note that the effect dust on the solar collector, when dust increase the temperature of solar collector decrease because. Figures (3 and 4) show the measured temperature with local time of storage tank, the temperature decrease with dust because the temperature of solar collector decrease.

Figures (5 and 6) show the equivalent the temperature of absorbed plate against time with and without dust, when the dust increased the temperature of absorbed plate decreased because exiguity absorbed solar radiation.

Figures (7, 8,9 and 10) Explain solar energy collected in flat plate collector and energy stored in the tank, these parameter change with local time. The energy decreased when the collector is containing in dust.

Figures (11 and 12) shows the Energy lost from the solar collector to the environment with dust. Figure (13) explain the change in efficiency through January and February month for solar collector.

## 6. Conclusion:

*The following conclusions may be concluded:*

- 1-This research indicates that maintenance mechanism could be applied successfully in Iraq to keep the solar system as much as reliable. The succeeding of the system depend on the performance of flat plate collector.
- 2-The efficiency of solar collector is decreasing with the dust increasing.
3. To keep on efficiency of solar collector must be use the proper maintenance mechanism and regularly periodic.

## References:

- [1]. DIMITRIO Panapakidis "Solar Water Heaters Basics" University of Strathclyde in Glasgow. 1997.
- [2]. S. T. Ahmed "Theoretical and Experimental Study of a forced Circulation Solar Water Heater "University of technology. Baghdad. 1978..
- [3]. Close,D.J. "The performance of solar water heaters with natural circulation,J.solar energy,Vol.6,pp.33-40,1962.
- [4]. Phillips, W.F. and Cook,R.D. "Natural Circulation of a flat-plate collector to hot liquid storage tank. ASME paper No. 1-53, pp. 1-5, 1975.
- [5]. Thomas. Mueller, Lars STAUDACHER ,"Design and Maintenance Guidelines", ALTENER, 2002.
- [6]. Nimmo, B., Pearce, J. and Clark. "An analytical and experimental study of pumped solar water heaters, Sun Mankind's future source of energy, pp. 907-911,1978.
- [7]. Gupta, C.L. and Garg, H.P "System design in solar water heaters with natural circulation ", solar energy , Vol.12, pp. 163-182, 1986.
- [8]. Antonis. M. Psarompas ,"Energy Performance Assessment ",University of Strathclyde, Glasgow 2001.
- [9]. Ari Rabl "Active solar collectors and their applications", Oxford University. 1985.
- [10]. D.B. CAMPEEL, *Maintenance and Operation of Active Solar Heating Systems*, July, 1990.
- [11]. MODULE 2.2 "Thermal analysis of the collector to estimate the collector Efficiency and heat removal factors",. Paper at Int. Thermal Analysis of Flat Plate Collectors. 1998.
- [12]. "Solar water heating system requirements", section 2: solar water heating, Energy Thrust of Oregon, Inc, V22, 2007.
- [13]. " Solar and efficient water heating " , A technology Roadmap, u.s. department of energy, 2005.

## EFFECT OF DIFFERENT METHODS BONDING BETWEEN ABSORBER PLATE AND TUBES FOR FLAT PLATE SOLAR COLLECTOR ON EFFICIENCY FACTOR

Ass.Prof Dr.Saad T. Hamidi  
Energy & Renewable Energies Technology Center  
University of Technology

### ABSTRACT

The present work involves a theoretical study to investigate the effect of deferens's methods joint between absorber plate and tubes for flat plate solar collector on efficiency factor. The solution procedure is performed three type flat plate collector used three types bonding absorber plate with riser tubes (Absorber plate–tube upper bond configuration, Absorber plate–tube side bond configuration and Absorber plate –tube lower bond configuration) with different distance between riser tubes. The analysis of mathematical model and solved using collector program. The results at the same defined dimensions and parameters for the solar collector shows that the maximum values of (efficiency factor is 0.963, efficiency removal factor is 0.945 and absorber temperature is 57.7 C) at Absorber–tube side bond configuration. From the results can be said that the Absorber – tube side bond configuration is better.

Keywords: Solar energy, Flat plate collector, Material, Absorber, Solar heating

### تأثير طريقة الربط المختلفة بين سطح الامتصاص والانابيب لمجمع شمسي مستوي السطح على معامل الكفاءة

#### الخلاصة

العمل الحالي ينطوي على دراسة نظرية لتقييم تأثير طرق الربط المختلفة بين صفحية الامتصاص والانابيب لمجمع شمسي مستوي السطح على عامل الكفاءة . تنفيذ اجراءات الحل من ثلاث انواع لمجمع مستوي السطح بأستد انواع لربط سطح الامتصاص مع الانابيب المسندة ( أنابيب مرتبطة الشكل على أنابيب مرتبطة الشكل اسفل سطح الامتصاص ) مع مسافات مختلفة بين الانابيب تحليل الموديل الرياضي الحل باستخدام برنامج كوليكر . لمجمع شمسي محدد الابعاد والعوامل أظهرت القيم العليا (معامل الكفاءة 0.963 0.945 57.7 درجة مئوية ) عند الانابيب المرتبطة الشكل بجانب سطح الامتصاص . من النتائج يمكن القول الانابيب المرتبطة جانبا مع س

## NOMENCLATURE

| Symbols     | Definition                                                     | Units             |
|-------------|----------------------------------------------------------------|-------------------|
| $A_c$       | Area of solar collector                                        | $m^2$             |
| $C_b$       | Welding thermal conductivity                                   | $W/m.^{\circ}C$   |
| $C_p$       | Specific heat of water                                         | $J/kg.^{\circ}C$  |
| $D$         | External diameter of tube                                      | $m$               |
| $D_i$       | Internal diameter of tube                                      | $m$               |
| $F_R$       | Removal factor of solar collector                              | -                 |
| $F'$        | Efficiency factor of solar collector                           | -                 |
| $G$         | Mass flow per unit area                                        | $kg/sec.m^2$      |
| $h_w$       | Wind heat transfer coefficient                                 | $W/m^2.^{\circ}C$ |
| $h$         | Heat transfer coefficient between fluid and internal tube wall | $W/m^2.^{\circ}C$ |
| $H$         | solar radiation incident on horizontal surface                 | $W/m^2$           |
| $H_T$       | solar radiation incident on the solar collector                | $W/m^2$           |
| $K$         | Thermal conductivity                                           | $W/m.^{\circ}C$   |
| $L$         | Riser length                                                   | $m$               |
| $\dot{m}$   | Mass flow rate of water                                        | $kg/sec$          |
| $\dot{m}_c$ | Mass flow rate of water passing through the solar collector    | $kg/sec$          |
| $\dot{m}_L$ | Load water flow rate                                           | $kg/sec$          |
| $m_s$       | Mass of water in the tank                                      | $kg/m^2$          |
| $N$         | Number of glass covers                                         | -                 |
| $n$         | Number of risers                                               | -                 |
| $Q_{Coll}$  | Solar energy collector                                         | $W$               |
| $Q_{Load}$  | Thermal energy drawn from the thermal tank                     | $W$               |
| $Q_{CLoss}$ | Energy lost from the solar collector to the environment        | $W$               |
| $Q_{Stor}$  | Energy stored in the tank                                      | $W$               |
| $R$         | Ratio of total solar radiation                                 | -                 |
| $S$         | Solar energy absorbed                                          | $W$               |
| $s$         | Inclination angle of the solar collector                       | degree            |
| $t$         | Time                                                           | hr                |
| $T_a$       | Air temperature                                                | $^{\circ}C$       |
| $T_{f,i}$   | Inlet water temperature tor solar collector                    | $^{\circ}C$       |
| $T_{f,o}$   | Outlet water temperature from solar collector                  | $^{\circ}C$       |
| $T_{f,m}$   | Mean external temperature from solar collector                 | $^{\circ}C$       |
| $T_{p,m}$   | absorber plate mean temperature                                | $^{\circ}C$       |
| $T_p$       | Temperature of absorbed plate                                  | $^{\circ}C$       |
| $T_s$       | Temperature of water tank                                      | $^{\circ}C$       |
| $T_{s1}$    | Temperature of water tank at the beginning of hour             | $^{\circ}C$       |
| $T_{s2}$    | Temperature of water tank at the end of hour                   | $^{\circ}C$       |

## 1. INTRODUCTION

Today, solar heating is becoming more important than ever before. Natural gas and oil which are burned to heat our homes and water are limited. As reserves of gas and oil shrink, these fuels become more expensive. If more people began using solar heating systems, fossil fuels such as oil and gas would become less expensive and last longer. Burning natural gas and oil in our heating systems also causes air pollution. So if more people used solar energy to heat the air and water in their homes, our environment would be cleaner. Solar energy collectors are special kind of heat exchangers that transform solar radiation energy to internal energy of the transport medium. The major component of any solar system is the solar collector.. Kalogirou [1] developed six ANN models for the prediction of standard performance collector equations coefficients, wind and no-wind conditions, the incident angle modifier coefficients at longitudinal and transverse directions, the collector time constant, the collector stagnation temperature and the collector capacity were considered. The study based on a steady-state operation conditions. The thermal performance of flat-plate solar collector is strongly related to the flow distribution through the absorber tubes, Fan et al. [2] investigated experimentally and theoretically the flow and temperature distribution in a solar collector panel with an absorber consisting of horizontally inclined fins. Numerically, the flow and heat transfer in the collector panel were studied by the means of CFD calculations. Experimentally, the flow distribution through the absorber evaluated by means of temperature measurements on the backside of the absorber tubes. Their results showed a good agreement between the CFD results and the experimental data at high flow rates. However for small flow rates, large differences appeared between the computed and measured temperatures. This disagreement is most likely due to the oversimplification of the solar collector model. Augustus and Kumar [3] developed mathematical model to predict the thermal performance of an unglazed transpired collector, also known as perforated collector- a new development in the solar collector technology. But there is a host of literature on glazed solar collectors. Sopian et al. [4] conducted an experimental study on the thermal performance of a non-metallic unglazed solar water heater integrated with a storage system. Gorla [5] performed an analysis based upon the two-dimensional finite element method to characterize the performance of solar collectors. Selmi et al. [6] performed a CFD simulation of flat plate solar energy collector with water flow. The CFD model was validated with experimental results. Janjai et al. [7] developed a mathematical model for simulating the performance of a large area plastic solar Collector. Lecoecue and Lalot [8] applied neural network technique to predict the thermal performance of a solar flat plate collector.

The objective of the present work is the influence of the different bonding absorber plate with riser tubes for flat plate solar collector and investigation these affect on efficiency factor, efficiency removal factor ,absorber temperature and mean water temperature .Used three types bonding absorber plate with riser tubes (upper, side and lower bond) with different distance between riser tubes . We analyzed and calculated the mathematical model using Kolektor program to solved the model under defined dimensions and parameters for flat-plate solar collector.

## 2. THEORETICAL MODELING

The thermal performance of the solar collector water heating system can be described by the energy balances on the collector absorber plate and the water in the collector flow tubes. The following assumptions are made in order to simplify the thermal analysis of the system in developing the steady state model [9]

- collector performance is under steady state conditions
- flow tubes are parallel to each other and temperature gradients around tubes are negligible
- the temperature drop between the top and bottom of the collector absorber plate and glazing is negligible
- heat flow is one dimensional through the covers as well as through the back insulation
- thermo-physical properties of the materials are independent of temperature
- heat loss from the front and back of the absorber are to the same ambient temperature

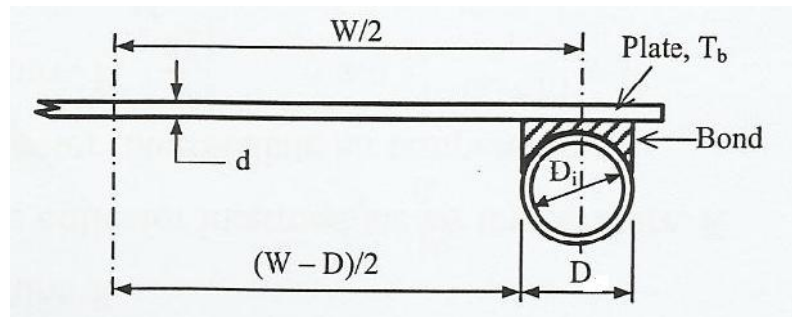


**Figure 1.** Absorber plate and tube

Consider the absorber plate with tube configuration as shown in **Figure 1**. The distance between the tubes is  $W$ , the tube diameter is  $D$ , and the absorber plate thickness is  $d$ . Base on the above assumptions, the plate above the bond is at some local based temperature,  $T_b$ . The region between the centerline separating the tubes and the tube base can then be considered as a classical fin problem. The fin of length  $(W-D)/2$  is shown in **Figure 2**.

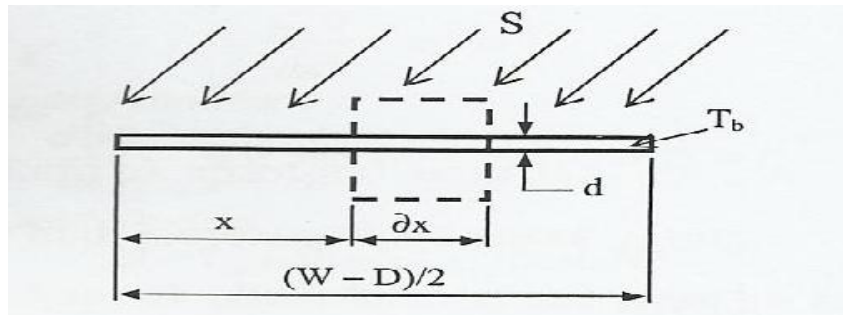


**Figure 2.** Fin element

and an elemental region of width  $dx$  for a unit length in the flow direction is shown in **Figure 3**.  $S$  represents  $\tau_{\text{gl}} I$ , the absorbed solar energy per unit area ( $\text{W/m}^2$ ).

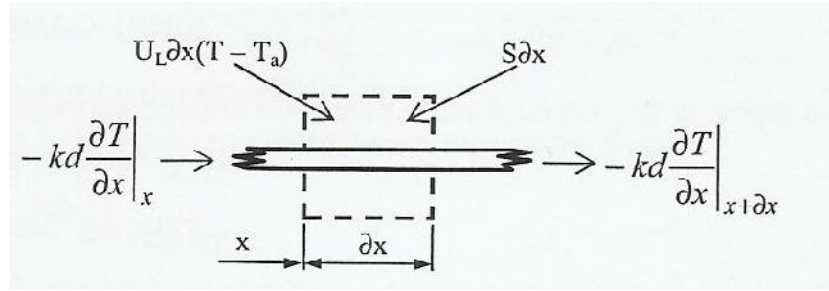


**Figure 3.** Energy balance on fin element

An energy balance on this element yield:

$$Sdx + U_L dx(T_a - T) + (-kd \frac{dT}{dx})|_x - (-kd \frac{dT}{dx})|_{x+dx} = 0 \quad (1)$$

Dividing through by dx and finding the limit as dx approaches zero yields:

$$\frac{d^2 T}{dx^2} = \frac{U_L}{kd} \left( (T - T_a) - \frac{S}{U_L} \right) \quad (2)$$

The two boundary conditions necessary for this second order differential equation are symmetry at the centerline and known root temperatures [9]:

$$\frac{dT}{dx} \Big|_{x=0} = 0 \text{ and } T \Big|_{x=(W-D)/2} = T_b \quad (3)$$

If we define

$$m^2 = \frac{U_L}{kd} \quad (4)$$

and

$$\Theta = T - T_a - \frac{S}{U_L} \quad (5)$$

Eq. (2) becomes

$$\frac{d^2 \Theta}{dx^2} - m^2 = 0 \quad (6)$$

which has the boundary conditions

$$\frac{d\Theta}{dx} \Big|_{x=0} = 0 \text{ and } \Theta \Big|_{x=(W-D)/2} = T_b - T_a - \frac{S}{U_L} \quad (7)$$

The general solution is then

$$\Theta = C_1 \sinh mx + C_2 \cosh mx \quad (8)$$

The first boundary yield  $C_1=0$  ,and the second boundary condition yields :

$$\Theta = T_b - T_a - \frac{S}{U_L} = C_2 \cosh mx \quad \text{or}$$

$$C_2 = \frac{T_b - T_a - \frac{S}{U_L}}{\cosh m(W - D)/2}$$

The constant C1 and C2 can be found by substituting the boundary conditions Eq. (7) into the general solution, Eq. (8). The results are:

$$\frac{T - T_a - \frac{S}{U_L}}{T_b - T_a - \frac{S}{U_L}} = \frac{\cosh mx}{\cosh m(W - D)/2} \quad (9)$$

This equation gives the temperature distribution in the x-direction at any give y.

The energy conducted to the region of the tube per unit of length in the flow direction can be found by evaluating Fourier's law at the fin base [9].

$$q_{fb} = -kd \left. \frac{dT}{dx} \right|_{x=(w-D)/2}$$

$$q_{fb} = \frac{kdm}{U_L} [S - U_L(T_b - T_a)] \tanh m(W - D)/2 \quad (10)$$

Eq. (10) account for the energy collected on only one side of a tube; therefore, for both sides and substitution of Eq. (4), the energy collection is

$$q_{fb} = (W - D)[S - U_L(T_b - T_a)] \frac{\tanh m(W - D)/2}{m(W - D)/2} \quad (11)$$

It is convenient to use the concept of a fin efficiency to rewrite Eq. (11) as

$$q_{fb} = (W - D) F [S - U_L(T_b - T_a)] \quad (12)$$

$$F = \frac{\tanh m(W - D)/2}{m(W - D)/2} \quad (13)$$

The function 'F' is the standard fin efficiency for straight fins with rectangular profile. The useful gain of the collector also includes the energy collected above the tube region. The energy gain for the tube region is

$$q_t = D[S - U_L(T_b - T_a)] \quad (14)$$

Accordingly, the useful gain for the collector per unit of length in the flow direction becomes:

$$q_u = q_{fb} + q_t$$

$$q_u = [(W - D)F + D][S - U_L(T_b - T_a)] \quad (15)$$

The useful gain from Eq. (15) must be transferred to the fluid. The resistance to heat flow to the fluid results from the bond and the fluid to tube resistance [9]. The useful gain can be expressed in terms of these two resistances as:

$$q_u = \frac{T_b - T_f}{\frac{1}{h_{fi}fD_i} + \frac{1}{C_b}} \quad (16)$$

where  $D_i$  is the inside tube diameter and  $h_{fi}$  is the heat transfer coefficient between the fluid and the tube wall. The bond conductance,  $C_b$  can be expressed as [9]:

$$C_b = \frac{k_b b}{\langle} \quad (17)$$

The bond conductance can be very important in accurately describing the collector performance and generally, it is necessary to have good metal-metal contact so that the bond conductance is greater than 30 W/mK and preferably the tube should be welded to the fin.  $T_b$  can be eliminated from consideration in order to obtain an expression for the useful gain in terms of known dimensions, physical parameters, and the local fluid temperature. Solving Eq. (16) for  $T_b$ , substituting it into Eq. (15), and solving the result for the useful gain per unit length, we obtain:

$$q_u = WF'[S - U_L(T_{fi} - T_a)] \quad (18)$$

where  $F'$  is the collector efficiency factor and is given by

Different absorber configurations result in appropriate equations.

1. Upper bond of absorber to riser pipes the efficiency factor is given as

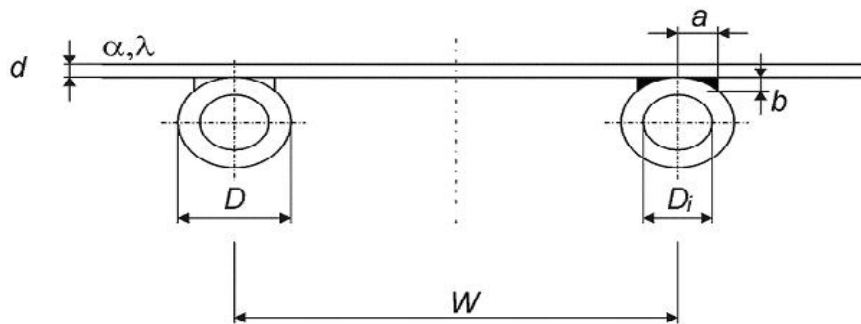


**Figure 4.** Upper bond absorber plate with riser tubes

$$F' = \frac{\frac{1}{U_L}}{W \left[ \frac{1}{U_L [D + (W - D)F]} + \frac{1}{C_b} + \frac{1}{f D_i h_{fi}} \right]} \quad (19)$$

2. Middle bond of absorber to riser pipes the efficiency factor is given as

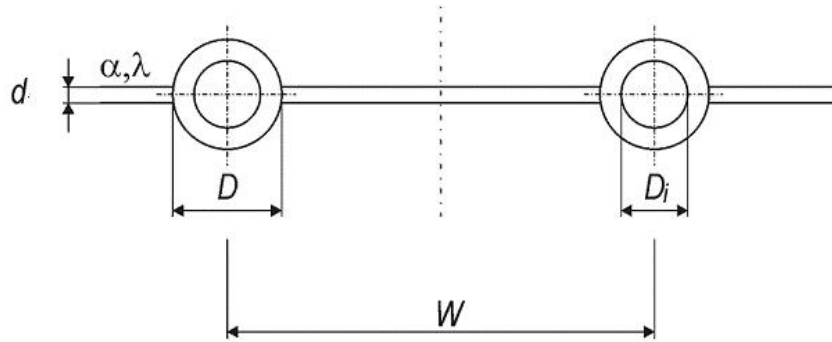


**Figure 5.** Side bond absorber plate with riser tubes

$$F' = \frac{\frac{1}{U_L}}{W \left[ \frac{1}{U_L [D + (W - D)F]} + \frac{1}{f D_i h_{fi}} \right]} \quad (20)$$

3. Lower bond of absorber to riser pipes the efficiency factor is given as

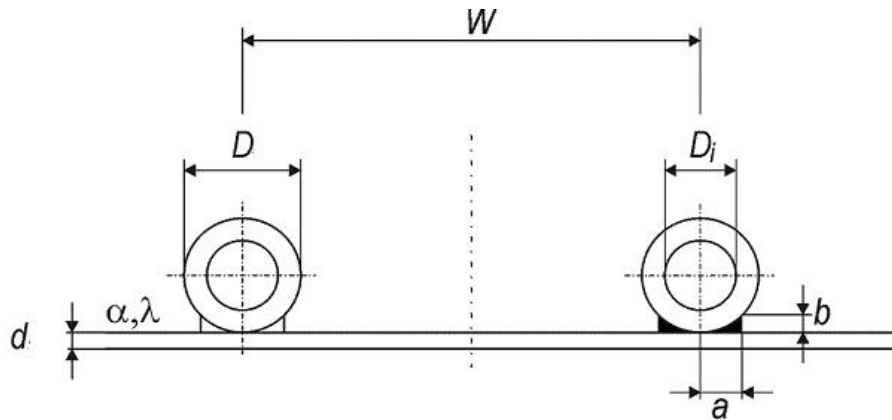


**Figure 6.** Lower bond absorber plate with riser tubes

$$F' = \frac{1}{\frac{WU_L}{fD_i h_{fi}} + \frac{1}{\frac{D}{W} + \frac{1}{\frac{WU_L}{C_b} + \frac{W}{(W-D)F}}}} \quad (21)$$

If collector has a length 'L' in the flow direction and the number of tubes in the collector is 'n' then the heat gained by the collector ( $Q_C$ ) is found by multiplying Eq.(18) by Ln:

$$Q_C = WLn F' [S - U_L (T_{fi} - T_a)] \quad (22)$$

or

$$Q_C = A_C F' [S - U_L (T_{fi} - T_a)]$$

where,  $A_C = WLn$ , the total collector area (m<sup>2</sup>).

The useful energy gained by fluid flowing in the collector tubes ( $Q_U$ ) is obtained by multiplying Eq. (20) by the collector flow factor ( $F''$ ) [10]:

$$Q_U = A_C F' F'' [S - U_L (T_{fi} - T_a)] \quad (23)$$

The collector heat removal factor ( $F_R$ ) is the product of collector efficiency factor ( $F'$ ) and collector flow factor ( $F_R$ ), therefore, Eq. (21) can be written as:

$$Q_U = A_C F_R [S - U_L (T_{fi} - T_a)] \quad (24)$$

The overall heat loss coefficient is a complicated function of the collector construction and its operating conditions [11,12] , given by the following expression

$$U_L = U_t + U_b + U_e \quad (25)$$

To calculate the coefficient of thermal losses from the lower surface and sides of solar collector, as the sides of solar collector isolated the same material,  $U_b$  ,  $U_e$  becomes as:

$$U_b = \frac{K}{L} \quad (26)$$

$$U_t = \left( \frac{N}{\left( (344/T_p) [(T_p - T_a)/(N + f)]^{0.31} + \frac{1}{h_w} \right)} + \frac{\dagger (T_p + T_a)(T_p^2 + T_a^2)}{[v_p + 0.0425N(1 - v_p)]^{-1} + [(2N + f - 1)/v_g] - N} \right)^{-1} \quad (27)$$

$$f = (1.0 - 0.04h_w + 5.0 \times 10^{-4} h_w^2)(1 + 0.058N)$$

$$h_w = 5.7 + 3.8V$$

The specification of the flat plate collector is summarized in **Table (1)**.

|                                                 |             |
|-------------------------------------------------|-------------|
| Fluid temperature                               | 25 C        |
| Solar irradiation                               | 800 Watt/m2 |
| Ambient temperature                             | 20 C        |
| Relative humidity                               | 50%         |
| Wind speed                                      | 2 m/s       |
| Collector slope                                 | 45 degree   |
| Gross height of collector                       | 2 m         |
| Gross width of collector                        | 1 m         |
| Gross area of collector                         | 2 m         |
| Absorber glazing gap thickness                  | 20 mm       |
| Glass thickness                                 | 4 mm        |
| Normal solar transmittances of glass            | 0.92        |
| Normal solar reflectance of glass               | 0.06        |
| External and internal surface emissive of glass | 0.85        |
| Thermal conductivity                            | 0.8 W/mK    |
| Thermal conductivity of cooper tube material    | 390 W/mK    |
| Length of riser tube                            | 2 m         |
| Number of riser tube                            | 5-12        |
| Distance between riser tubes                    | 83-200 mm   |
| Tube external diameter                          | 10 mm       |
| Tube internal diameter                          | 8 mm        |
| Average bond width                              | 3 mm        |
| Average bond thickness                          | 3 mm        |
| Bond thermal conductivity                       | 300 W/mK    |
| Bond thermal conductance                        | 300 W.mK    |
| Collector mass flow rate                        | 0.04 Kg/s   |

### 3. RESULTS AND DISSCUSION

- **Figure 7.** Show influence of distance between riser tubes (80-200 mm) on efficiency factor with different bond absorber plate with riser tubes (upper ,middle and lower bonds) .Its notes the values for efficiency factor at upper bond absorber plate with riser tubes between (0.847-0.962), middle bond (0.848-0.963) and lower bond (0.847-0.962), also the results indication that the efficiency factor decreasing with increasing distance between riser tubs.

- **Figure 8.** Show influence of distance between riser tubes (80-200 mm) on efficiency heat removal factor with different bond absorber plate with riser tubes (upper ,middle and lower bonds) .Its notes the values for efficiency factor at upper bond absorber plate with riser tubes

between (0.820-0.938), middle bond (0.833-0.945) and lower bond (0.831-0.944), also the results indication that the efficiency heat removal factor decreasing with increasing distance between riser tubes.

- **Figure 9.** Show influence of distance between riser tubes (80-200 mm) on absorber temperature with different bond absorber plate with riser tubes (upper ,middle and lower bonds) .Its notes the values for absorber temperature at upper bond absorber plate with riser tubes between (37.4-57.69 C), middle bond (36.15-56.65 C) and lower bond (36.28-55.89 C), also the results indication that the absorber temperature increasing with increasing distance between riser tubes.

#### 4. CONCLUSION

- From the results can be say that the side absorber plate with riser tubes is better than upper and lower bond for efficiency factor , efficiency removal factor , and the absorber temperature.

#### REFERENCES

- [1] Kalogirou S., "Prediction of flat-plate collector performance parameters using artificial neural networks", Solar Energy, 80, pp.248-259, 2006
- [2] Fan J., Shah L., and Furbo S., " Flow distribution in a solar collector panel with horizontally inclined absorber strips", Solar Energy, 81, pp.1501-1511, 2007
- [3] Augustus M. and Kumar S., " Mathematical modeling and thermal performance analysis of unglazed transpired solar collectors", Solar Energy, 81, pp.62-75, 2007
- [4] K. Sopian, M. Syahri, S. Abdullah, M.Y. Othman, B. Yatim," Performance of a non-metallic unglazed solar water heater with integrated storage system", Renewable Energy,vol. 29, pp.1421–1430, 2004
- [5] Gorla, R.S.R, "Finite element analysis of a flat plate solar collector", Finite Elements in Analysis and Design, vol.24, pp. 283-290, 1997
- [6] Selmi, M., Al-Khawaja, M.J., and Marafia, A., "Validation of CFD simulation for flat plate solar energy collector", Renewable Energy, vol.33, pp. 383-387, 2008
- [7] S. Janjai, A. Esper, W. Muhlbauer, "Modelling the performance of a large area plastic solar collector", Renewable energy, vol. 21, pp. 363-376, 2000
- [8] S. Lecoeuche and T, S. Lalot, "Prediction of the daily performance of solar collectors", International Communications in Heat and Mass Transfer,vol.32, pp. 603–611, 2005
- [9] Bukola O.Bolaji," Mathematical modeling and experimental investigation of collector efficiency of a thermosyphonic solar water heating system", UEM .pp. 55-63, 2011
- [10]Mullick SC, Samdarshi SK.,"An improved technique for computing the top heat loss factor of flat-plate collector with a single glazing', ASME J Sol Energy Eng..pp. 262-270, 1988
- [11] Malhotra A, Garg HP, Palit A.,' Heat loss calculation of flat-plate solar collectors", J Thermal Eng 2, pp.59-62, 1981.
- [12] P. K. C. Pillai and R. C. Agarwal," An Analytical Approach for Opimising a set of and values for Solar Energy Applications", Energy Conv. and Mgmt.20 , pp. 205- 212 , 2005

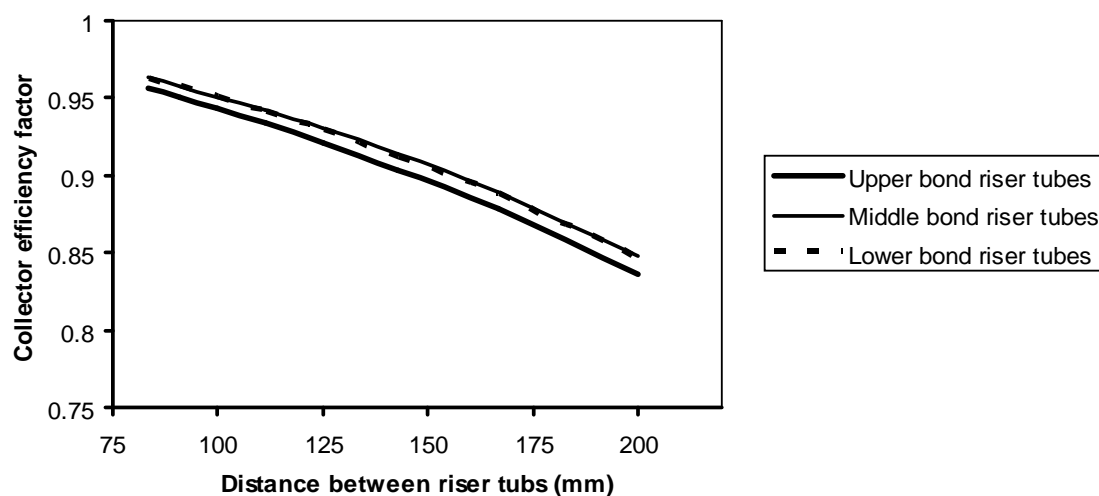


**Figure 7.** Relation between distance riser tubes and collector efficiency factor

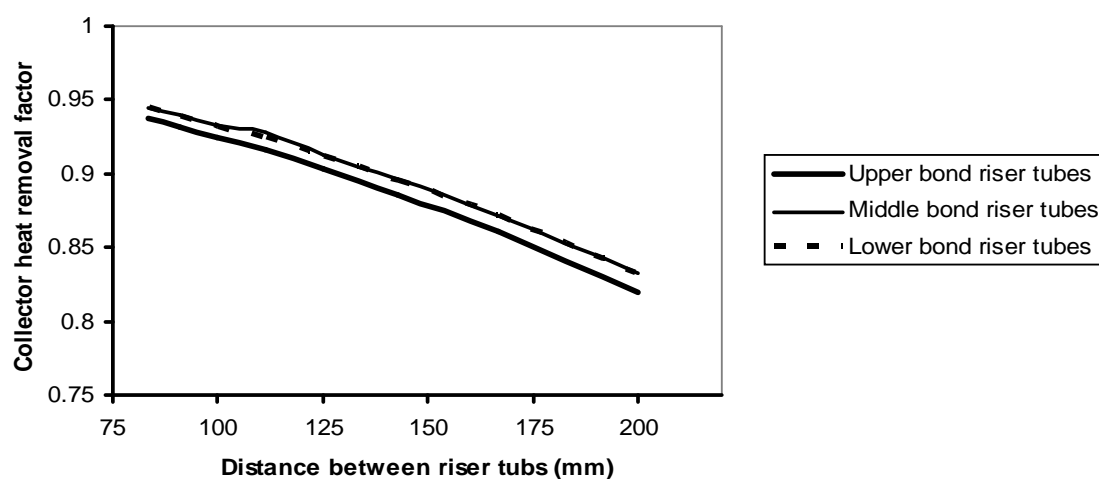


**Figure 8.** Relation between distance riser tubes and heat removal factor

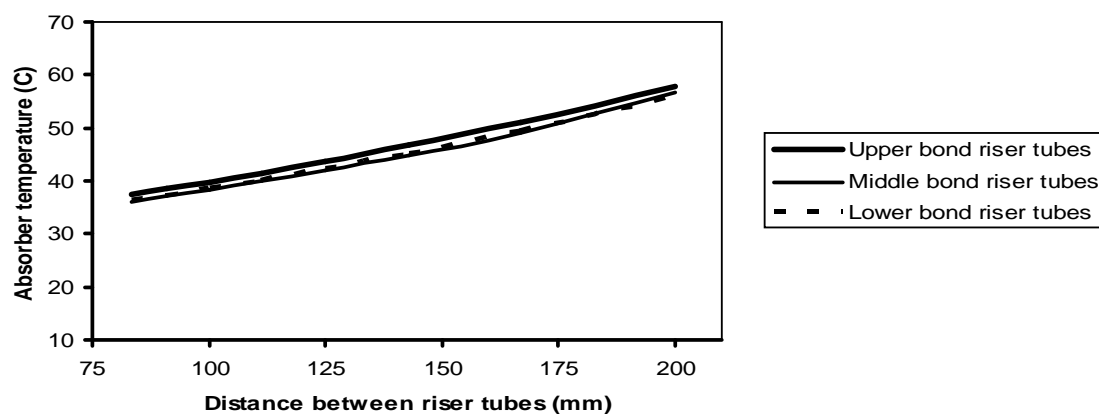


**Figure 9.** Relation between distance riser tubes and absorber temperature

## Numerical Assessment of Thermal Energy and Flow of Nanofluids in a Horizontal and an Inclined Tube Filled with a Porous Medium

**Dr. Khalid Faisal Sultan**

**Lecture**

**Electromechanical. Eng. Dept**

**University of Technology**

**E- mail: [ksultan61@yahoo.com](mailto:ksultan61@yahoo.com)**

### **Abstract**

Porous media have considerable importance in improvement of thermal energy and storage. This research include theoretical study of mixed convection heat transfer of flow through a horizontal and an inclined tube filled with a porous medium by using nanofluids. The theoretical study includes the derivation of governing equations for the flow and heat transfer through porous media employing the Darcy flow model under condition of applying uniform heat flux on the tube. One type of filling material were used as porous medium glass beads ( $d_p=8\text{mm}$ ). The energy equation was first solved using (ADI) method, and then the momentum equations and continuity equation were combined as the pressure correction formula and solved by the simple algorithm. The numerical results represented by a stream function contours, isotherms for different values of Rayleigh number ( $Ra=10^3, 10^5, 10^6$ ), volume fraction ( $\phi=1, 2.5$  and  $5\%$  vol), type of nanofluid, tube angles of inclinations ( $\theta=30^\circ, 60^\circ$  and  $90^\circ$ ) and peclet number ( $Pe=10$ ) as well as the change of average Nussult number with Rayleigh number, volume fraction, type of the nanofluid. The numerical results show that the effect of natural convection appears at the region from the start of the tube. Results reveal also that the nanoparticles concentration does not have significant effect on the secondary flow, the distribution and development of the velocities of tangential and radial component of the secondary flow ,on the peripherally average skin friction coefficient and on the porous media. As well as the average of the heat transfer increasing significantly by increases of the particle volume fraction and Rayleigh number. Also, the type of nanofluid is a key factor for heat transfer enhancement where the high values are obtained when using Ag, Cu, and  $\text{TiO}_2$  nanoparticles respectively (55%, 37%, 22%). Moreover Nussult ratio factor are used to indicated the flow field and the heat transfer inside the tube.

**Key wards: Nanofluid, NUR factor, Porous medium, and nanoparticles.**

## التقييم العددي في الطاقة الحرارية والجريان للموائع النانوية في انبواب أفقي ومائل مملوء بوسط مسامي

د. خالد فيصل سلطان

مدرس

قسم الهندسة الكهروميكانيكية  
الجامعة التكنولوجية

### الخلاصة

الوسط المسامي ذو أهمية في تحسين انتقال الحرارة وتخزينها تم في هذا البحث إجراء دراسة نظرية على انتقال الحرارة بالحمل المختلط والجريان من خلال نانوية الحجم . اشتقاق المعادلات الحاكمة للجريان وانتقال الحرارة من خلال الوسط المسامي جريان وتحت ظرف فيض حراري منتظم . تم استخدام نوع واحد من الوسط المسامي وهو خرز زجاجية بقطر (8mm). معادلة الطاقة أولا باستخدام طريقة (ADI) ومن ثم ربط معادلات الزخم بمعادلة الاستمرارية لتكوين معادلة تصحيح الضغط والتي تم حلها باستخدام خوارزمية (SIMPLE). ومثلت نتائج هذه الحلول لمختلف زوايا ميلان الانبواب وقيم عدد راييلي ونسب الحجم ونوع المائع الفائق الدقة بمخططات دالة الجريان ودرجة الحرارة وتغير قيم عدد نسلت المعدل بتغير قيم عدد رالي ( $Ra=10^3, 10^5, 10^6$ ) ( $=1, 2.5 \text{ and } 5 \text{ vol}\%$ ) الفائق الدقة وقطر الجزيئية الفائقة الدقة . بينت نتائج الحل العددي أن الجريان الثانوي الناتج عن الحمل الحر له تأثير هام على عملية انتقال الحرارة وان أعظم تأثير له يكون عند الموضع الأفقي لأنبوب ويتناقص تأثيره بزيادة ميلان . بينت ان تركيز الجزيئات ليس له تأثير هام على الجريان الثانوي توزيع ونمو السرعة القطرية والمماسية وضحت أن معدل انتقال الحرارة يزداد طبقا إلى زيادة نسب الحجم ورقم راييلي على دقات نانوية الحجم هو المفتاح الرئيسي للتحسين انتقال الحرارة حيث كانت أعلى قيم لذلك في حالة  $Ti_2O, Cu, Ag$  (22%, 37%, 55%) على الترتيب  $NuR$  لإظهار مجال الجريان وانتقال الحرارة داخل الانبوب.

### NOMENCLATURE

| Symbol         | Name                                            | Unit        |
|----------------|-------------------------------------------------|-------------|
| r              | radius of tube                                  | m           |
| Pe             | Peclet number                                   | —           |
| $Cp_{nf}$      | Specific heat of nanofluid at constant pressure | kJ/kg.k     |
| g              | Gravity acceleration                            | $m/s^2$     |
| G              | Dimensionless gravity acceleration              | —           |
| h              | Heat transfer coefficient                       | $W/m^2.k$   |
| p              | Pressure                                        | $N/m^2$     |
| $R, \theta, Z$ | Dimensionless cylindrical coordinates           | —           |
| Nu             | Nusselt number                                  | —           |
| S              | Relaxation factor                               | —           |
| t              | Temperature                                     | $^{\circ}C$ |
| $U_r$          | Radial velocity component (r)                   | m/s         |
| $V_t$          | Tangential velocity component (w)               | m/s         |
| W              | Axial velocity component (z)                    | m/s         |
| $k_{nf}$       | Thermal conductivity of the nanofluid           | W/m.k       |
| P              | Dimensionless pressures                         | —           |

|          |                                |    |
|----------|--------------------------------|----|
| $P_{mf}$ | Prandtl number for Nano fluid  | —  |
| $P_z$    | Dimensionless pressure drop    | —  |
| $d_p$    | Particle diameter              | nm |
| ADI      | Alternating direction implicit | —  |

### Creak Symbols

|             |                                                |          |
|-------------|------------------------------------------------|----------|
|             | Angle of inclination of tube                   | degree   |
| $r_{nf}$    | Thermal diffusivity of the nanoluid            | $m^2/s$  |
| $S_{nf}$    | Thermal Expansion Coefficient of the nanofluid | 1/K      |
| $\mu_{nf}$  | Dynamic viscosity of the nanofluid             | Kg/m.s   |
| $\nu_{nf}$  | Kinematic viscosity of the nanofluid           | $m^2/s$  |
| $\rho_{nf}$ | Density of the nanofluid                       | $kg/m^3$ |
|             | Vorticity                                      | 1/s      |
|             | Stream function                                | $m^2/s$  |
|             | Volume fraction                                | Vol%     |

### Superscript

|    |                                                           |
|----|-----------------------------------------------------------|
| mt | Number of radial points in the numerical mesh network     |
| nt | Number of tangential points in the numerical mesh network |
| s  | Solid                                                     |
| w  | Wall                                                      |

## 1.Introduction

Nanofluid, a name conceived by Choi [1] in Argonne National laboratory, are fluids consisting of solid nanoparticles with size less than 100nm suspended with solid volume fraction typically less than 4%. Nanofluid can enhance heat transfer performance compared to pure liquids. Nanofluids can be used to improve thermal management system in many engineering application such as transportation, micromechanics and instrument, HVAC system and cooling devices. Recently, many investigators studied nanofluid convective heat transfer in different geometry both numerically and experimentally (Maiga et al. [2]; Heris et al. [3]; Duangthongsuk and Wongwises [4]; Santra et al.[5]; Nguyen et al. [6]. For numerical simulation, two approaches have been adopted in the literature to investigate the heat transfer characteristics of nanofluids, single phase model and two phase model. Another approach is to adopt the Boltzmann theory Wang and Mujumdar [7]. In single phase model, a uniform volume fraction distribution is assumed for nanofluids. In other words, the viscosity and thermal conductivity of nanofluids are formulated by volume fraction and nanoparticle size then continuity, momentum and energy equations are solved for nanofluids. In two phase model, the volume fraction distribution equation is added to other conservation equations. Many investors used single and two phase models for investigating the flow and heat transfer of nanofluids Behzadmehr et al. [8]; Lee and Mudawar [9]; Mirmasoumi and Behzadmehr [10]. Buongiorno [11] introduced seven slip mechanisms between nanoparticles and the base fluid. He showed that the Brownian motion (movement of nanoparticles from high concentration site) and thermophoresis (movement of nanoparticles from the high temperature site to the low temperature site) have effected significantly in the laminar forced convection of nanofluids. Based on this finding, he developed non-homogeneous two – component equations in nanofluids. Heyhat and Kowsary [12] used Buongiorno's equations for investigating the effect of particles migration on flowand convective heat transfer of

nanofluids flowing through the circular pipe. Results show that the non-uniform distribution leads to a higher heat transfer coefficient while the wall shear stress is decreased. Therefore, the particle migration can play an important role in improvement of the heat transfer coefficient in convective heat transfer in nanofluids.

In recent papers, written by Kuznetsov and Nield [13 – 15], the Buongiorno's model was applied to the Horton–Rogres – Lapwood problem (the onset of convection in a horizontal layer of a porous medium uniformly heated from below). Both Brownian motion and thermophoresis give rise to cross-diffusion terms that are in some way analogous to the familiar Sort and Dufour cross-diffusion terms that arise with a binary fluid. Nield and Kuznetsov [16] introduced an analytical treatment of double-diffusive natural convection boundary layer flow in a porous medium saturated by nanofluid. They used the Buongiorno's equation for modeling the nanofluid and Darcy model for porous medium. The result showed a decrease in the reduced Nusselt number associated with an increase in the thickness of the thermal boundary layer an increase in Brownian motion parameter, buoyancy ratio, thermophoresis parameter, modified Dufour parameter, and a decrease in regular buoyancy ratio. The analytical treatment of double-diffusive natural convection boundary layer flow of a nanofluid past a vertical plate was also studied by Kuznetsov and Nield [17]. Investigation of mixed convective heat transfer of nanofluids in an horizontal and an inclined a porous tube has not been considered completely in the literature and this challenge is generally considered to be an open research topic that may require more study.

The aim of this study is to investigate the effects of nanoparticle concentration on thermal energy and flow of nanofluids in a horizontal and an inclined tube filled with a Porous medium.

## 2. Problem Description and Governing Equation

The theoretical analysis current is derivation of governing equations the flow of nanofluids in circular tube section and filled with porous media (consist of glass beads ( $d_p=8$  mm)). This analysis adopted Darcy model to find a governing equations [18], which is assumed the homogeneous Porous media and symmetric (Isotropic), any that the properties of the porous media such as porosity and thermal conductivity coefficient does not depend on the direction and solid material in thermal equilibrium with nanofluid passing through at any point within the porous media and Reynolds number localized calculated on the basis of mean velocity through the Porous media and particle diameter does not exceed (10).

Figure (1) as shows the nanofluid enter the tube with uniform velocity ( $u_i$ ) and temperature ( $t_i$ ) with assuming the components velocity in the direction ( $r, w, z$ ) is ( $u_r, u_t, u_z$ ) respectively Based on the assumptions above, the equations of conservation of mass, momentum and energy flow in hydro dynamic and fully developing cylinder coordinates can be written as follows.

### Continuity Equation

$$\frac{1}{r} \frac{\partial}{\partial r} (r u_r) + \frac{1}{r} \frac{\partial}{\partial w} (u_t) + \frac{\partial}{\partial z} = 0 \quad (1)$$

## Momentum Equation

According to the Darcy law done neglected non – Darcy effects which including the inertia force effect, boundary effect, channeling effect ,thermal diffusion and assumed an inclined angle of the tube ( $\alpha$ ) from horizontal axis. according to the assumptions mentioned the velocities components in cylindrical coordinate as follows:

$$u_r = \frac{-k}{\mu} \left( \frac{\partial P}{\partial r} - g \cos w \cos r \right) \quad (2)$$

$$u_t = \frac{-k}{\mu} \left( \frac{\partial P}{\partial w} + g \cos w \sin r \right) \quad (3)$$

$$= \frac{-k}{\mu} \left( \frac{\partial P}{\partial z} \pm g \sin w \right) \quad (4)$$

## Energy Equation

$$u_r \frac{\partial t}{\partial r} + \frac{u_t}{r} \frac{\partial t}{\partial w} + \frac{\partial t}{\partial z} = e \left[ \frac{1}{r} \frac{\partial}{\partial r} \left( r \frac{\partial t}{\partial r} \right) + \frac{1}{r^2} \frac{\partial^2 t}{\partial w^2} + \frac{\partial^2 t}{\partial z^2} \right] \quad (5)$$

The properties of nanofluid (fluid containing suspended nanoparticles) are defined as follows:

Effective thermal conductivity [19]

$$\frac{k_{nf}}{k_f} = \left[ \frac{k_s + (n-1)k_f - (n-1)(k_f - k_s)\Phi}{k_s + (n-1)k_f + (k_f - k_s)\Phi} \right] \quad (6)$$

Where n is a shape factor and equal to 3 for spherical nano particles.

Thermal diffusivity [20].

$$r_{nf} = \frac{k_{nf}}{(1-\Phi)(\dots Cp)_f + \Phi(\dots Cp)_s} \quad (7)$$

Thermal expansion coefficient [21].

$$S_{nf} = \left[ \frac{1}{1 + \frac{(1-\Phi)\dots_f}{\Phi\dots_s}} \frac{S_s}{S_f} + \frac{1}{1 + \frac{\Phi\dots_s}{(1-\Phi)\dots_f}} \right] \quad (8)$$

Specific heat [21 ].

$$Cp_{nf} = \frac{(1 - \Phi)(...Cp)_f + \Phi(...Cp)_s}{(1 - \Phi)..._f + \Phi..._s} \quad (9)$$

Effective viscosity [22].

$$\sim_{nf} = [123\Phi^2 + 7.3\Phi + 1] \quad (10)$$

### 3. Boundary Conditions

The B.C of the model is derived based on the Darcy model . It is assumed that the boundaries slip with a symmetry about the vertical axis of the tube.

$$\frac{\partial T}{\partial R}(1, w, Z) = 0.5, \quad \frac{\partial T}{\partial w}(R, 0, Z) = 0, \quad \frac{\partial T}{\partial w}(R, f, Z) = 0$$

$$\text{Inlet } (Z = 0), \quad T(R, w, 0) = 0$$

$$\frac{\partial \Xi}{\partial R}(R, 0, Z) = 0 \quad \Xi(R, f, Z) = 0$$

$$\frac{\partial \Xi}{\partial R}(R, f, Z) = 0 \quad \Xi(R, 0, Z) = 0$$

### 4. Grid Testing and Code Validation

Basically, the flow region associated with the polar coordinates (R, w) is divided into a grid network which contains the following dimensions  $\Delta R \times \Delta w$  for one division. Figure (2) shows nodes divided on a regular basis in the tangential direction w while irregularly divided radial direction (R) where the nodes focused and be close more near to the surface of the tube. These nodes focused at the wall using the zoom factor ( ) and where each partition in the radial direction (R) from the center of the tube can be calculated as follows:

$$\Delta R_{i+1} = u \Delta R_i \quad (11)$$

Selected value ( = 0.95) [23], which is generally used to give the desired focus of the nodes near the wall. The number of divisions and nodal points, in this case, will be (mt×nt) and [(mt+1) × (nt+1)] , respectively, where mt refers to the number of divisions in R direction which changes from (m=1) to (m=mt) and equals to (1 /  $\Delta R$ ) , while (nt) refers to the number of divisions in w – direction which changes from (n=1) to (n= nt) and equals to (f /  $\Delta w$ ) for one half of the tube because of the flow symmetry about the vertical line of the tube . Figure (3) demonstrates the influence of number of grid points for attest case of fluid confined within the present configuration at  $Ra=10^4$  and =0, it is clear that, the grid system of (40\*55) is fine enough to obtain accurate results and guarantees. The present code was test for grid independence by calculating the average Nusselt number around the perimeter of the tube Therefore, adopted a grid system of (40\*55).

## 5. Numerical Implementation

The governing equation in the cylindrical coordinates (equations 1, 2, 3,4and 5) as well as boundary conditions were discretized by finite difference method. In this study the finite difference equation were derived by using central difference approximation for the partial derivatives except the convective terms for which upwind difference formula was employed. Derivative at the boundary were approximated by three point forward and backward difference. The alternating direction implicit (ADI) method was employed for the solution of energy fields, while relaxation method was employed for stream function calculation. A time increment  $\Delta t = 10^{-5}$  has been used for  $Ra=10^3, 10^5$  and  $10^6$ . In order to evaluate how the presence of the nanofluids affect the heat transfer rate around the perimeter of tube according to the parameters Rayleigh number to plect number, nanoparticles volume fraction, and theta it is necessary to observe the variation of the Local Nusselt number on the perimeter of tube . In generalized coordinate the local and average Nusselt number defined as the local Nusselt number around the perimeter of tube will be as follows:

$$Nu_{nt}^{k+1} = \frac{Nu^k}{\Delta R} [3T_{mt,n}^k - 4T_{mt-1,n}^k + T_{mt-2,n}^k] \quad (12)$$

The mean Nusselt number around the perimeter of inner cylinder at location (k+1) is deduced by integrating local Nusselt number as follows:

$$Nu^{k+1} = S Nu^K + (1-S) \frac{2}{f} \int_0^f Nu_{nt}^{k+1} dW \quad (13)$$

The Nusselt number is used to calculate the surface temperature at the location (k+1), but it is found that the boundary conditions causes unstable state in the solution at the value of relaxation factor ( $S = 0$ ). Therefore; relaxation factor ( $S = 0.8$ ) is used for stability considerations [23]. The above integral was calculated using Simpson's rule 1/3 method.

## 6. Results and discussion

Numerical results have been performed systematically for tube to investigate the parametric influences on the heat transfer and nanofluid flow patterns through horizontal and inclined tube filled with saturated porous medium . The heat transfer rate of the problem considered in the present study.

For a given  $Ra, Pe$  and three different values of the  $Ag$  (25nm),  $Cu$  (30nm) and  $TiO_2$ (50nm) particles volume fractions (1, 2.5 and 5% vol), Contours of dimensionless

secondary  $\left( \frac{UD}{r_{nf}}, \frac{VD}{r_{nf}} \right)$  and contours of dimensionless temperature  $\frac{(t - t_b T) k_{nf}}{q_w D}$  at fully

developed region are presented for three volume fraction percent (1, 2.5 and 5 % vol) and Rayleigh number ( $Ra=10^3, 10^5, 10^6$ ), Peclet number ( $Pe=10$ ) and  $\theta = 0$  (horizontal) in figs. (7), (8) and (9). The nanofluid rises to top of the tube filled with saturated porous medium and falls slowly toward the centerline tube because of buoyancy force. Therefore, a

secondary flow patterns appears at the tube cross section which creates a circular cell. Its position depends on the balance of the buoyancy force and the inertia of the secondary flow at the vertical plane (symmetry plane). the presence of porous media (glass beads with nanofluids) lead to more vortices. The effects of nanoparticles concentration on the secondary flow and isotherms are shown in figs. (8). Adding Ag (20nm), Cu (30nm) and TiO<sub>2</sub> (50 nm) nanoparticles in distilled water increases the effective thermal conductivity of the nanofluids and therefore the molecular heat diffusion is augmented.

For a given  $Ra=10^5$ ,  $Pe=10$ ,  $\theta=0$ (horizontal) and different volume particle fraction (1, 2.5 and 5%vol) nanofluid temperature becomes more uniform by increasing nanoparticles concentration for UHF. While the center of secondary flow is located top and bottom of the horizontal axis to eddies formed. The circulation strength is similar approximately between nanofluids and distilled water. It can be noticed as different  $\theta$ ,  $Pe=10$ ,  $Ra=10^5$  (glass beads ( $d_p=8\mu m$ )) and  $\theta=0$  (horizontal) of small second eddy formed by side the main eddy which is pushed upward and rendered unsymmetrical. The isotherms tend to become horizontal, especially in the regions away from the wall of tube, approximating the temperature distribution in a stably stratified nanofluid.

The secondary flow does not significantly change despite of higher heat flux needs to keep the Rayleigh number constant for higher particles concentration. It is expected that the heat transfer process in horizontal position is better than other angles of inclinations because of the stronger secondary flow associated with free convection which behave so as to reduce temperature difference in the tube.

Figs.(9) show the isotherms lines contour for  $Pe=10$ ,  $\theta=90^\circ$  (vertical), and  $Ra=10^4$ , for UHF. As can be seen from this figure, it is impossible to represent the secondary flow by plotting a diagram describes streamlines since stream function is equal to zero. This is a guide for accuracy of the numerical method used in solution of the governing equations of flow. The figure show on the right hand side the isotherms contour that are nearly circular and have the same center located exactly at the center of tube further indicate little influence of the convective flow on heat transfer.

Plot the contours of the stream and isotherms lines for the different inclination angles of tube ( $\theta=30^\circ, 60^\circ, 90^\circ$ ), peclet number ( $Pe=10$ ) and Rayleigh number ( $Ra=10^4$ ) can preview the form of secondary flow to clarify the impact of changing inclination angles of tube as shown in the fig. (9) on the left side. Also it can be seen the secondary flow center to be close to the wall at the horizontal position and move away gradually from the wall increase the values of inclination angles of the tube toward the vertical position. The maximum deformation in the isotherms lines and unsymmetrical about the horizontal axis of the tube. isotherms be a concentric circles perfectly with the centerline tube ( $\theta=90^\circ$ ) because of the fading effect of free convection on flow field in the tangential & radial direction and as a result of weak secondary flow currents and limited on acceleration the nanofluid velocity near the heated wall in thermally fully developed region.

The strength of secondary flow for three types of the nanofluids(Ag (20nm) - distilled water), (Cu (30nm) - distilled water) and (TiO<sub>2</sub> (50nm) - distilled water) and which be larger

than distilled water while the same behavior for the isotherms because of adding the nanoparticles in distilled water increase the effective thermal conductivity of the nanofluids and therefore the molecular heat diffusion is augmented and the nanofluid temperature becomes more uniform by increasing nanoparticles concentration. The nanoparticle Ag (20nm) is smaller than both nanoparticles Cu (30nm) and TiO<sub>2</sub> (50nm) which rendered enhancement heat transfer for the nanofluid (Ag (20nm) - distilled water) is higher than both nanofluids (Cu (30nm) - distilled water) and (TiO<sub>2</sub>(50nm) - distilled water).

Fig.(10) exhibit the change in radial velocity of the nanofluid (Cu – DW) with horizontal axis of the tube as ( $d_p=8\text{mm}$ (glass beads),  $Pe=10$ ,  $\phi = 5\%$  vol ,different Ra number ( $2 \times 10^4$ ,  $4 \times 10^4$ ) and locations along the tube. When decreasing of the Ra number the radial velocity were very small at the entrance of the tube ( $Z = 0.001, 0.01, 0.015$ ) then started increases clarity at move away from the entrance ( $Z = 0.05, 0.1$ ) due to increases strength of the secondary flow arising from the impact of natural convection. The increasing strength of the radial velocity and reverse the direction to become toward the center in the regions near of the tube surface while reversed direction the center in the regions far from the surface at the values ( $Z=0.2, 0.5$ ). When increasing of the Rayleigh number the radial velocity were similar to the previous situation with the rise in the values to this velocity for the same locations along the tube.

Fig (11) reveal the change in tangential velocity of the nanofluid for the same boundary condition in radial velocity. The tangential velocity equal to zero near the center of tube and increasing in the opposite direction to the center whenever strayed from it. This increase to access maximum value at the surface of tube. the tangential velocity increasing with Ra number increase be the same previous pattern at Ra number ( $Ra=4 \times 10^4$ ).

Fig.(12) depict the change in radial velocity of the nanofluid (Cu – Dw ) with vertical axis to same B.C above. The direction of this component towards the center of the tube at locations near the top surface of tube. The increased intensity and lower then close to zero at the center of the tube and reverse direction away from the center. The distribution pattern similar but more strongly as we move away from the entrance of the tube until access to ( $Z=0.1$ ) . When increasing of the Rayleigh number the same pattern but larger values due to increased intensity of secondary current. The radial and tangential velocity group in fig.(13) for three types of nanofluids be approximately convergent velocities and not change significant to mention in radial and tangential velocity profile group for the three types of the nanofluids.

Fig. (14) Shows the axial profile of the peripheral average for Nusselt number with different inclination angles of the tube ( $\theta = 0^\circ, 30^\circ, 45^\circ, 60^\circ, 90^\circ$ ), Rayleigh number ( $Ra=10^5$ ), Peclet number ( $Pe=10$ ) and volume fraction ( $\phi = 5\%$  vol). On the left and right side shown clearly that the increasing of the Nusselt number and when be horizontal position was higher than the vertical position at the same values of the Rayleigh number ( $Ra = 10^5$ ) due to the considerable influence of free convection currents at the horizontal position and the reason behind this is due to the buoyancy force which driven secondary flow depended on the magnitude of eddy as function of flow which determines value magnitude of each of the

radial and tangential velocity, which in turn depends on the magnitude of inclination of the tube . So the buoyancy force be in the case of the maximum value and decrease gradually when the change to the vertical position. As it is clearly seen increasing the Rayleigh number augments the buoyancy force and enhances Nusselt number at the fully developed region.

Fig.(15) represents the peripherally average skin friction coefficient to nanofluid (Ag (20nm),Cu(30) - distilled water) at constant Rayleigh number ( $Ra=10^5$ ), Peclet number ( $Pe=10$ ), volume fraction ( $\phi=0, 1, 5$  vol%) and different inclination angles of the tube ( $\theta=0^0, 30^0, 45^0, 60^0, 90^0$ ). In spite of augmenting the Nusselt number by increasing the nanoparticles concentration, the skin friction does not change. As it was seen in the previous figures, the velocity profiles and the secondary flow are not significantly affected by the nanoparticles concentration. Also at the high of the Rayleigh number by increasing the nanoparticles volume fractions does not have significant effect on Cf. In general, increasing the tube inclinations augments the flow acceleration near wall and consequently higher skin friction occurs.

## 7. Conclusion

The conclusions can be drawn from the results of theoretical study were as follows:

1. Three types of nanofluids, with 20 nm ,30 nm and 50 nm particles showed higher thermal energy rate than the base fluid.
2. The nanoparticles concentration does not have significant effect on the secondary flow, radial and tangential velocity profile , on the peripherally average skin friction coefficient and on the porous media.
3. Flow strength and thermal energy rate are increasing generally in nanofluid case comparing with pure fluid case.
4. The type of nanofluid is a key factor for thermal energy enhancement.
5. Nusselt ratio factor increase generally with Ra at constant  $\phi$  and increases with  $\phi$  at constant Ra.
6. Skin friction coefficient is augmented by increasing the tube inclinations.
7. The thermal energy rate increasing with decrease the nanoparticles size.
8. The metallic nanoparticles give higher thermal energy enhancement than nano metallic particles (oxides) due to the high thermal conductivity of metallic nanoparticles.

## Reference

- [1] Choi, S.U.S.: Enhancing thermal conductivity of fluid with nanoparticles. Dev. Appl Non – Newtonian Flows 66, 99–105 (1995).
- [2] Maiga, S.E.B., Nguyen, C.T., Galanis, N., Roy, G.: Heat transfer behaviors of nanofluid in a uniformly heated tube. Superlattices Microstruct. 35, 453–462 (2004).

- [3] Heris, S.Z., Etemad, S.Gh., Esfahani, M.N.: Experimental investigation of oxide nanofluid laminar forced flow convective heat transfer. *Int. Comm. Heat Mass Transf.* 33, 529–535 (2006).
- [4] Duangthongsuk, W., Wongwises, S.: Heat transfer enhancement and pressure drop characteristics of TiO<sub>2</sub>-water nanofluid in a double-tube counter flow heat exchangers. *Int. J. Heat Mass Transf.* 52, 2059–2067 (2009).
- [5] Santra, A.K., Sen, S., Chakraborty, M.: Study of heat transfer due to laminar flow of copper–water nanofluid through two isothermally heated parallel plates. *Int. J. Therm. Sci.* 48, 391–400 (2009)
- [6] Nguyen, C.T., Galanis, N., Polidori, G., Fohanno, S., Pota, C.V., Beche, A.L.: An experimental study of confined and submerged impinging jet heat transfer using Al<sub>2</sub>O<sub>3</sub>-water nanofluid. *Int. J. Therm. Sci.* 48, 401–411 (2009)
- [7] Wang, X.Q., Mujumdar, A.S.: Heat transfer characteristic of nanofluid: a review. *Int. J. Therm. Sci.* 46, 1–9 (2007).
- [8] Behzadmehr, A., Saffar-Avval, M., Galanis, N.: Prediction of turbulent forced convection of a nanofluid in tube with uniform heat flux using a two phase approach. *Int. J. Heat Fluid Flow* 28, 211–219 (2007).
- [9] Lee, J., Mudawar, I.: Assessment of the effectiveness of nanofluid for single-phase and two-phase heat transfer in micro-channels. *Int. J. Heat Mass Transf.* 50, 452–463 (2007).
- [10] Mirmasoumi, S., Behzadmehr, A.: Numerical study of laminar mixed convection of a nanofluid in a horizontal tube using two-phase mixture model. *App. Therm. Eng.* 28, 717–727 (2008).
- [11] Buongiorno, J.: Convection transport in nanofluid. *ASME J. Heat Transf.* 128, 240–250 (2006).
- [12] Heyhat, M.M., Kowsary, F.: Effect of particle migration on flow and convective heat transfer of nanofluids flowing through a circular pipe. *ASME J. Heat Transf.* 132, 062401 (2010).
- [13] Kuznetsov, A.V., Nield, D.A.: Thermal instability in a porous medium saturated by a nanofluid: Brinkman model. *Transp. Porous Media* 81, 409–422 (2010a)
- [14] Kuznetsov, A.V., Nield, D.A.: Effect of local thermal non-equilibrium on the onset of convection in a porous medium layer saturated by a nanofluid. *Transp. Porous Media* 83, 425–436 (2010b).
- [15] Kuznetsov, A.V., Nield, D.A.: The effect of local thermal non-equilibrium on the onset of convection in a porous medium layer saturated by a nanofluid: Brinkman model. *J. Porous Media* 14, 285–293 (2011a).
- [16] Nield, D.A., Kuznetsov, A.V.: The Cheng-Minkowycz problem for double-diffusive natural convective boundary layer flow in a porous medium saturated by a nanofluid. *Int. J. Heat Mass Transf.* 54, 374–378 (2011).
- [17] Kuznetsov, A.V., Nield, D.A.: Double-diffusive natural convective boundary-layer flow of a nanofluid past a vertical plate. *Int. J. Therm. Sci.* 50, 712–717 (2011b).
- [18] L. Badea, M. Discacciati, and A. Quarteroni. Numerical analysis of the Navier - Stokes/Darcy coupling. Technical report, Ecole Polytechnique Fédérale de Lausanne, IACS-CMCS, (2008).
- [19] Y. Xuan, W. Roetzel, "Conceptions for heat transfer correlation of Nano fluids", *Int. J. Heat Mass Transfer* (43) 3701–3707 (2000).
- [20] Barozzi, Sabbagh, G.S., Zanchini, et al, "Experimental investigation of combined forced and free convection in Horizontal and inclined tubes". *Meccanica* 20, 18–27.

- (1985).
- [21] Khanafer, K., Vafai, K., Lightstone, M., "Buoyancy – driven heat Transfer enhancement in a two dimensional Enclosure utilizing Nano fluids.Int. J. Heat Mass Transf. 46, 3639–3653.(2003).
- [22] Maiga, S.E., Nguyen, C.T., Galanis, N., Roy, G., "Heat transfer behaviors of Nano fluids in a uniformly heated tube". Super Lattices Micro structure. 35 (3-6), 543–557. (2004).
- [23] Anderson, D. H., "Computational fluid mechanics and heat transfer", Hemisphere.Washington, DC,(1984).
- [24] Mohammed,A.T., Mixed convection heat transfer in a horizontal tube filled with porous media.ph. D. Thesis, University of Technology(2000).
- [25] Carlo. N, Guidice .S.D, " Finite element analysis of laminar mixed convection in the entrance region of horizontal annuli duct "Numerical, Heat Transfer , Part A,29, PP 313 – 330 , (1996).

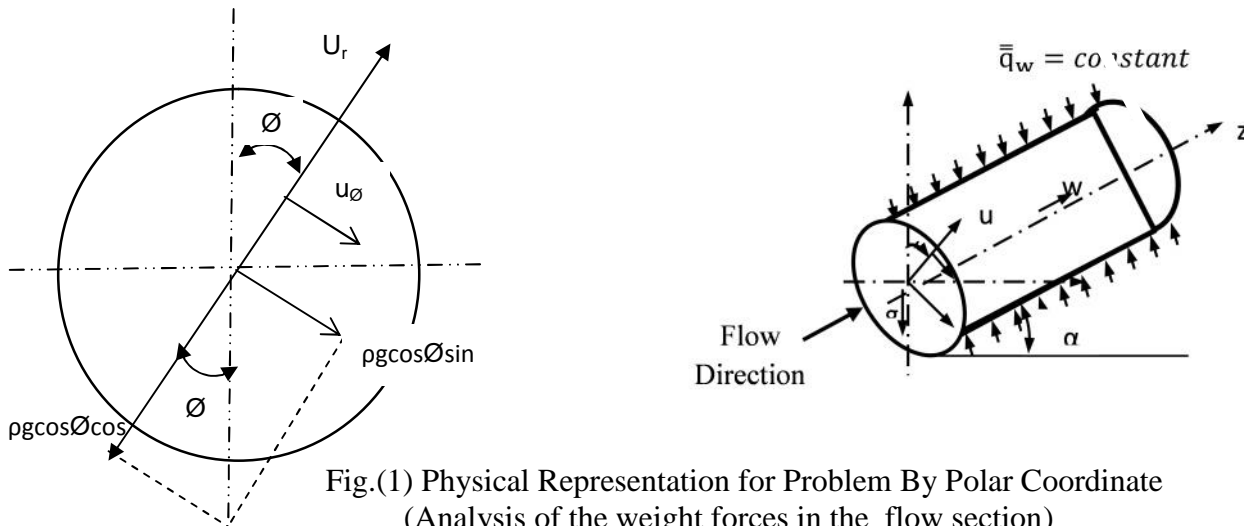


Fig.(1) Physical Representation for Problem By Polar Coordinate  
(Analysis of the weight forces in the flow section)

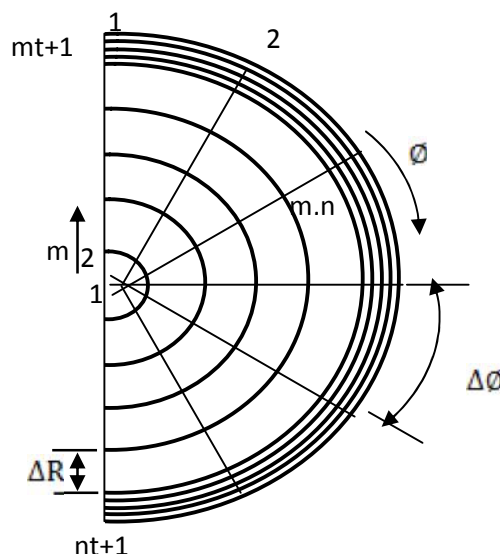


Fig. (2) Mesh network for flow region Representation

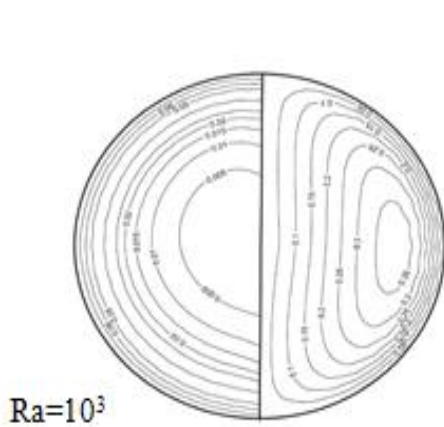


Fig (3) stream and isotherms lines [24]  
in the tube filled with porous medium

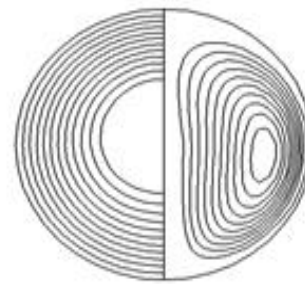


Fig (4) Present work of the stream and isotherms  
lines in the tube filled with porous medium

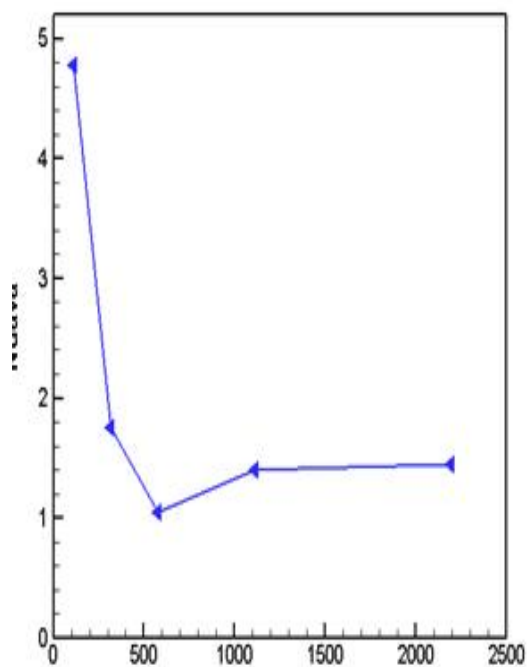


Fig (5) Grid Size Study for  $Ra=10^4$ ,  $\Phi=0$

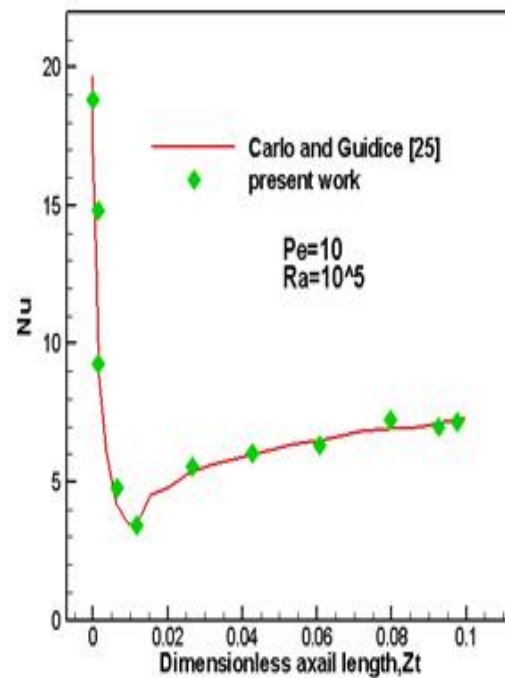


Fig (6) comparison of the present results (Nusselt  
number) with the results of Carlo and Guidice [25]

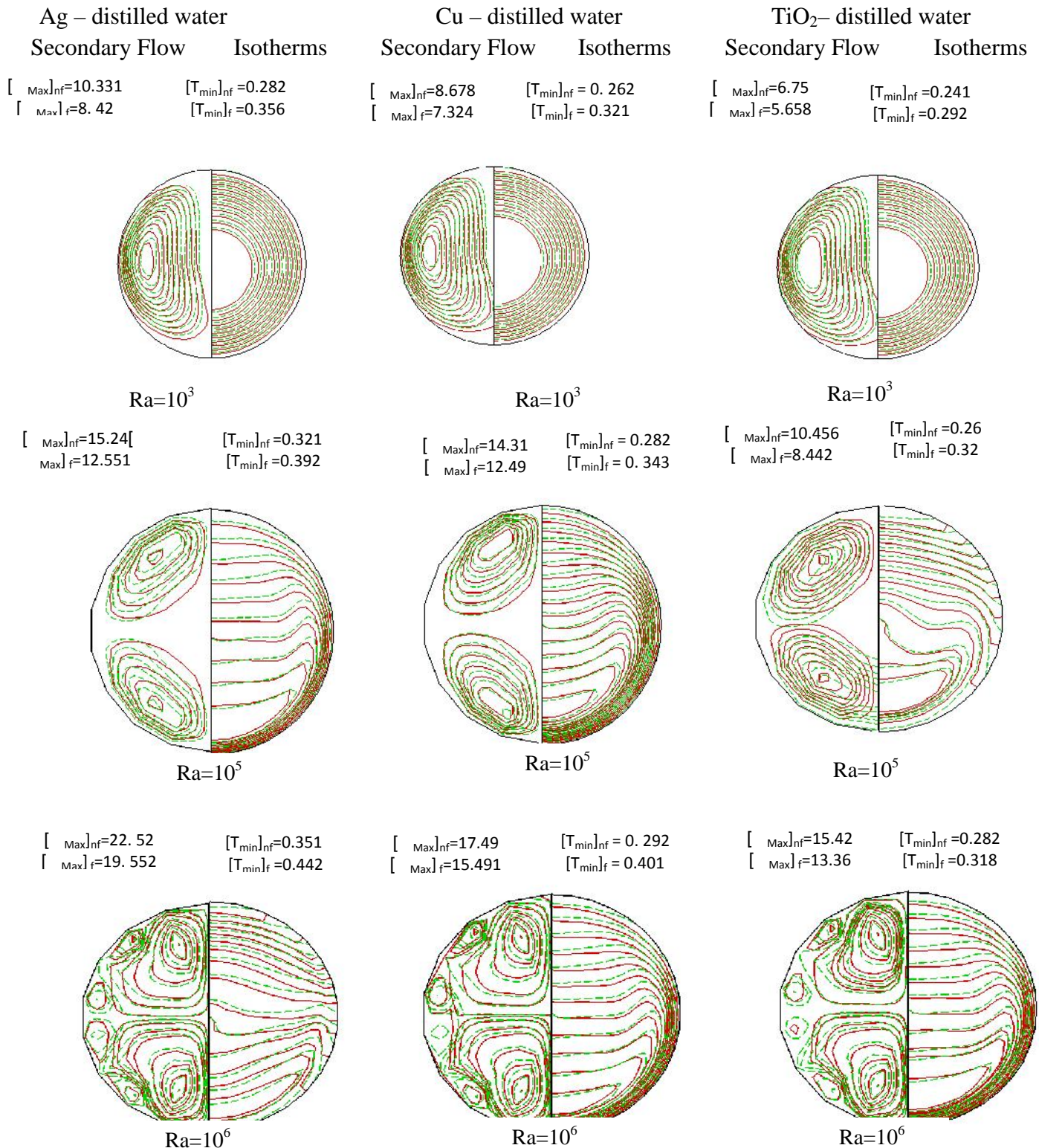


Fig.(7) : Secondary flow (on the left) and Isotherms (on the right) for Ag,Cu , TiO<sub>2</sub> – distilled water nanofluids (—) and water (---) with different Ra , Pe=10 ,  $\theta=0^\circ$  (Horizontal) ,(glass beads(dp=8mm)) and UHF

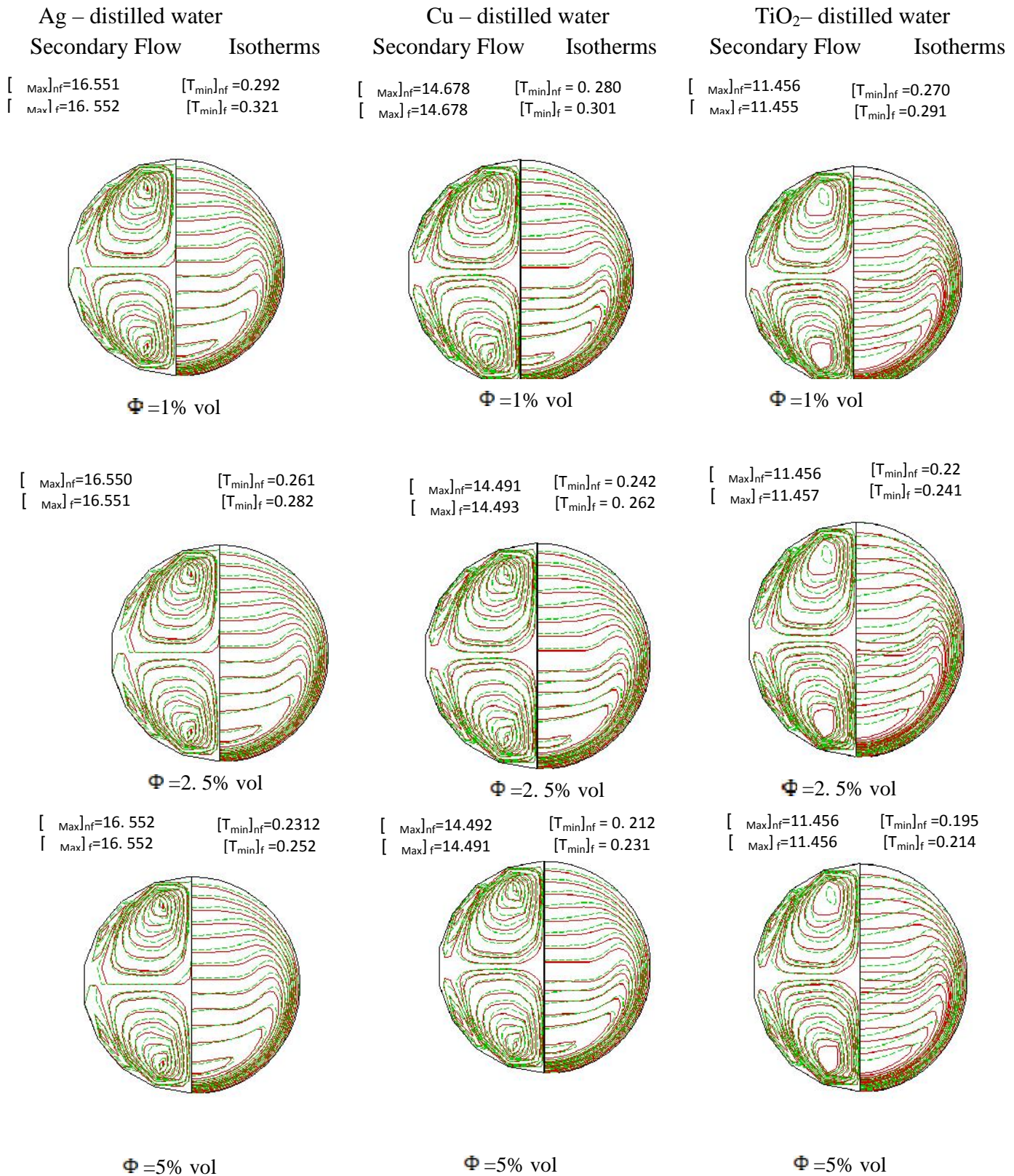


Fig.(8) : Secondary flow (on the left) and Isotherms (on the right) for Ag,Cu , TiO<sub>2</sub> – distilled water nanofluids (—) and water (---) with different  $\Phi$ , Pe=10 , Ra=10<sup>4</sup>,  $\theta=0^\circ$  (Horizontal), (glass beads(dp=8mm)) and UHF

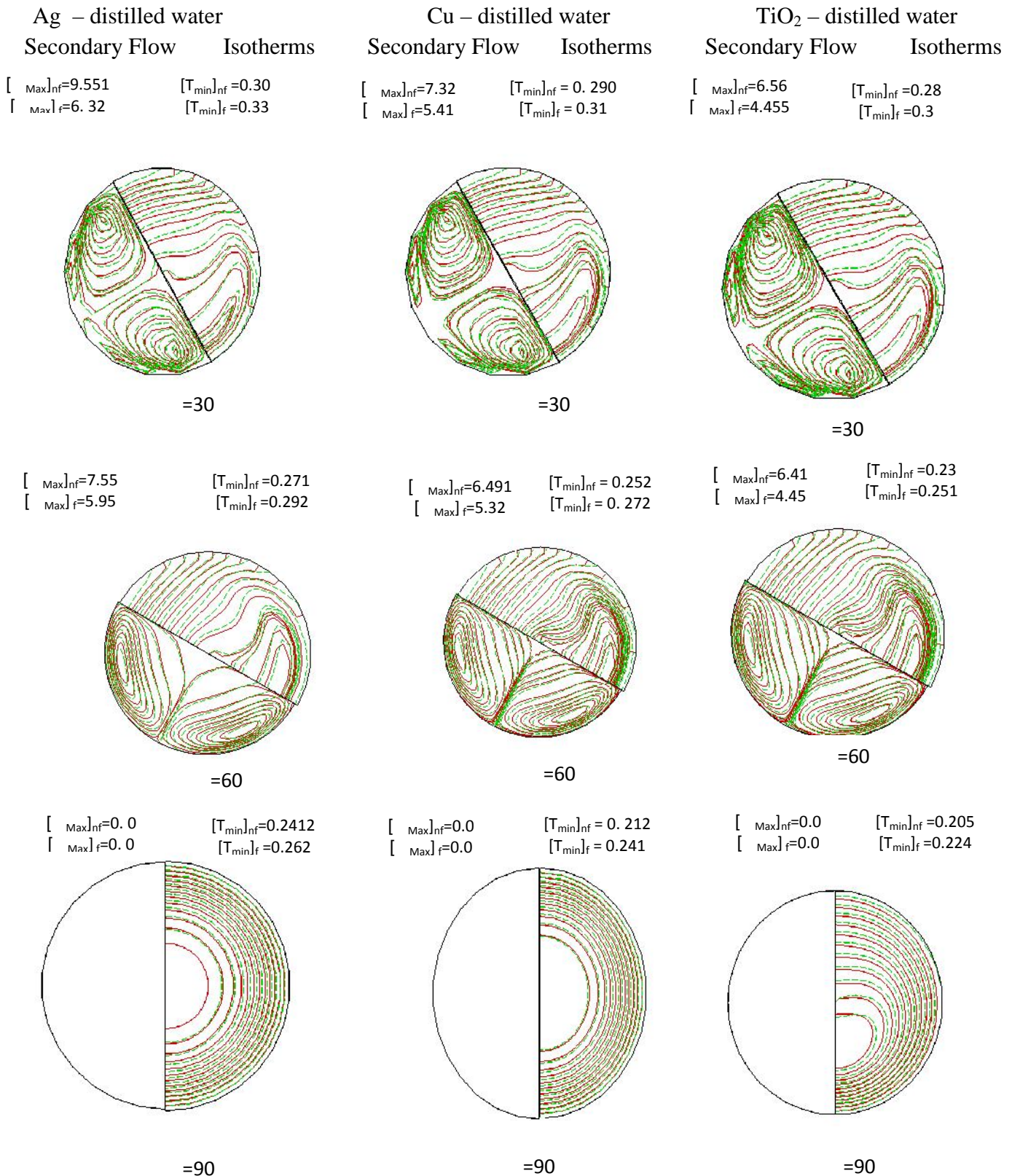
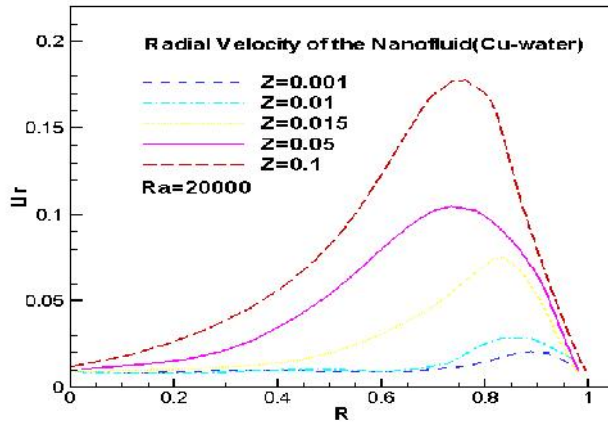


Fig.(9) : Secondary flow (on the left) and Isotherms (on the right) for Ag, Cu , TiO<sub>2</sub> – distilled water nanofluids (—) and water (---) with different , Pe=10 , Ra=10<sup>4</sup>, (glass beads(dp=8mm)) and UHF

Cu – distilled water



Cu – distilled water

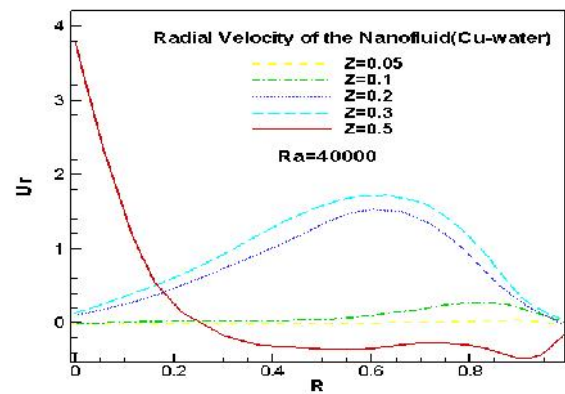
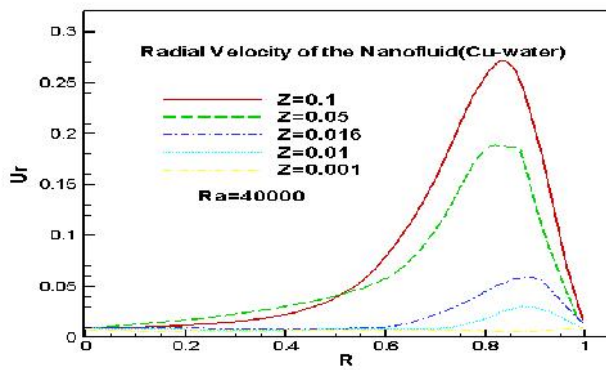
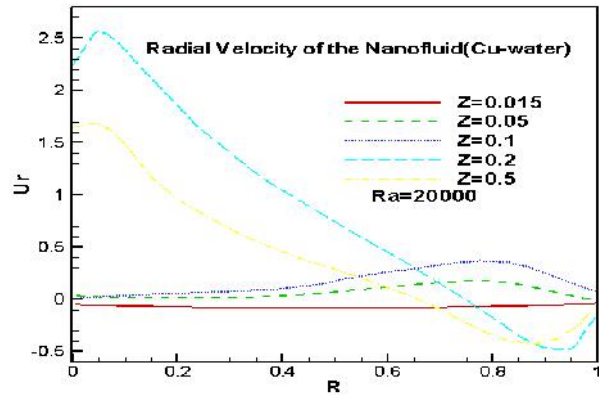


Fig. (10): Changing radial velocity of the nanofluid (Cu – distilled water) with **horizontal** axis to  $Pe=10$ ,  $\Phi=5\%$  vol ,(glass beads( $dp=8\mu m$ )) at different  $Ra$  and position on the length of the tube

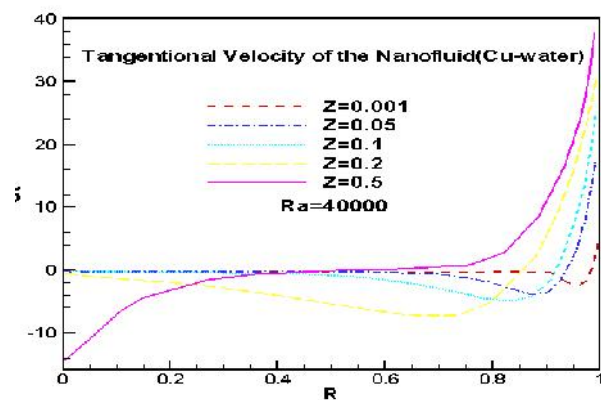
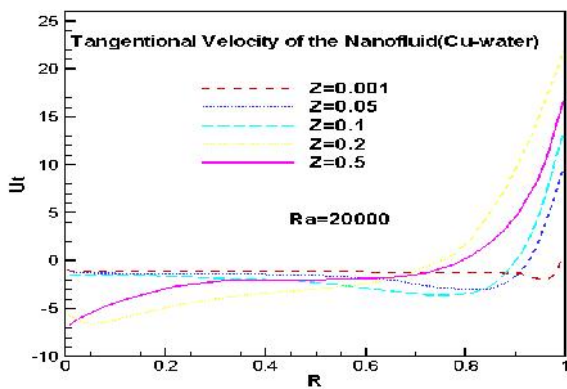
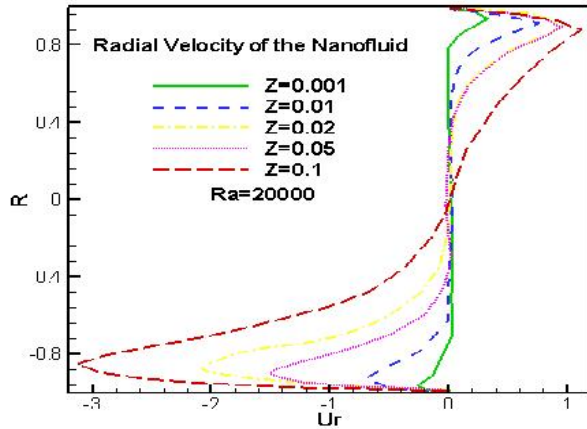


Fig. (11): Changing tangential velocity of the nanofluid (Cu – distilled water) with **horizontal** axis to  $Pe=10$ ,  $\Phi=5\%$  vol ,(glass beads( $dp=8\mu m$ )) at different  $Ra$  and position on the length of the tube

Cu – distilled water



Cu – distilled water

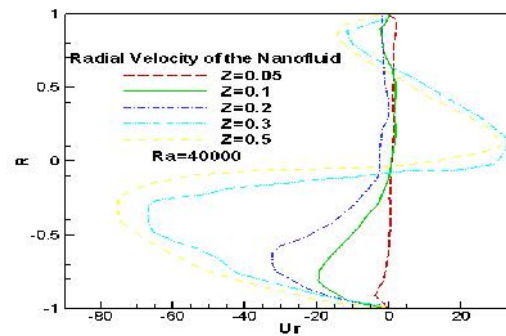
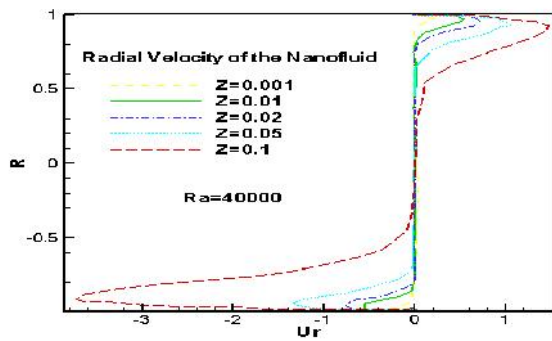
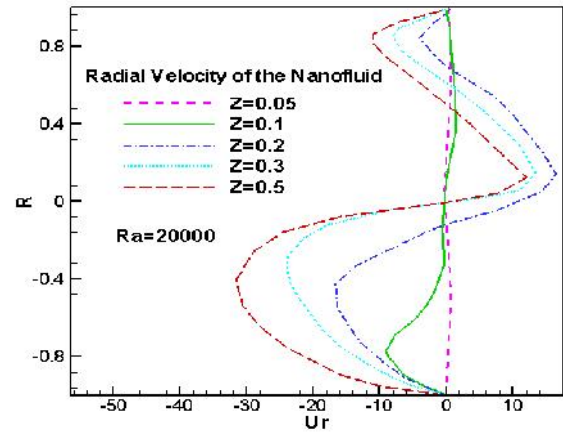


Fig. (12): Changing radial velocity of the nanofluid (Cu –distilled water) with **vertical** axis to  $Pe=10$ ,  $\Phi=5\%$  vol (glass beads( $d_p=8\mu m$ )) at different  $Ra$  and position on the length of the tube

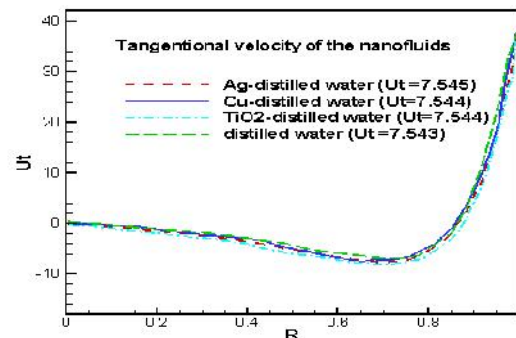
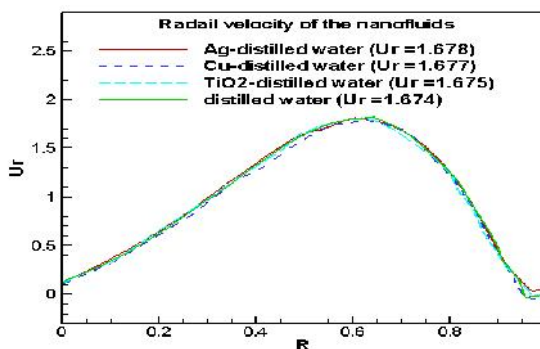
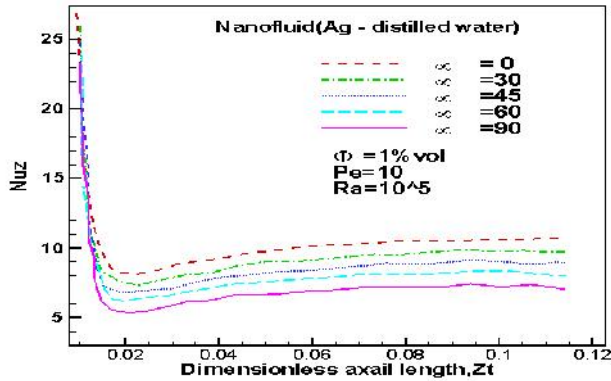
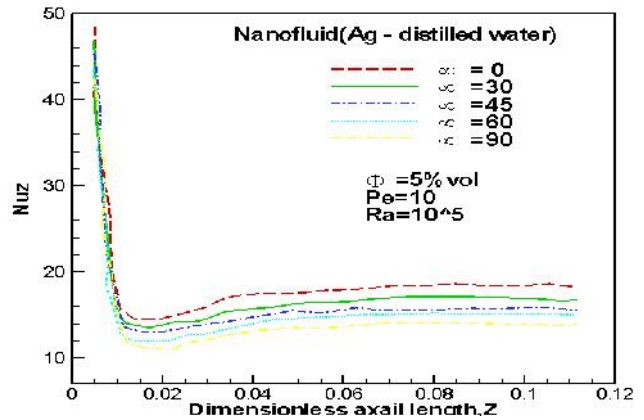


Fig. (13): Groups changing radial and tangential velocity of the nanofluids (Ag,Cu,TiO<sub>2</sub> – distilled water) with **horizontal** axis to  $Pe=10$ ,  $\Phi=5\%$  vol , $d_p=8\mu m$  at different  $Ra$  and position on the length of the tube

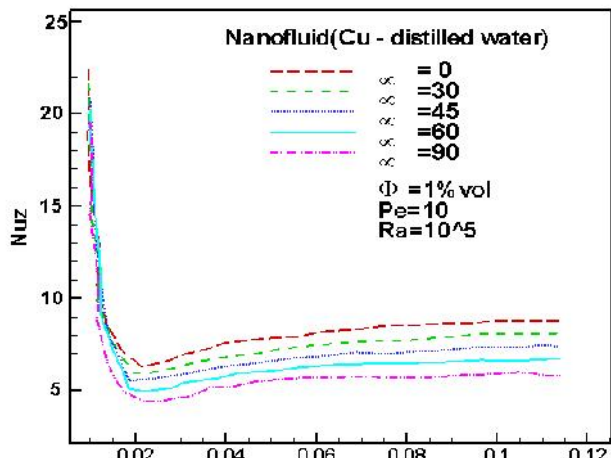
Ag – distilled water



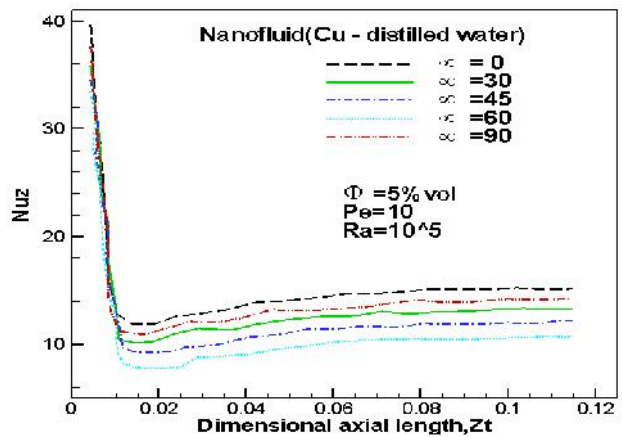
Ag – distilled water



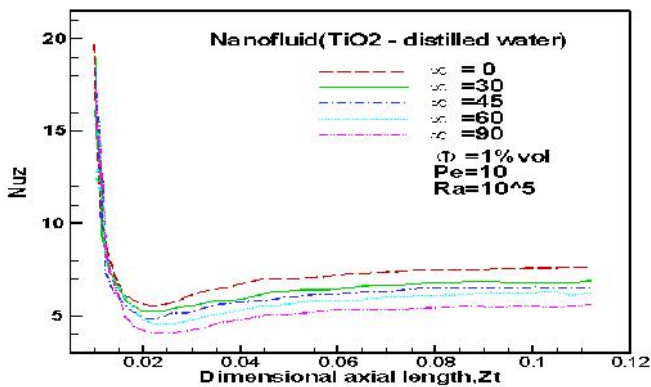
Cu – distilled water



Cu – distilled water



TiO<sub>2</sub> – distilled water



TiO<sub>2</sub> – distilled water

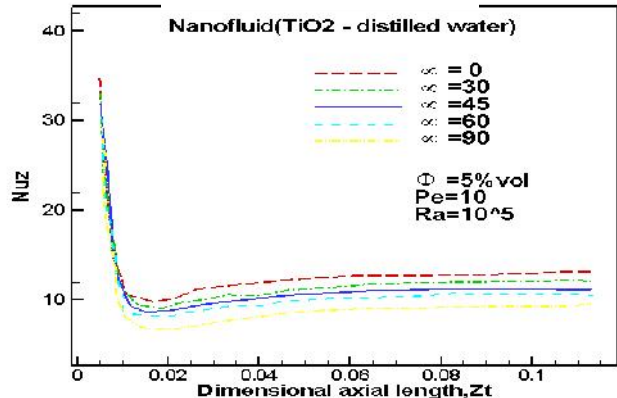
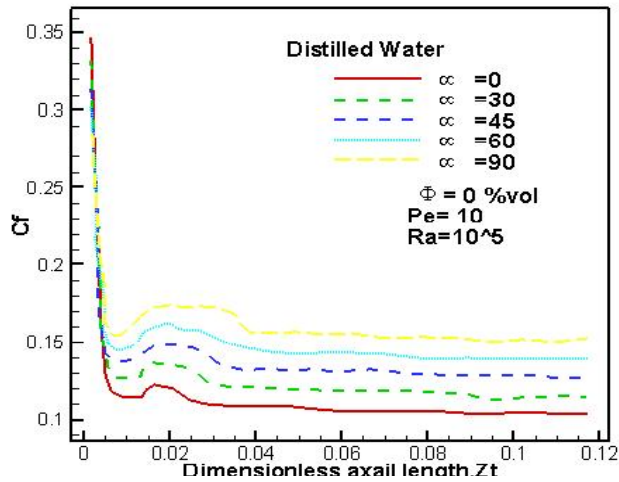
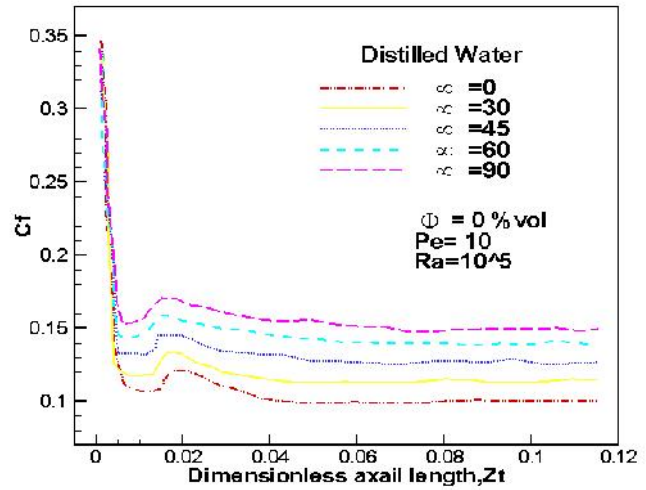


Fig. (14): Axial profile of the peripheral average Nusselt number to UHF (Ag ,Cu and TiO<sub>2</sub> – distilled water ) nanofluids with different angles,  $Ra = 10^5$  , glass beads( $dp = 8\text{mm}$ ),  $Pe = 10$ ,  $\Phi = 1\% \text{ vol}$  and  $5\% \text{ vol}$

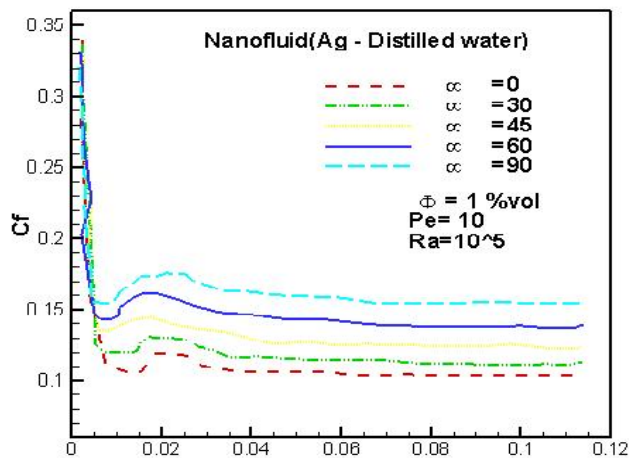
Distilled water



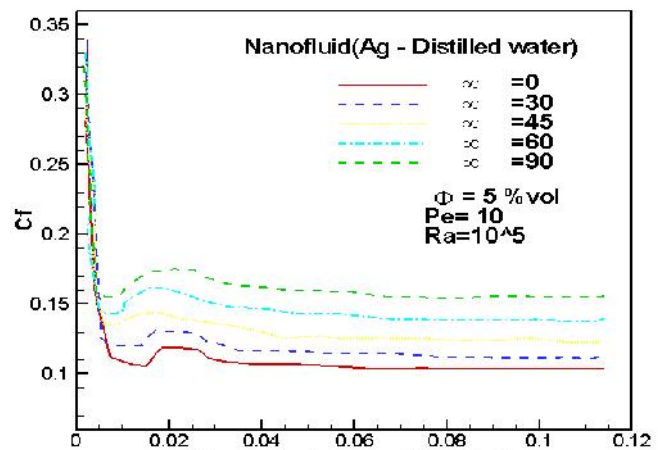
Distilled water



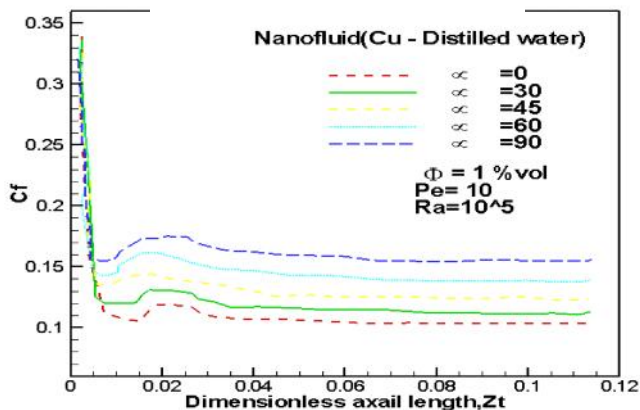
Ag – Distilled water



Ag – Distilled water



Cu – Distilled water



Cu – Distilled water

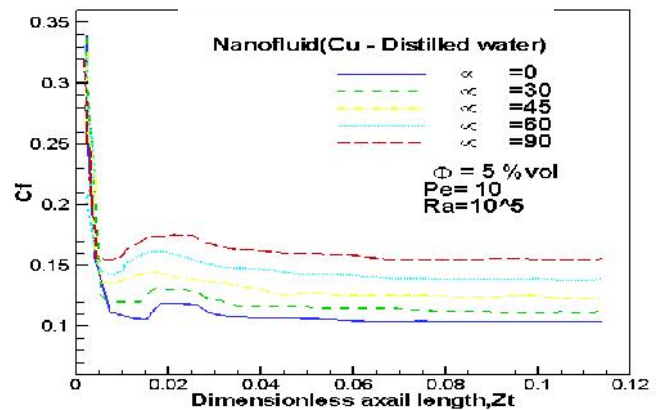


Fig. (15) : Axial profile of the peripheral average skin friction coefficient to UHF (Ag,Cu – distilled water) nanofluids with different angles,  $Ra=10^5$ , glass beads( $dp=8\text{mm}$ ),  $Pe=10$ ,  $\Phi=1\% \text{vol}$  and  $5\% \text{vol}$

## دراسة تقييمية للعوامل المؤثرة على كفاءة خلايا الوقود باستخدام النمذجة والمحاكاة

د. م جمال محمد حمد

الجامعة التكنولوجية – مركز تكنولوجيا الطاقة والطاقة المتجددة

### الخلاصة

يقدم هذا البحث عرضا لأنواع خلايا الوقود وخصائص كل نوع منها والمقارنة فيما بينها لتحديد أيهما أفضل والأكثر استخداما من ناحية الكفاءة والكلفة، بعد ذلك تم التطرق بشكل مفصل للعوامل المؤثرة على أداء الخلية منها ما يتعلق بتركيب الخلية نفسها ومنها ما يتعلق بظروف التشغيل. (Matlab)

تبين من خلال هذه الدراسة أن سمك طبقة المصعد ودرجة حرارة التشغيل لها التأثير الأكبر على أداء الخلية مقارنة

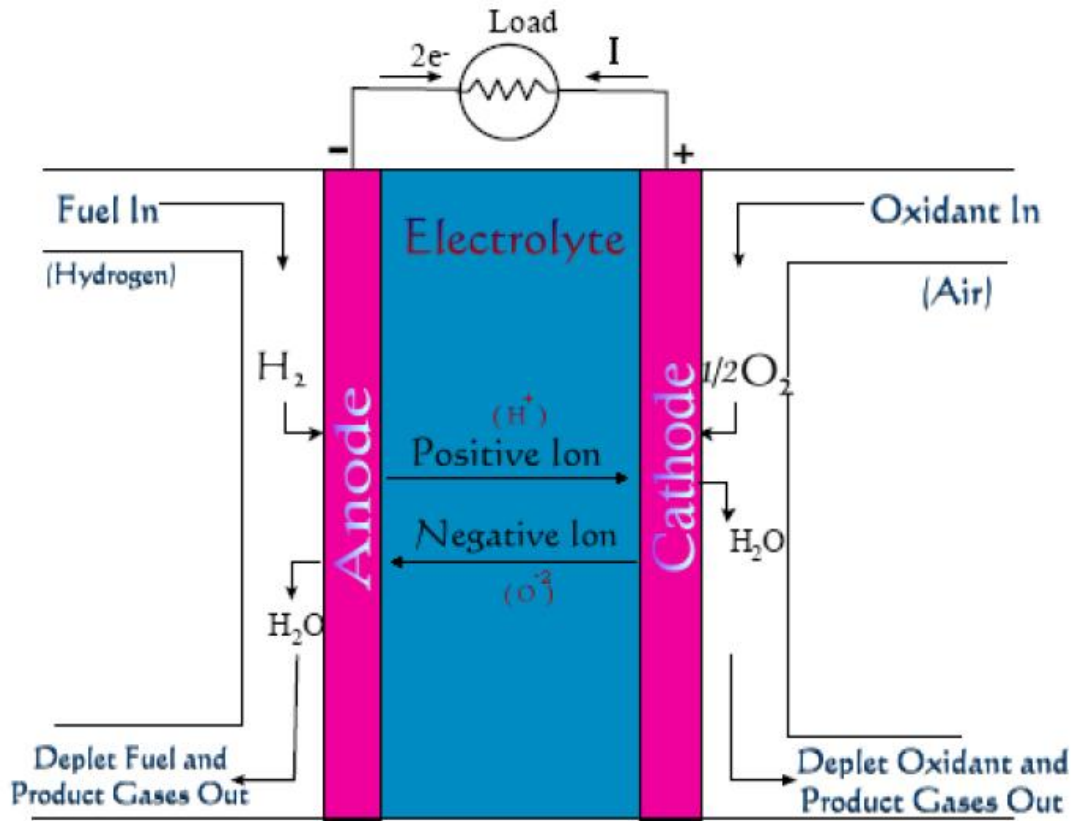
## Study evaluation the affected parameters on efficiency of fuel cells by using simulation

### Abstract

This study provides an overview of fuel cell types, characteristics and features, and then compares them to select the best for use in the field of performance and cost. Study of all structural and operational parameters, that affect of performance of cell. By use matlab program to simulated the supposing experiment. Appear for this study the thickness of the anode and operational temperature had a major effect of performance than that another parameters.

## المقدمة

يعمل الوقود على تحويل الطاقة الكيميائية التي يحويها الى طاقة كهربائية وذلك بطريقة كهروكيميائية، والتركيب البنوي للخلية يتكون من كهروليت محصور بين المهبط (مجرى الهواء) وال ( ) ( 1 - ) يوضح تركيب خلية الوقود.



( 1 - ) تركيب خلية الوقود وتفاعلاتها

يمر الوقود بشكل مستمر في المصعد (السالب) بينما تمر المادة المؤكسدة في المهبط (الموجب) وغالبا مايزود بالهواء، حيث يبدأ التفاعل الكيميائي عند الاقطاب ويقوم الكهروليت بنقل الايونات بين الاقطاب بالاضافة الى دوره بمنع الاختلاط بين الوقود والهواء.

وقد تم تصنيف خلايا الوقود استنادا الى نوع الكهروليت المستخدم والذي بدوره يحدد درجة حرارة التشغيل ونوع حامل

يمكن تصنيف خلايا الوقود حسب درجة حرارة العمل الى

1 - خلايا درجات الحرارة المنخفضة Low temperature fuel cell

2 - خلايا درجات الحرارة المرتفعة high temperature fuel cell

ل يحتاج الى معالج وقود خارجي (External reformer)

ومن أمثلتها AFC, PAFC, PEMFC

اما النوع الثاني لايحتاج الى معالج وقود خارجي فهي قادرة على معالجة الوقود الهيدروكربوني الخفيف مثل الميثان وتحويله الى هيدروجين بشكل مباشر بوجود بخار الماء مما يؤدي الى زيادة كفاءة الخلية بنسبة 14% .

#### انواع الخلايا:

1 – خلايا الوقود القلوية (AFC)

يستخدم هذا النوع من الخلايا هيدروكسيد البوتاسيوم (KOH) ككهروليت، وتتراوح درجة حرارة التشغيل ما بين (25-100) $^{\circ}\text{C}$  لكنها غالية الثمن حيث تستخدم في التطبيقات الفضائية لخفة وزنها ولا تعمل الا على الهيدروجين الصافي.

2 – خلايا حامض الفسفور (PAFCO)

يستخدم هذا النوع من الخلايا حامض الفسفور ككهروليت وتتراوح وتتراوح درجة حرارة العمل ما بين  $180-220^{\circ}\text{C}$ .

3 – خلايا الكربونات المنصهرة (MCFC)

الكهروليت المستخدم في هذا النوع كربونات الليثيوم والبوتاسيوم ( $\text{LiNaCO}_3$ ) او كربونات الليثيوم والصوديوم ( $\text{LiKaCO}_3$ ) وتبلغ درجة حرارة التشغيل لها  $600-650^{\circ}\text{C}$  .

4 – خلايا غشاء التبادل البروتوني (PEMFC)

الكهروليت المستخدم هو غشاء تبادل بروتوني مصنع من بوليمر حامض الكبريتيك المفلور (Fluorinated sulfuric acid polymer)

5 – خلايا الاوكسيد الصلب (SOFC)

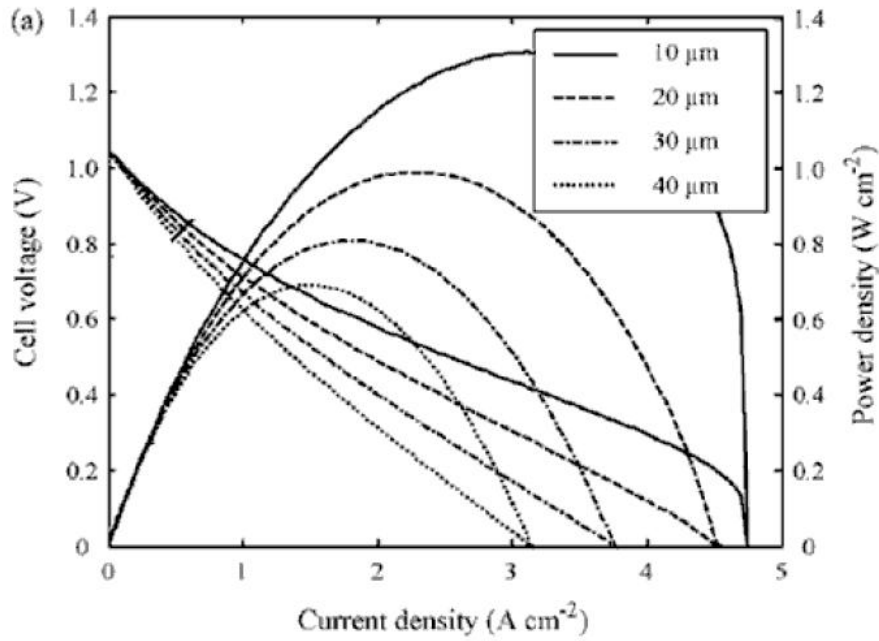
يستخدم ثاني اوكسيد الزركونيوم المثبت باوكسيد الايتريوم ( $\text{Y}_2\text{O}_3 - \text{stabilized ZrO}_2$ )  $600-1000^{\circ}\text{C}$  .

#### النتائج والمناقشة

يعتمد عمل الخلية على العديد من العوامل منها ما يتعلق بظروف العمل كدرجة الحرارة والضغط ونوع الوقود، ومنها ما يتعلق بتركيب الخلية كالاقطاب والكهروليت، وكل واحد من هذه العوامل يلعب دورا كبيرا في تحديد كفاءة اداء الخلية وهذه العوامل:

1 – سمك الكهروليت:

لدراسة تأثير سمك طبقة الكهروليت يتم تثبيت سمك طبقة كل من المهبط والمصعد، وقد وجد بانه كلما انخفض سمك طبقة الكهروليت ازدادت قيمة كثافة التيار مما يعني تحسن اداء الخلية كما هو واضح في المخطط والذي يبين كذلك زيادة تأثير ضياعات المصعد التركيزية (2 – ) .

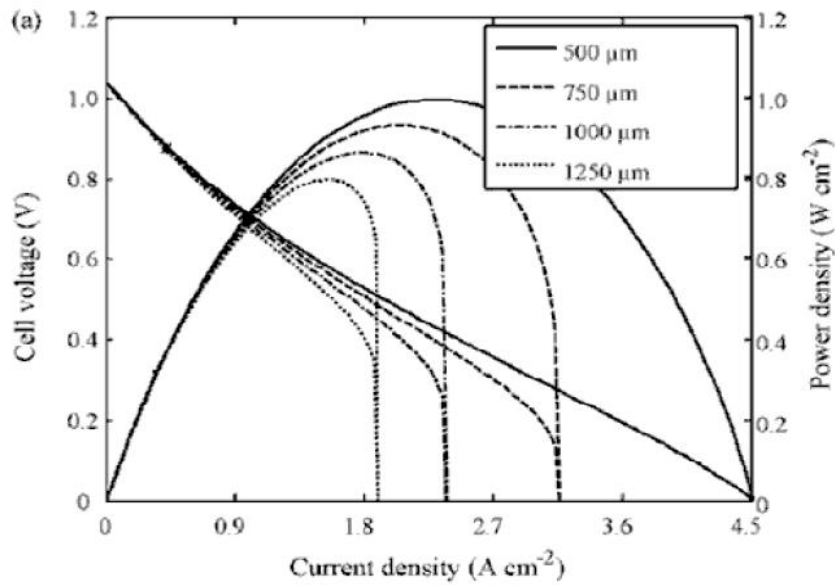


( 2 - ) ثير سمك طبقة الكهروليت على كفاءة الخلية

2

– سمك المصعد:

مع ثبات سمك كل من المهبط والكهروليت فان زيادة سمك طبقة المصعد يؤدي الى زيادة ضياعات التركيز وبالتالي داء الخلية وكما موضح في (شكل-3).



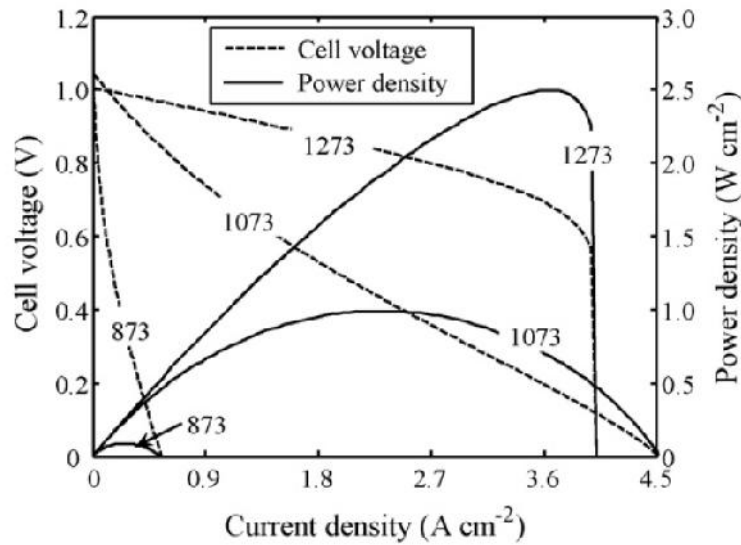
( 3 - ) تأثير تغير سمك طبقة المصعد على كفاءة الخلية

### 3 - سمك المهبط:

لا يوجد تأثير واضح عند تغير سمك طبقة المهبط على اداء الخلية حيث ان الضياعات الاومية والتركيزية تتغير بشكل طفيف وغير مؤثر.

### 4 - درجة الحرارة:

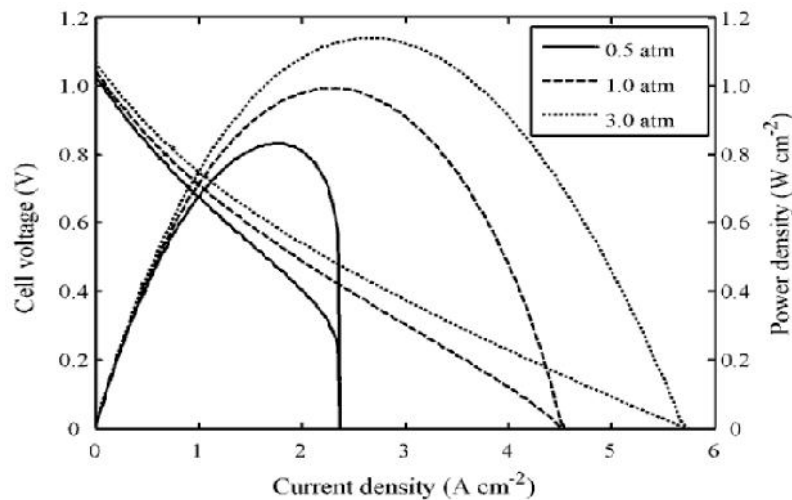
يتناسب اداء الخلية تناسباً طردياً مع درجة حرارة التشغيل، ( 4 - ) يبين تأثير تغير درجة الحرارة على اداء الخلية.



( 4 - ) تأثير تغير درجة حرارة التشغيل على كفاءة الخلية

### 5 - الضغط:

ان زيادة ضغط التشغيل يؤدي الى زيادة اداء الخلية ولكن هذا الاداء ينخفض عند زيادة الضغط الى حد معين او ما يسمى د نيرست وكما موضح في (شكل- 5).



( 5 - ) تأثير تغير ضغط التشغيل على كفاءة الخلية

## 6 – بالوقود:

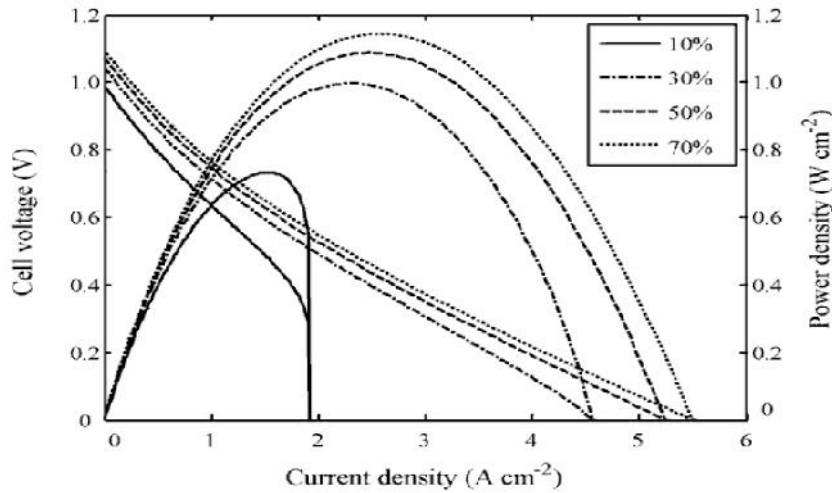
ان كمية الوقود التي تتفاعل داخل الخلية يعبر عنها مايسمى بعامل الانتفاع ويعبر عنه رياضيا

$$K_f = \frac{H_2(\text{in}) - H_2(\text{out})}{H_2(\text{in})}$$

عند زيادة عامل الانتفاع بالوقود زيادة عالية يؤدي الى انخفاض جهد الخلية حيث تحدث ضياعات تركيزية عالية ، وقد وجد عمليا ان افضل نسبة لعامل الانتفاع بالوقود هي 85% .

## 7- تركيب الوقود:

يعتبر تركيب الوقود عاملا اساسيا ومؤثرا على اداء الخلية مق ( 6- ) ادناه نلاحظ بانه كلما زادت نسبة الهيدروجين كلما ازداد اداء الخلية وتنخفض ضياعات التركيز.



( 6 – ) تأثير تغير نسبة الهيدروجين على كفاءة الخلية

## References

1. "Fuel cell", Springer Science, Business Media, LLC, USA, 2006.
2. B.J. Holland, J.G. Zhul and I. Jamet, "Fuel Cell Technology and application".
3. Prof.Hashem Orkozagh and Mas.Mohammad Mosavi" Study of the Characteristics of PEM. Fuel Cells, and its Dynamic Operation" Damascos university journal.2009.
4. Hydrogen Fuel Cell Engines and Related Technologies: Rev 0,December 2001.
5. Bouziane MAHMAH . Abdelhamid M'RAOUI . Maïouf BELHAMEL. Hocine BENMOUSSA " Experimental Study and Modelling of a Fuel Cell PEMFC Fed Directly with Hydrogen / Oxygen" June 2006 – Lyon France.
6. Yang ,C. " Introduction to Fuel Cell Science and Engineering "Lecture 5 Fuel Cell Fundamentals. Hydrogen Economy , TTP 289 -2002.
7. U.S. Fuel Cell Council ,www.usfcc.com.

## دراسة وتحليل للجدوى العلمية والاقتصادية باستخدام الطاقة النظيفة بديلاً عن مصد الطاقة التقليدية

المهندس: وليد خالد حسين  
الجامعة التكنولوجية  
مركز تكنولوجيا الطاقة والطاقات المتجددة

م.م وفاء محمد عزيز سلمان  
هيئة التعليم التقني  
معهد الإدارة /

### الخلاصة:

في هذا البحث تم عرض مصادر الطاقات المتجددة وبالتحديد منظومات الطاقة الشمسية وتوضيح جميع الجوانب العملية والبيئية التي تؤثر عليها بالإضافة الى تجارب الدول في هذا المجال و اسباب اللجوء الى الطاقة الشمسية واستخداماتها عالمياً .

و يتلخص هذا البحث بدراسة الجدوى العلمية والاقتصادية لمنظومات الطاقة الشمسية وتحليلها عن طريق دراسة تطبيقات المنظومات الغير تقليدية (الطرق الحرارية و الفوتوفولتائية) واخذ مثال لكل منهما على حده ومقارنتها بمنظومات الطاقة التقليدية ففي حالة (الطرق الفوتوفولتائية ) تم اخذ بناية دائرة حكومية كنموذج واحتساب القدرة الكهربائية اللازمة لها وبعد ذلك تم احتساب كلف المنظومات التقليدية (المولدات الديزل ) اللازمة لتشغيل البناية ومن ثم احتساب كلف الخلايا الشمسية لتوليد نفس القدرة الكهربائية .

اما بالنسبة للطرق الحرارية تم اخذ السخان الكهربائي كنموذج لمنظومات الطاقة التقليدية مع احتساب الكلف اللازمة لشراء وتشغيل مليون سخان كهربائي وكذلك احتساب الكلف اللازمة لشراء وتشغيل مليون سخان شمسي.

مما تقدم تم استخلاص النتائج والجدوى الاقتصادية والعلمية عن طريق المقارنة بين مصادر الطاقة التقليدية ومصادر الطاقة المتجددة لكل منظومة على حدة وايضاح جميع العوامل المؤثرة في عمل المنظومات واستخلاص المناقشة النهائية والتوصيات.

### 1- المقدمة:

تشكل الطاقة ركنا أساسيا في البناء الاقتصادي لجميع الدول ، حيث أصبح مقدار استهلاك الطاقة مؤشرا على تقدم تلك الدول بسبب استخدامها في جميع المجالات لذلك فأن الترشيح في استهلاك الطاقة التقليدية والبحث في ايجاد البدائل أصبح أمرا ضروريا [1]. ان الشمس هي مصدر أغلب الطاقات على الكرة الأرضية بصورة مباشرة أو غير مباشرة . ذكرت الشمس في ( 26 ) آية في القرآن الكريم وأفردت لها سورة خاصة هي سورة الشمس لأهميتها لدى الخالق عز وجل [2]. يتحول في الشمس ( 600 ) مليون طن من الهيدروجين الى هيليوم محررا طاقة تكفي ساعة منها استهلاك العالم بأكمله لمدة عام كامل ورغم هذا الفقدان في كتلة الشمس وتحولها الى طاقة قد يتراءى للبعض ان الشمس تتعرض للفناء ولكن لا داعي للقلق فأن عظمة الخالق جعلت كتلة الشمس (  $10 \times 10^{27}$  ) طن عندها تكفي لعشرة بلايين سنة [3] . يواجه سكان الأرض اليوم أكثر التحديات صعوبة على مر التاريخ متمثلة بالارتفاع الملحوظ بدرجات الحرارة نتيجة الانبعاثات للغازات الماصة للحرارة مثل ( ثاني أكسيد الكربون ، الميثان ، ثاني أكسيد الكبريت ، أكسيد النيتروز ،

والهالوكربونات). لذلك فإن استغلال الطاقة الشمسية هي أحد الخيارات المتميزة للعالم ولذلك أصبحت في عصرنا الحالي دخلاً قومياً لبعض البلدان. يتمتع العراق بمناخ جيد ومعتدل ويستلم اشعاعاً شمسياً لفترة تزيد على ( 3500 ) ساعة سنوياً وعليه فإن الفرص والامكانيات واسعة لاستغلال هذه الطاقة بأقصى درجات الفعالية والكفاءة حيث يقع العراق ضمن الحزام الشمسي الذي يستلم كمية من الإشعاع الشمسي يصل معدله (5,6- 7) كيلو واط ساعة/المتر المربع [4]. يعتبر العراق في طليعة الدول المصدرة للنفط ويمتلك ثاني أكبر احتياطي من النفط الخام (112 مليار برميل) و لكون الطاقة أعلاه قابلة للنضوب لذلك فإن الكنز الحقيقي للعراق هو الطاقة الشمسية وليس النفط ولا لابد من ترشيد استهلاكنا للنفط والنظر باهتمام الى استغلال الطاقة المتجددة في العراق (الطاقة الشمسية تحديداً) ، كل المعلومات أعلاه تعطي العراق المؤهلات اللازمة لاستغلال الطاقة الشمسية في العراق [5]. مما تقدم فإن هناك عدة تطبيقات لاستخدام الطاقة الشمسية منها:

اولا - الطرق الحرارية لتحويل الطاقة الشمسية

أ - التحلية والتعقيم للمياه

ب - التدفئة والتبريد (تسخين المياه للأغراض المنزلية والصناعية)

ج - التقنيات الحرارية لتوليد الكهرباء

ثانيا - الطرق الفوتوفولتائية ( توليد الكهرباء )

## 2- اسباب اللجوء الى استخدام الطاقة الشمسية :-

اولا- الزيادة في معدلات استهلاك الطاقة :

الزيادة في اعداد السكان والاختلاف بأساليب التكنولوجيا الحديثة في مختلف الأنشطة الحياتية أدى الى زيادة في استهلاك الطاقة سواء في المدينة او في الريف كما ازدادت الحاجة الى الطاقة في جميع القطاعات الانتاجية المختلفة للزيادة والتوسع في استعمال الآلات والأجهزة وانتاج السلع لقطاعي الزراعة والصناعة وكذلك وسائل النقل. يوضح الجدول رقم ( 1 ) الاستهلاك العالمي للطاقة ويتضح منه ان اجمالي ما استهلكه العالم من الطاقة عام 1990 على سبيل المثال قد بلغ ( 4,8 مره) قدر استهلاكه عام 1950[6].

جدول رقم (1) الاستهلاك العالمي من الطاقة حسب مصادرها الأولية (1950- 1990)  
( الوحدة : مليون ب/ي بترول مكافئ)

| السنة | زيت  | غاز طبيعي | فحم  | نووية | مائية | المجموع |
|-------|------|-----------|------|-------|-------|---------|
| 1950  | 9.1  | 3.3       | 20.9 | -     | 1.8   | 35.1    |
| 1960  | 21.6 | 8.1       | 30.0 | -     | 3.6   | 63.3    |
| 1970  | 46.4 | 18.6      | 32.7 | -     | 6.1   | 104.2   |
| 1973  | 57.0 | 22.0      | 34.1 | 1.0   | 6.8   | 120.9   |
| 1979  | 64.1 | 26.1      | 40.4 | 3.1   | 8.4   | 142.1   |
| 1980  | 61.6 | 26.7      | 41.0 | 3.5   | 8.6   | 141.4   |
| 1985  | 58.5 | 31.0      | 47.4 | 7.0   | 10.4  | 154.3   |
| 1989  | 65.0 | 35.7      | 46.3 | 9.4   | 11.1  | 167.5   |
| 1990  | 64.9 | 36.4      | 45.9 | 9.6   | 11.3  | 168.1   |

ثانياً- حماية مصادرها الطبيعية:

ان الاتجاه نحو استغلال الطاقة المتجددة يقلل من استنزاف المصادر الغير متجددة مثل النفط، والفحم الحجري والابتعاد عن الطاقة النووية لان اللجوء للطاقة النووية يعزز من استنزاف كمية هائلة من المياه، وبالمقابل اللجوء للطاقة الشمسية يقلل من استهلاك 16000 جالون من الماء سنوياً.

ثالثاً:- الاستقلالية في الطاقة:

بالاعتماد على الشمس، بالتالي نتحرر من الاعتماد على الآخرين المزودين للطاقة الغير متجددة مثل الغاز والنفط الثقيل لأنها طاقة متوفرة في معظم دول العالم.

رابعاً:- عوامل اقتصادية:

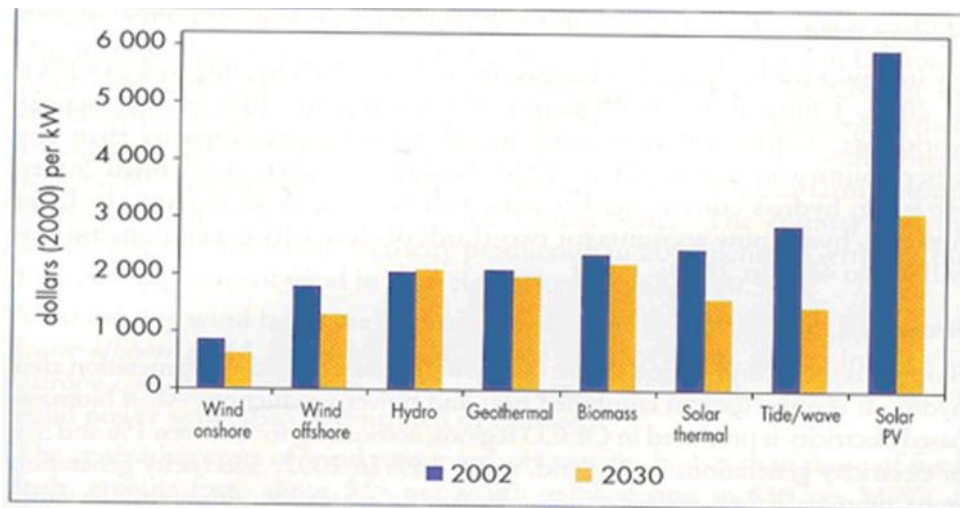
ان الطاقة الشمسية اقتصادية في كثير من الاستخدامات، وذات عائد اقتصادي كبير وذلك لضمان استمرار توافرها وبسعر مناسب وانتظام هذا السعر. ويعتمد على نوع النظام المراد استخدامه وكمية الطاقة المستهلكة.

خامساً:- عوامل بيئية:

نظيفة ولا تلوث البيئة، وتحافظ على الصحة العامة لأنها لا تحدث أي ضوضاء، أو تترك أي مخلفات ضارة تسبب تلوث البيئة. ان استهلاك 980 كيلو وات شهرياً يؤدي لإحداث ضرر بيئي كبير حيث كل منزل يفرز 7.4 طن من ثاني أكسيد الكربون، وهذا يعادل 185 طن من الغاز ثاني أكسيد الكربون خلال ال 25 سنة. ولا ننسى بأن هذا الغاز سبب رئيسي في مشكلة الاحتباس الحراري، وله مؤثرات أخرى لانقراض الكثير من الحيوانات [7].

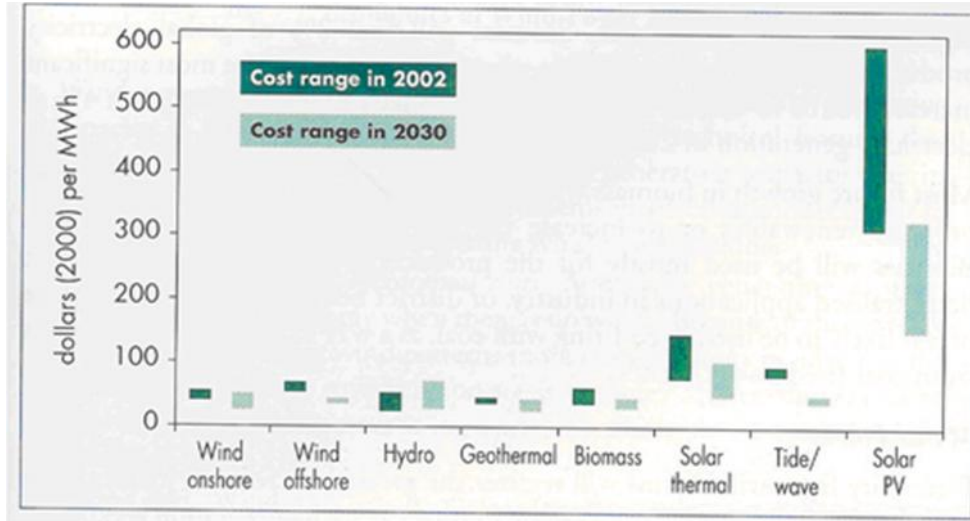
سادساً:- سعي العالم الى استغلال الطاقات المتجددة وتقدمه في هذا المجال:

أ- يسعى العالم جاهدا الى استثمار الطاقات المتجددة بكل اشكالها ويبين الشكل ادناه قيم الكلف التي ينفقها العالم لاستغلال هذه الطاقات وخصوصا الطاقة الشمسية التي تمثل النسبة الاكبر وكما موضح في الشكل رقم (1). [5].

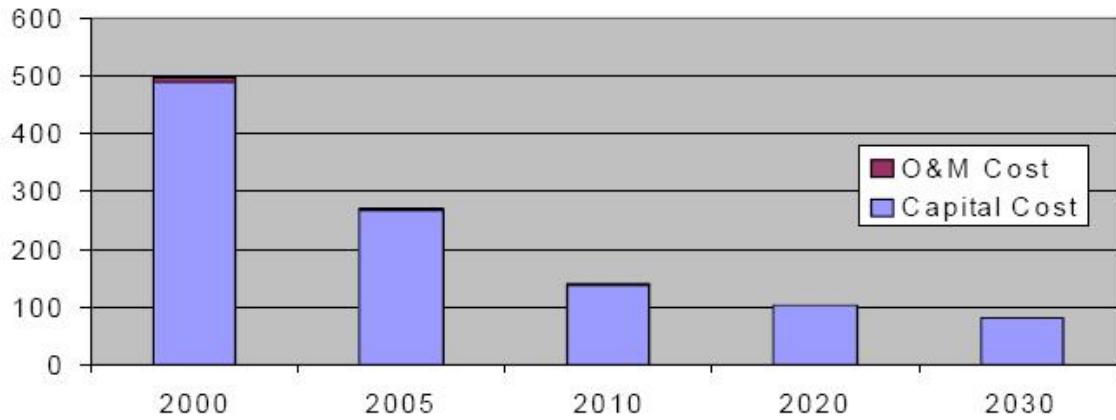


شكل رقم (1) كلف الاستثمار العالمي في مجال الطاقات المتجددة للأعوام (2030-2002)

ب- تتسع كلف انتاج الطاقة عالميا من الطاقات المتجددة وخصوصا في الدول المتقدمة حيث تنفق هذه الدول مبالغ طائلة وعالية جداً ولكن على فرض ان هذه الكلف سوف تصل الى ما دون الصفر مع مرور الزمن نتيجة الاستفادة الكبيرة من هكذا مشاريع وكما موضح في الشكل رقم (2) [5].



شكل رقم (2) نطاق كلف الانتاج من مصادر الطاقة المتجددة (2030-2002)



شكل رقم (3) انخفاض كلفة الوحدة الواحدة للطاقة بمرور الزمن [6]

ومن الجدير بالذكر ان الحاجة قائمة الى الطاقة الشمسية في بعض المناطق الخالية من مصادر الطاقة تقريبا والتي تشكو من صعوبة نقل الطاقة اليها او كلفة الصعوبات المختلفة ونقل الوقود لإنتاج الطاقة وخاصة في المناطق النائية والتي تحتاج الى اقامة مشاريع يتطلب ايجاد مصادر طاقة لتشغيلها [6].

### 3- استخدامات الطاقة الشمسية في الزراعة والري:-

أ- تحلية الماء لاستخدامات الارواء باستخدام الطاقة الشمسية :  
استخدامات الطاقة الشمسية لتقطير المياه تجربة قديمة ابتدأ بكتابتها عالم كيميائي عربي سنة 1551 وفي عام 1589 قام (الكيميائي بلابورتا) بشرح مجالات الاستخدام وفي عام 1862 قام لافواسير بتجربة استخدام عدسات كبيره بتركيز وتسلط الطاقة الشمسية. في اليونان وخليج المكسيك هناك وسائل عديدة تستخدم الطاقة الشمسية في تجهيز الماء الصحي بالاستناد الى نوعية التنفيذ والظروف المناخية [7].

ب- استخدامات الطاقة الشمسية في تشغيل منظومات الري:  
في العراق نجح مجموعة من الاساتذة والباحثين في وزارة التعليم العالي والبحث العلمي في هيئة التعليم التقني من انجاز البحث ( استخدام الطاقة المتجددة في تشغيل منظومات الري بالتنقيط باستخدام السيطرة الحديثة ) والتطبيق العملي له حيث

تم استخدام الطاقة الشمسية بدلا عن الطاقة الكهربائية في تشغيل منظومات الري والتنقيط وان الدراسة مستمرة في هذا المجال حيث تم زراعة 10 دوانم من الارض كتجربة في قرية اولاد مسلم بن عقيل (ع) ضمن قضاء المسيب في محافظة بابل. ادناه جدول يوضح مقارنه بين مضخة تقليديه تشتغل بالديزل ومضخة تشتغل بواسطة الطاقة الشمسي [7].

جدول رقم(2) : مقارنه بين المضخات التقليدية و المضخات العاملة بالطاقة الشمسية.

| نوع التشغيل    | الايجابيات                                                                                      | السلبيات                                                                                                                                                                                                                         |
|----------------|-------------------------------------------------------------------------------------------------|----------------------------------------------------------------------------------------------------------------------------------------------------------------------------------------------------------------------------------|
| الطاقة الشمسية | اقل صيانه<br>لا توجد صرفيات وقود<br>سهولة التركيب<br>بسيطة وموثوقة<br>ممكن تصنيعها لتكون متنقلة | - ذات كلفة عالية أجمالا<br>- ذات طاقة منخفضة في الجو الغائم<br>- تشتغل في اوقات شدة الاشعاع الشمسي بين الساعة التاسعة صباحا والثالثة بعد الظهر                                                                                   |
| الوقود         | ذات كلفة معتدلة<br>ممكن حملها<br>مجربه كثيرا وتتوفر خبره في تشغيلها                             | - تحتاج الى صيانة وتبديل اجزاء بشكل مستمر<br>- الصيانة غير الكفوة تقلل من عمرها<br>- تتطلب كلفة عالية بتوفير الوقود وتجهيز مستمر<br>- ينتج عن تشغيلها ضوضاء ، اوساخ ودخان<br>- تحتاج اشراف ومراقبة وزيارة لموقع النصب بشكل مستمر |

#### 4- الحسابات الرياضية والكلف للمنظومات:

اولا:- الالواح الشمسية ( الطاقة الشمسية الفوتوفولتائية ) :- تم اختيار دائرة معينة كنموذج للعمل والتطبيق ومن ثم نقوم بجولة ميدانية على الغرف الموجودة لإحصاء عدد الاجهزة وانواعها ومقدار ما تستهلكه من طاقة كهربائية كما موضح في الجداول (3,4,5) ومن ثم احتساب كلف تشغيل هذه البناية عن طريق:

أ- المصادر التقليدية للطاقة ( مولد ديزل ) .

ب- الالواح الشمسية الفوتوفولتائية.

مقدار ما تستهلكه الدائرة من طاقة كهربائية:-

- قسم الصيانة والعقود

جدول رقم (3) معدل استهلاك الطابق الثالث للدائرة من الطاقة الكهربائية

| ت                                                   | اسم الموقع       | عدد<br>الشمعات | عدد<br>المراوح | عدد اجهزة<br>الحاسوب | عدد<br>التلفزيونات | اضافات<br>اخرى | مقدار<br>التيار | مقدار تقريب التيار<br>للحد الاعلى |
|-----------------------------------------------------|------------------|----------------|----------------|----------------------|--------------------|----------------|-----------------|-----------------------------------|
| 1                                                   | مهندسين المدني   | 16             | 2              | 1                    | 0                  | 0              | 4.9             | 5 امبير                           |
| 2                                                   | مهندسي الميكانيك | 11             | 2              | 1                    | 0                  | ثلاجة          | 4.4             | 4.5 امبير                         |
| 3                                                   | المطبخ           | 11             | 2              | 1                    | 1                  | ثلاجة          | 5               | 5 امبير                           |
| 4                                                   | الحمامات         | 8+4 ص          | 0              | 0                    | 0                  | 6 مفرغات       | 6.6             | 7 امبير                           |
| 5                                                   | الممر            | 13             | 5              | 0                    | 0                  | براد           | 5.85            | 6 امبير                           |
| 6                                                   | المخزن           | 16             | 3              | 0                    | 0                  | 0              | 4.7             | 5 امبير                           |
| 7                                                   | الفنيين          | 16             | 2              | 0                    | 1                  | 0              | 4.8             | 5 امبير                           |
| 8                                                   | الادارية         | 16             | 2              | 3                    | 0                  | 0              | 5.7             | 6 امبير                           |
| 9                                                   | الحاسبة          | 8              | 2              | 4                    | 0                  | 0              | 4.6             | 5 امبير                           |
| 10                                                  | السكرتارية       | 8              | 2              | 0                    | 1                  | براد           | 3.95            | 4 امبير                           |
| 11                                                  | المدير           | 12             | 2              | 0                    | 1                  | ثلاجة كبيرة    | 5.3             | 5.5 امبير                         |
| مجموع استهلاك قسم الصيانة للتيار الكهربائي كحد اعلى |                  |                |                |                      |                    |                |                 | 58 امبير                          |

• قسم المشاريع

جدول رقم (4) معدل استهلاك الطابق الثاني للدائرة من الطاقة الكهربائية.

| ت                                                    | اسم الموقع        | عدد<br>الشمعات | عدد<br>المراوح | عدد اجهزة<br>الحاسوب | عدد<br>التلفزيونات | اضافات<br>اخرى | مقدار<br>التيار | مقدار تقريب التيار<br>للحد الاعلى |
|------------------------------------------------------|-------------------|----------------|----------------|----------------------|--------------------|----------------|-----------------|-----------------------------------|
| 1                                                    | المهندسين         | 8              | 2              | 6                    | 0                  | ثلاجة          | 6.3             | 6.5 امبير                         |
| 2                                                    | وحدة الخرائط      | 16             | 4              | 1                    | 0                  | ثلاجة          | 6.6             | 7 امبير                           |
| 3                                                    | الفنيين والحرفين  | 12             | 4              | 7                    | 0                  | ثلاجة          | 8.6             | 9 امبير                           |
| 4                                                    | الحمامات          | 12 ص           | 0              | 0                    | 0                  | 6 مفرغات       | 6.6             | 7 امبير                           |
| 5                                                    | الممر             | 7              | 7              | 0                    | 0                  | براد           | 5.85            | 6 امبير                           |
| 6                                                    | مخازن             | 24             | 6              | 6                    | 1                  | ثلاجة          | 12.3            | 12.5 امبير                        |
| 7                                                    | الدراسات          | 8              | 2              | 3                    | 1                  | ثلاجة          | 5.4             | 5.5 امبير                         |
| 8                                                    | الادارية          | 8              | 2              | 4                    | 0                  | 0              | 3.6             | 4 امبير                           |
| 9                                                    | غرفة المدير العام | 8              | 1              | 1                    | 1                  | ثلاجة          | 4.4             | 4.5 امبير                         |
| 10                                                   | السكرتارية        | 8              | 1              | 0                    | 1                  | 0              | 2.7             | 3 امبير                           |
| 11                                                   | المعاون           | 12             | 3              | 1                    | 1                  | ثلاجة كبيرة    | 6.3             | 6.5 امبير                         |
| 12                                                   | المراسم           | 24             | 6              | 10                   | 1                  | ثلاجة          | 14.1            | 14.5 امبير                        |
| 13                                                   | ممر المراسم       | 4              | 0              | 0                    | 0                  | 0              | 0.8             | 1 امبير                           |
| مجموع استهلاك قسم التصاميم للتيار الكهربائي كحد اعلى |                   |                |                |                      |                    |                |                 | 87 امبير                          |

• الورش و الاستعلامات

جدول رقم (5) معدل استهلاك الطابق الارضي للدائرة من الطاقة الكهربائية.

| ت                                             | اسم الورشة      | عدد<br>الشمعات | عدد<br>المراوح | عدد اجهزة<br>الحاسوب | عدد<br>التلفزيونات | اضافات<br>اخرى | مقدار<br>التيار | مقدار تقريبي التيار<br>للحد الاعلى |
|-----------------------------------------------|-----------------|----------------|----------------|----------------------|--------------------|----------------|-----------------|------------------------------------|
| 1                                             | التكييف         | 12             | 0              | 0                    | 1                  | ثلاجة كبيرة    | 4.3             | 4.5 امبير                          |
| 2                                             | القاعة الرئيسية | 28             | 2              | 1                    | 0                  | ثلاجة          | 7.8             | 8 امبير                            |
| 3                                             | الصحيات         | 8              | 2              | 0                    | 1                  | براد           | 3.95            | 4 امبير                            |
| 4                                             | الاستعلامات     | 4              | 1              | 0                    | 1                  | براد           | 2.65            | 3 امبير                            |
| مجموع استهلاك الورش للتيار الكهربائي كحد اعلى |                 |                |                |                      |                    |                |                 | 20 امبير                           |

إذن مجموع ما تستهلكه البناية من كهرباء=165 امبير في حالة (Full load) ولكن تعتبر هذه القيمة بعيدة عن مقدار الاستهلاك الحقيقي للتيار لأنها تفترض عمل جميع الاجهزة الكهربائية في نفس الوقت وبأقصى كفاءة. معدل استهلاك التيار الحقيقي من 100- 150 امبير وقد تم الحصول على هذه النتيجة عن طريق اخذ القيمة المعدل للتيار بعد ضربها بقيمة المصحح:-

معدل الاستهلاك الحقيقي =مقدار التيار - (عدد الغرف \* مقدار التيار%100)

معدل الاستهلاك الحقيقي=165-(0.01\*165\*28)

معدل الاستهلاك الحقيقي= 165-46.2

معدل الاستهلاك الحقيقي=118.8 امبير.

فيما يلي جدول ملحق يبين ما تستهلكه الاجهزة من تيار كهربائي وحسب القراءة التقريبية التي تم الحصول عليها من الأميتر :-

جدول رقم (6) معدل استهلاك الاجهزة من الطاقة الكهربائية.

| ت | اسم الجهاز        | مقدار سحب الكهرباء ب الواط | مقدار سحب الكهرباء ب الأمبير |
|---|-------------------|----------------------------|------------------------------|
| 1 | الشمعة الكبيرة    | 50 واط                     | 0.2 امبير                    |
| 2 | الشمعة الصغيرة    | 40 واط                     | 0.2 امبير                    |
| 3 | المروحة السقفية   | 100-55 واط                 | 0.5 امبير                    |
| 4 | الحاسبة المنضدية  | 100 واط                    | 0.5 امبير                    |
| 5 | تلفزيون مع ستلايت | 120 واط                    | 0.6 امبير                    |
| 6 | الثلاجة الكبيرة   | 250-160 واط                | 1.3 امبير                    |
| 7 | الثلاجة الصغيرة   | 150-120 واط                | 0.75 امبير                   |
| 8 | مفرغة الهواء      | 100-50 واط                 | 0.7 امبير                    |

أ- الديزل:

• يتم اختيار مولد ديزل لسد حاجة البناية من التيار الكهربائي وعلى ضوء هذا الاختيار سيتم حساب معدل المبالغ المصروفة لشراء ونصب وتشغيل المولد لمدة سنة كاملة ومن ثم احتساب معدل المصروفات لمدة خمس سنوات ، يعتبر المولد الديزل ذو مقدار توليد (80 K.V) كاتم للصوت المولد المثالي لتوليد ما يكافئ (155) امبير والذي يسد حاجة الدائرة من التيار الكهربائي المطلوب.



Q20S

وقد تم اختيار نوع (كاتم للصوت) لكي تكون منظومة توليد الكهرباء بالديزل اقرب الى المنظومة الشمسية المختارة من ناحية (الصوت والاهتزاز والضوضاء بصورة عامة).

وفيما يلي احصائيات المبالغ المدفوعة لشراء ونصب وتشغيل وصيانة المولد الديزل ويمكن تقسيمها الى:-

1- الموجودات او المصروفات الثابتة:- وهي المبالغ التي يتم صرفها عند شراء ونصب المولدة فقط كما موضح في الجدول (7) وتعتبر ثابتة وتشمل:-

جدول رقم (7) الموجودات الثابتة لمنظومة الديزل

| السعر          | التفاصيل                                                                                   |
|----------------|--------------------------------------------------------------------------------------------|
| 12600000 دينار | • شراء مولد كاز حجم (80.K.V) نوع بيركنز كاتم للصوت مع اجرة التوصيل والجينج اوفر الخاص بها. |
| 750000 دينار   | • نصب المولد ويشمل:-                                                                       |
| 250000 دينار   | • بناء الصبه مع السقيفة بمساحة (2*3)م                                                      |
| 125000 دينار   | • شراء خزان ماء وخزان كاز مع القاعدة سعة (1000) لتر                                        |
|                | • تسليك انابيب الماء والكاز واسلاك الكهرباء مع الربط                                       |
| 13725000 دينار | المجموع                                                                                    |

2- الموجودات او المصروفات المتغيرة:- وهي المبالغ المدفوعة لتشغيل المولدة بعد النصب وتعتبر متغيرة نسبيا بسبب تغير اسعار المواد واجور العمل بصورة عامة وسوف نقوم بحساب المصروفات المتغيرة لمدة سنة واحدة كما موضح في الجدول التالي:

جدول رقم (8) معدل استهلاك منظومة الديزل خلال سنة واحدة من مصاريف

| نوع العمل                                  | مدة العمل                                                      | السعر                                | اجرة العمل لفترة محددة        | اجرة العمل خلال سنة واحدة |
|--------------------------------------------|----------------------------------------------------------------|--------------------------------------|-------------------------------|---------------------------|
| • شراء كاز                                 | 150 لتر يوميا كحد ادنى للعمل (24) ساعة                         | 600 دينار للتر الواحد مع التوصيل     | 900000 دينار باليوم الواحد    | 32400000 دينار            |
| 2-تبديل دهن                                | 50 لتر لكل 10 ايام                                             | 2500 دينار للتر الواحد مع التوصيل    | 125000 دينار لكل (10) ايام    | 4500000 دينار             |
| 3-تبديل فلاتر (الدهن،الكاز، الهواء) عدد(5) | (5)فلاتر لكل (10) ايام (2) فلتر دهن،(2) فلتر كاز (1) فلتر هواء | 30000 دينار للفلتر كمعدل مع التوصيل  | 150000 دينار لكل (10) ايام    | 5400000 دينار             |
| 4-رواتب موظفي التشغيل عدد(3)               | ما يقارب 1000000 دينار اجور العاملين كمعدل للشهر الواحد        | مهندس =450000 فني=350000 مشغل=200000 | 1000000 لكل (30) يوم كحد ادنى | 12000000 دينار            |
| مجموع المصاريف لمدة سنة واحدة              |                                                                |                                      |                               | 54300000 دينار            |

#### ملاحظات:-

- جميع المصاريف المحسوبة تقريبية ولكن بالحد الادنى لقيمتها الحقيقية.
- تم اختيار اسعار افضل الانواع لكل مفردة موجودة لضمان عمل المولد بصورة جيدة ولمدة طويلة.
- تم اهمال اجرة صيانة المولد في حال عطل احد الاجزاء على افتراض ان المولد سوف يعمل بصورة جيدة لمدة سنة كاملة وبمعدل 6-8 ساعات يوميا.
- تم اهمال اجور صيانة الاسلاك والقواطع والانابيب على فرض عملها بصورة جيدة لمدة سنة كاملة.
- تم اهمال الارتفاع والانخفاض الحاصل في اسعار الكاز والدهن والفلاتر خلال السنة وتم اخذ المعدل مع التوصيل بالحد الادنى.
- تم افتراض ان المولد سوف يعمل بمعدل توليد ( 100- 150 ) أمبير اي اقل من قدرة المولد العليا لضمان طول عمر المولد.

• والان سوف نقوم بحساب مصاريف المولد الديزل لمدة خمس سنوات للاستفادة منها في دراسة الجدوى على افتراض ثبات الاسعار بالرغم من ان اسعار النفط ومشتقاته في صعود متواصل خلال الوقت، وعلى افتراض عدم عطل اي جزئ من منظومة الديزل خلال خمس سنوات، وهذه حالة مثالية ولا يمكن تحقيقها.

مجموع المبالغ المدفوعة لمدة خمس سنوات=المصروفات الثابتة+{5\*(المصروفات المتغيرة لمدة سنة واحدة)}

المجموع =13725000 دينار + {5\*(54300000 دينار)}

المجموع لمدة خمس سنوات = 284775000 دينار

اي ما يقارب 300 مليون دينار عراقي.

5- لو افترضنا ان المنظومة تعمل 25 سنة كحد أدنى فان الكلف التي تم حسابها لخمس سنوات ستتضاعف خمسة مرات :-  
 $1,500,000,000 = (5 * 300,000,000)$

ب- منظومة الطاقة الكهربائية الشمسية:-



وبصورة عامة تم اختيار مكونات المنظومة من:-

1- نوع الألواح الشمسية و المقوم العاكس Inverter والمثبتات والاسلاك وجميع التوصيلات الى حد الصامولات

تؤخذ من نفس النوع وشرط ان تكون غربية المنشاء وذات ضمان لا يقل عن خمس سنوات.

2- البطاريات (deep-cycle).

5- ملخص العروض لمجموعة من الشركات المعروفة ووفقا لأجود المواصفات مع الضمان واجور العمل مع النقل والاستيراد تبين ان سعر الواط الواحد يتراوح بين 5-10 دولار .

لذلك فأن :-

• كل 220 واط تعطي تقريبا 1 أمبير وبما ان سعر الواط \$10 كحد اعلى اذن:

سعر الامبير=  $10 * 220 = 2200$  ← كلفة انتاج الامبير الواحد تقريبا = \$2200

وبما اننا نحتاج الى ما يقارب 130 امبير لسد استهلاك الدائرة

اذن كلفة المنظومة=(سعر الامبير \* عدد الامبيرات)

$2200 * 130 = \$286000$  أي ما تعادل 343200000 دينار عراقي مع الربط كحد اعلى

• او ان سعر الواط \$7 كحد ادنى:-

سعر الامبير  $220 * 7 = \$1540$  ← كلفة انتاج الامبير الواحد تقريبا

اذن كلفة المنظومة  $1540 * 130 = \$200200$  أي ما يعادل 240240000 دينار عراقي اقل كلفة لمنظومة عالية الجودة مع الربط.

• او ان سعر الامبير \$8 وهو العرض المتوسط تقريباً ويمثل معظم العروض التي تم الحصول عليها.

سعر الامبير  $220 * 8 = \$1760$  ← كلفة انتاج الامبير الواحد تقريبا

اذن كلفة المنظومة  $1760 * 130 = \$228800$  أي ما يعادل 274560000 دينار عراقي.

ثانياً- الطرق الحرارية لتحويل الطاقة الشمسية :

تم اختيار منظومة السخان الشمسي كمنظومة اقتصادية تعمل بمبدأ الاستفادة من الطاقة الحرارية الشمسية بصورة مباشرة ومقارنتها بالسخان الكهربائي التقليدي

في أدناه احتساب مبسط كمية الطاقة الكهربائية التي سيتم تخفيضها:

أ- السخان الكهربائي ( الطرق التقليدية):

تحتاج المنازل ودوائر الدولة بصورة عامة الى سخان كهربائي يستهلك ما يقارب 2 كيلو واط من الطاقة الكهربائية، وعلى فرض استخدام 1000,000 (مليون ) سخان شمسي تكون النتائج:-



1- الكلفة الاساسية:

سعر السخان الكهربائي حالياً في الاسواق المحلية مايقارب \$100 تقريباً

الكلفة الاساسية =  $100 \$ * 1000000$

= \$100.000.000

2- كلف التشغيل: يستهلك السخان الكهربائي بصورة عامة 2 كيلو واط

استهلاك السخانات من الطاقة الكهربائية =  $1000000 * 2000$  واط

= 2000.000.000 واط

اي ما يعادل 2000 ميكا واط

كلفة التشغيل = كلفة انشاء محطة لتوليد 200 ميكا واط

تقدر سعر انشاء 1ميكا واط تقريباً بـ \$1000000

كلفة التشغيل = 2000ميكا واط \* \$1000000

= \$2000000000

اذن كلفة التشغيل 2 مليار دولار مع اهمال كلفة الوقود والصيانة للمحطة وكلفة تشغيل المحطة ككل

اي ما يعادل 2,500,000,000,000 دينار عراقي

ب- السخان الشمسي: على افتراض استخدام مليون سخان شمسي



كلفة مليون سخان شمسي = كلفة الشراء والنصب فقط.

كلفة السخان بما يكافئ 2 كيلو واط = \$340

كلفة مليون سخان = \$340 \* \$1,000,000

= \$340,000,000 اي ما يعادل 425,000,000,000 دينار عراقي

##### 5- الجدوى الاقتصادية والمناقشة :-

الحالة الاولى: المقارنة بين المصادر التقليدية للطاقة ( مولد ديزل) و الألواح الشمسية الفوتوفولتائية لغرض تشغيل دائرة بقوة 125 امبير وكما مبين في الجداول (9,10) :

أ- من الناحية المالية:-

جدول رقم (9) مقارنة بين منظومة الديزل والمنظومة الشمسية من ناحية مصاريف

| التفاصيل                                | منظومة الديزل       | المنظومة الشمسية     |
|-----------------------------------------|---------------------|----------------------|
| 1- كلفة الشراء والربط                   | 13725000            | 274560000            |
| 2- كلفة الرواتب والموظفين لمدة سنة      | 12000000 ل(3)موظفين | تقدر ب 6000000 ل(1)  |
| 3- كلفة الرواتب لمدة خمس سنوات          | 60000000            | 30000000             |
| 4- كلفة الرواتب لمدة 25 سنة             | 300000000           | 125000000            |
| 5- كلفة التشغيل لمدة سنة                | 54300000            | لا شيء ماعدا الرواتب |
| 6- كلفة التشغيل لمدة 5 سنوات            | 271500000           | لا شيء ماعدا الرواتب |
| 7- كلفة التشغيل لمدة 25 سنة             | 1357500000          | رواتب وبطاريات فقط   |
| 8- مجموع المدفوعات المتوقعة لمدة 25 سنة | 2-1,5 مليار         | 0,5-0,2 مليار        |

ب- من نواحي أخرى:-

جدول رقم (10) مقارنة بين منظومة الديزل والمنظومة الشمسية من نواحي أخرى

| التفاصيل               | منظومة الديزل | المنظومة الشمسية             |
|------------------------|---------------|------------------------------|
| 1- البيئة              | ملوثة ضارة    | صديقة                        |
| 2- عدد الموظفين        | كثير          | اقل                          |
| 3- البناء              | تحتاج         | لا تحتاج                     |
| 4- المساحات            | اشغال         | استغلال                      |
| 5- الطاقة              | زائلة         | دائمة دوام الحياة            |
| 6- حرارة الجو والابنية | زيادة         | تقليل ( بسبب التظليل والعزل) |
| 7- المصاريف            | تبذير         | توفير                        |
| 8- الانحباس الحراري    | زيادة         | تقليل                        |
| 9- اسعار الوقود        | زيادة دائما   | لا تحتاج                     |
| 10- التطوير والاستثمار | لا يوجد       | يوجد                         |

#### المناقشة للحالة الاولى:

نلاحظ من الجدول رقم (9) ان منظومة الطاقة الشمسية الفوتوفولتائية توفر ما يقارب المليار ونصف المليار دينار عراقي على مدى 25 سنة تقريبا وعلى فرض ان منظومة الديزل ( التقليدية ) تم اهمال اجرة صيانة المولد في حال عطل احد الاجزاء على افتراض ان المولد سوف يعمل بصورة جيدة لمدة سنة كاملة وبمعدل 6-8 ساعات يوميا مع اهمال ارتفاع الوقود وعلى فرض ان المولد الديزل سيعمل بنفس كفاءته لمدة 25 سنة. نلاحظ من الجدول رقم (10) ان منظومة الطاقة الشمسية الفوتوفولتائية هي الافضل والامثل للاستخدام من جميع النواحي المذكورة انفاً.

#### الحالة الثانية:

المقارنة بين منظومة السخان الشمسي كمنظومة اقتصادية تعمل بمبدأ الاستفادة من الطاقة الحرارية الشمسية بصورة مباشرة والسخان الكهربائي التقليدي:

جدول رقم (11) مقارنة بين منظومة السخان الكهربائي و منظومة السخان الشمسي من ناحية الكلفة.

| التفاصيل                                | منظومة السخان الكهربائي | منظومة السخان الشمسي |
|-----------------------------------------|-------------------------|----------------------|
| 1- كلفة الشراء والربط                   | \$100.000.000           | \$340.000.000        |
| 5- كلفة التشغيل لأول مرة                | \$2.000.000.000         | لا شيء               |
| 8- مجموع المدفوعات المتوقعة لمدة 25 سنة | \$2.100.000.000         | \$340.000.000        |

أ- من نواحي أخرى:-

جدول رقم (12) مقارنة بين السخان الكهربائي والشمسي من نواحي أخرى

| التفاصيل             | منظومة السخان الكهربائي                                      | منظومة السخان الشمسي           |
|----------------------|--------------------------------------------------------------|--------------------------------|
| 1- البيئة            | ملوثة ضارة بسبب توليد الكهرباء<br>اللازم له بالطرق التقليدية | صديقة                          |
| 4- المساحات          | اشغال                                                        | استغلال                        |
| 5- الطاقة الكهربائية | تستهلك طاقة كهربائية كبيرة                                   | لا تستهلك طاقة كهربائية        |
| 7- المصاريف          | كبيرة بسبب التشغيل                                           | شبه معدومة نسبياً              |
| 8- آلية العمل        | يحول الكهرباء الى طاقة حرارية                                | يحول الطاقة الشمسية الى حرارية |

نلاحظ من الجدول رقم (11) ان كلفة شراء السخانات الشمسية تزيد بمقدار ثلاثة اضعاف كلفة شراء السخانات الكهربائية ولكن كلفة شراء وتشغيل السخانات الشمسية هي اقل من كلفة شراء وتشغيل السخانات الكهربائية. وهذه الاحصائية تمثل الفروقات في كلف التشغيل الاولى ومع تقدم الزمن فإن الكلف تزداد بالنسبة للسخان الكهربائي وذلك بسبب الزيادة الحاصلة في اسعار الوقود بالإضافة الى كلف الصيانة والتشغيل . ويوضح الجدول رقم (12) الجوانب الايجابية الاخرى للسخانات الشمسية مقارنة بنظيرتها الكهربائية.

#### 6- الاستنتاجات:-

- 1- مما تقدم اعلاه نلاحظ ان منظومة الطاقة الشمسية الفوتو فولتائية توفر اكثر من مليار ونصف المليار دينار عراقي للبنية الواحدة تقريباً اي ما يعادل \$ 1,200,000 وعلى مدى 25 سنة وهذا المبلغ لا يمكن الاستهانة به
- 2- توفر منظومة الطاقة الشمسية الحرارية في تطبيق السخان الشمسي ما يعادل \$1,760,000,000 وهذا مبلغ كبير جداً.
- 3- يمتلك العراق ثاني أكبر احتياطي للنفط الخام ( 112 مليار برميل) ، ولكن استمرار النضوب لهذه الطاقة سوف يلجأ العلم مستقبلاً الى الطاقة الشمسية وبالنظر لمتن العراق بنسبة عالية من الاشعاع الشمسي الذي يصل معدله ( 5,5 – 7 ) كيلو واط . ساعة / المتر المربع وفترات سطوع شمسي مقدارها ( 2800 – 3300 ) ساعة / سنة كان لا بد من الوقوف والاهتمام بهذا الموضوع حيث يعتبر العراق من البلدان الغنية بالطاقة الشمسية.
- 4- يتمتع العراق بمعدل عالي من الفقر في مجال الطاقة حيث يعيش اكثر من 30% من سكان العراق في مناطق ريفية ونائية محرومة من الامدادات والخدمات الاساسية للطاقة ( وكذلك الحال حالياً في المدينة ) مما أدى الى تدهور الاوضاع الاجتماعية وانخفاض مستوى التعليم والرعاية الصحية والتنمية لذلك تعتبر حلول الطاقة الشمسية هية الحل الامثل لهكذا مشكلات.
- 5- لا توجد سياسة واضحة للطاقة في العراق وعدم ادراج الطاقات المتجددة( الطاقة الشمسية) كجزء متكامل من سياسة الدولة.
- 6- محدودية التمويل المخصص للطاقة الشمسية من المصادر الوطنية مقارنة" مع الاستثمار الضخم للنظم التقليدية مع غياب جلب الاستثمار في هذا المجال
- 7- عدم وجود سياسة ترشيد للطاقة في العراق ولا يوجد تشريع يلزم هذه السياسة باستخدام الطاقة المتجددة كما معمول به في دول العالم بما فيها الدول العربية المجاورة.
- 8- انخفاض الوعي العام في مجال الطاقة الشمسية وتقنياتها وجدواها
- 9- الاسعار الابتدائية المرتفعة لمنظومات الطاقة الشمسية يؤدي الى العزوف عن استخدامها ولكن تكمن جدواها الاقتصادية في اعمارها الطويلة
- 10- لا يوجد تنسيق عملي بين المراكز العلمية المتخصصة في مجال الطاقة المتجددة

- 11- تم تنفيذ بعض مشاريع الطاقة الشمسية بشكل انفرادي وبدون دراية بالجدوى الاقتصادية لذلك تعتبر ان العامل الاقتصادي هو عامل اساسي في أي مشروع ويجب الانتباه له.
- 12- حقيقة الحروب والصراعات الآن تهدف الى امتلاك الطاقة لانه لاهية بدونها والخوف من نضوب البترول ( 5 أو 10 ) عقود يجعل العالم يلهث من أجل البديل (و الطاقة الشمسية متوفرة لدينا).
- 13- الاستفادة من تجارب الدول في هذا المجال كما نلاحظ ان دول الجوار التي تتوفر فيها الطاقة الكهربائية بمصادرها التقليدية سبقت العراق باتخاذ التدابير المختلفة في استخدام الطاقات المتجددة و منها الطاقة الشمسية ابتداء من اكبر المجمعات السياحية والإدارية في دبي حتى وصلت إلى أن ابن البادية الذي يحمل خلية شمسية على دابته لاستعمال الطاقة الكهربائية أينما ذهب.
- 14- الاستغناء ولو بصورة جزئية عن الحاجة لمولدات الكهرباء والتي تتميز بكلف باهظة الثمن (سعر المولدة ووقود وزيت وصيانة وموصف صيانة وتشغيل) إضافة الى المخاطر الناجمة عن الوقود ونقله وتداوله.
- 15- استغلال مساحات مهدورة مثل أسطح البيوت والمدارس والمباني العامة .
- 16- التلوث الناجم عن استخدام النفط ومشتقاته لإنتاج الطاقة الكهربائية فعلى سبيل المثال أنه للحصول على كيلو وات في الساعة باستخدام الفحم ينطلق في الهواء 1,5 باوند من أكسيد الكربون و 0,2 باوند من ثاني أكسيد الكربون و 0,2 من أكسيد الكبريت و 0,25 باوند من النتروجين.
- 17- التخلص التدريجي من الانحباس الحراري من خلال تخفيض نسبة ثاني أكسيد الكربون.
- 18- يمكننا استغلال الطاقات البديلة عوضاً عن استخدام النفط ومشتقاته وكذلك الفحم في عمليات توليد الطاقة الكهربائية والتي يزداد سعرها يوماً بعد يوم وتعرض للتقلبات السريعة طرذاً مع التقلبات السياسية العالمية.
- 19- بعد نصب منظومة الطاقة الشمسية والمعدات اللازمة تصبح الكلفة مجانية وتلك المعدات تخدم لفترات تزيد عن 25 عاماً باستثناء البطارية.
- 20- مشكلة الغبار حيث برهنت البحوث والدراسات الجارية حول هذا الموضوع ان أكثر من 50% من فعالية الطاقة الشمسية تفقد في حالة عدم تنظيف الجهاز المستقبل لأشعة الشمس لمدة شهر.
- 21- مشكلة الخزن للطاقة الشمسية والاستفادة منها أثناء الليل أو الأيام الغائمة أو المغبرة ويعتمد هذا التخزين على طبيعة وكمية الطاقة الشمسية ونوع الاستخدام وفترة الاستخدام.
- 22- مشكلة التآكل في المجمعات الشمسية الحرارية بسبب الأملاح الموجودة في المياه المستخدمة في دورات التسخين.

#### المصادر

1. المصري ، رضوان عبدالغني، " دراسة استخدام الطاقة الشمسية لتسخين مياه المسابح الخارجية " ،المؤتمر الثالث، الهندسة الميكانيكية والصناعية الأردني، JMIEC، 1999.
2. Al. Saad, Mohammed. A., " Monthly Performance of Solar Water Heater for Jordan". Dirasat, Vol.x11, No.1, pp.129-149, (1985).
3. Al. Saad, Mohammed. A., Habali, S.M., Hijazi, M., Rabadi, N., " An Inexpensive & Reliable Solar Water Heater for Jordan". Dirasat, Vol.x11 No.1, pp.111-129, (1985).
4. Wei Liu, Jan H.Davidson, F.A.Kulack, and Susan C.Mantell, "Natural Convection of a Horizontal Tube Heat Exchanger Immersed in a Tilted Enclosure", ASME Journal of Solar Engineering and Solar 2002 Conference.
5. عبد الرحمن قهوجي دراسة عن أداء المجمعات الشمسية الخازنة الطباقية في ترشيد استهلاك الطاقة في المنازل في مناطق مختلفة من العراق " ،مجلة هندسة الرافدين ،المجلد 2 ،العدد 4 ،نوفمبر 1994.
6. ASHRAE. 2000. Solar Energy Equipment. Chapter 33. Standard 97-2000 (Reaffirmed 2000).
7. Al. Essa, Abdullah.H."Side By Side Comparison Of Two Types Of Integral Collector / Storage Systems", M.sc, Thesis, College of Engineering, University of Mosul-Iraq, 1993.

### دراسات الجدوى من استخدام مولد 1MW يعمل بالألواح الشمسية الفوتوفولتائية في منفذ عرعر الحدودي

رئيس مهندسين أقدم  
أحمد عبد الجبار محمود أبو الهدى  
وزارة العلوم والتكنولوجيا / دائرة الطاقات المتجددة  
بغداد- العراق

#### الخلاصة:

دراسات الجدوى من إنشاء محطة كهربائية في منفذ عرعر الحدودي ذات قدرة 1MW تعمل بالألواح الشمسية الفوتوفولتائية وبيان أفضلية نصب مثل هكذا محطات في المنافذ الحدودية بالنسبة للربط خارج الشبكة الوطنية أو ربطها مباشر الى الشبكة الوطنية علما أن أغلب المنافذ الحدودية العراقية الرئيسية موصولة بالشبكة الوطنية، وأن المحطات ذات القدرات المتوسطة والكبيرة يفضل ربطها مباشر الى الشبكة الوطنية وتكون ذات جدوى اقتصادية وذلك بإنتفاء الحاجة الى عمليات خزن الطاقة (البطاريات) والتي تعتبر مكلفة جدا. وتم حساب كلف الأضرار البيئية بالنسبة لمولد قدرته 1MW يعمل بوقود الكازأويل مستعينا بالبرنامج المعد من قبل الوكالة الدولية للطاقة الذرية .

### Feasibility studies for use generator 1MW photovoltaic solar panels in ARAR border port

Ahmed Abdul-Jabbar Mahmud  
Ministry of Science and Technology/Renewable Energy Directorate  
[Ahmed\\_abualhuda@yahoo.com](mailto:Ahmed_abualhuda@yahoo.com)  
Baghdad-Iraq

#### abstract:

Feasibility studies to create a power station in port ARAR border, capacity 1MW working in photovoltaic solar panels and statement preference monument like so stations at border crossing points for connecting stand alone or on grid, note that most border crossings major Iraqi connected to the national grid, and the stations with medium and large capacity preferably linked directly on grid to be economically feasible by preclusion need energy storage (batteries), which are very expensive. The cost was calculated for environmental damage ability 1MW generator with gasoil fuel the help of the program prepared by the International Atomic Energy Agency (IAEA).

## 1. المقدمة:

تواجه الدول النامية في الوقت الحالي العديد من تحديات الطاقة تتلخص بشكل رئيسي في :

- أ. الطلب على الطاقة بشكل متزايد
  - ب. المخاوف من ارتفاع أسعار الوقود
  - ج. إجراءات التكيف مع تغيرات المناخ
- مع تمتع الدول العربية بتوافر معدلات مرتفعة من الإشعاع الشمسي تتراوح بين 4 إلى 8 كيلوواط ساعة/م<sup>2</sup>/يوم، كما تنحصر كثافة الإشعاع الشمسي المباشر بين 1700 إلى 2800 كيلوواط ساعة/م<sup>2</sup>/السنة، مع غطاء سحب منخفض يتواجد بنسبة 10% إلى 20% على مدار العام بما يسمح بالاستخدام بشكل فعال مع التقنيات الشمسية المتوافرة حالياً.

## 2. الجدوى البيئية للمشروع

لكل مشروع آثار بيئية موجبة أو سالبة ،لذا فإن تقييم الآثار البيئية للمشروع يساعد في تقديم التوصيات بخطوات منع أو تقليل الأضرار البيئية الناتجة عن أي مشروع وزيادة المنافع البيئية الإيجابية . وكذلك تأثير البيئة على المشروع وهذا يقرر المضي قدماً في المشروع أو التوقف عنه.

## 3. الأنشطة التي لها علاقة بالمشروع

- من المنتجات البديلة لتوليد الطاقة على مستوى المؤسسات الحكومية أو لأغراض الطوارئ هو استخدام المولد الذي يعمل على الوقود (الكازاويل) وتتصف هذه المولدات الكهربائية بالمساوئ الآتية:
- أ. تستهلك كميات كبيرة من الوقود ( كلفة الوقود عالية ) .
  - ب. التلوث البيئي من احتراق الوقود والتداول الخاطئ للوقود ومنظومات التبريد بالمياه وغيرها.
  - ج. الاستهلاك السريع للمحركات، وضعف في الصيانة والخدمة.

## 4. دراسة الجدوى الفنية والاقتصادية: [1]

- أ. حساب معدل شدة الإشعاع الشمسي في منطقة عرعر الحدودي:

تم حساب شدة الإشعاع الشمسي في منفذ عرعر الحدودي عن طريق موقع ناسا ( $4.2 \text{ kWh/m}^2/\text{d}$ )

(NASA Surface meteorology and Solar Energy: RET Screen Data

Latitude 41.02 / Longitude 30.99 was chosen for ARAR)

- ب. تكاليف إنشاء محطة (1MW) تعمل بالألواح الشمسية الفوتوفولتائية في منفذ عرعر الحدودي تعمل خارج

الشبكة الوطنية (stand alone):

- (1). لغرض حساب كلفة المحطة وملحقاتها تم إجراء الحسابات حسب الاعتبارات التالية: [1]

- (أ). ساعات التشغيل 7 ساعات في اليوم و 365 يوم في السنة  
(ب). البطاريات المستخدمة 12 فولت 200 أمبير ساعة ، عمر النضيدة 5 سنوات  
(د). قدرة اللوح الشمسي 150 واط 24 فولت ، عمر اللوح الشمسي 25 سنة  
(و). Day of autonomy=1 ، زاوية ميل اللوح 45 درجة شتاء و 33 درجة صيفا  
(ز). المشروع سيقام على أرض ملك للدولة ولا تدخل قيمة الأرض ضمن الحسابات  
(2). إجمالي تكاليف الاستثمار (التكاليف الثابتة)

| ت | التفاصيل                                                                | القيمة (دولار) |
|---|-------------------------------------------------------------------------|----------------|
| 1 | مباني وإنشاءات هندسية تقام على أرض مساحتها بحدود (51750) م <sup>2</sup> | 250,000        |
| 2 | ألواح شمسية (150W 24V) عدد 17124 (1.3 دولار سعر الواط)                  | 3,424,800      |
| 3 | بطارية (Deep cycle) (12V 200Ah) عدد 5720 سعر البطارية 200 دولار         | 1,144,000      |
| 4 | ملحقات المنظومة (مسيطرات الشحن ، العواكس والمواد الخاصة بالمحطة)        | 1,000,000      |
| 5 | مواد وأعمال ميكانيكية لنصب الخلايا والمواد الملحقة بالمحطة              | 250,000        |
| 6 | وسائط نقل ومصاريف أخرى                                                  | 150,000        |
|   | المجموع بالدولار                                                        | 6,218,800      |

(3). إجمالي التكاليف السنوية (المتغيرة)

| ت | التفاصيل                                          | القيمة (دولار) |
|---|---------------------------------------------------|----------------|
| 1 | قطع غيار وصيانة (تشمل تبديل النضائد) وأجور وغيرها | 320,000        |

(4). تقييم المشروع بمعايير الربحية التجارية: [ب]

(أ). متوسط صافي التدفقات النقدية السنوية:

• سعر كيلو واط ساعة (20 سنت) (1Kwh =20 Cent)

الإيرادات السنوية بالدولار = 0.2 دولار × 1000 كيلوواط × 7 ساعة × 365 يوم = 511,000 دولار

متوسط صافي التدفقات النقدية السنوية (الأرباح) = الإيرادات - الكلف السنوية = 191,000 دولار

(ب). حساب معيار فترة الاسترداد:

معيار فترة الاسترداد = كلفة الاستثمار \ متوسط صافي التدفقات النقدية السنوية = 32 سنة

(ج). معيار معدل العائد المتوسط على رأس المال المستثمر:

معيار معدل العائد المتوسط = (الربح × 100 %) \ كلفة الاستثمار المبدئي = 3 %

(د). معيار العمر الافتراضي للمشروع :

|   |                                             |         |
|---|---------------------------------------------|---------|
| 1 | الاندثار السنوي للمباني والإنشاءات الهندسية | 12,500  |
| 2 | الاندثار السنوي للمعدات التي تعمل في المحطة | 250,000 |
|   | مجموع الاندثار السنوي                       | 262,500 |

معيار العمر الافتراضي للمشروع = الكلفة الاستثمارية \ الاندثار السنوي = 25 سنة

(5). تكاليف شراء كهرباء من مولد يعمل بوقود الكازاويل :

كلفة الحصول على ( 1MWh ) طاقة كهربائية لمدة سبع ساعات من المولدات التي تعمل على وقود الكازاويل (شراء الطاقة الكهربائية من مولدات الديزل) كالتالي :

1 ميكرواوط تعادل تقريبا 4545 أمبير (1,000,000 واط \ 220 فولت)

4545 أمبير  $\times$  10 دولار  $\times$  12 شهر = 545,400 دولار (شراء 2555 ميكرواوط ساعة سنويا)<sup>1</sup>

(أ). كلفة الأضرار البيئية : [ج]

جدول يوضح مقدار الضرر الكلي الذي تسببه الملوثات بوحدة الدولار لكل كيلوغرام

| Fuel/Tech | PM10 العوالق | Nox النترات | Sox السلفات |
|-----------|--------------|-------------|-------------|
| Diesel    | 1.70         | 0.63        | 0.43        |

جدول يمثل كميات الملوثات بوحدة gram/kWh الناتجة من حرق أنواع الوقود

| كمية الملوث / نوع الوقود | PM10 العوالق (g/kWh ) | Nox g/kWh النترات | Sox السلفات (g/kWh ) |
|--------------------------|-----------------------|-------------------|----------------------|
| Diesel( Gasoil)          | 77.8                  | 1.5               | 20                   |

الأضرار البيئية محسوبة على أساس الانبعاثات الجوية الضارة للبيئة الناتجة من حرق الوقود (Gasoil) وهي السلفات والنترات والعوالق وغيرها ومجموع هذه الأضرار على الصحة البشرية تحسب كما يأتي :  
كمية الطاقة المنتجة بوحدة kWh سنويا = 1 كيلوواط  $\times$  7  $\times$  365 يوم = 2555 كيلو واط ساعة

• السلفات  $SO_x = 2555000 \times 20 = 51000$  كيلو غرام

الكلفة =  $0.43 \times 51000 = 22,000$  دولار

مجموع الملوثات 255,000 كيلو غرام ، كلف معالجة الملوثات أكثر من 350,000 دولار سنويا .

إذن الكلفة الكلية التقريبية =  $(350,000 + 545,000) = 895,000$  دولار سنويا

ج. تكاليف إنشاء محطة (1MW) تعمل بالألواح الشمسية الفوتوفولتائية في منفذ عرعر (On Grid):

(1). إجمالي التكاليف (التكاليف الثابتة):

| ت | التفاصيل                                                                     | القيمة (دولار) |
|---|------------------------------------------------------------------------------|----------------|
| 1 | مباني وإنشاءات هندسية تقام عليها المحطة مساحتها بحدود (22145) م <sup>2</sup> | 100,000        |
| 2 | خلايا شمسية (SOLAR PANEL) (150W 30V) عدد 8000                                | 1,560,000      |
| 3 | ملحقات المنظومة (العواكس والمقاييس والكيبلات وغيرها من مواد)                 | 650,000        |
| 4 | مواد وأعمال ميكانيكية لنصب الخلايا والعواكس والمواد الملحقة بالمحطة          | 100,000        |
| 5 | وسائط نقل ومصاريف أخرى                                                       | 120,000        |
|   | المجموع بالدولار                                                             | 2,530,000      |

(2). إجمالي التكاليف السنوية (المتغيرة):

| ت | التفاصيل              | القيمة (دولار) |
|---|-----------------------|----------------|
| 1 | قطع غيار وصيانة وأجور | 45,000         |

<sup>1</sup> (سعر بيع الأمبير الواحد من المولدات الأهلية 10\$، تعمل 7 ساعات في اليوم ولمدة شهر لعام 2012)

د. مقارنة بين كلف الاستثمار في محطة ( 1M ) وتقييم المشروع بالربحية التجارية

| الجدوى الاقتصادية            | 1MW Stand alone       | 1MW connect on Grid    |
|------------------------------|-----------------------|------------------------|
| متوسط عمل المنظومة           | 7 ساعات باليوم الواحد | 4.2 ساعة باليوم الواحد |
| كلفة إنشاء المنظومة          | 6,555,200 دولار       | 2,530,000 دولار        |
| إجمالي التكاليف السنوية      | 320,000 دولار         | 45,000 دولار           |
| صافي التدفقات النقدية السنوي | 191,000 دولار         | 216,600 دولار          |
| معيان فترة الاسترداد         | 34 سنة                | 11.5 سنة               |
| معيان معدل العائد            | 3 %                   | 8.6 %                  |
| العمر الافتراضي              | 25 سنة                | 25 سنة                 |
| النتائج                      | لا توجد جدوى اقتصادية | توجد جدوى اقتصادية     |

5.الاستنتاجات:

أ. لا توجد جدوى اقتصادية من استخدام التقنية الفوتوفولتائية لمولد قدرته ( 1MW ) يعمل لوحده ( stand alone ) خارج الشبكة الوطنية في منطقة عرعر الحدودي بالنسبة للمستثمرين كون خزن الطاقة عن طريق البطاريات ذات تكلفة عالية جدا والمستثمر يهمل الربح والخسارة بالدرجة الأولى ،أما بالنسبة للدولة فهي توازن بين المنفعة الاجتماعية وتقدير الكلفة .

ب. تستخدم التقنية الفوتوفولتائية في المولدات المنزلية الصغيرة أما في المحطات الفوتوفولتائية المتوسطة والكبيرة يكون الربط مباشر الى الشبكة الوطنية للتخلص من البطاريات وتقليل الكلفة ،ولا يفضل استخدام التقنية الفوتوفولتائية في المحطات ذات السعات التوليدية الكبيرة كونها مكلفة لذا يتم استخدام المركبات الشمسية.

6.المصادر :

- استخدام برنامج ( PV SET ) المعد من مركز تكنولوجيا الطاقة المتجددة.
- دراسة الجدوى الاقتصادية وتقييم المشاريع (مشروع الإصلاح الإداري العراقي / ترابط).
- SIMPACT برنامج رياضي لحساب وتقدير التغيرات البيئية نتيجة الانبعاثات الضارة والصادرة من محطات الطاقة المعد من الوكالة الدولية للطاقة الذرية .

## 7. الملاحق

ملحق (أ) مواصفات مولد قدرة 1MW يعمل بالطاقة الشمسية والحسابات باستخدام برنامج ( PV SET )

| Specification                  | Value                      | Description     | Specification                      |
|--------------------------------|----------------------------|-----------------|------------------------------------|
| Total power                    | 1 MW                       | Solar Panel     | MonoCrystalline Solar Panel        |
| Average Irradiation            | 4.2 KWh/m <sup>2</sup> day |                 | (Peak Power) Pmax 150 W            |
| Hours per Day                  | 7                          |                 | (Maximum Power Voltage) Vmp 30 V   |
| Day per Week                   | 7                          |                 | (Maximum Power Current) Imp 5.0 A  |
| Total Energy                   | 7 MW/day                   |                 | (Open Circuit Voltage) Voc 36 V    |
| Efficiency of inverter         | 0.85                       |                 | (Short Circuit Current) Isc 5.55 A |
| Efficiency of charger          | 0.9                        |                 | Module Dimensions (1333*813*35) mm |
| Tolerance of solar panel       | 5%                         | Storage Battery | Maxima 200Ah 12V                   |
| Days of Autonomy               | 1                          |                 | Rated Voltage 12 V                 |
| Efficiency of Battey           | 0.8                        |                 | Rated Capacity 200 Ah              |
| Depth of Discharge             | 0.75                       |                 | Dimension (50*25*25) cm            |
| Number of PV                   | 17124 pcs                  |                 | Temperature Range (C) -20 To +60   |
| Number of Batteries            | 5720 pcs                   |                 | Weight of Battery 60 Kg            |
| Inverter Sizing                | 1300 kw                    |                 |                                    |
| Solar charge controller sizing | 53221 A                    |                 |                                    |
| Active Area of PV Array        | 16758.84 m <sup>2</sup>    |                 |                                    |

### ملحق (ب) حساب مساحة المحطة

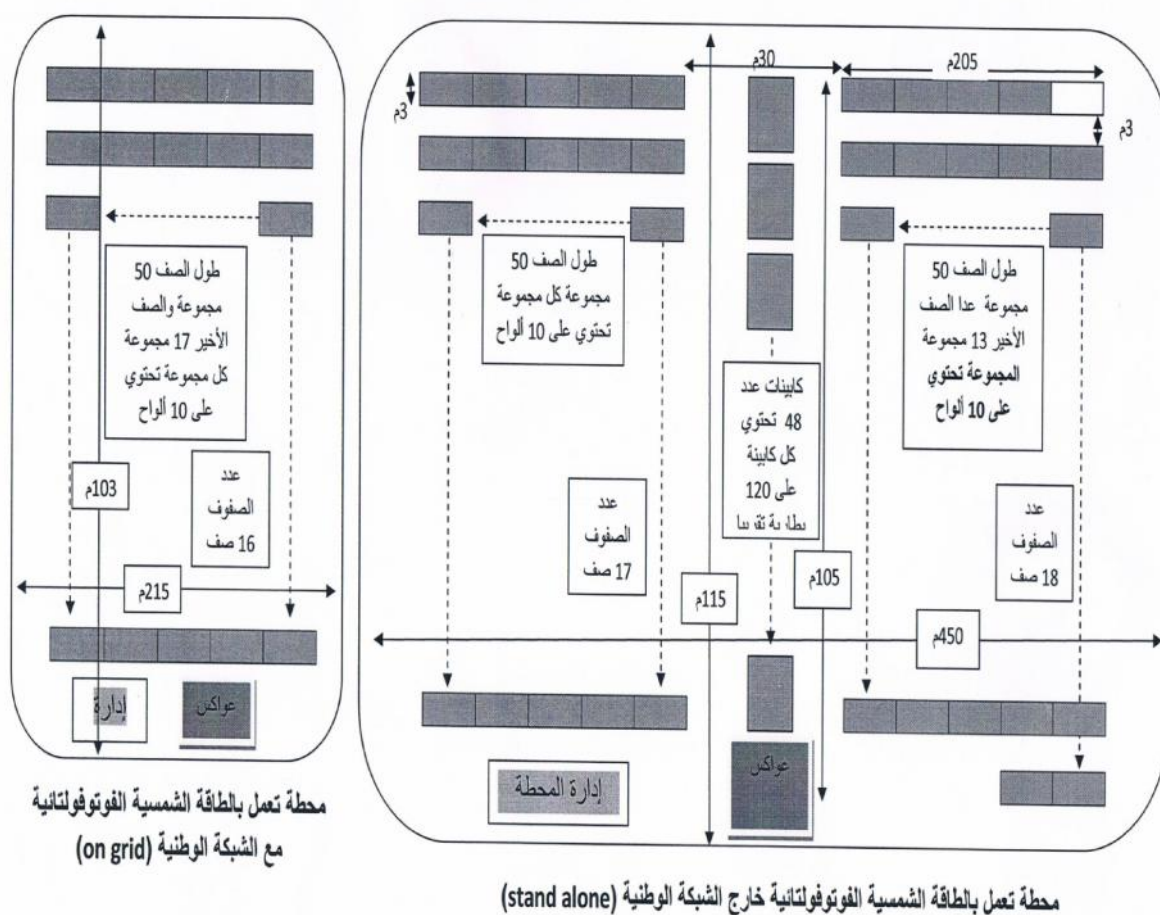
#### • حساب مساحة المحطة (1Mw stand alone) ، عدد الألواح الشمسية 17124

يتم تقسيم الألواح إلى مجاميع تحتوي كل مجموعة على 10 ألواح شمسية (5×2)  
عرض مجموعة الألواح  $2 \times 1.333 = 2.666$  متر عدد تقرب إلى 3 م عند الربط  
طول مجموعة الألواح  $5 \times 0.813 = 4.065$  متر تقرب إلى 4.1 م عند الربط  
يتألف الصف من 100 مجموعات (طول 450 متر) عدد الألواح 1000 لوح  
ويكون الصف 50 مجموعة متصلة وبعدها فاصل 40 متر وبعدها تكمل الصف 50 مجموعة.  
طول 50 مجموعة (  $4.1 \times 50 = 205$  متر )  
طول المحطة  $5 + 205 + 30 + 205 + 5 = 450$  متر  
تتألف المحطة من 17 صف مكون من 100 مجموعة وصف واحد يتكون من 13 مجموعة  
وبهذا يكون عدد الألواح الشمسية 17130 لوح  
يوجد طريق بين صف وآخر عرضه 3 متر لغرض تنظيف الألواح والتخلص من الظل  
المسافة بين السياج الخارجي والألواح 5 متر  
عرض المحطة  $5 + 3 \times 17 + 3 \times 18 + 5 = 115$  متر  
المساحة الكلية للمحطة  $115 \times 450$  متر عرض طول  $51750$  متر مربع  
طول السياج المحيط بالمحطة  $(450 + 115) \times 2 = 1130$  متر

#### • بنفس الطريقة حساب مساحة المحطة (1Mw on grid) : عدد الألواح الشمسية 8000

طول المحطة  $5 + (50 \times 4.1) + 5 = 215$  متر ، عرض المحطة  $5 + (31 \times 3) + 5 = 103$  متر  
تتألف المحطة من 16 صفوف مكون من 50 مجموعة  
المساحة الكلية للمحطة  $103 \times 215$  متر (عرض)  $22145$  متر مربع  
طول السياج المحيط بالمحطة  $(215 + 103) \times 2 = 636$  متر

ملحق (ج) مخطط يوضح فرق المساحة لمحطات توليد الطاقة الكهربائية باستخدام الخلايا الشمسية الفوتوفولتائية



## اللجنة العليا المشرفة

أ.د. امين دواي ثامر/ رئيس الجامعة التكنولوجية

أ.د. محمد يحيى جاسم العاني / مساعد رئيس الجامعة للشؤون العلمية

أ.م.د. علي هادي عبد المنعم/ مدير مركز تكنولوجيا الطاقة والطاقات المتجددة

## اللجنة التحضيرية

أ.م.د. علي هادي عبد المنعم/ مركز تكنولوجيا الطاقة والطاقات المتجددة / رئيسا

د. قصي عبد الجبار جواد / مركز تكنولوجيا الطاقة والطاقات المتجددة

د. جعفر علي كاظم / مركز تكنولوجيا الطاقة والطاقات المتجددة

د. جمال محمد حمد / مركز تكنولوجيا الطاقة والطاقات المتجددة

د. مهدي علي عبد الحسين/ مركز تكنولوجيا الطاقة والطاقات المتجددة

د. ضياء الدين حسين علوان/ الكلية التقنية –

/ .

ضياء نجم عبد الامير/ مركز تكنولوجيا الطاقة والطاقات المتجددة

كاظم حسين صفر/ جامعة النهرين

وليد خالد حسين/ مركز تكنولوجيا الطاقة والطاقات المتجددة

## اللجنة العلمية

أ.د. محسن جبر جويج/ جامعة النهرين

أ.م.د. علي هادي عبد المنعم/ مركز تكنولوجيا الطاقة والطاقات المتجددة

أ.م.د. عبد الجبار نعمة خليفة/ جامعة بغداد

أ.م.د. عباس زغير سلمان/ مركز تكنولوجيا الطاقة والطاقات

أ.م.د. عبد القادر داود فيصل / مركز بحوث النانو تكنولوجي

د. محمد احمد صالح/ وزارة الكهرباء

## اللجنة التنظيمية

. سلافة اسماعيل ابراهيم

. . حيدر شريف مهدي

. .

. . ايمان علي احسان شيت

. .

ميثم طارق مهدي

## الجهات الساندة للمؤتمر

جامعة النهرين

الكلية التقنية –